Université de Montréal

Understanding cone photoreceptor dystrophies: from animal models to engineered patient-derived retinal tissues

Par

Andrea Barabino

Programme de biologie moléculaire, Faculté de médecine,

Université de Montréal

Thèse présentée en vue de l'obtention du grade de doctorat

en biologie moléculaire

Avril 2021

Université de Montréal

Unité académique : département de biologie moléculaire, Faculté de médecine

---

A été évaluée par un jury composé des personnes suivantes

Dr. Massimiliano Paganelli
Président-rapporteur

Dr. Gilbert Bernier
Directeur de recherche

Dr. Przemyslaw(Mike) Sapieha
Membre du jury

Dr. Thomas Durcan
Examinateur externe

Résumé

La vision est considérée comme un des sens les plus importants, prenant en charge environ 80% des perceptions que nous recevons dans notre vie quotidienne. Les photorécepteurs de type cônes sont responsables de la vision centrale de haute résolution et en couleurs, et leur dégénérescence est souvent la cause de la perte de vision dans les maladies dégénératives rétiniennes (RDs). Les RDs sont un groupe hétérogène de maladies affectant des millions de personnes dans le monde, qui pour le moment sont pour la plupart sans aucune option thérapeutique.

Les modèles animaux sont extrêmement utiles pour étudier le développement ou la dégénérescence de la rétine, ainsi que pour comprendre les mécanismes moléculaires des maladies génétiques héréditaires affectant les photorécepteurs. La modélisation des maladies dégénératives et du développement peut être particulièrement difficile, spécialement dans le cas de maladies humaines rares et complexes pour lesquelles aucun modèle animal exhaustif n'est disponible. De nos jours, la génération et le maintien de modèles de maladies humaines permettant une analyse approfondie du mécanisme moléculaire représente un grand défis . La technologie des cellules souches possède un grand potentiel dans la modélisation des maladies et représente un outil puissant pour générer des modèles évolutifs, sans l'utilisation d'animaux qui peuvent illustrer plus précisément les phénotypes cliniques de maladies humaines complexes.

Nous avons développé un protocole pour différencier les cellules souches pluripotentes (PSCs) en feuillets rétiniens (RSs), qui sont des tissus polarisés et multicouches contenant des photorécepteurs cône et exprimant les marqueurs spécifiques du segment externe (OS), du cilium connecteur (CC) et du noyau.

En utilisant à la fois des modèles de souris et des modèles humanisés à base de cellules souches, nous avons étudié le rôle de BMI1 dans les photorécepteurs matures. La protéine du groupe Polycomb Bmi1 est connue pour ses fonctions neuroprotectrices en contrôlant la sénescence et l'apoptose, et est exprimée à la fois dans le progéniteur rétinien et les neurones, mais on en sait peu sur son rôle spécifique dans la rétine adulte. Elle a été récemment associée à des troubles

neurodégénératifs d'apparition tardive, et elle pourrait avoir un rôle dans la pathologie des RDs d'apparition tardive, comme la dégénérescence maculaire liée à l'âge (DMLA).

Nous avons montré que les photorécepteurs cône et les neurones bipolaires sont générés normalement mais subissent ensuite une dégénérescence rapide chez les souris Bmi1$^{-/-}$ par nécroptose associée à Rip3. La dégénérescence était associée à des anomalies de compactage de la chromatine, à l'activation des répétitions en tandem et au stress oxydatif. De plus, nous montrons que BMI1 est préférentiellement exprimé dans les cônes au niveau des foyers hétérochromatiques dans la rétine humaine. Son inactivation dans les cellules souches embryonnaires humaines (hESCs) a altéré la différenciation terminale du cône et a entraîné des anomalies de compactage de la chromatine, l'activation des répétitions en tandem et l'induction de P53. Ces résultats fournissent un mécanisme expliquant comment une carence en Bmi1 conduit à la dégénérescence des cônes et révèlent des fonctions biologiques conservées et des différences pour Bmi1 dans la biologie des photorécepteurs entre la souris et l'homme.

En utilisant un modèle humain basé sur les cellules souches pluripotentes induites (iPSCs), nous avons ensuite étudié le processus dégénératif chez les patients atteints de ciliopathies, un groupe de maladies génétiques hétérogènes affectant les protéines impliquées dans la structure et la fonction du cil primaire, qui sont fréquemment accompagnée d'une dégénérescence rétinienne.

Nous générons des feuillets rétiniens dérivés d'iPSCs à partir de patients atteints de deux ciliopathies, les syndromes de Meckel-Gruber (MKS) et de Bardet-Biedl (BBS). Les photorécepteurs ciliopathiques présentaient des altérations communes significatives dans l'expression de centaines de gènes de développement. De plus, ils ont montré plusieurs anomalies dans la formation et le maintien du cilium interne, le positionnement du centriole mère, l'activation d'une réponse au stress aux protéines mal repliées, instabilités génomiques et l'accumulation de dommages à l'ADN.

Cette étude révèle comment la combinaison des technologies de reprogrammation cellulaire et d'organogenèse avec le séquençage de nouvelle génération permet d'élucider les mécanismes moléculaires et cellulaires impliqués dans les troubles dégénératifs et développementaux de la rétine humaine. La même approche, combinant la différenciation en RSs avec des techniques de

séquençage du génome à large spectre, pourrait être appliquée pour modéliser de nombreuses maladies génétiques, développementales et dégénératives affectant les photorécepteurs. Il peut également aider à élucider les mécanismes moléculaires sous-jacents à ces maladies, au criblage de médicaments de composés ayant des effets thérapeutiques potentiels et à prédire les effets secondaires des médicaments.

Mots-clés : Cellules souches, rétine, photorécepteurs, cônes, ciliopathies, MKS, BBS, BMI1, iPSC, neurodégénérescence.

Abstract

Vision is considered the most important sense, taking on about 80% of the perceptions we receive in our everyday life. Cone-photoreceptors are responsible for high-resolution central vision and color discrimination, and their degeneration is frequently the cause of vision loss in retinal degenerative diseases (RDs). RDs are a heterogeneous group of diseases affecting millions of people worldwide, which at the moment are mostly without any therapeutic option.

Animal models are extremely useful in studying the retina's development or degeneration and understanding the molecular mechanisms in inherited genetic disease affecting photoreceptors. Modeling human developmental and degenerative diseases can be particularly challenging, especially in the case of rare and complex diseases where no exhaustive animal models are available. Generation of sustainable human disease models that allow in-depth analysis of the molecular mechanism is one of the big challenges nowadays. Stem cell technology holds great potential in disease modeling and represents a new powerful tool for generating scalable and animal-free models that can more accurately illustrate clinical phenotypes of complex human diseases.

We developed a protocol to differentiate pluripotent stem cells (PSCs) into retinal sheets (RSs), which are polarized, multi-layered tissues containing cone photoreceptors and expressing outer segment (OS), connecting cilium (CC), and nuclear specific markers.

Using both mouse and stem cells-based humanized models, we first investigate the role of BMI1 in mature photoreceptors. The Polycomb group protein Bmi1 is known for its neuroprotective functions by controlling senescence and apoptosis and is expressed in both retinal progenitor and neurons, but little is known about its specific role in the adult retina. It has been recently linked to late-onset neurodegenerative disorders, and it could have a role in the pathology of late-onset RDs, such as Age-related Macular Degeneration (AMD).

We showed that cone photoreceptors and bipolar neurons are generated normally but then undergo rapid degeneration in Bmi1$^{-/-}$ mice through Rip3-associated necroptosis. Degeneration was associated with chromatin compaction anomalies, activation of tandem-repeats, and

oxidative stress. Furthermore, we show that BMI1 is preferentially expressed in cones at heterochromatic foci in the human retina. Its inactivation in human embryonic stem cells (hESCs) impaired cone terminal differentiation and resulted in chromatin compaction anomalies, activation of tandem-repeats, and P53 induction. These findings provide a mechanism explaining how Bmi1 deficiency leads to cone degeneration and reveal conserved biological functions and differences for Bmi1 in photoreceptor biology between mouse and man.

Using an induced Pluripotent Stem Cells (iPSCs) based human model, we then investigate the degenerative process in patients with ciliopathies, a group of heterogeneous genetic diseases affecting proteins involved in primary cilium structure and function frequently accompanied by retinal degeneration.

We generate iPSC-derived retinal sheets from patients affected by two ciliopathies, Meckel-Gruber (MKS) and Bardet-Biedl syndromes (BBS). Ciliopathic photoreceptors displayed significant common alterations in the expression of hundreds of developmental genes. Moreover, they showed several anomalies in the formation and maintenance of cilia, the mother centriole's positioning, the activation of a stress response to misfolded proteins, genomic instabilities, and DNA damage accumulation.

This study reveals how combining cell reprogramming and organogenesis technologies with next-generation sequencing enables the elucidation of molecular and cellular mechanisms involved in human retinal degenerative and developmental disorders. The same approach, combining photoreceptor sheet differentiation and wide-genome expression profile, could be applied to model many genetic, developmental, and degenerative diseases affecting photoreceptors. It may help elucidate the molecular mechanisms underlining these diseases, drug screening of compounds with potential therapeutic effects, and predict drug side effects.

Keywords: Stem cells, retina, photoreceptors, cones, ciliopathies, MKS, BBS, BMI1, iPSC, neurodegeneration.

Table of Contents

List of figures

1. INTRODUCTION

3. RESULTS

3.1 Retinal development anomalies and cone photoreceptors degeneration upon Bmi1 deficiency

3.2 Deregulation of neuro-developmental genes and primary cilium cytoskeleton anomalies in iPSC retinal sheets from human syndromic ciliopathies

4. DISCUSSION AND PERSPECTIVE

List of acronyms and abbreviations

5mC: 5-methylcytosine
9cRA: 9-cis retinal
ABCA4: ATP-Binding Cassette transporter 4
ALMS: Alström Syndrome
AMD: Age-related Macular Degeneration
ANRIL: Antisense Non-coding RNA in INK4 locus
ar: autosomal recessive
arCRD: autosomal recessive Cone-Rod Dystrophy
arRP: autosomal recessive RP
ARS: Axenfeld-Rieger syndrome
ASPM: Abnormal Spindle-like microcephaly-associated protein
ATG: autophagy-related
AVSD: Atrioventricular Septal Defect
BAB: Blood-Aqueous Barrier
BB“s”: Basal Body“s”
BBS: Bardet Biedl Syndrome
BDNF: Brain Derived Neurotrophic Factor
bFGF: basic Fibroblast Grow Factor
BMI1: B lymphoma Mo-MLV insertion region 1 homolog
BMP“s”: Bone Morphogenetic Protein“s”
BOR: Branchio-Oto-Renal
BRB: Blood-Retinal Barrier
Cas: CRISPR associated system
CC“s”: Connecting Cilium“s”
CCD“s”: Coiled-Coil Domain“s”
CD“s”: Cone Dystrophie“s”
CDKs: Cyclin-Dependent Kinases
CEP290: Centrosomal Protein 290kDa
CFAP: Cilia and Flagella Associate Proteins
CFAP: Primary Ciliary Dyskinesia
Chk2: Checkpoint kinase 2
CIHR: Canadian Institute Health Research
CNV: Copy Number Variation
COMMD3: Copper Metabolism gene MURR1 Domain 3
Congenital Stationary Night Blindness 2A (CSNB2A)
Cpfl1: Cone photoreceptor function loss 1
Crb1: Crumbs homolog 1
CRD“s”: Cone-Rod dystrophy“es”
CRISPR: Clustered Regularly Interspace Short Palindromic Repeats
CRISPRa: CRISPR-Cas9-based gene activation
CRPT: Carpenter Syndrome
Crx: Cone-rod homeobox
CSRCS: Comité de Surveillance de la Recherche sur les Cellules Souches
CSs: Centriolar Satellites
CTM: chetomin
DAI: DNA-dependent Activator of Interferon regulatory factors
DDR: DNA Damage Response
DHA: Docosahexaenoic Acid
DIV: Days *In vitro*
Dkk1: Dickkopf-related protein 1(Dickkopf-1)
DNMTs: DNA methyltransferases
DSBs: Double-Strand DNA Breaks
EGFP: Enhanced Green Fluorescent Protein
Elovl4: Very-long-chain fatty acids-like 4
ER: Endoplasmic Reticulum
ERG: Electroretinogram
ESC: Extra Sex Comb
ESCs: Embryonic Stem Cells
ESCS: Enhanced S-cone Syndrome
eSpCas9: Cas9 of Streptococcus Pyogenes
ESRD: End-Stage Renal Disease
EYA: Eyes Absent
EZH1/2: Zest Enhancer
FCS: Fetal Calf Serum
FDR: False Discovery Rate
FZD: Frizzled
GABA: gamma-Aminobutyric acid
GO: Gene Ontology
GSK3: Glycogen Synthase Kinase 3
H2Aub: ubiquitination of H2A
H3K27me3: triple histone H3 methylation on lysine 27
H3K4me3: triple methylation on lysine 4 of histone H3
H3K9ac: acetylation on lysine 9 of histone H3

H3K9me3: triple methylation on lysine 9 histone H3
HDAC: Histone Deacetylases
hESCs: human ESCs
HLS: Hydrolethalus Syndrome
HOTAIR: HOX transcript antisense intergenic RNA
HSP“s”: Heat Shock Protein“s”
IF: Immunofluorescence
IFT: Intraflagellar Transport
IGDS: Iridogoniodysgenesis Syndrome
IGF1: Insulin Grow Factor
IHC: immunohistochemistry
INL: Inner Nuclear Layer
IPL: Inner Plexiform Layer
iPSC: induced Pluripotent Stem Cells
IS“s”: Inner Segment“s”
JBTS: Joubert Syndrome
JNCL: Juvenile Neuronal Ceroid Lipofuscinosis
JSRD: Joubert Syndrome and Related Disorders
KLF4: Kruppel Like Factor-4
KO: Knockout
LC3/Atg8: Lipidation of microtubule-associated protein 1 light chain 3
LC3: Lipidation of microtubule-associated protein 1 light Chain 3
LCA: Leber’s Congenital Amaurosis
LIF: Leukemia Inhibitory Factor
LncRNA: long noncoding RNA
lncRNA“s”: Long non-coding RNA“s”
L-Opsin: Long-wave Opsin
LRAT: Lecithin Retinol Acyltransferase
LRFs: Luminance Response Functions
LSFMP: Light-Sheet Fluorescence Microscopy
LZTFL1: Leucine-Zipper Transcription Factor-Like 1
MAK: Male Germ Cell-Associated Kinase
MD“s”: Macular Degeneration“s”
MDM2: Mouse Double Minute 2
mEpiSC“s”: mouse Epiblast Stem Cell“s”
MERTK: MER Proto- Oncogene Tyrosine Kinase
mESCs: mouse ESCs
MIPE: Mechanism Interrogation Plate
MKS: Meckel-Gruber Syndrome
MMEJ: Microhomology-Mediated End Joining
M-NS RDs: Monogenic Non-Syndromic RDs
M-opsin: Medium-wave opsin
M-S RDs: Monogenic Syndromic RDs
MTT: Methyl Thiazol Tetrazolium
NB“s”: Nuclear Bodie“s”
Nec-1: Necrostatin
Nesprin-2: Nuclear envelope spectrin repeat protein 2
NHEJ: NonHomologous End-Joining
NIC: Nicotinamide
NPHP: Nephronophthisis
Nrl: Neural retina leucine zipper
NS: Non-Syndromic
NSERC: Natural Science and Engineering Research Council of Canada
OCT: Optimum Cutting Temperature
OCRL: Oculocerebrorenal Syndrome of Lowe
OFF: OFF-center
OLM: Outer Limiting Membrane
ON: ON-center
ONL: Outer Nuclear Layer
OPC“s”: Oligodendrocyte Progenitor Cell“s”
OPL: Outer Plexiform Layer
Opn1mw: Opsin 1 Medium-wave
Opn1sw: Opsin 1 Short-wave
OR: Ocular Retardation
ORDs: Outer Retinal Dystrophies
OS“s”: Outer Segment“s”
Otx2: Orthodenticle Homeobox 2
OV“s”: Optic Vesicle“s”
PC: Polycomb
PCD: Primary Ciliary Dyskinesia
PcG: Polycomb Group
PCM: Pericentriolar Material
PDE: Phosphodiesterase
PFA: Paraformaldehyde
PH: Polyhomeotic
PHS: Pallister-Hall syndrome
PKD: Polycystic Kidney Disease
PMC: Periciliary Membrane Complex
PNA: Peanut Agglutinin
polyUb-K48; Polyubiquitin chains at lysine 48

POU5F1/OTC4: Octamer binding Transcription Factor-4
PR“s”: Photoreceptor“s”
PRC: Polycomb Repressive Complex
PRPF3: Pre-mRNA Processing Factor 3
PRR: pattern recognizing receptors
PSC: Posterior Sex Combs
PSCs: Pluripotent Stem Cells
PTMs: Post-Translational Modifications
QC: Quality Control
qPCR: quantitative RT-PCR
RA: Retinoic Acid
RCD“s”: Rod-Cone Disease“s”
rd: retinal degeneration
RD“s”: Retinal Degenerative diseases; Retinopathies; retinal dystrophies
RDH5: Retinol Dehydrogenase 5
rds: retinal degeneration slow
RGC“s”: Retinal Ganglion Cell“s”
RHIM: RIP Homotypic Interaction Motif
RHO: Rhodopsin
RIPK: Receptor-Interacting Protein Kinase
RNAseq: RNA sequencing
Rorb: RAR-related orphan receptor β
ROS: Reactive Oxygen Species
RP: Retinitis Pigmentosa
RPC“s”: Retinal Progenitor Cell“s”
RPE: Retinal Pigmented Epithelium
RPE65: RPE-Specific Protein 65kDa; Retinoid Isomerohydrolase
RPGR: Retinitis Pigmentosa GTPase Regulator
RPGRIP: RPGR interacting protein
RS“s”: Retinal Sheet“s”
SAG: Smoothened Agonist
SAM: Sterile Alpha Motif
SFEB: Serum-Free Floating culture of Embryoid Bodies
shBMI1: small hairpin RNA against BMI1
Six3OS: Six3 Opposite Strand transcript
SLSN: Senior-Løken Syndrome
SMO: Smoothened
SNVs: Single Nucleotide Variations
S-opsin: Short-wave opsin
SOX2: Sex Determining Region Y-box 2
SUZ12: Zest Suppressor 12
SVZ: Subventricular Zone
T3: Rriiodothyronine
TALEN“s”: Transcription Activator-Like Effector Nuclease“s”
TBCC: Tubulin Specific Chaperone C
TEM: Transmission Electron Microscopy
TET: Translocation Methylcytosine Dioxygenases
TF“s”: Transcription Factor“s”
TGFβ: Transforming Growth Factor-β
Thrβ2: Thyroid receptor β2
TLRs: Toll-Like Receptors
TR: T3 receptor
TrxG: Trithorax
TZ: Transition Zone
USH: Usher Syndrome
USH1: USH type I
VEGF: Vascular Endothelial Growth Factor
VIP: Vasoactive Intestinal Peptide
WGS: Whole Genome Sequencing
XLRS: X-linked Juvenile Retinoschises
ZFN“s”: zinc-finger nuclease

“Above all, don't fear difficult moments. The best comes from them.” – Rita Levi-Montalcini

Acknowledgments

First of all, I would like to thank my research director, Dr. Gilbert Bernier, for sharing all his know-how with me and having best supported and guided me during my Ph.D. I will always be grateful for his support and all his teaching.

Special thanks go to Roy Hanna for his friendship and his moral and scientific support, and without which, I do not know if I would have ever managed to get this far.

I also thank my friend Anthony Flamier with whom I have shared countless hours in cell culture and who has been my reference in stem cell biology.

I also want to thank Katia Mellal for all her loving support and all her help over the past few years of thesis; Rimi Hamam, who has always managed to get me back in a good mood and refuel during blood sugar or caffeine drops; and Boris Tripied for all his help with cell culture and the excellent company in the many hours spent in the white room.

I would also like to thank all of my thesis jury Dr. Mike Sapieha, Dr. Thomas Durcan, and Dr. Massimiliano Paganelli, for their help in realizing my thesis and for their wise advice.

I also thank all my other colleagues who have come and go during these long years and with whom I have shared both good and exciting moments and difficult times that we have constantly surpassed by supporting each other.

I cannot fail to mention all my friends and roommates for their support and make my stay in Montreal unforgettable.

Finally, I especially thank my mother, father and, sister, and all my family for their love and support and for having always believed and sustained me throughout my life and in all critical choices.

Last but not least I want to thank my dear grandmother, whom I could not say goodbye to and who has always been the first to encourage me, belief in me, and made me become the man I am.

1. INTRODUCTION

Many have wondered which of the five senses: sight, taste, smell, sound, or touch, is the most essential in humans, or rather, which sense we are most afraid of losing. To this question, most people answer vision. We can say that sight is considered by far the most important sense, taking on about 80% of the perceptions we receive in our everyday life (1).

The eyes are the organ of the visual system that allows the detection of light. They also have some other vision-independent functions related to photoreception, such as the regulation of circadian rhythms (2,3). Photoreception seems to date back over 500 million years. The eye's common phylogenetic origin theory is widely accepted and considers the Pax6 gene one of the key factors (4–7). The simplest type of "eye," also found in unicellular microorganisms, is called eyespot and consists of photosensitive proteins capable of responding to light stimuli. The eyespots do not allow vision but only the presence or absence of light, which is sufficient to regulate circadian rhythms and light periods. During evolution, this type of primordial eye gradually changed to form a "cup" type of invagination that allowed to identify the direction of origin of the light by exploiting different impact angles (8,9). Finally, the eye has evolved by further invaginating and reducing the opening towards the surface and forming what we call pinhole camera eye, which can distinguish shapes, and which is the basis of complex visual systems (10,11).

Further evolution was the lens, or crystalline lens, appearance, which is characteristic of what we call complex eyes, including human eyes. Complex eyes have continued to evolve and adapt to

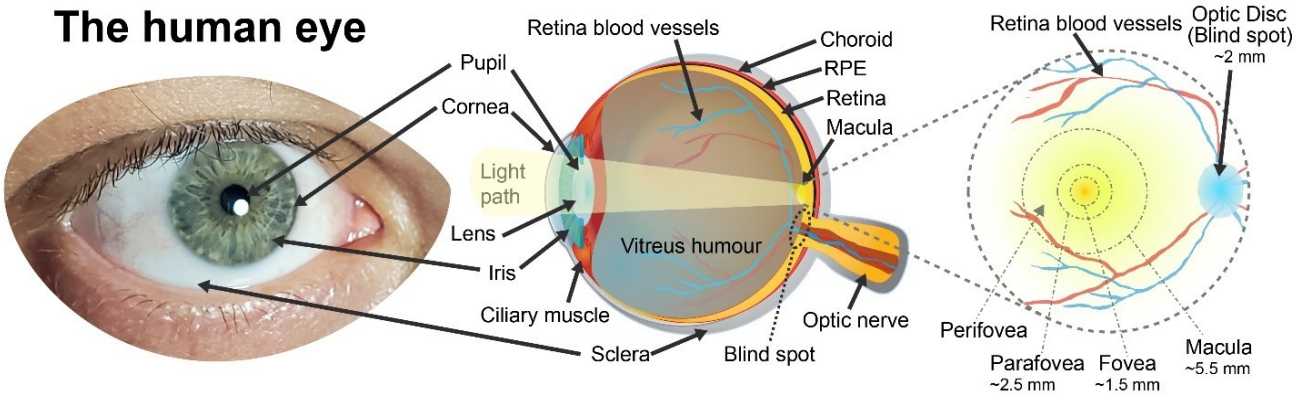

Figure 1: The eye anatomy

different species' needs but maintain universal operating principles and structures (9).

Anatomically, a complex vertebrate eye consisting of the cornea, iris, pupil, vitreous, lens, retina, pigmented tissue, and optic nerve (Figure 1) (12,13).

The principle of eye functioning is similar to that of a camera. The light hits the eye surface, called the cornea, which acts as the first focus and directs the light inside the eye. The iris, the colored part of the eye, automatically adjusts the pupil's opening, which is the hole in its center, controlling how much light penetrates the bottom of the eye, as a shutter controls the opening of a camera. Once past the pupil, the light immediately meets the lens, which is entirely transparent. Like camera autofocus, it automatically adjusts the focus on approaching objects, always concentrating the light on the right plane on the bottom of the retina (14). The vitreous is a dense solution that fills the eye cavity while maintaining constant intraocular pressure, thus preventing retinal detachment and the eye from collapsing (15). The retina is part of the nervous system; it consists of a thin layer covering the eye's inner surface, responsible to captures the light, which is converted into visual perception through a complex neuronal pathway in the Cerebral Cortex (16,17). Other essential parts of the vertebrate eye are the sclera, the white outer wall of the eye that borders and protects the eye, and the choroid, a layer rich in blood vessels between the retina and the sclera. The ciliary body located behind the iris contains the muscles responsible for the lens's movement that adjusts the focus (18).

1.1 Overview of retinal composition, structure, and function

The retina is an overturning of the nervous system organized as a multi-layered neuro-vascular tissue consisting of alternating layers of neurons and synapses (Figure 2).

This system is nourished by retinal and choroidal circulation, which provides neuronal sustenance and waste elimination. The only avascular part of the retina is the outer nuclear layer (ONL), where the photoreceptors (PRs) reside (16). The light passes through the entire retina before being absorbed by the photosensitive pigments present in the PRs (Figure 2) (19).

PRs can be considered the functional units of the retina. The pigments called opsins are stacked in hair-like structures to maximize their surface and respond to light by initiating a nerve impulse (13). There are two types of PRs, the cones and the rods (Figures 1, 6) (20). The rods express

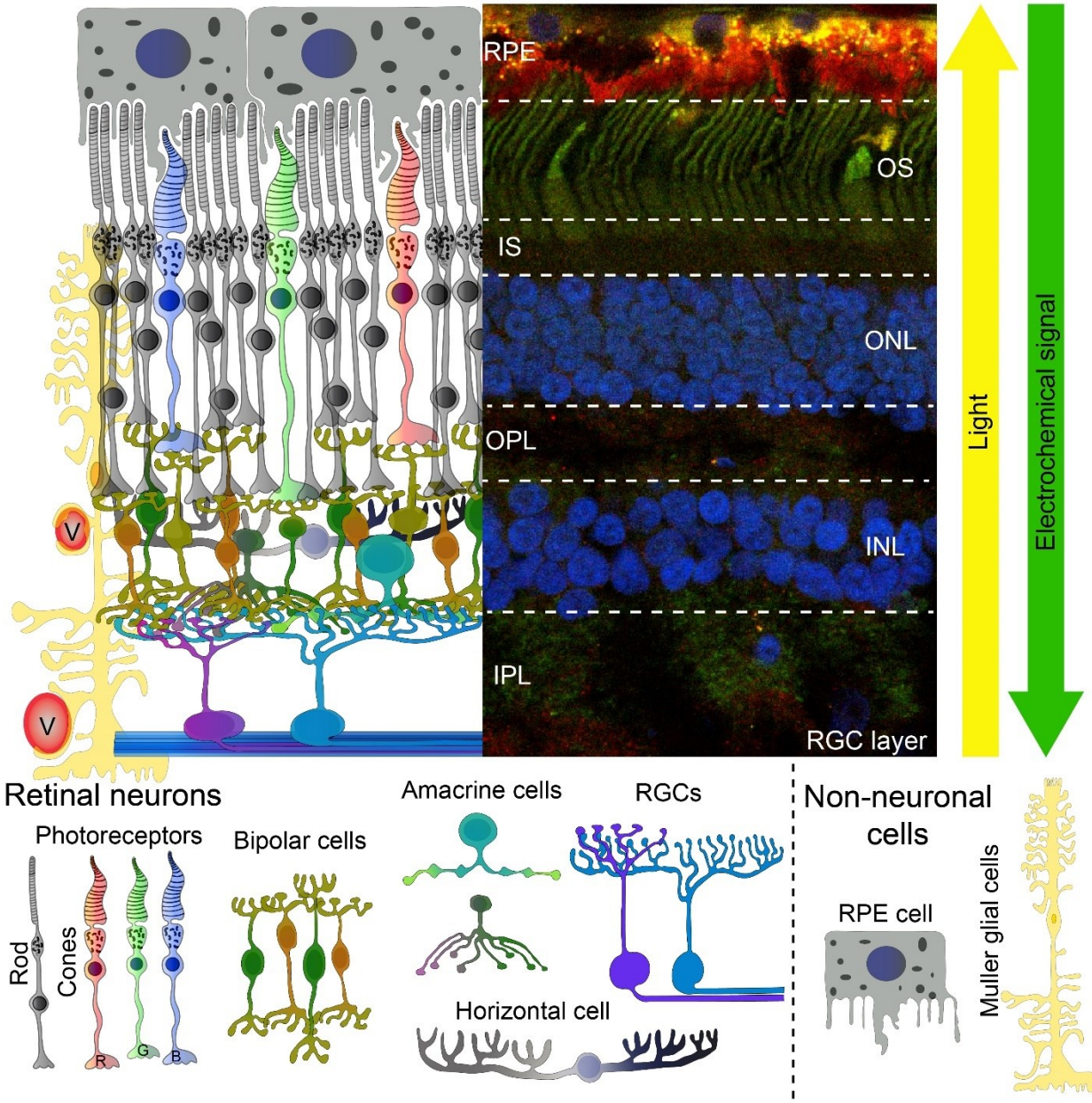

Figure 2: Structure and cell types of the vertebrate retina

rhodopsin, which is the most sensitive pigment and absorbs around 500 nm. Rods are responsible for night and achromatic vision and are the most numerous PRs in the retina, although their proportions vary from species to species. Cones are responsible for visual acuity, defined as the ability to distinguish precise details. Cones are divided into subclasses based on the type of opsin expressed, which differ in their sensitivity to photons of different wavelengths, which are therefore perceived as different colors. Short-wave opsin (S-opsin) absorbs light at a wavelength of 430 nm, which is perceived as a blue, medium-wave opsin (M-opsin) at 530 nm and

corresponds to the green color, while the long-wave Opsin (L-Opsin) absorb at 560 nm in the red spectrum (Figure 3) (19,20). It is no coincidence that the color system most used in graphics and monitors is based on the *RedGreenBlue* system, better known as RGB.

The position and quantity of the cones and the proportions between the different types of cones are very variable in different species (21,22).

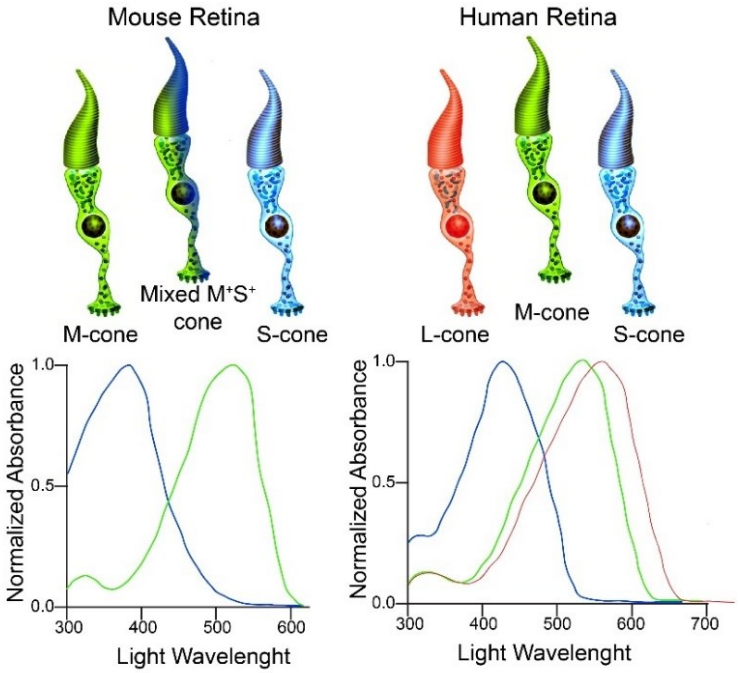

Figure 3: Cone types in the human and mice retina

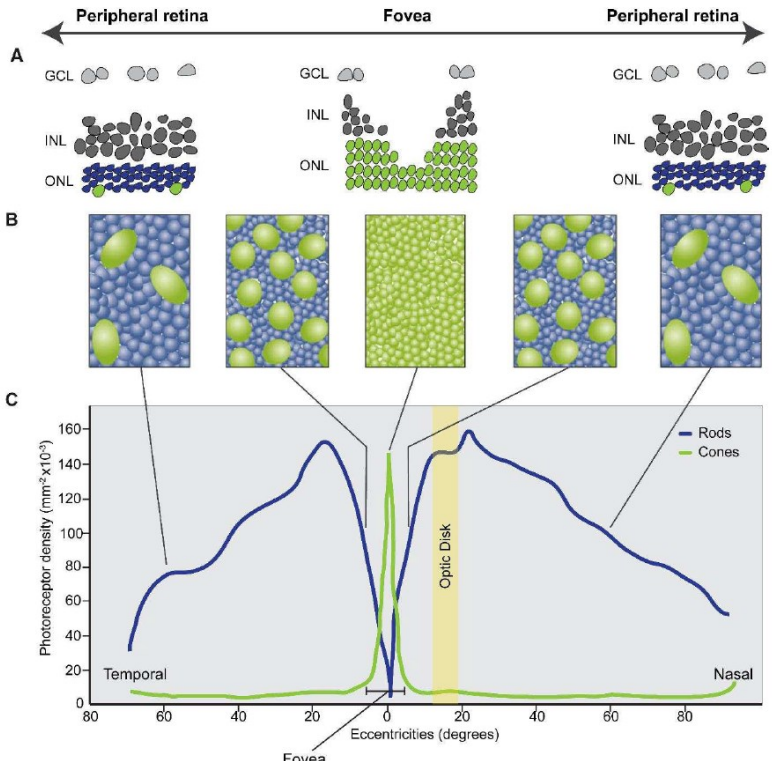

Figure 4: Photoreceptors density and distribution in the human retina (1201)

In humans and some other higher primates, cones are highly concentrated in a small high-acuity area of about 5 mm in diameter called the macula (Figures 1, 4).

The macula is further divided into the peri macula, perifovea, and fovea, a small point of the retina of about 1.5 mm (Figure 1) (23). The fovea's central region has an area free of rods of about 300-600 µm, which is perfectly aligned with the lens's axis and has the maximum resolution (Figures 1, 4) (24). PRs convert the light into an electrochemical signal and pass it to the second order of neurons called bipolar cells since they possess two sets

of synapses extending from the central body. The soma of bipolar cells, together with the horizontal cells and the amacrines, reside in the inner nuclear layer (INL). Bipolar cells and horizontal cells contact the PRs in the outer plexiform layer (OPL), and then the bipolar cells transfer the output signal to the ganglion cells via ribbon synapses contained in the inner plexiform layer (IPL) (Figure 2) (25). Bipolar cells can be divided into two classes: ON-center (ON) end OFF-center (OFF) based on the type of receptor possessed, either metabotropic or ionotropic. The first type is active when the light is on, and therefore when the set of PRs that define its reception field receive the light and are hyperpolarized and release less glutamate. Instead, the bipolar OFF-center cells are active when the light is off in the center of their receptive field, and the PRs are depolarized (Figure 6).

There are 12 known types of bipolar cells. While there is only one type of bipolar cell for rods, of the ON type, cones have five types of OFF cells and six types of ON cells (26,27). While the receptor field of rod bipolar cells is relatively large to increase sensitivity to light and is ''insensitive to color", instead the field of cone bipolar cells is smaller and is sensitive to the colors, thus contributing to cones' high-resolution color-vision (Figure 6) (25,28).

Horizontal cells from pre and postsynaptic connections with the PRs in the OPL. By modulating the response of the PRs in their "center of action" with the surrounding PRs. This way, they indirectly help bipolar cells to increase brightness and contrast, generating more detailed images (Figure5) (29,30).

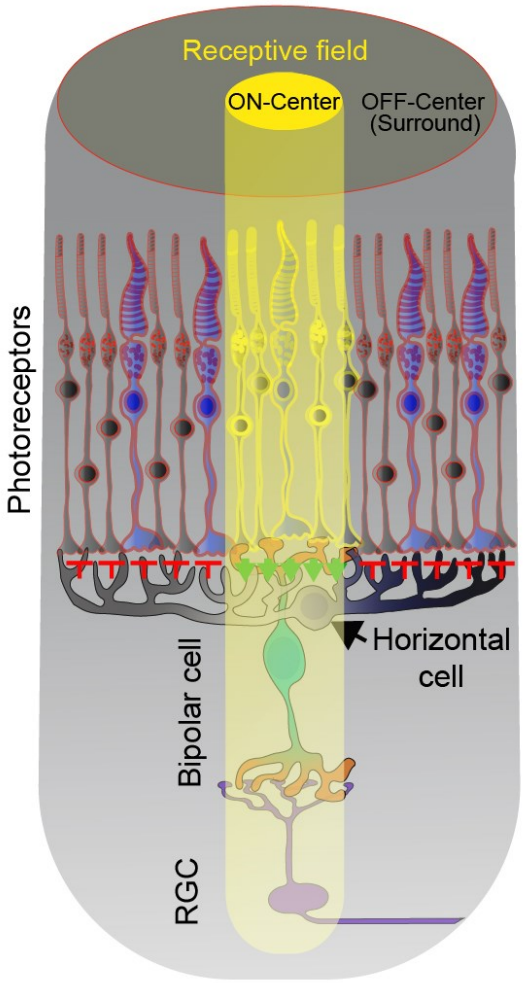

Figure 5: Receptive field in the retina

ON and OFF-center signal transmission. Horizontal cells connects to PRs and bipolar cells in the visual field and in the surrounding area to help modulate their response

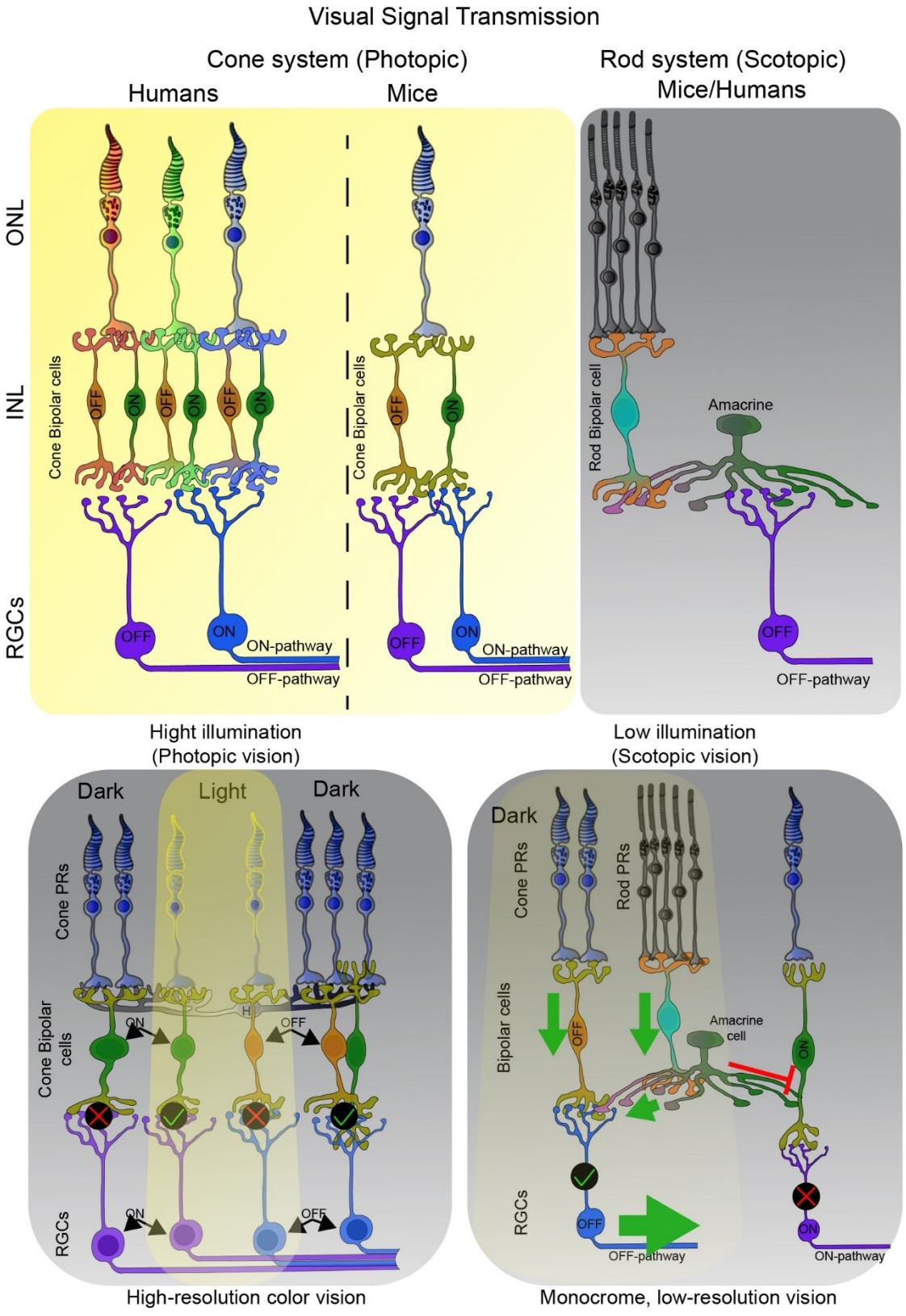

Figure 6: Visual signal transmission in human and mice retina

Amacrine cells regulate the signal transfer from bipolar to ganglion cells, providing a direct vertical link between the two and transferring information necessary to detect movement. They also have a function similar to horizontal cells by providing lateral connections between types of neurons of the same species. Instead of communicating with different PRs, amacrine cells connect different bipolar cells, thus increasing the center-background effect in the receptive fields of the ganglion cells and regulating the interaction between scotopic (night time) or photopic (daylight) response (Figure 6) (31,32).

The signal then arrives at the third order of neurons, the ganglion cells, which receive the stimulus from the bipolar and amacrine cells, and then transfer it to the visual cortex (Figure 6).

The axonal extensions of ganglion cells are collected in an area of the retina devoid of PRs called "blind spot" where they exit the Retinal Ganglion Cell (RGC) layer and form the optic nerve (Figure 1, 4) (33). The optic nerve transmits the signal in the form of action potential to various brain regions such as the thalamus, hypothalamus, and midbrain (34).

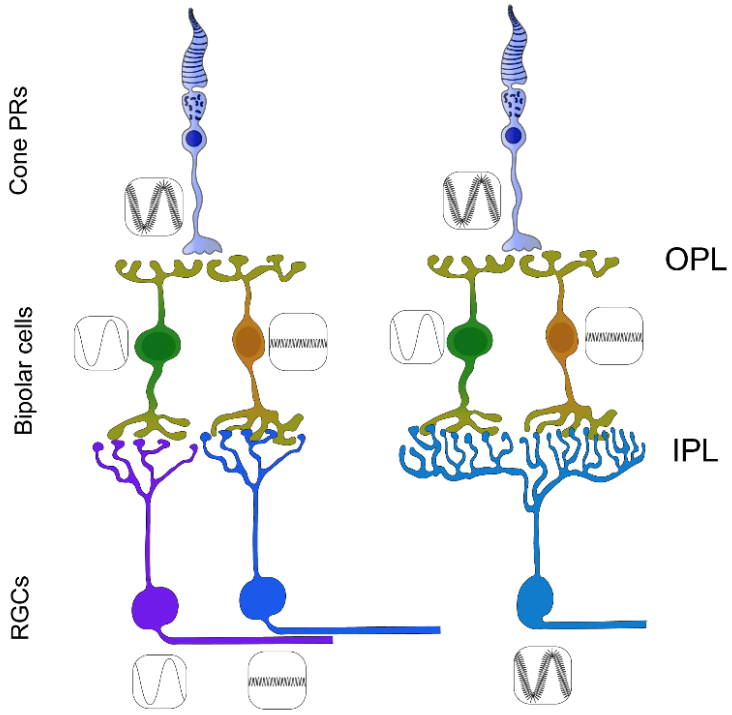

Figure 7: Cone signal transmission (inspired by (25))

How transient and sustained bipolar cells decompose the output of a cone. The resulting high- and low-frequency channels can contact narrowly stratified ganglion cells (left), in which case the two frequency bands are transmitted via separate, parallel channels to the brain. Broadly stratified ganglion cell (right) receives input from both types of bipolar cells and has a broadband response.

RGCs can transmit visual information related to shape and movement to the brain and include other additional functions that contribute, for example, to the regulation of circadian rhythms and the pupil reflex to light. Unlike most other non-primate mammals, such as mice, where RGCs are arranged in a monolayer and uniformly distributed along the retina, the density of these cells in the human retina can vary by a factor of 100 (35). More than 50% of the ganglion cells are

located in the macular and peri-macular region in the human retina, representing an average of 6% of the retina's total surface (36). This massive concentration of ganglion cells in the macular area reflects the high proportion of the central nervous system dedicated to high-resolution central vision.

Maintaining the retina's integrity depends on the non-neuronal support cells, including astrocytes, glial Muller cells, and cells of the Retinal Pigmented Epithelium (RPE) (Figure 2).

The bodies of glial Muller cells reside in the INL, and from there, they can reach every part of the retina. Like the glia in the central nervous system, they offer nutritional and mechanical support for the retina's neurons. They also ensure the nerve tissues' isolation, protection, and proper functioning by recycling neurotransmitters such as glutamate and gamma-Aminobutyric acid (GABA) and eliminating debris and waste substances. They also reabsorb potassium from the extracellular environment and regulate exchanges between the vascular system and neurons, thus contributing to the brain-blood barrier (37,38).

RPE is formed by a single layer of densely packed pigmented hexagonal cells covering the retina's external layer and divides the neural retina from the choroid (39). The microvilli of the apical part of the RPE cells welcome the PRs' outer segments, helping their function and survival by engulfing the outer part of the OSs, which are in continuous destruction due to the exposure to oxidative stress generated by the photoreception process (40,41). RPE has a broad spectrum of functions. First, it provides mechanical support by absorbing the scattered light thanks to its melanin granules, and then it provides a physical barrier between blood and the retina that contributes to the retina's immune privilege. Besides, RPE supplies nutrients to the PRs, eliminates water and metabolites and controls the ionic potassium homeostasis (39,42). Also, it contributes to the regulation of the visual cycle in various ways, including the release of signal molecules and various factors such as Insulin Grow Factor (IGF1), basic Fibroblast Grow Factor (bFGF), and Vascular Endothelial Growth Factor (VEGF) (43). Dysfunctions in the RPE are the cause of some cases of Retinitis Pigmentosa (RP) and Macular Degeneration (MD) (44–46).

1.2 Developmental genetics of the eye

The vertebrate eye is generated from several embryonic sheets, including neuroepithelium, superficial ectoderm, and extracellular mesenchyme. The neuroepithelium generates the retina, the optic nerve, the iris, and the ciliary body, while the surface ectoderm gives rise to the lenses, the epithelium of the cornea, and the eyelids. Finally, the mesenchyme forms the cornea's endothelium, the stroma, the vitreous, the sclera, blood vessels, and muscles (13,16).

In this chapter, we will describe the initial stages of the development of the eye (common to most of the eyes of the different species), and then we will focus on the retina and, more particularly, the human and mouse retina.

The development of the eye starts from a single group of cells located centrally in the front part of the brain, which during the neurulation is divided into two parts, giving rise to two separate optic pits (Figure 8 Top). The optic pits then mature into optic vesicles during the closure of the neural tube (end of fourth weeks in the human, embryonic day 9.5 in the mouse) (13). Fine regulation between canonical and non-canonical WNT pathways and the FGF pathway plays an essential role in this initial stage. Loss- and gain-of-function experiments in model organisms have identified Transcription Factors (TFs), such as Pax6, Rax (also called Rx), Lhx2, Otx2, Sox2, Six6, and Six3, involved in early eye patterning and retinal developmental (Figure9) (47–55). Rax null mice do not form optic vesicles and, therefore, eyes (53). This condition is called anophthalmia and has also been observed in humans due to mutations in *OTX2*, *PAX6*, and *SOX2* (56–60). The optic vesicles protrude from the brain towards the surface ectoderm, while from the opposite side, towards the lumen, it remains in contact with the frontal part of the brain through the optic stalk that will give life to the optic nerve (Figure 8 central part). When the optic vesicle comes into contact with the ectoderm, the optic vesicle gradually begins to invaginate, giving shape to the optic cup, the internal part of which will give rise to the retina while the most external one will generate the RPE (13). One of the key factors in the invagination process leading to the optic cup's formation seems to be the paracrine signaling generated by Retinoic Acid (RA) following the activation of *Raldh2* (61,62). Also, LHX2 seems to be an essential factor in this invagination process and works in part by regulating the Bone Morphogenetic Protein (BMP) signaling

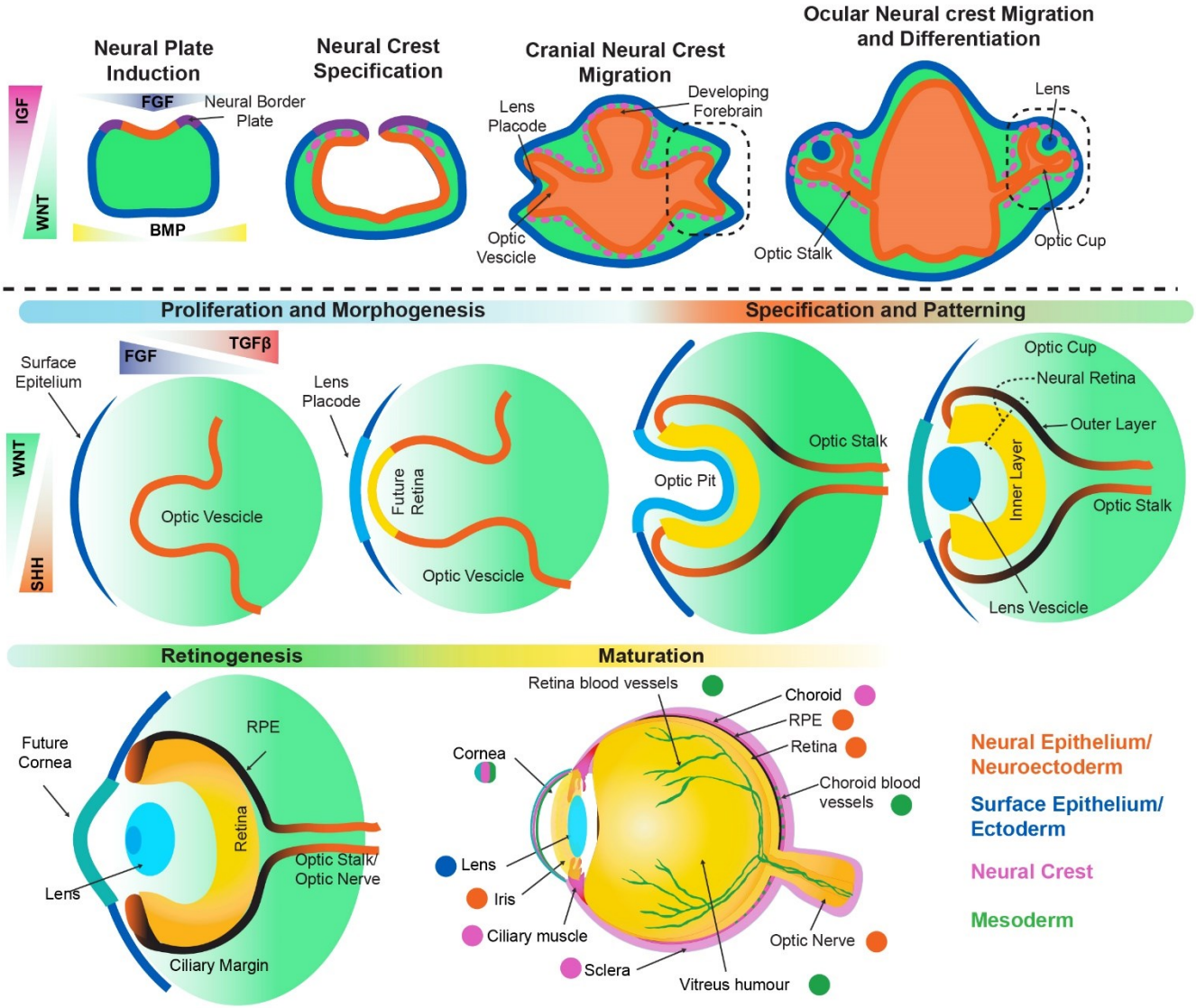

Figure 8: Overview of eye and retina development

pathway. It seems to act in an autocrine manner in the optic neuroepithelium and in a paracrine way in the ectoderm, where it guides the lens's formation (55,63). In both Lhx2$^{-/-}$ and Raldh2$^{-/-}$ mice, the invagination process fails, and the eye's development remains incomplete without forming the optic cup. The optic cup's central part will generate the iris and the ciliary body while the ectoderm in the front part gradually thickens, giving rise to the lens placode. It then separates from the ectoderm to form the lens's vesicle at the optic cup's opening, which will later mature in the lens (9). After detachment of the lens vesicle, the surface ectoderm forms the cornea (Figure 8 bottom).

Dand5 (Coco), belongs to the Cerberus/DAN/Gremlin superfamily initially identified as BMPs' antagonists responsible for the dorsal/ventral axis formation during development (64–67). As the Nodal/Activin pathway, the BMP signaling pathway is part of the Transforming Growth Factor-β (TGFβ) signaling network (68–71). Some members of the Cerberus/DAN/Gremlin superfamily are expressed in the endoderm and mesoderm and act as secreted inhibitors of both BMP and Nodal/ Activin ligands (Figure 9) (65,66). Coco functions as a TGFβ-ligand antagonist in the ectoderm and, supplied maternally, is one of the earliest expressed antagonists of TGFβ signaling (72). Coco physically associates with BMP and Activin/Nodal proteins, inhibiting signal transduction. The repression of COCO leads to expression in the left lateral plate mesoderm of PITX2, considered one of the most significant TFs controlling early eye development and a role in retinal cell type specialization (73,74). PTX2 is expressed in almost all retinal tissue during early eye development but is almost absent in the retina in later stages. Inversely, COCO is highly expressed in the neural retina until later when PRs are generated (Figure 10) (75).

Subsequent differentiation and rearrangement of the cells in the optic cup according to a meticulously orchestrated sequence of events ultimately gives rise to the eye (Figure 8 bottom).

The neural retina differentiation process is orchestrated by autonomous factors (76). As previously mentioned, the outer layer cells are committed to forming RPE during the optic cup formation. RPE formation is directed by the interaction of this outer layer of the optic cup with the periocular mesenchyme, which stimulates a signal cascade directed by activin A and TGFβ (Figure 8, 9) (77). FGF signaling inhibits this process, thus favoring the formation of the neural retina. In KO mice for Fgf9, the RPE expands at the retina's expense, while the ectopic expression of Fgf9 in the RPE progenitors causes the formation of a second neural retina instead of the RPE (78,79).

The cells of the inner layer of the optic cup form the neural retina. In this stage, the retinal progenitor cells (RPCs) expand and differentiate into the five types of neurons and 1 type of glial cell (Figure 9) (13,54).

In humans, neural retina differentiation starts at the end of week 6 of gestation, while cone and rod PRs are first observed at week 9 of gestation (Figure 9) (20). Retinal development continues

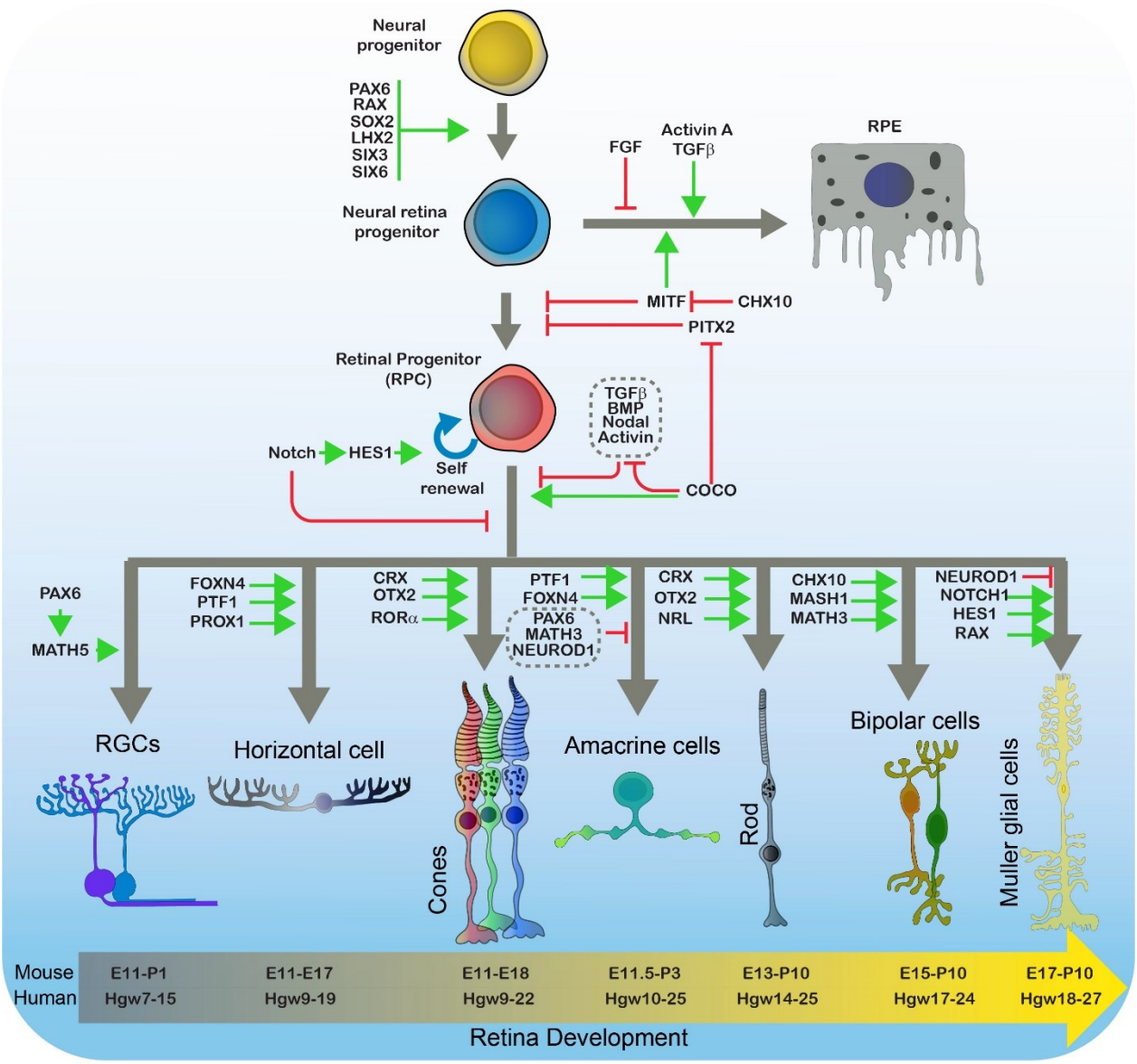

Figure 9: Cell types specification during retina development

until the 8th month, and the macula becomes fully functional only after birth. In the mouse, the corresponding process starts at E12 and is finished two weeks after birth when the eyelids open (80). The peculiar ability of RPCs to generate the diverse class of neurons in sequential order during retinal development is thought to be modulated by an intrinsic transcription factor molecular program and by extrinsic cues. It seems to be well conserved among many species (81–85). In this process, the ganglion cells are the first to be formed, followed by the amacrine cells, cone PRs, and horizontal cells. Bipolar cells and rod PRs form at later stages (Figure 9). Continuous support of RPCs is necessary for the proper formation of the retina; the progenitor cell renewal

process seems to be regulated by the basic helix–loop–helix TFs Hes1 a downstream target of the Notch signaling pathway (Figure9) (83). Hes1$^{-/-}$ embryos show a severely impaired cell proliferation of the RPCs in the neural retina with recessive ocular retardation (OR).

OR is characterized by blindness associated with microphthalmia, cataractous lens, thin and poorly differentiated retina, and lack of the optic nerve. In both mice and humans, OR is observed in homozygous mutations in the homeobox transcription factor CHX10, also called VSX2 (86,87). Further analysis determined that Chx10 is required to maintain mammalian neural retinal identity through the repression of *Mitf* (Figure 9) (88).

One of the master regulators of RGCs differentiation is Math5, a transcription factor induced through PAX6 (Figure 9) (89,90). RGCs are significantly reduced in Math5$^{-/-}$ mice while they are almost all lost, and accompanied by a severe loss of all other retinal cell types, in the Math5$^{-/-}$/Brn3b$^{-/-}$ mice (91).

Amacrine cell differentiation starts slightly earlier than horizontal cells, but they have many classes of TFs in common. Foxn4 induction is sufficient to induce amacrine cell differentiation, and the same results are obtained with simultaneous inhibition of Pax6 with Neurod1 or Math3. Math3$^{-/-}$/ Neurod1$^{-/-}$ mice also show preferential loss of amacrine cells over horizontal ones, while total inhibition of Ptf1 or Foxn4 causes total loss of horizontal cells and reduction of amacrine (83,92,93). Prox1 is another crucial factor involved in generating horizontal cells (Figure 9) (94).

Bipolar cells are interneurons that relay information from PRs to RGCs, and probably for this reason, they appear later in mouse development. Nearly all bipolar cells are generated postnatally when both RGCs and PRs are completely developed (Figure 9) (95–97). Chx10 is expressed in RPCs and is essential in bipolar cell generation as they are almost absent in Chx10$^{-/-}$ retinas (86,98,99). The differentiation of bipolar cells is also dependent on Mash1 and Math3 since, in the corresponding double Knockout (KO) mice, bipolar cells are completely lost (26,100,101). Prox1 is an early bipolar marker, but it also has a vital role in the functionality and survival of mature PRs (94,102). PRs and bipolar cells both express Otx2 (Figure 9). The generation and

differentiation of bipolar cells are complicated by different ON and OFF subtypes (103). Bhlhb4 and Vsx1 are respectively ON- and OFF- bipolar cell TFs required for bipolar cell specification (31).

1.2.1 Photoreceptor lineage specification

PRs require a specific set of TFs to define their cell type identity and subtypes (104). PR progenitors and precursors express Orthodenticle Homeobox 2 (*Otx2*) and Cone-Rod Homeobox (*Crx*) genes. Conditional deletion of *Otx2* or *Crx* in the developing mouse retina impairs PRs' fate, leading to PRs conversion into amacrine cells (83,105,106). Crx is indispensable for PRs terminal differentiation and maintenance, and if mutated, it causes severe human retinal diseases (104,107–109). PRs can be of two types: cones and rods. Rods are involved in achromatic night vision, and cones are involved in daylight color vision.

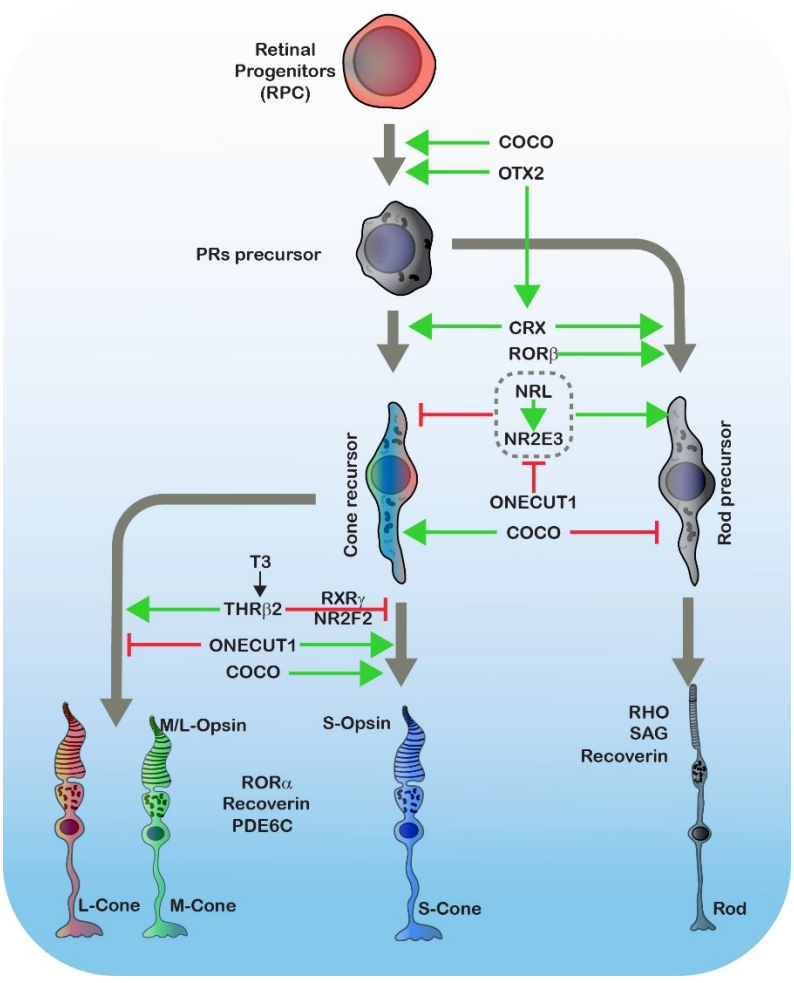

Figure 10: Photoreceptors lineage specification

PRs follow an S-cone (cones containing S-opsin) default pathway during development, which is determined by Crx and thyroid receptor β2 (Thrβ2, encoded by *Thrb*) (Figure 10) (22). Crx induces expression of Opsin 1, Short Wave Sensitive (*Opn1sw* encoding S-opsin) by default, whereas Thrβ2 suppresses it and induces expression of Opsin 1, Medium Wave Sensitive (*Opn1mw* encoding M-opsin) (106,110,111). On the other hand, expression of neural retina leucine zipper (Nrl), RAR-related orphan receptor β (*Rorb*), and Notch1 inhibit cone formation

while promoting rod genesis (Figure 10) (112–116). The orphan nuclear receptors Nr2e3 is also a key regulator of rod fate by stimulating the expression of rod-specific genes (117,118).

In mice, if one of these genes, *Nrl*, *Rorb*, or *Nr2e3* is mutated, the resulting retinas contain no rods and instead show an abundance of PRs with cone-like features that mainly express S-opsin (114,115,118). Also, the nuclear hormone receptor RXRγ promotes the production of M/L-cones at the expense of the S-cone (Figure 10) (119–121).

Many extrinsic factors have been shown to regulate PRs neurogenesis and differentiation, including Fgfs, Wnts, Shh, RA, and thyroid hormone (T3). Gradients of these signaling molecules are associated with differential expression of photoreceptor-specific opsins (121–123). While the patterns of rod and cone PRs vary among animal models, the use of these gradients seems to be broadly conserved between species (22).

Onecut1 is a TF expressed in subsets of RPCs and Otx2-expressing cells early during development, while later is also present in horizontal and ganglion cells (Figure 10) (102,124). Onecut1 overexpression results in the formation of excess cones at the expense of rods. In mice that lack Onecut1, cones are only modestly reduced by the end of development (125). Most of the cones in these mutants express high levels of S-opsin, and few cones express M-opsin, similar to *Thrb2* null mice. Thus, the synergic action of Onecut1/2 and Otx2 is needed for physiological M-cone subtype development.

1.3 Introduction to the primary cilium

Primary cilia were first described at the beginning of the '60s on fibroblasts and smooth muscle cells (126). Since then, these organelles have been observed on almost every cell type of the human body. Primary cilia are usually non-motile cytoplasmic appendages of a microtubule-based framework that extends from the cell surface and are essential for normal developmental and physiological functions (127,128). Cilia are present in approximately all cell types but were traditionally described in epithelial cells. The ciliary axoneme is anchored and develops from a specialized centriole called the basal body (BB) that operates as a microtubule-organizing center. The BB is composed of a symmetric and radial arrangement of nine triplets of microtubules, whence the external doublets of microtubules of the axoneme extend (Figure 11). The axoneme is a structure formed by aligned alpha and beta-tubulin microtubules arranged in a radial array of 9 doublets. Primary cilia can be distinguished from motile cilia for the absence of a central pair of microtubules. While motile cilia have a "9+2" structure, non-motile primary cilia lack this central pair, so define as a "9+0" structure (129). The entire axoneme is covered by a membrane continuous with the plasma membrane of the cell. Cilia are generally formed during the G0/G1 phases of the cell cycle, but they can also be observed during the S/G2 phases (130). Cilia formation, also called ciliogenesis, is restricted to these phases because, during mitosis, the BB generates one of the two centrosomes essential for mitotic spindle formation during cell division (131).

1.3.1 Cilia, basal bodies, and centrosomes

Primary cilia and mitotic spindle have a common origin, the centrosome. Although the term centrosomes are best known for their role in cell division, where it orchestrates microtubule arrays during mitosis, they are also responsible for the organization of microtubules responsible for polarity, shape, and cell motility in differentiated cells.

Centrosome and cilia biogenesis, function, and maintenance are regulated by physiological stimuli and are largely influenced by the cell cycle (132,133).

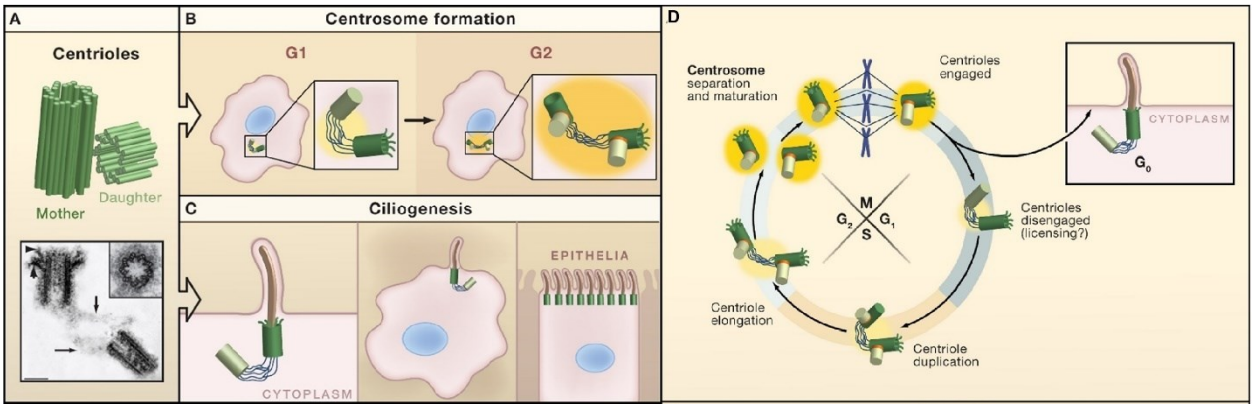

Figure 11 Schematic representation of centriole behavior during the cell cycle (1202)

In non-replicative cells, the centrosome forms the basal body that acts as a template for the cilium assembly, while during mitosis, the centrosome duplicates itself and generates the spindle poles, which orchestrate the formation of the mitotic spindle. The mitotic spindle is responsible for the segregation of chromosomes and the orientation of the cell division.

Both cilia and mitotic spindle require for their assembly an efficient transport along the microtubules mediated by molecular motors and cargo proteins. More and more evidence shows that many ciliary proteins have a dual and independent role in these two systems. Indeed, many of them localize both to the basal body, centrosomes, and as well as to other organelles (134).

The centrosomes constitute the Microtubule Organizing Center (MTOC) and are formed by one or two centrioles embedded in a protein matrix called Pericentriolar Material (PCM) in which the γ-tubulin ring complex (γ-TURC) and related γ-tubulin complexes provide temporal and spatial control over the growth of nascent microtubules (135). The minus (-) end of the microtubules are incorporated in the centrosome, while the Plus (+) ends, which can grow by adding new tubulin molecules, are free in the cytoplasm.

Centrosomes duplicate when the cell enters into the cell cycle. Centrosome duplication starts with the separation of the two centrioles during the G1 phase of the interphase. Then in the S phase, the centrioles duplicate, generating two mother-daughter centriole pairs, which can be distinguished by the fact that only the mother carries appendages. Once formed during the early S phase, new centrioles elongate throughout the S and G2 phases.

The two pairs of centrioles remain together until the cell enters mitosis. When the mitosis starts, the two centriole pairs (or centrosomes) migrate in opposite directions. As centrosomes move apart, the mitotic spindle begins to form, and the microtubules grow as the centrosomes move farther away. At the middle of mitosis, the two centrosomes would have reached the opposite side of the cells taken the name of spindle poles (136). There are three types of spindle microtubules: astral microtubules, which radiate outward and contact the cell membrane, thus positioning the spindle in the cell. Interpolar microtubules originating from the two opposite poles overlap with their plus (+) ends in the midzone. The last type of microtubules are the kinetochore microtubules which have their plus ends attached to sister chromatids at the centromere region (kinetochore). The number of microtubules attached to a kinetochore varies between species, but at least one microtubule from each pole attaches to the kinetochore of each chromosome. During metaphase, the mitotic spindle is now complete, and the chromosomes align along the cell equator. The spindle assembly checkpoint (SAC) controls that chromosomes are correctly attached to the mitotic spindle before continuing with the anaphase (137). During the anaphase, each chromosome's sister chromatids separate and move to opposite poles of the cell, and each chromatid becomes an independent chromosome. Chromatid's separation and the movement of the chromosomes are driven by changes in the length of the kinetochore microtubules. Astral microtubules anchored to the cell membrane also contribute to the separation pulling the poles further apart. Finally, interpolar microtubules slide past each other, adding additional pulling force to the chromosomes.

During telophase, the chromosomes arrive at the cell poles, and the mitotic spindle is disassembled.

Finally, during cytokinesis, the cell membrane pinches in at the cell equator, forming a cleavage furrow until the parent cell completely splits into two identical daughter cells. The furrow direction depends on the position of the astral and interpolar microtubules during anaphase, which is controlled by the parent centrosome's positioning. After exiting the cell cycle, the centrosome acquires the competence for the initial process of ciliogenesis, where the mother centrioles become the basal body. The basal body can migrate and anchor to the cell surface or dock ciliary vesicles, which elongate and eventually fuse with the plasma membrane depending

on the cell/cilia type. Despite the great interest in the subject, the system that regulates the transition from the centrosome to the basal body remains to be fully understood.

1.3.1.1 Control of centriole number

Perturbations of the mitotic spindle or centrosomes number can generate several errors during mitosis leading to chromosome missegregation or failure in cytokinesis that can eventually trigger programmed cell death mainly driven by p53. P53 seems of central importance to prevent centrosome overduplication. Inactivation of p53 in human cells favors multipolar spindle formation and tetraploid cells while rarely generating aneuploidy (138). Centrosome amplification is frequently observed in human cancers, where it constitutes one of the primary causes of the chromosomal instability typical of tumor cells.

Centrosome amplification can arise through several independent pathways. It can reflect deregulation of the centrosome cycle due to centriole overduplication generated by multiple rounds of duplication in the same S phase or excessive centriole multiplication (due to simultaneous formation of multiple centrioles from the pre-existing centriole pair). It could also reflect a failure of cell division, which can generate a tetraploid cell with four centrosomes. Centrosome amplification can also arise through cell fusion due to the action of fusogenic viruses. The evidence available so far indicates that deregulation of centrosome duplication and cell division failure represent the most common causes of centrosome amplification (138,139).

The maintenance of a constant number of centrioles is regulated by numerous factors that guarantee two types of controls. The control over the cell cycle guarantees that the centriole duplication occurs only once for each division of division, while the control of the copies number ensures that only one new daughter centriole is formed alongside each mother (140). Many cell-cycle regulatory proteins such as cyclins and cyclin-dependent kinases accumulate at centrosomes during the S phase (141). Both DNA replication and centrosome duplication require the hyperphosphorylation of the retinoblastoma (RB) protein and the activation of cyclin-dependent kinase 2 (CDK2) (142–144). Other kinases such as PLK1, PLK2, PLK3, TKK/MPS1, GMNC/Geminin are also central in this process (140,145–148). During G2 / M transition, the key

mitotic kinases Aurora-A, Cdk1 / Cyclin-B, and Polo family members accumulate at centrosomes. The mitotic activation of Cdk1 is first detected at centrosomes (149,150).

The control of the number of copies is also strictly regulated. The new centrioles are kept tightly bound to the parent centriole from their formation during the S phase until late mitosis. This bond prevents reduplication, and the process of separating the new centrosomes, called disengagement, is a necessary step for a new duplication (151). Although the precise mechanism of the disengagement process is still to be clarified, ESPL1, PKL1, PKL4, and SASS6 have been shown to play a central role in this process (152–154).

1.3.2 The photoreceptor primary cilium

PRs are sensory neurons that generate electrical responses when stimulated by light. PRs have long served as an outstanding model for elucidating fundamental principles of neuron function and sensory transduction (155). Advances in ciliary biology and the realization that PRs are also an excellent model for studying targeting, trafficking, and ciliary protein dynamics have brought even more interest in these cells. How phototransduction proteins traffic from the inner segment (IS) to the OS is an area of active research (156–158).

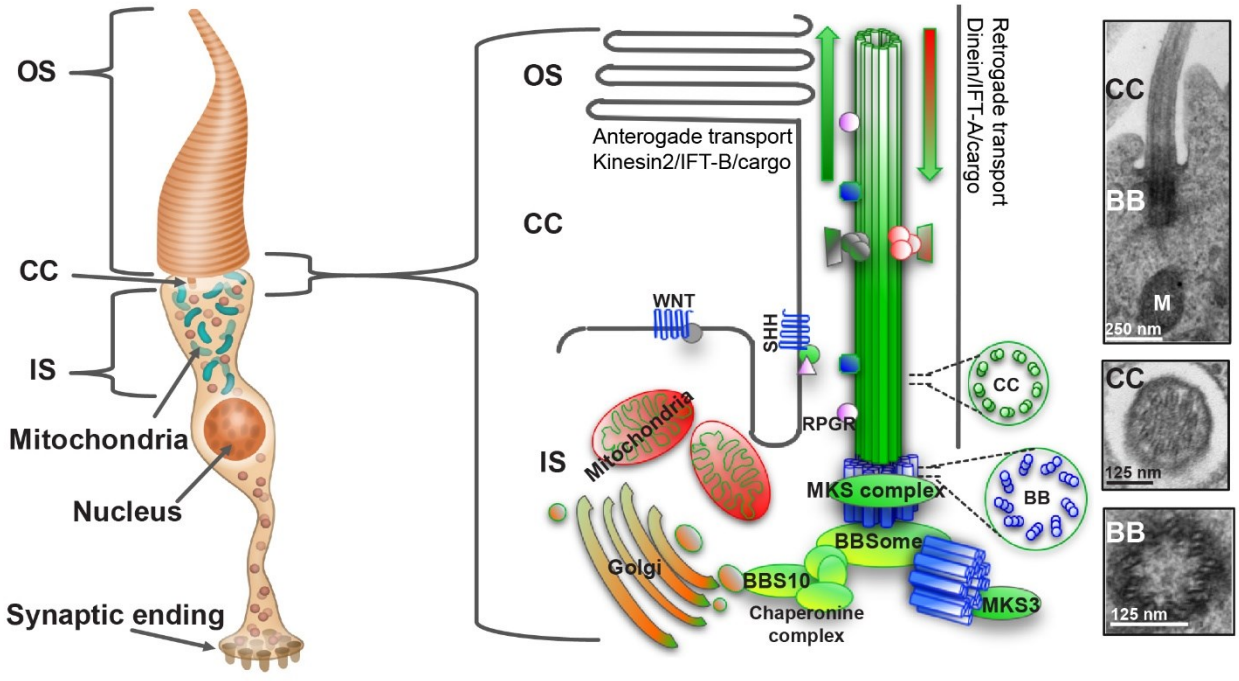

Figure 12: The photoreceptor's Connecting Cilium

Representation of the PR's CC with the reference of a few of its major components treated in this thesis. On the right, representative TEM images of iPSC-derived PRs CC and BB at 60 Days of differentiation.

Defective ciliary trafficking can cause PRs cell death (159). The PRs' primary cilium is a modified and unique type of sensory cilium and has an intracellular location (Figure 12) (160). Its most outer part constitutes the OS which contains membranous discs arranged in a coin-stack-like configuration filled with pigments densely packed within the disc lamellae (161). The high density of photosensitive proteins and their ordered alignment regarding the light path enhance the probability of capturing an incident photon. This highly organized and complex structure captures photons and produces electrical responses (42). The PRs have a high energy demand, and the IS is where all metabolism, biosynthesis, and endocytosis occur. The IS is rich in mitochondria and other organelles, including the endoplasmic reticulum (ER) and Golgi, necessary to produce and transport the component to build and maintain the OS (162,163). The CC is a complex structure responsible for the interactions between OS and IS, and it is the only connection between these two components (160). PRs cilium is a structure with an extremely high flow of lipids and proteins. It has been estimated that every minute more than 2000 opsins are transported from the IS to the OS (164). In terms of molecular composition and morphology, the CC shares common features with primary cilia. The CC is essential in PRs physiology, and, therefore, its dysfunction contributes to retinal degeneration (165).

1.3.2.1 Structure and functions

PRs ciliogenesis starts when the BB reaches the plasma membrane and anchors to it. Fibrous structures cross-link each microtubule doublet to the overlying plasma membrane to stabilize the BB in its proper position. The axonemal microtubules are anchored at the BB located at the distal end of the IS. The axoneme extends from the BB and represents the "spine" of the OS, and it extends distally to about half of the OS length (Figure 12) (166).

1.3.2.1.1 The axoneme and ciliary transport machinery

Cilia lack the necessary apparatus for protein synthesis. For this reason, all proteins required for ciliary generation and function must first be transported to the base of the cilia in specific vesicles (165). Post-Golgi vesicles are delivered to the CC, then the proteins destined to the OS need to be sorted between axoneme, lamellar disc region, and the plasma membrane.

This cargo system's precise mechanism is still not fully understood but seems to involve specific trafficking motif recognized by complexes such as the Intraflagellar Transport (IFT) machinery (161). This complex was first identified in Chlamydomonas flagella for leading the building process of the rising cilia. The IFT is a bidirectional cargo transport system from the base to the tip of the cilia (anterograde) and back to the base (retrograde) (Figure 12) (167). The IFT supports the trafficking carried by the cargo proteins that are the molecular motors that actively move along the axoneme (168). Kinesin-II is responsible for the anterograde transport and is associated with IFT-B proteins, while cytoplasmic dynein 2, assisted by the IFT-A proteins, is in charge of the retrograde one (169). Conditional deletion of a kinesin-II subunit KIF3A disrupts OS formation and opsin trafficking (170,171). Several IFTs have been localized to the photoreceptor CC, including IFT88, IFT57, IFT52, IFT140, and IFT20 (166). IFT88 was the first of the family recognized as indispensable for the ciliogenesis and the cilia's correct function. Ift88-deficient mice showed a highly perturbed OS development and a complete absence of CC, which caused PRs death (164). Similarly, the Ift140 KO caused incorrect opsins trafficking that resulted in their accumulation in the IS. IFT20 is the only component of the family that is also found outside the cilium. It is associated with the Golgi and is responsible for transporting essential components to the cilium base (172). For this reason, Ift20-deficient mice show an accumulation of opsins around the Golgi (173).

IFT components recognize specific motifs present in CC, OS, and integral membrane proteins. For this reason, defects in the transport of one protein do not generally affect the transport of others, suggesting that their transport occurs independently. The VxPx motif at the rhodopsin's carboxyl terminus is necessary for the correct sorting of rhodopsin into transport carriers from the Golgi towards the CC and then to the OS; when mutated, it causes autosomal dominant RP in human patients (157,174,175). This motif is also present in cone opsins and is recognized from transport proteins as the small GTPase Arf4, ASAP1, Rab11, and FIP3 (159).

Actin and myosin are also an essential part of this system and are present in PRs IS, CC, and OS, and their malfunction causes PRs degeneration (169). For example, Actin depolymerization promotes PRs death, while myosin mutants show transport defects from the IS to the OS. Myosin defects cause numerous diseases, including the human Usher syndrome (USH) (176). The USH1G

protein acts as a scaffold of the ciliary/periciliary USH protein network in PRs. It is associated with microtubules representing the transport routes for protein delivery toward the cilium (17,177,178).

1.3.2.1.2 Connecting Cilium and the Basal Body

The CC-associated proteins are also crucial for the correct trafficking to the OS. One of the first described is RP1, responsible for 5–10% of all RP cases. RP1 is a large protein localized at the CC, mainly in the nascent OS, in both rods and cones (179). RP1 also seems to bind and stabilize microtubules in the axoneme. Rp1 KO mouse model shows swollen OS with abnormal formation and alignment of the discs (180–182). The Retinitis Pigmentosa GTPase regulator (RPGR) is important for PRs' physiology. Mutations in *RPGR* cause severe and progressive retinal dystrophy. RPGR and its related protein, RPGRIP (RPGR interacting protein), are found in amacrine cells and CC and OS of rods and cones. Rpgr KO mice have shown reduced quantities of rhodopsin in rods and mislocalization of opsin in cones preceding their degeneration, suggesting a role for RPGR in the trafficking of proteins through the CC from IS to the OS (183,184).

The mother centriole, which is the oldest centriole inherited during mitosis, becomes the BB during ciliogenesis. The mother centriole is distinguished from the daughter centriole by appendages on its distal end and is required to initiate the primary cilium generation (185). The BB docking is the process that allows the mother centriole to bind the cell membrane, thus triggering ciliogenesis. This process requires the apical actin cytoskeleton web organization, a process involving the RhoA GTPase, an active signaling mechanism that regulates BB placement (186–188). Centriolin/CEP110/CNTRL is a protein associated with the mother centriole (189). In the centrosome, Centriolin is found at both ends of the centrosomal tube, including the site of centrosome duplication. However, in the daughter centrosome, it is present only at the closed end. Centriolin seems to interact with Rab11 to promote the mother centriole's correct localization and maintenance (190). Mutations in Centriolin in humans can cause ciliopathies as Atrioventricular Septal Defect (191). Centrins are calcium-binding proteins associated with the centrosome, that are present in both rods and cones. Mammalian PRs have four isoforms of centrins that localize at the CC and BB. These centrins seem to have a role in the alignment of the photoreceptor's OS. Centrins were shown to interact with Transducin, regulating its light-

dependent translocation from the OS to the IS (192). In addition to the IFT machinery, four major complexes have been identified to take part in ciliary trafficking: the BBSome, the MKS complex, and two NPHP complexes, all located in the Transition Zone (TZ) (Figure 12) (193,194).

1.3.2.1.3 Transition Zone

The TZ is a specialized ciliary domain present at the cilium base that acts as a "ciliary gate" (160). The TZ represents a structural intermediate between the BB and the axoneme, responsible for regulating ciliary traffic. Diverse ciliary proteins accumulate at the TZ in wild-type cells, suggesting that the TZ is a waypoint for proteins entering and exiting the cilium. Electron micrographs of the TZ have identified Y-shaped structures, called Y-links, with the stem anchored at the microtubule doublets and the two arms attached to the ciliary membrane (195). TZ proteins generally show a long-term stable association at the ciliary base, whereas the BBSome appears to be more dynamic (193).

Meckel-Gruber syndrome (MKS) and Nephronophthisis (NPHP) complexes are two of the several complexes that localize with TZ (194,196–198). Dysfunctions in TZ's function can modify the ciliary membrane's composition with delocalization of the transmembrane signal proteins, which cause in humans a subset of ciliopathies such as NPHP, Joubert syndrome (JBTS), and MKS (193,199,200). NPHP and MKS complex components form nested rings comprised of nine-fold doublets with a more proximal localization in the TZ than the BBSome.

1.3.2.1.4 BBSome

The BBSome is physically and functionally connected to the other complexes located in the TZ (Figures 12, 22) (201). The BBSome is a stable octameric protein complex with a central role in primary cilia function and homeostasis, and its malfunction causes severe ciliopathies such as Bardet-Biedl syndrome (BBS). BBSome plays a key role in mediating molecular/vesicular transport in and out from the primary cilium, regulating intraciliary trafficking, and interacting with the IFT machinery (202–204). It functions as a cargo adapter that recognizes a set of membrane-bound ciliary and signaling proteins and links them to the IFT machinery (202). The BBSome is also implicated in the assembly and stabilization of the IFT machinery, and its dysfunction has variable effects in different organisms (172,204–207). The BBSome was first discovered in 2007 through

biochemical purification of BBS4-containing complexes from mammalian cells. It comprises seven highly conserved BBS proteins (BBS1, BBS2, BBS4, BBS5, BBS7, BBS8, and BBS9) and a novel protein, BBIP10, each present in stoichiometric amounts. Additional BBS proteins have functions in the BBSome assembly, including cilia targeting of BBSome proteins, proper identification of BBSome cargoes, and some other extra-ciliary roles (Figure 22) (208). BBSome complex binds with pericentriolar material 1 (PCM1) and Rabin8, a guanosine exchange factor for RAB8A (203,209). BBSome assembly appears to be an orderly and sequential process initiated by a complex composed of BBS7, BBS chaperonins-like proteins (BBS6, BBS10, and BBS12), and the CCT/TRiC complex, which acts as a scaffold for the addiction of the further BBSome subunits (202,210,211). Apart from BBS5, which contains two pleckstrin homology domains and binds phosphatidylinositol 3-phosphate, the BBSome subunits do not contain any informative domains. It is not clear how the interplay between BBSome and membrane actually works. In the retina, it has been reported that BBS5 can be phosphorylated through light stimulation by protein kinase C, which causes the release of Arrestin1 into the OS membranes (212). Many BBS proteins that are not part of the BBSome have been shown to be indispensable for its correct function. Among these, BBS3/Arl6 is an Arf-like GTPase, and BBS11/TRIM32 functions as an E3 ubiquitin ligase (213,214). BBS3/ARL6 localizes to the BB and ciliary membrane. It interacts with BBS1 in its active GTP-bound form, allowing the transport of the BBSome to the cilium (215). Three BBS proteins, BBS6, BBS10, and BBS12, have similar motifs to type II chaperonins, and they localize to centrosomes and BBs (216,217). These chaperone-like proteins seem to be only required for the assembly of the BBSome (218). The chaperonin-like BBS proteins are structurally analogous to the CCT family of group II chaperonins. However, they seem to have lost both the ATP-dependent folding activity of canonical CCT chaperonins and the ability to make CCT-like oligomeric complexes. They play a pivotal role in the initial steps of the BBsome assembly (211). Recent work has demonstrated that BBS6, BBS10, and BBS12 are key factors in this process by stabilizing BBS7 (the first protein to be incorporated) and driving its interaction with six canonical CCT chaperonins (CCT1-5 and CCT8), which are responsible for the folding process (219,220). Rather than having an active role of chaperonins, it would appear that BBS6, BBS10, and BBS12 act as a linker to promote the interaction of CCT proteins to their substrates as part of the transitory

BBS/CCT/TRiC-chaperonin complex (218). BBS10 seems to mediate the interaction of the BBS6-BBS12-BBS7 pre-complex with the CCT proteins to finally form the BBS/CCT/TRiC-chaperonin complex (203,211). Mutations in the leucine-zipper transcription factor-like 1 (LZTFL1), encoded by *BBS17*, occasional cause BBS (219,221,222). It is found in the cytosol, and it is not enriched at the BB or the cilium. LZTFL1 interacts with the BBSome through the binding of its C-terminal to BBS9 (Figure 22) . When LZTFL1 expression is inhibited, there is no observable effect on cilia length or formation, while LZTFL1 deletion cause increasing translocation of BBSome proteins to the cilium. Surprisingly, LZTFL1 downregulation can rescue BBSome localization to the cilium also in cells depleted for BBS3 and BBS5 (223). More recently, have been reported few cases of BBS with hypomorphic mutations in two new genes, *BBS13* and *BBS14*, also known as *MKS1* and Centrosomal protein 290 kDa (*CEP290*) (224–227).

CEP290 is part of the centriolar satellites (CSs), electron-dense granules that accumulate around centrosomes and centrioles in the pericentriolar material. CEP290 is required for BBS4 localization to the CSs necessary for the BBSome formation and its recruitment to the cilium (228,229).

1.3.2.1.5 MKS complex

MKS complex is restricted to the distal half of the TZ, where are situated the Y linkers, advancing the hypothesis that the MKS complex directly associates with them (193,230,231). Studies using murine epithelial cells and embryos indicate that the MKS complex delimits the ciliary membrane and acts as a diffusion barrier at the cilium base (194,196). B9D1, TCTN2, and TMEM231 are components of the MKS complex, and they all cause MKS phenotype when mutated (196–198,232,233). B9d1 and Tmem231 are needed to localize part of MKS complex components to the TZ, in different cells and tissues. This process is required to maintain ciliary protein composition *in vitro* and *in vivo* (199). The MKS3/TMEM67 protein is not an integral part of the MKS complex, but it seems to interact with it (234,235). MSK3 localizes to the TZ at the primary cilium base and the cell membrane in ciliated cells (231). Human MKS3 has 995 amino acid residues containing four functional domains: a signal peptide, a cysteine-rich repeat region, three transmembrane domains, and a coiled-coil domain from N- to C-terminus (235,236). The extracellular cysteine-rich repeat region is similar to the cysteine-rich domain of the Frizzled (FZD) protein family, which is implicated in canonical and non-canonical Wnt signaling pathways, both

frequently perturbed in ciliopathies (237,238). The coiled-coil domain seems to interact with other proteins, such as nuclear envelope spectrin repeat protein 2 (Nesprin-2) (236). MKS3 has been linked with centrosome migration to the apical cell membrane during early ciliogenesis and with the control of centrosome organization (Figure 12) (239,240).

1.3.2.1.6 NPHP complex

Several proteins are part of the NPHP complex, and NPHP1, NPHP2, NPHP3, NPHP4, NPHP6, and NPHP8, have been found to interact with each other (241–244). NPHP complex localizes to the ciliary compartment border and seems to have a gatekeeper-like functional role controlling the entry and exit of proteins at the cilium (245). RPGRIP1L is also a part of the NPHP complex and has been demonstrated to interact with NPHP1 directly (246–248). In *C. Elegans*, a homolog of RPGRIP1L is required for the localization of both the NPHP and MKS complexes at the TZ (194,249). Mutations in RPGRIP1L disrupt Smoothened (SMO) accumulation at the TZ in both *C. Elegans* and vertebrates. SMO is an essential mediator of the vertebrate Hedgehog signaling pathway, and it requires the TZ proteins B9D1, TMEM231, and TCTN2 to accumulate within the ciliary membrane (196,197,199). Consequently, loss of any of these proteins leads to Hedgehog-associated developmental defects (198,250).

1.3.2.1.7 Cilia and flagella associate proteins

Cilia and flagella associate proteins (CFAP) family is another class of proteins associated with the primary cilia, although they were first discovered in flagella and motile cilia (251–253). Mutations in these proteins are one of the leading causes of Primary Ciliary Dyskinesia (PCD) that cause sterility in men and affect women's fertilization capacity (254). These patients' symptoms are variable and are associated with various clinical manifestations, including RD (255). Mutations in *DNAAF1*, *CFAP300*, *CFAP298/C21orf59* were shown to cause PCD, and cells with mutations in these genes, have immotile cilia that either lack the outer and inner dynein arms or have severe defects in these structures (256–259). Apart from the role of a few components of the CFAP family, little is known about their role in the primary cilium. Members of the CFAP family seem to be involved in microtubule/spindle formation in the meiotic cell cycle (260). CFAP54 and C21orf2/CFAP410 have a critical role in the proper assembly and function of mammalian cilia and

flagella. Reduced levels of functional CFAP410 induced abnormal cilia formation with subsequent PRs degeneration, leading to autosomal recessive RP (arRP) and autosomal recessive cone-rod dystrophy (arCRD) (261).

In this thesis, we are interested in the role of CC components, such as the BBSome and MKS complex, in PRs development, function, and survival. More precisely, we confirm previous evidence on the functions of MKS3 and BBS10 and reveal new possible roles of these proteins during ciliogenesis and in the maintenance of genomic stability.

1.4 Retinal dystrophies

Retinopathies, also called retinal dystrophies or Retinal Degenerative Diseases (RDs), are diseases causing retina degeneration. Visual impairment can arise from the loss of PRs, defects in synaptic transmission between PRs and bipolar cells, or loss of ganglion cells or other retinal cell types. RDs caused by loss of PRs are the most frequent and are called Outer Retinal Dystrophies (ORDs) (262).

RDs can also be divided into two broad groups – stationary (congenital) and progressive (degenerative) (263,264). Stationary RDs are usually present during infancy or early childhood, and symptoms usually remain unchanged throughout life. In progressive RD, associated symptoms worsen over time. However, the age of onset and the progression rate can vary considerably from one person to another. Progressive RDs usually develop in late childhood or early adulthood. Affected people commonly experience gradual vision loss that may lead to blindness. Dystrophies caused by the progressive loss of PRs account for averaging half of the total blindness cases in the developed countries (262,265). These conditions can be caused genetically or acquired later in life. Simple inherited diseases affecting the retina are defined as monogenic non-syndromic RDs (M-NS RDs). Their phenotype is restricted to the eye since they are almost entirely linked to PRs and RPE-specific genes. M-NS RDs affect more than 2 million people worldwide, and the onset time and disease progression are mainly driven by genetic risks. RP is a congenital stationary night blindness, Leber's congenital amaurosis (LCA), and rod-cone disease (RCD) are all part of this class and are caused by inherited rare mutations (Figure 13) (262,266).

Monogenic retinal dystrophies can also be a part of a syndromic condition where the ocular phenotype can be associated with symptoms affecting other tissues (267,268). These conditions, named monogenic syndromic RDs (M-S RDs), include USH and BBS syndromes (224,269,270). M-S RDs are primarily associated with ciliary dysfunction and are characterized by pleiotropic effects on multiple organs and tissues. In addition to the retinal phenotype, the most common symptoms include obesity, polydactyly, mental retardation, deafness, renal abnormalities/deficiency, and metabolic disorders (Figure 21). Monogenic RDs' inheritance can be dominant, recessive, or X-linked (266,271).

Complex retinopathies (complex RD), such as AMD, are caused by a combination of both genetic and environmental factors. Complex RDs, in comparison to simple monogenic RDs, are typically characterized by later onset and are caused by a combination of age-related variations, common or rare genetic mutations, and other risk factors such as gender, lifestyle, and smoking (266,271).

Classical categorization of retinal dystrophies can be defined as a phenotype-centric classification that takes into account the type of PRs that are primarily affected. This classification can divide retinal dystrophies into three major groups: Generalized RD, rod-dominant RD, and cone dominant RD (Figure 14-16).

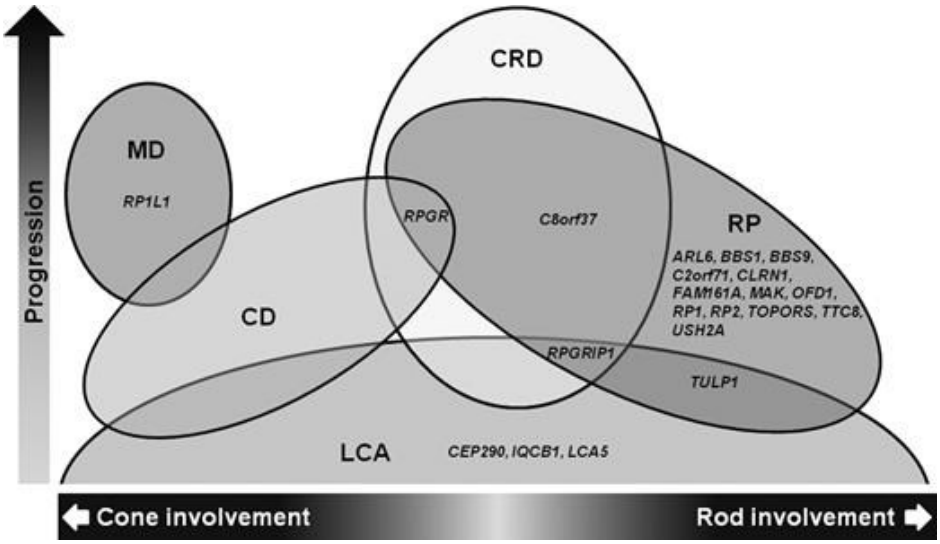

Figure 13: Schematic representation of phenotypic and genetic overlap among non-syndromic retinal ciliopathies (276)

1.4.1 Phenotype-centric classification of RDs

1.4.1.1 Generalized RDs

Generalized photoreceptor diseases are characterized by the early loss of both cone and rod PRs (272,273). In this category, the best-known disease is LCA, a severe congenital RD with an incidence of about 1 for 40.000 newborns (274,275). LCA is the most aggressive form of early-onset retinal blindness and typically becomes evident in the first year of life. It is characterized by reduced visual function with abolished or severely reduced rod and cone functions, photophobia, absent

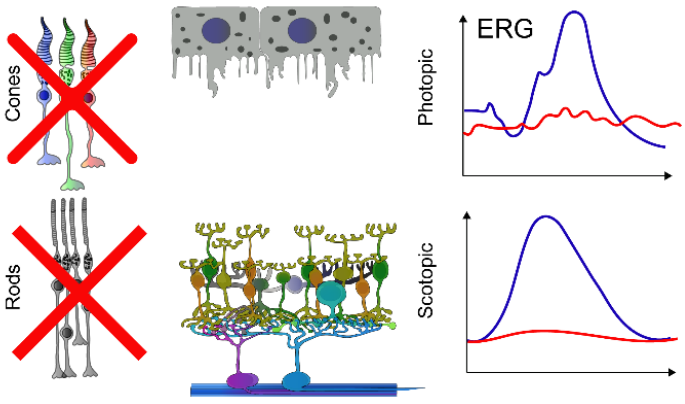

Figure 14: Generalized Retinal Degeneration

pupillary responses, and hyperopia (276). Currently, more than 16 genes have been identified mutated in LCA patients, with a mode of inheritance, mostly autosomal recessive (277). These causative genes mostly refer to retina-specific genes such as *GUCY2D, RPGRIP1, RDH12, SPATA7, AIPL1, RD3, CRB1, CRX, IMPDH1, IQCB1, KCNJ13*, and *LCA5*. Mutations in the CEP290 and the RPE-Specific Protein 65kDa (RPE65) also cause LCA (274,278,279). Given the severity of the condition, it is one of the most extensively studied inherited retinal disorders. Gyrate atrophy (causal mutation in the *OAT* gene) and Choroideremia (causal mutation in *CHM* gene) are the two other major forms of non-syndromic generalized photoreceptor diseases with an estimated incidence rate of 1:50000 (275,280). CRD is generally classified in the generalized RDs group, but it can also be classified in the cone-dominant RD when rods degeneration starts later than cones, but the border between the two can be clouded (272,273). For example, in this context, patients carrying causal C8orf37 mutations vary from a classic RP phenotype with night blindness followed by concentric loss of visual field to a CRD with electroretinogram (ERG) responses of both cone-rod severely reduced or nonrecordable (281).

1.4.1.2 Rod-dominant RDs

RP is the most common form of rod-dominant disease. It is also known as progressive pigmentary retinopathy and is sometimes considered a CRD when degeneration of cones is observed early in the disease progression (282,283). It is a class of genetically heterogeneous diseases with clinically similar phenotypes involving progressive degeneration of the retina. The onset and progression of the disease vary between patients (284). However, it typically starts with rod PRs dysfunction that arises into night blindness, followed by progressive mid-peripheral vision loss, which could eventually affect macular and foveal regions, resulting in complete blindness (282,285,286). RP incidence is 1 in 4000, with about 1.2 million affected individuals worldwide (283). Disease-causing mutations can

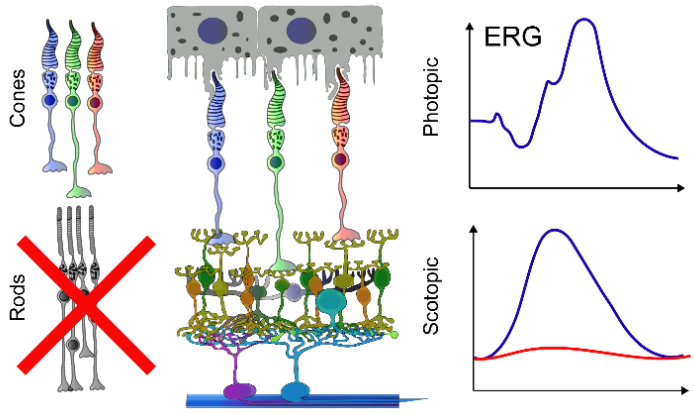

Figure 15: Rod-dominant Retinal Degeneration

be inherited in an autosomal recessive (50 to 60%), autosomal dominant (30 to 40%), and X-linked way (5 to 15%), and mutations in several genes can be either dominant or recessive (287–289).

Recent advancement in Whole Genome Sequencing (WGS) techniques has enabled the discovery of many new mutations and genes responsible for RP, with now nearly 60 genes and more than 3000 mutations involved in non-syndromic RP (280,282). Although the molecular function of a considerable number of RP-associated genes has been deeply investigated, the correlations between the phenotype and the genotype are not fully understood. Most causative mutations in non-syndromic RPs affect PRs-specific genes such as Rhodopsin (RHO), covering around 25% of the autosomal dominant cases and making it the most commonly mutated gene (174,284). Some RP cases are generated from mutations in RPE-specific genes, such as the Retinoid Isomerohydrolase (*RPE65*), the Lecithin Retinol Acyltransferase (*LRAT*), the Retinol Dehydrogenase 5 (*RDH5*), or the MER Proto- Oncogene Tyrosine Kinase (*MERTK*) (279,290–292). Mutations in one of these genes lead to a dysfunctional RPE, which causes reduced phagocytosis with an insufficient clearance of photoreceptor OS that causes degeneration and loss of PRs.

Mutations in *RPE65* can cause RP or LCA (279). RP is diagnosed to patients with PRs degeneration with good central vision within the first decade of life, whereas the diagnosis of LCA is reserved for patients born blind or who have lost vision during the first few months after birth. This variation and apparent overlap in their severity undermine the classic RDs' taxonomy, suggesting that some LCA cases represent one extreme of a spectrum of diseases, for the most part, categorized as RP.

Interestingly, the genes coding for the pre-mRNA processing factor 3 (*PRPF3), PRPF8,* and *PRPF31* are implicated in around 10% of the autosomal dominant cases. These genes are ubiquitously expressed even though the phenotype observed in patients is restricted to the retina (293–295). Since the splicing activity is essential in almost all cell types, it is unclear why mutations in PRPF genes cause a retinal-specific disease and the specific retinal cell type(s) first affected by these mutations.

Although RP is more commonly restricted to the retina, it can also be part of a syndromic disorder in 25% of its cases (283,296). Among the syndromic forms of RPs, we have USH and BBS (270,297).

On the other hand, some BBS cases show MD instead of RP, which makes the understanding and classification of these diseases even more elusive (298,299).

1.4.1.3 Cone-dominant RDs

Cone-dominant diseases, such as MDs, cone dystrophies (CDs), and CRDs, all lead to severe visual impairment. About 20 and 10 different genes are currently responsible for non-syndromic progressive cone-rod dystrophies and monogenic macular dystrophies, respectively (275,280). The damage in MDs is restricted to the macula, whereas in CRDs, the progressive loss of cone PRs is followed by loss of rod PRs, which cause a diminution of the visual acuity, accompanied by successive loss of peripheral vision and night blindness, which eventually leads to complete vision loss (262,300). Perifoveal atrophy of the outer retina with the "bull's eye" effect is typically observed in these cases (Figure 17) (265,272,273). Alternatively, cone function decreases gradually in CDs, while rod functions are initially normal but can slightly diminish over time. CDs are characterized by color vision disturbance and photophobia, which brings to legal blindness before the third or fourth decade of life (263).

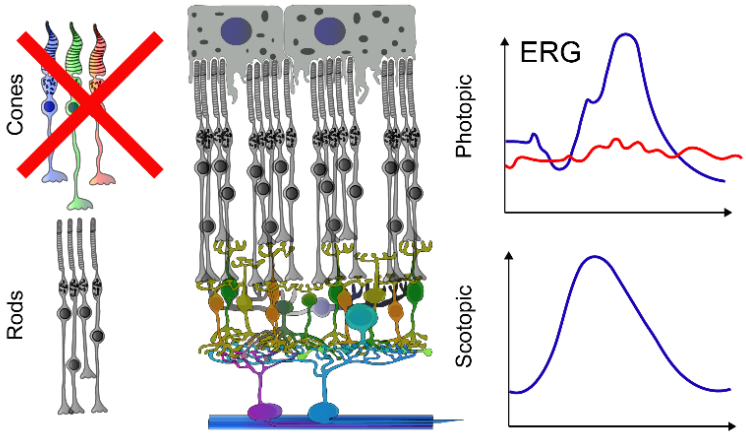

Figure 16: Cone-dominant Retinal Degeneration

MDs can further include a broad set of diseases as Stargardt's Disease, Sorsby Fundus Dystrophy, X-linked Juvenile Retinoschisis, BBS, and others. Stargardt disease has an autosomal recessive inheritance due to mutations in the ATP-binding cassette transporter (*ABCA4*) gene (301). It is the most common form of inherited juvenile MD, with about 1 in 9000 individuals affected (302,303). Rare cases of Stargardt-like disease inherited as a dominant trait are due to mutations in the Elongation Of Very Long Chain Fatty Acids 4 (*ELOVL4*) gene (304).

AMD develops late in life and is considered a complex RD. It has a complex origin as it is caused by a combination of risk factors, including genetics, aging, environmental factors, and lifestyle

(305). AMD is considered one of the most relevant among hundreds of human retinal diseases, affecting more than 8% of the world population aged 45–85 years. AMD cases in 2020 have almost reached 2 million, and this number is predicted to increase to 2.8 million by 2040 (306,307). As most of the RDs, AMD is neither preventable nor curable, representing one of the major causes of irreversible blindness. The underlying processes leading to AMD are not entirely understood. However, it includes single-gene mutations, which represent risk factors, complemented with complex gene-metabolic-environment interaction, resulting in extracellular remodeling, abnormal angiogenesis, chronic inflammation, oxidative stress, and defective lipid metabolism, many of which are common age-induced physiological and anatomical changes (Figure 18) (305,308,309).

Interestingly, while more than 66% of the genes implicated in monogenic and simple MDs forms are caused by mutations in genes involved in visual functions such as phototransduction, ciliary transport, and retinal recycling, only 7% of AMD risk genes are involved in vision-related functions, but rather tend to affect tissue homeostasis processes (Figure 19). These mechanisms play a role in many non-retinal tissues, suggesting that AMD-affected genes strongly correlate to non-retinal phenotypes (310). For example, many AMD risk genes are linked to the kidney, skin, coronary arteries, and heart dysfunctions. They have also been related to diabetes and neural and metabolic symptoms supporting the theory that AMD could be considered a systemic disease (268,311,312).

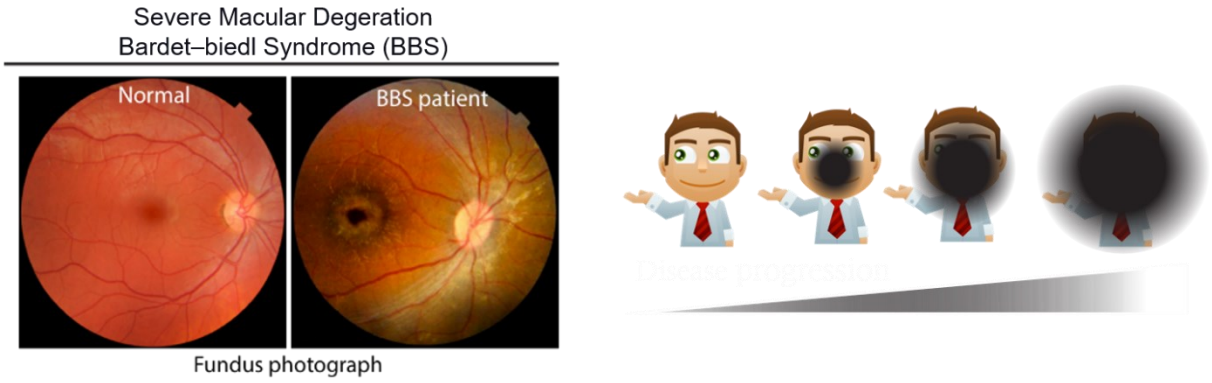

Figure 17: Macular Degeneration in the human retina (adapted from (313))

1.4.2 Molecular/anatomical classification of RD

Due to frequent overlap of phenotype and high diagnostic variation, classical categorization of retinal dystrophies based on phenotype can be confusing in many cases. Another problem related to the classical system in understanding complex diseases, such as multisystemic and age-related diseases, is that genes related to these diseases are expressed in many tissues, and often their vision-related functions are unknown (268,308,311). Thanks to the advancing of next-generation sequencing that allows precise mapping of genomes in patients, the molecular basis of pure monogenic RDs has expanded, and nowadays, more than 200 genes have been linked to RDs (314,315). Interestingly, only half of these genes are mainly expressed in PRs, while the remaining 50% of genes are, more or less, ubiquitously expressed (Figure 19) (266,308).

Even though specific PR genes can be identified thanks to the linkage with known diseases, their specific function cannot be established by simple association. Basic research must be carried out to establish their function and localization, both in the physiological and physiopathological context. More recently, technological and bioinformatic advancements associated with sophisticated and innovative experimental approaches have allowed incredible progress in identifying photoreceptor components (20,158). Their function, modulation, interaction in and between different complexes, and their arrangement in signaling cascades have been amply described, although it is far to be complete (158). Furthermore, their physiological function in the retina and during pathogenesis has been described for most genes. Since proteins mutated in different diseases often interact or are part of the same complex, this has allowed a new classification based on their molecular, physiological, and anatomical characteristics. This classification could represent a significant advance in developing new and more effective therapies (316,317).

Considering the sizeable phenotypic overlap caused by different mutations, it is evident that many different RDs are interconnected (Figure 21). When we divide RDs according to their genetic origin, they are included into three groups: M-NS RD, M-S RD, and complex RD (Figure 18 C). Interestingly these three groups have a slight overlap of the causal genes, suggesting that they are implicated in different biological mechanisms and pathways or are expressed in different cells or cell regions (Figure 18 C). If RDs associated genes are assigned to groups based on their

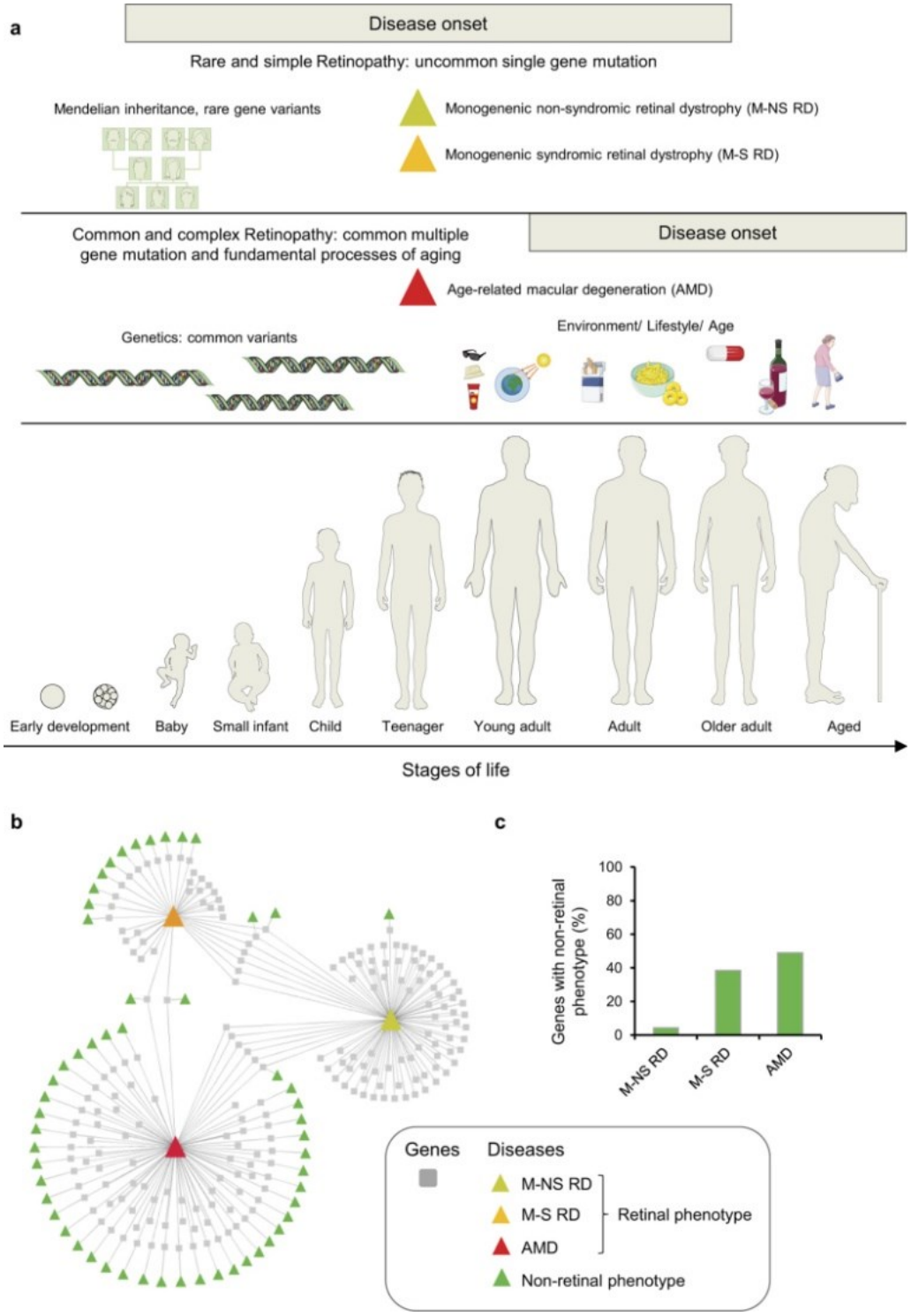

Figure 18: Principal differences between simple and complex retinal dystrophies (RD) and disease-gene network (266)

(a) Monogenetic non-syndromic and syndromic RDs are mainly driven by rare genetic variation. The disease onset can be very early, if the infant is born blind or develops severe vision loss soon after birth. Vision loss can also develop later in life. Complex retinopathies, such as age-related macular degeneration (AMD) have a later onset in life and are caused by a combination of common genetic risk factors, ageing and environmental/ lifestyle factors. (b) Disease/phenotype-gene network of 208 genes related to RD. Boxes represent genes and triangles diseases or phenotypes. Monogenic non-syndromic RD are colored in yellow, monogenic syndromic RD are colored in orange, and AMD in red. Green triangles represent diseases or phenotypes that manifest in tissues outside the eye (non-vision related). (c) Percentage of genes with a non-retinal phenotype for M-NS RD, M-S RD, and AMD.

biological function and retinal compartments, this results in a protein process network arranged

hierarchically in six main classes (266,308) (Figure 19).

1) Visual homeostasis with processes such as phototransduction, ciliary trafficking, neurotransmission, phagocytosis of outer segment disks, retinal development, and the visual retinoid cycle.

2) Tissue integrity (extracellular matrix turnover, angiogenesis, transepithelial transport, and apoptosis).

3) DNA and protein homeostasis.

4) Protection system, including the innate immune system (inflammatory and complement system processes) and biological systems such as the antioxidative system, which can counteract oxidative stress.

5) Metabolism.

6) A class with unknown proteins and those related to general signaling processes.

Most of the M-NS RDs related proteins are included in few classes of retina-specific processes. Some other ubiquitous processes are implicated in these diseases, such as regulation of splicing/gene expression, extracellular matrix turnover, complement pathway, protein homeostasis, and lipid metabolism, which are in line with the involvement of RPE and choroid in some cases of retinal dystrophies, in particular in the context of RP (287,289,318).

M-NS and M-S RDs overlap for different genes and processes, although most of the genes related to M-S RD are linked to proteins implicated in ciliary trafficking (Figure 19) (165,289,319). Even if cilia are present in most cells, this class of proteins is included in the retinal-specific processes because of their importance in PRs biology. However, primary cilia are present in more than 98% of the cells in our body, and for this reason, it is not strange to think that these PRs ciliary proteins have a role outside the retina, so causing syndromic manifestation (237). The functional and anatomical overlap between complex and Simple RDs is minimal, suggesting that these types of conditions have distant origins and must, therefore, be considered separately in particular when developing new therapeutic solutions.

As in M-NS RD, some complex RDs, such as AMD, are related to Choroidal/RPE genes, mainly implicated in extracellular matrix turnover and protein homeostasis (79). Few other common

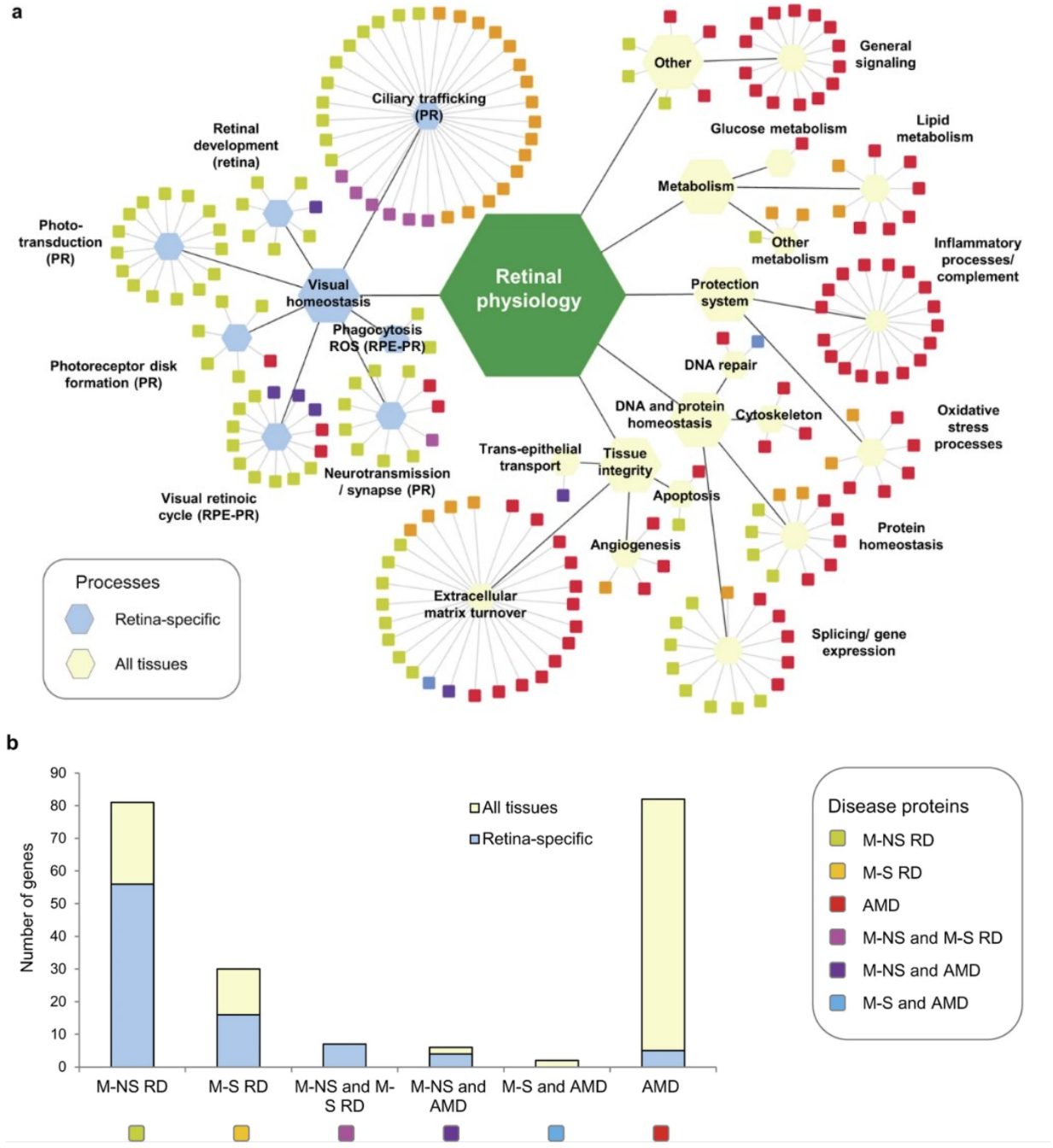

Figure 19: Functional classification of 208 RD genes and association to cell types or tissue compartments where this function contributes to vision-related tasks or to keeping the tissue integrity (266).

(a) Boxes represent the 208 RD genes, which are coloured according to their RD disease classification. Genes are boxed according to their functional classification and assigned to either the retinal cell type where this process plays a role, or to functions affecting other retinal compartments and retinal tissue development and integrity, or to presumably cell general functions. (b) Statistic of proteins in the different disease classes and their association to retina- specific and cell and tissue general functions.

processes between complex and M-NS RDs are the spicing/gene expression group and other general signaling proteins, mostly a group of proteins with unknown functions (293,320).

The vast majority of complex RDs proteins are not specific to the retina but are ubiquitously expressed and profoundly linked to processes with a role in homeostasis in multiple tissues. Regardless of their localizations, some of these diseases exclusively affect the eye, but the reasons are in most cases unknown, making them a hotly debated topic (311).

These ubiquitous processes include general signaling, cytoskeleton, chaperones, Golgi function, DNA repair, apoptosis, and oxidative stress.

1.4.2.1 Ubiquitous processes implicated in RDs

1.4.2.1.1 The cytoskeleton

The cytoskeleton is a cardinal component for both eukaryotic and prokaryotic cells. In addition to providing a structural scaffold for the cell, its modulation plays a fundamental role in many processes, including cell division, intracellular and vesicle transport, adhesion, migration, endocytosis, force transmission, response to external forces, and adaptation of cell shape and cell layer geometry to external and internal factors (296). A robust connection between the intracellular cytoskeleton and the extracellular matrix is indispensable for the polarization and function of RPE and other retinal cells (40,45,296,321). Among all the cells in the body, neurons are the type of cell more extensively studied in the cytoskeleton`s context. In the PRs, cytoskeleton and associated proteins are a fundamental part of the ciliary structure, which, as mentioned above, is indispensable for their function and survival. The cytoskeleton is also indispensable for the RPE cells to fulfill all their functions, including its daily phagocytosis of the shed photoreceptor OS's tips and intracellular processing and recycling of their constituents. Impairments of these cytoskeletal structures that affect PRs or RPE architecture result in an unfunctional retina and are at the origin of different retinal diseases, including AMD (45,322).

The retina is a metabolically active structure continuously targeted from the light and, therefore, also exposed to high levels of oxidative stress (41). In the retina's specific case, the most abundant type of stress is the photo-oxidative stress, which is continuously controlled by specific systems

in PRs and RPE cells (46,323). Defects in the RPE cause a decreased in its phagocytic and antioxidant properties, which trigged a reaction between cellular metabolites and free radicals, causing deposits of lipofuscin and ceroid. PRs are the major oxygen users in the retina; if the system responsible for the clearance fails and is unable to balance radicals' production, this triggers a mechanism that inevitably brings to PRs cell death. Furthermore, the degenerating PRs can release these oxygen reactants with a deleterious effect on the surrounding PRs, causing a "chain effect" (323). Oxidative stressors play an essential role in the pathogenesis of RDs and particularly in AMD and other age-related RDs (46,324). Oxidative stress represents a potential therapeutic target that is often poorly explored (325,326).

1.4.2.1.2 Genomic instability and DNA repair system

Photo-oxidative stress can trigger cell death in PRs. However, this process is usually preceded by genomic instability and activation of the DNA repair system (327–330). In PRs, excessive oxidative stress triggers waves of DNA fragmentation, causing elevated activation of DNA-repair mechanisms that tempt to rescue the damaged cells. If the damage is too severe or the DNA repair machinery is not functioning correctly, cells undergo apoptosis. The DNA-damage machinery's improper activity can be caused by mutations in its specific components or by a physiological decrease of the DNA repair system with age. So maintaining or activating the cell's endogenous system can, in some cases, be a possible therapeutic solution for rescue PRs and other neuronal cells. In other cases, hyperactivation of certain factors may be the cause of the degeneration (331,332). This is the case of the *AAG* gene implicated in some RP cases. AAG has an essential role in snipping DNA bases that toxic agents have damaged. Under certain conditions, this protein is "hyper-activated" and cuts too quickly for the rest of the repair system to keep up, then causing the cell to enter apoptosis (333,334). In this case, AAG inhibition has proven to prevent degeneration.

1.4.2.1.3 Response to misfolded proteins

Another critical process for PRs' function and survival is the response to misfolded proteins. This function is operated by the family of molecular chaperones (335,336). PRs OSs need continuous maintenance, and for this reason, they need a particularly effective and active system of

specialized chaperones to respond to the peculiar requests of light-sensitive PRs (335). Some chaperones are implicated in opsin's biogenesis and response to opsin misfolding (337,338). Some components of the crystalline family, initially discovered in the lens, have chaperone functions. More than 20 types of crystallin proteins are present in the retina (339–342). The α-crystalline family has common motifs with the heat shock proteins (HSP) family of molecular chaperones and appears to be implicated in OS renewal (339,342). Other proteins of the HSP family, such as DNAJB1/HSP40 and DNAJB2/HSJ1b, are expressed at exceptionally high levels in the retina compared to other tissues, and DNAJB2 co-localizes with Rhodopsin at its production site (343,344). It is clear that the retina has specialized molecular chaperones that are essential for visual function, and they may be manipulated to combat protein misfolding diseases (345). The weight of chaperones in the retina is confirmed by the multiplicity of diseases caused by loss-of-function of specific chaperones, emphasizing their importance in many aspects of photoreceptor biology. *MKKS/BBS6*, *BBS10*, and *BBS12*, if mutated, cause Bardet–Biedl syndrome. Since these ciliary proteins have homology with type II chaperonine, they have recently been included within the chaperonopathies (216,219,220,346–348).

AIPL1 is a TPR protein causing LCA, with blindness at birth due to massive retinal degeneration. AIPL1 is an HSP70/HSP90 co-chaperone implicated in the modulation of the nuclear translocation of NUB1, in the facilitation of protein farnesylation, and the biogenesis and post-translational regulation of phosphodiesterase (PDE) subunits (345,349–351).

Finally, *RP2*, one of the leading genes implicated in x-linked RP, also has homology to tubulin specific chaperone C (TBCC), which is involved in tubulin biogenesis (352–354)

1.4.3 Ciliopathies: a broad spectrum of diseases

Cilia are involved in a wide-ranging of biological processes; therefore, it is not surprising that the lack or loss of cilia or the production of shorter, fewer, or unfunctional cilia manifest as multi-symptomatic disorders called ciliopathies. Ciliopathies are a heterogeneous group of genetic diseases caused by aberrations in ciliogenesis (cilia assembly and maintenance) and functional and structural cilium defects. Ciliopathies can be classified into two large groups, syndromic and non-syndromic (165,237). Since primary cilium is particularly vital in the developmental process,

ciliopathies often include complex multi-organ developmental defects, which result in a poor quality of life with early death for many patients. At the moment, there are no treatments that can improve the symptoms of these patients. Understanding the mechanisms underlying these diseases and identifying causal mutations are necessary to develop effective therapies (276). Recently clinical trials based on gene therapy for patients with LCA caused by mutations in the ciliary gene *ABCA4* are under evaluation and have brought great hopes for the cure of monogenic RDs (355,356).

Given their functional and structural diversity, immotile primary cilia or motile cilia/flagella dysfunction causes different pathologies. Since most of the known ciliopathies concern dysfunction of the primary cilium, the term ciliopathies is reserved for the cases where the primary cilium is affected. Defects in motile cilia, on the other hand, are defined as PCD (357). PCD is a genetically and clinically heterogeneous condition. At the moment, more than 40 motile cilia genes have been confirmed as the cause of PCD. The phenotype is variable with chronic respiratory infections from early in life, progressive upper respiratory problems with loss of lung function, conductive hearing problems, subfertility, and infrequent hydrocephalus. 50% of PCD patients also manifest left-right axis abnormalities, and in some cases, symptoms overlap with ciliopathies such as RP (358,359).

Ciliopathies affecting primary cilium are much more abundant than PCD. Thanks to the increased efficiency of sequencing techniques and other technological advancements, the unveiling of previously unknown genes' molecular functions and localization have caused previously uncharacterized diseases to fall in this class. Nowadays, more than 190 genes have been identified as responsible for 35 different ciliopathies, and more than 240 other genes are considered potential candidates (360,361). Phenotypic and genetic heterogeneity is often observed in these diseases. The relation between ciliary genes and ciliopathies is way more complicated than what is illustrated by classical Mendelian genetics and has been recently at the center of numerous reviews (361–363). While PCD is generally associated with highly destructive mutations that cause null allele effects, ciliopathies are often caused by a combinational effect of lighter hypomorphic mutations. This probably contributes to these diseases' peculiar heterogeneity, creating further difficulties in identifying the causal mutations (237,360,364). For these reasons, genetic

diagnostic rates of severe primary ciliopathies remain around 44% using whole-exome sequencing (317,361) and reach 62% using targeted gene panel sequencing (365,366), with an average of 50% of cases that remain undiagnosed. In an attempt to further define the phenotypic and variant spectrum of ciliopathies, a group of researchers exploited the highly consanguineous nature of the Saudi population, which facilitates the occurrence of these recessive disorders and their mapping to the underlying variant. They found that splicing variants in that population accounted for 22.6% of all variants, consistent with the previous observation of a high percentage of splicing variants in ciliopathies, including noncanonical splicing variants (367). Some genes are associated with a specific ciliopathy. For example, *USH1C* and *USH1F* are associated exclusively with Usher Syndrome, and *RP1* and *PRPF6* mutations are associated only with RP. In other cases, a single gene can be associated with a broad spectrum of ciliopathies (234,368). For example,

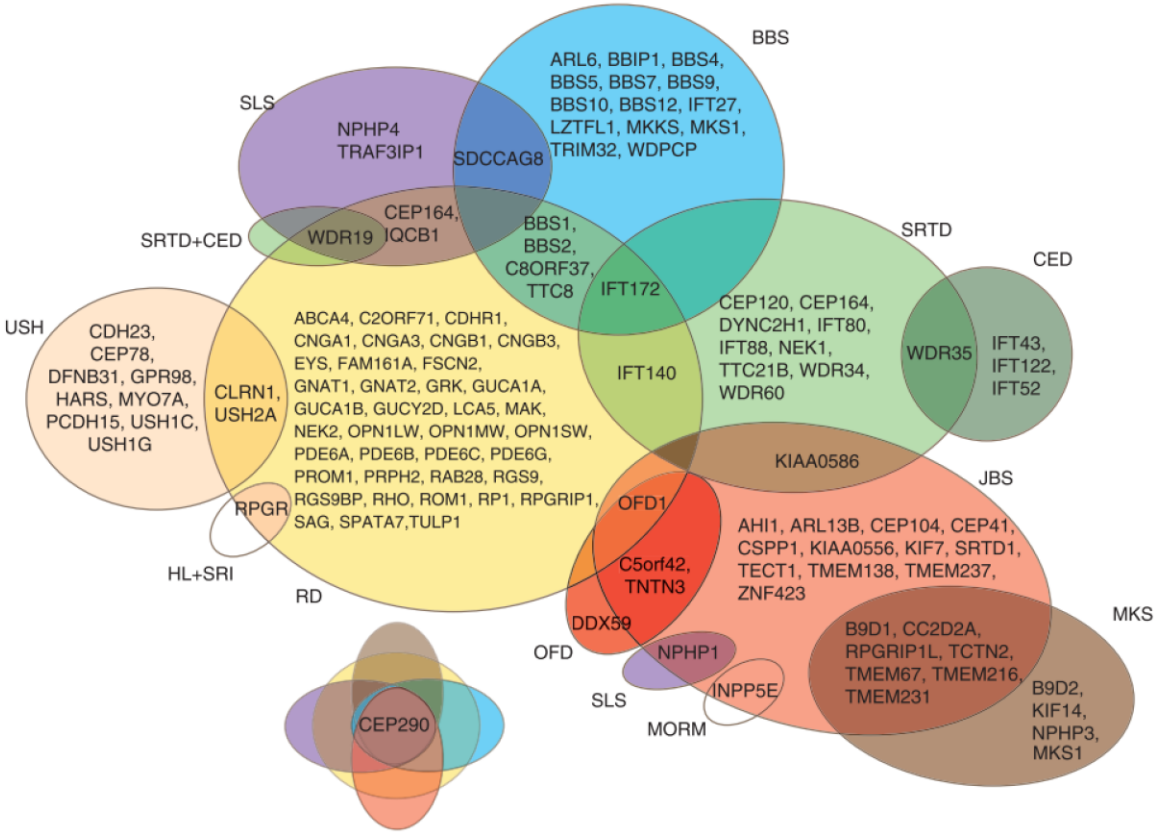

Figure 20: Genetic overlap between different forms of ciliopathy (319).

BBS, Bardet–Biedl syndrome; CED, cranioectodermal dysplasia ; HL þ SRI, hearing loss and sinorespiratory infections; JBS, Joubert syndrome; MKS, Meckel–Gruber syn- drome; MORM, mental retardation, truncal obesity, retinal degeneration, and micropenis; OFD, oral-facial- digital syndrome; RD, retinal degeneration—nonsyndromic; SLS, Senior–Løken syndrome; SRTD, short-rib thoracic dysplasia; USH, Usher syndrome.

mutations in a subset of BBS genes have been identified in some MKS cases, and *vice versa*, mutations in MKS genes have been observed in some patients with BBS (234,369). *CEP290* probably represents the most striking example of genes that, when mutated, can cause multiple different phenotypes. *CEP290* mutations in humans can cause perinatal lethal MKS, severe JBTS, BBS, and non-syndromic LCA or RP, which only affects the retina (Figure 20) (278,370,371). The extremely high variability of the phenotype caused by *CEP290* mutation is still elusive. Another subset of TZ genes, including *B9D1*, *TCTN2, TMEM231*, and *RPGRIP1L*, are known to cause MKS, and mutations in most of these genes also cause JBTS (Figure 20) (372).

Reduction of the costs and the advancement of new sequencing technologies has allowed more extensive access to these technologies, permitting the realization of projects such as the 100'000 genomes project. The 100'000 Genomes Project offers an excellent opportunity to discover new ciliary genes and identify new orphan ciliopathies in those patients with mutations not yet identified (372). Individuals with a diagnosis of CRDs, MDs, and RPs have been recruited for this

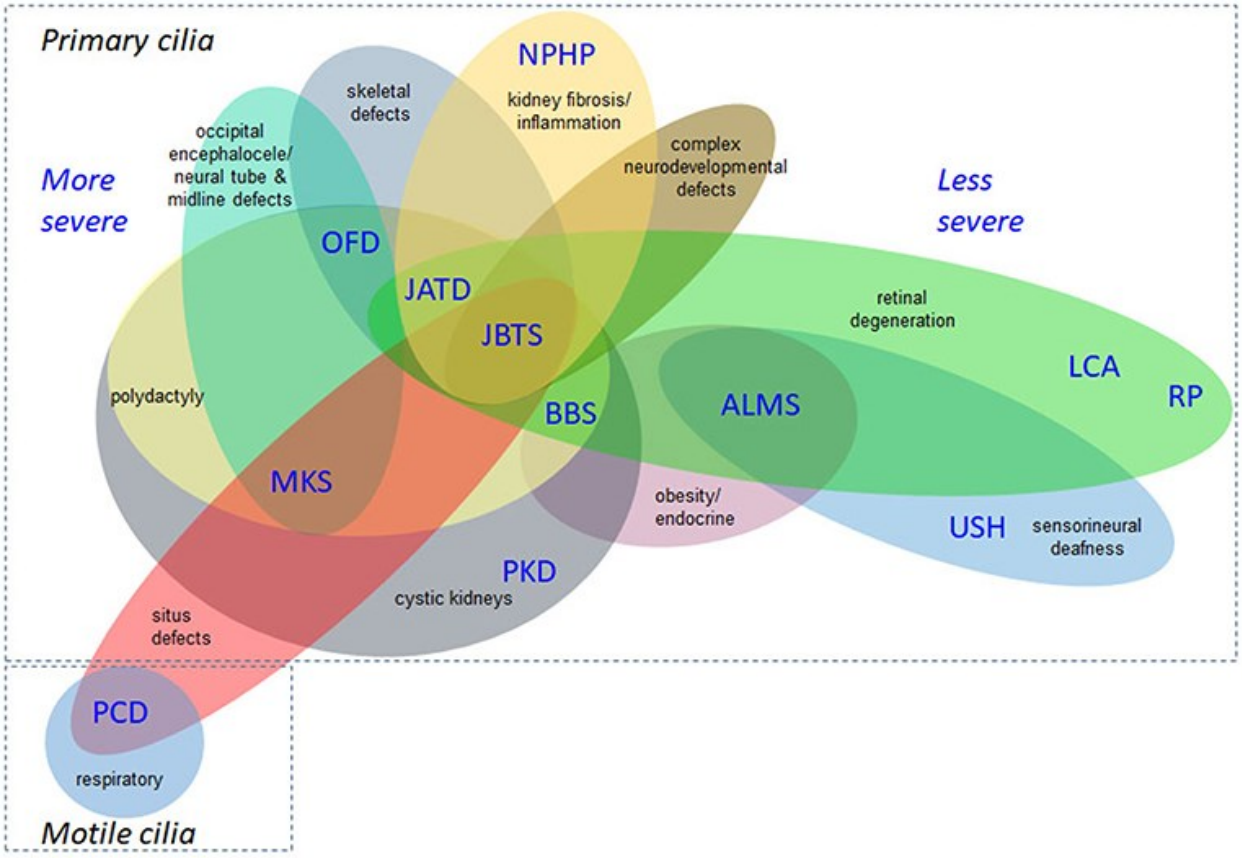

Figure 21: Phenotypic overlap between different forms of ciliopathies (361)

project. It can be estimated that around one-third of these patients have retinal dystrophy owing to a retinal photoreceptor cilium defect (361). Patients with other dysmorphic and congenital abnormalities with features overlapping ciliopathy phenotypes have been included in this large study and could be undiagnosed ciliopathies. A large proportion of patients with disease classified as unexplained monogenic fetal disorders, neurological or neurodevelopmental disorders, intellectual disabilities, ophthalmological disorders, which are all been included in the 100'000 Genomes project, are also likely to be undiagnosed ciliopathies (266).

The systematic analysis of such a large number of samples, with the inclusion of unaffected parents or close relatives, and detailed patient information, may in the future allow the identification of new pathogenic variants or additional gene modifiers. It has been proposed that genetic variants associated with primary causal mutations may be the basis of the high phenotypic and genetic variability (245). Some patients diagnosed with ciliopathies have already been associated with multiple genetic variants in ciliary and ciliopathy-associated genes, thus supporting the proposed implication of a complex additive or multiplicative genetic effect, which can contribute to this vast phenotypic variability (245). The high percentage of patients affected by ciliopathies with biallelic candidate variants shows that the non-Mendelian model needs to be invoked to cover most cases (367,373,374). Within the widely accepted Mendelian inheritance context, the role of modifiers has also drawn importance on the Non-Mendelian inheritance of these disorders (375–377).

Understanding the mechanisms by which mutations, or sets of mutations, contribute to specific phenotypes is central to understanding pathological mechanisms and develop effective clinical strategies.

1.4.3.1 Non-syndromic ciliopathies

Non-syndromic (NS) ciliopathies can affect different organs, where the eye and the kidney are the most commonly touched. The most commonly known non-retinal NS ciliopathies are Polycystic kidney disease (PKD) and Nephronophthisis (NPHP).

PKD is a group of monogenic disorders characterized by the presence of multiple cysts, primarily in the kidney and other organs such as the liver, pancreas, and seminal vesicles in a minority of

the cases (378,379). PKD is inherited in an autosomal dominant or recessive fashion (380). The dominant form of PKD is caused by a mutation in either of two genes, *PKD1* or *PKD2* (381). Late-onset PKD is one of the most common genetic causes of chronic kidney disease, with an incidence of 1:400–1:1,000, while the recessive and neonatal form is rarer, with an incidence of 1 in 20,000 (379).

Caroli disease is a rare form of inherited NS ciliopathy. It is distinguished by cystic dilatation of the bile ducts within the liver (382). Isolated or simple Caroli disease affects an isolated portion of the liver and is transmitted as an autosomal dominant trait. Its complex form is more diffused, associated with polycystic kidney disease, portal hypertension, and congenital hepatic fibrosis. This form is transmitted as an autosomal recessive trait and is often called "Caroli syndrome" (383,384).

NPHP is a cystic renal condition with an autosomal recessive inheritance caused by mutations in *NPHP1–8* genes (244,385). It is characterized by corticomedullary clustering of cysts and tubulointerstitial fibrosis. Depends on the disease's onset, it can be classified as infantile, juvenile, and adolescent (386). It is the most frequent known genetic cause of end-stage renal disease (ESRD), or more simply kidney failure, in young patients. NPHP is more commonly associated exclusively with renal histopathology, while some patients have additional symptoms which overlap with other ciliopathies, which generally include PRs degeneration in the form of LCA or RP (380).

1.4.3.1.1 Non-syndromic retinal ciliopathies

RD is one of the most common phenotypes among ciliopathies. It ranges from cone and cone-rod dystrophies to global severe retinal dystrophy and congenital ocular disabilities (319,387). RP is frequently associated with other symptoms in syndromic ciliopathies such as USH (RP and deafness), BBS (RP, obesity, polydactyly, and developmental delay), and Alport syndrome (RP, deafness, and renal glomerular dysfunction) (Figure 21) (197,270,299,388). Although RD is frequently present as one of the clinical features of syndromic ciliopathies, it manifests more often as an isolated disease without additional features.

One-third of non-syndromic RDs cases involve a defect in a ciliary protein, emphasizing the importance of this small but indispensable structure in PRs' function, development, and survival (Figure 19) (266). This number may be even more significant as a large part of RDs' cases remain still undetermined, and it would not be surprising that many of these cases concern abnormalities in ciliary proteins. As far as 2012, almost 90% of autosomal recessive (ar) CD, 60% of arCRD, 50% arRP, and 30% of arLCA cases still need a genetic explanation. With the advancement of large-scale sequencing techniques in the last decades, many other cases have been resolved, but we are still far from covering their totality (316).

More than 30 ciliary genes have been confirmed to be the genetic cause of RP, and these explain almost 50% of the genetic causes in RP. Among the most frequent causes of RP are mutations in the *USH2A, EYS, RPGR*, and *RP1* genes, and between them, the *USH2A p.Cys759Phe* mutation is the most common globally, while [*p.(Ser1653fs)* in *EYS*] is the most frequent in the Japanese population (389,390). Mutations in the *RP2* gene account for around 15% of cases of X-linked RP (354). RP2 contributes to the PRs ciliary trafficking by regulating proteins' transport from their production site through the CC to the OS (166). Curiously, despite being ubiquitously expressed, patients with *RP2* mutations exhibit no extra-retinal phenotypes (296).

At present, little more than 25 genes are known to cause LCA, and at least 9 of them are ciliary genes. Some other genes identified mutated in these patients, such as *CCT2* and *CRB1*, are not considered in these numbers since their mechanism is still poorly understood, but both proteins localize at the cilium and/or interacts with ciliary complexes, therefore, are most likely part of this group (391–394). Five ciliary genes (*CEP290, IQCB1, LCA5, RPGRIP1*, and *TULP1*) explain 23% of all solved LCA cases (277,278). An intronic mutation (*c.2991+1655A→G*) in *CEP290*, which creates a robust splice-donor site and inserts a cryptic exon into the mRNA, is the most frequent cause of LCA (395,396).

In CDs and CRDs, only about 5% of the cases are due to mutations in ciliary genes *(RPGR, RPGRIP1, RAB28*). C8orf37 is another protein that may have a ciliary function, but it is not considered in this category due to its unknown mechanism of action. However, it localizes to the photoreceptors' CC and, when mutated, gives rise to an early-onset autosomal recessive CRD or RP phenotype

with early macular atrophy that occasionally can be accompanied by other symptoms such as polydactyly (397).

Furthermore, the relatively low number of ciliary genes in CD and CRD is probably also due to many cases still unresolved, which in the case of CD reaches almost 90% of the total cases (177,274,398,399). CDHR1 represents another excellent example of a potential ciliary protein with unknown function that can lead to retinitis RP, CD, and CRD (400,401). *CDHR1* gene is part of the cadherin family, and its product is found in several tissues, with the highest abundance in the retina, where it predominantly localizes at the CC, at the junction between IS and OS of rod and cone PRs (402–404).

CEP78 encodes a centrosomal protein that is required for the regulation of centrosome-related events during the cell cycle. If *CEP78* is mutated, it can result in CRD associated with hearing loss or USH (405).

The case of MDs is fascinating. Despite MD's recurrent presence between syndromic ciliopathies symptoms, very few ciliary genes have been associated with NS MD, but it may be due to the large proportion of unresolved cases. Recently a genetic variant of *WDR19* has been found in three unrelated families, all presenting NS Stargardt disease (367). WDR19 represents the first ciliary gene linked to the Stargardt disease phenotype. Mutations in another ciliary gene, *RP1L1*, have been described in Japanese patients with occult MD, which is a particular form of MD characterized by deterioration of macular function with a healthy ophthalmoscopic appearance of the fundus (406,407). Abnormal spindle-like microcephaly-associated protein (ASPM) has been associated with some cases of AMD. ASPM is considered a member of a novel family of ASH (ASPM, SPD-2, Hydin) domains. These domains are present in proteins associated with cilia, flagella, and centrosomes. Currently, ASPM is under investigation to confirm its role as a ciliary protein (408,409).

CD, CRD, LCA, MD, and RP are generally described as distinct clinical entities, but they are often difficult to distinguish because they often share common genetic origins. The first example in this way is *RPGR* which is responsible for 70–80% of X-linked RP cases where result in a severe phenotype with early visual loss (184,227,398). Although *RPGR* mutations cause mostly X-linked

RP, it has found mutated in other RDs, including CRD, CD, and atrophic MD. Several additional *RPGR* gene mutations have been confirmed in people with syndromic diseases, which display, in addition to the progressive vision loss, a combination of other symptoms such as hearing loss, chronic respiratory problems, sinus and ear infections (410). It is still unclear how mutations in *RPGR* can cause such an extreme variety of disorders and is a field of active research. Some studies have shown that some specific *RPGR* mutations affect the ciliary structure in non-retinal cells, including cells of the inner ear and the respiratory tract (410,411).

Growing evidence shows that RPGR regulates actin turnover and rhodopsin trafficking, but the molecular mechanism remains to be fully elucidated (227,412,413).

Furthermore, RPGR may regulate protein entry to the cilia since it is known to interact with the scaffold protein Whirlin, encoded by the *DFNB31* gene, in the CC of PRs. Whirlin is a critical component of the periciliary membrane complex (PMC) that seems to facilitate the migration of rhodopsin and other ciliary and OS components to the CC. Whirlin, if mutated, causes USH Type 2, a recessive syndromic form of RP with non-congenital sensorineural deafness (414,415).

Another example is *CRB1*, a component of the Crumbs family, well-known regulators of apicobasal polarity. Mutations in *CRB1* are a frequent cause of RP, LCA, and CRD (391,393). More than 200 different disease-causing mutations have been reported in *CRB1*, mainly affecting its extracellular domain (416). In the retina, CRB1 is expressed in both PRs and Muller glia; it is localized at the cilium base, where it is thought to participate in cell-cell adhesion at the retinal outer limiting membrane (OLM) through its extracellular domain (417). Its dysfunction disrupts cell-cell adhesions and the OLM leading to defects in retinal lamination. CRB1 precise function is not fully understood yet, and the broad spectrum of its phenotype is still obscure.

FSCN2, locate at the IS and to the calyceal processes of PRs. In the Japanese population, mutations in *FSCN2* have been shown to cause RP, AMD, and CD in an autosomal dominant manner (389,418,419). It has been demonstrated that the *208delG* mutation, which causes a highly variable phenotype in humans, results in a classical RP phenotype with progressive retinal degeneration in mice. Interestingly the exact same mutation causing RP in most patients was found in Chinese families that did not present any phenotype, thus taking the concept of

phenotypic variability to the extreme. The cause of the resistance in these subjects remains obscure (420).

PROM1 gene encodes the protein prominin (also known as CD133) that is expressed on the plasma membrane in most cells and localizes to cellular protrusions, including cilia and microvilli. In both rod and cone PRs, PROM1 localizes to the base of the OS where regulates disc morphogenesis (421). Loss of prominin provokes disorganization of the OS's discs. Its dysfunction causes a wide range of retinal dystrophies, including early onset of severe autosomal recessive RP, Stargardt disease, macular dystrophy, and cone-rod dystrophy (422,423).

These pieces of evidence show the recent advances in unraveling the mechanisms behind NS retinal ciliopathies, but it also demonstrates the long way to go to fully understand the complex relationships between genotype and phenotype in this rapidly expanding class of diseases.

1.4.3.2 Syndromic ciliopathies

Syndromic ciliopathies are multi-systemic and typically affect different organs as the brain, kidney, skeleton, and eyes. BBS, Carpenter syndrome (CRPT), Hydrolethalus syndrome (HLS), JBTS, Oculocerebrorenal syndrome of Lowe (OCRL), MKS, MORM syndrome, Pallister-Hall syndrome (PHS), Senior-Løken syndrome (SLSN) are included in this class (255,424). They are multi-allelic diseases with high phenotypic and genetic heterogeneity (255,374).

JSRD and MKS are allelic at several loci (*CEP290, TMEM216, TMEM67, RPGRIPL1, CC2D2A*) but show remarkable differences in the outcomes (Figure 21) (361,425).

BBS and MKS are rare developmental diseases defined by multiple developmental anomalies, retinal degeneration, polydactyly, genito-urinary defects, and cognitive impairment (426). Whereas MKS is fatal at birth, BBS is among the most severe ciliopathies compatible with life. MKS and BBS show a strictly different outcome; however, MKS master-genes such as *MKS1* and *MKS3/TMEM67* have also been found in some BBS patients, pointing out, once again, the interconnections between different ciliopathies (234,427).

1.4.3.2.1 Joubert syndrome

JBTS is a rare genetic disorder that principally affects the cerebellum, an area of the brain responsible for balance and coordination, and it is frequently associated with RP (428). JBTS, like many other ciliopathies, is a very variable and heterogeneous syndrome with a known mutation in over 30 genes that frequently overlaps with other ciliopathies (165,429,430). The symptoms can vary enormously, even among members of the same family. A characteristic feature of the disease is the "molar tooth sign." It results from the irregular development of structures in the back of the brain and got its name because, by MRI, the abnormality resembles the cross-section of a molar tooth (368). Most affected individuals have intellectual disabilities that can range from mild to severe. They present hypotonia, ataxia, respiratory problems, and abnormal eye movements and may include PRs degeneration with progressive vision loss. Additional symptoms are kidney and liver disease, skeletal abnormalities, polydactyly, endocrine problems, and facial morphogenetic abnormalities (Figure 21) (428). A combination of the characteristic features of JBTS in association with other supplementary symptoms represents a group of heterogeneous diseases that together are named Joubert Syndrome and Related Disorders (JSRD) (431). JBTS usually has an autosomal recessive pattern of inheritance, but some cases of JBTS are inherited in an X-linked recessive pattern (432).

1.4.3.2.2 Bardet-Biedl syndrome

BBS is a disorder associated with obesity, kidney disease, and RD. It is characterized by a mixture of morphogenetic and developmental defects combined with obesity and the degeneration of some organs (Figure 21) (269,297). Despite the presence of polydactyly at birth in most patients, the average age of diagnosis is nine years old. At this time, retinal degeneration becomes apparent, which is added to the diagnosis of obesity that generally occurs within the first five years of life. Some other common additional symptoms are renal, cardiovascular, and skeletal abnormalities, including a broad spectrum of craniofacial and dental deformations, often accompanied by loss of senses such as vision and taste (433). Just under 50% of the patients are considered mentally retarded.

At present, 25 genes have been identified to cause this syndrome. *BBS1* and *BBS10* represent the most commonly mutated gene, with an incidence of about 25% and 20%, respectively, followed

by *BBS12*, responsible for about 10% of cases (220,434). The genetic cause of the disease remains to be determined in about 25% of cases.

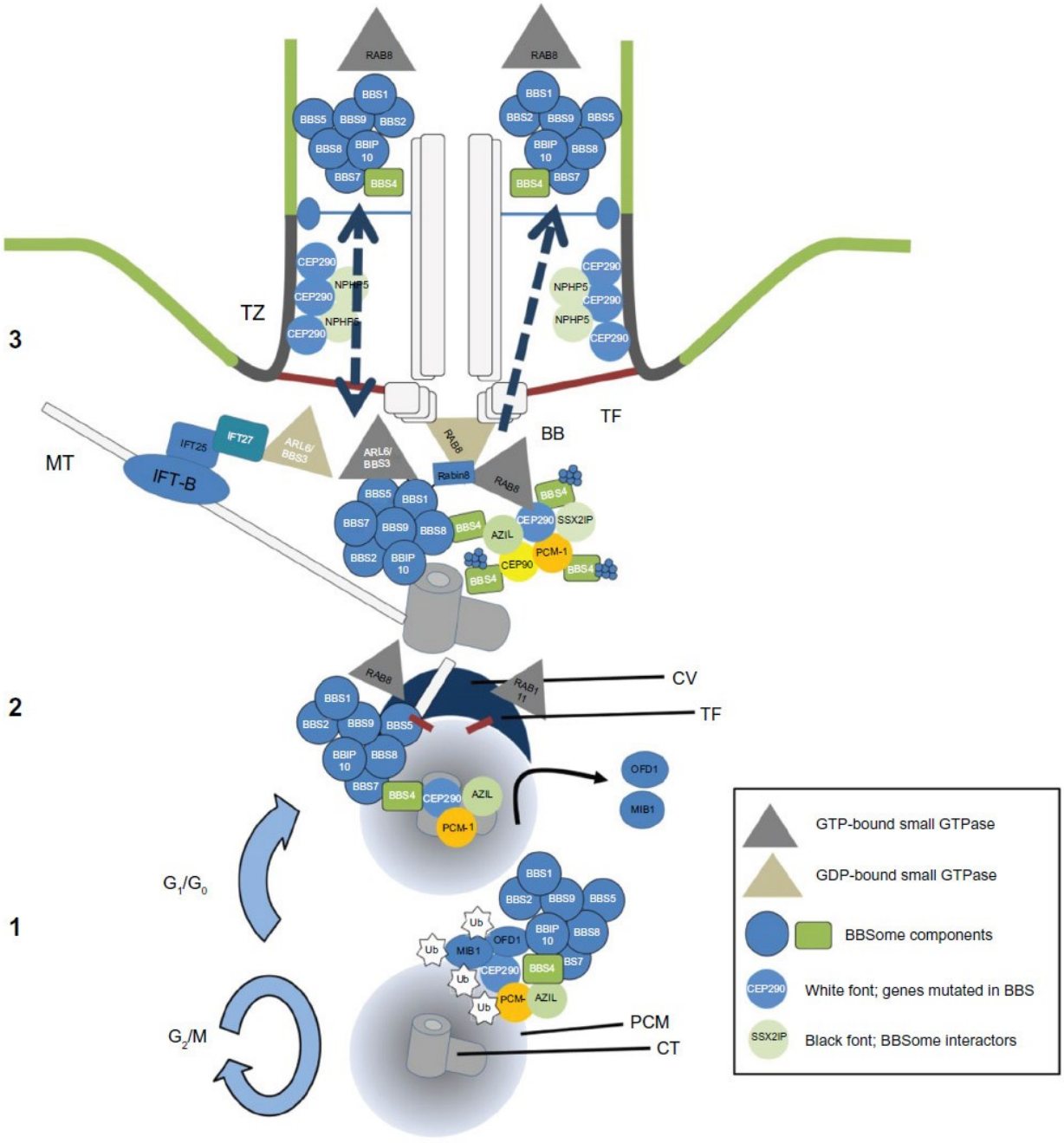

Figure 22: The BBSome (201)

(1) Remodeling of centriolar satellites. (2) The basal body is transported to the membrane. (3) Regulatory network of BBSome loading into the cilium. Abbreviations: BB, basal body; BBS, Bardet–Biedl syndrome; CSs, centriolar satellites; CT, centrosome; CV, ciliary vesicle; IFT, intraflagellar transport; MIB1, mindbomb E3 ubiquitin protein ligase 1; MKS, Meckel–Gruber syndrome; MT, microtubular; NPHP, nephronophthisis; OFD1, oral facial difital syndrome protein 1; PCM, pericentriolar material; TF, transition fibers; TZ, transition zone; UV, ultraviolet; TPR, tetratricopeptide

Mutated genes associated with BBS includes: *BBS1* (434), *BBS2* (435,436), *ARL6/BBS3* (437), *BBS4* (438), *BBS5* (439,440), *MKKS/BBS6* (348,441), *BBS7* (442), *TTC8/ BBS8* (443), *BBS9* (444), *BBS10* (211,218,220), *TRIM32/BBS11* (445), *BBS12* (211,219), *MKS1/BBS13* (234), *CEP290/BBS14* (234,278), *WDPCP/C2ORF86/BBS15* (446,447), *SDCCAG8/BBS16* (448), *LZTFL1/BBS17* (221,223), *BBIP1/BBS18* (202,449), *IFT27/BBS19* (450–452), *IFT74/BBS20* (168,453,454), *C8orf37/BBS21* (397,455), *IFT172* (456,457), *CEP19* (458), *TMEM67/MKS3* (234), and *SCLT1* (459) (Figure 20). The genes found to be mutated in BBS patients are not all components of the BBSome complex. The full dynamic of how the BBSome and the other BBS proteins interact is still unclear. It is now known that some of these proteins can directly regulate the cellular localization of the BBSome. Three of the 25 genes currently linked to BBS encode chaperonin-like proteins (MKKS/BBS6, BBS10, and BBS12). Therefore, these BBS cases can also be considered as chaperonopathies (211,218). Remarkably, up to 50% of clinically diagnosed BBS cases can harbor disease-causing mutations in one of these three genes, highlighting the pathological impact of chaperone defects in genetically heterogeneous syndromes such as BBS. Interestingly, BBS families with deleterious variants in *MKKS/BBS6*, *BBS10*, or *BBS12* genes generally display more severe phenotypes than families with mutations in the BBSome core components (211,460).

Moreover, mutations in some BBS genes can cause NS retinal ciliopathies; for example, a splice-site mutation in a retina-specific exon of *BBS8* causes NS RP (320,461).

“Gene modifiers” are defined as genes that do not represent the primarily causative mutation but instead can increase the disease penetrance. Modifiers' role seems important in BBS pathogenesis as they can cause an exacerbation of the phenotype, probably contributing to the high heterogeneity of the symptoms. Modifier genes include *CCDC28B, MKS1, MKS3, C2ORF86, KIF7, AR*, and *PDE6B* gene, most of which can also act as primary causal genes (433,462). In some patients, heterozygous BBS3 mutations have been shown to act as a modifier for BBS1 mutations (361). Some studies have proposed that the common *RPGRIP1L* (A229T) allele may function as a modifier gene affecting the retinal phenotype, which could explain the variability of symptoms ranging from MD and CRD to RP in ciliopathies such as BBS, JBTS, and MKS (463,464).

1.4.3.2.3 Meckel-Gruber syndrome (MKS)

MKS is a lethal autosomal recessive congenital syndrome, probably the most severe among known ciliopathies, caused by primary cilia dysfunction during early embryogenesis. MKS has a worldwide incidence of 1:140000 live births, which is highly variable among different populations. It can reach 1:9000 in Tatars, Hutterites, and Finnish, with a peak of 1: 1300 registered in Gujarati Indians between 1976 to 1982 (465,466). Most individuals with MKS die before or shortly after birth, typically due to Kidney failure or respiratory problems. MKS displays a high clinical variability that can include central nervous system malformations (occipital encephalocele and other posterior fossa defects), cystic dysplastic kidneys, hepatic bile duct proliferation, pulmonary hypoplasia, polydactyly, and liver fibrosis. The ocular phenotype is highly variable, ranging from early PRs degeneration and abnormal eye development to clinically absent globes (464,467–469). Retinal dysplasia, cryptophthalmos, cataracts, and hypoplasia have also been reported. The retina has been described as dysplastic with foci of rosette-like structures and abundant glial cells (466). Other additional symptoms can vary widely between cases, usually affecting the development and morphogenesis of the face, heart, bones, urinary system, and genitalia. MKS cases have also been reported with neural tube defects in which the neural tube failed to close completely during early embryonic development (466,470).

13 disease-associated genes has been identified: *MKS1* (471,472), *TMEM216/MKS2* (473), *TMEM67/MKS3* (235,472), *CEP290/MKS4/BBS14* (370), *RPGRIP1L/MKS5* (242), *CC2D2A/MKS6* (432,474), *NPHP3/MKS7* (241), *TCTN2/MKS8* (475), *B9D1/MKS9* (232,425), *B9D2/MKS10* (250), *TMEM231/MKS11* (476,477), *KIF14/MKS12* (478–480) , and *TMEM107/MKS13* (481).

Some studies have found some BBS genes mutated in fetuses diagnosed with MKS. A more in-depth study showed cleft lip/palate symptoms and pancreatic and epididymal cysts characteristic of MKS and generally absent in BBS. On the other hand, these cases did not present the typical liver ductal plate anomaly or encephalocele, considered a constant in MKS. The precise origin of the particular severity in these cases remains unknown (234,369). These cases have now been included in the MKS-like syndromes (369). It can be that mutations not yet identified in genes related to MKS, gene modifiers, or high-frequency pathogenic variants may be responsible for the additional features. Otherwise, this suggests a genetic interaction between BBS and MKS

(426,427). Some genes frequently mutated in MKS are also allelic in JSRD, with which it shares several features (Figures 21, 23) (366,369).

In MKS, autosomal recessive inheritance is widely accepted, and locus heterogeneity has been proposed to be at the base of the highly variable clinical phenotype (482). Numerous examples support this transmission mode, including the concordance between homozygous twins, the frequency between siblings, indifference to sex, and increased incidence in consanguinity cases. Nevertheless, the tremendous phenotypic variability makes it presumable that, as in BBS, the presence of accessory mutations on gene modifiers may contribute to its broad phenotypic spectrum.

This work investigates the molecular mechanism underlying retinal developmental abnormalities and PRs degeneration in patients with syndromic ciliopathies such as MKS and BBS. Through WGS analysis, we identify the causal mutations. Using a human *in vitro* model, which allows in-depth analysis of patient-specific PRs, we reveal similarities and differences between these two syndromes and their retinal transcriptional profile.

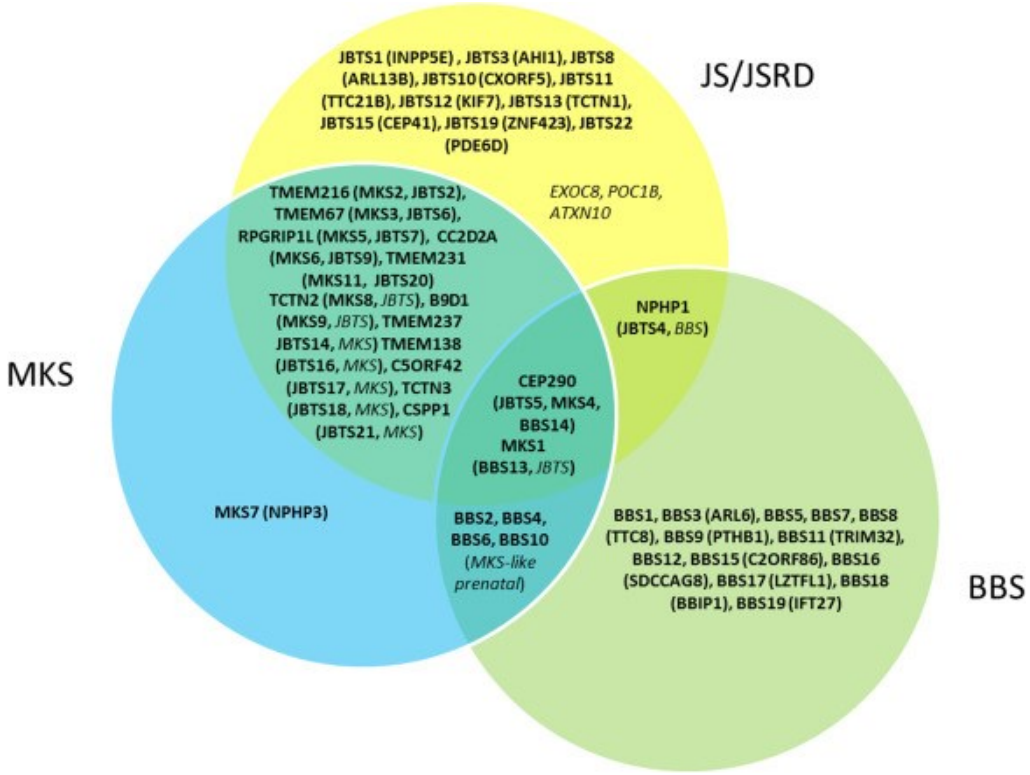

Figure 23: Genetic overlap between MKS, BBS, and JSRD (366)

1.5 Aging and epigenetics in RDs

A limitation of the classical molecular medicine approach to study complex RD diseases such as AMD is that the classical molecular medicine approach misses the contributions of normal aging processes, environmental factors, and lifestyle to the pathology. Many changes occur in the eye and all other tissues during aging from both anatomical and physiological prospects. In the retina have been observed changes in choroidal capillary diameter and density, RPE cell structure and composition, and Bruch's membrane thickness. RPE cell defects include decreased number of cells in the posterior pole, decreased melanin content, decreased cytoplasm volume, and

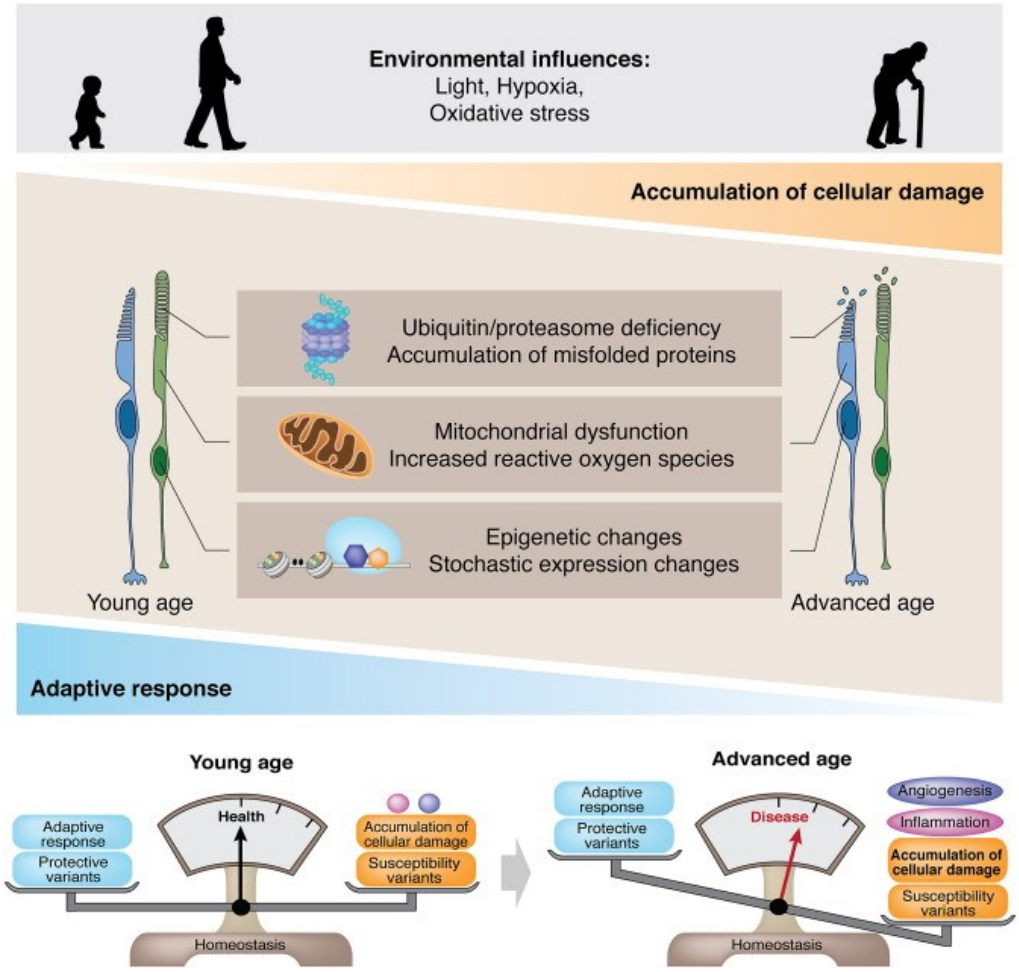

Figure 24: Interplay between aging and disease in the retina (1203).

The environment influences photoreceptor homeostasis throughout life. The cell adaptive response helps maintain a balanced homeostasis. As the adaptive response becomes insufficient to overcome "insults" to the system, damage accumulates in aging photoreceptors. Major metabolic failure is observed for the ubiquitin-proteasome system and mitochondria. Epigenetic changes and stochastic changes in gene expression combined with the presence of susceptibility variants, eventually tilt the equilibrium towards the disease state. At which point, inflammation and angiogenesis become pathologic, further aggravating disease manifestations.

increased lipofuscin content (23,483). These changes can affect the different processes, including the transport of nutrients, metabolites, and waste products between compartments. Other aging-related changes affect the extracellular matrix turnover and the release of pro-inflammatory cytokines that cause a transition to a pro-inflammatory state (484,485).

Peculiar features of complex RD diseases are their genetic heterogeneity and high variability in the onset, progression, and visual activity outcome. This heterogeneity can be observed even between monozygotic twins, denoting the impact of factors other than genetics on the pathogenesis of these diseases (Figure 24) (486–488). Some adult-onset disorders may also be linked to dysregulated embryonic development, but the mechanisms underlying this association remain poorly understood (489–491).

Even though over the last decade, advances in sequencing technologies have tremendously enhanced our ability to identify genes that, when mutated, cause both syndromic and non-syndromic RD, our understanding of the pathophysiology of photoreceptor loss is still incomplete, and the contribution of epigenetic changes in the context of late-onset RDs is unclear (492–494).

Thus, to fully understand complex RDs, a functional-centric approach is insufficient as it does not consider the physiological variation necessary to identify new critical therapeutic targets. Likewise, merely focusing on the physiological/anatomical variation provides only limited information for components and molecular pathways underlying the pathology's mechanism, particularly in AMD, where only a limited number of genes have a retina-specific expression (266).

A combinatorial approach that considers the functional, anatomical, and physiological aspects allow viewing diseases as consequences of a disturbance in tissue homeostasis, highlighting the interdependence between different cells and tissues (Figure 24).

1.5.1 The epigenome and its modulation

As in the other tissues of the organism, during retinal neurogenesis, the RPCs respond to intrinsic and extrinsic signals that regulate critical processes such as proliferation and differentiation to precisely control cell fate determination (495). The same factors are also responsible for maintaining the cell identity of somatic cells. The postnatal and adult retina is susceptible to an

aberrant gene's expression because of its minimal cellular regeneration and turnover capacity. These intrinsic factors consist of TFs and epigenetic regulators, including DNA methylation, histone modifications, and Long non-coding RNAs (LncRNAs) (494).

TFs are proteins responsible for transcribing the genetic information from DNA into RNA by binding to a specific DNA sequence. TFs include a vast number of proteins that initiate and regulate genes transcription (496). TFs act alone or in complexes with other proteins to promote (as an activator) or block (as a repressor) the RNA polymerase recruitment to specific genes.

In general, mutations of retinal-specific TFs give birth to striking phenotypes and malformations. The well-known phenotypes for loss of function of PAX6, CRX, and NRL, which respectively give absence or formation of small eyes, absence of PRs, and absence of rods (cone only retina), have been highly characterized, and their pathways demarcated (497). As described before, in most cases, RP is inherited as a Mendelian trait, with a transmission modality which is autosomal recessive in 30% of patients, autosomal dominant in 20%, X-linked in 10% of cases. More than 40% of RP patients did not show a Mendelian inheritance. Interestingly, most of these cases are late-onset and sporadic cases, in most of which the origin is unknown (497–499).

Some TFs have been linked to late-onset degenerations, thus advancing a more complex role of these TFs in maintaining healthy tissue in adulthood, and that germline mutation can cause adult-onset diseases. The *ZNF408* gene encodes a TF thought to be implicated in DNA binding (500). Homozygous mutations in this gene have been identified in different unrelated families as the cause of late-onset RP (498). Some other sporadic cases with late-onset RP have been linked to a homozygous nonsense mutation in *SAMD11* and *SAMD7*. These proteins contain a Sterile alpha motif (or SAM) domain, which has a primary role in RNA binding and protein-protein interactions during signal transduction and transcriptional regulation (501,502). SAMD11 is predominantly expressed in developing PRs and the adult pineal gland (503). It has been shown that SAMD11 interacts with CRX and is implicated in CRX-mediated transcriptional regulation in the retina, playing an essential role in promoting rod fate and maintenance. Smad7 is a nuclear protein expressed in many tissues and seems to interact with the polycomb protein complex 1 (PRC1) and with the E3 ubiquitin ligase SMURF2. SMAD7 has a DNA-binding transcription factor activity and

can block TGFβ1 and activin pathways and promote embryonic stem cells' (ESCs) self-renewal (504,505).

DNA methylation is an essential transcriptional regulation mechanism that can control gene expression in time and tissue-specific manners by transferring a methyl group onto the C5 position of the cytosine to form 5-methylcytosine (506). DNA methylation occurs at the level of cytosines when they precede a guanine in regions called CpG islands, which are G-rich sequences generally present at the promoter's level. DNA methylation controls gene expression by inhibiting the binding of TFs to the DNA or by recruiting complexes involved in gene regulation (506,507). The DNA methylation pattern along the genome is variable and dynamic during development, thanks to DNA methylase and demethylase's ability to orchestrate the process. In a fully developed organism, differentiated cells develop a distinctive and stable methylation pattern that regulates the transcription of tissue-specific genes (507). DNA methyltransferases (DNMTs) are responsible for the methylation of cytosine into 5-methylcytosine (5mC). DNMT1 is responsible for preserve DNA methylation patterns during DNA replication, whereas DNMT3a and DNMT3b are involved in *de novo* methylation (506). In contrast, DNA demethylation is an active multistep process mediated by at least eleven Translocation Methylcytosine Dioxygenases (TET) (508).

TET3 is a crucial factor for DNA demethylation and retina regeneration. It can reprogramming RPE cells to regenerate the chick's retina after injury, revealing that active DNA demethylation could represent a potential epigenetic target to regenerate the retina in mammals (509,510).

Histone modifications are covalent post-translational modifications (PTMs) of histone proteins, including methylation, phosphorylation, acetylation, ubiquitylation, and sumoylation. The PTMs made to histones can impact gene expression by altering chromatin structure or recruiting histone modifiers. Due to their impact on chromatin structure and DNA accessibility, histones are critical regulators of all major chromatin-related processes, including DNA transcription, replication, and repair (511). Histone modifications are a critical regulatory system at every stage of embryonic development and in adults, and they can be modulated by a large number of regulators that can activate or prevent transcription. Histone modifications are essential for regulating different pathways and processes during embryonic development, such as body

patterning, organogenesis, and differentiation (512). The maintenance of pluripotency in stem cells is also regulated in this way (513). Histone modifications are essential for the continuous maintenance of cell fate during adulthood, tissue homeostasis, and repair (514–516). In adults' tissues, they act in a concerted manner to induce or stabilize cell-specific fate through inductive signals and tissue-specific TFs. Chromatin is defined by all the factors coating genomic DNA. DNA wraps over a length of 147 bases around an octamer of 4 histones (H2A, H2B, H3, and H4) (Figure 25). Each histone has an N-terminal fragment that extrudes from the structure, which is permissive to various post-translational modifications, and these changes will dictate how the genome will be condensed (517–519). These enzymes capable of modifying histones are divided into two categories: the writers that add post-translational modifications and the erasers that remove them. The proteins that recognize specific histone modification(s) but do not edit them are named readers. The leading writers are methyltransferases and acetyltransferases, while demethylases and histone deacetylases (HDAC) are the major erasers (520). Polycomb group (PcG) and Trithorax (TrxG) proteins are also key players in maintaining these domains (521). These modifications allow the DNA to have a conformation, either relaxed to promote transcription or condensed to inhibit the transcription of specific genes or to replicate or repair its DNA. Because of their significant impact on the chromatin, the most studied histone modifications are the triple methylation on lysine 4 of histone H3 (H3K4me3), the triple histone H3 methylation on lysine 27 (H3K27me3), triple methylation on lysine 9 histone H3 (H3K9me3), acetylation on lysine 9 of histone H3 (H3K9ac) and the ubiquitination of H2A (H2Aub).

H3K4me3 and H3K9ac are activators because they are generally found at the promoter level and activate transcription. These marks constitute the open chromatin, also called euchromatin. The H3K27me3 mark is also found at the promoter level, but it suppresses gene transcription and constitutes the facultative heterochromatin. H3K9me3 marks the constitutive heterochromatin, a repressive mark mainly enriched in poor transcribed regions like the telomeric and peri-centromeric regions (522,523). Finally, the role of H2Aub has been debated for a long time. It is highly dynamic and primarily responsible for gene silencing, although more recently, it has been shown to accumulate in areas of damaged DNA and on actively expressed genes (524). In ESCs, early mouse embryos, and adult cells, a subset of H3K27me3 marks are present together with the

active chromatin mark H3K4me3, and these regions are called bivalent chromatin domains (525–527). These bivalent domains play a crucial role in maintaining pluripotency by keeping the expression of developmental genes repressed in the absence of differentiation signals and are capable of rapid activation following stimulation (521).

Histone modification's importance in the retina's context has been proven through pharmacological and genetic inactivation of key enzymes that participate in this process (494,495). Furthermore, changes in histone marks are observed during aging and age-related retinal diseases suggesting their involvement in the disease pathogenesis. SIRT1 exhibits decreased expression during physiological aging and in age-related diseases, and maintaining its activity seems to protect retina and RPE cells against light or oxidative damage (528). Changes in histone acetylation through HDACs activity also seem to be involved in the early stages of retina degeneration in some age-related cases (529).

The epigenome includes all of the epigenetic changes governing genome expression and maintenance. Consequently, epigenetics does not stop with the modification of DNA and histones. lncRNAs are an integral part of the epigenome and consist of various RNA species not translated into proteins. lncRNA are generally longer than 200 nucleotides and can even reach more than 100 kilobases (510,530). Several lncRNAs are also subject to specific post-transcriptional modifications such as splicing, polyadenylation, and 5' capping, similar to conventional mRNA processing. They are emerging as critical regulators in gene expression networks. They control chromatin architecture by promoting or preventing chromatin modifiers' recruitment and regulating inter-and intra-chromosomal interactions. LncRNAs can control nuclear architecture coordinating Nuclear Bodies (NBs) formation, which are dynamic membraneless RNA-protein complexes associated with the nuclear matrix. NBs included nucleoli, Cajal bodies, nuclear speckles, Polycomb bodies, and paraspeckles. LncRNA can control transcription in the nucleus by modulating mRNA stability, forming R-loops, interfering with the Pol II machinery, and regulating alternative gene splicing (531). Several lncRNAs are also exported to the cytoplasm, where they regulate mRNA turnover, modulate translation directly acting on the ribosome, and interfere with post-translational modifications (532,533). Many retinal homeodomain factors critical during retinal development have lncRNAs associated with their

transcriptional unit, including *Six3, Pax6, Six6, Vax2, Otx2, Pax2*, and *Rx* (510). For example, the *Six3* opposite strand transcript (Six3OS) is expressed in the developing mouse retina, where it plays an essential role in retinal cell specification. Six3OS does not directly control Six3 expression levels, but instead, it regulates Six3 activity by recruiting histone modification enzymes to Six3 target genes (530,533,534). Various lncRNAs have been shown to recruit Polycomb proteins to particular loci to modify chromatin states and repress gene expression. Some well-documented examples include *XIST*, the antisense non-coding RNA in *INK4 locus (ANRIL), MALAT1*, and the *HOX* transcript antisense intergenic RNA (*HOTAIR*) (535).

1.5.2 The Polycomb Group (PcG) proteins and their role in the retina

Polycomb repressive complexes (PRC) maintain transcriptional repression of genes encoding crucial developmental regulators through chromatin modification. TrxG and PcG proteins have a central role in maintaining bivalent domains (521). Most PcG proteins constitute two multimeric repressive complexes capable of binding DNA to specific regions and reshaping the chromatin locally. These complexes, called PRC1 and PRC2, are involved in the gene silencing of many developmental processes (Figure 25, 26) (536,537). PRC1 and PRC2 complex are recruited to their target sites by a set of DNA binding proteins, where they inhibit the activated form of RNA polymerase II preinitiation complex using repressive methylation marks.

PRC1 core complex contains a quartet of PcG proteins: Polycomb (PC), Posterior sex Combs (PsC), Polyhomeotic (PH), and RING domain. PRC1 is responsible for the ubiquitination of H2A to lysine 119 through B lymphoma Mo-MLV insertion region 1 homolog (BMI1) activity, which binds to DNA and RING1, so permitting the ubiquitination reaction (Figure 25) (538). While ubiquitination was initially identified as the key mechanism in marking misfolded or surplus protein molecules for degradation, it soon became clear that it is far more than just a general mechanism to mark obsolete proteins for degradation. Indeed, ubiquitination is now recognized as a highly regulated, flexible, and reversible process that can signal multiple responses, from degradation to changes in activity, re-localization, or changes in the histone code. This high bandwidth in signaling power is achieved by the complex nature of the ubiquitin signal itself, which reflects the ubiquitin mark on the substrate protein and the length and architecture of the ubiquitin chain (539).

Ubiquitin modifications are assembled by a hierarchical cascade comprising ubiquitin-activating enzymes (E1), ubiquitin-conjugating enzymes (E2), and ubiquitin-ligating enzymes (E3). The E3 ligase is responsible for substrate and target lysine specificity and determines the linkage type within the poly-ubiquitination chain, aided by the E2 enzyme (539,540).

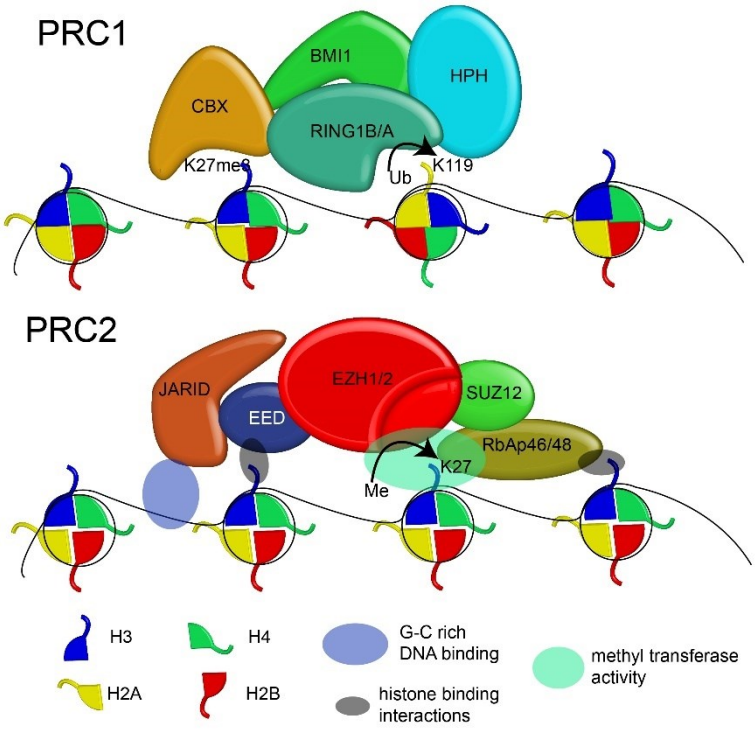

Figure 25: Polycomb Repressive Complexes

The PRC2 complex target genes are different from those recognized by PRC1. PRC2 consists of three proteins that are Zest Enhancer (EZH1/2), Zest Suppressor 12 (SUZ12), and Extra Sex Comb (ESC). SUZ12 binds to the promoter of target genes, and EZH1/2 is responsible for the tri-methylation of H3K27 thanks to its methyltransferase domain (537,541). The H2Aub and H3K27me3 marks have the effect of condensing the chromatin and suppress gene expression (542). Contrary to PcG, TrxG forms a complex that includes the methylase MLL1, which can catalyze H3K4me3 modifications in order to maintain transcriptionally active chromatin (543). H3K27 methylation is relatively stable, and it maintains long-term transcriptional repression. However, lysine demethylases such as JMJD3 and UTX specifically demethylate H3K27, resulting in activation of genes associated with animal body patterning, inflammation, and, ultimately, the resolution of bivalent domains (542).

PRC1/2 colocalize almost perfectly in embryogenesis, and there is strong evidence that gene repression upon PcG is obtained by a synergistic interaction between PRC1 and PRC2 (543,544). PRC1-2 are essential for embryonic development via the repression of *HOX* genes. Their embryonic KO phenotypes are similar, with posterior homeotic transformations due to misexpression of this set of genes (545,546). This function of PcG was first described in Drosophila in 1978 (547). In addition to their role in development, PcGs have also been associated with

cancer, indicating that PcG proteins may be dynamically recruited to new target genes (548,549). Since then, PcGs have been intensively studied for their involvement in the differentiation process, cellular identity determination, and pathologies such as cancer (550,551). Polycomb-dependent tumorigenesis has been linked to non-canonical pathways such as JAK/STAT and the *CDKN2A locus*, encoding two tumor-suppressor proteins $p16^{INK4A}$ and $p14^{ARF}$ that act on both pRb- and p53-dependent mechanisms (552–555).

In the retina, perturbation PRC1 and PRC2 complexes affect retinal progenitors and seem to lead to disruption of postnatal homeostasis. Consequently, it could lead to postnatal retinal degeneration from aberrant de-repression of a subset of usually silenced genes (556). A good example concerning the role of polycomb proteins in RD is the PRC2 subunit Ezh2. Ezh2 trimethylates H3K27me3, a repressive histone mark that is known to persist into adulthood (557,558). If EZH2 is removed or its function is compromised, it can no longer maintain the methylation of histone H3K27 on the promoter region of its target genes, including SIX1, causing their over-expression. SIX1 is vital for the eye's formation during embryonic development, and its abnormal expression in the mature retina causes the aberrant gene expression that contributes to the degeneration and ultimately to PRs death (535,559). Moreover, *Ezh2* KO in the mouse retina, using a *Chx10-Cre* construct that allows normal development of the retina to the perinatal period, still causes progressive photoreceptor degeneration postnatally, linking for the first time an in utero events to juvenile and adult-onset vision loss (535).

1.5.2.1 The PRC1 complex

PRC1 is dynamically recruited to new target genes varying from its canonical embryonic ones during development and adulthood. This implies a wave of deployment during early and late embryogenesis and later in infancy and adulthood, where PRC1 components are recruits to novel target genes (546).

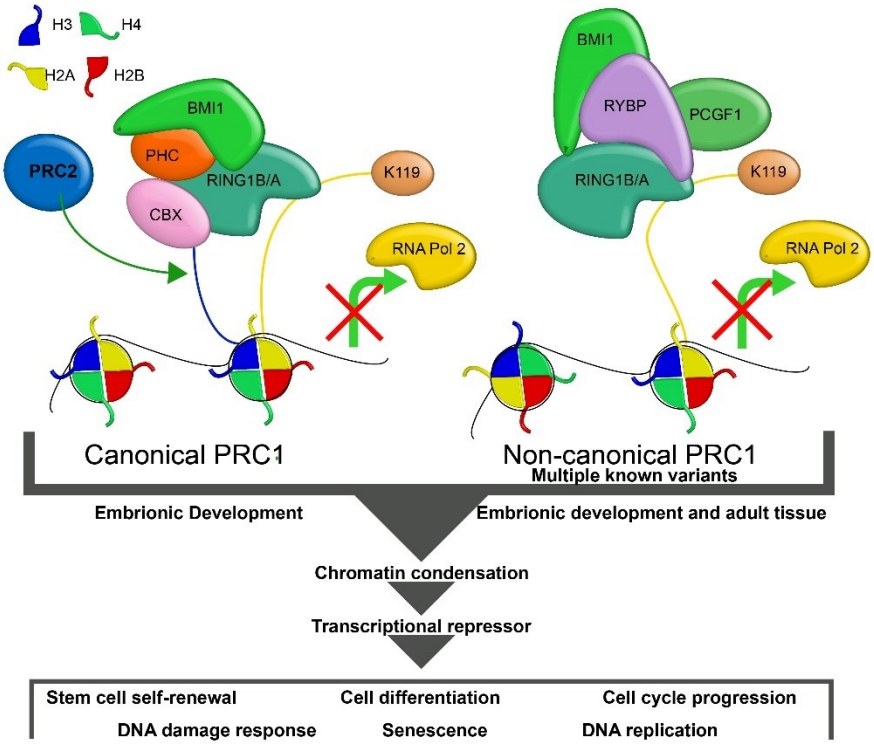

Figure 26: Canonical and non-canonical PRC1 complexes

During embryonic development, the PCR1 component strongly colocalizes with RING1B and H3K27me3, silencing canonical target genes using a classic chromatin remodeling mechanism (Figure 26). Contrarily, in differentiated cells, PCR1 seems to target non-canonical target genes without the need for RING1B or H3K27me (560,561). Deletion of *Ring1b* in mice results in severe developmental defects and embryo lethality, whereas KO of *Ring1b/Rnf2* in zebrafish led to developmental defects such as incomplete differentiation of cranial neural crest cells and severe craniofacial defects (562). Furthermore, recently has been reported a case of syndromic neurodevelopmental disabilities due to mutation on RING1 that affects its catalytic domain activity. PRC1 also binds with RING1B without H3K27me3 on non-canonical targets in both drosophila and mammals (563,564). This new set of target genes includes hundreds of genes in the eye discs. These new PRC1 targets are strongly enri-ched in genes regulating the cell cycle, DNA repair, cell polarity, and cytoskeletal organization. Many of these genes play key roles in cell signaling, signal transduction, and cell proliferation, and they are also involved in cancer-related pathways such as the Notch pathway.

Several PcG members can act as tumor suppressors, and PRC1 may be present at a large subset of sites in the absence of H3K27me3 (560,565).

1.5.2.1.1 BMI1

BMI1 is the core component of PRC1. BMI1 is a 37 kDa protein that contains 326 amino acids highly conserved in mammals (Figure 26) (566). It is encoded by a gene located on chromosome 10 containing ten exons. Upstream *BMI1* there is another gene called Copper Metabolism gene MURR1 Domain 3 *(COMMD3*), which can be transcribed with BMI1, but this fusion protein's function is mostly unknown.

PRC1's primary activity is the monoubiquitination of H2A at Lys119, in which BMI1 plays an essential role as a catalyst, stimulating the E3 ligase activity of RING1B (567). It also mediates the compaction of chromatin, independently of its ubiquitylation activity (Figure 26) (568).

BMI1 was first discovered in 1991 for its involvement in lymphoma in cooperation with MYC (569–571). In 1999, the authors also demonstrated that BMI1 makes it possible to block senescence thanks to the repression of the *INK4A / ARF locus* (572). BMI1 is expressed in most tissues, but it is particularly enriched in hematopoietic and neural stem cells (573). It is also overexpressed in lung cancer, colorectal cancer, medulloblastoma, glioblastoma, and neuroblastoma (566,574,575). Defects in self-renewal and proliferation observed upon *Bmi1* knockdown were found to be mediated by cell cycle inhibitors p16, p19, and p21 (550,572,576). $p16^{Ink4a}$ inhibits the CDK4/6, cyclin kinase responsible for phosphorylation of pRb during the cell cycle (577). The hypophosphorylated pRb can bind and repress the transcriptional activation of E2F, repressing its target genes responsible for S-phase entry, thus causing cell cycle arrest and senescence.

BMI1 is a key factor for the control of p53 activation, which regulates a wide variety of stress responses, from apoptosis to senescence. More recently, new roles of p53 in the adaptation to metabolic and oxidative stress have also been described. P53 acts mainly as a transcription factor, repressing and activating many target genes (578). Another p53 function, independent from its transcriptional activities, is regulating apoptotic signals at the mitochondria (579). P53 activation leads to numerous responses such as cell cycle arrest, senescence, and apoptosis to prevent the cell from replicating. Key to p53 regulation is the control of the stability of the p53 protein,

orchestrated mainly through a network of ubiquitination reactions where BMI1 plays an essential role (580).

MDM2 and its homolog MDMX are critical negative regulators of p53. In the absence of BMI1, p19ARF/p14ARF binds the p53 ubiquitin ligase MDM2, preventing MDM2 from inducing p53 proteasomal degradation. P53 then blocks cell cycle progression by inducing the expression of p21, which in turn binds and inhibits different cyclins such as CDK2, CDK1, and CDK4/6 and promotes apoptosis through various mechanisms. Thus the effect of BMI1 suppression of the INK4a/ARF locus results in the inhibition of apoptosis and promotion of cell cycle progression (580). Interestingly, inactivation of $p16^{Ink4a}$ and $p19^{ARF}$ or directly of the INK4a/ARF locus partially rescues the self-renewal and the ratio of the neural stem in the central and peripheral nervous systems in $Bmi1^{-/-}$ mice, showing that BMI1 repression of the *Ink4a-ARF* locus is critical to maintaining self-renewal of neural stem cells (573,581).

However, the partial rescue of the $Bmi1^{-/-}$ phenotype through ablation of $p16^{Ink4a}$ and $p19^{ARF}$ suggests supplementary target genes and additional functions for BMI1.

BMI1 is also able to regulate some cyclins directly. In fact, it has been proven that the oncogenic activity of BMI1 and MYCN in neuroblastoma pathogenesis and progression is largely due to their capacity in maintaining cyclin E1 levels (582).

Overexpressing BMI1 in healthy cells does not allow transforming or immortalizing the cell but gives it a significantly longer lifespan (572). By inhibiting the INK4A / ARF locus expression, BMI1 promotes proliferation and self-renewal of cells. Conversely, the loss of BMI1 induces senescence of cells via the p16INK4A and p53 pathways (583).

BMI1 and RING1A also regulate the cell cycle through the ubiquitination of chromatin-associated proteins bound to promoters. This modification is necessary for the expression of marked genes once the cells enter G1. Their depletion, which causes the inactivation of mitotic bookmarking by ubiquitination, is deleterious to progression through G1, cell survival, and proliferation (584).

The BMI1 protein contributes to stem cell pluripotency and oncogenesis via multiple functions, including its newly identified role in DNA damage response (DDR). BMI1 Ubiquitination of H2A at

lysine 119 is not only central as an epigenetic regulator during development, but it is also important during DNA damage; in fact, BMI1 also confers radio-resistance to glioblastoma cancer stem cells by recruiting DNA repair machinery to sites of double-strand breaks (DSBs) and UV lesions (585–587). BMI1 and RING1B are rapidly recruited to sites of DNA damage and contribute to the ubiquitination of H2A and γH2AX (588–590). Recruitment of γH2AX to DSBs (γH2AX foci) promotes the assembly of repair factors, thus facilitating DSB repair (591,592). Therefore, BMI1 contributes to maintaining genome integrity and resistance to genotoxic therapeutic reagents by assisting the HR-mediated repair of DSBs (593,594).

The sustained localization of BMI1 to damage sites is dependent on intact ATM and ATR and requires H2AX phosphorylation and recruitment of RNF8. RNF8 and RNF168 functions are also required for proper localization of 53BP1, although the exact mechanism is unclear (595–597). ATM activation cause also phosphorylation of ATM targets, including γH2AX, CHK2, and p53. In the absence of BMI1, several proteins dependent on ubiquitin signaling, including 53BP1, BRCA1, and RAP80, are impaired in recruitment to DSBs (588).

It has been reported that BMI1 can also directly associate with NBS1, required for ATM activation, altering its binding capacity with ATM and causing decreases of the DNA damage-induced G2/M checkpoint (598).

Recently, BMI1 has been found downregulated in late-onset Alzheimer patients, and BMI1 KO in human post-mitotic neurons resulted in amyloid-beta peptide secretion and deposition, p-Tau accumulation, and neurodegeneration. Mechanistically, BMI1 seems required to repress *MAPT* transcription and prevent GSK3beta and p53 stabilization, which otherwise resulted in neurodegeneration (599).

1.5.2.2 BMI1 in the postnatal brain and retina

Little is known about BMI1's role in the adult human brain and retina, and most of the research in this field has been done in mouse models. Bmi1 null mice are viable but not healthy, and their lifespan is highly reduced. They show axial skeleton defects, reduced postnatal growth, reduced brain size, with decreased proliferation of cortex and subventricular zone (SVZ). The neuronal phenotype includes impaired cerebellar formation, loss of synapsis connections, axon

demyelination, as well as a deficit of glutamate transporters with a subsequent neurodegenerative process (600). Bmi1−/− mice are also characterized by lens cataracts, cortical neuron apoptosis, p53 activation, and accumulation of oxidative damage characteristic of a progeroid phenotype (601). Bmi1 reduces p53 protein levels by directly inducing its polyubiquitination and proteasomal degradation (602). This progeroid mouse model overexpresses p16, a canonical senescence biomarker, both in retinal neurons and retinal endothelial cells but not in neuroglial cells, and affected cells tend to undergo cellular senescence. BMI1's direct target P16 has also been found highly overexpressed in old-age human retinas compared with middle-age retinas, supporting a correlation between cellular levels of p16, senescence, and retinal aging (603,604). Cellular senescence has been implicated in age-dependent eye diseases, such as AMD and glaucoma (46,605–607). Heterozygous Bmi1 mutant mice (Bmi1+/−) develop normally; however, they have a reduced lifespan and present age cognitive deficits and neurodegeneration, sharing similarities with Alzheimer's disease (608). A meta-analysis of more than 300 genome-wide association studies identified the *INK4a/ARF locus*, which encodes p16, as the genomic locus that is genetically linked to the highest number of age-associated pathologies, including type 2 diabetes (609).

The eyes of Bmi1 null mice are smaller but develop all the retinal layer and eye structures with no major observable phenotype. Bmi1 does not seem to be required for the proliferation of the main RPC population in the developing retina. Instead, it seems required for the proliferation and postnatal maintenance of the most immature RPCs situated at the retinal ciliary margin. Bmi1 overexpression in RPCs induces chromatin remodeling, causing their conversion into long-term RPCs with increase proliferative capacity and stem cell characteristics (610). Bmi1 expression level thus discerns immature progenitor/stem cells from the predominant RPC population during retinal development (610).

Interestingly, Bmi1 is also expressed in some mature retinal neurons, including PRs, introducing the concept that it might be relevant for their postnatal maturation or maintenance (601). On the other hand, it has been shown that genetic Bmi1 deletion significantly delays cell death, generating the most potent PRs rescue that was ever achieved for the rd1 mouse model (611). In this context, BMI1 retinal toxicity seems to be independent of the

classical Ink4a/Arf pathways and seems to be independent of its phosphorylation status, highlighting the complexity surrounding the Bmi1 biology *in vivo* (612).

Much remains to be revealed on the role of BMI1 in retinal neuronal cells, particularly its role in the degeneration process in the adult and aging retina.

Here we investigate BMI1's role in the postnatal mouse retina and human PRs, focusing on postnatal cone maturation, maintenance, and survival. We show the implication of both the classical Ink4a/Arf pathway and alternative pathways independent from p16 and P53 activation during PRs degeneration. We then show partially conserved BMI1 function in the retina between mice and humans.

1.5.3 Mechanisms of cell death in retinal neurons

Cell death in neurons, retinal cells, and other specialized cells can have many faces. The cell death process in highly specialized cells has been at the center of constructive debates to understand the molecular mechanisms that guide this process. More recently, many apoptosis-independent cell death pathways have been described. These unconventional and alternative mechanisms are a "hot topic" and have been extensively reviewed (613–615). Understanding these mechanisms can be crucial to develop therapeutic strategies for RDs and other degenerative diseases. Investigating the mechanistic events orchestrating cell death in retinal neurons, especially PRs, is not only crucial for a better understanding of RDs, but it may be relevant to understand neuronal cell death mechanisms in other non-retinal diseases.

Here, we will briefly discuss the most relevant types of cell death in the context of RDs: necrosis, apoptosis, necroptosis, and autophagy (Figure 27).

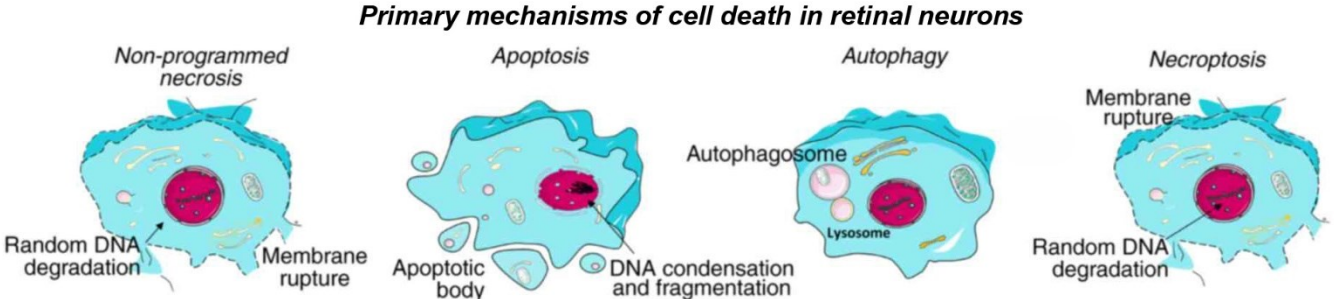

Figure 27: Cell death modalities and their key features (modified from (615))

1.5.3.1 Non-programmed necrosis

Irreversible cell injury to cells invariably leads to cell death. Non-programmed necrosis is aroused by several external factors: infection, toxins, oxygen deprivation or hypoxia, extreme environmental conditions such as heat, radiation, exposure to ultraviolet irradiation, and physical injury. It is generally considered a passive process that needs minimal energy and does not require de novo macromolecular synthesis (616).

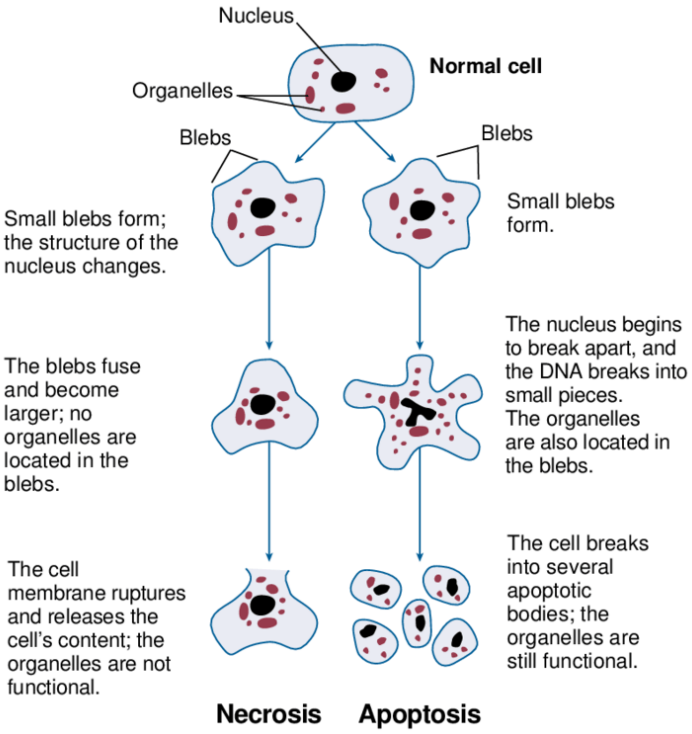

Figure 28: Structural changes of cells undergoing necrosis or apoptosis (1204)

Necrosis begins with cytoplasmic swelling, digestion of the chromatin, disruption of the plasma and organelle membranes without severe chromatin condensation, and random degradation of the DNA. Then, the ER vacuolizes, and the membranes and organelles collapse entirely. Finally, the cell lyses, scattering its intracellular content, causing inflammation and activation of the immune response (Figure 28).

Non-programmed necrosis is frequently observed in ischemia, trauma, and some forms of neurodegeneration (615).

1.5.3.2 Apoptosis

Apoptosis can represent a cell suicide or a murder. Cells can commit suicide when they are deprived of any incoming survival signal in the form of trophic factors or when they recognize extensive and unfixable DNA damage, which triggers an intrinsic cascade of signals leading to cell death. Cells murder other cells to clear out unneeded cells or eliminate potentially self-attacking immune cells; in this case, they generate extrinsic signals that affect the surrounding cells (617,618).

Either of these processes constitutes programmed cell death. The highly regulated cooperation between the apoptotic process and the generation of new cells is a cardinal point for embryonic development. Apoptosis is also a physiological and continuous process in many tissues, such as the intestines, liver, and blood (619).

Apoptosis includes a series of firmly controlled events. It is distinguished by cell shrinkage, membrane blebbing, positional organelle loss, collapsing of the cytoskeleton, nuclear envelope disassembling, and DNA condensation and fragmentation with the release of apoptotic bodies. Three different signaling pathways have been established to trigger apoptosis: The extrinsic (death receptors) pathway, the intrinsic (mitochondrial) pathway, and the perforin/granzyme pathway (Figure 28) (620).

Apoptotic cells do not induce inflammation, but they release signaling proteins and apoptotic bodies to induce phagocytosis and remove the debris. Failure in the apoptotic process can lead to more damaging necrotic cell death or trigger neoplastic formation (615–617).

Different proteins are essential for the apoptotic process, and they are divided into three principal categories. The 'killer proteins' are represented by the caspases, which have been extensively studied, and their cascade process characterized. The second category includes the 'destruction proteins,' which digest DNA, fragment the cell, and break down the cytoskeleton. Finally, we have the 'engulfment proteins' that elicit and promote phagocytosis by other cells (620).

1.5.3.2.1 DNA damage and apoptosis

Apoptosis is the preferred mechanism of cell death in case of DNA damage (621,622). Different proteins, such as the Polycomb protein BMI1, can activate P53 directly or through the *INK4A* locus (594). P53 is a master regulator of DNA damage response, and when activated, it binds to promoters of target genes to promote DNA repair, apoptosis, or cell cycle arrest (Figure 29) (623).

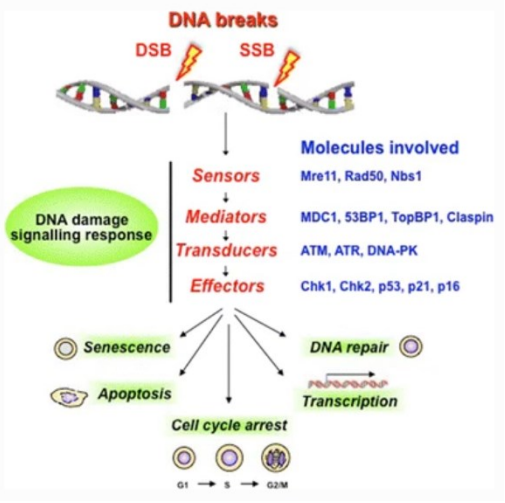

Figure 29: DDR signaling cascade activated in response to SSBs and DSBs (1205)

DNA damage generally causes DNA breaks that activate the DNA damage response (DDR) and DNA repair pathways to repair the damage. If the damage is effectively repaired, the cell continues its cycle, while if the damage is insurmountable, this causes the activation of apoptosis or senescence (624). DNA repair pathway is essential for protecting the DNA from breaks and promoting long-range DNA end-joining via the nonhomologous end-joining (NHEJ) DNA repair mechanism. NHEJ is the primary DNA repair mechanism used during CSR. Microhomology-mediated end joining (MMEJ) is an error-prone repair mechanism for DSBs, which relies on exposed microhomologous sequence flanking broken junction to repair the damage, and it can also contribute to repairing the DNA breaks (625). P53 counteracts the transcription of many G2-specific genes to contribute to the maintenance of the G2 arrest. In contrast, Mdm2 and Wip1 perform a negative regulation on p53 to maintain the reversibility of a G2 arrest (626–629).

Mdm2 is the main E3 ubiquitin ligase that targets p53 for proteasomal degradation and inhibits its function as a transcription factor, whereas Wip1 dephosphorylates both p53 and Mdm2 to promote p53 degradation (630–632). P53 levels fluctuate in response to DNA damage, and during the reparation process, this oscillatory pattern of p53 expression results in distinct cell fate outcomes that can induce senescence, apoptosis, or reentering in the cell cycle if the damage is resolved. Besides, p53 itself is known to bind DNA double-strand breaks, advancing a possible role in DNA damage detection (633). Another transcription-independent proapoptotic function carried out by the cytoplasmic p53 fraction is to induce mitochondrial outer membrane permeabilization during p53-dependent apoptosis (634,635). When DNA damage could not be resolved, p53 is stabilized and activate its transcriptional function to promote the expression of pro-apoptotic genes, notably *Puma and Noxa* (623,636). Puma and Noxa inactivate the anti-apoptotic Bcl2-family proteins and activate Bax or Bak to cause cytochrome C release from the mitochondria, leading to the activation of caspases (617,637). In addition to p53, the mammalian genome encodes two other related TFs, p63 and p73, which also appear to stimulate pro-apoptotic gene expression (621,622).

The DDR pathway includes proteins such as ATM, NBS1, γH2AX, MDC1, RNF8, RNF168, 53BP1, and RIF1. MDC1 cooperates with H2AX to promote cell cycle arrest and recruit DNA repair factors at the DNA break (638). The interaction between γH2AX and MDC1 is required to recruit different

factors at the DDR machinery, including 53BP1, BRCA, NBS1, and phosphorylated ATM, and for foci's formation (638,639). Further deposition of the MRN–ATM complex surrounding the break can amplify the ATM-dependent γH2AX signal at the break. ATM is also required for the ATM-dependent phosphorylation of downstream factors, including Chk1 and Chk2 (Figure 29) (624).

DNA-damage Checkpoints proteins such as Chk1 and Chk2 play essential roles in the self-renewal, maintenance, and quiescence of somatic mammalian stem cells. They are also implicated in diseases such as cancer and aging (640). DNA-damage checkpoints generally help extend lifespan by controlling carcinogenesis, while in other situations, such as during aging, DNA-damage checkpoints proteins may participate in the degenerative process. Chk2 is a stable protein expressed throughout the cell cycle. It appears mostly inactive in the absence of DNA damage, but it is rapidly activated in response to double-strand DNA breaks (DSBs), mainly by ATM (641,642). In contrast, Chk1 protein is more liable, is generally activated by ATR, and is restricted mainly to S and G2 phases (642).

1.5.3.3 Necroptosis

Almost until the end of the twentieth century, only two types of cell death were known, apoptosis and necrosis, where their main difference was that the first is regulated by precise and defined molecular pathways, while the second results from chaotic and unregulated cell death. Nowadays, however, it is clear that even the necrotic process can be regulated by precise molecular pathways, which has been named necroptosis (643–646). Although initially there was a tendency to call all types of programmed necrosis with this term, in reality, the term necroptosis refers to programmed necrotic death dependent on receptor-interacting protein kinase-3 (RIPK3) considered the molecular switch of this process (613). Necroptosis seems to have evolved as a defense against intracellular infection (647,648). Recently, it has gained considerable importance from the pathophysiological point of view, having been associated with a variety of diseases such as myocardial infarction and stroke (649,650), atherosclerosis (651), ischemia-reperfusion injury (652,653), pancreatitis (644,646,654), inflammatory bowel disease (655,656) and some other clinically common disorders (657). Necroptosis can be triggered by various cytokine, death receptors, Pattern Recognizing Receptors (PRR), cell surface Toll-Like Receptors (TLRs) (658–660), DNA-dependent Activator of Interferon regulatory factors (DAI) (661,662), and other signals. It is

trigged upon caspase-8 inhibition by pharmacological treatment and genetic manipulation (663). In the context of PRs degeneration upon retinal detachment, it has been shown that treatment with a pan-caspase inhibitor (such as z-vad-fmk) reduces the apoptotic process, while it induces necroptosis and, therefore it does not stop the degeneration (664).

At the molecular level, necroptosis is operated through a highly regulated complex called the "necrosome". Necroptosis induction promotes the recruitment of proteins containing a RIP Homotypic Interaction Motif (RHIM), which subsequently recruit and activate the receptor-interacting protein kinase (RIPK) 3 also containing an RHIM domain (643,649,656,657). RIPK1 and RIPK3 are part of the necrosome complex and are activated by autophosphorylation. RIPK3 subsequently phosphorylates MLKL, resulting in MLKL oligomerization through the interaction of its coiled-coil domains (CCD) (654,665–667). Oligomerized MLKL is transported to the plasma membrane, where it executes necroptosis by regulating ion channels and increasing membrane permeabilization (666,668). Beclin1 is a core protein of the autophagy process, and it is inhibited in apoptotic conditions by active caspases' cleavage. In turn, Beclin1 acts as a switch between necroptosis and autophagy, inhibiting necroptosis when the autophagic process is activated. Beclin1 binds to the CCD of MLKL during autophagy, which prevents MLKL oligomerization and the plasma membrane's perforation, thus preventing necroptosis (669).

1.5.3.4 Autophagy

Autophagy is a form of regulated cell death, initially described as a Type II cell death, that mechanistically depends on the autophagic machinery (670). Are now known different subtypes of autophagy (671). It is a process by which damaged cells compartmentalize and digest themself, providing a more controlled elimination with less stress for the neighboring cells (670,672–675). An isolation membrane is generated during autophagy in the cytoplasm, which surrounds cytosolic cargos to create an autophagosome. Autophagosomes then fuse with lysosomes leading to the digestion of engulfed material, allowing macromolecules to be recycled. This complex process is carried out by dedicated proteins, including more than 30 autophagy-related (ATG) proteins, proteases such as cathepsins, and other proteasomal proteins (676,677).

Autophagy is indispensable to many processes at the physiological level, including development, immunity, and aging (678). Apoptotic and autophagic machinery are highly interconnected during developmental cell death and are required for proper embryonic development (675). Defects in autophagy have also been associated with embryonic lethality, developmental defects, and multiple pathological disorders, including neurodegeneration, cancer, and cardiovascular disorders (672,678–682). Autophagic cell death is frequently induced when apoptotic pathways are inhibited or if apoptosis is blocked (683,684). However, in most cases, autophagy appears to be associated with pro-survival processes more than the execution of cell death. It seems to act as a form of adaptation to stress, hence mediating cytoprotective, rather than cytotoxic, effects, thus reducing the impact during the activation of other cell death mechanisms. Autophagy seems indispensable under specific settings to carry out other cell death mechanisms (685–690). Blocking autophagy with pharmacological or genetic interventions usually has a nefarious effect, accelerating, rather than delaying, stress-induced cell death. For example, autophagy is observed in degenerating PRs exposed to oxidative stress where Lipidation of microtubule-associated

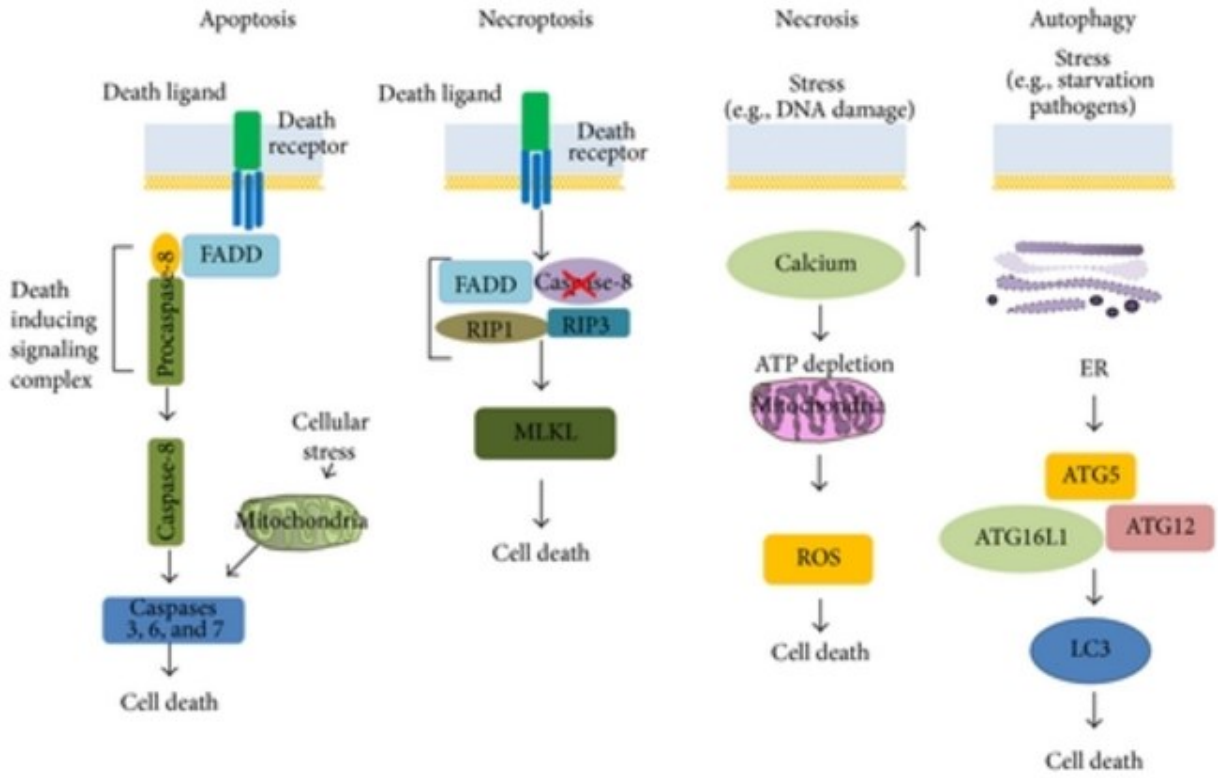

Figure 30: Overview of cell death mechanisms (1206)

protein 1 light chain 3 (LC3/Atg8) seems to initiate apoptosis or generate apoptosis-independent cell death if apoptosis is blocked (323). In this context, blocking both apoptosis and autophagy does non rescue the phenotype and brings to a more aggressive degeneration by necrosis (691).

In this thesis, we use mouse and human *in vitro* models to investigate the molecular mechanisms that drive PRs degeneration in the context of BMI1 deletion and in patients with RDs.

1.6 Modeling outer retinal degenerative diseases

For thousands of years, "scientists and doctors" have used animal models to study anatomy, physiology, and pathology. The earliest documented animal studies date back to before 300 BC in Greece and Alexandria of Egypt (692). Aristotle's research of animals is collected in different manuals, which include detailed illustrations and descriptions that have been admired for their meticulous and illuminating characterization of more than 500 different kinds of mammals, birds, fish, amphibians, reptiles, insects, cephalopods, and many other invertebrates (693). Otherwise, the first publications about RD date back to the first half of the last century (694,695). After only a few years, the firsts natural mouse models of retinal degeneration, rd (retinal degeneration), and rds (retinal degeneration slow) were identified and published (696–698). These animals showed Mendelian hereditary transmission and have been extremely useful in understanding PRs degeneration mechanisms. Only in the 1980s, the causal mutations in these two models have been identified in *Pde6b* (rd mice) and *Prph2* (rds mice) genes (696,698). Hundreds of mutations that cause retinal degeneration have been identified ever since (699).

Unquestionably the discovery that exogenous DNA can be introduced by homologous recombination in mouse embryonic cells and the consequent development of recombination technologies that allow the insertion (knock-in) or deactivation (knock-out) of one or more genes has enormously increased the number of animal models available (700–703). The incredible technological advancement in the field of gene editing has led to the development of site-specific programmable nucleases such as zinc-finger nucleases (ZFNs), transcription activator-like effector nucleases (TALENs), and most recently Clustered regularly interspace short palindromic repeats (CRISPR)/CRISPR associated systems (Cas) has expanded even further the number of animal models for inherited RDs (703–707).

While the first animal models were beginning to become available, the concomitant advancement of sequencing techniques developed in the 1970s by Frederick Sanger, Nobel price in chemistry along with Wally Gilbert and Paul Berg, as pioneers of the DNA sequencing technique, allowed the isolation of more and more causal mutations in patients suffering from genetic diseases, including RDs (708–710). This has allowed an enormous expansion in the availability of human

inherited RD models with the most disparate mutations. Of course, this does not exclusively include rodents, although they are the most commonly used. To date, an enormous variety of natural and transgenic vertebrate models are available to study retinal function and disease, such as macaque, dog, cat, pig, sheep, chicken, and zebrafish (711,712).

Large animal models such as monkeys and pigs are preferable for preclinical and surgical studies for their more considerable resemblance to humans in the context of eye dimensions and anatomy. Some non-human primates, but not all, are of particular interest in studying MDs because they possess a macula similar to the human one (713). On the other hand, large animal models have numerous disadvantages, including high costs, handling difficulties, low reproductive capacity, and slower development. Zebrafish has been extensively used in research due to its high reproductive capacity, ex vivo development that allows easy genetic manipulation, and characteristic transparency that allows easy visualization of embryonic development. Otherwise, the eye's structure, retina, and PRs' anatomy and genetics differ significantly from the human one (711,712).

Mouse models are undoubtedly the most extensively used and characterized and possess numerous advantages. Maintenance, housing, and breeding are cheap and well mastered. They have copious offspring with short generation time and fast development (714). Furthermore, the mouse genome is extensively sequenced and characterized (532,703). Compared to other species, mice have a higher number of natural mutations and are particularly prone to genetic manipulation. They are also evolutionarily close to humans, with a 79% identity in the aminoacidic sequence of proteins involved in inherited RD, even higher than larger species such as pigs (711).

1.6.1 Mouse models of inherited RDs

The use of mutant mouse models, either naturally occurring or generated by genetic modification, has significantly contributed to our knowledge of PRs components and functions, the physiological processes that regulate vision, and the pathophysiological mechanisms underlying RDs. Besides recapitulating human photoreceptor dystrophies, KO models have been valuable for dissecting gene products' role in phototransduction and development. Furthermore, they are

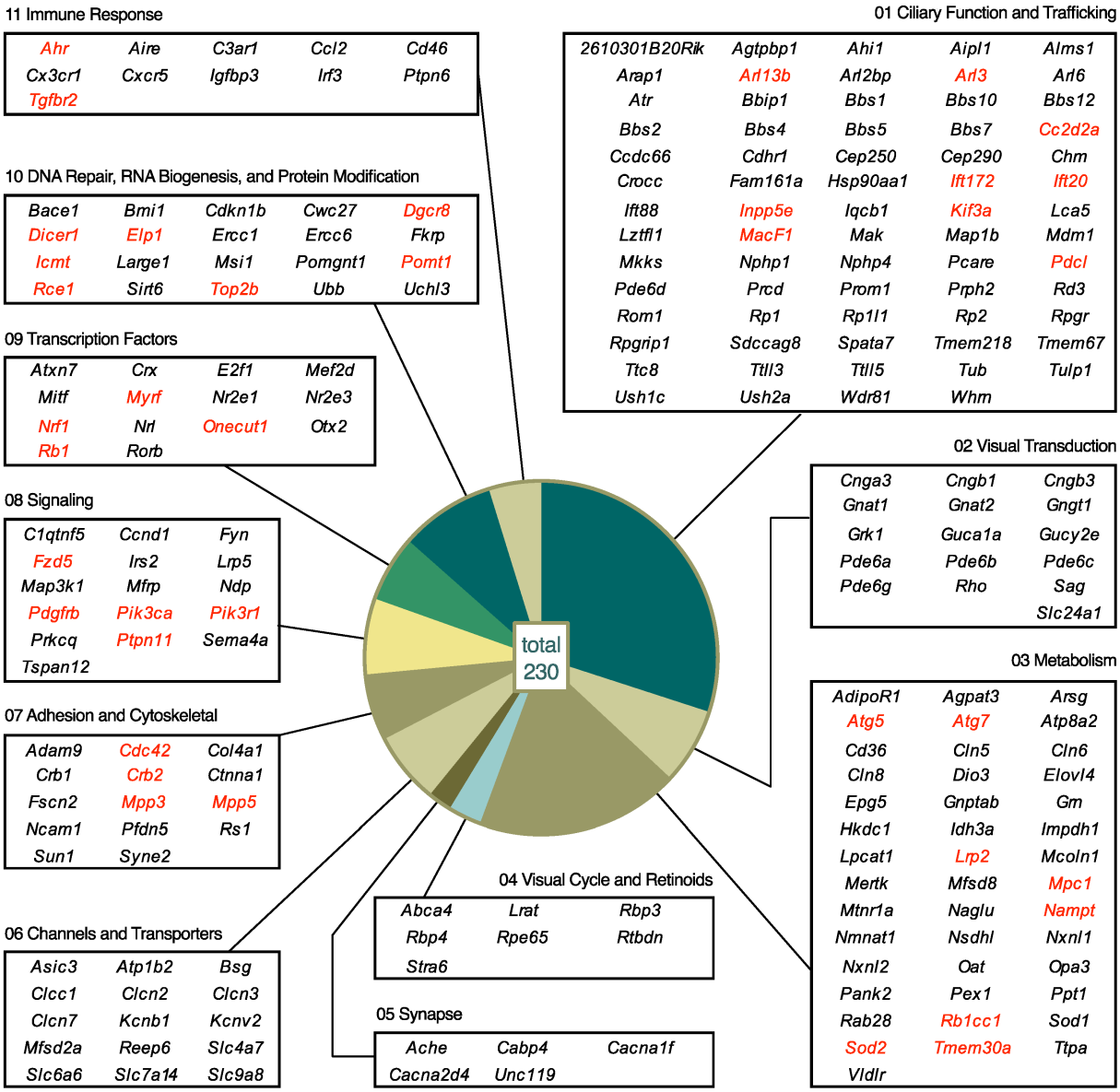

Figure 31: Genes associated with PR cell loss in monogenic mouse models of retinal degeneration (RD) (756)

Genes identified by combined review of the Mouse Genome Informatics (MGI) database and articles from a PubMed query assigned to the indicated functional categories. Genes for which mutant alleles are available only in the conditional form are displayed in red. Conditional alleles were included only in instances where germline null alleles resulted in embryonic, prenatal or postnatal lethality.

extremely useful in other applications such as drug screening and toxicity testing, and several of these models have allowed the development of novel treatments, such as gene augmentation therapies that are now in clinical trials (355,715).

The current availability of mutant mice is impressive, and The Jackson Laboratory has the world's most extensive collection of mutant mouse models. This mice collection includes models with

variations and disorders affecting every portion of the eye, including the cornea, lid, iris, lens, and retina (716). Available mouse models of inherited RDs incorporate many different diseases such as RP, LCA, CRD, and CD (703,717). The term “MDs mouse models” is occasionally inappropriately used for mouse models with mutations in genes linked to MDs cases in humans. Since mice do not have a macula, we will primarily refer to them as CDs in this chapter. To date, 230 genes linked to RDs have been isolated or generated in mice, and they can be divided into 11 categories (Figure 31): Ciliary Function and Trafficking; Visual Transduction; Metabolism; Visual Cycle and Retinoids; Synapse; Channels and Transporters; Adhesion and Cytoskeletal; Signaling; Transcription Factors; DNA Repair, RNA Biogenesis, and Protein Modification; Immune Response (699).

Of the 273 human retinal degenerative disease genes in RetNet (718), which have mouse homologs, 110 are available in mouse models, including germline and conditional mutants. There are 120 additional genes in which mutations cause PRs degeneration in mice but are not yet been linked to human RDs (Figure 32). Since the cause of a large part of human RDs still needs to be genetically explained, these genes could represent not yet identified RD gene candidates.

Two gene categories are particularly related to this study: Ciliary Function and Trafficking, and DNA Repair, RNA Biogenesis, and Protein Modification

Ciliary genes are the biggest gene group causing RDs in humans (Figure 19), and it is not surprising that the largest group of genes causing RDs in mice are part of this same category (Figure 31).

As described before, perturbation of BB-TZ-CC proteins and complexes such as MKS, NPHP, BBSome, PCM, and IFT machinery can cause syndromic and nonsyndromic manifestation, which often include retina degeneration. In most cases, the effects of the mutations in humans are phenocopied in the mouse.

RDs mouse models with ciliary dysfunction include various genetically modified models and a good number of naturally occurrent models such as rd3 (*Ush2a*), rd5 (*Tub*), rd9 (*Rpgr*), rd16 (*cep290*).

Mice with mutations in components of the MKS and NPHP complexes such as Nphp1, Nphp4, Ahi1, Iqcb1, Tmem67, and Cep290 generally do form PRs, but they often display

abnormal OS morphogenesis (198,719,720). Retinas in these mutant mice quickly degenerate e, resulting in complete ONL disruption within one month of age. Interestingly, rd16 mice, caused by a deletion in the Cep290 c-terminal domain have a longer disease progression than the knock-out mice (720,721). The use of these different mouse models can help understand the tremendous phenotypic variability in patients harboring mutations in these genes, which, in the case of *CEP290*, vary from LCA to BBS, MKS, and JBTS (225,722,723).

BB and PCM proteins such as ALMS1, CC2D2A, and C8ORF37, which are known cause of ciliopathies, has been mutated in mice. *ALMS1* encodes a protein that localizes at the BB, and when disrupted, it results in the Alström syndrome (ALMS) (724,725). Mice with frame-shift or nonsense mutations both recapitulate human ALMS disease features such as obesity, diabetes, and neurosensory deficits associated with normal vision at birth and postnatal slow PRs degeneration. This model has served to better understand Alms1 functions and its role in PRs' homeostasis and survival (726).

Genetic mutations in *CC2D2A*, which encodes a component of the subdistal appendages of mother centrioles and basal bodies, have been observed in patients with MKS, JBTS, BBS, and M-NS RDs (224,428,432). Knock-out of *Cc2d2* in mice causes embryonic lethality, while drug-induced deletion in adult mice causes a slow PRs degeneration unveiling its role in PRs homeostasis (727).

Targeted mutations of some genes causing USH in humans result, in mice, in a late-onset and prolonged progression of PRs degeneration and nonprogressive hearing impairment, mimicking the visual and hearing deficits in USH patients (177). Homozygous Ush2a knock-out mice have normal retinas at 10 months of age and lose 70% of their PRs by 20 months of age (414,728). In contrast, other USH gene mutations isolated in humans show no phenotype in mice.

Mutations in the TZ-associated protein, RPGR, are the most frequent cause of x-linked RP, but they can also cause other RDs with variable phenotypic outcomes (265,359,729). The naturally occurring rd9 model and the $Rpgr^{-/-}$ mice have a similar late onset and slow PRs degeneration (730). These models and other Rpgr mutants harboring different hypomorphic mutations allowed major break-throws on the disease mechanism and the understanding of RPGR functions. These

models make it possible to develop therapeutic strategies such as *RPGRORF15* gene replacement with AAV vectors to treat x-linked RP, actually in preclinical evaluation (731–733).

Different components of the BBSome complex have been disrupted or modified in mice to understand their function and role in BBS and other associated ciliopathies characterized by a complex and heterogeneous phenotype (269,424). Disruption of any BBSome complex proteins such as Bbs1, Bbs2, Bbs4, Bbs7, Bbip1, Ttc8, and Arl6, and its regulators Lztfl1, Mkks, Bbs10, and Bbs12 partially recapitulates BBS syndrome. The phenotype is generally associated with selective cilia dysfunction, renal cysts, deficits in olfaction, and obesity that increases with age (436,734–736). In the retina has been observed reduced ribbon synapses and a slow and moderate PRs' degeneration (737–741). The absence of defects in ciliogenesis and the moderate degenerative process in PRs, observed in some mouse mutants, has suggested some functional redundancy amongst the BBSome components in mice, thus highlighting some of the mice models' limits in modeling human diseases.

IFT component also has been extensively modified in mice. Most IFT proteins, such as Ift122, Ift88, Ttc21b, Ift172, Ift80, cause embryonic lethality when disrupted, attributable to ciliary-related disturbances in hedgehog signaling (742–749). These findings helped to understand the integral role of cilia and IFT machinery during embryogenesis (161,742). Hypomorphic and conditional alleles were needed for elucidating the roles of IFT components in retinal disease. Mice with a hypomorphic mutation in Ift88 are viable and exhibit disorganized OSs and early and progressive PRs degeneration, which cause complete ONL loss in 3 months (750). Rod-specific ablation of Ift172 causes an accumulation of rhodopsin in the cell soma and delocalization of other ciliary proteins, such as Rp1, leading to rapid PRs degeneration (751). Conditional depletion of Ift20 in M-cones also results in opsin mislocalization and cone degeneration. These mouse models have greatly supported the understanding of ciliary trafficking and IFT components' function in cone and rod PRs (752).

DNA Repair, RNA Biogenesis, and Protein Modification are all processes that significantly impact every aspect of organisms' physiology, from the development to tissue specification and aging (753–755). Generally, when their components are not functioning correctly, it can affect many

other genes' functions, thus generating major abnormalities in several tissues. For this reason, mutations associated with these processes usually cause embryonic lethality in mice, and naturally occurring viable mutations are rare (756). For example, genes associated with PRs degeneration in humans, such as the RNA splicing genes *Bnc2, Prpf3, Prpf8, and Prpf31*, the DNA repair gene *Ercc1*, and the miRNA processing genes *Dicers1* and *Dgcr8* are all embryonic lethal in knock-out mice, and for this reason, the adult and age-related phenotypes are not easily accessible (699,757,758). The use of heterozygous mice or the generation of drug-induced, conditional, or hypomorphic mutations has been necessary to study their function in adult tissues and their age-related implication. In the retina, most mutations in these genes result in PRs degeneration. Some knock-out models for this class of genes, such as Msi1/Musashi1 and Bmi1, which play central roles in posttranscriptional gene regulation and DNA repair, are viable, although their lifespan is reduced and present different developmental abnormalities (566,610,759). They are, therefore, suitable for studying the role of these proteins in mature neurons, such as PRs, and during the aging process. On the other hand, the phenotype observed in these mice suggests a possible compensatory effect during embryonic development.

To support the importance of the DNA repair machinery in non-dividing cells such as PRs, mutant mice for Top2b, responsible for creating DSBs during transcriptional activation, have shown to be indispensable during postnatal PRs development and maturation (760,761). These results suggested that the DNA repair system is needed to repair DNA damage that occurs during transcription of actively transcribed genes, which is necessary for PRs maintenance and survival. Mice harboring mutations in genes implicated in DNA repairs such as *Sirt6, Cwc27, Ubb, Lmo7, Uchl3, Ercc1,* and *Ercc6* are characterized by a consistent accumulation of DNA damage and DSBs that correlate with a relative slow PRs degeneration progression (762–766). Atr gene product localizes at the cilia of PRs and is therefore included in the ciliary gene category (category 1, Figure 31), and its human homolog has been associate with RDs (767). Atr has also been shown to have an essential role in the DNA damage response (630). Atrtm1Ofc mice have a faster disease progression compared to other mutant mice of the same class, probably related to the extra functions of Atr in ciliogenesis or cilia maintenance (351,767).

Since the retina is characterized by a high expression of splice variants, mutations of mRNA splice components greatly impact retinal neurons' physiology (293,768–770). Mutations in PDAP1, PRPF3, PRPF6, PRPF8, and PRPF31 all-cause autonomous PRs degenerations in humans, and some of their mice models efficiently recapitulate the phenotype (293,771). Mice with hypomorphic mutation of the mRNA splicing gene, *Cwc27*, show reduced lifespan and present a moderate late-onset photoreceptor degeneration similar to what was observed in human patients (772). On the other hand, Prpf3 and Prpf8 mice with a humanized heterozygous allele and Prpf31$^{-/-}$ mice do not display PRs degeneration, as observed in humans, but instead show late-onset RPE degeneration (293,294,771).

A substantial part of the available mouse models can recapitulate the human disease phenotype and permit mechanistic and therapeutic studies.

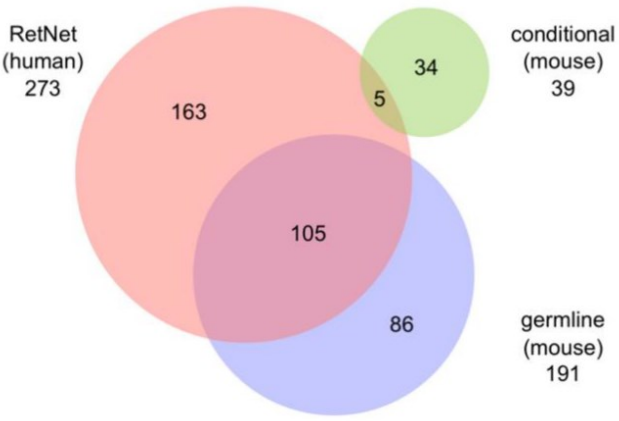

Figure 32: Overlap between gene implicated in mouse and human RDs (756)

1.6.1.1 Mouse models of cone degeneration

Despite the massive number of RDs' mouse models, the vast majority of them involve rods or generalized PRs degenerations, which are more representative for RPs and LCA cases (773). The number of cone-specific degeneration models are limited (774). With cone-specific degenerations, we consider models characterized by initial cone cell death, which may or may not be followed by rod cell death (775).

Cone degeneration is usually driven by two different mechanisms: non-cell-autonomous and cell-autonomous.

Non-autonomous cone degeneration is caused by the secondary effect of mutations affecting neighboring cells such as rods, Müller, and RPE cells.

In the *Rpe65*^{R91W} knock-in mouse, the wild-type murine codon is substituted with a humanized one harboring a mutation observed in patients with LCA with early-onset s-cone dysfunction and

rod desensitization (776,777). This mouse model displays a severe and rapid cone-specific degeneration and almost complete loss of cones at p30 that correlate to the human phenotype (778,779). Curiously this phenotype was even more severe than what was observed in the naturally occurring $Rpe65^{rd12}$ or the full knock-out mice $Rpe65^{-/-}$ (778,780,781).

In the $Rpe65^{-/-}$ mouse, RPE cells' inability to recyclate 11-cis retinal, while in the chromophore-deficient model, $Lrat^{-/-}$, RPE cells do not produce 11-cis retinal. Both models show similar phenotypes with early and severe S-cone degeneration combined with a slow and moderate reduction of rods function (782,783).

Cell-autonomous cone degeneration is generally due to mutations is in cone-specific genes. However, in some cases, distinguishing the cone-autonomous effect of mutations could be challenging, especially when the affected genes are expressed in both rods and cones. Naturally occurring cone-specific models are rare, but genetic editing has helped in this context (774). The use of alternative strategies such as conditional knock-out models offers a better understanding of cone physiology and disease. Below we present some examples of mouse models with cone-specific degeneration and the strategies adopted to overcome limitations in this field.

$Cpfl3^{Gnat2}$ is a naturally occurring model of cone degeneration due to a single base missense mutation in Gnat2, which encodes the α-subunit of cone transducing (784). $Cpfl3^{Gnat2}$ mice have a very early loss of cone functions without any visible cell death (785). These mouse models have served for the first cone-targeted gene therapy. AAV-mediated reintroduction of the healthy allele has proven to be sufficient to restore cone function and visual acuity, taking one step closer to a possible cure for achromatopsia (784,786). $Gnat2^{tm1Erica}$ harbors a different mutation in Gnat2; it has shown a similar but more severe phenotype with cone degeneration starting before the first year of life (787).

The naturally occurring $Cpfl5^{Cnga3}$ have the same phenotype as the $Cnga3^{-/-}$ (785). Cnga3 localizes to the plasma membrane of the cone's OS, where it interacts with cones-specific CNG channels to regulate calcium homeostasis, which is indispensable for phototransduction. Both mice have no recordable photopic light response with progressive cone degeneration (785,788). As described in patients with achromatopsia due to *CNGA3* and *CNGB3* mutations, rods function is

unaltered initially but starts a slow and progressive degeneration later (around one year of age in the mice), when cones are almost entirely lost (789–791). Most of the mice with null mutations in other subunits of the CNG channels have a similar disease progression, but they can vary in the onset (789,792).

Mouse models with mutations in the elongation of very-long-chain fatty acids-like 4 (*Elovl4*) gene show features resembling human Stargardt macular dystrophy with cone degeneration preceding rods (793–795). While homozygous knock-out mice die perinatally due to severe skin permeability defects, heterozygous mice show no apparent phenotype (794,796–798). Heterozygous mice expressing a truncated form of Elovl4 mimics several aspects of the human disease such as lipofuscin accumulation, RPE atrophy, accumulation of subretinal debris, and PRs degeneration (799). Surprisingly, rod- or cone-specific knock-out of Elovl4 does not result in retinal degeneration and only mildly influences function (800). These results have suggested that protein dysfunction, not its loss, is the cause of the retinal phenotype.

ABCA4 is a PR-specific transmembrane protein participating in the clearance of all-trans-retinal from the OS. When mutated in humans, it causes RDs such as RP and Stargardt disease (302,303). $Abca4^{-/-}$ mice have a deficit in all-trans-retinal clearance with an accumulation of lipofuscin in the RPE, increased oxidative stress, and activation of the complement (801,802). However, no PRs degeneration is observed in these mice up to 1 year of age (802)

Homozygous $Guca1a^{tm1.1Hunt}$ mice, which have a *Glu155Gly* missense substitution identical to one found associated with severe dominant cone dystrophy, resulting in rapid loss of cones and subsequently rods (265,803). The cause of the disease seems to be due to a defect in calcium-sensing and perturbed homeostasis, leading to constitutive activation of the guanylyl cyclase, which leads to cytotoxic accumulation of cGMP (804).

Eye physiology is also influenced by the action of several hormones (805). Mouse models mutant for genes responsible for the metabolism of the T3, such as $Dio3^{-/-}$, show a deleterious effect specifically on cone photoreceptors. These models have helped understand the role of triiodothyronine (T3) on cone cell fate determination, maintenance, and survival (806,807).

Congenital stationary night blindness 2A (CSNB2A) is an X-linked retinal disorder characterized by impaired vision with variable outcomes (808,809). It is caused by the absence or loss of function of the voltage-gated calcium channel protein CACNA1F (810). Cacna1f$^{-/-}$ mice have served to understand better the role of the Cacna1f in cone PRs' physiology and disease (811,812). Interestingly the effects of both knock-out and missense mutation have greater severity in mice than what was observed in patients. Both, Cacna1f$^{-/-}$ and Cacna1f^{G305X}, show unregistrable photopic function, ONL degeneration, and disruption of cone PRs' synaptic terminals (811,813). Recently, a new naturally occurring mouse model harboring a new mutation in *Cacna1f*, called Cacna1f^{nob9}, has displayed an even more severe phenotype than the knock-out mice (814).

A strategy to study cone-specific gene functions, which are also expressed in other retinal cells such as rods, is to generate conditional cone mutations (815). The Rp2^{MKO} mouse allowed studying the cone-autonomous effect of Rp2 detection, which resulted in the abnormal extension of cones' OSs with abnormal ultrastructure and disorganized disks (353,354,816,817). This model has shown to be a great tool for understanding cone morphological defects and cone-autonomous degeneration mechanisms during RP progression and has helped develop targeted gene therapies (818).

We now have access to a large number of models for studying cone degeneration. A limitation of using nocturnal animal models such as mice in modeling cone physiology and disease is that mice have only about 3% of cones, thus causing particular difficulties in evaluating the cone-autonomous mechanism of degeneration (711). The cone-only Nrl$^{-/-}$ mouse model has brought a significant advance in this regard (819). NRL is the rod-specific transcription factor responsible for repressing cone-specific genes to drive rod fate (104,115). Similar to the rd7^{nr2e3} mice, which naturally do not form any rods and instead form hybrid PRs, the absence of Nrl causes all photoreceptor precursors to differentiate into S-cones (115,820,821). However, the retina of Nrl$^{-/-}$ mice is not entirely healthy. It has lamination problems with the formation of rosettes and waves (819). Furthermore, partial and transient cone degeneration is generally observed between 1 and 4 months, followed by long-term persistence of remaining cones (821).

Conversely, transgenic mice that express Nrl under the control of the *Crx* promoter give rise to a rod-only retina without lamination defects (822). Interestingly, introducing the T3 receptor (TR)-β2 in *Nrl*$^{-/-}$ mice resulted in M-cones' generation instead of S-cones (820). This has advanced the hypothesis that S-cones follow a differentiation program "by default," while NRL and TR-β2 are responsible for determining the alternative PRs fates (Figure 10) (104,820).

The Nrl$^{-/-}$ model is therefore very attractive to study mutations causing cone degeneration in humans. Furthermore, it can be used to study cone degeneration mechanisms and facilitate the development of targeted therapies to rescue cone death (819).

Indeed, it has been used for the generation of double mutants to study the role of specific genes in the context of cone degeneration. Nrl$^{-/-}$ /Grk1$^{-/-}$ have been served to study the involvement of cone degeneration in Oguchi disease, a rare form of congenital and stationary night blindness which may be accompanied by progressive later-onset central vision loss (823–825). The Nrl$^{-/-}$ /Grk1$^{-/-}$ mouse model has served to understand that Grk1 inactivation can effects cones autonomously, also in the absence of rods (826).

A last interesting example is the Elovl4 mutation. ELOVL4 is found mutated in Stargardt disease 3, a rare, early-onset, and aggressive form of MD (793,795). Several mouse models have been generated to investigate the role of the *ELOVL4* disease-causing mutations, but all these models fail to recapitulate the early-onset cone degeneration observed in patients. These differences were supposed to be due to the reduced density of cones in the mouse retina. A group investigated the effect of *ELOVL4* mutations in the Nrl$^{-/-}$ retina trying to overcome the limits given by the scarcity of cones in other models. Unfortunately, they were still unable to show any visible cone cell death, highlighting the differences between men and mice regarding PRs physiology and genetics (796).

1.6.2 Limitation of mouse models in RDs modeling

The current mouse models are very helpful in studying cone physiology and pathophysiology. However, mouse models do not always reflect what is observed in humans. Animal models' failure to recapitulate the human phenotype occurs, with a large part of mouse models that only partially mimic the human phenotype. Sometimes the phenotype is absent or widely differs from the

human one. For this reason, certain limitations have to be considered when using these mice for research.

First, among mammals, trichromatic color vision is a privilege of some primates such as humans, macaque, and marmoset, which are also characterized by the presence of the macula in the temporal area (figure 33) (827–830). Most terrestrial mammals, including mice, are dichromatic (831–833).

Mice lack L-cones, and they also possess bivalent cones expressing both M and S-opsin that have never been described in primates. Furthermore, 'true S-Cones' are only a minority of the total cones in the mouse retina, and they are localized in the naso-ventral part (figures 3, 6) (834,835).

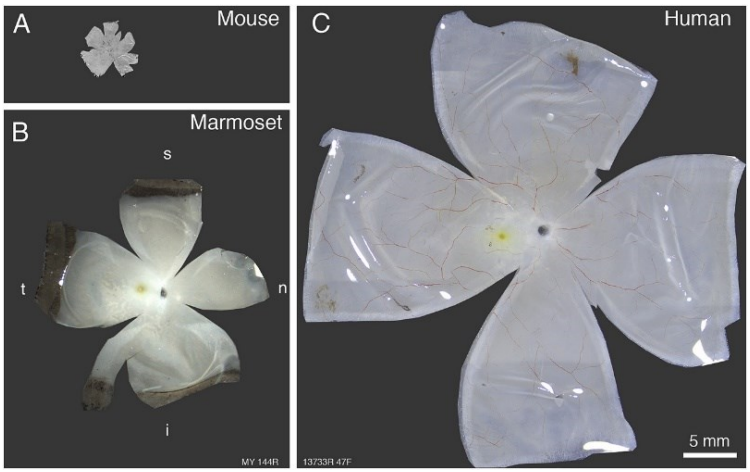

Figure 33: Comparison of primate and rodent retinas (713)

Images of retinal whole mount preparation from mouse, marmoset and human. The image of the mouse retina was kindly provided by Silke Haverkamp. The scale bar applies to all images. The macula (yellow) is located in temporal retina in marmoset and human.

Although the retina's neuronal architecture is comparable among different vertebrates, PRs' quantity and distributions vary considerably (80,713,836). PRs patterns, also called mosaicism, have been refined during evolution to fit the animal's unique behavior (diurnal or nocturnal) and its lifestyle (prey or predator) in order to maximize the efficiency of the visual information to the specific needs of the species and their natural environment (21,22,828,837). Mouse's ability to distinguish color is restricted to the ventral retina (838). Furthermore, mice lack the macula, which is present only in humans and some other non-human primates (16,839,840).

These differences can cause bias and difficulty when modeling retinal diseases, particularly when the primary affected cells are cones, such as MDs (774).

Moreover, PR's anatomy differs from the human one. The structures called calyceal processes located at the TZ of human PRs are not present in mice. Proteins such as USH1G, USH1C, MYO7A,

CDH23, and PCDH15, which are mutated in USH, colocalize with caliceal processes at the base of the CC of human PRs (841). The mechanisms underlying PRs degeneration in USH type I (USH1) remain largely unknown because mutant mice lacking these proteins do not display any retinal degeneration. Several animal models of USH have been created after the spontaneous mutations in the mouse Ush1g have been identified (842). Each one of these mice, including $Ush1C^{-/-}$ and $Ush1d^{-/-}$ successfully recapitulates the deafness, vestibular dysfunction, and hearing loss observed in patients, but everyone fails to show RD even though some of them show signs of a mild perturbation of the visual function (843–846).

Another interesting case refers to the eyes absent (*EYA*) gene family, which is a group of TFs involved in the development and DNA repair (559,847–849). Four known *Eya* genes exist in vertebrates (*Eya1-Eya4*). They have been initially discovered in *D. Melanogaster* to cause severe embryonic defects and absence of eyes (847–850). Only EYA1 has been linked to disease in humans, where it seems to interact with SIX1. It causes the branchio-oto-renal (BOR) syndrome, characterized by congenital cataracts and ocular anterior segment anomalies (851). $Eya1^{ED}$ mice contain a damaging deletion in Eye1 and show severe skeletal and craniofacial defects, absence of kidneys, parathyroid glands, thymus, and ears, but no sign of ocular defects (852). Similarly, $Eya3^{-/-}$ mice and zebrafish show no effect on ocular or brain development and morphogenesis (850).

EYS is a ciliary gene frequently mutated in arRP in humans (389,853). It has a homologous in Drosophila, while in mice, and more in general in rodents, Eys is disrupted and has accumulated a large number of mutations causing multiple reading-frame shifts (854,855). It is one of the few human retinal genes completely absent in rodents, highlighting the genetic discrepancy between humans and mice in the retinal context.

Finally, mice have a short life span and mostly live all life in a pathogen-free environment. These parameters cannot be underestimated, particularly in the context of those diseases, such as AMD, diabetic retinopathy, glaucoma, and other complex diseases, where aging, immune system, epigenetic and environmental factors are crucial (493,711).

On the other hand, work over many decades has overcome some limitations, improving laboratory mouse models for human aging (856,857). It has been shown that mice can develop impairments and diseases during aging, just like humans (741,858). Furthermore, this age-related phenotype is attributable to genetic factors, which are mostly conserved among vertebrates (859). This knowledge made it possible to manipulate these factors in mice (856,859). Now are available mouse models of premature aging diseases such as Progeria and Werner syndrome and age-related disorders such as Alzheimer's disease, diabetes, and AMD (608,860–862).

However, such research has focused chiefly on the genetic basis of aging, and we are still far from fully understand the aging process and the complex mechanisms involved (857).

More work and better tools are necessary to unveil pathophysiological pathways underlying age-related and complex diseases and overcome the difficulties associated with intrinsic species-related differences (863).

In this thesis, we use ko and heterozygous BMI1 mice, characterized by shortened life and age-related neurodegeneration, to investigate its role in the postnatal retina as it has been found expressed in RPCs during embryonic retinal development. We also use double and triple KO mice where the BMI1 deficiency is accompanied by the inhibition of key factors of the apoptotic process and DNA damage response to determine the molecular mechanism leading to cone degeneration.

1.7 Modeling Retinal dystrophies using pluripotent Stem Cells

1.7.1 Pluripotent stem cells: history and origins

Understanding the underlying mechanisms of human disease is essential for developing effective therapies, but this process can be challenging due to the lack of relevant animal models. The concept that animal research is a poor predictor of humans' physiology is not new (864). More than a thousand years ago, Avicenna, a Persian philosopher and scientist, considered by many to be the father of modern medicine, had declared the need to study man instead of animals. Although more or less genetically similar to humans, species-specific differences are inevitable. These differences create difficulties in transposing the results obtained during research or preclinical tests on animals to their human application, often causing conflicts resulting in clinical trial failure (865–872). Of course, replacing animal models has always been considered unthinkable for obvious ethical implications of human experimentation, at least until very recently (873).

Stem cell glossary	
Stem cell	Undifferentiated cells or partially differentiated cells that can differentiate into various types of cells and proliferate indefinitely to produce more of the same stem cell.
Cell fate	A cellular state characterized by a unique combination of stable gene expression patterns and their downstream functional effects. Also referred to as 'cell type', 'identity' and 'terminal differentiation'.
Cell specification	The process by which a cell acquires its fate. This process can have several steps, or intermediates, before reaching the final stable gene expression state that defines a given cell fate.
Commitment	The point during specification when a cell becomes constrained to execute a specific gene expression profile (often repressing alternative fates). This event may greatly precede the full gene expression state that characterizes a cell fate.
Stem Cell Potential	The range of fates available to a cell.
Progenitor	A proliferative cell that can give rise to one or more distinct cell fates.
Precursor	A non-proliferative (i.e. postmitotic) cell that does not yet express all the characteristics of a mature cell type. This includes cells that have not committed to a fate.
Embryonic Stem Cell (ESC)	pluripotent stem cell derived from the inner cell mass of a blastocyst,
induced Pluripotent Stem Cell (iPSC)	pluripotent stem cell generated from a somatic cell
Reprogramming	The process that involves the conversion of a somatic cell into an iPSC

Table 1: Stem cell glossary

The term stem cell appears for the first time in the scientific literature in 1868 in the works of the renowned German biologist Ernst Haeckel (874,875). Haeckel, who was one of the major supporters of Darwin's theory of evolution, initially used the term "Stammzelle" (stem cell in

German) to indicate the ancestral single-celled organism from which all the more complex organisms evolved according to his theories (874,876). Later, focusing mainly on embryology, he used the same term "Stammzelle" to indicate the fertilized egg, which can generate all the mature organism cells (877).

Subsequently, in 1892 Haeckel and Boveri independently define some cells originating from the zygote with the term stem cells. Boveri took up and expanded Haeckel's definition of stem cells as a fertilized egg, extending it to other cells generated later in the differentiation process (878). On the other hand, Haeckel describes for the first time the asymmetric division that characterizes stem cells (879).

Doctors and scientists have always tried to understand the tissue generation process. Two discoveries that occurred in the early 1960s revolutionized the understanding of how the organism repairs and develops. Between 58 and 62, Gurdon successfully conducted the first nuclear transfer experiments in frogs by transferring a nucleus of an intestine epithelial cell in a denuclearized egg cell, thus proving that it could give life to a whole organism (880,881). He demonstrates for the first time that cellular specialization is reversible. Simultaneously, Till & McCulloch discover that the tissue repair process is carried out by a limited group of cells capable of self-renewal and differentiate into different types of more specialized cells (882). This was elegantly demonstrated by showing that a bone marrow transfer was sufficient to save mice treated with lethal doses of radiation and by observing that the injected cells were capable of clonal expansion *in vivo* and *in vitro* (882–884). These cells were later baptized with the name hematopoietic stem cells (885,886).

Thomson and its colleagues have brought another significant advance in the field. They discover that hESCs can be isolated from the embryo, and these cells have an illimited self-renewal capacity, and therefore are not subject to senescence, besides being capable of generating any cell in the organism (887). This has led to the need to classify cells based on their potency, which refers to their varying ability to differentiate into specialized cell types (Figure 34). Cells with higher potency can generate more cell types than those with lower potency (888,889). Totipotent cells can differentiate into all adult organism tissues, including extraembryonic tissues such as the

placenta; this state is specific to the zygote (890,891). The state of totipotency is unstable, and it is already lost at the blastocyst stage. The blastocyst's inner cell mass cells are the ESC cells, which are pluripotent and can form all the organism cells (892). PSCs are also transient and restricted to the first part of embryonic development. These cells lose part of their replication and differentiation capacity along the developmental process and become progenitor cells. Both progenitors and adult stem cells, responsible for regenerating tissues in the adult organism, are considered multipotent (893,894). These often have specific names; hematopoietic, mesenchymal, and neural stem cells are some examples. These cells have a limited capacity of differentiation, which is specific to their *niche* (886,895,896). Finally, we have the unipotent cells, which have lost all proliferative and differentiation capacities. These include somatic cells, which are mature and fully differentiated, and precursor cells, which are not entirely differentiated but are already committed to a certain fate.

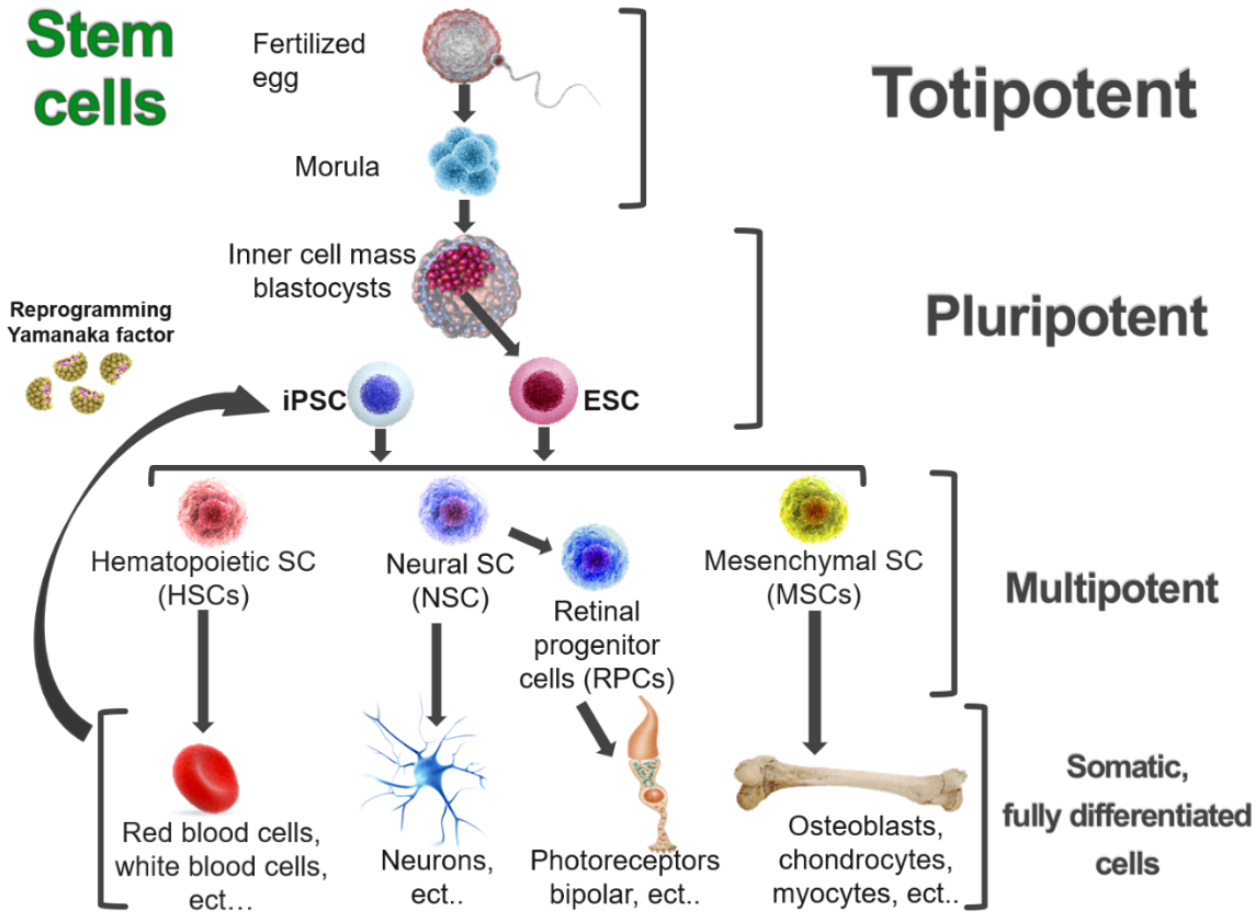

Figure 34: Stem cells types and their differentiation potential

1.7.1.1 Induced Pluripotent stem cells

For a long time, one of the *dogmas* of biology has been that these somatic cells have lost the information necessary to follow other fates, and the specialization process was irreversible. Cloning experiments made by Gurdon have been reproduced in other species, including mammalian, and altogether have paved the way for what is arguably the most significant medical discovery of our century. Yamanaka and Takahashi demonstrate that in both mice and humans, somatic cells can be reprogrammed back to a pluripotent state, similar to that of ESC, by reintroducing a limited number of TFs (897,898). These genes were named reprogramming factors, or Yamanaka factors, and were initially reduced to POU5F1/OTC4 (Octamer binding transcription factor-4), SOX2 (Sex determining region Y-box 2), KLF4 (Kruppel Like Factor-4), and MYC (Figure 35). This discovery introduced the concept of iPSCs. IPSC's use overcomes many ethical problems related to the use of ESC and human embryos, creates new opportunities to study diseases, and opens new frontiers for diagnostic procedures, drug screening, and clinical practice (899,900). The enormous impact of this discovery led to the re-writing of biology textbooks and the establishment of new research fields. Many advancements have been made since then on various fronts. New reprogramming factors capable of substituting the original ones have been discovered, reducing the number of factors required, or improving efficiency or safety (901–903). Reprogramming techniques were also ameliorated (900). Nowadays, we have the availability of small molecules able to replace some of the reprogramming factors or to improve the overall reprogramming efficiency (904–910), integration-free vectors (911–914), miRNA, and reprogramming factors in the form of mRNA or proteins (915–918), all of which reduce or eliminate the risks related to the introduction of exogenous DNA (Figure 35). More recently, the use of CRISPR-Cas9-based gene activation (CRISPRa), which offers direct targeting and expression of endogenous genes instead of introducing exogenous ones, has pushed the concept of integration-free gene expression modulation to the extreme (919).

Some significant advancements in stem cell biology comes from analyzing the differences between mouse ESC (mESCs) and hESCs. mESC can form germline chimeras while hESC are not. The discovery that mouse epiblast stem cells (mEpiSCs), which can be isolated from the post-implantation epiblast, have similar characteristics to hESc have lead to the proposal that exists

more than one pluripotent state in the epiblast (920,921). These two pluripotent states are called naïve (or ground) and primed states, representing the distinct cellular identities of pre-and post-implantation epiblast cells, respectively (922). These two stem cell states possess distinct epigenetic signatures, and unlike primed SCs, naive SCs do not yet show the deactivation of the x chromosome and have a more pronounced relaxation of the chromatin. The factors required to maintain these two cell types in culture vary significantly. *In vitro* culture of Naïve SCs require serum / LIF or 2i / LIF medium (two inhibitors (i) for MEK and GSK3) along with leukemia inhibitory factor (LIF). Instead, primed SCs require Activin and FGF signaling (920,921). To date, we are able, by adapting the reprogramming process, to directly derive both these states starting from somatic cells of different species, just as we are able to pass from one state to another simply by varying the culture conditions and factors (small molecules and proteins recombinants) to which they are exposed (923,924). Reprogramming techniques have also been successfully used to drive a somatic cell's cell fate directly into a different one without passing through the pluripotent state, in a process called transdifferentiation or lineage reprogramming (925–927).

Since their potential was revealed, iPSCs have been widely used in clinical and research studies, including regenerative medicine, drug discovery, drug cytotoxicity, and, last but not least, disease modeling (900). iPSCs have sparked new hope for hitherto incurable diseases and tissue regeneration. Stem cells first entered the clinical stage in 2016, and now in 2021, there are more than 5,000 registered clinical trials involving stem cell research, which are rapidly moving through the process (715,928). Among the organs involved in these trials, the eye is undoubtedly one of the most targeted due to a series of favorable characteristics that make it particularly fit for this purpose, especially in this initial proof-of-concept stage. Notably, they are immune-privileged and have a series of natural barriers, including the blood-retinal barrier (BRB) and the blood-aqueous barrier (BAB), which isolate them, limiting the possible spread of transplanted cells (929). Moreover, unlike the other organs, the eyes are easily accessible and can be monitored with non-invasive techniques (930–932).

1.7.1.1.1 Generation, characterization, and application of iPSCs

iPSC technology generates new means to investigate inherited diseases, such as diabetes, neurological diseases, and retinopathies, by directly looking to patient-specific cells generated *in vitro* (318,933–936).

For this purpose, patients' somatic cells, which carry the patient's genetic information, can be used to generate patient-specific iPSCs (933). These somatic cells can be obtained with minimally invasive techniques, as skin biopsy, blood, or even urine samples are sufficient as a starting material for iPSC generation (458,937).

A typical pipeline requires several stages:

1. isolation and expansion, of patient's somatic cells (1-15 days),
2. reprogramming in iPSCs (approximately 30 days),
3. collection and quality control of clones (approximately 30 days),
4. expansion of selected clones (variable according to the desired initial quantity of cells),
5. differentiation (variable according to the protocol used and the level of maturation required).

iPSC generation is conducted through the reprogramming process extensively summarized by numerous reviews (900,938,939). The clones are then selected through strict quality control, including morphology, expression of pluripotency genes, karyotype, and the ability to differentiate in all embryonic layers (888,892,940,941). iPSCs may harbor different types of

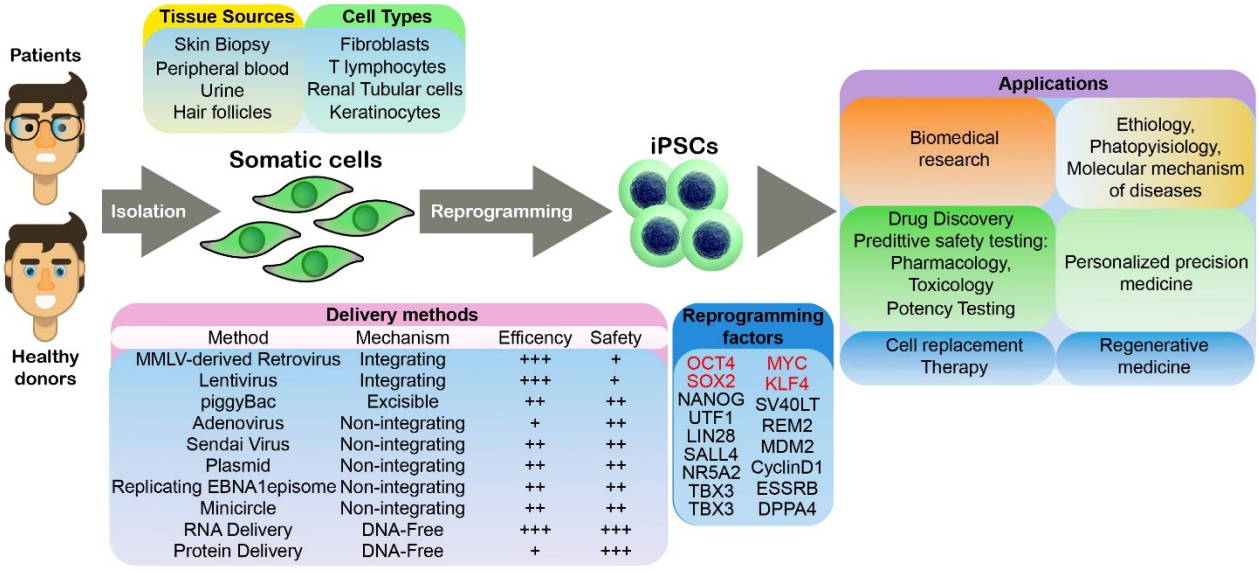

Figure 35: Generation and applications of iPSCs

genetic variations such as single nucleotide variations (SNVs), subchromosomal copy number variation (CNV), and including aneuploidy (417,942–944). These variations can be introduced into the iPSCs from different sources during their generation and maintenance (944). WGS of the parental somatic line and the clones are generated and highly advisable to determine if any genetic abnormalities occur during these processes. It is also highly advisable to carry out periodic quality controls, including WGS, in long-term maintenance cultures and batches of differentiated cells (945). Rigid quality controls (QCs) are necessary for iPS cells intended for use in clinical practice to ensure their safety, and they are also essential to ensure the authenticity of the results and absence of bias in the context of disease modeling and drug screening (940,946).

iPSCs are generally not used as they are, apart from rare cases such as studying their biology and pluripotency mechanisms (900,947). This is particularly true in the clinical context, where their residual presence represents a potentially life-threatening risk (936,943). Once the iPSCs are generated and verified, the next step is to differentiate them in the desired cell type.

PSCs' fate needs to be driven into the desired cell types in order to exploit their potential. This process is generally achieved by mimicking the molecular signaling pathways identified by studying embryonic development of the tissue/cells of interest (948,949). Differentiation strategies and protocols are tailored on a case-by-case basis according to the desired cell type, their maturation level, and the required purity grade (936). It is, therefore, a highly variable process that is generally multistep and time-consuming. Today, hundreds of differentiation protocols have been published to generate the most diverse cell types in the body (512,950).

1.7.2 Generation of retinal cells from Pluripotent Stem Cells

As previously discussed, retinal degeneration arises from the loss of PRs or RPE, which is the leading cause of irreversible blindness with limited effective treatment options. iPSCs represent an excellent platform to investigate normal and pathological retinal development and mechanism of degeneration and are a valuable source of retinal cells for clinical applications and drug screening (951). The generation of specific somatic cells from pluripotent stem cells can be obtained with different strategies.

Somatic cells can be obtained by spontaneous differentiation of stem cells upon withdrawal of the factors necessary to maintain the pluripotent state. Spontaneous differentiation generates several different cell types belonging to the three embryonic sheets. These cells can be isolated, passed, and maintained in culture and purified by repeated manual isolation and passaging. RPE cells are the retinal cell most well-characterized and easiest to obtain by PSC differentiation. RPE cells were initially obtained with these techniques without adding particular factors to drive their fate. Of course, this type of strategy has numerous limitations, such as low efficiency and high variability. Furthermore, many cell types, such as PRs, cannot be obtained with these techniques.

The design of protocols to correctly drive the stem cells' fate in the wanted direction requires an excellent knowledge of embryonic development and of the developmental genetics of the cells and tissue of interest.

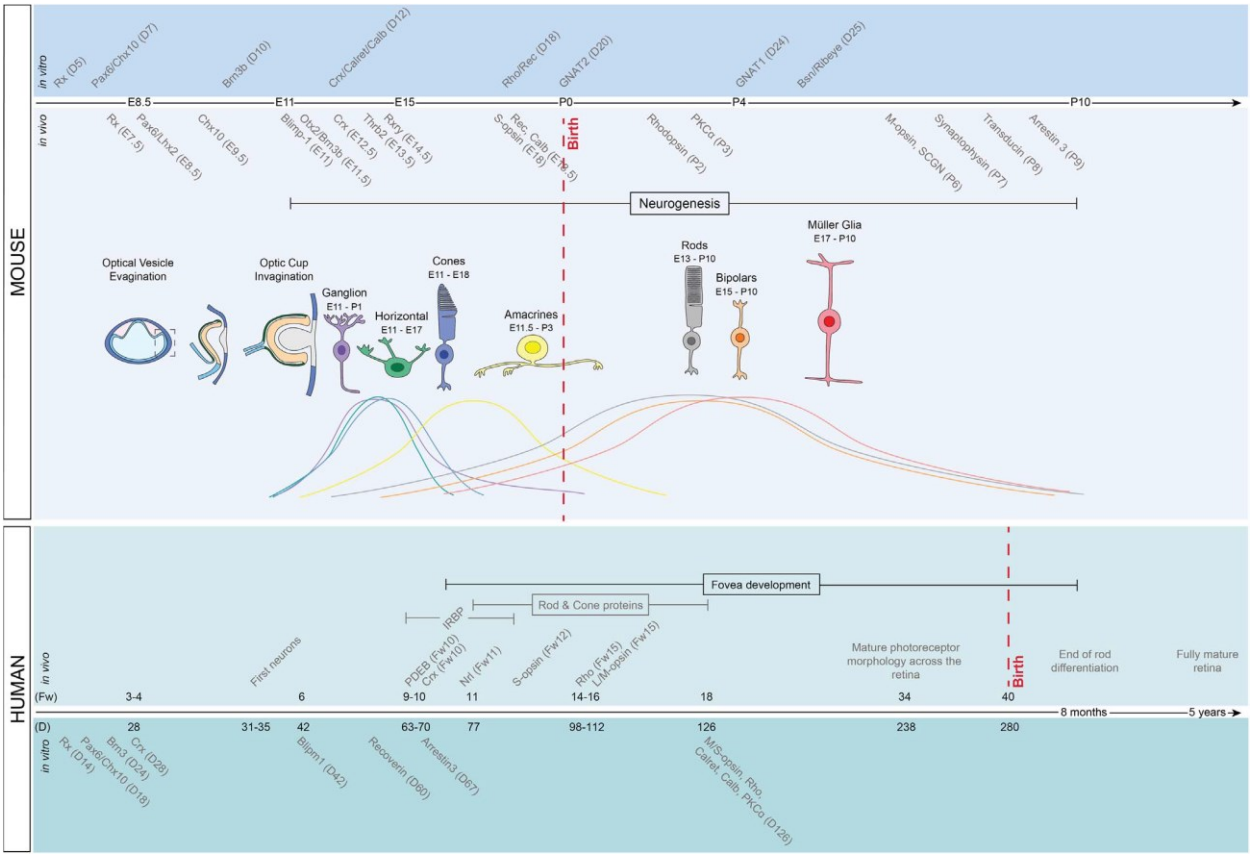

Figure 36: Comparison between in vivo and in vitro retinal development in human and mice (1207)

The use of factors capable of stimulating the expression of specific genes or signaling pathways has vastly improved differentiation efficacy and permitted the generation of specific cell types otherwise impossible to obtain by spontaneous differentiation.

RPE cells, retinal progenitors, PRs, and other retinal cells can now be generated from ESCs or iPSCs by mimicking developmental processes in a stepwise fashion *in vitro (Figure 36)* (952–954).

1.7.2.1 RPE cells differentiation

RPE cells have been first generated from PSCs by spontaneous differentiation consequent to the removal of bFGF from the culture medium. Protocols to differentiate human iPSC lines into RPE cells were successfully established by multiple groups (955–961), and similarity between RPE generated using this strategy, and human fetal RPE, was determined by gene expression profiling (935,958). With these basic protocols, the initial pigmentation typically appeared 25-30 days after the start of differentiation but can vary considerably between batches, and their quantity was not sufficient for their isolation and purification up to 60–90 days after bFGF depletion. Though these populations of RPE cells have hexagonal geometry, pigmentation and are positive for markers such as Best1, MITF, ZO-1, and PDF, and show phagocytosis potential comparable to fetal-derived RPEs, they begin to express hallmarks of terminally differentiated RPE, such as RPE65, only after eight months in culture (935,954,957).

A significant improvement in the RPE cell generation was obtained by adding nicotinamide (NIC) and Activin A to the PSC culture (78,962). This method significantly increases the generation of RPE cells by enabling the formation of abundant clusters of pigmented cells only after 40 days in culture. Additional factors introduced as retinal-inducing factors are noggin, RA, and sonic hedgehog (963–966). More recently, emulating RPE development cues proved useful for generating rapid RPE-directed differentiation in as little as 14 days. Homogenous cultures of RPE cells can be produced in 20 days showing an accelerated differentiation and morphogenesis compared to their *in vivo* development (956,967,968). This was obtained by adding IGF1, Dickkopf-related protein 1 (Dkk1), Vasoactive Intestinal Peptide (VIP), and FGFR1 inhibitor (SU5402) to the previously used ingredients (noggin, bFGF, NIC, and Activin A).

Although easily obtainable, most efficient RPE differentiation protocols rely on complex, stepwise treatments and the addition of growth factors. The use of small molecules chetomin (CTM), an inhibitor of hypoxia-inducible factors, allowed upregulating RPE markers MITF, OTX2, and PMEL17. Its combination with NIC efficiently induces directed-RPE differentiation in multiple hESC and hiPSCs. Typical RPE morphology is achieved within two weeks, and pure monolayers of functional RPE can be obtained following a single passage (969).

All these researches permit the *in vitro* generation and deep characterization of PSC-derived RPE, which have been efficiently applied in RDs modeling and drug screening. Furthermore, they laid the groundwork to develop new therapies for the treatment of MD due to RPE dysfunction, with more than 16 clinical trials between phase I-II at the end of 2020 (970,971).

1.7.2.2 Neural retina and photoreceptors differentiation from PSCs

Unlike RPE, neural retina cells are more difficult to obtain and generally require more complex protocols. Pure populations of a single retinal cell type are challenging to obtain since their differentiation process is more sensitive, finely regulated, and dependent on cell-cell interactions. Furthermore, neural retina cells, such as PRs, are post-mitotic and can only be amplified at early differentiation steps when their fate is not entirely determined yet. During the early development of the neural retina, RPCs proliferate, increasing the progenitor pool size. When they reach a certain maturation level, RPCs begin to divide asymmetrically, giving rise to different cell types, which can adopt several fates during development. Later, a highly coordinated differentiation process driven by intrinsic and extrinsic factors permits the generation of the seven different mature cell types of the neural retina and all their sub-types in the proper proportions (972,973).

The generation of RPCs is mandatory in almost all protocols for generating neural retina cells and can be achieved by aggregating stem cells into spheroids, in adherence or suspension, or through highly packaged adherent single layer cultures.

1.7.2.2.1 The origins of the retinal differentiation protocols

One of the first successes in generating neural retina cells has been carried out from mouse ESCs in a mixed system starting from a serum-free floating culture of embryoid bodies (SFEB system), which are then plated on polylysine coated dishes during differentiation (952). Following a

multistep process starting with the anteriorization of neural fate through the inhibition of Wnt and Nodal signaling pathways using Dkk1 and Lefty-A recombinant proteins, they were able to generate RPCs. They are subsequently pushed to differentiate into Rax+ cells by treatment with activin-A and serum with an efficiency of around 16%. These cells did not efficiently differentiate into PR precursors unless they were co-cultured with cells derived from an embryonic mouse neural retina at E17.5. Interesting only Rod-specific markers were observed, and there was no evidence of cones' presence (952).

One year later, another group successfully generated PRs from hESCs and hiPSCs using a similar strategy based on sequential specification and intermediate SFEB step (974). As forebrain development requires inhibition of both WNT and BMP pathways, this time, DKK1 has been associated with Noggin, a potent inhibitor of BMP, in the presence of IGF1, bFGF, and proneural medium supplements (B27 and N2). Analysis of retinal markers revealed a preferential presence for ganglion and amacrine precursor cells, while immature PRs' markers, CRX, and NRL were expressed in approximately 10% of cells (974). However, less than 0.01% of the cells expressed mature PRs' markers, S-Opsin, and RHO (974).

Also in this case, PRs generated from iPCS or ESC cells did not fully maturate *in vitro*. Their final differentiation could be facilitated through transplantation into the mouse retina subretinal space, where they could partially restore light response in a cone-free $CRX^{-/-}$ mouse (975).

Subsequently, progressive improvements have been made to the protocol. Takahashi and Sasai Labs differentiated Mouse and monkey ES cells into Crx + photoreceptor precursors from Rx + retinal progenitors by treating with a Notch signal inhibitor (953,954).

Further application of FGF, Shh, taurine, and RA allowed further maturation into rod and cone PRs. In these conditions, CRX+ cells were identifiable after 90 days in culture, and their number increase reaching about 10% and 20% after 120 and 170 days, respectively. Rod PRs (RHO+) begin to be observed at day 130 to reach about 9% after 200 days (953). Cone PRs (S-Opsin+ and L/M-Opsin+) could also be found close to RHO+ cells. Although time-consuming and inefficient, they have brought significant progress towards the production of more mature cells and the use of xeno-free culture conditions (954).

Other groups have used the same principle to design a chemically defined culture medium with the intent of lower costs, increasing reproducibility by reducing variability from batch to batch, thus increasing the potential for a possible clinical application. Non-biological small-molecules Y-27632, CKI-7, LDN193189, and SB-431542 have been efficiently used to inhibit Wnt, Nodal, and BMP4 downstream pathways SMAD and β-Catenin to promote retinal differentiation (954,976). Small molecules such as Dorsomorphin and XAV939 have been used instead of NOGGIN and DKK-1 to differentiate human iPSCs into retinal progenitors (977,978). Although these protocols have brought great progress towards the formation of xenon-free chemical-defined media, they have generally given lower yields than the protocols based on DKK1, Leftly-A, and Noggin(979). Following the same basic principle, many other groups have developed differentiation protocols making essential changes that have made it possible to improve the original protocol, speed it up or enrich the desired subpopulations (960,980–985).

A considerable improvement was made by the 3-stage differentiation protocol, which combines previously published strategies. With this protocol, hESCs and hiPSCs could be differentiated into about 16% of CRX + cells expressing late-stage differentiation markers (RHO, OPN1LW, and OPN1SW) already at day 45, which represents an enormous acceleration of the differentiation process (983).

Interestingly, the control cells treated only with N2 and B27 showed retinal differentiation, although less effectively than the complete medium. This proves the importance of these two components in the differentiation and survival of retinal cells. N2 and B27 are chemically-defined blood serum substitutes containing growth factors that promote neuronal cell survival and multiple hormones, such as insulin and progesterone (986–988).

Differentiation of retinal progenitors into PRs has been favored by adding specific factors such as FGF1 and FGF2, T3, and Shh, each one in a specific time window during the 2D step (985,989,990). These components were usually accompanied by the addition of taurine, RA, N2, and B27 supplements. Yanai et al. have generated more than 80% of CRX + cells after 17 days of culture using a similar 3D / 2D stepwise protocol and focusing on EBs' size variation in the 3D step. This

was obtained using EBs of an optimal starting size (200 µm composed of about 1000 cells) and their subsequent seeding on Matrigel with the addition of Taurine, FGF2, and T3 (985).

A 3 step method was also adopted from David Gamm's group, which added a third step of culture, allowing the selective sorting of self-forming neuroepithelial structures (977). Following differentiation of iPSC and ESC-derived EBs in cell suspension, retinal spheres were plated on laminin-coated plates. Forming neuroepithelial structures were manually picked to be cultured again in suspension. They observed that these neuroepithelial structures' gene and protein expression profiles reflect a differentiation state close to the optic vesicle (OV) stage of human retinal development (977). Authors also observed that in some, but not all, iPSC lines, early endogenous expression of DKK1 and NOGGIN was sufficient to induce the formation of OV-like structures without small molecules' addition antagonizing the BMP, TGFβ, and Wnt pathways. These results point out that cell lines' intrinsic characteristics may significantly affect the differentiation process.

These floating OV-like structures continue to differentiate towards the PR lineage, showing expression of CRX and RECOVERIN between days 45-60 of culture and RHO or S-opsin after 100 days (977,991).

1.7.2.2.2 3D organoids

In the same period, the Sasai Group published several articles that present an alternative protocol that removes the 2D step in adherence and focuses on a purely 3D and suspension culture (76,992). Sasai's laboratory is the pioneer in 3D retinal organoids, which were obtained primarily with mESCs but quickly reproduced with hESCs and then in hiPSCs (76,992,993). Under these conditions, starting from both mouse and human ES, they were able to replicate the first step of retinal morphogenes, including the evagination of the distal portion in the RAX-expressing areas, forming structures similar to optic placode. Consequently, the invagination of these structures leads to the generation of stratified neural retinal tissue reminiscent of the typical bilayered embryonic optic cup, with the inner part differentiating into the neural retina and the outer layer towards the RPE lineage. The process closely mimics the complex tissue interactions of *in vivo* retinogenesis. They elegantly demonstrate that optic-cup morphogenesis relies upon an

intrinsic self-organizing program that involves a stepwise and domain-specific regulation based on local epithelial properties. To generate retinal organoids, hESCs dissociated into single cells were reaggregated in low-cell-adhesion V-bottom 96-well plates at a density of 9,000–12,500 cells/well in retinal defined differentiation medium containing ROCK inhibitor (Y-27632). Human ESC needs the addition of WNT inhibitor (iWR1e) to counteract the caudalising signals caused by the high KO serum level necessary for their differentiation. Following a few days of culture, Matrigel is added to the culture medium and acts as a basement membrane to stimulate epithelial fate and structural development.

Stimulation of the SHH pathway by the smoothened agonist (SAG) in the presence of FBS improves the efficiency from 30-70% to more than 70% of total cells expressing early retinal marker, RAX at day 18 (992). These cells further differentiate into CHX10+/PAX6+ progenitors. Treatment with the glycogen synthase kinase 3 (GSK3) inhibitor CHIR99021, which acts as a WNT agonist, during days 18-21, when cells have already committed to a retinal fate, allows the generation of MITF+ RPE cells without disturbing CHX10 expression in the distal portion of the retinal epithelium. This process closely mimics the *in vivo* development of the optic cups. In these conditions, CRX+ PRs can be observed within neural rosettes by day 35, RECOVERIN expression is observable by day 60, while rods specific markers NRL and RHO start to be observed by day 120 (992).

The same group also published different modifications to the protocols to recapitulate complete eyecup morphogenesis or maximize PRs genesis. Interestingly, the step-wise induction-reversal method generates tissue aggregates with RPE at the margin of a central-peripherally polarized NR (994). They improve NR differentiation using timed BMP4 treatment at a low concentration between days 18 to 24. They also found that further inhibition of GSK3 and FGFR induced the transition from NR tissue to RPE and that removing this inhibition facilitated the reversion of this RPE-like tissue back to the NR fate (994).

Further adaptation and combination of recently published differentiation protocol could generate a higher yield of 3D optic cups. In order to improve the protocol, initial SFEBs cultured in the presence of N2 were transferred in Matrigel-coated dishes instead of laminin-coated ones.

Treatment with serum, taurine, and RA in specific time windows during the floating cultures promoted cell survival and differentiation, allowing the formation of 3D retinal cups that seemed properly laminated. Besides showing that in these conditions, they were able to obtain advanced PRs maturation with OS formation in 180 days, they also conducted patch-clamp recording demonstrating, for the first time, that PSC-derived PRs were capable of responding to light (993).

Unfortunately, these retinal organoids are generated at very low efficiency and depend on their successful dissection, one of the key yield-limiting points. This operation requires highly specialized personnel and generates enormous variability between various manipulators. Emitting dissection compromises the retinal identity of organoids with the overtake of non-retinal structures (995,996).

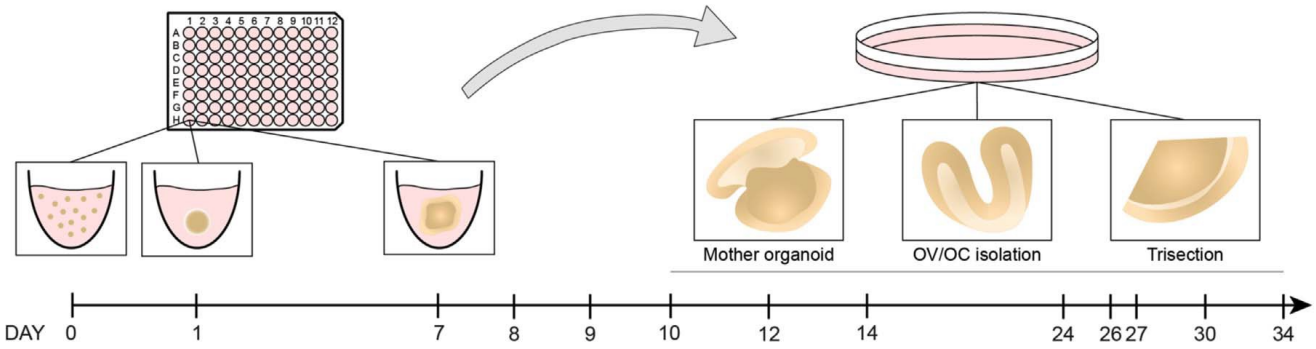

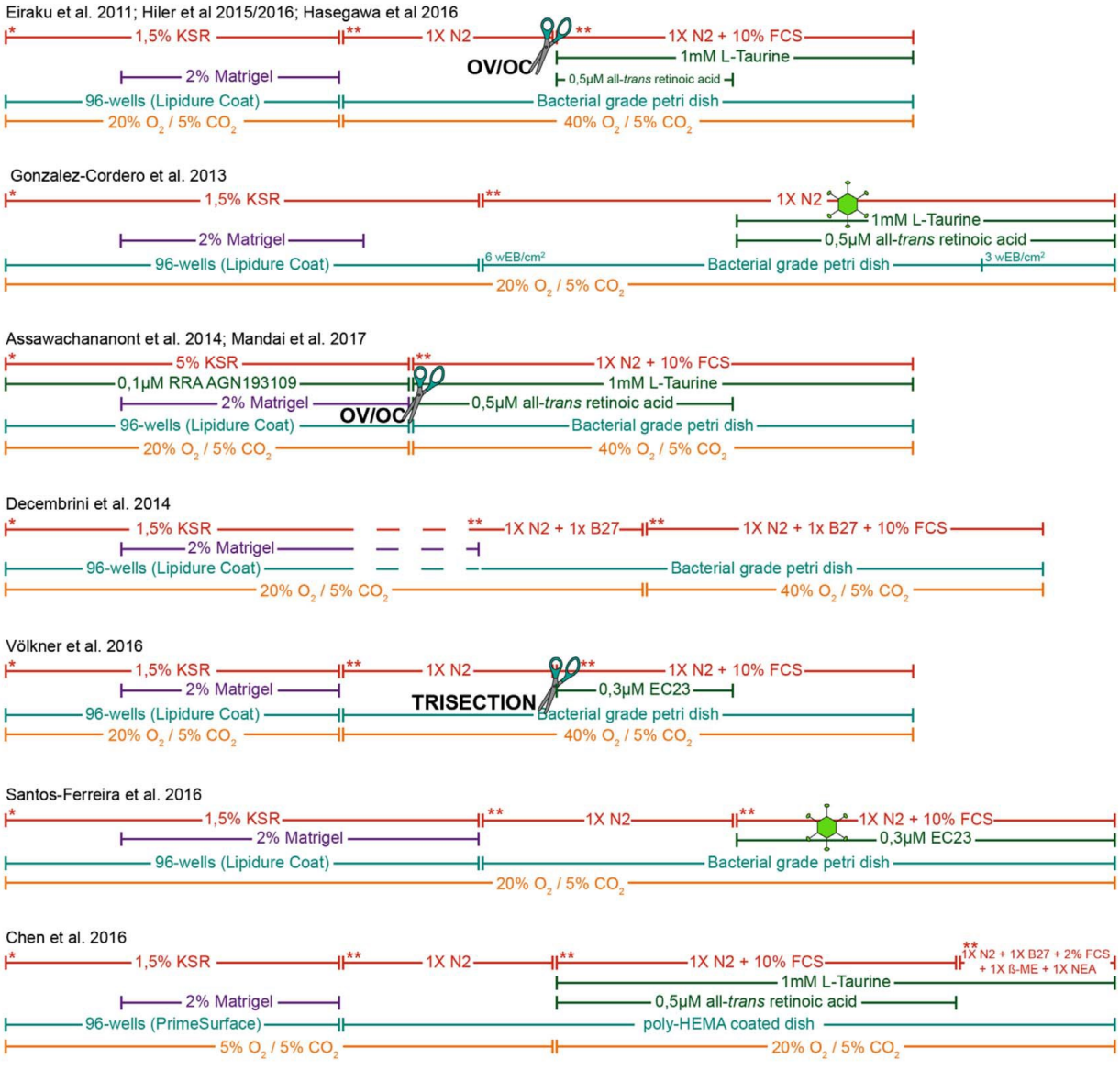

*RDM: GMEM + 1X NEA + 1X NaPyr + 1X ß-Me **RMM: DMEM/F12 + 1X P/S

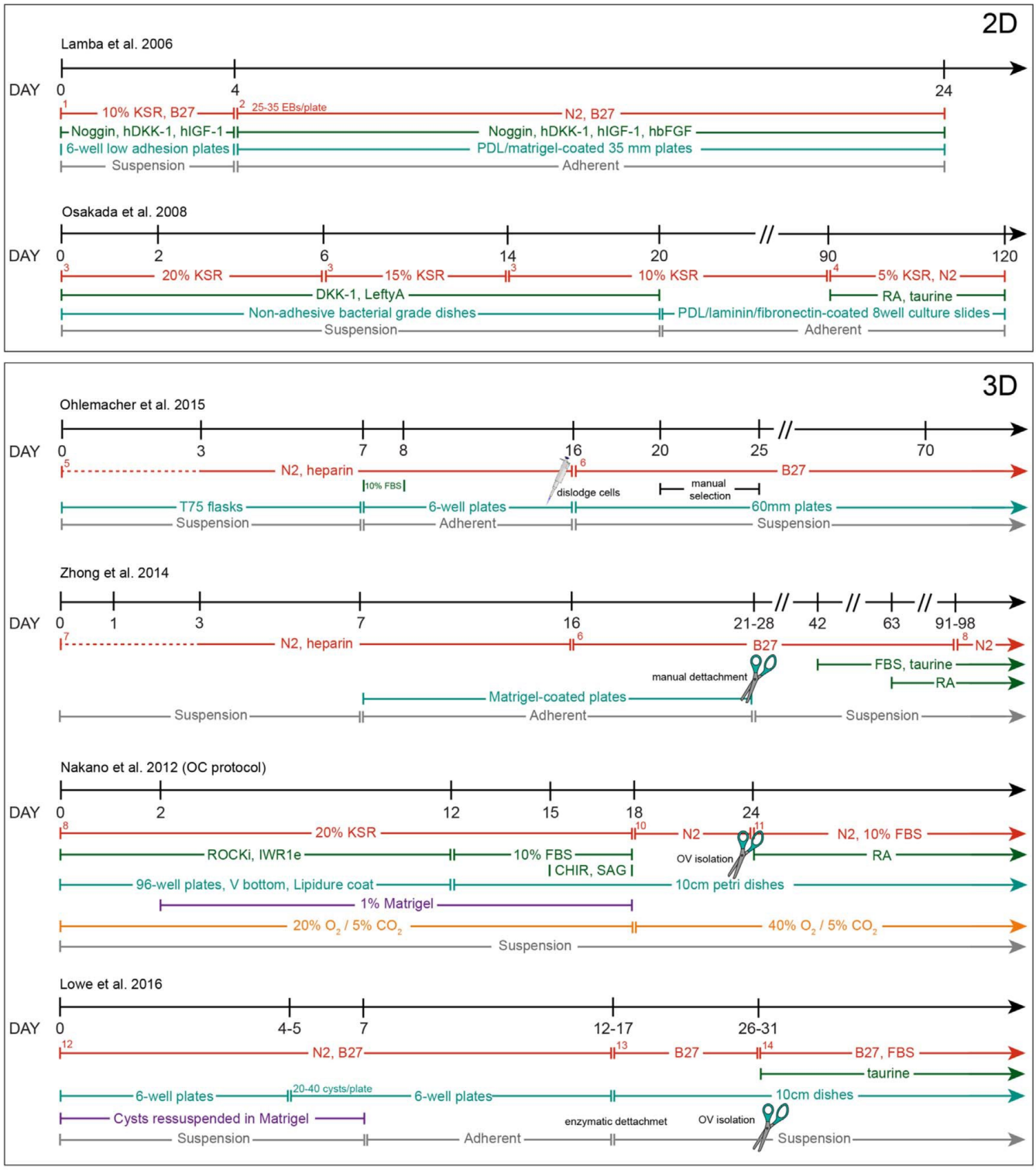

1 in DMEM/F12, 10% KSR, B27, 1ng/mL noggin, 1ng/mL Dkk-1, 5ng/mL IGF-1; **2** in DMEM/F12, B27, N2, 1ng/mL noggin, 1ng/mL Dkk-1, 5ng/mL IGF-1; **3** in DMEM/F12, 0.1mM B-Me, 0.1mM NEAA, 2mM L-glutamine, 20, 15 or 10% KSR; **4** in GMEM, 5% KSR, 0.1mM B-Me, 0.1mM NEAA, 1mM pyruvat, 1uM RA, 100uM taurine, N2, Pen/Strep; **5** gradual replacement of mTeSR1 with NIM = DMEM/F12, 1%N2, 1X NEAA, 2mg/mL heparin; **6** in RDM = DMEM/F12 3:1, 2% B27, 1X NEAA, 1% Pen/Strep, 1% antimycotic; **7** gradual replacement of mTeSR1 + blebbistatin with NIM = DMEM/F12, 1% N2, 1X NEAA, 2ug/mL heparin; **8** in RDM = DMEM/F12 3:1, N2, 1X NEAA, 1% Pen/Strep, 1% antimycotic; **9** in retinal diff medium = GMEM, 20% KSR, 0.1mM B-Me, 0.1mM NEAA, 1mM pyruvat, Pen/Strep; **10** in maturation medium 1 = DMEM/F12 Glutamax, 1X N2, Pen/Strep, Fungizone; **11** in maturation medium 2 = DMEM/F12 Glutamax, 1X N2, 10% FBS, 0.5uM RA, Pen/Strep, Fungizone; **12** in N2B27 medium = DMEM/F12+Glutamax and neurobasal medium 1:1, 0.5X B27, 0.5X N2, 0.1mM B-Me, 2mM Glutamax; **13** in medium 2 = DMEM/F12 3:1, 2% B27, 1X NEAA; **14** in medium 5 = DMEM/F12 3:1, 2% B27, 10% FBS, 100uM taurine, 1X NEAA, 2mM Glutamax.

Figure 37: Comparison between the main protocols to generate retinal cells from PSCs (1207)

Völkner et al. noticed that only a part of the neuroepithelium evaginated to form identifiable optic cups. He provides a protocol for unbiased trisection of the neuroepithelium early without affecting retinal cell differentiation (997,998). This protocol produced high numbers of large, stratified organoids committed to retinal fate (969,997,999).

Transcriptional analysis has shown that at day 37, CRX+ PRs appear in the basal or middle part of the neural retina and migrate to the apical side by day 67 (1000). CRX+/RECOVERIN+ PRs are firstly observed around day 50 and increase at day 120. NRL is first observed at day 70 and is robustly express in many CRX nuclei at day 90. Minimal S-opsin and no RHO or L/M-opsin were present until day 125-150 (992,1001). Retinal organoids with healthy PRs could be maintained in long-term culture. In these conditions, PRs' OSs start to be observable around day 160 and reached complete maturation at day 300 (993,999).

Retinal ganglion and amacrine cells start to be detected by day 37, while horizontal, ON-bipolar, and Müller glial cells appear in small numbers after 90 days in culture. The transcriptome profile, by RNA-seq, of developing human PRs was remarkably concordant with mRNA and immunohistochemistry data available for the human fetal retina, although the expression of many targets of CRX, including phototransduction genes, were exhibiting a significant delay (1000).

1.7.2.2.3 Further advancement in retinal differentiation protocols

With the idea of accelerating the differentiation process and reducing exogenous factors, Reichman et al. developed a retinal differentiation protocol that bypasses the EBs step. They have shown that human iPSCs in the absence of FGF2 allowed the endogenous production of DKK1 and NOGGIN, and the addition of N2 was sufficient to generate both RPE cells and self-forming NR-like structures in less than 15 days. These structures contained retinal progenitors expressing PAX6 and RAX. The NR-like structure can be manually dissected, and the derived floating cultures can generate all retinal cell types. With these conditions, CRX + and RECOVERIN + cells start to be observed between days 30 and 40, while S-Opsin, M-Opsin, and RHO were seen only after 80 days of culture (1002).

Lanza's Lab developed a four-step protocol able to induce a synchronized differentiation process to generate a homogeneous PR progenitor population for clinical use (1003). Adherent human PSCs cultured on Matrigel were directly induced to differentiate into retinal induction medium containing N2, B27, INSULIN, and NOGGIN. After four days, the medium changed to neural media, always in the presence of N2, B27, and noggin. After PSCs differentiation into eye field progenitors (PAX6+/RAX+) at day 19, cells were detached to form neural spheres in suspension culture to be then re-plated on Matrigel-coated surfaces to allow expansion and differentiation into RPCs. Cells continually expanded and formed neural rosettes, and after four passages (~90 days) more than 90% of cultured cells were positive for photoreceptor markers (CRX, NRL and NR2E3), with less than 10% of cells expressing the cell proliferation marker Ki67. Further maturation of these cells in the presence of RA, brain derived neurotrophic factor (BDNF), CNTF and DAPT, led to the generation of rod-like PRs, expressing RHO, RECOVERIN and PDE6 α, but lacking OS. The extra-ordinary use of CNTF in this protocol is interesting, as it is historically known to antagonize rod differentiation in rodents (1004,1005)

Robin Ali group proposes a modified 2D/3D protocol (1006) based on previous publications, where densely packed PSCs are pushed towards a neuronal fate through brief removal of FGF (993,1002). Self-forming optic cups became visible between 2-4 weeks when they are detached and grown in suspension. The differentiation media used was the same as described by Zhong et al., but, differentially, the RA was maintained, at lower doses, even after the first induction period. This allowed generating a higher population of cônes (18%), showing the formation of OS and pre-synaptic structures (1006).

Another protocol implementation was obtained by improving initial neural induction from SFEBs by replacing KO serum with E6 supplemented with B27 (without vitamin A) (999).

Although extremely elegant and useful in many applications, retinal organoids have been shown to have numerous limitations on several fronts. The presence of the whole retinal cells pull, the inability to control fate towards a specific cell type, the extremely long culture times, the variability between cell lines, and finally, the requirement of highly trained technical personnel have limited their use. Many groups have been interested in developing more straightforward,

reliable, and robust protocols for producing large quantities of PRs which would have greater potential in various fields such as clinical applications and drug screening. In this sense, more simple 2D, 3D-adherent, or mixed systems bear several advantages.

In 2015 we reported a protocol for a preferential differentiation of ESC toward S-cone PRs using the human recombinant protein COCO (Dand5), a member of the Cerberus gene family expressed in the developing and adult mouse retina (Annex 1) (1007). COCO has been shown to antagonize Wnt and ligands of the TGF-beta superfamily (which includes BMP and TGFβ) and acts in synergy with IGF1 (64,67,1008). In COCO's presence, the hESC line differentiates more effectively than with noggin and Dkk1, showing the expression of early retinal and PR genes *SIX6* and *CRX*, and phototransduction gene *OPN1SW* after only 21 days of culture. Under these conditions, 60-80% of the cells corresponded to S-cone PRs, despite OS's absence. The addition of T3 resulted in a mixed M / S-cone population but an overall decrease in the differentiation efficiency. The role of T3 signaling as a molecular switch between S and L/M-Cones generation has been later confirmed by other groups (1009,1010). This protocol represents an excellent improvement towards the generation of pure cone PRs, and even today, it is the protocol that generates the highest amount of cone PRs in the shortest amount of time without resorting to genetic mutations. On day 60, the cells show 3D self-organization and generate a reasonably uniform sheet with a thickness of about 5-10 nuclei showing an apical polarization of OS / IS components. Despite this, the PRs do not reach the same maturation levels obtained in 3D floating systems at the observed time points.

1.7.2.2.4 Improvements in photoreceptors generation

Once the basis for the generation of retinal cells has been established, subsequent studies are focused on improving the efficacy and control of cell fate to generate the desired subpopulations of PRs or obtain more mature and functional cells from them.

COCO was subsequently used to enhance PR precursor differentiation's efficiency in 3D retinal organoids (1011). COCO has also been used to induce preferential differentiation of cones in suspension cultures of primary mouse RPCs (1012).

The addition of COCO in the medium used to generate 3D retinal organoids increases the total yield of PRs in the early stages of differentiation, which favors the generation of cones at rods'

expense (1013). Conversely, Taurine and RA have been shown to act in an instructive and lineage-restricted manner early in the progenitor lineage hierarchy to produce rod-restricted progenitor (1014). On the other hand, RA treatment between 70-120 days has later been shown to stimulate PRs' final differentiation and maturation, generating all subtypes of PRs (1015).

Treatment of retinal organoids with RA + T3 from day 90 to 120 enhanced the generation of rod and S-cone PRs formation, while adding DAPT from day 28 to 42 combined with RA from day 30 to 120 enhanced the generation of L/M-cones at the expense of rods. RA associated with L-DOPA between days 90 and 120 also promoted S-cones' emergence at the expense of rod PRs (990). The use of 9-cis retinal (9cRA) instead of the more commonly used all-trans RA has recently accelerated PRs differentiation and improved morphogenesis (1016,1017).

Currently, also treatment with docosahexaenoic acid (DHA), known to activate the MAPK pathway and prevents photoreceptor apoptosis (1018), has been shown to promote the generation of rods at the expense of cones (1019).

Several groups have also demonstrated the usefulness of blocking Noch signaling to favor and accelerate PRs' generation. In the early stage, DAPT improves neuronal specification, while in the late stages of the differentiation protocol, it has been shown to force PRs precursors to commit to PRs cells (76,964,992,997,1020). However, it was observed that the use of DAPT preferentially favors the formation of cones to the detriment of rods, consistent with reports stating the necessity of Notch suppression for cone fate specification (113,116). Interestingly, a group reported preferential cone or rod differentiation in mouse retinal organoids by applying DAPT at specific stages early during differentiation, precisely day 12 for cones and day 16 for rods (1021).

Another important parameter that made it possible to improve the differentiation protocol is the manipulation of oxygen levels. It has been observed that cells maintained under hypoxia conditions (2% O_2) in the early stages are more favorable for efficient retinal differentiation (1022–1024). These conditions better mimic the physiological oxygen tension during embryonic development. Conversely, the long-term maintenance of these large three-dimensional structures, in the absence of a vascular system, requires higher oxygen levels reaching 40% O_2 and agitation systems such as micro-bioreactors (992,997,1025,1026). Bioreactors have been

shown to increase PRs generation yields compared to classic culture conditions. On the other hand, the stirring conditions are critical and must be finely controlled to promote oxygenation without damaging the cultures, particularly in the last phase of maturation, when OSs, which are extremely fragile, arises on the surface (1026).

One of the problems in generating retinal cells is the great variability between different PSC lines, to the point that some PSC lines are not capable of 3D self-organization, and the reasons are mostly unknown. It has been observed that these cell lines express a low endogenous level of DKK1, and the addition of exogenous fibronectin and DKK-1 in these cultures has been shown to improve the 3D organization and the entire differentiation process (1027).

Another group investigated the impact of the initial hPSC state for efficient retinal differentiation. The preconditioning of iPSC cultures by modulating TGF-beta and Shh signaling during the pluripotent state improved self-formation of 3D-neuroepithelium. This preconditioning method allows several feeder-free hPSC lines robustly differentiated into 3D-retinal organoids (1028).

Recently much work has been done to identify markers that can be used to purify the PR populations. Thanks to single-cell RNAseq studies that compared various regions of the adult human retina, different stages of human retina development, and various stages of differentiation of PSC-derived organoids, it has been possible to identify several potential markers and their precise expression pattern (1021,1029–1033). CD73 seems a promising surface marker to identify and purify PRs precursors in the early stages to obtain an enriched PRs population (964). This strategy has already been used effectively to purify PRs used for preclinical studies in rodents, where they were able to partially restore visual functions in ONL-deficient mice (1034–1036).

Accelerated PRs differentiation of hiPSC-derived retinal organoids has been obtained by contact co-culture with RPE, which has been shown to promote retinogenesis and PRs maturation, boosting the expression of PR's markers at different differentiation stages (1037)

A recent protocol that uses a minimal media composition and conditions adapted for long-term culture maintenance has been used to produce cone-rich human retinal, which show incredibly advanced maturation levels (1031,1038). For long-term cultures on day 22, Fetal Calf Serum (FCS)

(8%) was added to the medium, and organoids were cultured in 24-well plates on an orbital shaker. Between 6.5 and 11 months, PRs expressed mature PRs marker (S-Opsin, L/M-opsin, RHO) and shows protruding hair-like structures with elongated IS e OS. Furthermore, the ratio of cones: rods was as high as 2.8:1, reminiscent of the human macula (1031).

This year, NRL $^{-/-}$ gene-edited hESCs have allowed the generation of rod-deficient retinal organoids enriched in S-cone-like PRs (1039). Like the corresponding mouse model, these cultures hold enormous potential for screening for drugs with therapeutic potential and modeling specific cone diseases such as MDs.

In this thesis, we use a COCO-based differentiation method in combination with IGF1, bFGF, N2, and B27 supplements to generate PSC-derived cultures enriched in cone PRs, to investigate the molecular mechanisms underlying their degeneration.

1.7.3 Stem cell-based models of RDs

One of Stem Cells research's primary goals is to generate easily accessible human cells and tissues for their application in disease modeling and clinical practice. Human cell models offer significant advantages over animal ones, which occasionally fail to fully mimic human physiology. Many human primary cell lines, on the other hand, are not amplifiable or are only capable of a limited number of passages *in vitro*. PSCs can overcome these obstacles thanks to their self-renewal ability and their great differentiation potential. Patient-specific iPSCs have already been used to model various human diseases, from diabetes to neurodegenerative diseases such as Parkinson's and Alzheimer's (599,1040,1041).

Recent advances in iPSC biology and differentiation techniques have made it achievable to develop full-scale platforms to generate large quantities of various cell types for disease modeling, drug screening, and regenerative therapies.

As previously discussed, the retina and, more particularly, PRs' structure and distribution vary significantly from species to species. Furthermore, patients' retina biopsies are generally inaccessible or difficult to obtain, thus making studying the molecular mechanisms behind

inherited human RDs arduous. iPSCs have made this phytopathological and molecular investigation possible.

Human stem cells have been used to study embryonic eye development and retinogenesis by using 3D retinal organoids that closely mimic human development with a similar timeline. They have also been helpful in studying the function and development of retinal cells such as ganglion, bipolar, RPE, cell of the lens, and PRs (967,1002,1025,1042,1043). Recently, iPSC has been used to model various diseases such as RP, LCA, USH, and glaucoma (1044–1047).

While there are many publications for disease modeling using hiPSC-derived RPE cells, the number of publications involving PRs is more limited, reflecting the ease and challenges in their generation and maintenance. Among them, the great majority involve using 3D retinal organoids or 2D/3D mixed culture.

The choice of the differentiation protocol, the number of patients and controls, the enrollment rules, and the strategies adopted for the analyses must be intelligently planned to ensure the validity of the results using these models. These include, but are not limited to, the disease of interest, the weight and magnitude of the expected phenotype, the sensitivity of the assay techniques, and the heterogeneity inherent in the iPS cell lines, the variability derived from cellular reprogramming and *in vitro* culture condition during differentiation and maintenance.

Various strategies can be adopted to use iPSCs and ESCs to model RDs effectively; the main ones are summarized (Figure 38). There is no absolute best strategy, and each one offers its advantages and disadvantages. The choice of the most suitable strategy must be rationally planned after a careful case-by-case evaluation. Often two or more strategies can be used in combination to confirm or reinforce the results.

Here we summarize the principals' strategies for applying iPSCs in disease modeling, and we provide some examples for each group.

1.7.3.1 Application of patient-specific iPSCs in disease modeling

Patient-specific iPSCs offer a unique opportunity to directly investigate the molecular mechanisms behind human diseases in the patient's cells.

The most popular strategy is comparing cells generated from patients' iPSCs with those from healthy individuals. It requires using a "sufficient" number of samples from both controls and affected individuals to compensate for the genetic background variability. Generated cells have all the genetic and epigenetic signatures present in the patient, making them particularly representative of the individual and therefore suitable for studying rare genetic cases or developing personalized therapies. Patients' iPSCs are the favorite, or only, option for modeling complex and polygenic diseases, cases with not yet identified causing mutations, or those of unknown origin. When the number of available patients is minimal, such as rare diseases or rare genetic variants, it is recommended to use multiple clones per patient.

Recently, many high-rated journals have established guidelines for the number of patients and clones necessary for publication. Although they vary considerably depending on parameters such

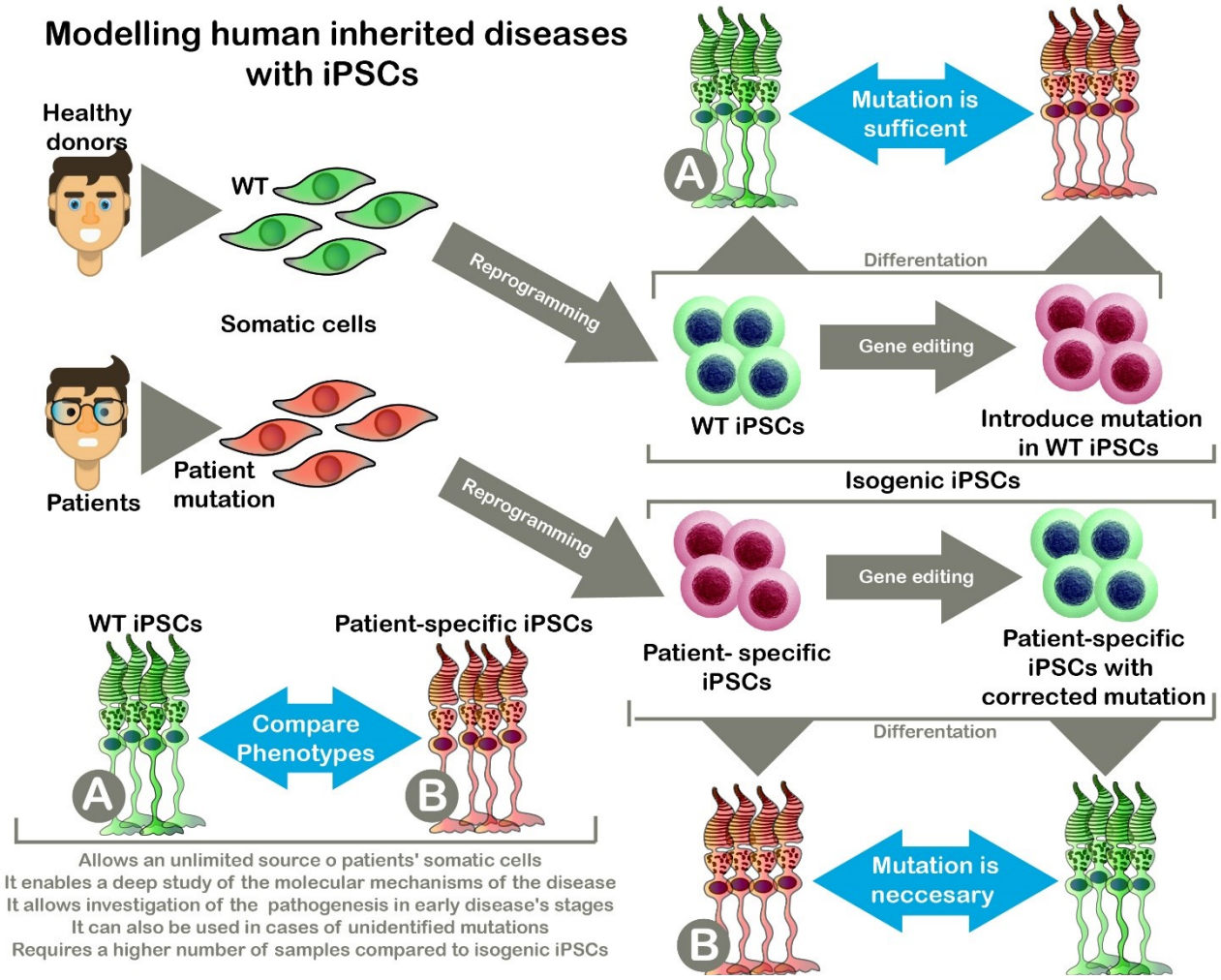

Figure 38: Strategies for disease modeling using PSCs

as the method of analysis, aspected outcome, biological effect studied, and experimental variability (1048)**,** evidence arose from transcriptomic profiles of undifferentiated iPSCs point out that four to six individuals per group provided a reasonable balance of sensitivity and specificity (1048,1049). However, these numbers are rarely reached at present. These guidelines provide essential resources for the design, analysis, and interpretation of future iPSC-based studies.

The first report on iPSC's use for modeling RDs comes from Takahashi's group at the RIKEN institute (1050). They obtained fibroblast cells from healthy individuals and five RP patients with distinct mutations in the *RP1, RP9, PRPH2*, and *RHO* genes and generated patient-specific iPSCs. They differentiated these iPSCs into rod PRs that express mature rod markers and exhibits electrophysiological properties. Similar to what happens *in vivo*, they observed a decrease in the number of rod cells in patient-derived cultures with distinct mutations. Furthermore, iPSC-derived PRs express oxidative and ER stress markers and respond differently to vitamin E treatment as observed in patients. For the first time, they demonstrated that patient-derived iPSCs could be used to interrogate RDs' pathophysiology, elucidate the underlying molecular mechanisms, and identify disease-causing mutations (1051).

Simultaneously, Tucker et al. use exome sequencing to identify a novel mutation in exon 9 of the male germ cell-associated kinase (*MAK*) gene as the presumed cause of disease in an isolated RP patient. They successfully generated iPSCs from patient fibroblasts and a healthy control and differentiated them into retinal precursor cells using a mixed 2D/3D method. Unfortunately, their model failed to show the developmental switch that allows the expression of the isoform containing the exon 9, as it happens *in vivo* during NR development, thus preventing the expected phenotype's appearance. This failure was mainly attributed to insufficient cell maturation. This study highlights current limitations in the applications of these models (1052).

Subsequently, the same lab, using NGS and Sanger sequencing, was able to identify the causal mutation in *USH2A*, which causes a frameshift with a premature stop codon, in a patient with RP. They efficiently generate multilayered optic cups from this patient and age-matched control. To overcome the limitations encountered previously, in addition to using an improved protocol, they transplant the PRs precursors into immunosuppressed mice in order to reach a more advanced

level of maturation. The cells developed into mature PRs that expressed PRs-specific proteins. These conditions allowed them to discover that USH2A mutation translates into post-developmental PRs degeneration triggered by protein misfolding and ER stress (984). This work sheds new light on the disease's mechanisms and lays the groundwork for further studies to develop effective gene correction therapies (1046).

Parfitt et al. effectively generate 3D optic cups from a patient with a homozygous mutation in *CEP290* (c.2991 + 1665A> G), a frequent cause of LCA. In this way, they demonstrated that RPE and optic cup neuroepithelium develop normally despite the incorrect splicing of *CEP290* and defects in ciliogenesis. These defects were more abundant in the optic cup than in RPE, thus explaining the preferred target for these structures in patients. They also showed a new antisense oligonucleotide's ability to block aberrant splicing, thus restoring the full-length *CEP290* transcript and restoring normal ciliogenesis and cilia trafficking. In this way, they demonstrate the versatility of iPSC-derived retinal organoids to discover the molecular mechanisms involved in RDs and develop effective clinical strategies (1001).

Another group uses iPSC-derived retinal organoids from four control individuals and six patients with RDs caused by *CEP290* mutation, including three with LCA and three with JSRD, to investigate the differential penetrance of *CEP290* mutations. They demonstrate that the reduction of CEP290 production in LCA patients impact cilia maturation. In contrast, the complete lack of CEP290 in JSRD patients caused decreased ciliogenesis, aberrations in the cilia structure, and increased SHH signaling pathways. This work demonstrates the correlation between ciliogenesis defects observed *in vitro* and the severity of patients' pathologies. They helped understand CEP290 role as a ciliary gatekeeper for transporting molecules in and out from the OS in human PRs (1045).

Stone's laboratory generated iPSCs and differentiated them into retinal organoids from a control donor and three patients with early-onset RP due to a mutation in *TRNT1*, a gene recently linked to PRs degeneration (1053). They observe a defect in autophagy characterized by increased expression of LAMP1, production of LC3-II, and lipidation of LC3-1. Finally, they detect elevated levels of oxidative stress, which seems to be the ultimate cause of PRs cell death, thus confirming what was hypothesized to be the cause of degeneration in patients (1054).

Megaw et al. use both mouse and hiPSC-based models to investigate the role of RPGR in PRs degeneration. With this intent, they generate iPSCs from two siblings with X-linked RP due to a mutation in *RPGR* (g.ORF15 + 689−692del4) and one unaffected close relative as control. They show that the mutation in RPGR prevents its physiological interaction with Gelsolin, which causes increased actin polymerization, abnormal OS formation, and PRs death. Moreover, the same abnormalities were found in both RPGR and Gelsolin KO mouse models, thus confirming their evidence. This report brings new insights into RPGR interactors' identity and its role in X-linked RP pathogenesis (1055).

Schwarz et al. generated iPSC-derived 3D optic cups from a patient with the *RP2* mutation (p. R120X). They show that cultures, despite the absence of detectable RP2, develop normally, but the PRs in the optic cups displayed reduced Kif7 staining at their cilia tips, suggesting that RP2 regulates specific trafficking kinesins to cilia tips. By screening active compounds, they found that PTC124 restored Kif7 levels at the tip of RP2 null cilia, thus representing an excellent candidate for future therapies. Overall, this work points out the utility of iPSC models in drug discovery (1056).

Recently Guo et al. recapitulated some of the phenotypes observed in patients with *USH2A* mutations using patient-specific iPSCs. Using 3D organoids from a single patient and age and sex-matched controls, they could show a range of defects, including abnormality in NR development and polarization, defects in ciliogenesis and PR’s morphology, aberrant expression of various PRs markers at both transcripts and protein level, and increased apoptosis. These data lead to a significant advance in the RP's molecular diagnosis and understanding the pathological role of USH2A mutations (1057).

Only very recently, another group has been successful in generating a model of late-onset RD. They generated iPSCs from peripheral blood mononuclear cells from a patient with late-onset RD harboring a mutation in *PDE6B*, identified by exome sequencing, and a control patient. To partially compensate for the limited number of samples, they generated three clones for each iPSC line. They then generated 3D retinal organoids, identified transcriptomic signatures at various time points via RNAseq, and confirmed their primary evidence by IF. They show that the phenotype's

appearance requires an extended culture period exceeding 200 days *in vitro* in line with patients' late-onset appearance of symptoms. They observed upregulation of TFs that promote rod development (SAG, NR2E3, and NRL), reflecting preferential rod development defects in the patient organoids. They also observed significantly increased cGMP levels in patients' PRs compared to controls, which could be one of the causes of the aberrations observed in both CC and synaptic connections. This work advances new evidence in the function of PDE6B in mature PRs and has its most significant impact in being the first report of a late-onset RD model (1058).

1.7.3.2 Disease modeling using human isogenic iPSCs

Another strategy to model inherited genetic diseases is to induce the desired mutation in a healthy iPSC or ESC line to compare two isogenic cell lines that share the same genetic background. Opposite to patient-specific iPSC lines, isogenic iPSC lines, created through gene editing approaches from well-characterized healthy subjects, bypasses the problems related to variations between cell lines. These differences include residual epigenetic memory, genetic background, incomplete programming, variable proliferation and differentiation potentials, aberrant transcription, and DNA methylation patterns (1059–1061). The isogenic iPSC approach reduces the number of samples required due to its high reliability and efficiency compared to traditional methods.

Thanks to the incredible technological advancement in cloning and site-directed mutagenesis techniques, such as TALENS and CRISPR-Cas9 systems and all their variants, theoretically, any genome locus can be changed with a single base precision (707,1062). At present, it is possible to induce complete gene KOs or generate a single site-specific point mutation, which can be either homozygous or heterozygous.

However, there are several limitations in the use of the isogenic iPSC line. First, the mutation of interest must be known to be reproduced, and polygenic or multifactorial diseases are generally inaccessible with these techniques. Furthermore, although these techniques are now economically accessible for most laboratories, the required manipulation still involves substantial investments and highly specialized technical personnel. Another major limitation of gene-editing is potential unintended and "off-target" effects, requiring multiple NGS analyses as quality

controls. Due to technical and analytical limitations, the complete exclusion of off-target mutations cannot be archived; for this reason, the use of multiple clones as biological replicates is still recommended. Engineered isogenic lines are gaining popularity to confirm the genotype/phenotype relationship observed with patients' iPSCs. In combination with 3D organoids, this strategy is also precious for studying specific genes' impact during the human retina's embryonic development.

Yoshida et al. used iPSCs derived from an RP patient to confirm a suspected RHO disease-causing mutation. They observed an increment of oxidative and ER stress in patients-derived organoids. Then they confirmed the pathogenicity of the patient's E181K RHO mutation by introducing it in an isogenic wild-type cell line expressing GFP under the control of the *NRL* promoter to facilitate further purification and analysis. Furthermore, they rescued patient-derived cells using HDAdV-mediated gene correction. Finally, they used their isogenic iPSC model to screen drugs capable of reducing ER stress, autophagy, and apoptotic markers, therefore suitable for therapeutic use (1063). This work provides exceptional guidance to compensate for a limited patients availability and the application of isogenic iPSCs to develop new treatments.

Similarly, Lane et al. investigate the role of RP2 in the pathogenesis of XLRP. Mutations in RP2 cause a severe form of RP, the mechanism of which remains somewhat obscure, and mouse KO models fail to recap the severity of the phenotype. With the intent to generate a representative model of the disease, they create an isogenic RP2 KO hiPSC line. Then they differentiated it together with the control and a patient iPSC harboring an RP2 mutation into 3D organoids. They clearly showed that both patient and RP2 KO line organoids displayed a decrease in RHO expression with a cell death peak around day 150, with a subsequent reduction in the thickness of the ONL already visible at day 180. They also demonstrated that the adenovirus-mediated reintroduction of RP2 could block apoptosis, rescue the degeneration, and re-establish the ONL thickness (1064).

Takahashi's lab used an engineered Nrl-GFP iPSCs and 3D retinal organoids to develop a chemically induced PRs degeneration model through treatment with 4-hydroxytamoxifen (4-OHT). The generative process recapitulates what was observed in organoids derived from RP

patients. Using this model, they develop a microscopy technique for real-time visualization of PRs degeneration using a GFP reporter. This drug evaluation system allows them to monitor the effect of drugs over extended periods in real-time, significantly reducing the number of samples required for this type of analysis, thus bringing significant advancement in drug screening platforms for RDs (1065).

Recently a group succeeded in the generation of a human NRL KO model (1031,1066). Mutations in NRL can cause various manifestations, from RP to enhanced cone syndrome. While the Nrl KO mouse model has been highly characterized (819,821), NRL's role in human PRs is not fully understood. To investigate the impact of the absence of NRL during human NR development at the molecular level, they generate an NRL KO hiPSC line and differentiate it and the isogenic control into 3D organoids. Consistent with the role of NRL in rod specification, its deactivation in retinal organoids leads to an increase in the two distinct cone subpopulations. Combining RNAseq and epigenetics analysis, as previously used in the context of the Nrl null mice (1067), they identify MEF2C as a potential new regulator of cone development. Interestingly, MEF2C has been previously identified as a regulator of rod fate, highlighting possible differences between mice and humans.

In addition to investigating the role of NRL in human PRs, this article represents an excellent alternative to increase cone generation during iPSC differentiation. This model could therefore be helpful to study cone dystrophies and to screen molecules with therapeutic potential for cone-specific degenerations such as CDs and MDs (1066)

1.7.3.3 Rescue patient-specific iPSCs using gene-editing

A final strategy that could be adopted to investigate or confirm the diseases' genetic origin is to correct the mutation directly in the patient's iPSCs in a rescue experiment.

It represents a mixture of the previous few strategies involving both patient-specific iPSCs and gene editing, thus bringing with it the advantages and disadvantages of both techniques.

It frequently represents a final and elegant confirmation of the mutation's pathological role and simultaneously confirms the degenerative process's reversibility and the gene correction

therapeutic potential. The major limitation in this approach is the gene-editing step, which, as previously mentioned, tends to be very laborious, in particular in the case of point mutations. For these reasons, the number of available examples remains minimal.

As anticipated previously, some groups have managed to restore PRs' physiological functions in different iPSC-based models by reintroducing the full-length gene via AAV or Lentiviral vectors.

Burnight et al. investigate the role of CEP290 in retinal degeneration. With this intent, they generate iPSCs from three LCA patients with mutations in CEP290. They showed that introducing the WT version of *CEP290* with a lentiviral vector was sufficient to restore the physiological length and number of cilia in two out of three patients' fibroblasts. Although the authors effectively differentiate patient-specific iPSCs into OTX2-positive RPCs and reintroduce the full-length version of CEP290 in these cells, they fail to show mature PRs or defects in ciliogenesis, thus highlighting challenges in PRs maturation and the generation of the CC in these differentiated cells (1068).

Wiley et al. generated iPSCs from two patients with confirmed mutations in CLN3 affected by Juvenile neuronal ceroid lipofuscinosis (JNCL), a childhood neurodegenerative disease characterized by severe early-onset central vision loss. This model shows that treatment with AAV2- CLN3 could restore full-length CLN production at both RNA and protein levels. Finally, they demonstrated that the injection of these cells in the subretinal space of immunosuppressed mice does not cause damage or toxicity, paving the road to future clinical trials using AAV gene therapy to treat JNCL and similar diseases. (1069)

Deng et al. generated iPSC from urine samples from three male patients with childhood night blindness diagnosed with RP harboring different *RPGR* frameshift mutations. They differentiate them into RPE cells and retinal organoids and observed multiple defects regarding localization, morphology, electrophysiological activity, and transcriptional profiling in differentiated PRs. Interestingly they observed ciliogenesis defects and shorted cilium in all undifferentiated iPSCs, RPE, and retinal organoids. They finally show that correction of these *RPGR* mutations is possible, and it is sufficient to restore to normal levels ciliogenesis, PR's structure and electrophysiological properties, and transcriptomic profile. This work successfully reproduces the phenotype observed

in patients harboring *RPGR* mutations using iPSC-derived 3D organoids and offers proof of concept that targeted gene therapy via CRISPR -Cas9 is feasible and could be helpful in the RP context (1070).

Huang et al. generate iPSCs from two X-linked juvenile retinoschises (XLRS) patients with RP1 mutations and two control donors. XLRS is characterized by retinoschisis, which is the separation of the retina layers, with consequent MD that can eventually affect peripheral vision. Using 3D retinal organoids, they could recapitulate the main features of XLRS, including retinoschisis, abnormality in OS, reduced transport between ER and Golgi, and deregulation in the expression of ciliary components. They also show that mutating RS1 in the control line mimics the XLRS phenotype. Therefore, using a single base resolution-editing approach, they demonstrate that the C625T mutation can be corrected effectively and precisely using CRISPR-Cas9, which can re-stabilize all pathological phenotypes, including retinoschisis and OS defects (1071).

To evaluate the therapeutic potential of gene-editing in USH and arRP with mutations in USH2A, Soriano et al. generate 3D organoids from two patients harboring the two most common mutations observed in these patients *c.2276G> T* and *c.2299delG*. Since the introduction of the full-length transcript is not possible due to its large size, gene correction for CRISPR-Cas9 is an attractive alternative. Using a Cas9 of Streptococcus Pyogenes (eSpCas9) with increased specificity, they could correct both mutations in the two patients' cells without detectable off-target effect, and this was sufficient to reverse the phenotype in iPSC-induced retinal cells (1046).

Similarly, Bohrer et al. use CRISPR-Cas9 to correct mutations in iPSC lines derived from two patients with Enhanced S-cone syndrome (ESCS) harboring mutations in NR2E3 (1072).

Overall, these works show the incredible advances in iPSC disease modeling since their disclosure in 2006. Although iPSCs, as all *in vitro* models, lack the microenvironment and biochemical context that retinal cells have *in vivo*, they only provide an in-depth and controlled molecular analysis of retinal cells during embryonic development, in the early stages of the pathological process, and during PRs degeneration, otherwise impossible to obtain in any *in vivo* animal models or patients. They also offer an excellent platform for monitoring therapeutic compounds' efficacy and toxicity in drug discovery platforms and preclinical studies. Despite their young age, iPSCs, combined with

next-generation sequencing and gene editing techniques, have already demonstrated their enormous potential from modeling RDs to their applications in regenerative medicine. This relatively new field is now in its exponential growth, and it is reasonable to think that it will represent one of the pillars of the “next modern medicine. “

In this thesis, we use both iPSC and ESC-based models to investigate the degenerative process in human PRs. We first study the rôle of BMI1 during PRs development and maintenance using control hESC lines treated with an shRNA to silencing gene function.

We then use iPSCs from patients with syndromic ciliopathies to study the associated retinal phenotype and investigate the molecular mechanism underlying PRs degeneration.

2. HYPOTHESIS AND OBJECTIVES

2.1 Hypothesis

RDs are a great burden on our society and are mainly without any therapeutic option.

This work's starting hypothesis is that the lack of treatment is partly due to the inadequacy of current animal models and interspecies differences that cause difficulties in studying the disease mechanisms, which is reflected in the failure of clinical trials.

Retinal cells for research and clinical use are extremely limited or difficult, if not impossible, to obtain in sufficient quantities. For this reason, nowadays, there is still a great need for retinal cells.

As valuable as animal models are, they could be flanked or partially replaced by humanized *in vitro* models, which can better recapitulate human physiology. PSCs technology now allows the generation of the desired population of human somatic cells *in vitro* and theoretically in unlimited quantities.

The Bmi1 polycomb protein is necessary for the survival of neurons in the cortex and is expressed in RPCs in the mouse embryonic retina, but little is known about its precise role in the mature retina. Since it is implicated in aging and neurodegenerative diseases, it could play a role in the degenerative process in RDs, thus representing a potential target to modulate PRs death.

The PRs CC is a very particular and indispensable structure for the continuous transport of molecules in and out of the PRs' OS. Diseases affecting the primary ciliary function end structure are called ciliopathies, a relatively recent and rapidly expanding class of heterogeneous conditions. Dysfunctions of ciliary proteins are now considered one of the most frequent causes of RDs. Delineate the components of the primary cilium and their specific functions, as well as understand the process of ciliogenesis and cilia maintenance, is essential to intervene effectively to find valid therapeutic solutions.

The PRs CC has been shown to have differences between humans and mice, and human models to study their dysfunction are limited to a few recent reports using iPSCs and 3D retinal organoids based on very technical and time-consuming protocols.

2.2 Objectives

In this thesis, we use mice and human PSC-based models to investigate the role of BMI1 in the postnatal retina and PRs survival.

We also provide proof of principle that patients' iPSC-derived retinal sheets can be used effectively to investigate the impact of mutations affecting CC components on PRs' development and survival. We finally show that this model can be used to evaluate compounds with potential therapeutic capabilities.

Objectives:

- Evaluation Of Bmi1's Role In The Mouse Postnatal Retina
- Modeling BMI1 Inhibitor in Photoreceptors Derived From Human Embryonic Stem Cells
- Improve protocol for Photoreceptors differentiation to generate 3D polarized sheets enriched in cones
- Generation of retinal sheets from patient-specific iPSCs
- Modeling human inherited retinal disease using patient-specific iPSCs
- Application of iPSC-derived retinal sheet in drug screening and personalized medicine

3. RESULTS

3.1 Retinal development anomalies and cone photoreceptors degeneration upon Bmi1 deficiency

Andrea Barabino[1£], Vicky Plamondon[1£], Mohamed Abdouh[1], Wassim Chatoo[1], Anthony Flamier[1], Roy Hanna[1], Shufeng Zhou[1], Noboru Motoyama[2], Marc Hébert[3], Joëlle Lavoie[3], and Gilbert Bernier[1, 4, 5 *]

[1] Stem Cell and Developmental Biology Laboratory, Hôpital Maisonneuve-Rosemont, 5415 Boul. l'Assomption, Montréal, Canada, H1T 2M4

[2] National Institute for Longevity Sciences National Center for Geriatrics and Gerontology 36-3, Gengo, Morioka, Obu, Aichi 474-8522, Japan.

[3] Department of Ophthalmology, Otorhinolaryngology and Cervico-Facial Surgery, Faculty of Medicine, Université Laval, Laval, Canada, G1V 0A6.

[4] Department of Neurosciences

[5] Department of Ophthalmology, Université de Montréal, Montréal, Canada, H3T 1J4

[£] Equal contribution

3.1.1 Abstract

Retinal development occurs through the sequential but overlapping generation of six neuronal and one glial cell type. Of these, rod and cone PRs represent the functional unit of light detection and phototransduction and are frequently affected in retinal degenerative diseases. During mouse development, the protein Bmi1 is expressed in the most immature RPCs and in differentiated retinal neurons, including cones. We show that Bmi1 is required to prevent cone PRs and bipolar neurons degeneration during post-natal eye development. Bmi1$^{-/-}$ mice's retinal phenotype was further characterized by loss of heterochromatin, activation of tandem-repeats, oxidative stress, and Rip3-associated necroptosis. Genetic inactivation of either Chk2 or p53 improved cone numbers in *Bmi1*$^{-/-}$ mice but could not overcome the progressive degenerative process. In the human retina, BMI1 was preferentially expressed in cones at heterochromatic foci. BMI1 inactivation in human ESCs was compatible with retinal induction but impaired cones' terminal differentiation. Despite this developmental arrest, BMI1-deficient cones recapitulated several anomalies observed in *Bmi1*$^{-/-}$ PRs such as loss of heterochromatin, activation of tandem-repeats, and p53 induction, revealing partly conserved biological functions during cone development between mouse and man.

3.1.2 Introduction

The distinct competence of RPCs to generate in sequential order the diverse class of neurons and a single glial cell type during retinal development is thought to be modulated by an intrinsic TFs molecular program and by extrinsic clues (81,82,85,1073). Loss- and gain-of-function studies in model organisms have revealed that the transcription factors Pax6, Rax (also called Rx), Lhx2, Otx2, Sox2, Six6, and Six3 are involved in early eye patterning and retinal developmental processes (47,50–54,1074–1076). Later on, specific sets of TFs define retinal cell type identity, including PRs (104). Photoreceptor progenitor and precursor cells express Otx2 and Crx, and conditional deletion of *Otx2* in the developing mouse retina impairs PRs fate BRCA1 tumor suppression occurs via heterochromatin-mediated silencing (105). In turn, Crx is required for terminal differentiation and maintenance of PRs and is mutated in human retinal degenerative diseases (107–109,1077–1079). PRs exist in two types, rods and cones. Rods are involved in low-intensity night vision, and cones are involved in high-intensity color vision. During development, PRs follow an S-cone default pathway, which is determined by Crx and Thrß2; Crx induces the expression of *Opn1sw* by default while Thrß2 suppresses it and induces the expression of *Opn1mw* (111,807). In turn, expression of *Nrl, RORbeta,* and *Notch1* inhibit cones formation, while both Nrl and RORbeta promote rod genesis at the expense of cones (113,114,116,1080).

Although the TFs dynamics during retinal development have been well described, the role of chromatin remodeling factors in retinal biology has been poorly explored (1081). PcG proteins form large multimeric complexes that silence specific target genes by modifying chromatin organization (1082). The PcG protein Bmi1 is a component of the PRC1, promoting chromatin compaction and gene repression through its mono-ubiquitin ligase activity on histone H2A at lysine 119 (567,1083,1084). *Bmi1*$^{-/-}$ mice show axial skeleton defects, reduced postnatal growth and lifespan, and progressive cerebellar degeneration (572,1085). Most Bmi1 functions in normal development and stem cell maintenance have been attributed to transcriptional repression of the *Cdkn2a* (also called *Ink4a/Arf*) locus, encoding for p16^{Ink4a} and p19^{Arf} (577,1082,1086). p16^{Ink4a} is a cyclin-dependent kinase inhibitor that blocks the activity of Cdk4/6 by preventing its association to cyclin D, which results in Rb hypophosphorylation and cell cycle arrest or senescence. p19^{Arf} binds and inhibits the activity of the E3-ubiquitin ligase mouse double minute

2 (Mdm2), which prevents p53 targeting for proteasomal degradation (577,1086). More recently, activation of the DNA damage protein checkpoint kinase 2 (Chk2) was found to contribute to several pathologies found in *Bmi1*$^{-/-}$ mice (1087). *Bmi1*$^{-/-}$ mice also develop a progeroid phenotype in the CNS characterized by lens cataracts, cortical neuron apoptosis, p53 activation, and oxidative damage accumulation (601). In the developing retina, it was found that Bmi1 is not required for the proliferation of the main RPC population but for proliferation and post-natal maintenance of most immature RPCs located at the retinal ciliary margin. *Bmi1* overexpression in RPCs with short-term proliferating activity induces chromatin remodeling and conversion into long-term RPCs with stem cell characteristics (610). *Bmi1* thus distinguishes most immature progenitor/stem cells from the main RPC population during retinal development (610). Notably, *Bmi1* is also expressed in differentiated retinal neurons, including PRs, raising the possibility that it may be important for their post-natal development or maintenance (601,610).

We report here that while retinal cell type genesis occurs relatively normally in *Bmi1*$^{-/-}$ mice, cone bipolar neurons and cone PRs rapidly degenerate during post-natal eye development through necroptosis. BMI1 was preferentially expressed in cones in the human retina, and BMI1 inactivation in human ESCs impaired CRX expression and cone terminal differentiation. The cellular phenotype was also associated with chromatin compaction anomalies, activation of tandem-repeats, and p53 induction, similarly to what was found in the *Bmi1*$^{-/-}$ mice. These findings revealed new and partly conserved biological functions for Bmi1 during cone PRs development between mouse and man.

3.1.3 Results

To investigate for a possible function of Bmi1 in retinal neuron differentiation, we performed immunohistochemistry (IHC) and immunofluorescence (IF) analyses on retinas from WT and *Bmi1*$^{-/-}$ littermates at postnatal day 30 (P30). This revealed that retinal organization and cell type genesis were possibly perturbed in *Bmi1*$^{-/-}$ mice (Figs. 1-2 and S1-S2). The distribution of syntaxin, which labels amacrine neurons, was abnormal, resulting in its focal accumulation in the inner nuclear layer (Figs. 1A and S2). The distribution of S-Opsin, which labels the cones' OS, was also perturbed (Figs. 1A and S1). In contrast, the overall intensity and distribution of Rhodopsin, which labels the outer segment of rods, was apparently normal. The total number of nuclei in the outer nuclear layer, which is a measure of the total number of PRs (mostly rods), was also comparable between the two genotypes (Figs. 1A-B and S2). We quantified the number of all major retinal cell types using specific antibodies (52,1088,1089). We found that the number of ganglion, amacrine, and horizontal cells was comparable between both genotypes (Figs. 1G-H and S2). On the other hand, the number of S-cones, as well as that of rod bipolar (Pkcα^{+}/Chx10^{+}) and cone bipolar (Chx10^{+}/Pkcα^{-}) neurons, was highly reduced in *Bmi1*-mutants (Figs. 1B and 2A-C). Amongst the two subcategories of cone bipolar neurons, T2 ON and T8 OFF neurons (labeled by Recoverin) were also nearly absent (Figs. 2G and S2).

To test if the observed reduction in cone numbers in *Bmi1*$^{-/-}$ mice resulted from a developmental defect or secondary to degeneration, we compared P12 and P30 mice. On retinal flat mounts, we found that S-Opsin^{+} and Peanut Agglutinin (PNA)$^{+}$ cone cells were equally abundant in the ventro-nasal region between WT and *Bmi1*$^{-/-}$ mice at P12, but not at P30, where they were significantly reduced in *Bmi1*-mutants (Figs. 1C-F and S1). The apparent over-representation of S-Opsin in the ventro-nasal region, in contrast to the dorso-temporal region, is due to the dual nature of mouse cone PRs, which frequently express both S-Opsin and M-Ospin (Fig. S4A) (1090). These analyses also highlighted a significant reduction in cone numbers in *Bmi1*$^{+/-}$ mice, revealing a gene-dosage effect (Fig. 1C-D). We performed labeling with an antibody against activated caspase-3 to test for apoptosis. However, positive cells were not observed in both WT and *Bmi1*$^{-/-}$ retinas at P30, suggesting that apoptosis is not the main mechanism of retinal cell death in *Bmi1*$^{-/-}$ mice (data not shown).

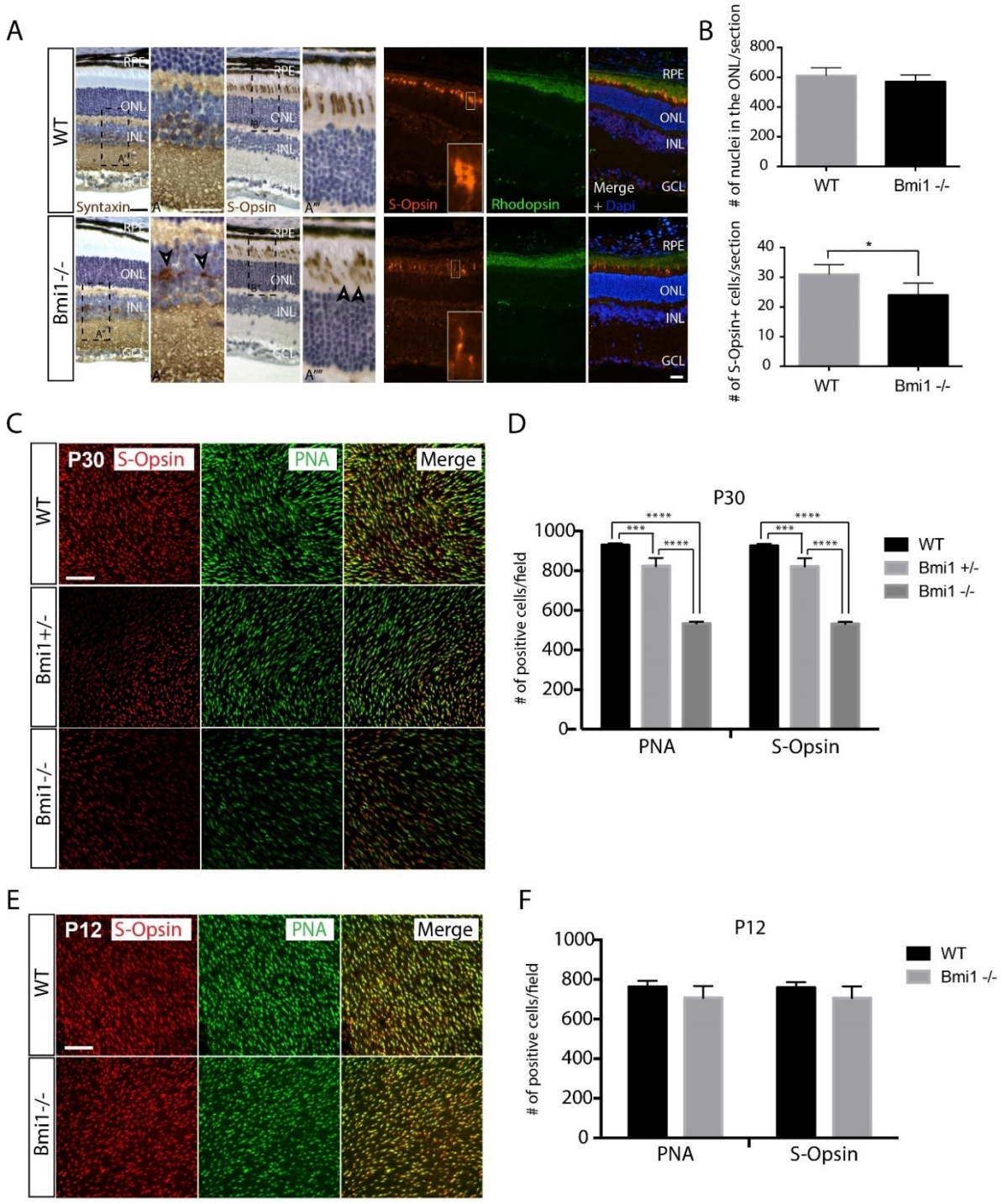

Figure 1: S-cones degenerate during postnatal eye development in Bmi1−/− mice.

*(A) Analyses of WT and Bmi1−/− retinas at P30. Abnormal distribution of syntaxin (arrowheads in A") and cone photoreceptor outer segments breaks in Bmi1−/− mice (arrowheads in A"") as visualized by IHC. Cone photoreceptor outer segments break but rod photoreceptors appear normal in Bmi1−/− mice, as visualized by IF. (B) Quantification of total number of photoreceptors (top) and S-cones (bottom). (C,E) Representative microscopy images from retinal flat-mount of WT, Bmi1+/− and Bmi1−/− mice at P30 (C) and WT and Bmi1−/− at P12 (E). Images were taken in the ventro-nasal part of the retina. (D,F) Quantification of S-cone photoreceptors (S-opsin+) and total cone photoreceptors (PNA+) at P30 (D) and P12 (F). RPE, retinal pigment epithelium; ONL, outer nuclear layer; INL, inner nuclear layer; GCL, ganglion cell layer. Scale bars: 40 µm. All values are means±s.e.m. *P≤0.05; ***P≤0.001; ****P≤0.0001; Student's t-test (B,F), two-way ANOVA (D).*

This is consistent with our previous findings, where differences in the number of caspase-3$^+$ cells were not observed between WT and *Bmi1*$^{-/-}$ retinas at P6 (610). To test for an altered retinal differentiation program, we performed quantitative RT-PCR (qPCR) on retinal extracts. While expression of the Bmi1-repressed locus *Cdkn2a* (encoding for the *p16*^{Ink4a} and *p19*^{Arf} transcripts) was increased in *Bmi1*$^{-/-}$ retinas (Fig. 2I) (581), no differences in the expression level of several retinal determination genes were observed between both genotypes.

We also investigated Bmi1 expression in the WT mouse retina at P30. While Bmi1 was expressed in nearly all retinal cell types, it was most abundant in Chx10$^+$ bipolar neurons (Fig. S5). In the outer nuclear layer, it was predominant in cones, not in rods, as further proved using the cone-only retina of *Nrl*-null mice (Fig. S3A) (1080). To test whether the cone degeneration phenotype was cell-autonomous, we performed dissociated retinal cultures from WT and *Bmi1*$^{-/-}$ mice at P1. Although the percentage of S-cones was comparable after 4 days *in vitro* (DIV) between both genotypes as revealed using Bmi1 and S-Opsin immunolabeling (Fig. S3B), it significantly decreased after 8 DIV and 12 DIV in the *Bmi1*$^{-/-}$ cultures, suggesting cell-autonomous degeneration of cones (Fig. S3C). Taken together, these observations revealed the predominant expression of Bmi1 in retinal neurons that degenerate in *Bmi1*$^{-/-}$ mice.

3.1.3.1 Cone function is severely perturbed in *Bmi1*$^{-/-}$ mice

To test the visual function, we performed ERG recordings of mouse retinal activity at P30. Examination of the ERG traces for the cone system revealed that cone activity was severely affected in *Bmi1*$^{-/-}$ mice when compared to WT (Fig. 3A-C). Notably, we observed a dose-dependent effect as cone activity was also perturbed in *Bmi1*$^{+/-}$ mice. When tracing the Luminance Response Functions (LRFs), significant genotypes-dependent differences were observed between WT, *Bmi1*$^{+/-}$ and *Bmi1*$^{-/-}$ mice for all four ERG parameters in photopic condition, namely the a-wave amplitude ($F_{2, 7}$ = 6.195, p = 0.028) (Fig. 2B and Table S1), the b-wave amplitude ($F_{2, 7}$ = 18.970, p = 0.001) (Fig. 3C and Table S1), the a-wave implicit time ($F_{2, 7}$ = 5.127, p = 0.043) (Table

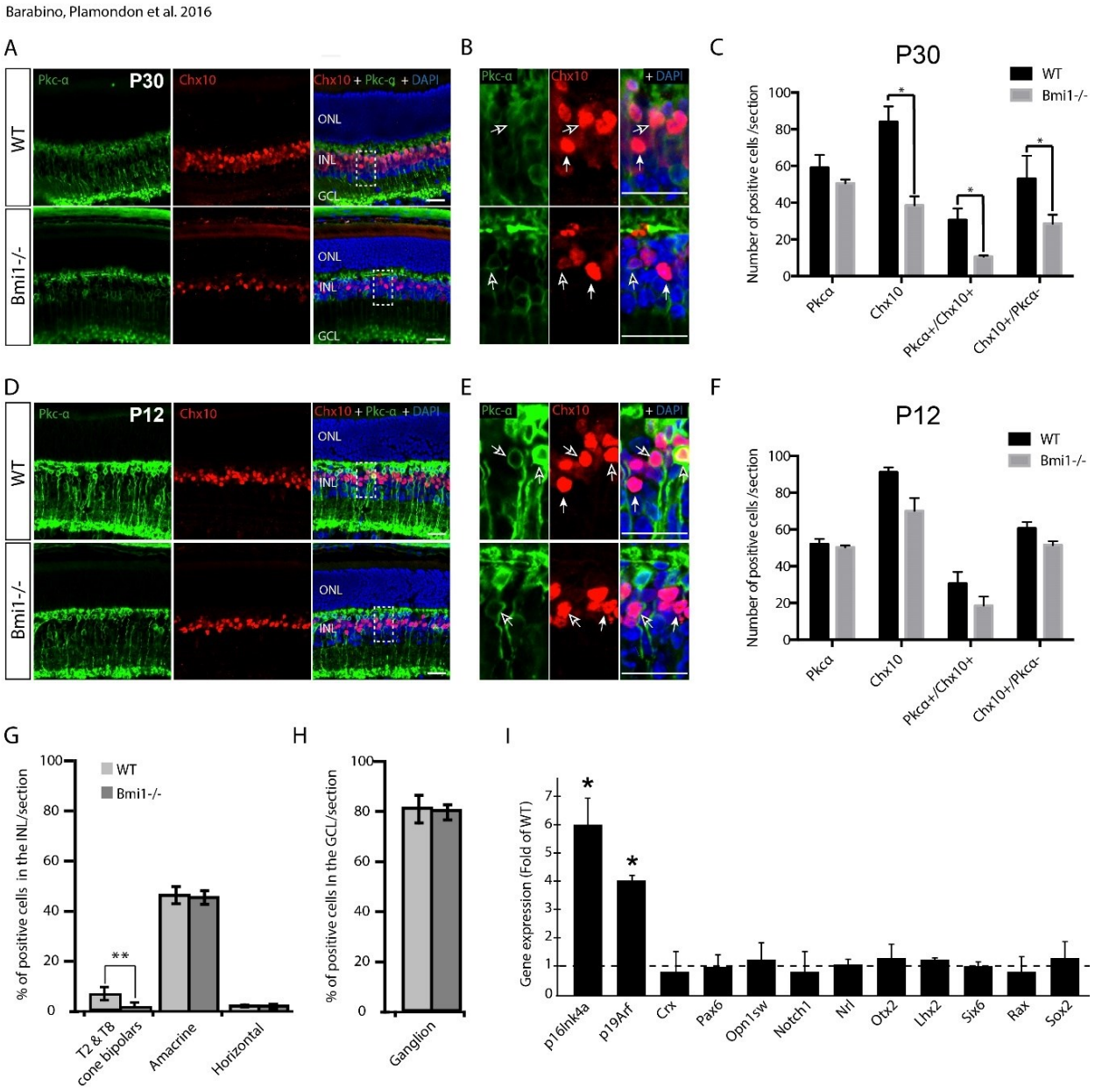

Figure 2: Bipolar neurons degenerate during post natal eye development in Bmi1−/− mice.

*(A,D) Representative images of WT and Bmi1−/− retinas at P30 (A) and P12 (D) labeled with antibodies against PKCα and Chx10. (B,E) Cropped images indicated by the respective dashed rectangles indicated in A and D. White filled arrows: cone bipolar cells (Chx10+/PKCα−). White-edged arrows: rod bipolar cells (Chx10+/PKCα+). Note the decrease in Chx10+ cells in Bmi1−/− retinas at P30. (C,F) Quantification of data acquired in A and D. (G) Quantification of T2-OFF and T8-ON cone bipolar cells (Recoverin+), amacrine cells (Pax6+) and horizontal cells (Calbindin+) in the INL. (H) Quantification of ganglion cells (Pax6+) in the GCL. (I) Gene expression analysis of WT and Bmi1−/− retinas at P30, where p16INK4a and p19ARF were used as positive controls. RPE, retinal pigment epithelium; ONL, outer nuclear layer; INL, inner nuclear layer; GCL, ganglion cell layer. Scale bars: 40 µm. All values are means±s.e.m. *P≤0.05; **P≤0.01; Student's t-test*

S1), and the b-wave implicit time ($F_{2,\ 7}$ = 20.852, *P* = 0.001) (Table S1). These results suggest that cone photoreceptor activity, as measured with the a-wave, and the cone bipolar cell activity, as

measured with the b-wave, were severely altered in *Bmi1*$^{-/-}$ mice. Also, rod activity was affected in *Bmi1*$^{-/-}$ mice, as observed by the lower b-wave amplitude when compared to WT mice, but the

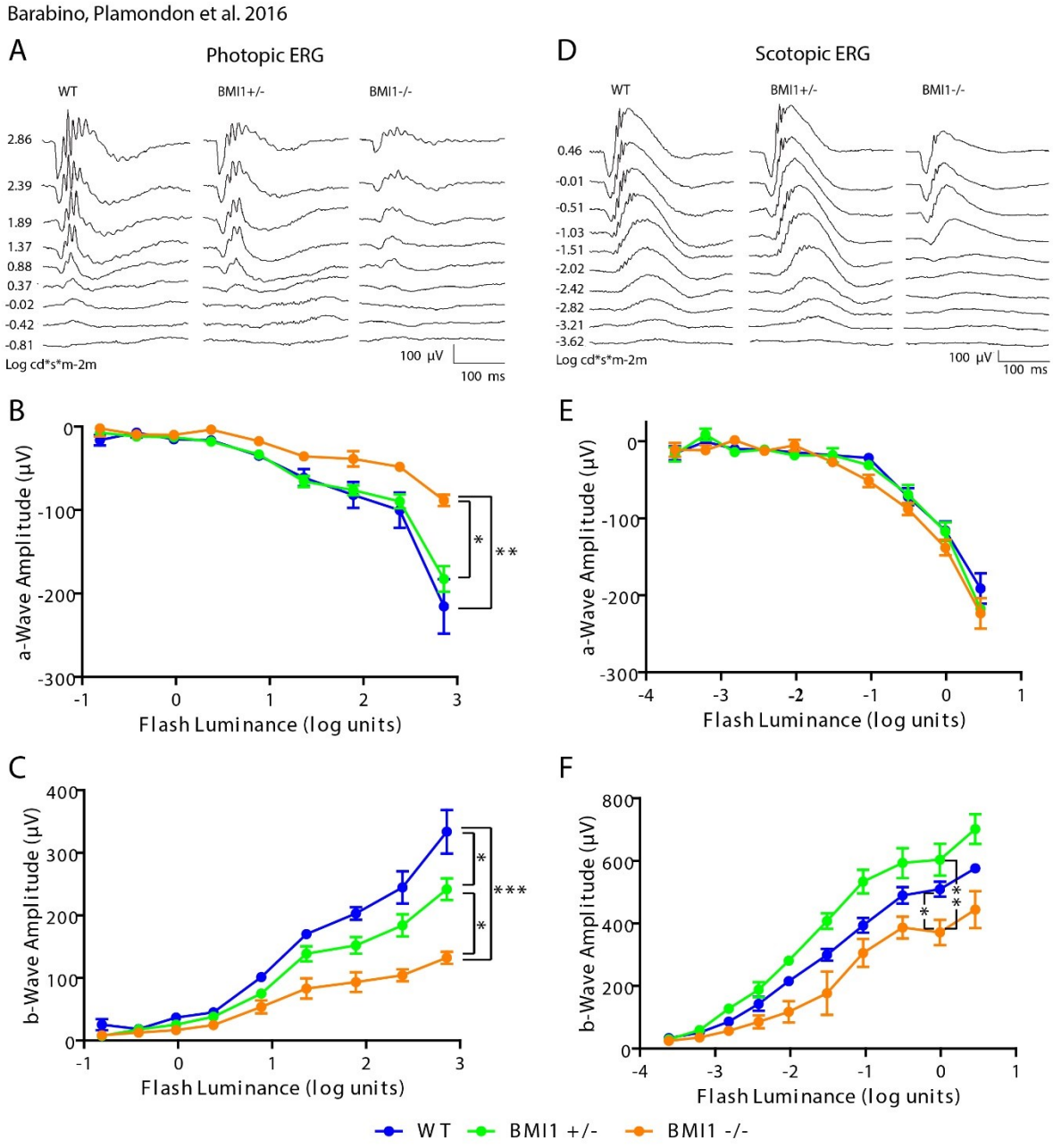

Figure 3: Cone and rod function is severely perturbed in Bmi1−/− mice.

ERG recorded in photopic (A-C) and scotopic (D-F) conditions. (A,D) ERG waveforms for WT, Bmi1+/− and Bmi1−/− mice. Luminance response function curve of a-wave (B,E) and b-wave (C,F) representing the dynamic electrical response from the cone (B,C) and rod (E,F) systems. Note the significant decrease in the retinal responses of Bmi1+/− mice and Bmi1−/− mice in photopic conditions for both the a-wave and b-wave amplitude at the Vmax compared with WT mice and the decrease of the b-wave amplitude at the Vmax in scotopic conditions in Bmi1−/− mice only the b-wave amplitude was found to be significantly different between WT and Bmi1$^{-/-}$ *mice ($F_{2,7}$ = 10.440, p = 0.008) (Fig. 3F and Table S1), suggesting that rod bipolar cell activity was affected in Bmi1*$^{-/-}$ *mice, but at a lower level in front of cones.*

difference was not significant for *Bmi1*$^{+/-}$ mice (Fig. 3D-F and Table S1). When analyzing the LRFs, only the b-wave amplitude was found to be significantly different between WT and Bmi1-/- mice ($F_{2, 7} = 10.440$, $p = 0.008$) (Fig. 3F and Table S1), suggesting that rod bipolar cell activity was affected in Bmi1-/- mice, but at a lower level in front of cones.

3.1.3.2 Loss of heterochromatin and necroptosis in *Bmi1*$^{-/-}$ cones

We next analyzed the retina of *Bmi1*$^{-/-}$ mice by Transmission Electron Microscopy (TEM) to search for ultra-structural anomalies at P30. In WT mice, the electron-dense heterochromatin of rods was preeminent, located in the center of the nucleus, and generally organized as a single large

Barabino, Plamondon et al. 2016

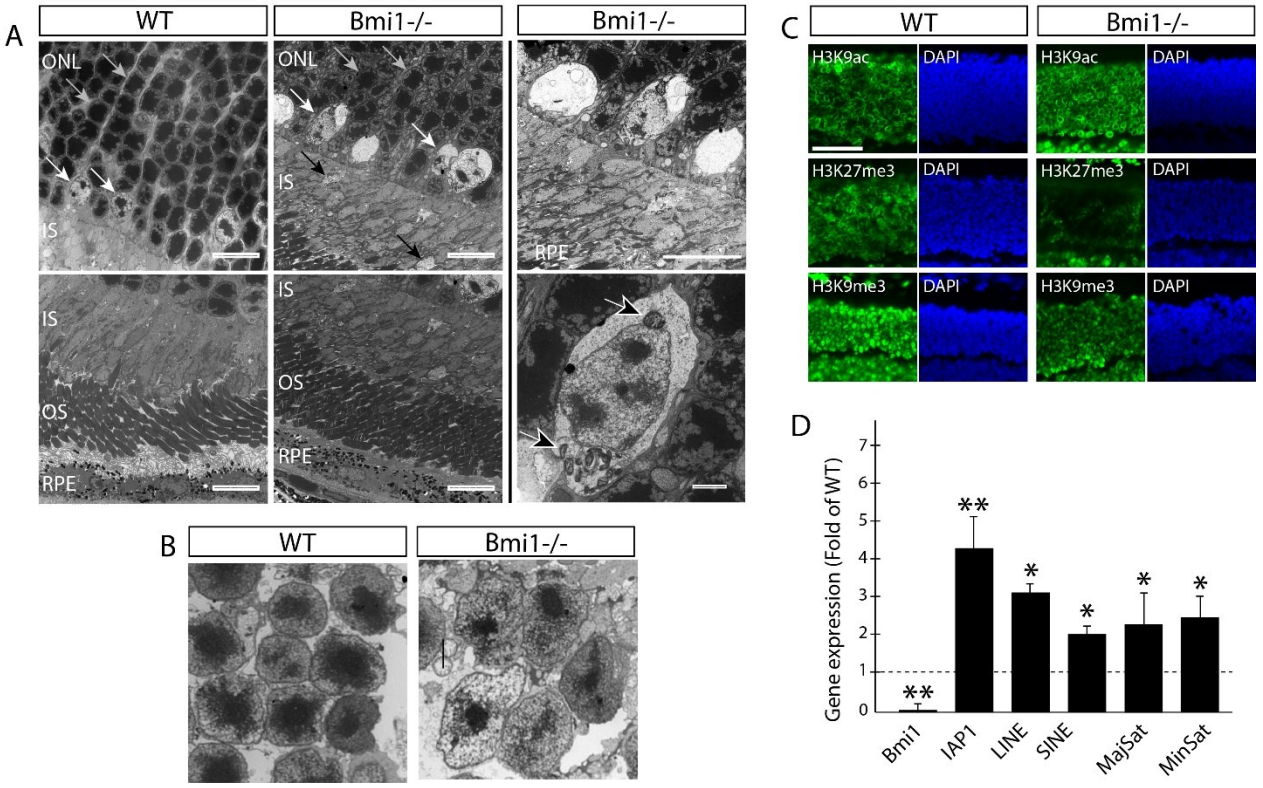

Figure 4: Cone necrosis, loss of heterochromatin and activation of tandem repeats in Bmi1−/− mouse retinas.

*(A) TEM on WT and Bmi1−/− retinas at P30. White arrows, cone photoreceptors; gray arrows, rod photoreceptors characterized by electron-dense heterochromatin organized as a single chromocenter; black arrows, degenerative cone cell bodies; white-edged black arrows, swollen mitochondria in cones. (B) TEM analysis of WT and Bmi1−/− rod photoreceptors at P15. (C) Analysis of histone modifications in WT and Bmi1−/− retinas by IF on sections at P25. (D) Quantitative PCR analysis of expression of repetitive DNA sequences in WT and Bmi1−/− retinas at P30. Bmi1 is used as a negative control and values are expressed as fold of WT value. RPE, retinal pigment epithelium; ONL, outer nuclear layer; OS, outer segment; IS, inner segment. Scale bars: 10 µm (A, left, center and top-right images); 2 µm (A, bottom-right image); 5 µm in B; 25 µm in C. All values are means±s.e.m. *P≤0.05; **P≤0.01; Student's t-test.*

chromocenter (Fig. 4A, grey arrows) (1091). In contrast, cone nuclei had 1-3 chromocenters that occupied a much-reduced nuclear surface (Fig. 4A, white arrows). Cone cell bodies were also located close to the junction with the inner segment in contrast to rod cell bodies, which were evenly distributed in the outer nuclear layer (Fig. 4A and S3A). In *Bmi1*$^{-/-}$ mice, the nucleus of rods appeared normal, but the chromocenter was slightly reduced in size and showed less condensation (see Fig. 4B for more details).

The cell body, IS, and OS of rods were apparently normal. In contrast, cones' cell body and nucleus were swollen and highly degenerative (Fig. 4A, white arrows). Accumulation of swollen mitochondria and fibrous material in the cell body of cones was also observed, suggesting necrotic cell death (also referred to as necroptosis) (Fig. 4A, white/black arrows in the high magnification image) (1092).

To further investigate the observed chromatin phenotype, we analyzed mice at P15, when chromatin condensation of immature rods is not yet completed. Marked differences in rod's heterochromatin condensation could be observed between WT and *Bmi1*$^{-/-}$ mice by TEM (Fig. 4B). By IF on retinal sections at P25, and using antibodies against "open" chromatin (H3K9ac), facultative heterochromatin (H3K27me3), and constitutive heterochromatin (H3K9me3), we found that the chromatin in the outer nuclear layer of *Bmi1*$^{-/-}$ mouse retinas was less condensed when compared to that of WT mice (Fig. 4B) (1093). The intergenic and pericentromeric constitutive heterochromatin contains numerous repetitive DNA sequences of retroviral origin that can be transcribed but generally silenced by heterochromatin formation (1093,1094). We thus compared the expression level of repetitive DNA sequences (*IAP1*, *Line*, *Sine*, *Major satellite repeats,* and *Minor satellite repeats*) between retinas from WT and *Bmi1*$^{-/-}$ mice by qPCR using RNA extracts first treated with DNaseI, since these transcripts are intron-less. We found increased expression of all tested repetitive sequences in *Bmi1*$^{-/-}$ retinas, consistently with the reduced heterochromatin compaction phenotype (Fig. 4C).

To investigate the mechanism of cell death, we measured the expression of genes known to mediate necroptosis (645,1095,1096). We found that the mRNA level of *receptor-interacting protein kinase 3* (*Ripk3*) significantly increased in Bmi1$^{-/-}$ retinas compared to WT (Fig. 5A). Rip3

protein accumulation in *Bmi1*$^{-/-}$ and *Bmi1*$^{+/-}$ retinas was confirmed by Western blot analysis (Fig. 5B). In these preparations, we noticed that Rip3 accumulation could be readily observed upon Ponceau staining of the nitrocellulose membrane. Furthermore, protein accumulation was present at ~20kDa in *Bmi1*$^{-/-}$ retinal extracts, suggesting "programmed" proteolytic cleavage (Fig. 5B).

To identify which retinal cell types were most affected, we performed IF analyses on sections. In both P12 and P30 *Bmi1*$^{-/-}$ retinas, we observed Rip3 immunolabeling in cones, but not in rods, and in neurons located in the inner nuclear layer, thus possibly corresponding to bipolar neurons (Fig. 5C-G). Rip3 immunolabeling was observed in the cell body and outer segment of cones at P12

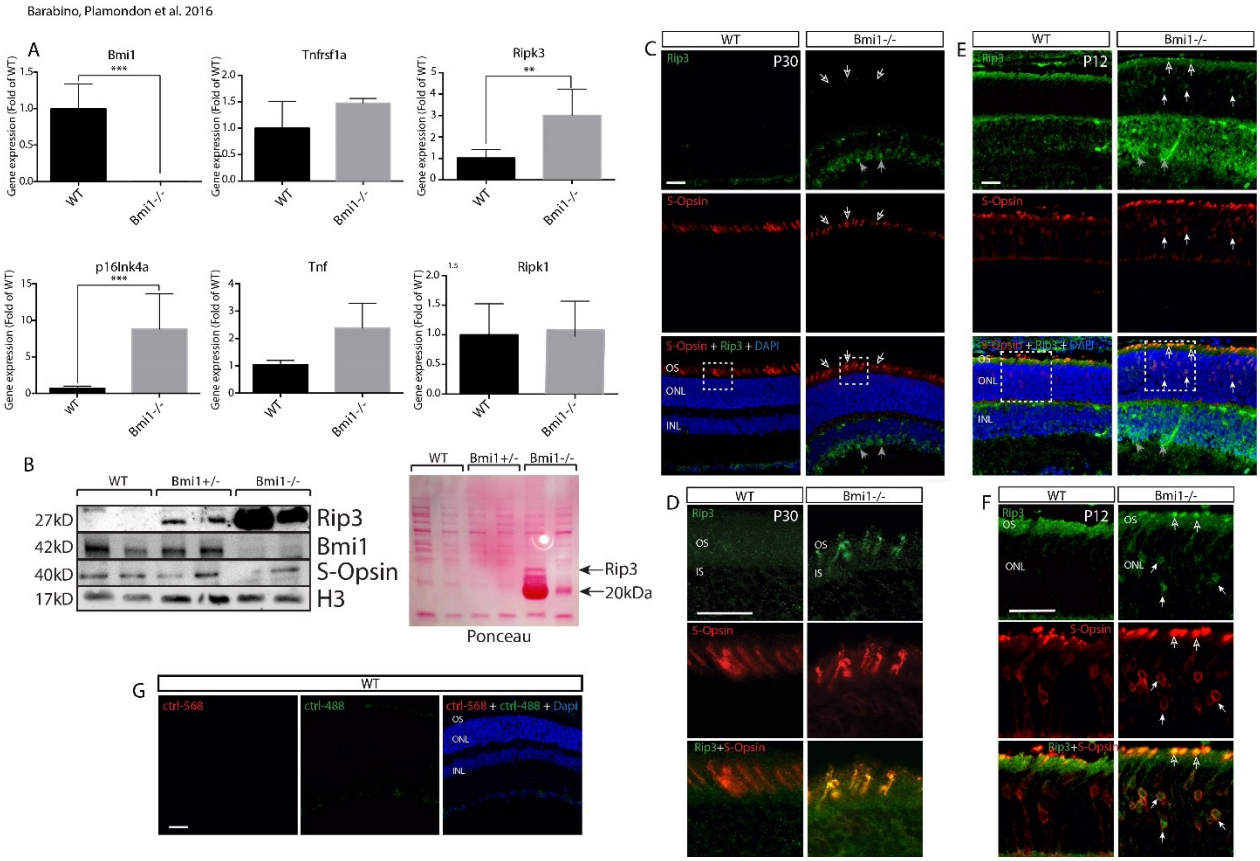

Figure 5: Cone degeneration in Bmi1−/− mice operates through necroptosis.

*(A) RT-qPCR analysis of Bmi1−/− and WT retinal extracts at P30; Bmi1 and P16Ink4a were used as internal controls. Values are expressed as fold of WT. (B) Western blot analyses of retinal extracts from WT, Bmi1+/− and Bmi1−/− mice. Note the gene dosage-dependent increase in Rip3 expression and the decrease in S-opsin expression in Bmi1−/− mice. Ponceau-red staining of the membrane is shown on the right. Histone H3 was used for protein normalization. (C-F) IF analyses on WT and Bmi1−/− retinas at P30 (C,D) and P12 (E,F). White-edged arrows, accumulation of Rip3 in S-cone outer segments; gray arrows, Rip3+ cells in the INL; white arrows, S-opsin+ cells with nuclear expression of Rip3 in Bmi1−/− mice at P12 not present at P30. (G) Control with secondary antibody only. INL, inner nuclear layer; ONL, outer nuclear layer; OS, outer segment; IS, inner segment. Scale bars: 40 µm. All values are means±s.e.m. **P≤0.01; ***P≤0.001; Student's t-test.*

(Fig. 5E-F), but was predominant in the outer segment of cones at P30 (Fig. 5C-D). Morphological anomalies of the cone OS were also easily visible in *Bmi1*$^{-/-}$ retinas at P30 (Fig. 5D). Taken together, these results revealed that necroptosis is the main mechanism of cone PRs cell death in *Bmi1*$^{-/-}$ mice.

3.1.3.3 *Chk2* or *p53* genetic deficiency can partially improve the *Bmi1*$^{-/-}$ retinal phenotype

To investigate additional molecular mechanisms leading to cone degeneration, we generated double-null mutants for the *Bmi1* and *p16*^{Ink4a}*/p19*^{Arf}, *p19*^{Arf,} or *Chk2* alleles. As previously reported, the *p16*^{Ink4a}*/p19*^{Arf} or *p19*^{Arf} mutant alleles did not rescue size or lifespan defects in

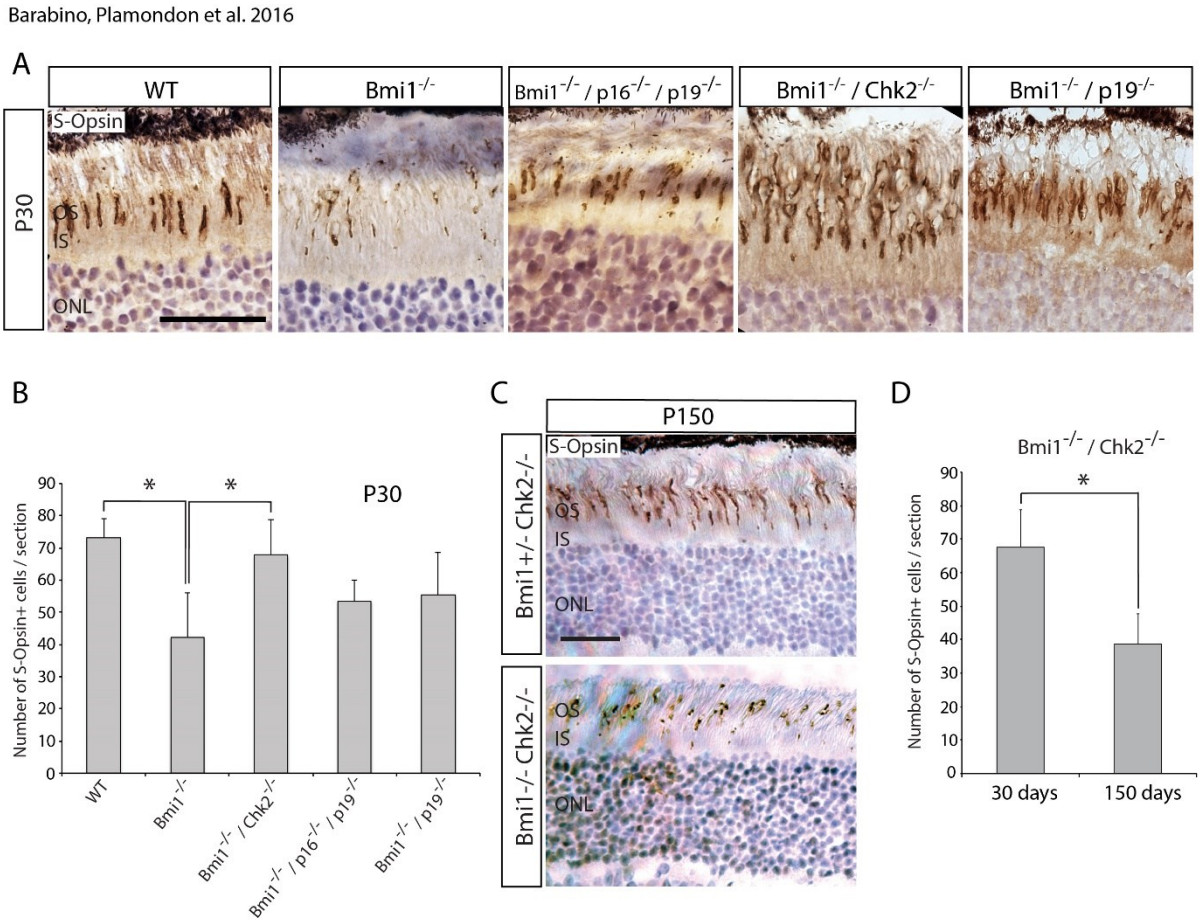

Figure 6: Chk2 genetic deficiency improves the Bmi1−/− cone degeneration phenotype.

*(A) Immunohistochemistry analyses of WT, Bmi1−/− and double mutant retinas at P30. (B) Quantification of the number of S-opsin+ photoreceptors per section for the five genotypes at P30 (n=4 mice for each genotype). (C) IHC analyses of retinas at P150. (D) Quantification of the number of S-opsin+ cells per field at P30 and P150. Scale bars: 40 µm. Quantifications are made from ×25 images. All values are means±s.e.m. *P≤0.05; Student's t-test.*

Bmi1-null mice (581). In contrast, insertion of the *Chk2* mutant allele improved size and lifespan in *Bmi1*-null mice, although *Bmi1*$^{-/-}$*/Chk2*$^{-/-}$ mice remained smaller than normal (Fig. S6).

Interestingly, the number of cones in *Bmi1*-null retinas at P30 was improved by the *Chk2* mutant allele, but not significantly by the *p16*^{Ink4a}*/p19*^{Arf} or *p19*^{Arf} mutant alleles (Fig. 6A-B). However, while the number of S-cones in *Bmi1*$^{-/-}$*/Chk2*$^{-/-}$ mice was improved, the outer segment's morphology remained highly abnormal (Fig. 6A). Analysis of *Bmi1*$^{-/-}$*/Chk2*$^{-/-}$ mice at P150 revealed severe depletion of S-cones, suggesting that *Chk2* deletion only provided a transitory rescue (Fig. 6C-D).

In cortical neurons of *Bmi1*-null mice, stabilization of p53 leads to accumulation of Reactive Oxygen Species (ROS) through repression of the *Nqo1, Gst1*α*,* and *Sestrin2* anti-oxidant genes (601,1097). p53 also promotes neuronal cell death through activation of *Apaf1*, *Fas/CD95,* and *Lpo* (1098). Bmi1 was also proposed to blocks ROS accumulation in blood cells and thymus through direct transcriptional repression of the pro-oxidant genes Cyp241a and Duox2 (1087). By qPCR analysis on retinal extracts, we found that the expression of anti-oxidant genes in *Bmi1*$^{-/-}$ mice was unchanged or increased (*Nqo1*), while that of pro-oxidant genes Cyp241a and Duox2 was increased (Fig. 7A). Notably, the expression of *Apaf1* and *Fas/CD95* was also increased in the retina of *Bmi1*$^{-/-}$ mice, consistently with the observed accumulation of p53 by Western blot (Fig. 7B). Among 200 offspring, we obtained expected numbers of WT, *Bmi1*$^{+/+}$*/p53*$^{+/-}$, *Bmi1*$^{+/+}$*/p53*$^{-/-}$, *Bmi1*$^{+/-}$*/p53*$^{+/-}$, *Bmi1*$^{+/-}$*/p53*$^{+/+}$, *Bmi1*$^{-/-}$*/p53*$^{+/+}$, and *Bmi1*$^{-/-}$*/p53*$^{+/-}$ mice, but a single *Bmi1*$^{-/-}$*/p53*$^{-/-}$ mouse (expected n = 12), for which size and viability were not improved. To evaluate the contribution of *p53* to the cone degeneration phenotype of *Bmi1*$^{-/-}$ mice, we performed double staining with S-Opsin and PNA, which labels the outer segment of all cones. By confocal microscopy, we reconstructed retinal sections in 3D to calculate the number of cones and evaluate their morphology. Interestingly, while the number of S-Opsin/PNA-positive cells was reduced in *Bmi1*$^{-/-}$*/p53*$^{+/-}$ retinas when compared to WT, it was improved in the unique *Bmi1*$^{-/-}$*/p53*$^{-/-}$ retina sample (Fig. 7C-D). However, S-Opsin labeling in the *Bmi1*$^{-/-}$*/p53*$^{-/-}$ retina remained fragmented and disorganized, suggesting improved survival but not morphology of S-cones (Fig. 7C). We also analyzed the samples using the MitoSoxRed reagent, which reacts with mitochondrial ROS on unfixed tissue. In *Bmi1*$^{-/-}$*/p53*$^{+/-}$ retinal sections, we observed robust

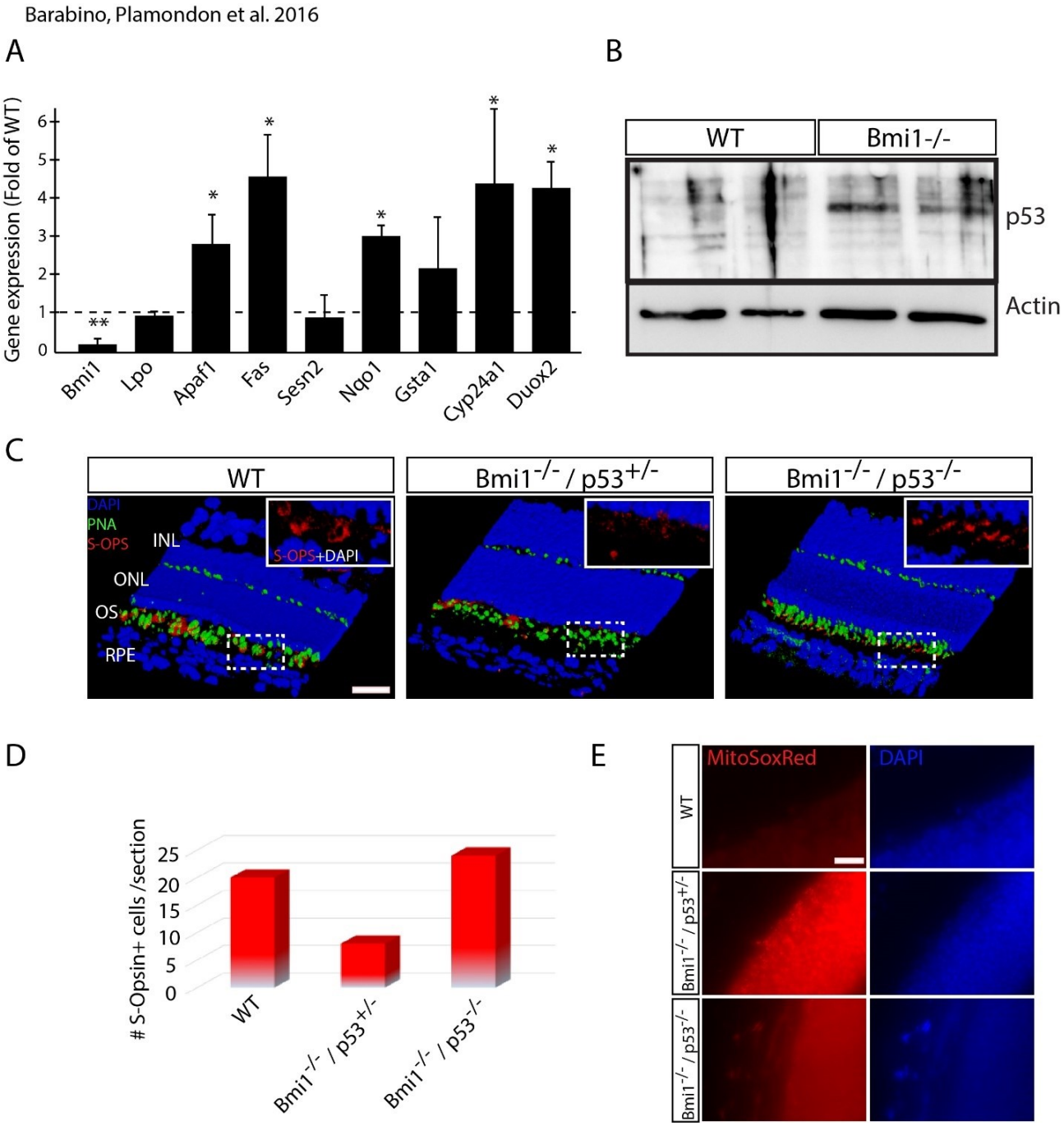

Figure 7: p53 genetic deficiency improves the Bmi1−/− cone degeneration phenotype.

*(A) Quantitative RT-PCR analysis of WT and Bmi1−/− retinal extracts at P30. Bmi1 was used as negative control and all values are expressed as fold of WT. (B) Western blot analysis of mouse retinas at P30 showing p53 accumulation in Bmi1 mutants. (C) 3D reconstruction by confocal microscopy analyses of WT, Bmi1−/−/p53+/− and Bmi1−/−/p53−/− retinas at P30. White box: detail of S-opsin in the outer segment in the dashed box. Note the lower immunoreactivity and the fragmentation of the S-opsin in Bmi1−/−/p53+/− mice and a rescue in the quantity of S-opsin in the Bmi1−/−/p53−/− even if it is still fragmented. (D) Quantification of S-opsin+ cells per section in WT, Bmi1−/−/p53+/− and Bmi1−/−/p53−/− mice. (E) IF analyses of WT and Bmi1−/− retinas at P30 stained with MitoSoxRed. Note the partial rescue in Bmi1−/−/p53−/− mice when compared with WT. RPE, retinal pigment epithelium; ONL, outer nuclear layer; INL, inner nuclear layer; OS, outer segment. Scale bar: 50 µm in C; 20 µm in E. All values are means±s.e.m. *P≤0.05; **P≤0.01; Student's t-test.*

fluorescence when compared to WT, suggesting increased mitochondrial ROS. Notably,

fluorescence was highly reduced in the *Bmi1*$^{-/-}$*/p53*$^{-/-}$ mutant retina but not completely restored to WT levels (Fig. 7E). These results revealed the partial contribution of *Chk2* and *p53* to the cone degeneration phenotype of *Bmi1*$^{-/-}$ mice.

3.1.3.4 BMI1 is enriched at heterochromatic foci in human cones

We previously reported on BMI1 expression in the human retina and down-regulation during aging (1099). Here we investigated BMI1 localization in human PRs. Using confocal IF analyses on adult human retinas, we observed punctuate BMI1 immunolabeling in the nucleus of PRs (Fig. 8A-C). In some cells that co-labeled with S-Opsin or M-Opsin, BMI1 immunolabeling was even more robust and present as multiple foci/nucleus (Fig. 8A). To characterize the BMI1

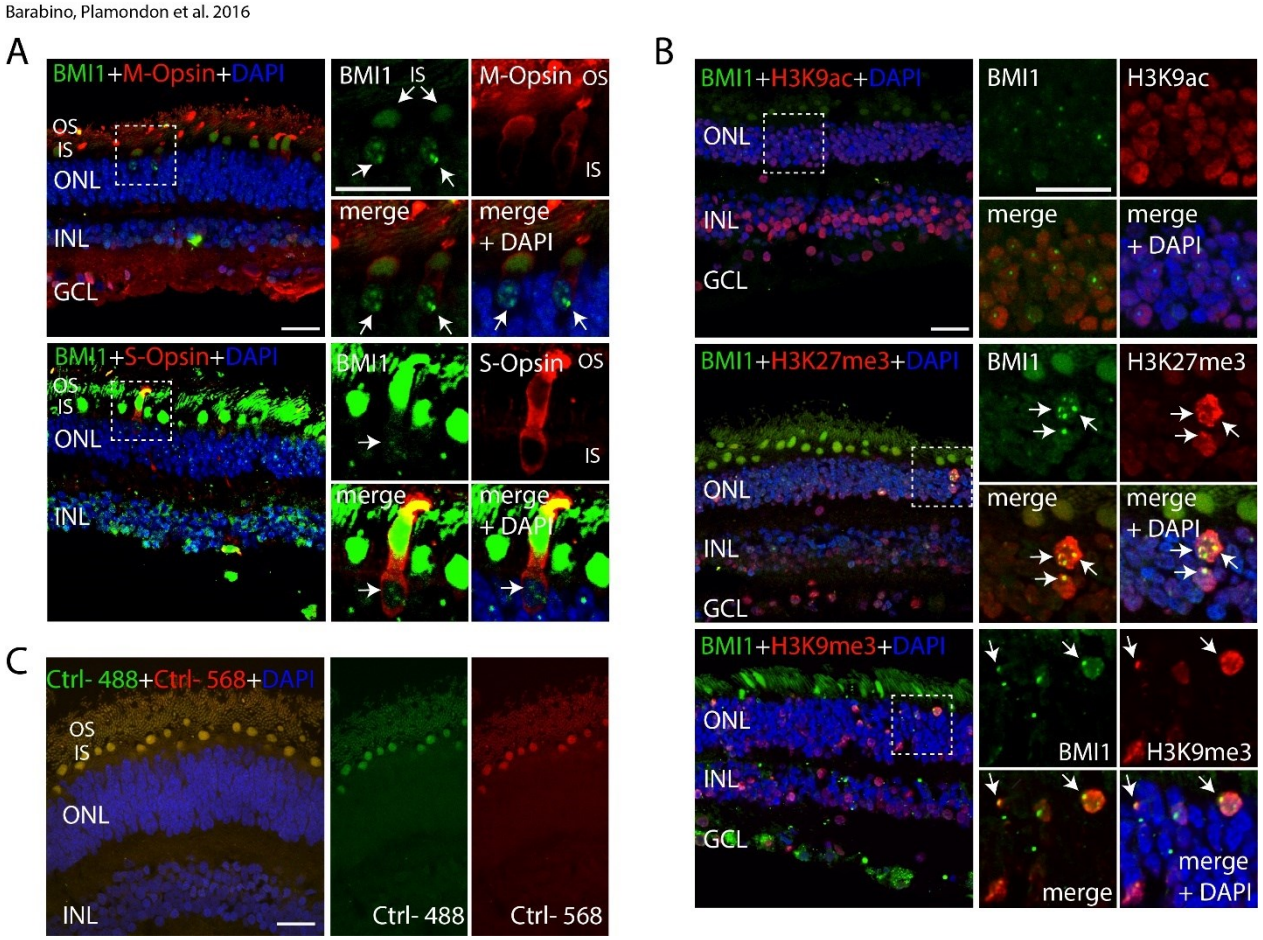

Figure 8: BMI1 is enriched at heterochromatic nuclear foci in human cones.

(A-C) Confocal IF analysis of BMI1 expression in the adult human retina. (A) BMI1 is expressed in the nucleus of M-opsin+ and S-opsin+ cones (arrows). (B) BMI1 is enriched at heterochromatic nuclear foci as shown by colocalization with H3K9me3 and H3K27me3 in cones (arrows). (C) Negative control with only the secondary antibody. Note the strong autofluorescence present in the IS and OS. ONL, outer nuclear layer; INL, inner nuclear layer; IS, inner segment; OS, outer segment; GCL, ganglion cell layer. Scale bars: 20 µm.

immunolocalization pattern on the chromatin of cones, we performed dual immunolabeling with antibodies directed against distinct histone modifications. While BMI1 did not co-localize with H3K9ac, it co-localized with H3K27me3 and H3K9me3, suggesting distribution at both facultative and constitutive heterochromatin in human cones (Fig. 8B).

3.1.3.5 BMI1 is required for human cone differentiation and chromatin integrity

To investigate BMI1 function during human cone development, we used a protocol allowing the differentiation of ~70% of hESC into cones (1100). This method results in the generation of immature S-cones expressing CRX, cone Arrestin (*ARR3*), and S-Opsin within 21 days (Fig. 9A, D, and E). Importantly, *in vitro* generated S-cones expressed BMI1, which also co-localized with H3K9me3 (Fig. 9A-B). We infected hESCs with a lentivirus expressing a small hairpin RNA against *BMI1* (shBMI1) or scramble sequence (shScramble) and performed hygromycin selection for 10 days (574). The hESCs were next differentiated into S-cones for 21 days. By Western blot analysis, we observed that BMI1 was not expressed at significant levels in naive hESCs, in contrast to *in vitro* differentiated cones (Fig. 9C). Histone H2Aub is the target of BMI1/RING1a/b biochemical activity (567,1083,1084,1101). Consistently, H2Aub was reduced in differentiated cones upon BMI1 knockdown (Fig. 9C). To confirm cone differentiation, we analyzed cells for S-Opsin and CRX expression (107–109,1077,1078). In control cells, S-Opsin and CRX expression was observed in greater than 70% of cells, as visualized by IF and Western blot (Fig. 9A and D). In contrast, S-Opsin and CRX expression was highly reduced in differentiated cones upon BMI1 knockdown (Fig. 9A and D). When using a hypomorphic construct against BMI1 that reduces BMI1 levels by ~50% (shBMI1 50%) (574), CRX expression in differentiated cones was reduced by ~25% when compared to control cells, suggesting a modest gene-dosage effect (Fig. 9D). Considering the role of p53 activation in the context of *Bmi1* deficiency, we investigated p53 expression (601). Using a pan-antibody against p53 that recognizes all family members i.e., p73, p63, and p53, we observed predominant expression of p73 in shScramble and shBMI1 50% cones (Fig. 9D) (1102). In contrast, p73 was lost in shBMI1 95% cones and associated with induction of p63 and p53 (Fig. 9D). It was previously proposed that one primary function of PcG proteins in mouse ES cells is to prevent differentiation through repression of lineage-specific homeobox genes such as PAX, SOX,

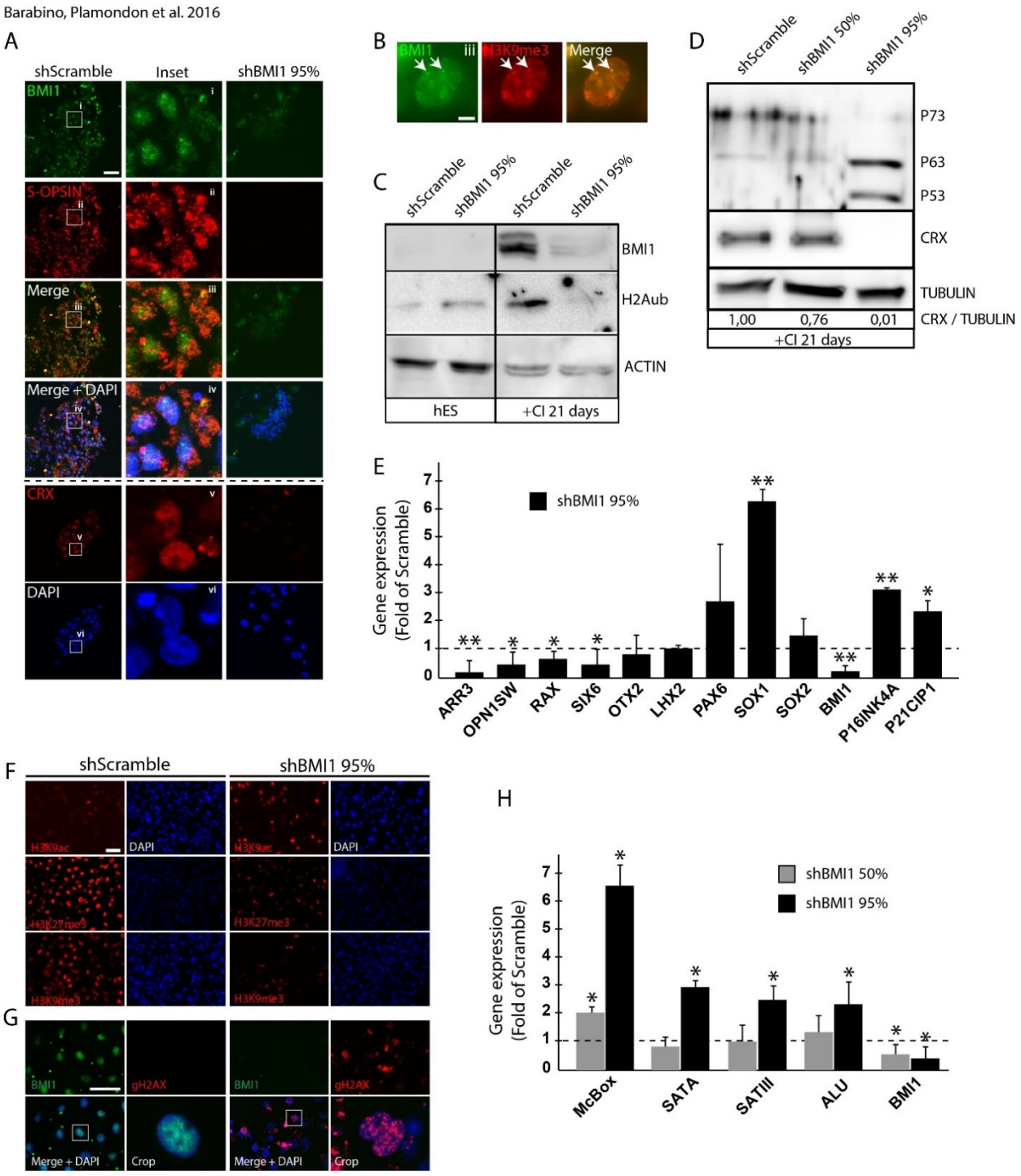

Figure 9: BMI1 is required for terminal differentiation, heterochromatin compaction and genomic stability of human cones.

*(A,B) IF analysis of hESCs differentiated for 21 days toward the cone photoreceptor cell lineage. (A) In controls (shSrcamble), BMI1 is expressed in the nucleus of S-opsin+ cells. In shBMI1 cells, BMI1, S-opsin and CRX expression were highly reduced when compared with controls. (B) Colocalization of BMI1 and H3K9me3 in cones (arrows). (C,D) Western blot analyses of hESCs and in vitro differentiated cones (+CI 21 days) infected with shScramble or shBMI1 viruses. Note that BMI1 knockdown affects histone H2Aub levels only in cones; BMI1 knockdown in human cones was accompanied by induction of p53. Quantification of CRX levels normalized to tubulin; note the dose-dependent reduction in CRX expression in BMI1 knockdown cells. (E,H) Quantitative RT-PCR analyses of in vitro differentiated cones for retinal markers (E) and repeat DNA sequences (H). BMI1 was used as negative control and values are expressed as fold of Scramble value. (F,G) IF analyses of hESC-derived cones (day 21). Scale bars: 20 µm in A,F,G; 2 µm in B. All values are means±s.e.m. *P≤0.05; **P≤0.01; Student's t-test.*

and LHX families (1103). To further characterize the cone differentiation phenotype, we analyzed

the cells by qPCR. We found that while the expression of cone-specific genes (*ARR3* and *OPN1SW*) and retinal homeobox genes (*RAX* and *SIX6*) was reduced by 50-75% in shBMI1 cells, expression of *SOX1* was increased by ~6 folds when compared to control cells (Fig. 9E).*SOX1* and *SOX2* are enriched in neural stem cells and retinal progenitors but are not expressed in PRs, thus providing a possible explanation for the defective terminal differentiation of cones upon BMI1 knockdown (54,1104–1107).

To investigate the effect of BMI1 knockdown on the chromatin of human cones, we performed IF analyses. BMI1 knockdown resulted in increased H3K9ac levels but reduced H3K27me3 and H3K9me3 levels when compared to control cells (Fig. 9F). BMI1 knockdown was also associated with the formation of γH2Ax foci, a histone modification characteristic of DNA double-strand breaks and genomic instability (Fig. 9G) (589,594,1108,1109). We observed the induction of repeat-DNA sequences in BMI1 knockdown cones consistently with the chromatin relaxation phenotype, with a modest gene-dosage effect when using the hypomorphic shBMI1 construct (Fig. 9H). These experiments revealed that BMI1 is required for terminal differentiation, heterochromatin compaction, repeat-DNA silencing, and genomic stability in human cones.

3.1.4 Discussion

We showed here that cone PRs and bipolar neurons are normally generated but then undergo rapid degeneration in *Bmi1*$^{-/-}$ mice, and this through Rip3-associated necroptosis. Selective retinal cell degeneration in *Bmi1*$^{-/-}$ mice also correlated with predominant Bmi1 expression in bipolar neurons and cone PRs. Cone number but not morphology in *Bmi1*$^{-/-}$ mice was partially rescued by either *Chk2* or *p53* deletion, implicating these additional pathways in neurodegeneration. BMI1 was expressed in human cones, where it localized at heterochromatic foci. BMI1 inactivation in hESC severely perturbed differentiation of cones, in contrast to the situation found in *Bmi1*$^{-/-}$ mice. However, BMI1-deficient human cones also presented common features with the *Bmi1*$^{-/-}$ mouse retinal phenotype, revealing partially conserved functions across species.

In previous work, it was proposed that *Bmi1* inactivation could prevent rod and cone PRs degeneration in *Rd1* mice, a model of RP (611). *Rd1* mice carry a mutation in *Pde6b*, which is only expressed in rods. Thus, cone degeneration in *Rd1* mice is thought to be secondary to the loss of trophic support provided by rods. Since rod PRs apoptosis in *Rd1* mice is preceded by cell cycle re-entry and cyclin-dependent kinase (CDKs) activation, it was suggested that loss of *Bmi1* provided neuroprotection by blocking CDKs activation and thus cell cycle re-entry of rods (611,1110,1111). Here we found that *Bmi1* deficiency was associated with the activation of several cell cycle inhibitors in the retina such as p16^{Ink4a}, p19^{Arf}, Chk2, and p53, consistently with Bmi1 general function at inhibiting the p16^{Ink4a}/CDK6/Rb and p19^{Arf}/p53/p21^{Cip1} pathways (1112). Thus, and taken in the context of the *Rd1* mutation, the proposed model is likely valid, but only in rods. Also, whether acute Bmi1 inhibition in *Rd1* mice can prevent rod degeneration remains to be demonstrated, as this would be more relevant to a clinical context. Interestingly, the outer segment of cones is abnormal in *Rd1*/*Bmi1*$^{-/-}$ mice, as shown using anti-S-Opsin labeling, suggesting rod-independent cone degeneration (611). This is consistent with our overall findings suggesting cell-autonomous degeneration of cones in *Bmi1*$^{-/-}$ mice.

Our genetic studies further revealed that *Chk2* or *p53* deletion could improve initial cone number in *Bmi1*$^{-/-}$ mice but not the outer segment morphology and progressive degeneration. This is consistent with previous work showing that in *Bmi1*$^{-/-}$ mice, *Chk2* inactivation improved several pathologies and lifespan and that *p53* inactivation prevented cortical neuron cell death

(601,1087). However, Bmi1 and p53 functions in the mouse retina, especially in cones, are apparently not identical to cortical neurons. For example, while p53-dependent apoptotic cell death was predominant in *Bmi1*$^{-/-}$ cortical neurons, it was not in *Bmi1*$^{-/-}$ cones, where we observed Rip3-associated necroptosis. At the molecular level, expression of the phase II anti-oxidant genes *NQO1* and *GST1*□ was also not reduced in *Bmi1*$^{-/-}$ retinas, in contrast to *Bmi1*$^{-/-}$ cortices. Since these are direct p53 targets, it suggests that p53 activity is distinct between the retina and brain in the context of *Bmi1* deficiency.

In recent years, necroptosis was revealed as an alternative cell death mechanism in many pathological contexts (645,1092). In the retina, it was found that cones, not rods, are especially vulnerable to necroptosis. For example, mutations in the cone-specific gene *PDE6C* result in Achromaptosis, a disease characterized by cone degeneration (1113). Using a zebrafish mutant for *pde6c*, it was shown that cone degeneration is mediated by rip1 and rip3, and that inhibition of necroptosis with necrostatin-1 can delay the disease process. Interestingly, necroptosis also operates in cones even when cone cell death is non-cell-autonomous, such as in

rd10 mice carrying a mutation in the rod-specific gene *pde6b* (1095). Here again, treatment of *rd10* mice with necrostatin-1 greatly improved the cone degeneration phenotype, bringing hope for possible pharmaceutical treatment of degenerative cone diseases.

Using directed differentiation of hESCs as a retinal development model, we demonstrated that BMI1 is required for the terminal differentiation of human cones. In contrast, the expression of retinal homeobox genes and *S-Opsin* was not altered in *Bmi1*$^{-/-}$ mouse retinas, revealing possible inter-species differences. However, these differences may be explained by compensation mechanisms operating during development in *Bmi1*$^{-/-}$ mice but not in *BMI1* knockdown cells or by the highly distinct experimental systems. For example, acute *Bmi1* inactivation in embryonic mouse cortical progenitors was shown to induce massive apoptosis, in sharp contrast to the situation observed in *Bmi1*$^{-/-}$ mice (576). Taken into a broader context, it is interesting to note that mice conditionally deficient for *Ezh2*, the catalytic subunit of the PRC2, which tri-methylates histone H3 at lysine 27, show reduced RPCs proliferation and increased apoptosis, but not post-natal degeneration of retinal neurons (1114). Likewise, mice deficient for *G9a*, which di-

methylates histone H3 at lysine 9, show increased RPCs apoptosis and persistent cell proliferation (1115). In both cases, inefficient repression of non-retinal genes such as *Six1* (*Ezh2* KO) or RPCs genes such as *Hes1*, *Chx10,* and *Lhx2* (*G9a* KO) perturbs the terminal differentiation of retinal cells. Thus, these two situations are similar to what we have observed in BMI1 deficient cones, where expression of *SOX1* was abnormally upregulated. At the chromatin level, it was demonstrated that rod PRs of mice deficient for all 3 linker histone H1 genes have reduced chromatin condensation and increased nuclear diameter (1116), a phenotype also similar to the one found in *Bmi1*$^{-/-}$ mouse PRs and BMI1-deficient cones. BMI1 functions at preventing heterochromatin loss and tandem-repeats expression in PRs also represent novel findings. Since constitutive heterochromatin is the most unstable portion of the mammalian genome (1117–1121), this could explain part of the genomic instability phenotype observed in BMI1 deficient cells (589,594,1108).

In conclusion, we demonstrated that Bmi1 expression in the retina is not required for retinal cell type genesis but essential to prevent bipolar neurons and cone PRs degeneration during post-natal development. Retinal cell death in *Bmi1*$^{-/-}$ mice was mediated by Chk2 and p53 on one hand and by Rip3-associated necroptosis on the other hand. Whether necroptosis is directly repressed by Bmi1 or indirectly mediated by the activity of p53 or Chk2 remains to be elucidated. Using an *in vitro* model of human cone development, we further demonstrated that BMI1 is required for the terminal differentiation of cones and maintenance of their genomic integrity. Further experiments, through BMI1 inactivation in terminally differentiated cones, should address whether BMI1 is important to prevent human cone PRs degeneration and/or cell type identity maintenance.

3.1.5 Materials And Methods

3.1.5.1 Ethic statement

The Animal Care Committee of the Maisonneuve-Rosemont Hospital Research Centre approved the use of the animals in this study. Post-mortem human eyes were provided by the Banque d'yeux du Québec du Centre Michel-Mathieu (http://www.maisonneuve-rosemont.org/pages/h/hopital/HMRCentreMichelMathieu.aspx) and were used with approbation of the Comité d'Éthique à la Recherche de l'Hôpital Maisonneuve-Rosemont. Human ESCs were used in accordance to Canadian Institute Health Research (CIHR) guidelines and approved by the Comité de Surveillance de la Recherche sur les Cellules Souches (CSRCS) of the CIHR.

3.1.5.2 Human specimens

Fresh eyes were provided by the Eye's Bank of Maisonneuve-Rosemont Hospital and used with permission of our institutes' ethical committee. Retinas were dissected and fixed in 4% paraformaldehyde, then cryopreserved in 30% sucrose and frozen until use.

3.1.5.3 Animals

Mice KO for *p53*, *p16^{Ink4a,}* or *p16^{Ink4a}/p19^{Arf}* were obtained from the Jackson Laboratory, Bar Harbor, Ma, USA. Wild-type mice of the C57BL/6 genetic background were obtained from Charles River, St-Constant, Canada.

3.1.5.4 Cell cultures

Cultures of retinal cells were obtained by dissecting the mice eyes at P5 in 1X oxygenated HBSS (Life Technologies) in order to extract only the neural retina. Retinal cells were then re-suspended and incubated 10 minutes at 37 ° C in the enzyme solution composed of 10ml 1X HBSS, 9.3 mg of Papain (Worthington), 1.6 mg of N-acetyl L-cysteine (Sigma), 0.5 mg of DNaseI (Roche), and 10µl EDTA 500mM (Fisher Scientific). After centrifugation cells were dissociated into Neurobasal^{tm} medium (Life Technologies) with 0.02µg/µl NGF (Invitrogen), 0.02 µg/µl BDNF (Invitrogen), 1% B27 (Invitrogen), 70µg/ml gentamycin (Invitrogen), 1% fetal bovine serum (Wisent), 0.5% glucose

(Sigma) and 10 µM Forskolin (Sigma). The cells were then spread and cultivated on coverslips treated with Poly-L-Lysine hydrobromide (Sigma) and BD Matrigel Matrix (BD Biosciences).

The hESC line H9 (WiCell) was cultured on BD Matrigel-coated plate (BD bioscience) with a daily change of mTeSR medium according to the manufacturer's instruction (Stemcell Technologies) (887). The H9 hESC line was first established on mouse embryonic fibroblasts (MEFs) and then cultured on Matrigel in mTeSR media. For S-cones derivation, undifferentiated hESC colonies expanded at near confluence were next cultured in DMEM-F12 media supplemented with 2% B27, 1% N2, 1% NEAM (Life technologies), 10 ng/ml IGF1, 10 ng/ml FGF2 (Peprotech), 10µg/ml Heparin (Sigma) and 30 ng/ml Coco (R&D Systems) for 21 days.

3.1.5.5 ERG recording and analysis

ERGs were recorded on mice (WT: n = 4; *Bmi1*$^{+/-}$: n = 3; *Bmi1*$^{-/-}$; n = 3) in photopic and scotopic conditions to assess the cone and rod systems activity, respectively, according to the procedure previously described (1122). A typical ERG trace is composed of the a-wave, which is a negative component originating from the PRs, and the b-wave, which is a positive component generated by the bipolar and Müller cells complex stimulation. Two major parameters can be derived from these waves: amplitude (µV) and implicit time (ms). By convention, the amplitude of the a-wave is measured from the baseline to trough, and the b-wave amplitude is measured from the trough of the a-wave to the peak of the b-wave. The implicit time of the waves represents the number of milliseconds at which the maximal amplitude is reached. For each of the four parameters, a photopic and scotopic LRF was generated, where the values of the parameters were plotted against flash luminance. Repeated measures analyses of variance with Bonferroni correction were performed to assess the difference between the three genotypes for each one of the parameters. All analyses were conducted using SPSS for Windows, version 22.0.

3.1.5.6 Immunohistochemistry and immunofluorescence

Tissues were fixed by immersion for 1 h at room temperature in 4% paraformaldehyde (PFA)/3% sucrose in PBS, pH 7.4. Samples were washed three times in PBS, cryoprotected in PBS/30% sucrose, and frozen in CRYOMATRIX embedding medium (CEM) (Thermo Shandon, Pittsburgh, PA) or in Tissue-Tek® optimum cutting temperature (O.C.T.) compound (Sakura Finetek, USA).

Otherwise, tissues were fixed in 10% buffered formalin and embedded in paraffin according to standard protocols. 5 to 12 µm thick sections were mounted on Super-Frost glass slides (Fisher Scientific) and processed for immunofluorescence or immunohistochemistry staining. For immunofluorescence labeling, sections were incubated overnight with primary antibody solutions at 4ºC in a humidified chamber. After three washes in PBS, sections were incubated with secondary antibodies for 1 h at room temperature. Slides were mounted on coverslips in DAPI-containing mounting medium (Vector Laboratories, CA). According to the manufacturer's instructions for immunohistochemistry labeling, slices were analyzed using the Vectastain® ABC kit (Vector). Peroxidase substrates used are the Vector® VIP (Pink) (Vector) and DAB (brown) (Sigma). Observations were made under a fluorescence microscope (Leica DMRE, Leica Microsystems), and images were captured with a digital camera (Retiga EX; QIMAGING; with OpenLab, ver.3.1.1 software; Open-Lab, Canada). Confocal microscopy analyses were performed using 60x objectives with an IX81 confocal microscope (Olympus, Richmond Hill, Canada), and images were obtained with Fluoview software version 3.1 (Olympus). 3D reconstructions were obtained with Fluoview software version 3.1 from 18-25 z-stack images. Primary antibodies used in this study are: sheep anti-Chx10 (1:250, Exalpha Biologicals), rabbit anti-Pax6 (1:500, Chemicon), mouse anti-Bmi1 (1:200, US Biological), rabbit anti-Bmi1 (1:150, US Biological), mouse anti-Syntaxin (1:200, Sigma), mouse anti-4D2 (Rhodopsin) (1:100, R. Molday, UBC), mouse anti-Gad65 (1:300, BD Pharmingen), rabbit anti-CORD2 (CRX) (1:300, Abcam), rabbit anti-S-Opsin (1:200, Invitrogen), rabbit anti-M-Opsin (1:100, Chemicon), Rip3 (1:250, Santa Cruz), rabbit anti-H3K9me3 (1:500, Abcam), rabbit anti-H3K9ac (1:300, Cell Signaling), rabbit anti-H3K27me3 (1:300, Cell Signaling), mouse anti-glutamine synthetase (GS) (1:100, Chemicon), rabbit anti-Pkcα (1:500, Sigma), rabbit anti-Calbidin (1:500, Chemicon), rabbit anti-Recoverin (1:1000, Millipore), mouse anti-γH2Ax (1:250, Millipore), rabbit anti-Cralbp (1:500, kindly given by Dr Saari's lab). Secondary antibodies are: donkey AlexaFluor488-conjugated anti-mouse (1:1000, Life Technologies), donkey AlexaFluor488-conjugated anti-rabbit (1:1000, Life Technologies), goat AlexaFluor594-conjugated anti-mouse IgM (1:1000, Invitrogen), donkey AlexaFluor633-conjugated anti-sheep (1:1000, Molecular Probes), goat AlexaFluor647-conjugated anti-mouse (1:1000, Life Technologies) goat AlexaFluor texas red-conjugated anti-rabbit (1:1000, Life

Technologies), donkey FITC-conjugated anti-mouse (1:300, Chemicon), goat FITC-conjugated anti-rat (1:300, Caltag Laboratories), donkey Rhodamine-conjugated anti-rabbit (1:300, Chemicon). Fluorescein labeled PNA (1:200, Vector laboratories) was used to stain the outer segment of PRs. Superoxide production was measured by red fluorescence intensity as described by standard protocol indicated by the manufacturer (MitoSoxRed mitochondrial superoxide indicator, Molecular Probes, U.S.).

3.1.5.7 Retinal dissection and eyes orientation

Eyes were labeled in the dorsal pole of the cornea by puncturing with a needle tip. Eyes were extracted, fixed in 4% PFA o/n, and stored in PBS. The retinas were marked by a small incision following the respective mark on the cornea. Retinas were then dissected as flattened whole-mounts by four radial cuts and processed for IF using the standard procedure as described above. Retinas were mounted between two coverslips that were attached to a slide by scotch tape, allowing flip-flopping of the retinas for analysis by microscope. For the preparation of the blocks for cryosections, eyes were marked as described above and oriented in blocks to maintain eye polarity.

3.1.5.8 Quantifications of retinal cell types

To collect sections from the ventral retina, blocks were trimmed up to the optic nerve, and sections were collected. Three successive images were taken on the nasal side for quantification from a set distance from the optic nerve. At least three different mice were used for each genotype (1 eye/animal), except for the *p53*$^{-/-}$*/Bmi1*$^{-/-}$ mouse, where only two eyes were available. Positive cells were counted manually using ImageJ software. For IF analysis, single analysis of the Green channel (488) and Red channel (568) were done to prevent filter overlap. To assess the general distribution of cones, whole-mounts were photographed with a 10x objective using a microscope Zeiss (Observer.Z1) equipped with a computer-driven motorized stage (VEXTA stepping motor), and individual frames were tiled to reconstruct the whole-mounts (about 36 images/retina) using AxioVision 4.8 software. For quantification of IF images, photos were taken with a confocal microscope equipped with a 60x objective. Three images were taken/sample, where n = 4 eyes/condition, at the same distance from the optic nerve in the naso-ventral portion

of the retina. PRs labeled with PNA or with S-Opsin and PNA were counted manually using ImageJ software. Quantifications of IHC experiments were performed in the same way but using images were taken with a microscope Zeiss (Observer.Z1) equipped with a 25x objective.

3.1.5.9 Quantitative RT-PCR

All primers were designed to flank individual exons and tested by PCR in RT+ and RT- control extracts. Total RNA was isolated using TRIzol reagent (Invitrogen). Reverse transcription (RT) was performed using 1 µg of total RNA and the MML-V reverse transcriptase (Invitrogen). Quantitative real-time PCR (qPCR) was performed using the Platinum SYBRGreen SuperMix (Invitrogen) and a real-time PCR apparatus (ABI Prism 7000). GAPDH was used as an internal standard for data calibration. The $2^{-\pi\,\pi\,Ct}$ formula was used for the calculation of differential gene expression. All experiments were performed at least in triplicates. Mouse primer sets used are:

Tnf-alpha (F) 5' AAAATTCGAGTGACAAGCCTGTAG 3'; Tnf-alpha (R) 5' CCCTTGAAGAGAACCTGGGAGTAG 3'; Tnfrsf1a (F) 5' GCCGGATATGGGCATGAAGC 3'; Tnfrsf1a (R) 5' TGTCTCAGCCCTCACTTGAC 3'; Ripk1 (F) 5' TGTCATCTAGCGGGAGGTTG 3'; Ripk1 (R) 5' TCACCACTCGACTGTGTCTCAG 3'; Ripk3 (F) 5' CTCCGTGCCTTGACCTACTG 3'; Ripk3 (R) 5' AACCATAGCCTTCACCTCCC3'; Bmi1 (F) 5'-GGAGACCAGCAAGTATTGTCCTATTTG-3', Bmi1 (R) 5'-CTTACGATGCCCAGCAGCAATG-3'; $p16^{Ink4a}$ (F) 5'-CAACGCCCCGAACTCTTTC-3', $p16^{Ink4a}$ (R) 5'-GCAGAAGAGCTGCTACGTGAAC-3'; $p19^{Arf}$ (F) 5'-GGCTAGAGAGGATCTTGAGAAGAGG-3', $p19^{Arf}$ (R) 5'-GCCCATCATCATCACCTGGTCCAGG-3'; Sox2 (F) 5'-TAAGGGTTCTTGCTGGGTTTT-3', Sox2 (R) 5'-AGACCACGAAAACGGTCTTG-3'; Lhx2 (F) 5'-GATCTCGCCTGGAAACAGAG -3', Lhx2 (R) 5'-TCGCTCAGTCCACAAAACTG -3'; Otx2 (F) 5'-AGAGGAGGTGGCACTGAAAA-3', Otx2 (R) 5'-TGACCTCCATTCTGCTGTTG-3'; Lpo (F) 5'-AGGTCTGTTGGCCAAGAATG-3', Lpo (R) 5'-ATGTTGATGGAAGCCAGGTC-3'; Apaf1 (F) 5'-TGCTCAGCGGATAAGAAGGT-3', Apaf1 (R) 5'TCCCAGAGCTTGAGGAAGAA-3'; Fas/CD95 (F) 5'-AAACAAACTGCACCCTGACC-3', Fas/CD95 (R) 5'CAACCATAGGCGATTTCTGG-3'; Nqo1 (F) 5'-TTCTCTGGCCGATTCAGAGT-3', Nqo1 (R) 5'GAGTGTGGCCAATGCTGTAA-3'; Gstα1 (F) 5'-CGCCACCAAATATGACCTCT-3', Gstα1 (R) 5'CCATGGCTCTTCAACACCTT-3'; Cyp241a (F) 5'-GGCGGAAGATGTGAGGAATA-3', Cyp241a (R) 5'GTTGTGAATGGCACACTTGG-3'; Duox2 (F) 5'-ACAAGGGGTGTATGCCTTTG-3', Duox2 (R) 5'-CACAGGTTGTGGTAGCGAAA-3'. Crx (F) 5'-CCTTCTGACAGCTCGGTGTT-3', Crx (R) 5'-

CCACTTTCTGAAGCCTGGAG)-3'; Sestrin2 (F) 5’-CCTCCTTTGTGTTGTGCTGT-3’, Sestrin2 (R) 5’-ACGGTTCTCCATTTCCTCCT-3’; Opn1sw (F) 5’-CAGCCTTCATGGGATTTGTCT-3’, Opn1sw (R) 5’-CAAAGAGGAAGTATCCGTGAC-3’; Rax (F) 5’-TGGGCTTTACCAAGGAAGACG-3’, Rax (R) 5’-GGTAGCAGGGCCTAGTAGCTT-3’; Six6 (F) 5’-GCAAGTAGCCGGGGTATGTG-3’, Six6 (R) 5’-CGACTCATTCTTGTTAAGGGCTT-3’; Nrl (F) 5’-CCCAGTCCCTTGGCTATGGA-3’, Nrl (R) 5’-ACCGAGCTGTATGGTGTGGA-3’; Notch1 (F) 5’-GATGGCCTCAATGGGTACAAG-3’, Notch1 (R) 5’-TCGTTGTTGTTGATGTCACAGT-3’; Pax6 (F) 5’-TGGCAAACAACCTGCCTATG-3’, Pax6 (R) 5’-TGCACGAGTATGAGGAGGTCT-3’; Gapdh (F) 5’-AGGTCGGTGTGAACGGATTTG-3’, Gapdh (R) 5’-TGTAGACCATGTAGTTGAGGTCA-3’;

Human primer sets used are:

PAX6 (F) 5'-AGATTTCAGAGCCCCATATTCG-3', PAX6 (R) 5'-CCATTTGGCCCTTCGATTAG-3'; ARR3 (F) 5'-CCCAGAGCTTTGCAGTAACC-3', ARR3 (R) 5'-CACAGGACACCATCAGGTTG-3'; SOX1 (F) 5'-AAAGTCAAAACGAGGCGAGA-3', SOX1 (R) 5'-AAGTGCTTGGACCTGCCTTA-3'; RAX (F) 5'-GGCAAGGTCAACCTACCAGA-3', RAX (R) 5'-GCTTCATGGAGGACACTTCC-3'; SIX6 (F) 5’-ACAGACTCCAGCAGCAGGTT-3’, SIX6 (R) 5’-AGATGTCGCACTCACTGTCG-3’; OPN1SW (F) 5’-TGTGCCTCTCTCCCTCATCT-3’, OPN1SW (R) 5’-GGCACGTAGCAGACACAGAA-3’; $P16^{INK4A}$ (F) 5’-GATCCAGGTGGGTAGAAGGTC-3’, $P16^{INK4A}$ (R) 5’-CCCCTGCAAACTTCGTCCT-3’; P21 (F) 5’-CCGAAGTCAGTTCCTTGTGG-3’, P21 (R) 5’-GTCGAAGTTCCATCGCTCAC3’; SOX2 (F) 5’-CACAACTCGGAGATCAGCAA-3’, SOX2 (R) 5’-CGGGGCCGGTATTTATAATC-3’; LHX2 (F) 5’-CCAAGGACTTGAAGCAGCTC-3’, LHX2 (R) 5’-TAAGAGGTTGCGCCTGAACT-3’; BMI1 (F) 5-AATCCCCACCTGATGTGTGT-3, BMI1 (R) 5-GCTGGTCTCCAGGTA ACGAA-3; GAPDH (F) 5’-(F) 5-TCACCAGGGCTGCTTTTAAC-3’, GAPDH (R) 5’- ATCCACAGTCTTCTGGGTGG -3’;

Primer sets for repetitive sequences were as described in (1123).

3.1.5.10 Lentiviral infection

The shRNA-expressing lentiviral plasmids were cotransfected with plasmids pCMVdR8.9 and pHCMVG into 293FT packaging cells using Lipofectamine (Invitrogen) according to the manufacturer’s instructions. Media containing viral particles were collected, filtered, and concentrated by ultracentrifugation. Viral titers were measured by serial dilution on 293T cells

followed by microscopic analysis 48 h later. For viral transduction, lentiviral vectors were added to dissociated cells before plating. Hygromycin selection (150 µg/ml) was added 48 h later.

3.1.5.11 Western blot

Total protein extracts were prepared in the Complete Mini protease inhibitor cocktail solution (Roche Diagnostics). Proteins contents were quantified using the Bradford reagent. Proteins were resolved in Laemmli buffer by SDS-PAGE and transferred to a 0.2µm Nitrocellulose Blotting Membrane (BioRad) that was exposed to the primary antibodies; mouse anti-Bmi1 (1:800, Millipore), mouse anti-H2Aub (1:1000, Millipore), mouse anti- βActin (1:1000, Abcam), p63, mouse anti-p73 (1:500, Abcam), mouse anti-p53 (1:500, Santa Cruz Biotechnology), goat anti-CRX (1:500, Santa Cruz Biotechnology), mouse anti-α-Tubulin (1:1000, Sigma), anti-Rip3 (1:1000, Santa Cruz Biotechnology), anti-Bmi1 (1:500, Abgent,), S-Opsin (1:400, Santa Cruz Biotechnology)., histone H3 (1:1000, upstate) Membranes were treated with corresponding horseradish peroxidase-conjugated secondary antibodies (Sigma) and developed using the Immobilon Western (Millipore).

3.1.5.12 Statistical analyses

Statistical differences were analyzed using Student's *t*-test for unpaired samples with equal SD using two-tailed P.value. For ERG experiments, analyses of variance were made by one-way ANOVA followed by Bonferroni's multiple comparisons test. For PRs quantification of flat-mount retinas, the analysis of variance was performed by two-way ANOVA followed by Tukey's multiple comparison test with 95% of confidence. Data are presented as mean ± standard deviation (error bars). Values are representative of at least 3 experiments. The criterion for significance (*P*-value) was set as mentioned in the figures.

3.1.6 Acknowledgment

We thank M. Van Lohuizen for the *Bmi1*$^{+/-}$ mice and A. Swaroop for the *Nrl*$^{-/-}$ mouse eyes. This work was supported by grants from the Natural Science and Engineering Research Council of Canada (NSERC), Antoine-Turmel Foundation for Macular Degeneration Research, and Foundation Fighting Blindness Canada. V.P. was supported by a fellowship from NSERC. A.F. was supported by Fellowships from Montreal University Molecular Biology Program and Réseau Vision du Québec.

3.1.7 Supplementary figures

Barabino, Plamondon et al. 2016

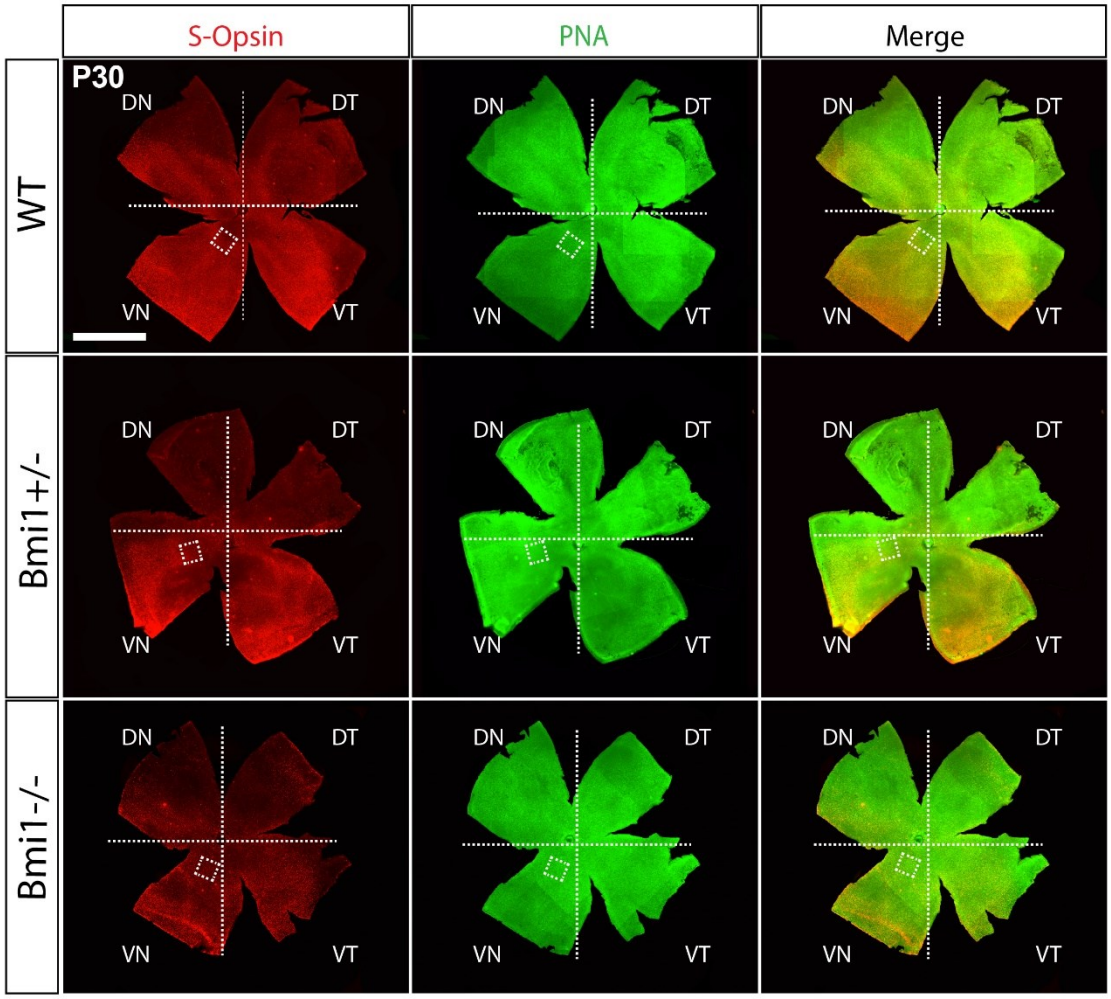

Figure S1

Figure S 1. Bmi1 is required for cone photoreceptor maintenance after birth

(A) Representative images from S-Opsin/PNA double-stained retinal flat mounts from WT, Bmi1$^{+/-}$ and Bmi1$^{-/-}$ mice at P30. Dorso-nasal (DN), dorso-temporal (DT), ventro-nasal (VN), ventro-temporal (VT). Scale bars: 1 mm.

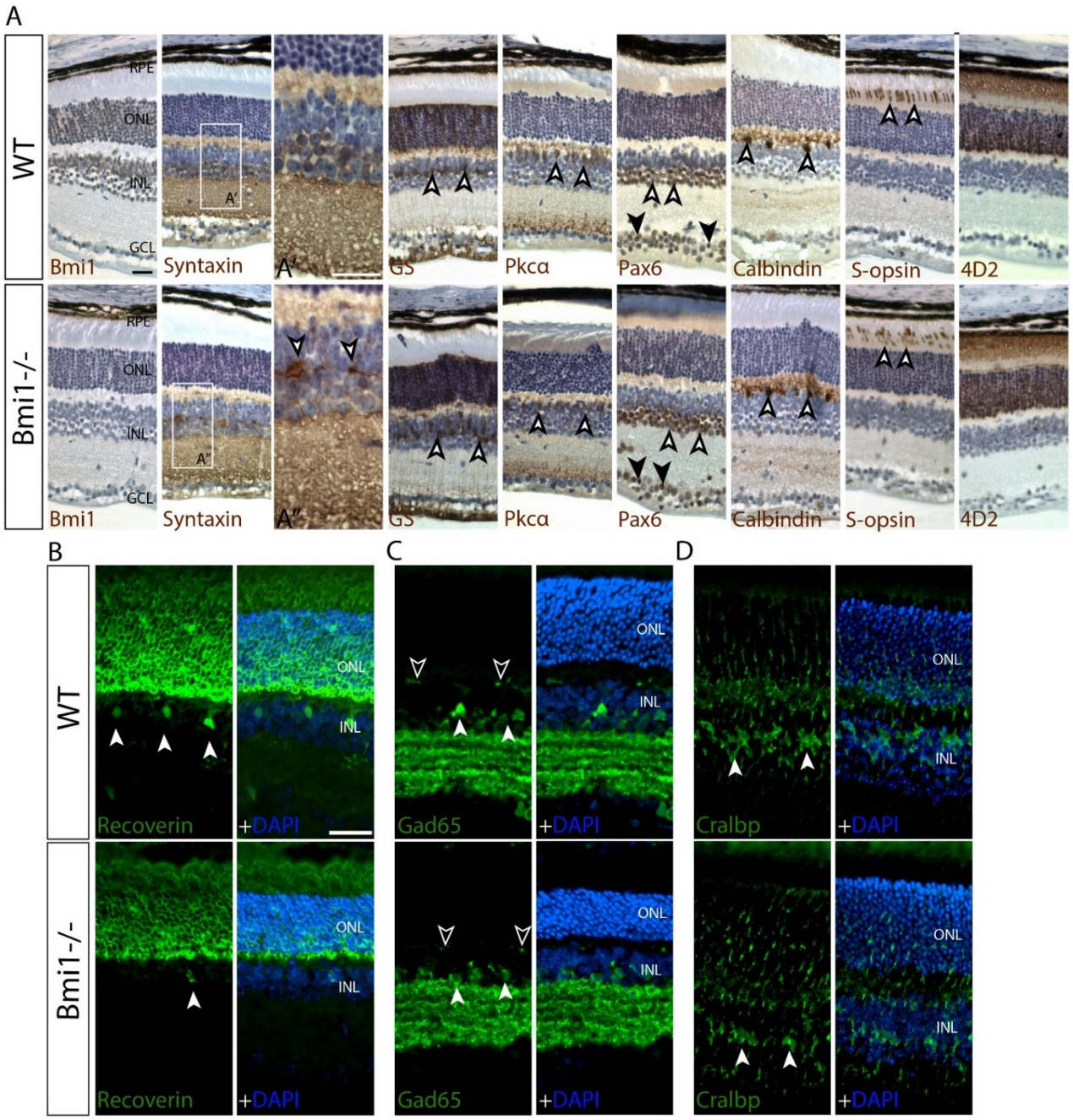

Figure S2

Figure S 2 Histological anomalies in Bmi1$^{-/-}$ mouse retinas

(A, B, C, D) IHC and IF analyses of WT and Bmi1$^{-/-}$ retinas at P30 using specific markers for different retinal cell types. (A', A'') crop of the area indicated by the respective dashed rectangles. Amacrine cells' membrane (Syntaxin), müller glial cells (Gs and Cralbp), rods bipolar cells (Pkcα), amacrine (white-edged arrows) and ganglion cells (black arrows) (Pax6), horizontal cells (Calbindin), c-cones (S-Opsin), rod photoreceptors (4D2), T2 OFF and T8 ON cone bipolar cells (Recoverin), amacrine cells (white arrows) and horizontal cells (white-edged arrows) (Gad65). Retinal pigmented epithelium (RPE); outer nuclear layer (ONL); inner nuclear layer (INL); and ganglion cell layer (GCL). Scale bars: 40µm.

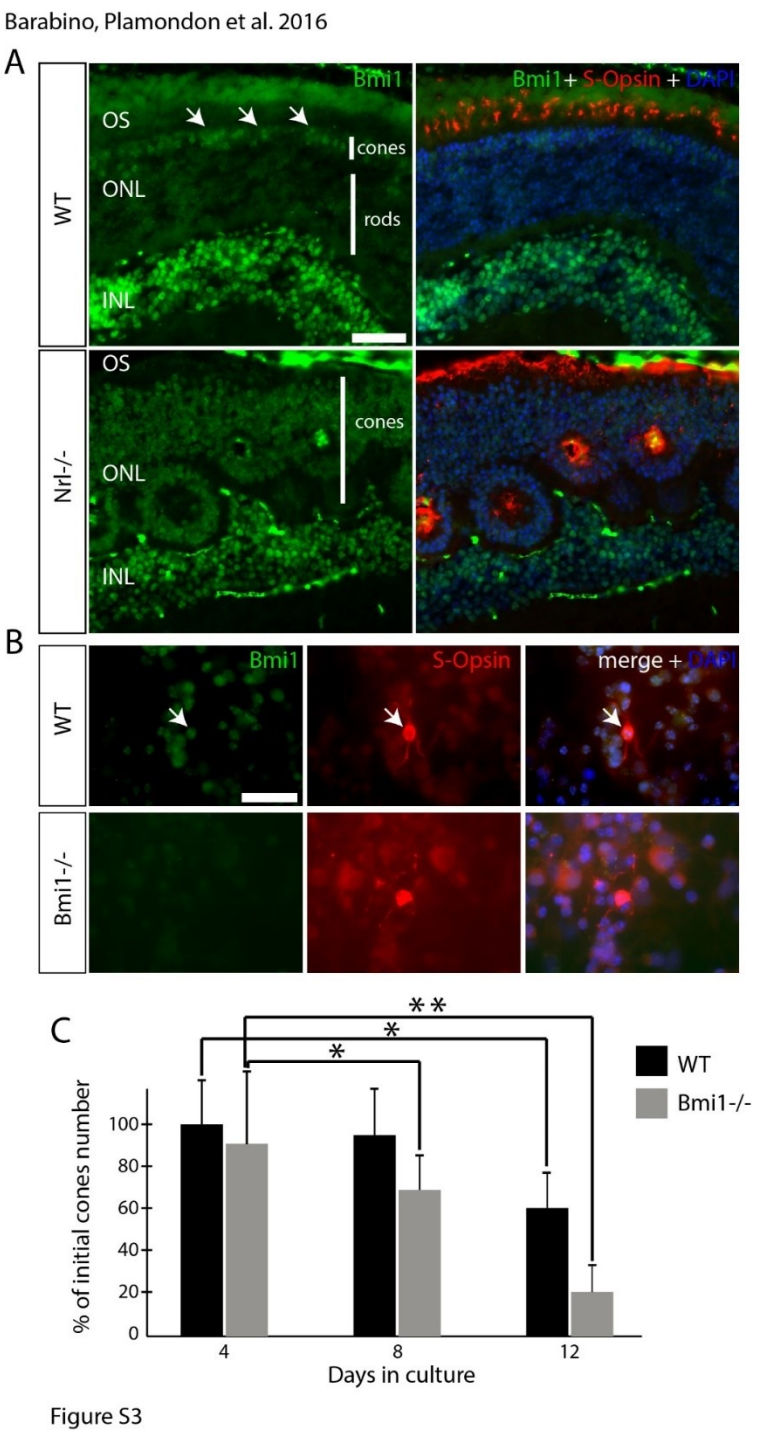

Figure S3

Figure S 3 Bmi1 is preferentially expressed in mouse cone photoreceptors

(A) IF analysis of WT and Nrl$^{-/-}$ mouse retinal cryosections at P30. Arrows: Note the preferential expression of Bmi1 in neurons of the INL and in cone photoreceptors located in the ONL (white arrows). In contrast, Bmi1 is evenly distributed in the cone-only ONL of Nrl$^{-/-}$ mice. (B) IF analysis of dissociated retinal cultures from WT and Bmi1$^{-/-}$ mice at P1 after 4 days in vitro (DIV). Note the expression of Bmi1 in WT cones labeled with S-Opsin, and the absence of Bmi1 in S-Opsin positive cells of Bmi1-mutants. (C) Quantification of S-Opsin positive cones in dissociated WT and Bmi1$^{-/-}$ retinal cultures, expressed as percentage of the initial cone number evaluated at 1 DIV. Outer nuclear layer (ONL); inner nuclear layer (INL); outer segment (OS). Scale bar: 50µm (A) and 20µm (B). WT n=4; Bmi1$^{-/-}$ n= 5. All values are mean ±SEM. (*) P ≤0.05; (**) ≤0.01; Student t-test.

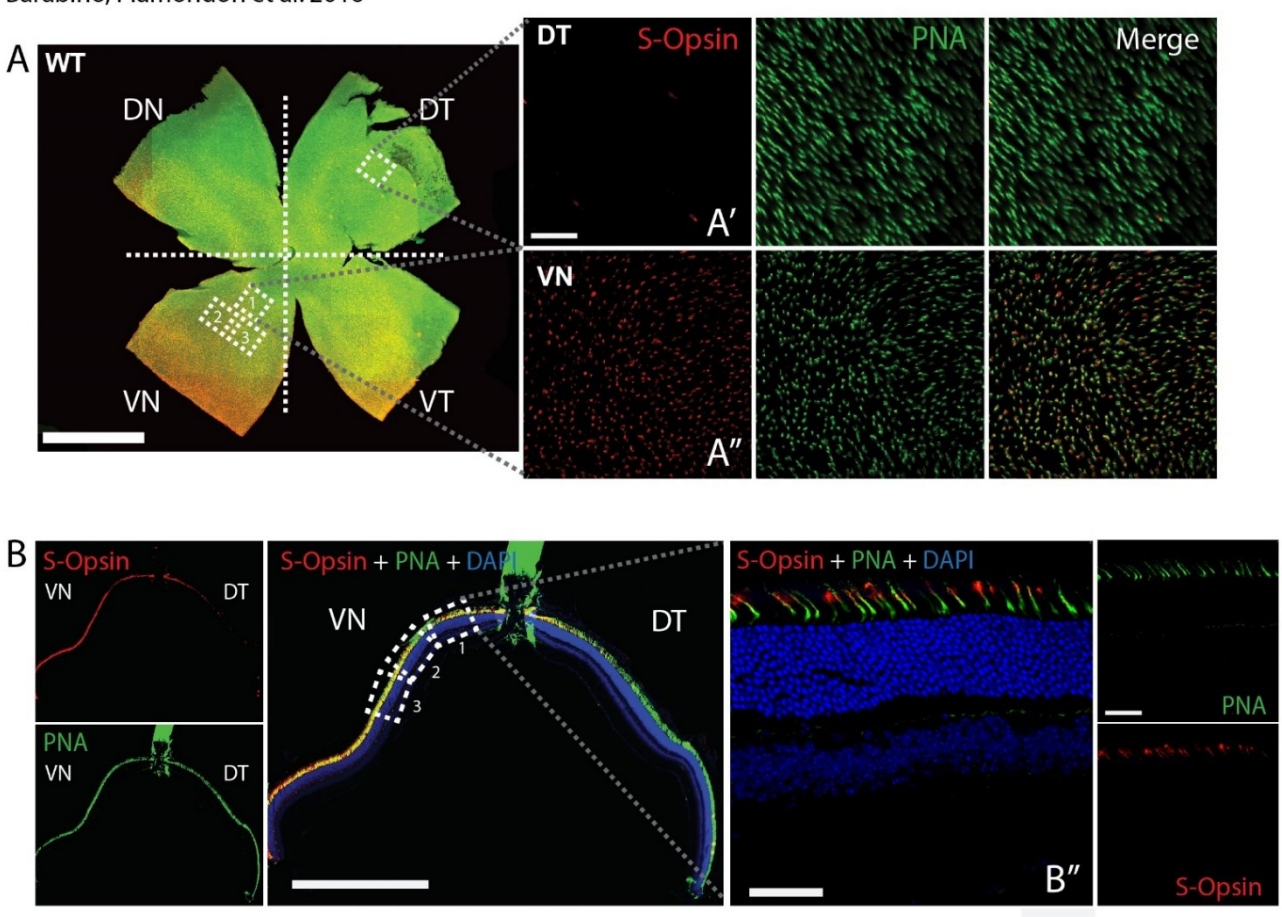

Figure S4

Figure S 4 Methodology for the quantification of photoreceptors and other retinal cells types

(A) Representative mosaic reconstruction from 10x images from S-Opsin/PNA double-stained retinal flat mounts from P30 WT mice. (A', A'') 60x confocal microscopy images from retinal flat mount of the DT (A') and from the VN (A'') portion indicate with dashed rectangles in (A). (A') Note the almost complete absence of S-cone (S-Opsin+ cells) in the DT portion where almost only M-pure cones are present. (A'') Note that in the VN portion approximately all cones express S-Opsin. The majority of these are dual-photoreceptors expressing both S and M Opsin and a minority of pure S-cone (data not shown). For PRs quantification, 3 images from the VN portion were quantified and averaged as shown by the dashed rectangles in (A). (B) 20x Mosaic Image of the whole retinal section at the level of the optic nerve of an orientated block. The eyes are oriented in the blocks in order to always have VN and DT in opposite positions with respect to the optic nerve on sections. For quantification on retinal sections, 3 consecutive images for sample (as shown by the boxes 1, 2, 3) were taken in the VN side, then quantified and averaged. (B') Representative 60x confocal microscopy image from retinal section used for quantification. Ventro-nasal (VN), dorso-temporal (TD). n= 3 to 6 retinas were used for genotype. Scale bars: (A) 1 mm, (B) 0,5mm.

Barabino, Plamondon et al. 2016

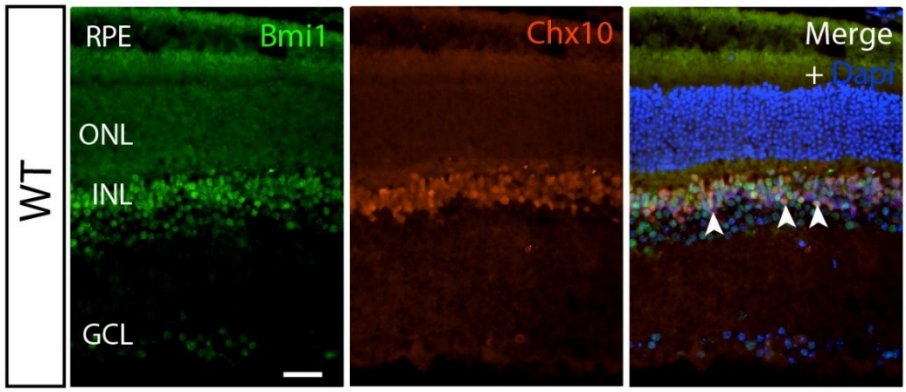

Figure S5

Figure S 5 . Bmi1 is highly expressed in bipolar neurons

IF analysis of a WT mouse retina (cryosections) using Chx10 and Bmi1 antibodies. Note Bmi1 expression in Chx10-positive cells of the INL. Retinal pigment epithelium (RPE); outer nuclear layer (ONL); inner nuclear layer (INL); ganglion cell layer (GCL). Scale bar: 20µm.

Barabino, Plamondon et al. 2016

Figure S6

Figure S 6 Chk2 deletion partially improves the Bmi1$^{-/-}$ phenotype

Bmi1$^{-/-}$ /Chk2$^{-/-}$ and Chk2$^{+/-}$ mice at P30. Note: Bmi1$^{-/-}$ /Chk2$^{-/-}$ mice were healthier than Bmi1$^{-/-}$ mice but remained smaller than Chk2$^{+/-}$ control mice.

Barabino, Plamondon et al. 2016

	Photopic system			Scotopic system		
	WT	+/-	-/-	WT	+/-	-/-
Overall a-wave amplitude	F(2,7) = 6.195, p = 0.028 *			F(2,7) = 1.297, p = 0.332 N.S.		
a-wave amplitude at Vmax	-215.4 ± 32.69 µV	-182.5 ± 15.29 µV	-88.35 ± 6.706 µV	-116.1 ± 12.17 µV	-117.4 ± 12.22 µV	-138.0 ± 10.05 µV
Comparison with the other groups (p-value)	+/- = 0.375 N.S.	WT = 0.375 N.S.	WT = 0.008 **	+/- = 0.939 N.S.	WT = 0.939 N.S.	WT = 0.226 N.S.
	-/- = 0.008 **	-/- = 0.039 *	+/- = 0.039 *	-/- = 0.226 N.S.	-/- = 0.281 N.S.	+/- = 0.281 N.S.
Overall a-wave implicit time	F(2,7) = 5.127, p = 0.043 *			F(2,7) = 0.596, p = 0.577 N.S.		
a-wave implicit time at Vmax	8.000 ± 0.4082 ms	8.667 ± 0.3333 ms	9.333 ± 0.3333 ms	21.75 ± 2.175 ms	19.67 ± 0.3333 ms	22.00 ± 2.517 ms
Comparison with the other groups (p-value)	+/- = 0.246 N.S.	WT = 0.246 N.S.	WT = 0.039 *	+/- = 0.484 N.S.	WT = 0.484 N.S.	WT = 0.932 N.S.
	-/- = 0.039 *	-/- = 0.275 N.S.	+/- = 0.275 N.S.	-/- = 0.932 N.S.	-/- = 0.464 N.S.	+/- = 0.464 N.S.
Overall b-wave amplitude	F(2,7) = 18.970, p = 0.001 ***			F(2,7) = 10.440, p = 0.008 **		
b-wave amplitude at Vmax	333.8 ± 34.78 µV	241.9 ± 17.30 µV	132.3 ± 9.479 µV	509.5 ± 24.04 µV	603.7 ± 51.01 µV	371.4 ± 40.36 µV
Comparison with the other groups (p-value)	+/- = 0.044 *	WT = 0.044 *	WT = 0.001 ***	+/- = 0.112 N.S.	WT = 0.112 N.S.	WT = 0.032 *
	-/- = 0.001 ***	-/- = 0.029 *	+/- = 0.029 *	-/- = 0.032 *	-/- = 0.004 **	+/- = 0.004 **
Overall b-wave implicit time	F(2,7) = 20.852, p = 0.001 ***			F(2,7) = 0.034, p = 0.966 N.S.		
b-wave implicit time at Vmax	27.25 ± 0.6292 ms	31.00 ± 1.000 ms	39.33 ± 2.848 ms	57.00 ± 1.472 ms	56.67 ± 1.453 ms	53.00 ± 2.517 ms
Comparison with the other groups (p-value)	+/- = 0.136 N.S.	WT = 0.136 N.S.	WT = 0.001 ***	+/- = 0.899 N.S.	WT = 0.899 N.S.	WT = 0.158 N.S.
	-/- = 0.001 ***	-/- = 0.010 **	+/- = 0.010 **	-/- = 0.158 N.S.	-/- = 0.217 N.S.	+/- = 0.217 N.S.

Table S1

Table S 1 Statistical analysis of ERG parameters

Global values from ERG experiment. Each parameter is analyzed by repeated measures ANOVA. The comparisons between the ERG parameters values at the Vmax are analyzed by one-way ANOVA. All values are mean ± SEM. N.S. = not significant; (*) P ≤ 0.05; (**) ≤0.01; (***) ≤0.001;

3.2 Deregulation of neuro-developmental genes and primary cilium cytoskeleton anomalies in iPSC retinal sheets from human syndromic ciliopathies

Andrea Barabino[1], Anthony Flamier[1,2], Roy Hanna[1], Elise Héon[3], Benjamin S. Freedman[4*], and Gilbert Bernier[1, 5, 6 **]

[1] Stem Cell and Developmental Biology Laboratory, Hôpital Maisonneuve-Rosemont, 5415 Boul. Assomption, Montreal, QC, H1T 2M4, Canada.

[2] Present address: Whitehead Institute for Biomedical Research, Massachusetts Institute of Technology (MIT), 455 Main Street, Cambridge, MA, 02142, USA.

[3] Hospital for Sick Children, Department of Ophthalmology and Vision Sciences, Program of Genetics and Genome Biology, 555 University av. Toronto, ON, M5G 1X8, Canada.

[4] Department of Medicine, Division of Nephrology, Kidney Research Institute, and Institute of Stem Cell and Regenerative Medicine, and Department of Pathology, University of Washington School of Medicine, Seattle, WA, 98109, USA.

[5] Department of Neurosciences, University of Montreal, Montreal, QC, H3C 3J7, Canada.

[6] Department of Ophthalmology, University of Montreal, Montreal, QC, H3C 3J7, Canada.

3.2.1 Abstract

Ciliopathies are heterogeneous genetic diseases affecting primary cilium structure and function. Meckel-Gruber (MKS) and Bardet-Biedl (BBS) syndromes are severe ciliopathies characterized by skeletal and neuro-development anomalies, including polydactyly, cognitive impairment, and retinal degeneration. We describe the generation and molecular characterization of human iPSC-derived RSs from controls, MKS (TMEM67), and BBS (BBS10) cases. MKS and BBS RSs displayed significant common alterations in the expression of hundreds of developmental genes and members of the WNT and BMP pathways. Induction of crystallin molecular chaperones was prominent in MKS and BBS RSs, suggesting a stress response to misfolded proteins. Unique to MKS photoreceptors was the presence of supernumerary centrioles and cilia and the aggregation of ciliary proteins. Unique to BBS photoreceptors was the accumulation of DNA damage and activation of the mitotic spindle checkpoint. This study reveals how combining cell reprogramming, organogenesis, and next-generation sequencing enables the elucidation of mechanisms involved in human ciliopathies.

3.2.2 Introduction

Primary cilia are typically non-motile cytoplasmic extensions of a microtubule-based structure that projects from the cell surface and are indispensable for normal developmental and physiological functions (127,128). The ciliary axoneme develops from and is anchored to a specialized centriole called the basal body (BB) that acts as a microtubule-organizing center. The BB is a symmetric radial arrangement of nine triplet microtubules from which the outer doublet of the axoneme's microtubules extends. Syndromic and non-syndromic ciliopathies represent a group of heterogeneous genetic diseases caused by mutations affecting the primary cilium's structure and function. Phenotypic and genetic heterogeneity is frequently observed in these diseases. The relationship between cilia genes and ciliopathies is far more complex than that described by classical Mendelian genetics and has recently been the focus of numerous reviews (362,363,1124).

Meckel-Gruber (MKS) and Bardet-Biedl (BBS) syndromes are rare developmental diseases characterized by multiple developmental anomalies, including retinal degeneration, digits, and genito-urinary defects, as well as cognitive impairment (211,234). While MKS is fatal at birth, BBS is one of the most severe ciliopathies compatible with life. MKS is a lethal autosomal recessive ciliopathy, presenting polycystic kidneys and severe eye/brain malformations, with over 13 disease-associated genes (235,242,471,1125). In contrast, BBS is a viable disorder associated with obesity and retinal degeneration (211,234) and with variants identified in over 22 genes, with *BBS10* representing the most commonly mutated gene (436,1126). MKS and BBS were, in principle, considered as two distinct clinical entities. However, the identification of hypomorphic mutations in *MKS1* and *TMEM67* in some BBS patients introduced the concept that BBS may represent a milder form of MKS (234). The MKS3 protein (encoded by *TMEM67*) is apparently not an integral part of the MKS complex but more likely to interact with it (234,235). MSK3 localizes to the TZ at the primary cilium base and the plasma membrane in ciliated cells (231). MKS3 has been associated with centrosome migration to the apical cell surface during early ciliogenesis and with the regulation of centrosome organization (239,240). The BB derives from the mother centriole, which distinguishes it from the daughter centriole by the presence of appendages on its distal end, allowing the primary cilium formation (185). Centriolin (also known as CEP110 or

CNTRL) is associated with the mother centriole (1127). Mutations in Centriolin can cause ciliopathies as Atrioventricular Septal Defect (AVSD) (191). Although many BBS-associated proteins are an integral part of the BBSome complex, BBS10 most likely interacts with the BBSome and shows sequence similarities with chaperones (220).

The vast majority of genes causing retinal degeneration involves a defect in a ciliary protein (RetNet). Molecular and cellular insights found in this work are potentially relevant to other ciliopathies and non-syndromic retinal disorders. Degeneration of PRs is often part of syndromic ciliopathies (387,1128). Retinal degeneration varies depending on the type of PRs that are primarily affected. Rods respond to dim light and are important for night and peripheral vision. Cones respond to intense light and are required for color, daylight, and high-resolution central vision (263). The inner segment and outer segment of PRs, which respectively represent the metabolic factory and the structure where phototransduction occurs, are connected by the CC, a modified intracellular version of the primary cilia (1129). The proteins synthesized in the inner segment are transported to the base of the CC in post-Golgi vesicles in an area also called the TZ, where they are associated with molecular transport complexes that allow bidirectional movement along the axoneme, called IFT (160,164). The IFT family and other BB-associated proteins, if mutated, may cause mislocalization and accumulation of outer segment proteins in the inner segment, causing PRs degeneration (164,1130). The RPGR, RP1, and RP2 proteins mainly localize at the CC's basal body, and mutations in these are a leading cause of RP (1131).

Though valuable, animal models have shown limitations in modeling retinal ciliopathies, with patient-derived induced pluripotent stem cells (iPSCs) representing a new opportunity for modeling human diseases (873). Structures like the macula, responsible for high-resolution central vision, are not present in most commonly used animal models. Moreover, the PR's ultrastructure between mice and humans differs at the TZ, an area adjacent to the CC. Here we found structures called calyceal processes, which are present in humans but not in mice. Likewise, the USH1G/1C proteins, which are mutated in USH, localize to the CC of human PRs but have no equivalent in rodents (841). We report here on the generation of iPSCs from MKS and BBS cases and on their differentiation into RSs containing cone PRs (1007). We found that RSs from MKS and BBS cases displayed common alterations in hundreds of developmental genes, including

homeobox and HOX genes, as well as genes of the WNT, NOTCH, and BMP signaling pathways. MKS PRs showed supernumerary cilia and centrioles and mislocalization of ciliary proteins. BBS PRs presented mitotic spindle checkpoint activation, DNA damage, and genomic instability. Both MKS and BBS PRs accumulated chaperones of the crystallin gene family, suggesting a cellular response to misfolded proteins and/or proteasome dysfunction. This study brings new molecular and cell biological information on the neuro-developmental and retinal degeneration anomalies associated with human syndromic ciliopathies.

3.2.3 Results

3.2.3.1 Generation and characterization of iPSC-derived retinal sheets

We have generated iPSCs from skin fibroblasts of three healthy volunteers ($Ctrl^{01}$, $Ctrl^{02,}$ and $Ctrl^{03}$), two unrelated MKS cases (MKS^{01} and MKS^{02}), and two unrelated BBS cases (BBS^{01} and BBS^{02}). The iPSCs expressed pluripotency markers, were able to form teratomas, and could be differentiated into embryoid bodies containing retinal RPE cells upon exposure to nicotinamide (Figure S1A-D). An external cilium was also observed in iPSCs using scanning electron microscopy (Figure S1B). By whole-genome sequencing of the parental fibroblast cell lines, we found that both BBS cases carried different mutations in *BBS10*, with a homozygous mutation causing a frameshift stop in the first case (c.271dup), and a compound heterozygous mutation in the second case (c.909_912del; c.687del) (Figure S1E-G). The MKS^{01} case carried compound heterozygous permutations at the TMEM67 locus (c.233G>A; c.1046T>C) predicted to be pathogenic (Figure S1E-G). We could not, however, confirm the disease-causing mutation in the MKS^{02} case.

Control, $BBS^{01/02}$, and $MKS^{01/02}$ iPSCs were differentiated for 60 DIV into RSs using the same methodology for hESCs (1007). Control RSs were analyzed by confocal immunofluorescence. 3D reconstruction imaging revealed the generation of a polarized, multi-layered tissue expressing OS (PNA and S-opsin), CC (acetylated α-tubulin and RPGR), and nuclear pan-photoreceptor (CRX) markers (Figure 1A), suggesting efficient differentiation into RSs. Using RNA sequencing (RNAseq), we compared the transcriptome of control RSs with that of the Human Retinal Development Atlas (16) and found that RSs clustered with human embryonic retinas at days 80 and 94. RNAseq data from control RSs were also compared with the top 50 most upregulated transcripts in adult human retina and the top 50 iPSC-specific transcripts (1132) (Figure 1B). Retinal and photoreceptor-specific transcripts, including *NR2E1*, *GRK1*, *CRX*, *PDE6H*, *RXRG*, *ROM1*, *CRB1*, *RPE65*, *PRPH*, *RP1*, *RCVRN*, *ABCA4*, and *GNAT1*, were significantly enriched in RSs. In contrast, iPSC-specific transcripts were lost in RSs, suggesting efficient cellular differentiation (Figure 1C). Despite the presence of rod-specific transcripts in RSs, we failed to detect rhodopsin protein expression using immunoblot or immunofluorescence.

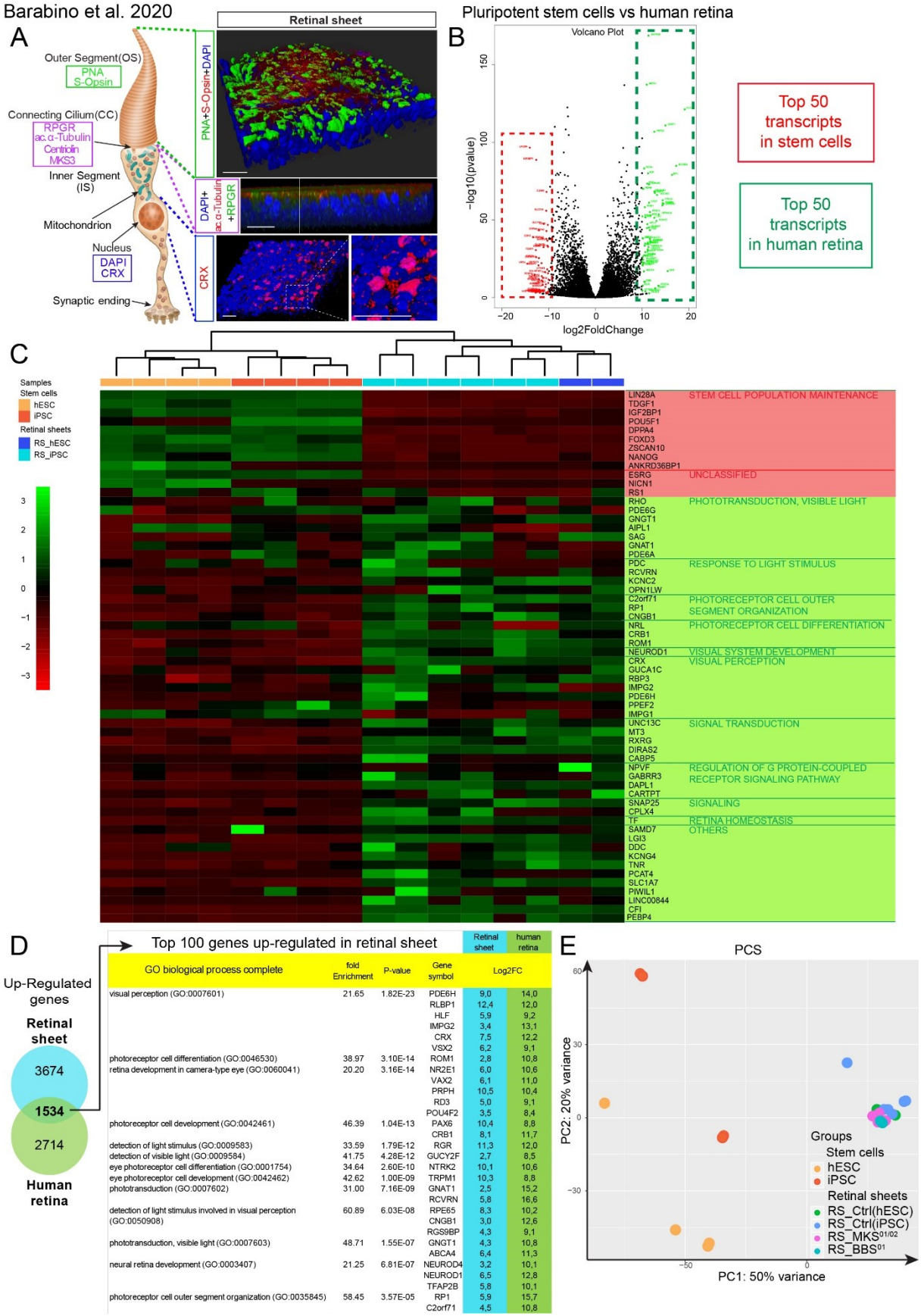
Barabino et al. 2020
A
Retinal sheet
Outer Segment(OS)
PNA
S-Opsin
Connecting Cilium(CC)
RPGR
ac.α-Tubulin
Centriolin
MKS3
Inner Segment
(IS)
Mitochondrion
Nucleus
DAPI
CRX
Synaptic ending
PNA+S-Opsin+DAPI
DAPI+
ac.α-Tubulin
+RPGR
CRX
Pluripotent stem cells vs human retina
B
Volcano Plot
−log10(pvalue)
log2FoldChange
Top 50
transcripts
in stem cells
Top 50
transcripts
in human retina
C
Samples
Stem cells
hESC
iPSC
Retinal sheets
RS_hESC
RS_iPSC
LIN28A
TDGF1
IGF2BP1
POU5F1
DPPA4
FOXD3
ZSCAN10
NANOG
ANKRD36BP1
STEM CELL POPULATION MAINTENANCE
ESRG
NICN1
RS1
UNCLASSIFIED
RHO
PDE6G
GNGT1
AIPL1
SAG
GNAT1
PDE6A
PHOTOTRANSDUCTION, VISIBLE LIGHT
PDC
RCVRN
KCNC2
OPN1LW
RESPONSE TO LIGHT STIMULUS
C2orf71
RP1
CNGB1
PHOTORECEPTOR CELL OUTER SEGMENT ORGANIZATION
NRL
CRB1
ROM1
PHOTORECEPTOR CELL DIFFERENTIATION
NEUROD1
VISUAL SYSTEM DEVELOPMENT
CRX
GUCA1C
RBP3
IMPG2
PDE6H
PPEF2
IMPG1
VISUAL PERCEPTION
UNC13C
MT3
RXRG
DIRAS2
CABP5
SIGNAL TRANSDUCTION
NPVF
GABRR3
DAPL1
CARTPT
REGULATION OF G PROTEIN-COUPLED RECEPTOR SIGNALING PATHWAY
SNAP25
CPLX4
SIGNALING
TF
RETINA HOMEOSTASIS
SAMD7
LGI3
DDC
KCNG4
TNR
PCAT4
SLC1A7
PIWIL1
LINC00844
CFI
PEBP4
OTHERS
D
Up-Regulated genes
Retinal sheet
3674
1534
2714
Human retina
Top 100 genes up-regulated in retinal sheet
GO biological process complete
fold Enrichment
P-value
Gene symbol
Log2FC
Retinal sheet
human retina
visual perception (GO:0007601)
21.65
1.82E-23
PDE6H 9,0 14,0
RLBP1 12,4 12,0
HLF 5,9 9,2
IMPG2 3,4 13,1
CRX 7,5 12,2
VSX2 6,2 9,1
photoreceptor cell differentiation (GO:0046530)
38.97
3.10E-14
ROM1 2,8 10,8
retina development in camera-type eye (GO:0060041)
20.20
3.16E-14
NR2E1 6,0 10,6
VAX2 6,1 11,0
PRPH 10,5 10,4
RD3 5,0 9,1
POU4F2 3,5 8,4
photoreceptor cell development (GO:0042461)
46.39
1.04E-13
PAX6 10,4 8,8
CRB1 8,1 11,7
detection of light stimulus (GO:0009583)
33.59
1.79E-12
RGR 11,3 12,0
detection of visible light (GO:0009584)
41.75
4.28E-12
GUCY2F 2,7 8,5
eye photoreceptor cell differentiation (GO:0001754)
34.64
2.60E-10
NTRK2 10,1 10,6
eye photoreceptor cell development (GO:0042462)
42.62
1.00E-09
TRPM1 10,3 8,8
phototransduction (GO:0007602)
31.00
7.16E-09
GNAT1 2,5 15,2
RCVRN 5,8 16,6
detection of light stimulus involved in visual perception (GO:0050908)
60.89
6.03E-08
RPE65 8,3 10,2
CNGB1 3,0 12,6
RGS9BP 4,3 9,1
phototransduction, visible light (GO:0007603)
48.71
1.55E-07
GNGT1 4,3 10,8
ABCA4 6,4 11,3
neural retina development (GO:0003407)
21.25
6.81E-07
NEUROD4 3,2 10,1
NEUROD1 6,5 12,8
TFAP2B 5,8 10,1
photoreceptor cell outer segment organization (GO:0035845)
58.45
3.57E-05
RP1 5,9 15,7
C2orf71 4,5 10,8
E
PCS
PC2: 20% variance
PC1: 50% variance
Groups
Stem cells
hESC
iPSC
Retinal sheets
RS_Ctrl(hESC)
RS_Ctrl(iPSC)
RS_MKS01/02
RS_BBS01

Figure 1: Generation of iPSC-derived retinal sheets.

(A) Representation of a cone PRs (left) and 3D reconstruction of a RS (right) with reference to the main compartments, Outer Segment (OS), CC (CC), Inner Segment (IS), and nucleus. For each compartment are indicated the main markers used in this paper: PNA and S-Opsin for the OS; Acetyl-α Tubulin and RPGR for the CC; CRX for the nucleus. Scale bars, 40 µm. (B) Volcano plot from RNAseq analyses between human retina (n=2 independent biological samples) and undifferentiated stem cells (n=4 iPSC; n=4 hESC, independent cell lines). The red points show the 50 most significantly downregulated genes (stem cell-related genes). The green points show the 50 most significantly upregulated genes (human retina-related genes). (C) Heatmap showing differential expression for stem cell and human retina related genes between undifferentiated stem cell lines (n=4 iPSC; n=4 hESC) and Ctrl RSs (n=8 from 3 independent iPSC and 1 hESC cell lines). Hierarchical clustering by Pearson's correlation clearly distinguishes the two groups. (D) Venn diagrams showing the intersection of significant genes differentially upregulated in control RSs (Ctrl01, Ctrl02, Ctrl03, hESC-Ctrl) and in the human retina. Gene Ontology Enrichment Analysis of the 100 most upregulated genes in RSs compared to undifferentiated iPSC that are also upregulated in the human retina (P-value <0,05). For every GO group, we indicated their fold enrichment, P-Value, and few representative genes. For every gene is indicated Log2FC in Ctrl_RSs (light blue) and in the human retina (green). (E) PCA between stem cells (iPSC, ESC), and RSs from control iPSC and hESC, and RS from MKS (n=4 from 2 patients) and BBS (n=2 from 1 patient). Notice how all RSs cluster together while PSC are more dispersed.

When comparing the entire gene dataset of undifferentiated iPSCs with that of adult human retinas and RSs, we found that 1534 genes were commonly upregulated in human retinas and RSs. Gene Ontology (GO) analysis of the top 100 genes revealed that these were primarily implicated in the detection of light stimuli, photoreceptor OS organization, photoreceptor development, and visual perception (Figure 1D). We also performed a principal component analysis of RSs and iPSC/hESC lines. While iPSCs and hESCs were generally scattered, RSs from all samples were grouped together, suggesting cellular differentiation toward a common lineage (Figure 1E). We next used immunoblot to test if RSs expressed photoreceptor-specific proteins. We found that Ctrl$^{01/02/03}$, MKS$^{01/02}$, and BBS$^{01/02}$ RSs were all expressing CRX (expressed in photoreceptor and in a subset of bipolar neurons) and S-opsin (expressed exclusively in cone PRs) (Figure 2A). Taken as a whole, these results suggested robust differentiation of iPSC lines into RSs.

3.2.3.2 Deregulation of neurodevelopmental genes in MKS and BBS retinal sheets

We compared RNAseq data from Ctrl$^{01/02}$, MKS$^{01/02,}$ and BBS^{01} RSs and found thousands of genes commonly dysregulated in ciliopathies (Figure 2B-C). 1597 genes were dysregulated in both BBS^{01} and MKS$^{01/02}$ samples when compared to controls (661 up-regulated, 936 down-regulated) (Figures 2D and 3A). Among the 661 commonly up-regulated genes, most were related to neural/retinal development (*DLX1*, *VSX1*, and *SIX6*), differentiation (*NEUROD4* and *ASCL1/MASH1*), and function (*SLC32A1* and *NTRK1*), while others were associated with ganglion and amacrine cell fate, suggesting premature and/or increased neurogenesis and perturbed retinal cell fate specification in ciliopathies (Figures 2E-G and S2A-D). Different homeobox genes,

including members of the HOX family, were also upregulated in both BBS^{01} and MKS$^{01/02}$ RSs

Barabino et al. 2020

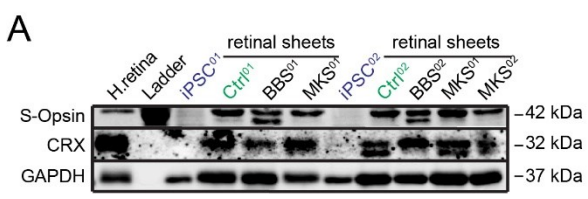

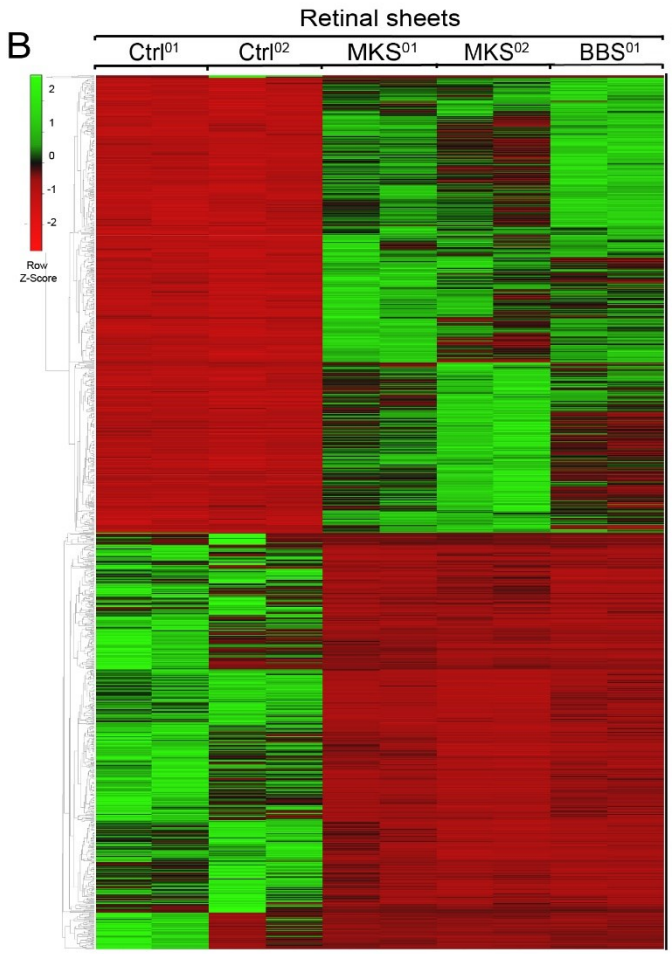

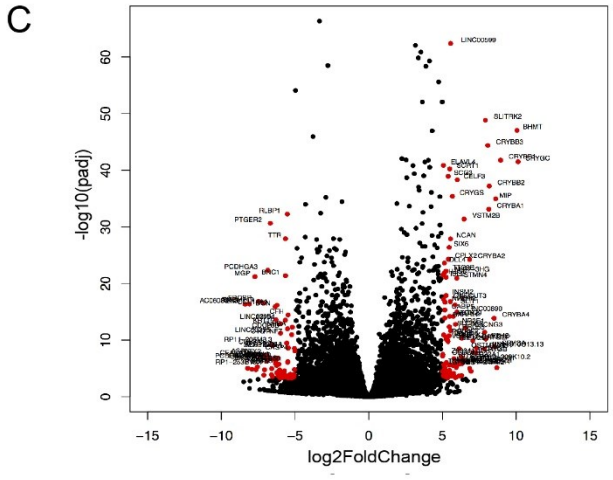

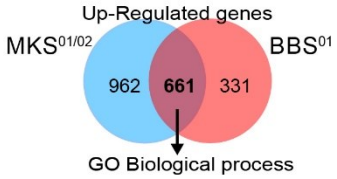

E

Neural retina function, development and morphogenesis	Gene Symbol	Log2FC MKS	Log2FC BBS
visual perception(GO:0007601)	GJA8	6,5	4,7
	GJA3	2,1	2,1
	RGS16	3,0	2,1
	IMPG2	4,6	3,1
	GUCY2D	3,6	3,1
	CHRNB2	4,1	3,5
	ZIC2	2,2	2,4
	MIP	8,4	8,7
	COL2A1	2,3	2,5
	VSX2	4,2	5,2
	RBP3	4,9	4,4
	CACNA1F	3,2	2,8
	PDC	4,6	4,4
	CLRN1	2,7	3,2
	RAX2	5,3	3,9
	NDP	5,3	3,2
	VSX1	5,5	4,6
	CNGA3	4,7	3,8
	RCVRN	4,3	4,3
	KCNJ10	3,8	4,4
phototransduction, visible light (GO:0007603)	AIPL1	3,9	3,3
	PDE6C	3,4	2,3
retinal cone cell development (GO:0046549	RORB	3,5	3,9
	DIO3	3,9	2,2
eye photoreceptor cell development (GO:0042462)	CRB1	3,3	3,6
	PRDM1	4,1	4,5
retina development in camera-type eye (GO:0060041)	TH	3,1	2,8
	GRM6	4,6	3,7
	NR2E1	6,3	4,6
	POU4F2	4,5	5,8
regulation of neural retina development (GO:0061074)	DLL4	4,6	5,8
	PTF1A	4,5	5,7
neural retina development (GO:0003407)	ATOH7	4,6	6,4
	SLC17A7	3,4	3,3
eye development (GO:0001654)	FOXE3	7,2	6,8
	SIX6	5,3	5,8
	SOX2	3,1	2,2
	RBP4	3,5	3,7
	CHRDL1	3,6	2,3
camera-type eye development (GO:0043010)	HES5	4,6	5,6
	PAX2	8,4	3,6
camera-type eye morphogenesis (GO:0048593)	AQP5	2,0	2,2

F

Retinal ganglion cell development	Gene Symbol	Log2FC MKS	Log2FC BBS
retinal ganglion cell axon guidance (GO:0031290)	ISL2	5,3	5,3
	ISL1	5,1	4,6
	SLIT1	6,3	3,4
	POU4F2	4,5	5,8
	NRCAM	3,9	2,7
optic nerve development (GO:0021554)	ATOH7	4,6	6,4
	PAX2	8,4	3,6
	NTRK1	3,4	4,2
	DRGX	3,1	3,6
	POU4F1	4,4	3,2

G

Amacrine cell development	Gene Symbol	Log2FC MKS	Log2FC BBS
amacrine cell differentiation (GO:0035881)	NEUROD4	5,4	4,9
	NEUROD1	4,8	5,3
	FOXN4	3,6	4,4
	PTF1A	4,5	5,7
positive regulation of amacrine cell differentiation (GO:1902871)	DLX1	6,7	4,6
	DLX2	4,9	3,4

Figure 2: Neuro-developmental anomalies in MKS and BBS retinal sheets.

(A) Immunoblot on extracts from a human retina (positive ctrl), undifferentiated iPSC (negative ctrl), and RSs from Ctrl01/02, BBS01/02, and MKS01/02 patients. (B) Heatmap of gene expression profile for differentially expressed genes between Ctrl01/02 (n=4 from 2 independent ctrl cell lines), MKS01/02 (n=4 from two independent MKS patients), and BBS01 (n=2 from one BBS patient) (P-value <0,0001, Up=log2FC>2; Down=log2FC<-2). Hierarchical clustering by average linkage with Kendall's Tau correlation clearly distinguishes control and patients' RSs. (C) Volcano plot from RNAseq analyses between Ctrl01/02 and all patient RSs. The red points show the most significantly dysregulated genes (log2FC>5 and p-value adjusted <0.001). (D) Venn diagrams showing the intersection of significant genes differentially upregulated in MKS01/02 (Blue, 1623 genes) and in BBS01 RSs (Red, 992 genes) (log2FC>2; P-value <0,05). (E-G) Gene Ontology Enrichment analyses of common differentially up-regulated genes between the two groups. Some of the main GO groups and subgroups are shown with some indicative genes and the respective Log2FC in MKS01/02 (orange column) and BBS01 RSs (green column) (P-value <0,05).

(Figure S2A). Defective NOTCH and/or WNT signaling is frequently associated with premature neurogenesis and/or cell cycle exit of neural progenitors (1133,1134). Hence, we found altered expression of genes of the WNT and NOTCH signaling pathways in both MKS and BBS RSs (Figure S2B-C). Further analyses suggested major deregulation of WNT signaling in ciliopathies toward the canonical pathway at the expense of the non-canonical one, which is known to play a role in planar cell polarity and cilia formation (Figure S2B) (321).

3.2.3.3 Alterations of genes involved in development, morphogenesis, and cilia formation

When analyzing genes commonly down-regulated in BBS^{01} and $MKS^{01/02}$ RSs, we found significant alteration of genes involved in development (112 genes) and/or morphogenesis (138 genes) (Figure 3A-C). We next grouped these genes among the most representative clusters and compared them by focusing on genes common to different organs/systems (Figure 3A-D). We found 5 developmental genes - *Noggin* (*NOG*), *SIX1*, *BMP4*, *CDH19, OSR1* - all involved in kidney, heart, ear, skeletal, circulatory, and retinal development (559,1135). Three of them, *NOG*, *SIX1*, and *OSR1,* were also present in most of the morphogenetic groups. Other genes such as *MSX1, TWIST1*, *SIX2*, *OSR2* were present in some of the morphogenetic and developmental groups (Figure 3B) (1136–1138). *PITX2* was one of the most downregulated developmental genes in both $MKS^{01/02}$ and BBS^{01} RSs (Figure 3D). Notably, a large number of genes involved in cilium assembly/organization and intraciliary transport were downregulated in MKS and BBS RSs (Figure S3A-C) (252). From these, 21 corresponded to the CFAP gene family (Figure S3B). We also found 962 genes upregulated and 684 genes downregulated only in $MKS^{01/02}$ RSs (Figure S3D-H). Among these, many were associated with the development and anterior-posterior pattern specification (Figure S3E, H). Several HOX family genes were also specifically upregulated only in $MKS^{01/02}$ RSs, in agreement with MKS being the most severe form of syndromic ciliopathy (Figure S3F).

Barabino et al. 2020

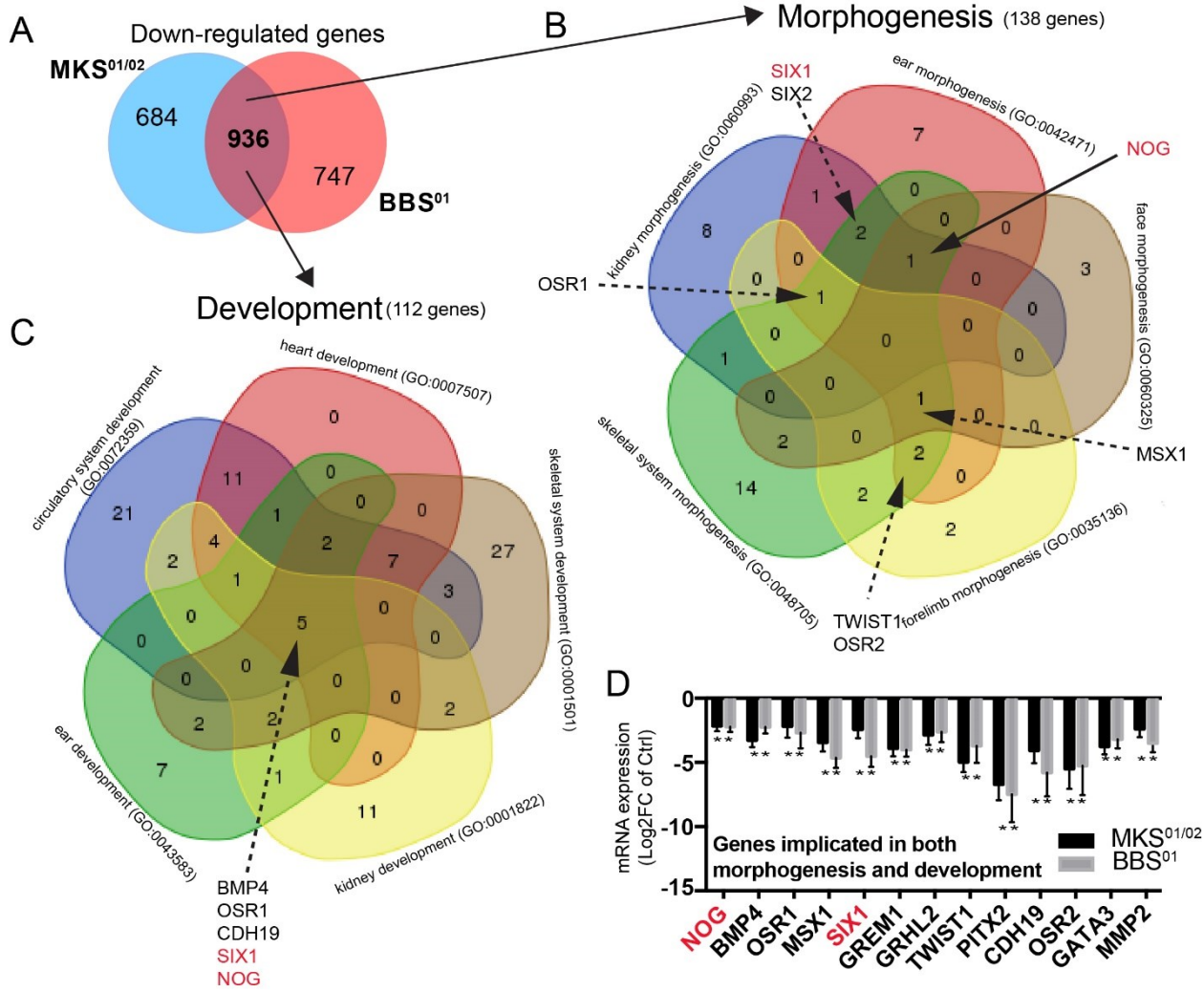

Figure 3: Reduced expression of genes involved in development and morphogenesis.

*(A) Venn diagrams showing the intersection of significant genes differentially down-regulated between MKS01/02 (Blue) and BBS01 RSs (Red). (B-C) Venn diagrams showing the intersection of significative downregulated genes belonging to GO groups involved in the morphogenesis (B) or in the development (C) of 5 organs/systems commonly affected in both MKS and BBS (log2FC>2; P-value <0,05). (D) Gene expression levels in BBS01 and MKS01/02 RSs at DIV60 of genes implicated in both development and morphogenesis. In red, the genes common to all 5 developmental groups with a role also in morphogenesis. All values are means ± SEM. * p<0.05, Student's unpaired t-test.*

3.2.3.4 Induction of the crystallin molecular chaperones in MKS and BBS retinal sheets

From the top 10 most upregulated genes common to BBS and MKS RSs, we found that 6 encoded members of the crystallin gene family (Figure 4A-S4C) (7). In non-lens tissues, these proteins work as molecular chaperones against protein misfolding. Using immunoblot and immunofluorescence, we observed specific accumulation of CRYBB1, CRYBB2, CRYBB3 in both the nuclear and cytoplasmic cell compartments of BBS^{01} and MKS^{01} PRs at DIV45 (Figures 4A-C and S4A-B). Polyubiquitin chains at lysine 48 (polyUb-K48) mark proteins for proteasomal

degradation, and poly-ubiquitylated proteins frequently accumulate in neurodegenerative

Barabino et al. 2020

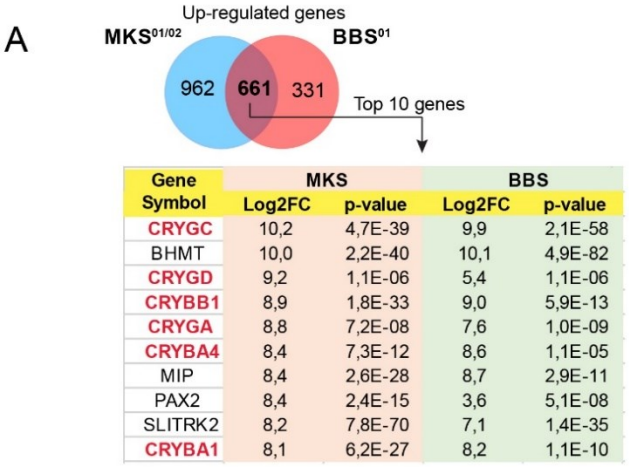

Gene Symbol	MKS		BBS	
	Log2FC	p-value	Log2FC	p-value
CRYGC	10,2	4,7E-39	9,9	2,1E-58
BHMT	10,0	2,2E-40	10,1	4,9E-82
CRYGD	9,2	1,1E-06	5,4	1,1E-06
CRYBB1	8,9	1,8E-33	9,0	5,9E-13
CRYGA	8,8	7,2E-08	7,6	1,0E-09
CRYBA4	8,4	7,3E-12	8,6	1,1E-05
MIP	8,4	2,6E-28	8,7	2,9E-11
PAX2	8,4	2,4E-15	3,6	5,1E-08
SLITRK2	8,2	7,8E-70	7,1	1,4E-35
CRYBA1	8,1	6,2E-27	8,2	1,1E-10

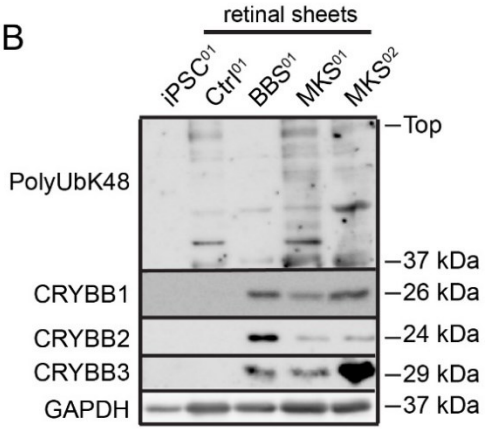

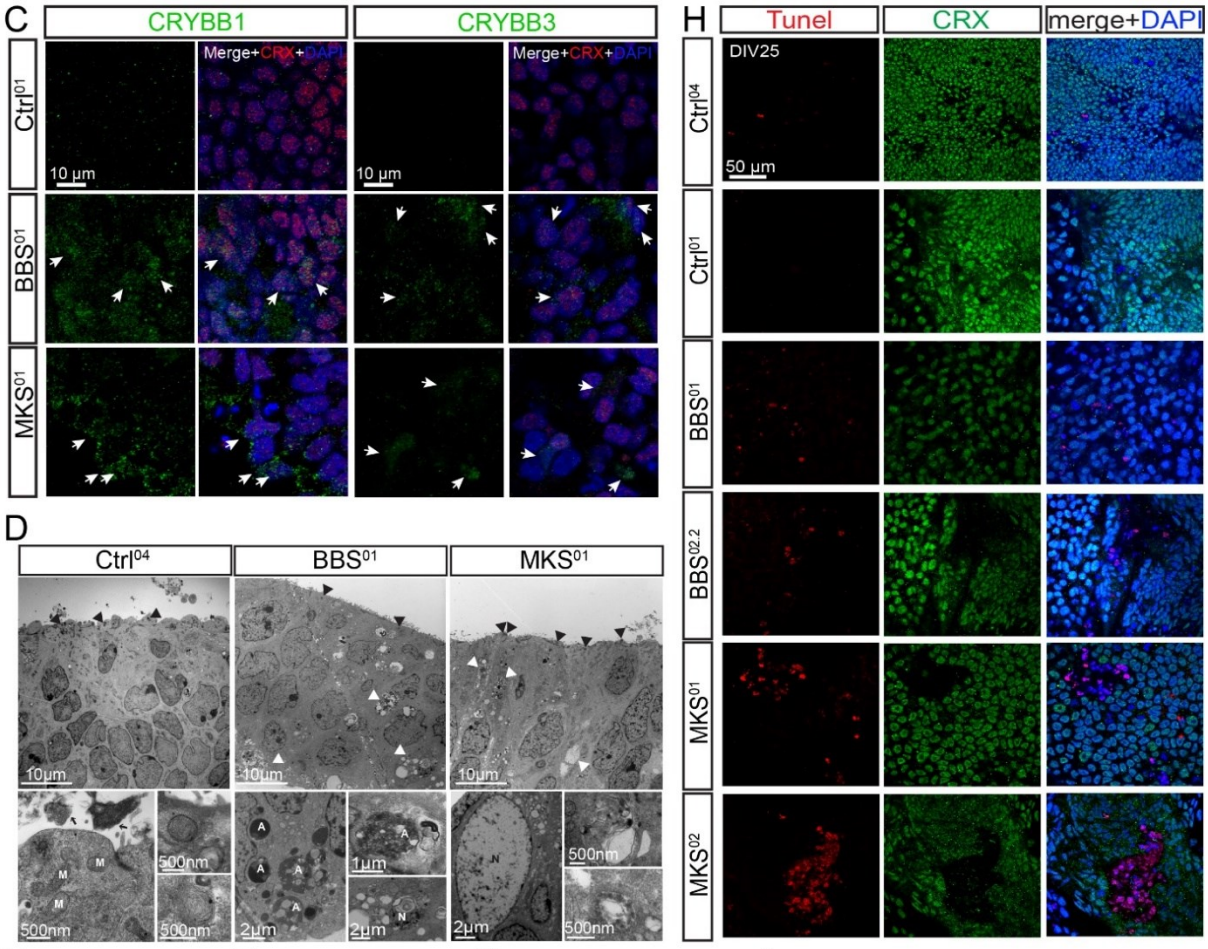

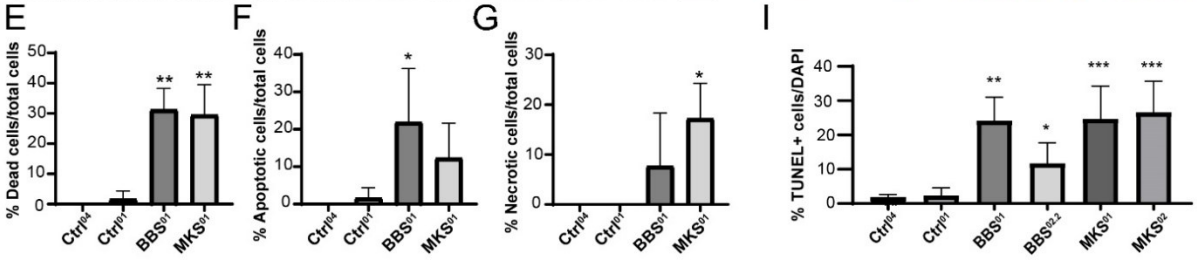

Figure 4: Induction and accumulation of crystallins in MKS and BBS retinal sheets.

*(A) Venn diagrams showing the intersection of significant genes differentially upregulated between MKS01/02 (Blue) and BBS01 RSs (Red) (log2FC>2; P-value <0,05), and the top 10 up-regulated genes common to the 2 groups with their respective Log2FC and p-value for each group. Genes members of the crystallin family are highlighted in red. (B) Immunoblot on extracts from undifferentiated iPSC and RSs. (C) Immunofluorescence (IF) representative images showing CRYBB1 and CRYBB3 accumulation in MKS01/02 and BBS01 CRX-positive cells at DIV45. Note the extracellular and intracellular accumulation of crystallin (white arrows). Scale bars: 10 µm. (D) TEM representative images of RSs at DIV60. BB (black arrowheads), dead cells (white arrowheads). For each condition at the bottom some high magnification images. In Ctrl04 we can observe IS structure with high density of mitochondria, BB near the apical surface, and marked gap junction. A beginning of OS with stack-like structures (black arrows) can be observed beyond the apical surface. Vesicles with laminar material are also observed near the surface. Large vesicles similar to lysosomes were particularly abundant in MKS RSs. M, mitochondria; A, apoptotic cells; N, necrotic cells. (E-G) Quantification of the percentage of total dead cells, apoptotic and necrotic cells observed by TEM at DIV60 (n = 3-4 fields for condition, an average of 24 cells for field. (H) IF representative images in dissociated cells culture at DIV20. Scale bar: 50 µm. (I) Quantification of the percentage of TUNEL-positive cells over total nuclei at DIV20 (n = 4-5 fields for condition, an average of 85 cells for field). n = 3 independent biological replicates for all experiments. All values are means ± SEM. *p < 0.05; **p < 0.01, ***p < 0.001 by one-way ANOVA test.*

diseases (336). When compared to control RSs, $MKS^{01,}$ and MKS^{02}, but not BBS^{01} RSs, presented increased polyUb-K48 levels, suggesting perturbed proteostasis (Figure 4B). Accumulation of misfolded proteins is frequently associated with neuronal cell death (1139). Accordingly, we observed increased expression of apoptosis and cell death-related genes in $MKS^{01/02}$ and BBS^{01} RSs (Figure S4D). Induction of photoreceptor cell death in MKS and BBS RSs was also confirmed using the TUNEL assay and TEM (Figure 4D-I, S4E-H). These results suggested a cellular response to misfolded proteins and increased cell death in $MKS^{01/02}$ and BBS^{01} PRs.

3.2.3.5 MKS photoreceptors are characterized by the presence of supernumerary centrioles

We performed cell biological analyses to study the structure of the cilium in MKS and BBS PRs. The centriole forms the primary cilium basement, and Centriolin marks the mother centriole and BB (185). Using an antibody against Centriolin, we found that when compared to controls, the number of centrioles per cell was higher in DIV60 $MKS^{01/02}$ PRs, but not in $BBS^{01/02}$ PRs (Figure 5A-B). This was confirmed by TEM (Figure 5C-D), and where cilia also appeared to be shorter in MKS (Figure 5C-D). While the total number of cells tended to be higher in MKS and BBS cultures, the difference was not significant (not shown). Notably, supernumerary centrioles were not observed in undifferentiated MKS^{01} iPSCs (Figure S5A-C), suggesting that the defect was cell-type specific.

We did not elucidate the pathogenic mutation in the MKS^{02} case. However, in the MKS^{01} case, the two identified mutations in *TMEM67* were predicted to generate a pathogenic but full-length variant of MKS3 (Figure S1G-H). Hence, we could observe by immunoblot the presence of MKS3 in $Ctrl^{01}$, $MKS^{01/02,}$ and $BBS^{01/02}$ RSs, and MKS3 levels were even slightly increased in MKS^{01} RSs

(Figure 5H). Using antibodies against Centriolin and MKS3, we performed confocal

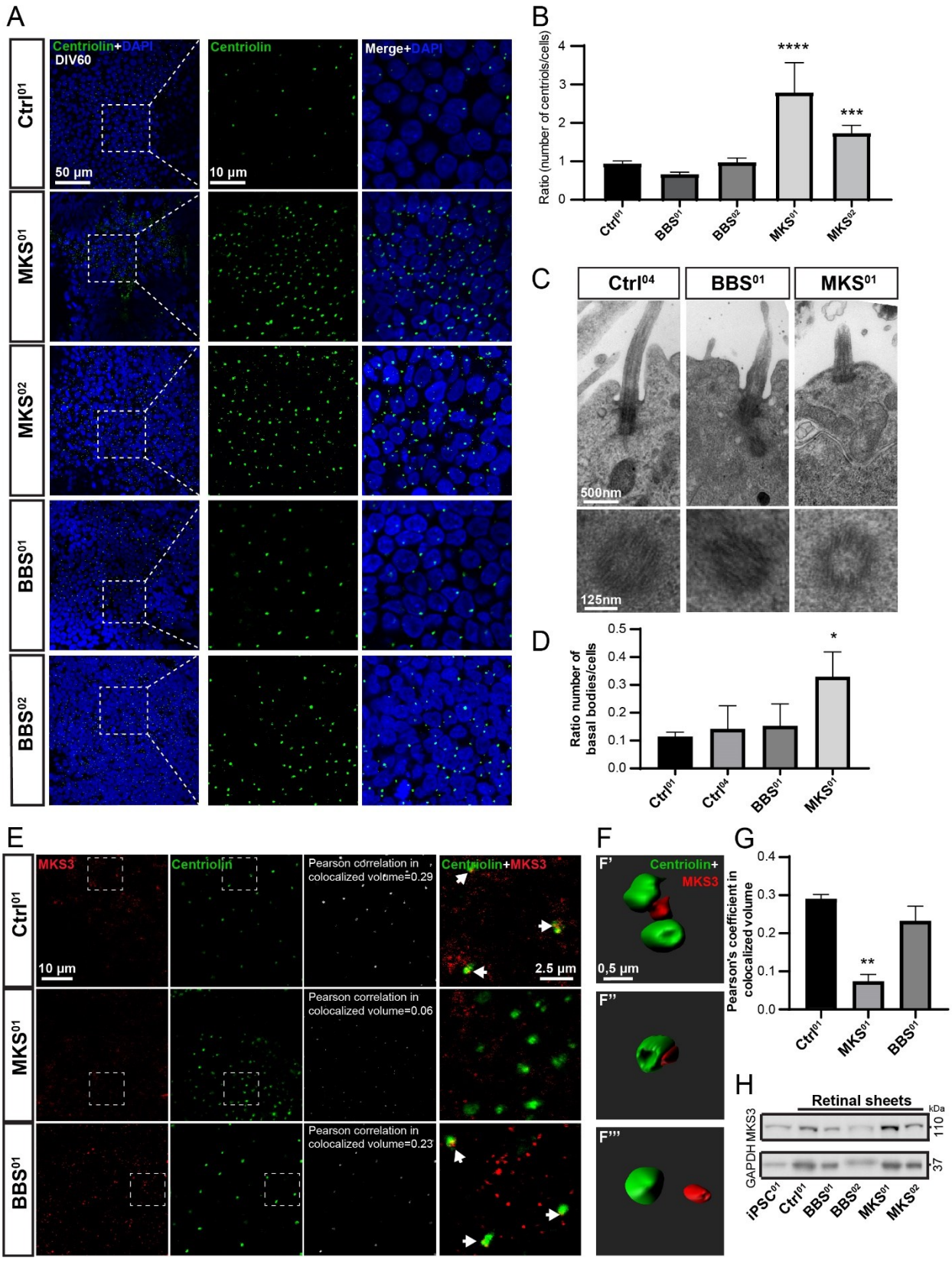

Figure 5: Supernumerary centrioles in MKS photoreceptors.

*(A) IF images of PRs at DIV60. Composed image from two focal planes (DAPI and Centriolin). Scale bar: 50 µm (left), 10 µm (right). (B) Quantification of the number of centrioles (Centriolin) per cell at DIV60 (n = 4 fields for condition, an average of 113 cells for a field). (C) TEM representative images of cilia and BB and its section (bottom). (D) Quantification of the ratio of BB/cells per field by TEM. (N=3-4 images for condition an average of 24 cells for a field. (E) IF images of dissociated PRs at DIV60. The white channel represents colocalized volume between Centriolin and MKS3 with the respective Pearson correlation value quantified in (G). On the right, high magnification images of the respective dashed square in each condition. (F) Representative surface rendering from 3D z-stack reconstruction of the three conformations observed between Centriolin and MKS3: BB and daughter centriole surrounding MKS3 (F'), MKS3 linked to Centriolin (F''), MKS3 and Centriolin unbound (F'''). Scale bar: 0,5 µm. (H) Immunoblot on extracts from iPSC and RSs. n = 3 independent biological replicates for all experiments. All values are means ± SEM. *p < 0.05; **p < 0.01, ***p < 0.001, ****p < 0.0001 by one-way ANOVA test.*

immunofluorescence imaging and 3D reconstruction on dissociated control PRs. We observed three different configurations between Centriolin and MKS3: BB and daughter centriole surrounding MKS3 (F'); MKS3 linked to the centriole (F''); and unlinked MKS3 and Centriolin (F''') (Figure 5F). Notably, while we observed that MKS3 was often in close association with Centriolin in control and BBS^{01} PRs (Pearson's coefficient correlation: 0.29 and 0.23), this association was near absent in MKS^{01} PRs (Pearson's coefficient correlation: 0.06) (Figure 5E-G). These results suggested defective interaction of MKS3 with the centriole in MKS^{01} PRs, possibly leading to the production of supernumerary centrioles (see the model in Figure S6).

3.2.3.6 MKS^{01} photoreceptors have smaller but supernumerary cilia and present abnormal accumulations of ciliary proteins

Using an antibody against acetylated α-Tubulin, we found that supernumerary centrioles in MKS^{01} PRs were also associated with an increasing number of cilia (Figure 6A-C). This phenotype was not observed in BBS^{01} PRs. We performed quantitative analyses of the images using IMARIS, which revealed that although more numerous, cilia in MKS^{01} PRs were shorter and thinner than normal (Figure 6D-E). Some rare giant cilia resembling a fusion of different cilia were also observed. The number of observed cilia was normal in undifferentiated iPSCs from MKS^{01} patients, suggesting cell-type specificity for this phenotype (Figure S5F-H). RPGR mostly labels the basal body of the CC (Figure 6F) (1140). Using confocal microscopy and 3D reconstruction, we observed that control RSs presented a relatively uniform immuno-labeling for RPGR proximal to the PNA-positive outer segment (Figure 6G). In contrast, MKS^{01} RSs were disorganized, as revealed by the unequal distribution of PNA. Furthermore, the signal for RPGR was mislocalized and tended to accumulate in aggregates. RPGR was also mislocalized in RSs from BBS^{01} patient (Figure 6G). These results

suggested supernumerary cilia, abnormal retinal tissue morphogenesis, and aggregation of ciliary proteins in MKS PRs.

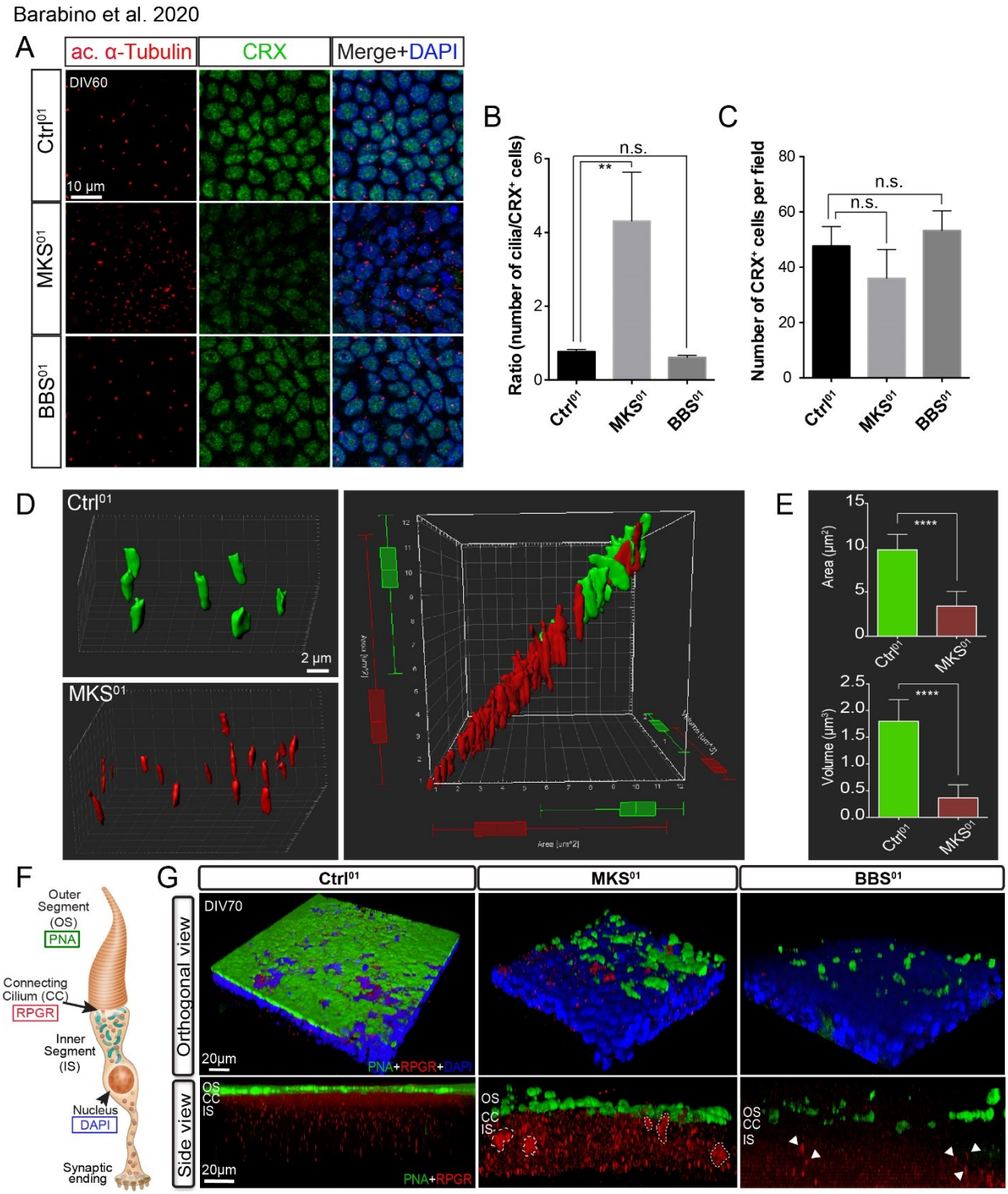

Figure 6: Supernumerary cilia and aggregation of ciliary proteins in MKS01 photoreceptors.

*(A) IF of PRs at DIV60. Composed image from two focal planes (DAPI and Acetyl-α Tubulin). Scale bar: 10 µm. (B-C) Quantification of the number of cilia (Acetyl-α Tubulin) per cell (B) and the number of CRX positive cells per field (C) in cells at DIV60 (n = 4 fields for condition, an average of 53 cells for a field). (D) Surface rendering 3D reconstruction from confocal z-stack images of Ctrl01 (green) and MKS01 (red) based on Acetyl-α Tubulin staining (left) Scale bar: 2 µm. A 3D plot of cilia (cilia from 3 images put together for each condition) based on area and volume (right). Notice how control cilia clustered together while MKS01 cilia are more heterogeneous, smaller, and more abundant (n = 2 independent experiments). (E) Quantification of area and volume of Ctrl01 and MKS01 cilia (ctrl n=20; MKS n=47). (F) Representation of a cone PR with reference to OS, CC, IS, and nucleus and the localization of the markers used in (G). (G) 3D z-stack reconstruction of RSs from IF images at DIV70. Dotted lines: intracellular aggregates of RPGR. White arrows: RPGR not polarized to the apical zone. n = 3 independent biological replicates for all experiments. Scale bars, 20 µm. All values are means ± SEM. ** p<0.01, **** p<0.0001, Student's unpaired t-test.*

3.2.3.7 BBS photoreceptors display mitotic spindle checkpoint activation and genomic instability

Significantly up-regulated genes in BBS^{01} RSs included markers of mitotic spindle checkpoint and microtubule cytoskeleton organization regulation (Figures 7A-B and S7B), suggesting possible genomic instability during mitosis. On the other hand, we observed the down-regulation of genes involved in extracellular matrix organization and tube development (Figure S7D). DIV15 photoreceptor progenitors were analyzed using specific antibodies. We found that the number of cells expressing the DNA damage response markers γH2Ax and 53BP1, and the activated mitotic checkpoint protein pChk2, were increased in $BBS^{01/02}$ samples, but not in control or $MKS^{01/02}$ samples (Figures 7C-G and S7E-H). This phenotype was, however, generally more severe in the BBS^{01} case than in the BBS^{02} case. We also observed the presence of very large nuclei in $BBS^{01/02}$ PRs that were also γH2Ax and pChk2-positive, suggesting possible arrest in the G2/M phase of the cell cycle. γH2Ax, a marker of DNA double-strand breaks, was also detected by immunoblot on whole-cell extracts in BBS^{01} RSs at DIV60 of differentiation, but not in control or MKS^{01} RSs (Figure 7H). Consistently, micronuclei, nuclear bridges, mitotic catastrophe, and nuclei having multipolar or monopolar spindles were more frequent in BBS^{01} PRs progenitors than in the MKS^{01} or control one. Nuclear bridges were detected in all conditions but tended to be more abundant in BBS^{01} PRs. Mitotic catastrophes were also significantly higher in BBS^{01} than in control cells, but they were also present in MKS^{01} cells (Figure 7I). We concluded that although MKS and BBS PRs shared a broad number of molecular and cellular alterations, they also displayed unique anomalies that may help explain the distinct phenotypes characterizing these disorders.

Barabino et al. 2020

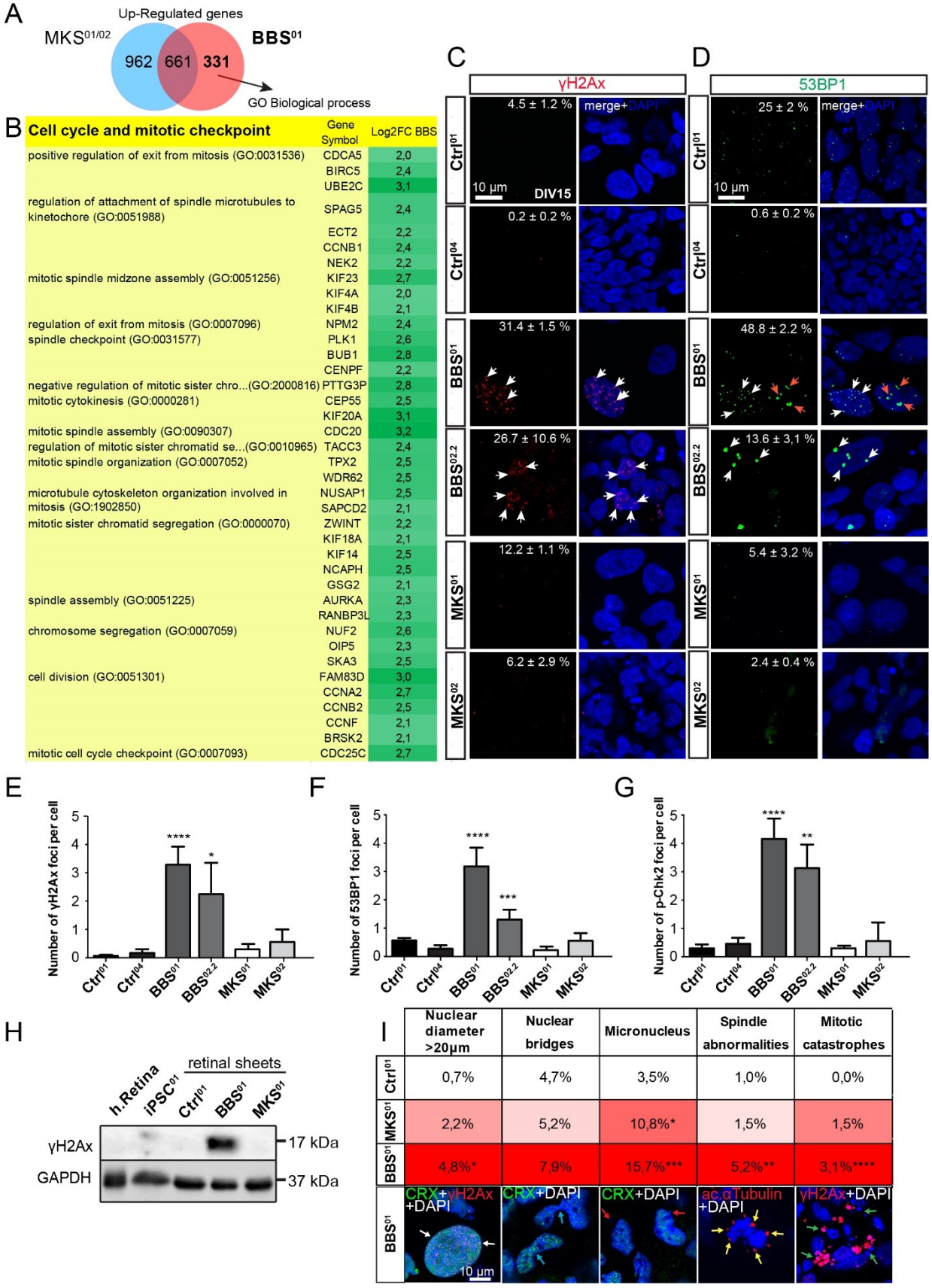

Figure 7: Activation of the mitotic spindle checkpoint and accumulation of DNA damage in BBS photoreceptors.

*(A) Venn diagrams showing the intersection of significant genes differentially upregulated in MKS01/02 (Blue) and BBS01 RSs (Red) (log2FC>2; P-value <0,05). (B) Gene Ontology Enrichment analyses of BBS01-specific differentially up-regulated genes. The main GO group and subgroups are shown. Some representative genes and the respective Log2FC (P-value <0,05) are indicated for each category. (C-D) IF images of PR progenitors at DIV15. The percentage of positive cells (more than 3 foci per cell) is indicated on the respective images (average n=253 cells for condition). Scale bar: 5 µm. (E-G) Quantification of the average number of foci per cell in PR progenitors at DIV15 (n>3 fields for condition, an average of 84 cells for a field). (H) Immunoblot on extracts from undifferentiated iPSC and RSs at DIV60. (I) Representative images for common mitotic abnormalities and the respective percentages of cells for each condition in PRs progenitors at DIV15. White arrows: giant nucleus; blue arrows: nuclear bridge; red arrows: micro-nuclei; Yellow arrows: multifocal spindle; green arrows: fragmented nuclei strongly marked by the anti-γH2Ax antibody. n = 3 independent biological replicates for all experiments. All values are means ± SEM. * p<0.05, ** p<0.01, *** p<0.001, **** p<0.0001, Student's unpaired t-test.*

3.2.4 Discussion

We generated iPSCs from control and ciliopathy cases and differentiated them into polarized 3D-adherent RSs that could recapitulate normal photoreceptor development and disease state, respectively. By whole-genome sequencing, we identified mutations in *BBS10* (BBS^{01} and BBS^{02} patients) and *TMEM67* (MKS^{01} case). Using RNA-seq analyses and high-resolution fluorescence microscopy, we were able to identify and study retinal developmental anomalies and photoreceptor degeneration processes that characterized MKS and BBS. Importantly, we could also distinguish specific pathological features that were either common or unique to the two syndromes.

Previous reports based on rare genetic cases suggested that BBS and MKS may represent a "unique disease" with two different degrees of severity (234,426). Using our *in vitro* model, we found that 60% of deregulated genes in BBS^{01} PRs and 49% of those in $MKS^{01/02}$ PRs were common between both diseases, although BBS and MKS cases studied here carried mutations in unrelated genes. Brain, eye, and bone malformations and polydactyly are common to MKS and BBS. Hence, we found deregulation of hundreds of neuro-developmental genes, most of them common to both ciliopathies. WNT, NOTCH, and HOX signaling pathways were highly affected, consistent with WNT and Notch's essential function in neural development and with the role of the *HOX* gene cluster in axial skeleton development and digit formation (147,1141,1142). Unexpectedly, we observed significant down-regulation of *NOG*, *BMP*, *SIX1*, *MSX1*, *TWIST*, *OSR1,* and *PITX2*. *NOG* and *BMP* are important for the nervous system, muscles, and bone development. In contrast, the others are required for the differentiation of intermediate mesoderm-derivative (gonads and kidneys) and limb buds (*OSR1*), in epithelial-mesenchymal transition (*TWIST*), in the development of the neck, ears, and kidneys (SIX1), and of oral structures (*MSX1*). *PITX2* is involved in the establishment of the left-right axis and morphogenesis of many organs (1143,1144). Mutations in *PITX2* are associated with Axenfeld-Rieger syndrome (ARS), iridogoniodysgenesis syndrome (IGDS), and sporadic cases of Peters anomaly, revealing his essential role in the eye's development (1145). Notably, polydactyly, craniofacial, neural, retinal, ocular, skeletal, and kidney anomalies are commonly observed in syndromic ciliopathies (426,1128). Thus, developmental defects

observed in peripheral organs and musculoskeletal structures of MKS and BBS patients were revealed in our gene expression profile analyses of RSs.

We found up-regulation of several apoptotic genes and genes of the beta and gamma-crystallin families in both MKS and BBS RSs. Alpha-crystallins are known to operate as molecular chaperones for misfolded proteins and can be found in ubiquitin-associated inclusions in neurodegenerative diseases (1146,1147). In contrast, the function of beta and gamma-crystallins in non-lens tissue is not well understood. Some studies have linked the expression of beta and gamma-crystallins to retinal diseases. It has also been observed that gamma and beta-crystallin production increases before photoreceptor cell death in animal models of RP and light-induced retinal degeneration (1148–1151). βB2-crystallin (*CRYBB2*) was shown to be strongly expressed in regenerating ganglion cells, where it may promote axonal regrowth (1152). Thus, although crystallins' exact role in neurodegenerative contexts remains to be clarified, our findings reveal robust activation of this pathway in PRs from ciliopathy patients.

In MKS^{01} PRs, we observed near absent co-localization of MKS3 with Centriolin, which may explain the presence of supernumerary centrioles. Cilia were also shorter and thinner than normal, suggesting cilia degeneration and/or abnormal formation and maintenance. Notably, it was shown that in mouse renal-tubule epithelial cells, reducing the level of MKS3 using siRNA impaired the number of cilia, whereas its complete loss caused elongated cilia (719). Multi-ciliated cells were also observed in MKS patients and in a rat model of MKS3 (1153). We also found that MKS^{01} RSs were highly disorganized and that the signal for RPGR was mislocalized and tended to accumulate in aggregates. BBS^{01} cells also showed abnormal RPGR localization. Unlike MKS^{01} PRs, however, RPGR was generally mislocalized at the basement of BBS^{01} PRs, suggesting abnormal transport or docking to the BB. This reveals both similarities and differences between the two syndromes.

Moreover, genes implicated in canonical WNT signaling were up-regulated, which was apparently at the expense of the noncanonical one. In polarized cells, the cilium grows at the apical side. During ciliogenesis, planar cell polarity and apical-basal polarity are necessary for docking of the centrioles at the plasma membrane and the correct formation and maintenance of PRs' BB

(447,1154). Taken as a whole, these observations suggest that hallmarks of the MKS phenotype previously reported in MKS patients and animal models were recapitulated at the cellular and molecular levels in $MKS^{01/02}$ RSs. Furthermore, we described for the first time the presence of supernumerary cilia and centrioles in $MKS^{01/02}$ PRs, which was associated with reduced co-localization of MKS3 with Centriolin in the MKS^{01} case, suggesting deficient interaction of the mutant MKS3 protein with centrioles. In the MKS^{02} case, which does not carry mutations in *TMEM67*, the number of centrioles/cells was about two folds higher than in controls and $BBS^{01/02}$ cases but was less severe than in MKS^{01}. It is not surprising that despite carrying mutations in different genes, MKS cases show highly related phenotypes at the cellular and molecular levels.

Previous reports have described cilia proteins with cilia-independent functions, including mitotic spindle generation and mitotic process regulation (129,363,1155). Unexpectedly, we found genomic instability in $BBS^{01/02}$ retinal progenitors and PRs, with the most prominent feature being the activation of the mitotic spindle checkpoint. This suggests a new and essential role of BBS10 in microtubule cytoskeleton organization during mitosis.

In summary, we have produced iPSCs from control, MKS, and BBS cases and differentiated them into RSs, allowing recapitulation of normal and pathological human retinal and PRs development *in vitro*. Molecular and cell biological analyses further revealed known and novel disease mechanisms associated with retinal ciliopathies, opening potentially new disease treatment avenues.

3.2.5 Methods

3.2.5.1 Generation, Maintenance, and Characterization of iPS Cells

Human PSc were used in accordance with the Canadian Institute Health Research (CIHR) guidelines and approved by the "Comité de Surveillance de la Recherche sur les Cellules Souches" (CSRCS) of the CIHR and Maisonneuve-Rosemont Hospital Ethic Committee. Fibroblasts MKS1, MKS2, BBS1, and BBS2 were obtained from clinically diagnosed individuals (Coriell Biorepository) (details of these cell lines and other cell lines used in this paper are in supplementary table) were reprogrammed by two rounds of overnight retroviral transduction with the four Yamanaka factors, OCT4, SOX2, KLF4, and c-MYC, using the pMIG vector set. Multiple clones from each patient were karyotyped (Cell Line Genetics) and frozen. A subset of these colonies was used for the study. Lines were established on mouse embryonic fibroblast feeders (Global Stem Cell GSC-6001G) in 20% Knock Out Serum Replacement, 1× nonessential amino acids, 1× Glutamax, 1× penicillin-streptomycin, 55 μM β-mercaptoethanol, DMEM-F12, and 10 ng/ml human fibroblast growth factor 2 (FGF2; Invitrogen) and restarted every ∼30 passages. For expansion ESC and iPSC were cultured on a Matrigel-coated plate (Corning, Cat# 354277) with a daily change of StemFlex medium according to the manufacturer's instruction (Gibco # A3349401). To generate teratomas, ~ 3 x 106 undifferentiated iPS cells were resuspended in 150 µl of a cold 50/50 mix of DMEM-F12 and Matrigel and implanted beneath the neck scruff of NOD-SCID immunodeficient mice. Tumors were harvested 12 weeks later and processed for histology analysis.

3.2.5.2 Differentiation of human ESC and iPSC into retinal sheets

The differentiation protocol was based on a previous study (Zhou et al., 2015). However, the recombinant COCO was used at 60ng/ml. iPSC and ES were dissociated using ReLeSR™ (Stem cell technologies, Cat# 05872) and platted on growth factor reduced Matrigel (Corning #356231) in StemFlex cell media (Gibco # A3349401) supplemented with ROCK inhibitor (Y-27632;10µM, Cayman Chemical #10005583). Upon 100% of confluency, the media was changed to CI60 Media [DMEM-F12 medium (Invitrogen) containing,1% N2, 2% B27, 10ng/ml IGF1 (peprotech, Cat#100-11), and 5 ng/ml bFGF (peprotech, Cat#AF-100-18B), 60 ng/ml COCO (R&D System, Cat#3047-CC-050), Heparin (Sigma, Cat#H3149]. The medium was changed every day. For single-cell IF

analyses, RSs were dissociated for 30min using Cell Dissociation Buffer (Gibco, Cat# 13151014) and resuspended in CI60 media supplemented with ROCK inhibitor (Y-27632; 10µM) and platted on growth factor reduced matrigel coated plates or chamber slides (Ibidi, Cat# 80826).

3.2.5.3 Fluorescence and Electron Microscopy

Cells were fixed with 4% PFA for 15 min and permeabilized with Triton X-100 for 10 min. Unspecific antigen blocking was performed using 2% BSA in PBST for 30 min. Cells were incubated with the primary antibody overnight at 4C in a humidified chamber (see dilutions in Table). Secondary antibodies were incubated 1h at room temperature. All secondary antibodies were tested alone or in combination to assay for possible non-specific background fluorescence. After incubation with the secondary antibody, slides were counterstained with DAPI. Pictures were taken using a confocal microscopy system (Olympus). Confocal microscopy analyses were performed using 60x objectives with an IX81 confocal microscope (Olympus, Richmond Hill, Canada), and images were obtained with Fluoview software version 3.1 (Olympus). 3D reconstructions were obtained with IMARIS station v8.4.1 (Bitplane). For electron microscopy, structures were scraped from the plate after 5 min of fixation, pelleted at 300g for 4 min, and the pellet was gently released by pipetting into 0.15 M sodium cacodylate trihydrate (Sigma) dissolved in water (pH 7.3) containing 4% formaldehyde and 2% glutaraldehyde (Electron Microscopy Sciences), post-fixed with osmium tetroxide solution (Sigma), dehydrated in serial ethanol dilutions (Sigma) and embedded in epoxy resin. Ultrathin sections (75 nm) were cut, mounted on 200 mesh copper grids, counterstained with uranyl acetate and lead citrate stains (Electron Microscopy Sciences), and examined in a JEOL JEM-1010 transmission electron microscope.

3.2.5.4 Quantification of immunofluorescence images

High magnification z-stack images of MKS3, Centriolin and acetylated α-Tubulin was used for 3D reconstruction. Using IMARIS station v8.4.1 (Bitplane) software with the Surpass optional module, volume and surface were rendered and quantified (Figure 6D-E). For Figure 5F the channel correlation in colocalized volume option was used to build the colocalization channel and then used for the Coloc Statistics.

3.2.5.5 RNA sequencing analyses

Total RNA from two independent biological samples (two distinct differentiation) for each cell lines was extracted using the RNeasy Mini Kit (Qiagen, Cat# 74104) according to manufacturer instructions including DNase treatment. RNA integrity was controlled using Bioanalyzer (Agilent) and two samples from each group with a RIN>8 were sequenced. 1 µg of total RNA was subjected to mRNA isolation using OligodT Dynabeads and libraries were prepared using Ion Total RNA-Seq Kit v2. Libraries were sequenced onto P1 chips from Ion torrent as unpaired to reach 40 million of reads for each sample. Raw sequencing files (FASTQ) were first trimmed to remove adapters and further validated using FASTQC v0.11.7. Reads were aligned onto hg19 using Hisat2 v2.1.0 with default parameters and sorted using samtools v1.9. Gene level counts were determined using featureCounts from subread package. Differential expression analysis was performed using DEseq2 package in R and volcano plot were generated using Tmisc and Calibrate R packages. FPKM values for each sample were calculated using Cufflinks v2.2.1. Heatmaps were generated with FPKM values using Heatmapper2. Gene Ontology was performed using PANTHER (Mi et al., 2010, 2012). Z-scores were computed for each row and clustered using average linkage and Pearson distance measurement method. For Gene-Set Enrichment Analysis (GSEA), differentially expressed genes were pre-ranked according to the log2 of fold change and a p-value < 0.05. Ranked lists were then subjected to GSEA with a classic scoring scheme, an enrichment score normalization and 1000 permutations. Publicly available RNA-seq used in this paper are found in the supplementary table.

3.2.5.6 Western Blot

Cell extracts were homogenized in the Complete Mini Protease inhibitor cocktail solution (Roche Diagnostics), followed by sonication. Protein material was quantified using the Bradford reagent. Proteins were resolved in 1x Laemelli reducing buffer by SDS-PAGE electrophoresis and transferred to a Nitrocellulose blotting membrane (Bio-Rad). Subsequently, membranes were blocked for 1h in 5% non-fat milk-1X TBS solution and incubated overnight with primary antibodies. Membranes were then washed 3 times in 1X TBS; 0.05% Tween solution and incubated for 1h with corresponding horseradish peroxidase-conjugated secondary antibodies.

Membranes were developed using the Immobilon Western (Millipore). Antibodies used are listed in supplemental experimental procedures.

3.2.5.7 Whole-genome alignment and variant calling.

Base calling was performed using Illumina HiSeq Analysis Software (HAS; version 2-2.5.55.1311). Reads were mapped to the b37 reference sequence using bwa-mem v0.7.12. Duplicate reads were removed using MarkDuplicates from Picard v2.5.0. Local read realignment around indels, base quality score recalibration (BQSR), variant calling with HaplotypeCaller, and variant quality score recalibration (VQSR), was accomplished using GATK v3.7.0. Resulting variant calls were annotated using a custom pipeline developed at TCAG based on ANNOVAR. Strategy for identification for pathogenic variant: 1. Filter out variants with read depth < 10; 2. Keep homozygous variant in more than 80% of the reads and heterozygous variant with 30%-70% of the reads with variants; 3. Keep variants with =< 1% population frequency; 4. Remove non-coding variants; 5. For coding variants: Keep Synonymous variants that can potentially affect splicing (spx_dpsi =<-4); Keep intronic variants that can potentially affect splicing (spx_dpsi =<-4); Keep loss of function mutation (frameshift substitution, frameshift insertion, non-frameshift substitution, non-frameshift deletion, non-frameshift insertion, stopgain, stoploss); Keep pathogenic missense mutation using pathogenicity scores; Sift =<0.05: Polyphen >=0.95; Ma >= 2; PROVEN =<2.5; ploylopPMam >=1; phylopVert100 >=1.5; CADD phred >=15; 6. Identify variants in cilia-related genes; 7. Use gnomAD and 1000 genome population frequency to further eliminate common variants; 8. Binary alignment map (BAM) validation on IGV.

3.2.5.8 Statistical Analysis

Statistical analysis was performed using GraphPad software (Prism 6). Statistical differences were analyzed using the Student's t-test for unpaired samples. Values are representative of at least 3 experiments. When comparisons were made using independent samples of equal size and variance following a normal distribution, significance was assessed using an unpaired two-sided Student's t-test. Where several groups were compared, significance was assessed by ANOVA and adjusted for multiple comparisons using the Bonferroni correction. Differential expression was

assayed using a log2 fold change statistical algorithm or one-way ANOVA with a p-value cutoff at 0.05. For gene ontology, a false discovery rate (FDR) cutoff of 0.01 was applied.

3.2.5.9 KEY RESOURCES TABLE

REAGENT or RESOURCE	SOURCE	IDENTIFIER	DILUTION WB	DILUTION IF	HOST
Antibodies					
Fluorescein labeled Peanut Agglutinin (PNA)	Vector laboratories	Cat#FL-1071	N/A	1/250	N/A
S-Opsin	SCB	Cat#sc-14363	1/250	1/200	Goat
RPGR	SCB	Cat#sc-14672	N/A	1/100	Goat
acetilated α-Tubulin	SCB	Cat#sc-23950	N/A	1/500	Mouse
Centriolin (C-9)	SCB	Cat#sc-365521	N/A	1/250	Mouse
MKS3 (EPR17187)	abcam	Cat#ab2020662	1/1000	1/500	Rabbit
CRX (CORD2)	abcam	Cat#ab78662	1/1000	1/300	Rabbit
CRYBB1 (A-8)	SCB	Cat#sc-374496	1/500	1/250	Mouse

CRYBB2 (B12)	SCB	Cat#sc-376006	1/500	N\A	Mouse
CRYBB3 (G-3)	SCB	Cat#sc-374374	1/500	1/250	Mouse
γH2Ax	Millipore	Cat#05-636	1/1000	1/250	Mouse
pChk2	CellSignaling	Cat#2661	N/A	1/100	Rabbit
TKK	SCB	Cat#sc-376842	N/A	1/200	Mouse
PCNA	abcam	Cat#ab18197	N/A	1/500	Rabbit
NANOG	abcam	Cat#ab21624	N/A	1/1000	Rabbit
OTC4	abcam	Cat#ab184665	N/A	1/500	Mouse
53BP1	Novus	Cat#nb100-304	N/A	1/500	Rabbit
GAPDH(D-6)	SCB	Cat#sc-166545	1/500	N/A	Mouse
PolyUBk48 (Apu2)	Millipore	Cat#05-1307	1/2000	N/A	Rabbit
MKS3	proteintech	Cat#13975-1-AP	N/A	1/100	Rabbit

REAGENT or RESOURCE	SOURCE	IDENTIFIER
Biological Samples		

Human eyes	Banque de tissus oculaires pour la recherche en vision (Centre de recherche du CHU de Québec-Université Laval)	NA
Chemicals, Peptides, and Recombinant Proteins		
ROCKi (Y-27632)	Cayman chem	Cat#10005583
Recombinant Human COCO Protein	R&D system	Cat#3047-CC-050
Recombinant human IGF-1	peprotec	Cat#100-11
Recombinant human FGF basic	peprotec	Cat#AF-100-18B
heparin	Sigma	Cat#H3149
Critical Commercial Assays		
TUNEL Alexa Fluor™ 488 Imaging Assay	Invitrogen	Cat#C10245
Deposited Data		
Indifferentiated IPS cells used in RNAseq analisys	GSE87273(1156); GSM3239684(1157); GSE98288(934).	SRX2186365; SRR7458274; SRR7458276; SRX2767163

Indifferentiated ESC cells used in RNAseq analisys	GSM1715067(1158); GSM3195634(1159); GSM2734431(1160).	SRR2069387; SRR7357230; SRR5905125; SRR5905126.
Human Retina used in RNAseq analisys	GSE94437(1132)	GSM2475287.
RNAseq Data of RSs (Ctrl$^{1/2/3}$, Ctrl^{4}(ES), MKS$^{1/2}$, BBS^{1}) (This paper)	GSE133247	GSM3903945; GSM3903946; GSM3903947; GSM3903948; GSM3903949; GSM3903950; GSM3903951; GSM3903952; GSM3903953; GSM3903954; GSM3903955; GSM3903956; GSM3903957; GSM3903958.

Whole genome Sequencing of MKS[1] and BBS[1] patients (This paper)	BioSample	SAMN13656497; SAMN13656498.
Experimental Models: Cell Lines		
Ctrl[01]_iPSC	In house (https://doi.org/10.1016/j.celrep.2018.04.097)	N/A
Ctrl[02]_iPSC	Lab. C. Beauséjour	N/A
Ctrl[03]_iPSC	Lonza	N/A
Ctrl[04]_iPSC	Coriell	AICS-0016
Ctrl_ESC (hESC line HUES9)	HSCI iPS Cell Core Facility	Cat#NIHhESC-09-0022
MKS[01] (Fibroblast cell line used to make in house iPSC)	Coriell	Cat#GM07214
MKS[02] (Fibroblast cell line used to make in house iPSC)	Coriell	Cat#GM07817
BBS[01] (Fibroblast cell line used to	Coriell	Cat#GM05948

make in house iPSC)		
BBS^{02} (Fibroblast cell line used to make in house iPSC)	Coriell	Cat#GM05950
BBS$^{02.2}$ (clone 2) (Fibroblast cell line used to make in house iPSC)	Coriell	Cat#GM05950
Software and Algorithms		
IMARIS station v8.4.1	Bitplane	N/A

3.2.6 Acknowledgments

This work was supported by grants from the Foundation Fighting Blindness Canada, National Science and Engineering Research Council of Canada (2017-05504), and Maisonneuve-Rosemont Hospital Foundation. AF, RH, and AB were supported by fellowships from the Molecular Biology Program of Université de Montréal. NIH Award K01DK102826 supported work in the Freedman laboratory. We thank Steve Breault, Anna Baccei, Joseph Bonventre for assistance with scanning electron microscopy and stem cell culture, Eric Pierce, Marc Consugar, and Erika Tavares for the mutational analysis and WGS, and Fabien Martinel for the photoreceptor graphics. G.B. and A.F. are co-founders of StemAxon^{TM} and its scientific advisory board members. The corporation was not involved in this study.

3.2.7 Supplementary figures

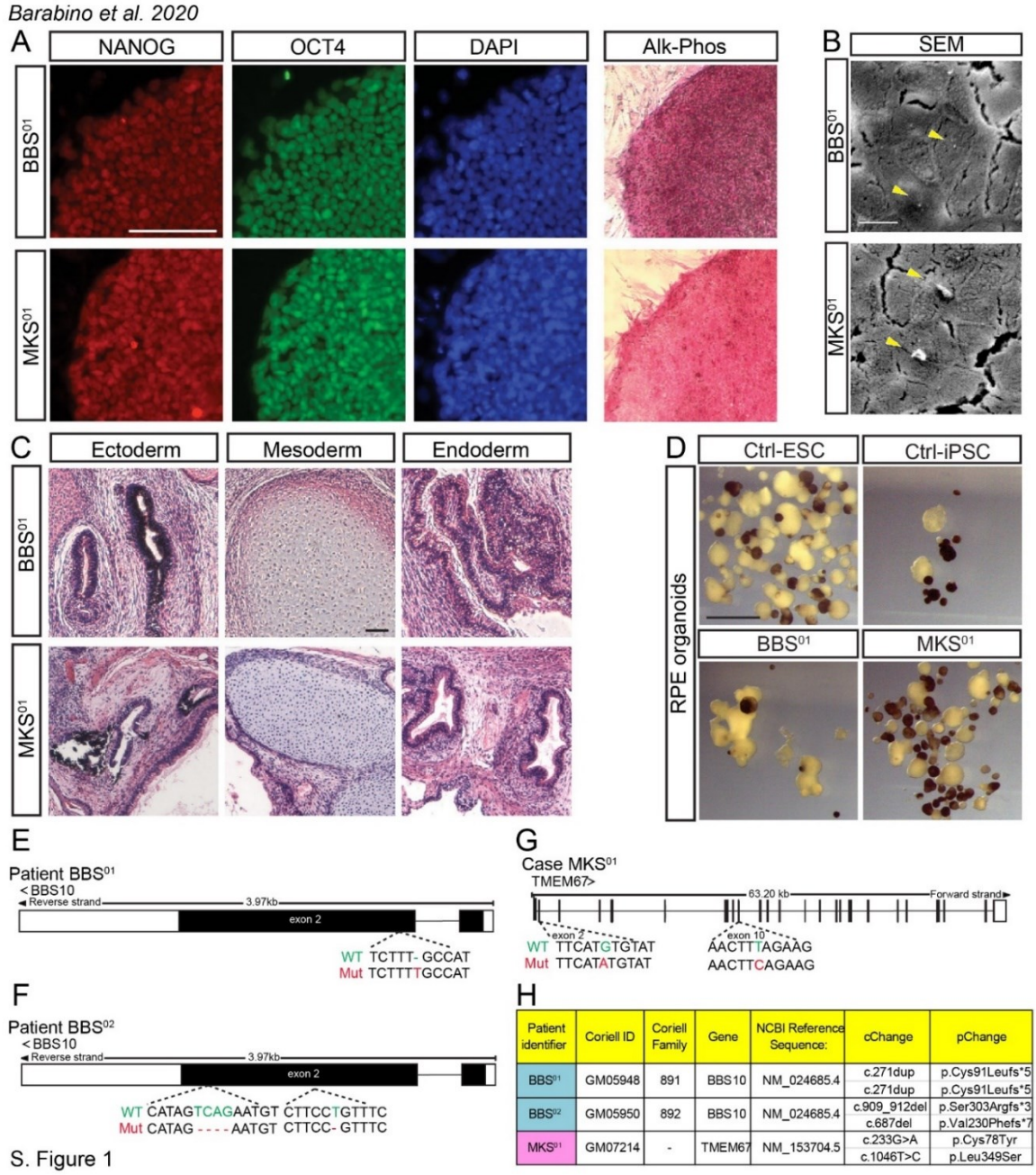

Patient identifier	Coriell ID	Coriell Family	Gene	NCBI Reference Sequence:	cChange	pChange
BBS01	GM05948	891	BBS10	NM_024685.4	c.271dup	p.Cys91Leufs*5
					c.271dup	p.Cys91Leufs*5
BBS02	GM05950	892	BBS10	NM_024685.4	c.909_912del	p.Ser303Argfs*3
					c.687del	p.Val230Phefs*7
MKS01	GM07214	-	TMEM67	NM_153704.5	c.233G>A	p.Cys78Tyr
					c.1046T>C	p.Leu349Ser

Figure S 1 Generation of iPSC cells and identification of the disease-causing mutations from patients affected by BBS and MKS (Related to Figure 1)

(A) Pluripotency marker expression (NANOG, OCT4, and Alkaline Phosphatase Live Stain) in iPSC derived from BBS^{01} and MKS^{01} patients. Nuclei stained with DAPI. (B) Representative images showing the surface of undifferentiated iPSC by scanning electron microscopy (SEM, arrows indicate cilia). (C) Teratoma sections obtained from BBS^{01} and MKS^{01} iPSC. (D) Dissecting microscope images of RPE organoids derived from control and ciliopathy iPS cell lines. (E-G) Schematics of the sequencing results for the four patients (BBS$^{01/02}$ and MKS$^{01/02}$). For each patient are indicated the schematic of the gene affected, the mutated loci with the exon number, the WT sequence in green and the mutated one in red. (H) Summary table of the mutations. For each patient are indicated the patient identifier, the Coriell ID of the fibroblasts of origin, Coriell family, gene name, NCBI Reference number, cChange, and pChange. Scale bars, 100 µm (A; C), 10 µm (B), 2 mm (D).

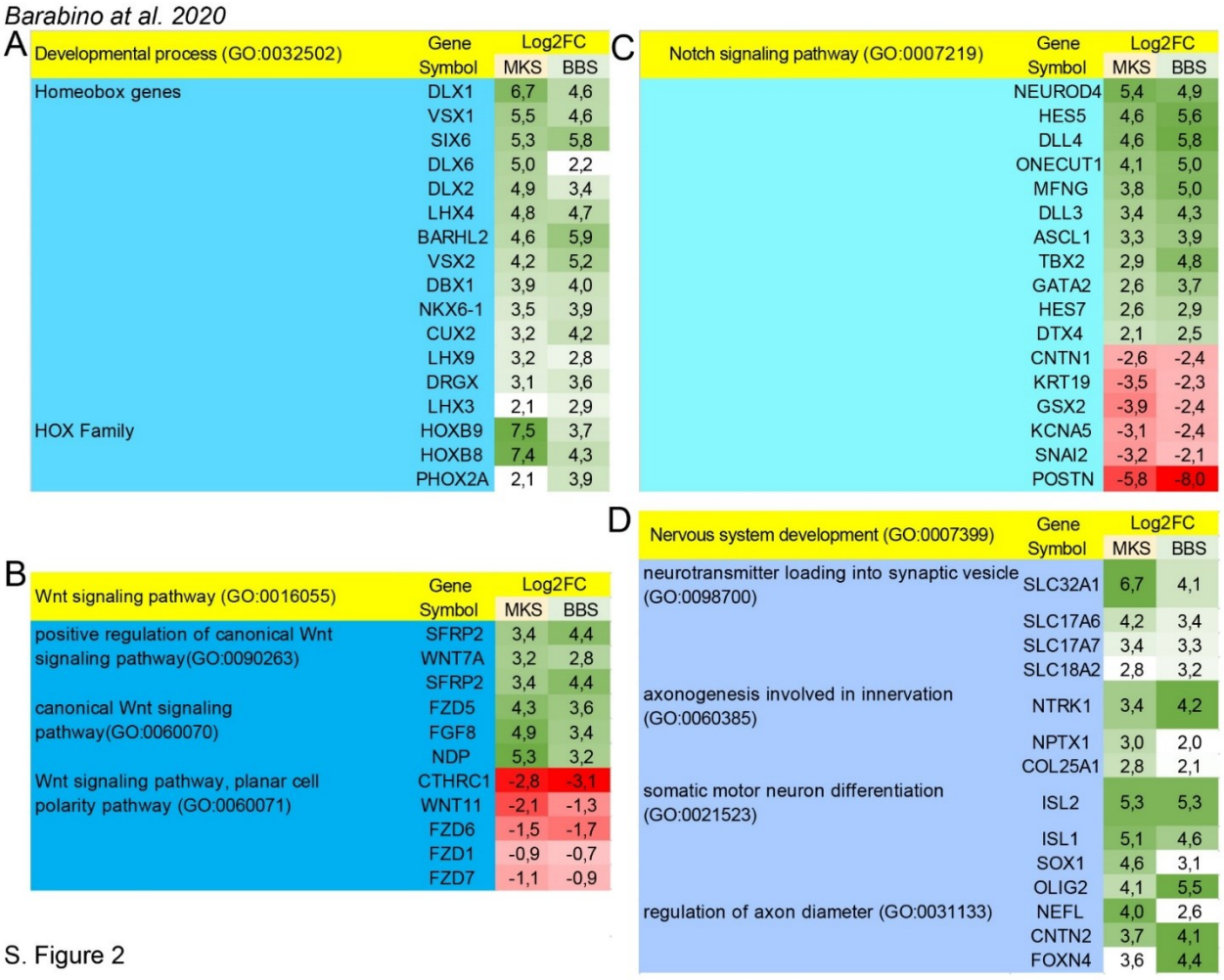

Figure S 2 Perturbed expression of Homeobox genes and WNT and NOTCH pathways in MKS and BBS RSs (Related to Figure 2)

(A-D) Gene Ontology Enrichment analyses of common differentially up-regulated and downregulated in the two groups. Some selected significantly enrich GO groups and subgroups are shown with a few representative genes and the respective Log2FC in MKS$^{01/02}$ and BBS^{01} vs Ctrl$^{01/02}$ RSs (P-value <0,05). Log2FC is also represented in a colorimetric scale from red (downregulated) to green (upregulated).

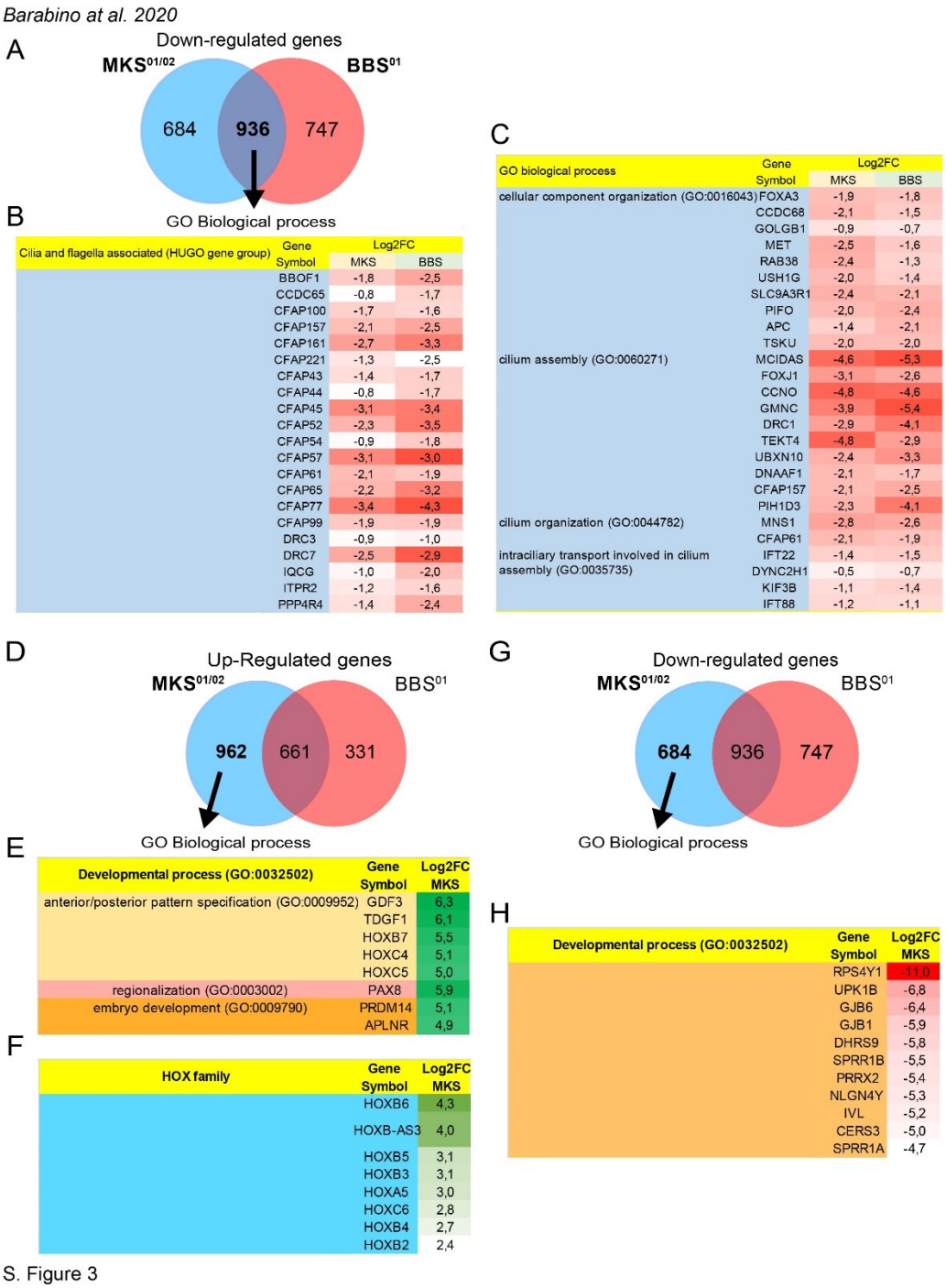

Figure S 3 Downregulation of genes responsible for cilia assembly, function and maintenance in BBS and MKS RSs and dysregulation of developmental genes in MKS RSs (Related to Figure 3)

(A) Venn diagrams showing the intersection of significant genes differentially downregulated in MKS$^{01/02}$ and BBS^{01} RSs (log2FC>2; P-value <0,05). (B-C) Some representative genes and the respective Log2FC (P-value <0,05) part of the cilia and flagella associated family (B), and other ciliary genes (C). The main GO group and subgroups are shown. Log2FC is also represented in a colorimetric scale from white (0) to red (-5,4). (D-H) Venn diagrams showing the intersection of significant genes differentially up-regulated (D) and down-regulated (G) between MKS$^{01/02}$ and BBS^{01} RSs. (E; F; H) Gene Ontology Enrichment analyses of MKS$^{01/02}$ specific differentially up-regulated (E-F) and down-regulated (H) genes. Selected GO group are shown. Some representative genes and the respective Log2FC (P-value <0,05) are indicated for each group. Log2FC is also represented in a colorimetric scale from white (0) to red (-11).

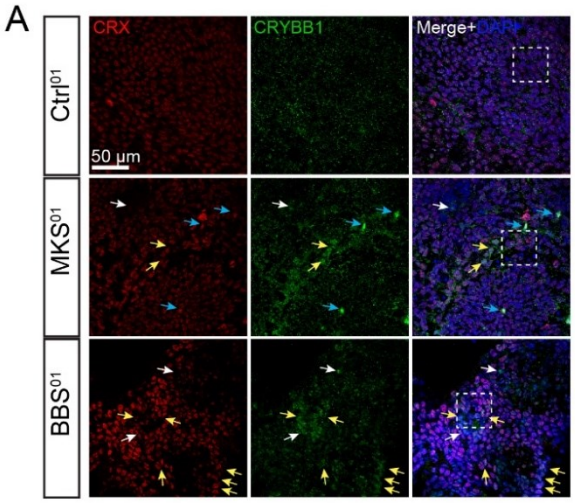

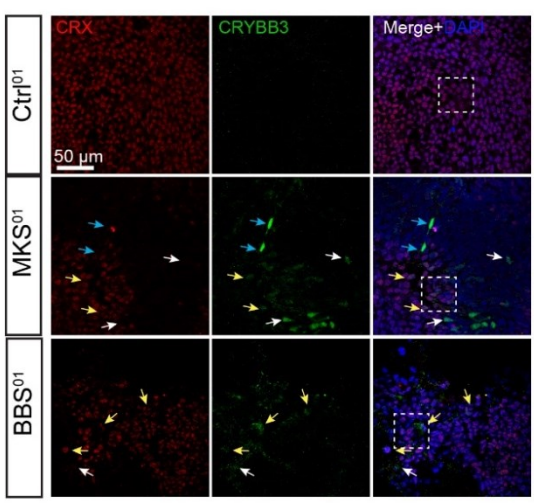

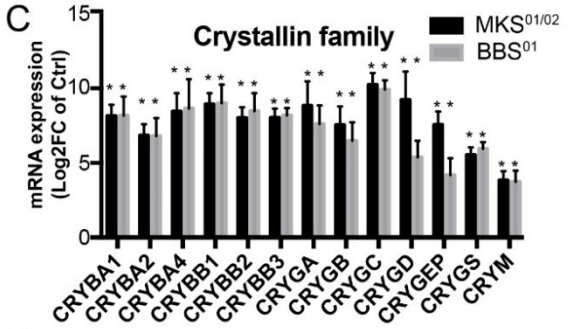

D

Apoptosis	Gene name	Log2FC MKS	Log2FC BBS
apoptotic process(GO:0006915)	ESPL1	2,1	2,7
	DIO3	3,9	2,2
	UNC5A	2,9	3,1
	TNFRSF9	4,9	2,8
	PTH2	7,3	8,7
	FGF8	4,9	3,4
	SFRP2	3,4	4,4
	CDCA7	3,2	2,7
	GADD45G	2,8	3,4
	UNC5C	2,2	2,8
	NSG1	2,8	2,8
positive regulation of neuron apoptotic process (GO:0043525)	PAK3	3,0	0,7
	JUN	2,0	1,4
	CDK5R1	2,4	2,0
	MYBL2	2,3	1,5
	RAPSN	2,3	1,9
	GRIK2	2,4	-0,4
positive regulation of neuron death (GO:1901216)	TLR4	4,8	-1,0
	GRIN2B	2,4	1,2
regulation of neuron apoptotic process (GO:0043523)	AGAP2	3,6	1,8
	MT3	3,0	0,5
	GRIN1	2,4	1,5
	FOXB1	2,0	-1,9
	NRP1	4,2	0,8
	ANGPT1	3,0	-2,8
	DRAXIN	3,2	1,8

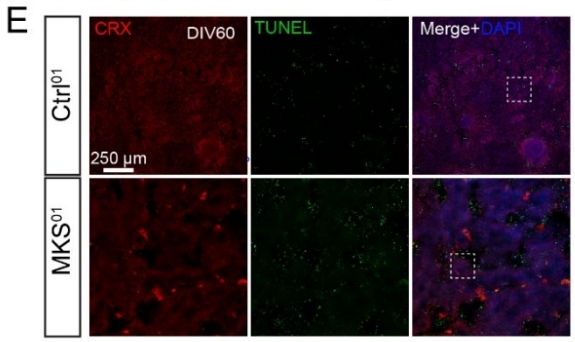

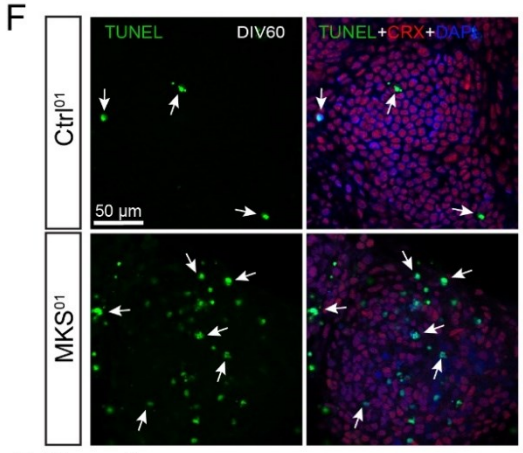

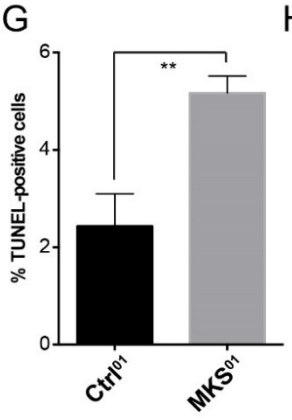

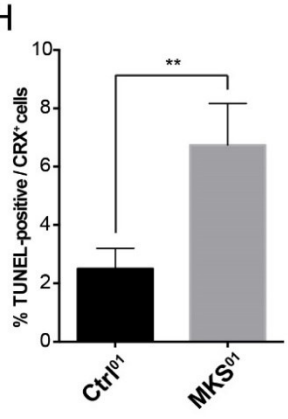

S. Figure 4

Figure S 4 Production of crystallin proteins and activation of apoptosis in MKS and BBS RSs (Related to Figure 4)

*(A; B; E) IF representative images used for quantification in figure 4 showing expression of CRX and CRYBB1 (A), CRYBB3 (B), at DIV45 and TUNNEL (E) at DIV60. Blue arrows, cells with strong nuclear expression of Crystallin proteins. Yellow arrows, CRX positive cells showing expression of Crystalline proteins. White arrows CRX negative cells with expression of Crystallin protein. Dotted square, a representative area used in high-resolution images in figure 4. (C) Gene expression levels of Crystallin family genes significantly upregulated in BBS01 and MKS01/02 RSs at DIV60. (D) GO group enriched in MKS01/02 and BBS01 RSs related to the apoptotic process. GO group names and some representative genes and the respective Log2FC. Non-significative Log2FC (P-value>0,05) are in red. (E, F) IF representative images in Ctrl01 and MKS01 dissociated PRs for CRX and TUNEL. (G, H) Quantification of the percentage of TUNEL-positive cells over total (G) or CRX+ (H) nuclei in Ctrl01 and MKS01 cells at DIV60 (n = 4 fields for condition, an average of 1057 cells for field). Scale bars: 50 µm (A, B, F), 250 µm (E). All values are means ± SEM. *p < 0.001, **p < 0.01, by Student's unpaired t-test.*

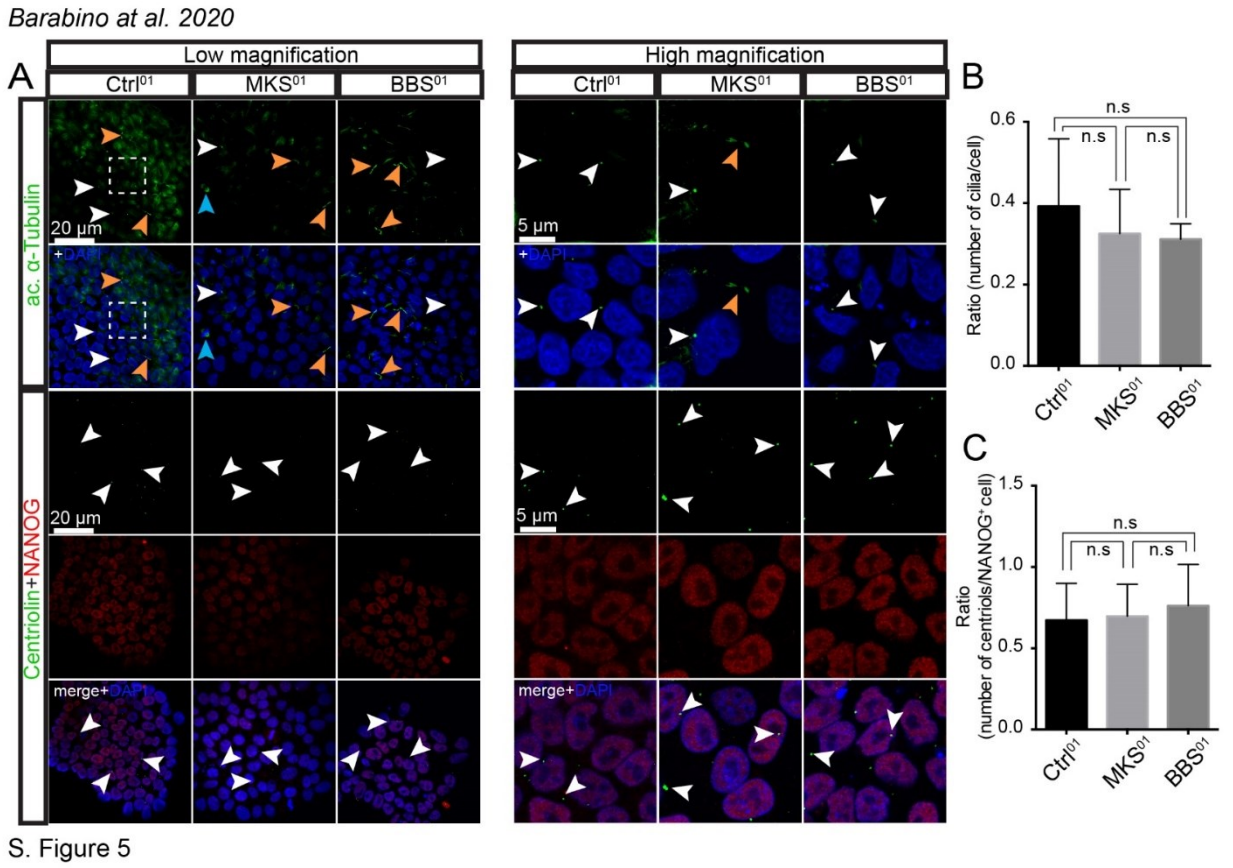

Figure S 5 Expression of Acetyl-α Tubulin and Centriolin in MKS and BBS undifferentiated iPSC (Related to Figure 5)

(A) Expression of Acetyl-α Tubulin, CNTRL, and pluripotency marker NANOG in Ctrl^{01}, MKS^{01} and BBS^{01} undifferentiated iPSC. (B-C) Quantification of the number of cilia (Acetyl α-Tubulin) per cells (B) and the number of centrioles (CNTRL) over NANOG positive cells per field (C) in Ctrl^{01}, MKS^{01} and BBS^{01} iPSC (n = 5 fields for a condition, an average of 12 cells for a field). Scale bars: 20 µm (A), 5 µm (A'). White arrowhead indicates cilia and centrioles. Orange arrows indicated midbody during cytokinesis that is not considered in the cilia quantifications. All values are means ± SEM., n.s. not significant, by Student's unpaired t-test.

Barabino et al 2020

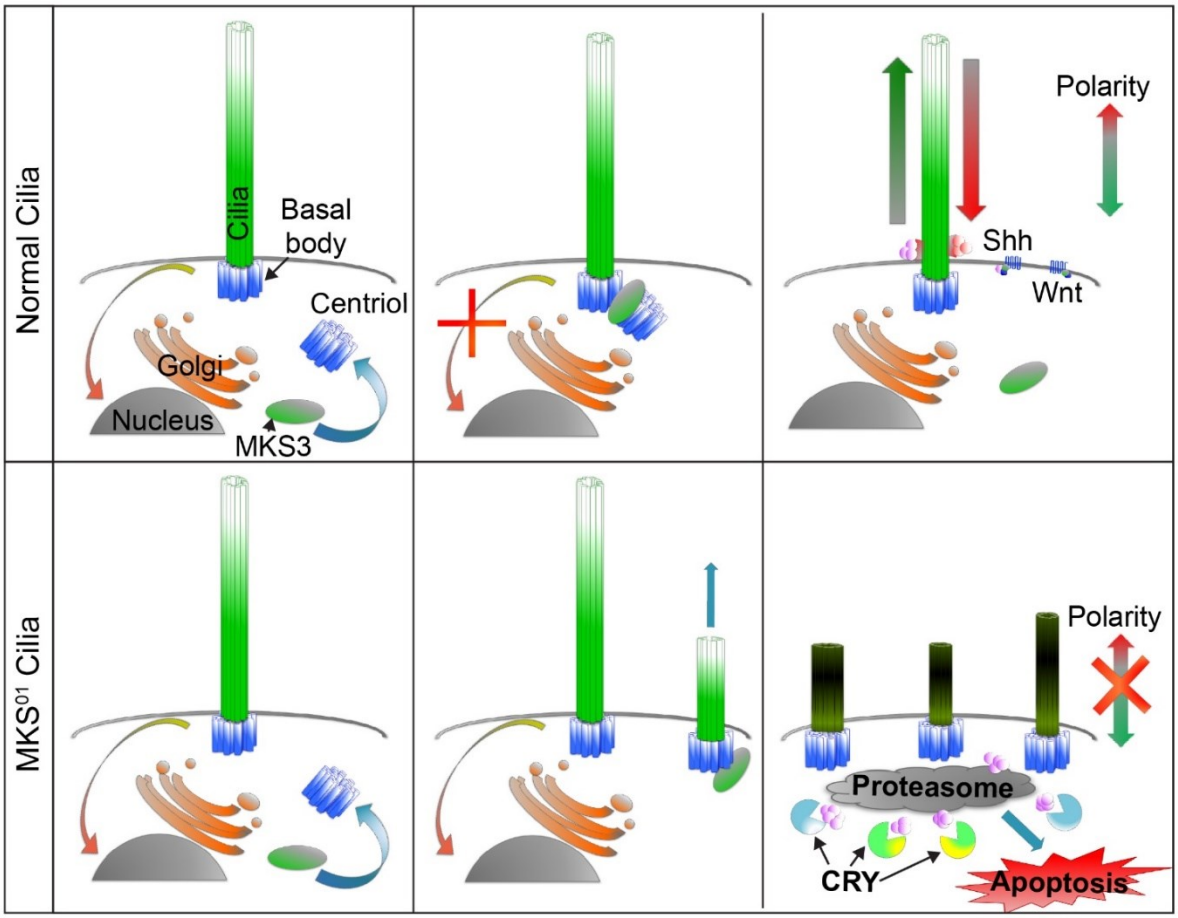

S. Figure 6

Figure S 6 Mutation in MKS3 protein causes the formation of small supernumerary cilia and aggregation of ciliary proteins (Related to Figures 5 and 6)

Graphic representation of the proposed model for the formation of supernumerary cilia in MKS^{01} photoreceptors.

Figure S 7 Activation of the mitotic checkpoint proteins and accumulation of DNA damage in BBS photoreceptor progenitors (Related to Figure 7)

(A; C) Venn diagrams showing the intersection of significant genes differentially up-regulated (A) and down-regulated (C) between MKS$^{01/02}$ and BBS^{01} RSs. (B; D) Gene Ontology Enrichment analyses of BBS^{01} specific differentially up-regulated (B) and down-regulated (D) genes. Selected GO group are shown. Some representative genes and the respective Log2FC (P-value <0,05) are indicated for each group. Log2FC is also represented in a colorimetric scale from white (0) to red (-6,3). (E) Expression of pCHK2 in Ctrl$^{01/04}$, MKS$^{01/02}$ and BBS$^{01/02.2}$ photoreceptor progenitors at DIV15. White arrows indicate positive cells. The percentage of positive cells (more than 3 foci per cell) for pCHK2 are indicated on the respective images (average n=159 cells for condition) Dotted squares represent representative area shown in upper images. Scale bar: 10 µm (Top); 50 µm (Bottom).

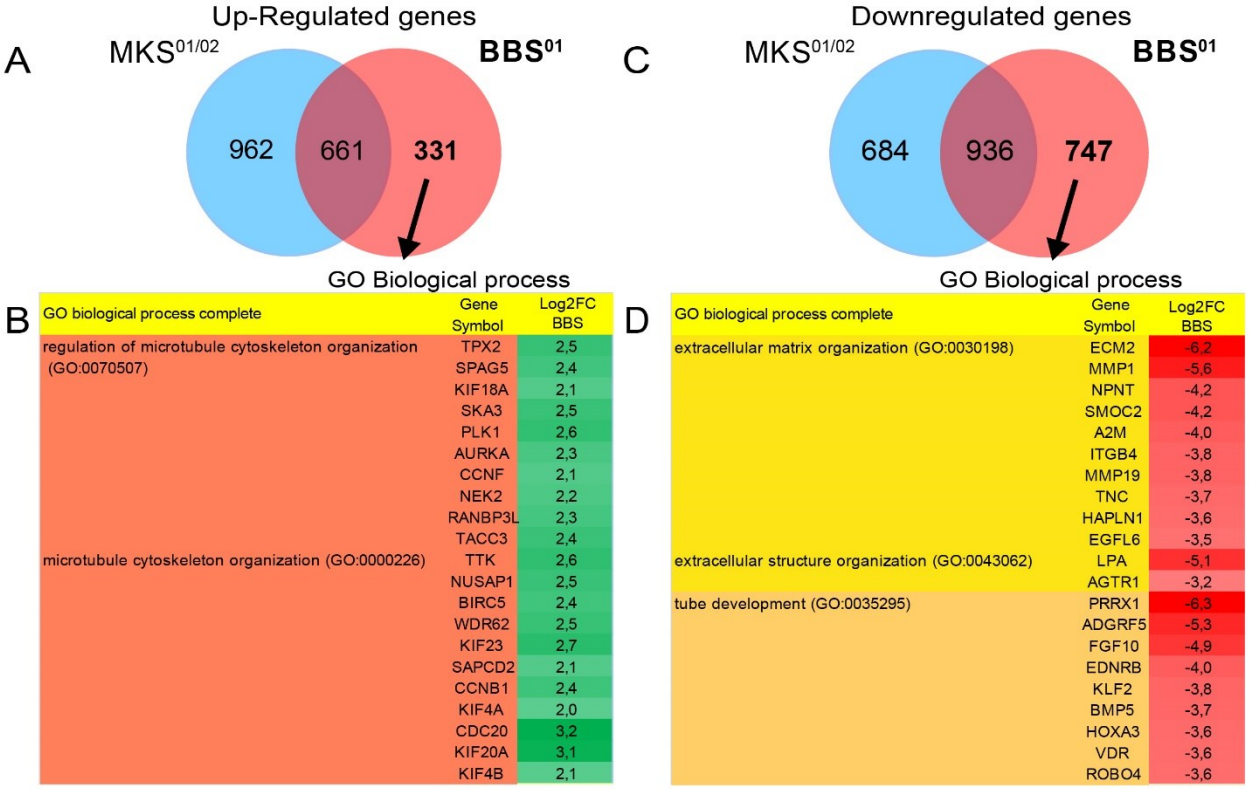
A
Up-Regulated genes
MKS01/02
BBS01
962
661
331
C
Downregulated genes
MKS01/02
BBS01
684
936
747
B
GO Biological process
GO biological process complete
Gene Symbol
Log2FC BBS
regulation of microtubule cytoskeleton organization (GO:0070507)
TPX2 2,5
SPAG5 2,4
KIF18A 2,1
SKA3 2,5
PLK1 2,6
AURKA 2,3
CCNF 2,1
NEK2 2,2
RANBP3L 2,3
TACC3 2,4
microtubule cytoskeleton organization (GO:0000226)
TTK 2,6
NUSAP1 2,5
BIRC5 2,4
WDR62 2,5
KIF23 2,7
SAPCD2 2,1
CCNB1 2,4
KIF4A 2,0
CDC20 3,2
KIF20A 3,1
KIF4B 2,1
D
GO Biological process
GO biological process complete
Gene Symbol
Log2FC BBS
extracellular matrix organization (GO:0030198)
ECM2 -6,2
MMP1 -5,6
NPNT -4,2
SMOC2 -4,2
A2M -4,0
ITGB4 -3,8
MMP19 -3,8
TNC -3,7
HAPLN1 -3,6
EGFL6 -3,5
extracellular structure organization (GO:0043062)
LPA -5,1
AGTR1 -3,2
tube development (GO:0035295)
PRRX1 -6,3
ADGRF5 -5,3
FGF10 -4,9
EDNRB -4,0
KLF2 -3,8
BMP5 -3,7
HOXA3 -3,6
VDR -3,6
ROBO4 -3,6

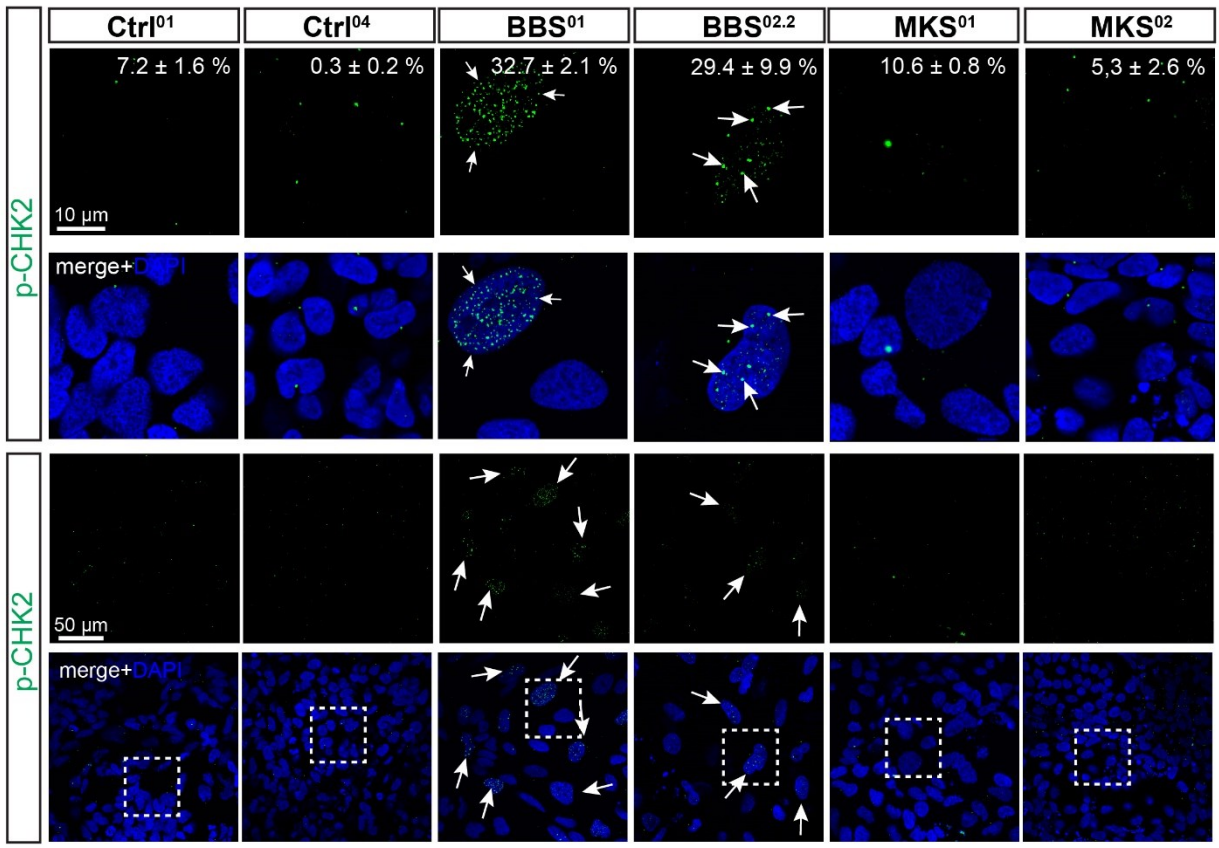
E
Ctrl01
Ctrl04
BBS01
BBS02.2
MKS01
MKS02
7.2 ± 1.6 %
0.3 ± 0.2 %
32.7 ± 2.1 %
29.4 ± 9.9 %
10.6 ± 0.8 %
5,3 ± 2.6 %
p-CHK2
10 µm
merge+DAPI
p-CHK2
50 µm
merge+DAPI

S. Figure 7

3.2.8 Contributions

A. Barabino and G. Bernier wrote the article.

A. Barabino did the cell culture and most of the experiments and analyses.

B. S. Freedman generated and characterized MKS and BBS iPSC lines and helped write the manuscript.

E. Héon helped identify the mutations through WGS and helped write the manuscript.

A. Flamier contributed to the bioinformatic analysis of the RNAseq and helped write the manuscript.

R. Hanna contributed to the bioinformatic analysis of the RNAseq and to the quantifications of ADN damage and helped write the manuscript.

4. DISCUSSION AND PERSPECTIVE

4.1 Discussion

Retinal degenerative diseases are a significant burden in modern society, and nowadays, there are no available therapies to slow down, stop, or reverse these diseases. The only exceptions are a limited number of clinical trials based on gene therapies using adenoviral vectors and RPE transplantation therapies using iPSCs. In 2021, more than 190 million people worldwide suffer from MDs without any treatment options, and it is expected to increase to 288 million by 2040. Importantly, these data exclude other forms of retina degenerations, such as LCA and RP, and other congenital, inherited retinal diseases (1161–1163).

Despite the great interest and capital invested in research and development in this domain, the large gaps in the comprehension of RDs and lack of available therapies reflect the complexity of the underlining molecular and physiopathological mechanisms, in addition to the inadequacy of the currently available models. Therefore, there is still a great need for eye and retinal cell sources for therapy and research applications.

Although extremely useful, animal models do not always reflect patients' defects. At best, they require further confirmation in human models, the lack of which causes a high risk of failure during the transition to human clinical trials or misinterpretation of research results.

As an alternative, hESCs and hiPSCs represent a theoretically unlimited source of retinal cells to be applied in disease modeling, drug screening, and regenerative therapies. iPSCs represent a very young and exponentially growing field with the potential to revolutionize various aspects of research and medicine (936).

4.1.1 Evaluation of Bmi1's Role in The Mouse Postnatal Retina

In the first part of this work, we investigate the role of BMI1 in the postnatal retina using a BMI1 KO mouse model. We observed that retinal cell development in KO mice occurs normally and found that BMI1 is mainly expressed in cones PRs and bipolar cell subsets in the adult mouse retina. Therefore, we have observed that both cone PRs and some subclasses of bipolar cells begin

to degenerate postnatally starting at day 10 and rapidly decrease in number by day 30. We have not looked further than day 30 since Bmi1 KO mice rarely survive beyond one month (Figure 1, 2 Chapter 3.1).

BMI1 contributes to stem cell pluripotency and oncogenesis via multiple functions. It is expressed at high levels in various types of cancer such as carcinomas, prostate cancer, glioblastoma, where its presence is often associated with a negative prognosis. It has also been implicated in regulating several varieties of somatic stem cells (573,1164–1166). BMI1 is also expressed at high levels in particular adult tissues, such as heart tissue and the nervous system. BMI1 regulates self-renewal, proliferation, and survival of cancer-initiating cells in different ways, but its main mechanism is the epigenetic repression of the CDKN2A tumor suppressor locus, which encodes the tumor suppressor genes $p16^{INK4A}$ and $p14^{ARF}$. More recently, the implication of BMI1 in the DNA damage response has been revealed, and it mostly relies on the ubiquitination of H2A and H2Ax at the damage site, promoting the repair of DSBs. Numerous BMI1 suppression and overexpression experiments have shown contrasting outcomes in different cell types. Therefore, BMI1's role can vary in different tissues and upon different stimuli. BMI1 can have different and independent functions even in the same cell, making the interpretation of its role in different situations challenging. For these reasons, the role of BMI1 must be carefully evaluated case by case.

We hypothesized that its role as a gene suppressor could mediate the effect of BMI1 on photoreceptors' survival. In its absence, ectopic gene expression could disrupt the postnatal maturation or maintenance of PRs and bipolar cells.

Another hypothesis is that its role in the survival of adult photoreceptors is linked to its function in response to DNA damage. Since the photoreceptors are long-living cells and are particularly exposed to oxidative stress, it is legitimate to think that these cells require an additional defense mechanism against DSBs and other forms of DNA damage. BMI activity in response to DNA damage is mainly linked to the activation of the CDKN2A locus, which encodes for $p16^{INK4A}$ and $p14^{ARF}$. These proteins activate downstream targets such as p53, p21, and Chk2, which play a critical role in the cell cycle progression, differentiation, senescence, and apoptosis. In our study, none of the double mutants mice $Bm1^{-/-}/p53^{-/-}$, $Bm1^{-/-}/Chk^{-/-}$, or $Bm1^{-/-}/p16^{-/-}/p19^{-/-}$

showed complete rescue of PRs degeneration (Figures 6, 7 Chapter 3.1). Therefore the role of BMI1 in adult cone PRs is only partially linked to its traditional role as an inhibitor of the CDKN2A locus.

Since we have observed a dose-response effect in heterozygous mice, which have a lifespan similar to WT mice, further long-term studies in heterozygous mice could distinguish between disparate roles of Bmi1during postnatal maturation versus its functions in PRs maintenance during aging.

We also observed that Bmi1 KO PRs degenerate primarily through necroptosis, a relatively new cell death mechanism whose primary components are Ripk1, Ripk3, and Mlkl (Figure 5 Chapter 3.1). Necroptosis seems confined to certain types of tissue that express Ripk3/Mlkl. In order to trigger apoptosis, caspase-8 blocks the necroptosis pathway by cleaving Ripk1 and Cyld (613,1167). It has been reported that retinal degeneration in different contexts can follow alternative pathways such as apoptosis, necroptosis, autophagy, pyrocytosis, and caspase-independent apoptosis (614). Autophagy, initially regarded as a suicidal mechanism, is a crucial cytoprotective system (670). It is rapidly activated after multiple stimuli and participates in the crosstalk between various cell demise modes (1168).

It has recently been shown that BMI1 can control autophagy in human cells (305,1169). Autophagy is an intracellular pathway where cytoplasmic constituents are delivered to the lysosomal pathway for degradation. It is not only a major pathway activated in response to cellular stress but is also essential for cytoplasmic turnover and to supply the structural and energy needs of cells (613).

Loss of autophagy led to progressive degeneration of rod photoreceptors demonstrating that basal autophagy is essential to the long-term health of rod photoreceptors and is a critical process for maintaining optimal levels of phototransduction proteins (691).

Recently BMI1 has also been shown to prevent the autophagic process in chronic myeloid leukemia (CML) cell lines, contributing to their clonogenic activity and proliferation. CCNG2/cyclin G2 has been identified as a direct BMI1 target responsible for activating the autophagic process (1170). Similarly, another group found that ovarian cancer cells deprived of BMI1 reduce their

proliferative capacity and induce autophagy. However, it was not mediated by CDKN2A / INK4 / ARF or CCNG activity in this context but rather through ATM depletion. Furthermore, they showed that targeting BMI1 engages the PINK1-PARK2-dependent mitochondrial pathway, which stimulates necroptosis-mediated cell death by activating RIPK1, RIPK3, and MLKL. Importantly, inhibition of autophagy or RIPK3 by genetic manipulation or pharmacological treatment rescues clonal growth in BMI1 depleted cells (1170). These observations reveal how BMI1 can take on distinct and well-defined roles in different types of cells.

However, the precise mechanism that links necroptosis and autophagy remains still unclear. Recently, it has been shown that autophagy can serve as a scaffold for the formation of the necrosome complex, which leads to Rip3 activation and Mlkl phosphorylation to cause cell necroptosis. However, autophagy may still promote caspase-dependent apoptosis when Rip3 expression is lacking (687,1169).

It seems that these pathways are linked together in a finely regulated process and do not act independently. We have observed a major necroptotic component and also activation of P53-dependent apoptosis in our Bmi1 KO model (Figures 6, 7 Chapter 3.1).

Ultimately, it seems legitimate to assume that combinatorial effects between these pathways determine the degeneration severity. It would be interesting to inhibit the different pathways, individually and in combination, to investigate their importance in more detail. The inhibition of necroptosis via small molecules such as Necrostatin (Nec-1), which blocks the activity of RIPK1, or using RNA-interference, could bring additional information on its importance in the degenerative process (649,653). Also, Rapamycin has been shown to inhibit necroptosis by an unknown mechanism. After induced retinal detachment, the treatment with caspase inhibitor z-vad-fmk (a pan-caspase inhibitor) could inhibit apoptosis but cause increased Ripk3 mediated necroptosis. Adding Rapamycin to the regimen allows inhibiting z-vad-fmk-induced necroptosis by inhibiting RIP-1 expression but finally promotes autophagy activation (664).

Inhibition of Ripk3 mediated apoptosis alone may cause a shift towards apoptosis and other types of cell death. The combined inhibition of multiple pathways such as Necrostatin plus Pifithrin (p53

inhibitor) or Chk2 inhibition could represent a potential treatment strategy to slow or prevent PRs degeneration.

4.1.2 Modeling BMI1 Inhibition in Photoreceptors Derived From Human Embryonic Stem Cells

The anatomical structure of the human and mouse retina are not identical, and the nature and structure of the PRs also vary; for example, the calyceal processes surround the CC and base of the OS and are absent in mouse PRs. Furthermore, mouse retinas possess dual PRs expressing both S-Opsin and M-Opsin absent in humans (Figure 3 Chapter 1). To investigate the role of BMI1 in adult human PRs, we first investigated its localization using postmortem human retinas. As observed in mice, we have confirmed a punctuate immunostaining that colocalizes with H3K9me3+ heterochromatin in both S and M cones PRs, and in some cells of the INL (Figure 8 Chapter 3.1). To overcome the limits of experimentation on human tissues and study the role of BMI1 during the development of human cones, we used our previously developed protocol with minor improvements. This protocol is mainly based on COCO recombinant protein activity that can inhibit all BMP, TGFb, and WNT signaling pathways. With this protocol, in 3 weeks, we can generate cultures consisting of around 70% of cones precursors. These cells express cone markers as CRX, cone arrestin, S-opsin, and ABCA4 (1007).

During the first ten days of differentiation, when cells start expressing early PR progenitor markers RAX and CHX10, we infected them with a lentivirus expressing an shRNA against BMI1, selected cells by hygromycin treatment then continued the differentiation until day 21. To evaluate the role of p53 activation in the context of BMI1 deficiency in human PRs, we used an antibody against p53 that also recognizes other family members, and we observed the induction of p53 and p63, while p73 was lost together with the PRs marker CRX (Figure 9 Chapter 3.1).

As in human post-mortem samples, also in hESC derived PRs precursors BMI1 colocalized with H3K27me3 and H3K9me3, suggesting distribution at both facultative and constitutive heterochromatin. As we observed in mice, we found an increase in H3K9 acetylation, accompanied by reduced H3K27 and H3K9 trimethylation and a notable induction of repetitive sequences of the genome, thus suggesting a reduction of heterochromatin compaction with

genomic instability as indicated by γH2Ax staining. Chromatin regulation abnormalities, observed in many diseases, lead to epigenetic gene regulation defects resulting in pathological gene expression programs (1171). Since one primary proposed function of the PRC complex in hESC is to prevent differentiation by repressing lineage-specific homeobox genes such as PAX, SOX, and LHX families, we looked at these genes' expression. SOX1, SOX2, and PAX6 were all increased, thus providing a possible explanation for the defective terminal differentiation of cones upon knockdown of BMI1 (Figure 9 Chapter 3.1).

These findings revealed new and partly conserved biological functions for Bmi1 in cone PRs development and survival between mouse and human. On the other hand, our system failed to observe RIP3K expression and activation of necroptosis. These differences may arise from interspecies differences but are more likely due to the *in vitro* system's limitations.

In vivo, cell death's fate is decided by a complex interaction of different autocrine, paracrine, and endocrine signaling and physical stimuli. *In vitro* systems lack many of these, probably causing a drift towards the predominant p53 dependent apoptotic process. Longer differentiation times reaching higher maturation levels, or the use of more complex systems such as 3D organoids containing a more varied cell population, could better reproduce these processes.

Furthermore, further studies are needed to fully understand BMI1 function in the retina, which seems to vary depending on the context.

It is interesting to note how the effect of BMI1 KO in mice causes postnatal death of cones, while in the context of Rd1 mice, knocking out Bmi1 significantly reduces and delays rod degeneration (2). Similar effects have been reported in other studies; inhibition of H3K27 trimethylation using DZNep has opposite effects on WT retinal progenitors and postnatal Rd1 PRs (3). Furthermore, silencing Ezh1/2 in MSNs and Purkinje cells causes progressive degeneration in WT mice while inhibiting Ezh2 in Atm $^{-/-}$ mice rescued Purkinje cell degeneration (4,5). Although their differential roles in various contexts remain somewhat elusive, it appears that polycomb proteins such Bmi1 and Ezh2 are essential for the generation and survival of newborn PRs and have a role during neurodegeneration in pathological contexts. The regulation of chromatin compaction seems highly related to the survival of PRs and other neurons.

Regulation of chromatin is essential for maintaining cell identity and function. Aberrant chromatin regulation is observed in many diseases, leading to defects in epigenetic gene regulation resulting in pathological gene expression programs. Chromatin deregulation often results in neurodevelopmental disorders and intellectual disabilities, frequently linked to physical and developmental abnormalities, but can also cause neurodegenerative diseases such as Parkinson's, Alzheimer's, Huntington's, Fragile X syndrome, or muscle wasting syndromes such as ALS (608,1171–1173). Acting on chromatin compaction can represent a potential new therapeutic strategy in some cases of RDs.

Little is known about the expression of BMI1 in human PRs in the context of late-onset retinal degeneration. Since BMI1 has been observed to have a neuroprotective role in cortical neurons, similar to what we observed in the retina, and its inhibition is sufficient to cause a phenotype that recapitulates Alzheimer's disease, acting on BMI1 could have a therapeutic potential to prevent degeneration in the context of late-onset RDs. While BMI1 overexpression is associated with some forms of cancer, no human disease is currently linked to mutations in BMI1. This is probably related to its essential role during development, which makes offspring with mutations in this gene inviable. On the other hand, epigenetic adjustments during aging can cause variability in its expression, thus taking part in the degenerative process. Small molecules able to modulate BMI1's expression and stability have recently been identified. It will be interesting to evaluate BMI1 activators and stabilizers' pharmacological potential in preventing PRs cell death, particularly in the context of late-onset RDs.

Chromatin compaction anomalies, activation of tandem repeats, and splicing defects have recently been associated with G4 structure formation in various in vitro cell culture models upon BMI1 repression, including human fibroblast iPSC-derived cortical neurons (1174). G4s are an alternative tertiary structure of DNA or RNA that seems to stall transcription, inducing gene repression, alternative splicing, and causing DNA instability. It is legitimate to think that this process could also be valid in the context of RDs and could represent an interesting research path to follow.

This work shows the potential of stem cell-based *in vitro* systems to study PRs degeneration and highlights some of their limitations. As powerful as these *in vitro* systems are, they cannot completely replace animal models, but they could significantly reduce their use. Humanized PSC-based models greatly expand the potential of *in vitro* modeling, and in combination with the more commonly used animal models, they represent a powerful tool for studying allelic variants or the effect of specific human mutations.

4.1.3 Modeling human inherited retinal disease using patient-specific induced pluripotent stem cells

Ciliopathies are a heterogeneous group of genetic diseases affecting primary cilium structure and function. They can be syndromic or non-syndromic and are characterized by developmental and morphogenetic abnormalities and a degenerative component. BBS and MKS are two syndromic ciliopathies involving the retina, among other tissues and organs. While MKS is embryonically lethal, BBS is one of the most severe ciliopathies compatible with life. In principle, MKS and BBS were considered two distinct clinical entities, but the identification of hypomorphic mutations in MKS1 and TMEM67 in some BBS patients introduced the concept that BBS may represent a "milder" form of MKS.

PRs possess a unique intracellular cilium, the CC, which originates from the centriolar structure called BB. It connects the OS, where phototransduction takes place, to the IS. The MKS complex and BBSome are two essential complexes associated with the BB and are necessary for the proper functioning of cilia

We first reported iPSCs generation from two patients with BBS and two cases with MKS, along with four healthy donors (Figure 2 Chapter 3.2). While there are only four previous reports of iPSC generation from BBS patients, three from the same group, for a total of 8 iPSC lines, none use these lines to investigate the retina's physiology (1175–1178). Furthermore, this is the first report, to our knowledge, of iPSCs generation from an MKS case. These numbers reflect the incidence of the two syndromes. The greater interest for BBS is justified as it is a viable but incurable disease that needs therapeutic options. On the other hand, the MKS complex has a central role in ciliogenesis and cilia maintenance, and the same genes mutated in MKS are responsible for viable

diseases, such as JSRD and BBS (Figure 22 Chapter 1). Studying these extreme cases, such as MKS, can help us better understand the functions of ciliary components, which is a key factor in developing more effective therapies.

We identified the causative mutations via WGS in both BBS patients and one of the two patients with MKS (Figure S1 Annex 3). Despite the incredible power of WGS techniques, we have not been able to find significant hits in one of the patients. The integration of healthy donors from the patient's close relatives could be a good way to help the identification of causative mutations in similar cases. Another possible strategy to overcome the unavailability of related controls is screening the potential hits obtained by WGS using the CRISPR-Cas9 system. Even if feasible, it currently remains a relatively inaccessible strategy for many laboratories, considering the resources necessary for generating multiple iPSC lines with single point mutations and the costs related to their CQ. On the other hand, the technologies and raw materials necessary for these applications become more accessible every year, allowing soon even wider access to this type of strategy, including academic laboratories with limited personnel and resources.

We then generated retinal sheets (RS) from BBS, MKS, and controls cell lines. We show, by both IF and TEM, the expression of mature markers (S-Opsin, CRX), polarization and onset of CC formation (RPGR and alpha-acetyl tubulin), as well as OS (PNA-S-Opsin) formation (Figures 1A, 4D Chapter 3.2). We have observed that these cells can generate fully mature PRs with elongated OS in around 150 days of differentiation (Figure 1 Chapter 4).

Transcriptome profiling of MKS and BBS retinal sheets allowed us to find common alterations in numerous genes related to ciliogenesis and ciliary components. We found alterations in the expression of hundreds of developmental genes, including several *HOX* genes as well as components of the WNT, NOTCH, and BMP signaling pathways (Figure S2, S3 Annex 3). Both diseases were also characterized by the accumulation of molecular chaperones from the crystallin family, suggesting a response to misfolded proteins and proteasome dysfunctions (Figure 4 Chapter 3.2).

To confirm degeneration in MKS and BBS RSs, we performed a TUNEL assay in both BBS and MKS PRs precursors. Using TEM, we showed that degeneration was still present in postmitotic PRs at

day 60 of differentiation. Moreover, we could also distinguish between necrotic and apoptotic cell death using TEM. Although there was both a necrotic and an apoptotic component in either disease, the former was predominant in MKS, while the latter was more prominent in the BBS RSs, thus highlighting the differences in the degenerative process between the two pathologies (Figure 4 Chapter 3.2; Figure S4 Annex 3).

Furthermore, we described unique characteristics and specific phenotypes of each syndrome.

Using antibodies against Centriolin and MKS3, we performed confocal immunofluorescence imaging and 3D reconstruction on control PRs to see the interplay between these two proteins. We observed three different configurations between Centriolin and MKS3. Notably, MKS3 was often found in close association with Centriolin in control and BBS PRs. This association was near absent in MKS, suggesting a defective interaction of MKS3 with the centriole in MKS PRs, possibly leading to the production of supernumerary centrioles (Figure 5 Chapter 3.2). We found that supernumerary centrioles in MKS PRs were also associated with an increasing number of cilia (Figure 6 Chapter 3.2). Using quantitative analyses of the 3D images, we observed that although more abundant, cilia in MKS PRs were shorter and thinner than normal. MKS RSs were disorganized, as revealed by the unequal distribution of PNA, and the signal for RPGR, which is frequently mutated in RDs, was mislocalized and tended to accumulate in aggregates (Figure 6 Chapter 3.2). We think that the lack of interaction between MKS and Centriolin could cause abnormal migration of the daughter centriole to the BB, which would cause supernumerary cilia to form. Lack of maintenance can cause dysfunction of the primary cilium with consequent mislocalization of ciliary and OS components, leading to PRs' degeneration (Figure S6 Annex 3).

Ciliogenesis and the cell cycle are intimately related, and the mechanisms of how these two phenomena are linked to each other have attracted considerable attention. Several cyclins, cyclin-dependent kinases, centrosomal protein (CEP family), molecular motors (myosin, kinesin (KIF family), and dynein), proteins of the intraflagellar transport (IFT family) machinery, and other related proteins were shown to play a central role in the regulation of these processes.

We found upregulation of many cell-cycle-related genes, such as cyclins and proteins contributing to centrosomes duplication during mitosis. These data suggest that basal bodies and

supernumerary cilia could also derive from mitotic abnormalities, failure in the cytokinesis, or centrosome overduplication. In our RNAseq results PKL1, PKL4, SASS6, and ESPL1 were all significantly upregulated in MKS. Although there are no known functions of MKS3 in the biogenesis and duplication of centrosomes, MKS3, like many other ciliary proteins, will likely adopt new functions during the cell cycle independent of those used during ciliogenesis.

It has been shown that overactivation or overexpression of Plk4 kinase can lead to the simultaneous formation of multiple centrioles around a single parent. This suggests that Plk4 overexpression creates multiple sites on "duplication-competent" parental centrioles (154). Similarly, overexpression of the centriole duplication protein SASS6 also induces the generation of extra centrioles (153).

Although anomalies in centrosome duplication could underlie the multiciliary phenotype observed in MKS, we have not observed extra cilia or centrosomes in cultured iPSCs, which are fast proliferating cells. Nevertheless, it is possible that these events are limited to a precise moment during cell differentiation or development and limited to a specific type of cell. The participation of mitotic anomalies with centrosome overduplication in retinal progenitors must be taken into consideration as a possible explanation for the presence of multiple cilia in MKS photoreceptors and merit further investigations

Although the precise molecular role of MKS remains unclear, these data bring new insights into its roles and functions, which largely remain unknown.

Interestingly in the MKS case harboring *TMEM67* mutations, the two identified heterozygous mutations were predicted to generate a pathogenic but full-length variant of MKS3. Hence, we could observe by immunoblot the presence of MKS3 in all RSs, and MKS3 levels were even slightly increased in MKS^{01} RSs (Figure 5 Chapter 3.2).

These results suggest abnormal retinal tissue morphogenesis, mislocalization, and aggregation of ciliary proteins in MKS PRs.

In BBS, we found mitotic spindle checkpoint activation, accumulation of DNA damage, and genomic instability. We notice an increase in DNA damage-response markers, γH2Ax and 53BP1,

and the mitotic checkpoint protein, p-CHK2, in PR progenitors at DIV15. Genomic abnormalities were present in both MKS and BBS RSs. However, they were more abundant in BBS. These included very large nuclei positive for gH2Ax and p-CHK2 that suggest possible arrest in the G2/M. Other abnormalities involve micronuclei, nuclear bridges, mitotic catastrophe, and nuclei having multipolar or monopolar spindles (Figure Chapter 3.2).

Control of centrosome number is essential for the fidelity of mitosis and maintenance of euploidy. Deregulation of centrosome numbers has long been proposed to contribute to genome instability and tumor formation, whereas mutations in centrosomal proteins have recently been genetically linked to microcephaly and other human diseases (131,1179). Contrary to MKS, BBS differentiated retinal cells did not show supernumerary cilia. Instead, they exhibit defects in the mitotic spindle, chromosomal aberrations with an accumulation of DNA damage, and a high frequency of tetrapolar/multipolar spindle and mitotic catastrophes, which are frequently due to aberrant centrosome duplication. In support of this hypothesis, we found numerous upregulated genes involved in mitotic spindle control and centrosome duplication, including several cyclins family members implicated in these processes, such as CCNA1, CCNA2, and essential kinases such as CDK1, CDKN1A/P21, CDKN2C, and CDKN2D.

Although many of these genes were overexpressed in both BBS and MKS, many were unique or more affected in BBS. For example, PKL1 was expressed only 2 -fold in MKS compare to controls, while BBS had an expression more than 6-fold higher. PLK1 and CDK1 function both as regulators of centrosome activity and in their maintenance (150,151).

Loss of centrosome integrity induces G1 — S arrest dependent on p38, p53, and p21 by a specific checkpoint that monitors the centrosome's functional integrity (1180). Accordingly, we observe induced apoptosis and activation of direct P53 targets, such as CDKN1A/P21. This effect can be a direct consequence of defects in centrosome maintenance and biogenesis. Otherwise, supernumerary centrosomes can contribute to the formation of multipolar spindles and thus to defective chromosome segregation.

We found upregulation of different centromere proteins such as CENPA, CENPE, CENPM, CENPF, INCENP, CENPK, CENPO, CENPV, INCENP, MKLP1 / KIF23, and PRC1. These proteins act at the

central spindle and midbody, where they have a central role in cytokinesis (489). All these genes have a dual role in mitotic spindle regulation and cilia biogenesis and were upregulated in our analysis—their overexpression support stalling of the cells in the G2 phase.

Interestingly, other proteins responsible for regulating centrosome replication in multiciliated cells, such as CCNO, Geminin (GMNC), MCIDAS, and DRC1, were expressed in control retinal sheets while highly downregulated in both MKS and BBS.

These observations suggest specific genomic instability in BBS PRs progenitors and a possible new role of BBS10 during mitosis.

To our knowledge, this is the first time that BBS10 is implicated in the mitotic process and thus merit further study. In normal cells, cilia are dynamically regulated during cell cycle progression. Cilia are present during G0 and G1 and are resorbed before mitotic entry to be reassembled after cytokinesis. It is logical to think that in a system as energetically efficient as the cell, some ciliary components, when not in use, are recycled during the mitotic process. Just as BB is converted into the centrosome, other ciliary components such as AURKA also play a different role during mitosis (1181,1182).

Although the concept is not new, we provide for the first time evidence of a new extra-ciliary role of BBS10 during cell division.

Interestingly, unlike all other known BBS proteins, including BBS6, another putative chaperonin, BBS10 is restricted to vertebrates. Within vertebrates, BBS10 is the fastest evolving BBS protein. In the BBS patients we analyzed, we found mutations in *BBS10* predicted to be damaging, which other groups had previously identified. While these are likely to be the underlying mutations, no molecular proof has ever been reported. All mutations found in the *BBS10* genes, the homozygous (*c.271dup*) in the first patient and the compound heterozygous (*c.909_912del; c.687del*) in the second one, are predicted to generate a premature stop codon and truncated transcripts (Figures S1E-G Annex 3). The *c271dup* variant has been reported in multiple affected homozygous and compound heterozygous individuals and has been classified as pathogenic by multiple clinical diagnostic laboratories. This pathogenic variant is predicted to cause the loss of normal protein function through protein truncation, as the last 633 amino acids of the BBS10 protein are lost and

replaced with four incorrect amino acids. The *c.909_912del* and *c.687del* mutations generate premature translational stop signals, p.Ser303Argfs*3 in the first and p.Val230Phefs*7 in the second case, which are not anticipated to result in nonsense-mediated decay. However, they are expected to disrupt the last 421 amino and 494 amino acids of the BBS10 protein, respectively. While some mutations in BBS10 seem to affect its ability to bind ATP and fold substrates, mutations in these regions have been shown to cause decreases in BBS10's interactions with BBS7, BBS9, and BBS12, indicating that these protein regions may be required for overall protein conformation. However, there are no supporting results about the actual state of these mutated proteins (220). It would be of greater interest to investigate how the protein structure and state vary in relation to the various mutations to define better the specific functions of the different portions of BBS10. It would also be interesting to investigate how these interfere with the interactions with other BBS proteins.

Furthermore, recent genetic studies argue that most of the patients with a *BBS10* mutation had potentially damaging mutations in other BBS-related loci, most of which are missense variants (26) and could presumably take part in the onset and severity of the disease (433).

Similarly, we found other variants in BBS-associated genes, such as *BBS1*, which could impact the disease, but based on bioinformatics analysis, they were inconclusive or not likely to be damaging. They would therefore require further investigation.

Although we managed to identify MKS3 by both WB and IF, we could not find any antibody that properly identified BBS10, causing limitations in our study. Identification of an antibody that specifically targets BBS10 is imperative for additional investigations.

A BBS10-specific antibody could provide new insight into the mutations' effect at the protein's transcriptional level, such as molecular weight and localization in physiological and pathological conditions. Furthermore, co-immunoprecipitation experiments would allow us to identify its interactors and variations in its complex's stability and composition during disease. BBS10 does not seem to be an integral part of the BBSome but rather interacts with it, and its precise mode of action remains relatively obscure.

A limitation of our study is that, aside from the RNAseq, which was performed on day 60, the rest of the experiments to study mitotic spindle defects were conducted before day 20 of differentiation, when the cultures' predominant population are the proliferative PRs' progenitors. Even at day 60, although most of the cells are postmitotic PRs and express markers of CC and OS, they do not correspond to a level of maturation comparable to that in patients. Although our data offer important insights into the role of BBS10 in the retina and, more precisely, in RPCs and immature PRs, further studies are needed to confirm its role in adult PRs. Longer differentiation times, exceeding 150 days, when PRs have fully matured and shown the formation of an elongated IS and OS similar to those seen in mature patient retinas (Figure 1 Chapter 4). This could offer us a better insight into the molecular mechanism behind the degeneration in adult individuals.

On the other hand, our study reveals that BBS has a strong developmental component, and probably, cones degeneration, which occurs early during childhood, is an effect of anomalies that occurred earlier during the development. Our findings point out that early intervention could delay, if not prevent, blindness in these patients. Differentiating the role of BBS10 during development and later in mature PRs is required to fully understand the degeneration mechanism and find the right therapeutic strategy. With this purpose, an iPSC line with an integrated inducible CRISPR-Cas9 system would permit to inactivate BBS10 efficiently and rapidly at different stages of the differentiation process.

The association of KO mice models for BBS10 could represent an excellent adjunct to confirm our results *in vivo* and more mature cells (Figure 4 Chapter 4) (1183).

This study reveals new biological and molecular information in the development and degenerative process associated with human ciliopathies. Moreover, this work provides a proof of principle that retinal sheets generated from patient-specific iPSCs can effectively summarize defects observed in patients, thus representing an exceptional tool for investigating molecular mechanisms directly in human cells, otherwise difficult to access. The same methodology could be applied to other RDs affecting cones such as Stargardt disease and other MDs. The association

of WGS and gene-editing techniques, iPSC technology, and retinal differentiation methods creates a unique opportunity to build platforms for disease modeling and drug screening.

4.1.4 Characterization of retinal sheets

In this thesis, apart from modeling RDs, we present a deep characterization of retinal sheets using protein analysis, high-resolution confocal microscopy, 3D z-stack reconstructions, and transcriptomic analyses (Figure 1 Chapter 3.2).

We show that by day 60, large portions of the cultures form a uniform 3D tissue-like sheet composed of 4-8 layers of CRX positive nuclei, showing apical polarization of CC and OS proteins and initiation of OS membrane formation (PNA labeling).

If these cells are grown in long-term suspension cultures, the PRs develop elongated CC and OS comparable to those seen in the adult human retina (Figure 1 Chapter 4).

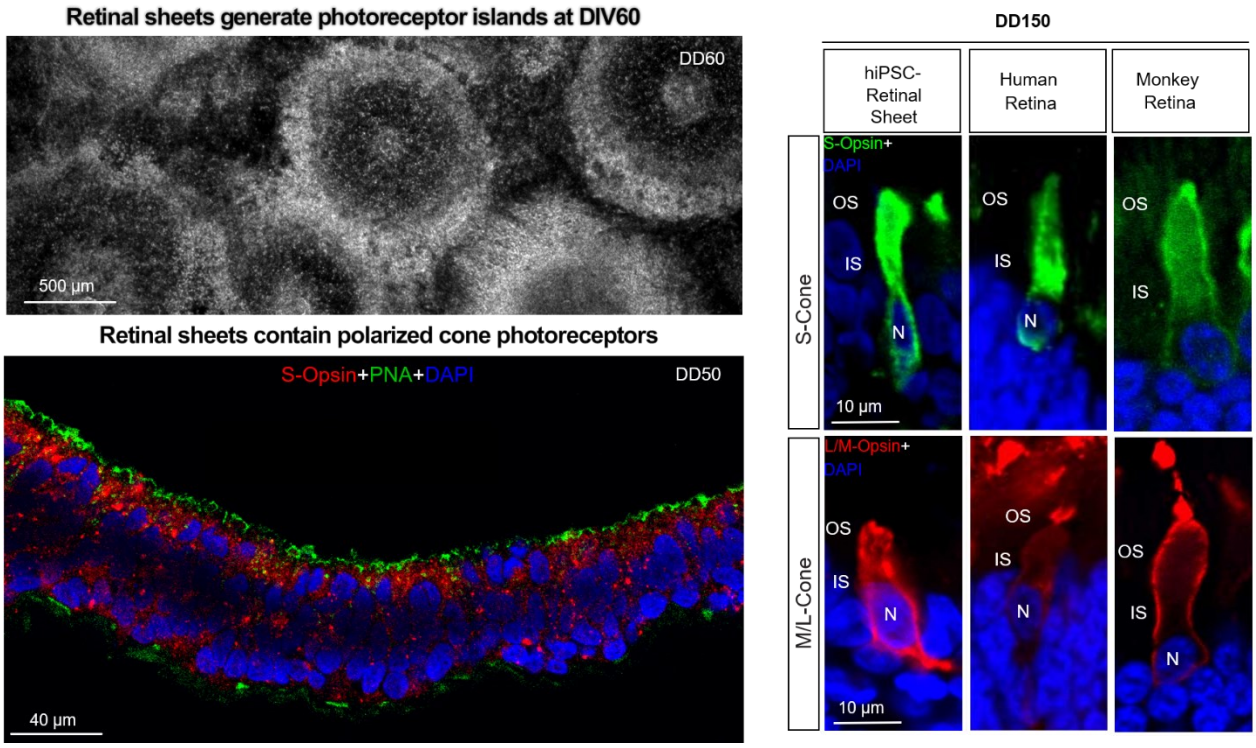

Figure 1: Polarization and long term maturation of iPSC-derived PRs

We also perform RNAseq transcriptomic analysis of differentiated retinal sheets from four control cell lines by comparing them to eight undifferentiated hPSCs (4 hiPSCs and 4 hESCs). This allows us to characterize their composition and level of differentiation better. iPSC-specific transcripts

were lost in RSs; in contrast, retinal and PR-specific transcripts were significantly enriched. Gene Ontology analysis on these genes categorizes them as PRs cell differentiation, PRs cell outer segment organization, visual perception, and phototransduction, thus suggesting efficient cellular differentiation into a retinal lineage (Figure 1C Chapter 3.2).

By comparing the transcriptomic profile of these differentiated cells from controls with the profile of various stages of human embryonic retinal development, we observed that day 60 retinal sheets correspond to 90-105 days of human embryonic development.

Although bulk RNA is exceptionally informative to speculate on the tissues' composition, a more detailed characterization of the diverse cell populations present in the RSs and their proportions can be obtained through single-cell RNAseq analysis currently underway in our laboratory.

4.2 Additional results and future prospects

Many questions remain to be answered or arise from this works, making this a valuable foundation for further studies. Furthermore, there are still many openings for further improvements in this young and fast-moving field.

Below, we present the future perspectives linked to this study and the different directions we intend to take. While some are more short-term or ongoing projects, others represent more theoretical ideas for improving future research. We also call attention to some reflection points that may be useful for implementing the use of stem cells in research and in its translation to the clinic.

4.2.1 Modeling retinal degenerative diseases using isogenic CRISPR-Cas9 edited iPSCs.

One of the major limitations of using patient-derived iPSCs is, as previously anticipated, the possible presence of a polygenic component or the presence of unidentified gene modifiers, which can cause erroneous interpretation of data or conclusions. Non-genetic differences between cell lines, such as gender, age, ethnicity, environmental conditions of the donor, reprogramming process, and iPSCs maintenance conditions (culture conditions and the number of passages), may equally affect the results.

Furthermore, the level of sensitivity of the techniques used and the parameters and databases applied in bioinformatics analyses can cause important data to go unnoticed, thus causing possible misinterpretations in identifying causing mutations.

While it can often be difficult to pinpoint potential causal mutations, providing definitive proof of their responsibility can be an even more daunting task.

While engineered animal models can often be helpful as further evidence, these transgenic or KO models can take a lot of time and resources to establish. They also have an inherent risk that protein function is not conserved between species, that the offspring is not viable, or that they do not reflect observations made in patients for other reasons.

Using a higher number of patients and controls can increase the results' sensitivity but remains prohibitive, when possible, causing most studies to be based on a limited number of patients.

Using iPSC isogenic lines is an elegant and efficient way to confirm disease-causing mutations and reduce the number of samples. As indicated in chapter 1.5, two strategies can be used: rescue the mutation in the patient iPSC line or reproduce the causing mutation or its effect in a control line. While the first offers further implications for clinical applications, induction of damaging mutations in control lines is easier to obtain.

Unlike site-specific correction, which can be very laborious and challenging to generate and require clonal isolations and multiple sequencing runs, gene KO or coarser destruction of specific domains by the CRISPR-Cas9 system can be induced at high efficiency so representing an attractive technique. It can be used to screen multiple mutations efficiently in shorter time frames. Mutations can be induced directly in iPSCs or in fibroblasts before being reprogrammed to facilitate the gene-editing process, as iPSCs are known to be particularly difficult to transfect with both episomal or viral construct (Figure 2 Chapter 4). In case it is desired to separate the gene/mutation's developmental functions from its role in mature cells, CRISPR KO can also be efficiently used at different steps during the differentiation process, including fully differentiated cells such as mature PRs.

Episomal Cas9 expression has numerous advantages and is often preferable in research in various applications. In general, it is faster, easier to implement, and requires less verification and QC. In some particular cases, the integration of the Cas9 in the genome may be preferable, offering a superior editing efficiency, as RNA guides alone can be delivered easier than larger plasmids.

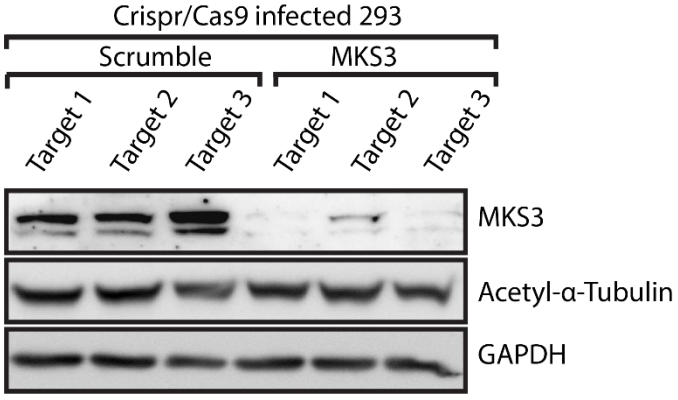

Figure 2: Generation of an isogenic TMEM67 KO line using CRISPR/Cas9 system

WB analisis of CRISPR/Cas9 edited 293 cells targeting 3 different loci on the MKS3 (TMEM67) gene. Edited cells can be reprogrammed into iPSC together with the non edited isogenic controls.

These cases include, for example, cells with low transfection efficiency (such as iPSCs), or hardly expandable (neuronal cells), or when a large number of guides need to be tested independently (CRISPR libraries). While constitutively Cas9 expression has shown to induce toxicity in iPSCs, integrating an inducible Cas9 in a safe harbor provides numerous advantages and represents an excellent strategy to adopt.

In light of these observations, we conclude that, behind the use of genetically engineered animal models, reproducing causing mutations in a control iPSC line could represent an effective strategy to confirm observations made in patient-specific cells, such as our observations on BBS and MKS cases. However, particularly in cases such as the MKS[1] one, which appears to express a defective but full-length version of MKS3, generating a KO mutation, although helpful and informative, is not the best strategy to investigate the mutation role.

It is now clear that when we talk about mutations in components of the cilium, different mutations on the same gene can cause significantly different outcomes, which can vary from non-syndromic MD to severe syndromic manifestation with developmental abnormalities and neonatal mortality.

Therefore, it is likely that an MKS3 KO will show essential differences from what has been observed in the patient's cells. The generation or correction of SNPs, deletion, or insertion at a single base resolution, is now possible but requires more workload and resources.

Since there is no clinical interest in treating MKS, to confirm the role of the mutation of interest using the CRISPR-Cas9 system, both precisely recreating the mutation in a control line and correcting the mutation in the patient-specific iPSC-line can be equally conclusive (Figure 38 Chapter 1).

Today new Cas9 variations are available, with increased specificity that offers better coverage and allows effective editing without recognizable off-target mutations. Despite this, not all areas of the genome are equally editable. Some areas remain particularly difficult to edit, and therefore, case by case, evaluations are required to define the editing's feasibility.

4.2.2 Application of Stem Cell-derived retinal tissue in drug discovery and HTS platforms

Despite major scientific and technological advancements and increasing investments in the field, there is still a high failure rate during drug development. The approval rate of new compounds relative to those initially undertaking clinical trials remains extremely low. Failure to prove drug efficacy is one of the main reasons for the early termination of clinical trials.

One of the contributing factors to this low success rate is partly due to inadequate animal models and over-simplistic 2D *in vitro* systems with limited predictive value. These systems often fail to be transferred to human trials because they poorly or partially recap human physiology and pathology. Immortalized human cell lines tend to be poor predictors, while primary human cell lines are often inaccessible or offer limited expansion *in vitro*. Furthermore, classical culture systems lack the dynamics present in a 3D environment, thus reducing their physiological relevance.

Together, iPSCs technology, advances in differentiation protocols, and 3D cell cultures that mimic embryonic retinal development can revolutionize the concept of *in vitro* models to apply in drug screening and toxicity tests. They represent exceptional tools to investigate the diseases' molecular mechanisms and evaluate potential treatments.

Although there are several examples of using iPSC-derived cells in drug screening, including cardiomyocytes, neurons, pancreatic islets, intestinal and kidney organoids, examples involving the retina are very limited and almost exclusively circumscribed to RPE cells.

Some pioneering studies have shown the potential of iPSC-based *in vitro* models to test compounds with therapeutic properties for RDs.

Chang et al. reported a viability test using H_2O_2 treatment to induce oxidative stress using AMD-patient iPSC-derived RPE, which exhibited reduced antioxidant activity compared to WT RPE cells. In an initial test-of-principle phase, they analyze a library of dietary supplements for retinal protection and natural compounds with an antioxidant effect and measure viability by methyl

thiazol tetrazolium (MTT) assay in 24-Well plate format. Thus, they determine that molecules like Curcumin can significantly reduce ROS in AMD-RPE cells (1184).

Schwarz et al. generated iPSC-derived 3D optic cups from one patient with the mutation *p. R120X* in the ciliary gene *RP2*, resulting in KIF7 accumulation at PRs cilia tip. Then, through a screening of a small number of selected molecules, they found that PTC124 was capable of restoring physiological levels of KIF7 in RP2 KO 3D organoids (1056).

Another group used rod PRs, generated from an RP patient with an E181K mutation in the Rhodopsin gene, and an isogenic control line where the same mutation was generated by gene editing. They used an adenoviral system to introduce NRL promoter-driven enhanced green fluorescent protein (EGFP) to purify the Rod population and bypass the poor differentiation efficiency. In this way, they observed a reduction in survival and increased ER stress and expression of apoptotic markers. Finally, they used this model to screen a small number of therapeutic reagents showing that Rapamycin, PP242, AICAR, NQDI-1, and Salubrinal could ameliorate the pathological effects of the mutation (1063).

Takahashi's lab also uses mouse iPSC-derived 3D organoids to establish a scalable chemical induction model of PRs degeneration via 4-OH treatment. For this purpose, they generate an engineered Nrl-GFP iPSC line and a live imaging system that allows the evaluation of the effects of drugs to promote PRs survival (1065).

Our experimental approach using retinal sheets generated from patient iPSCs, or isogenic mutant PSC lines, can be used to study specific mutations' roles during neural retina development or in adult PRs, and could be used for screening compounds with therapeutic properties.

4.2.2.1 Drug screening to rescue DNA damage and PRs degeneration in a BBS model of MD.

We have shown that retinal sheets from patients with ciliopathies efficiently recapitulate PRs degeneration and multiple genomic abnormalities as reflected in their transcriptomic profile.

Since BBS patients still need therapeutic options, we use patient iPSCs and our retinal sheet system to screen a limited number of targeted molecules in the context of RDs. BBS patient's cells

have shown ciliary dysfunctions, mitotic spindle checkpoint activation, DNA damage, and increased cell death (Figure 7 Chapter 3.2).

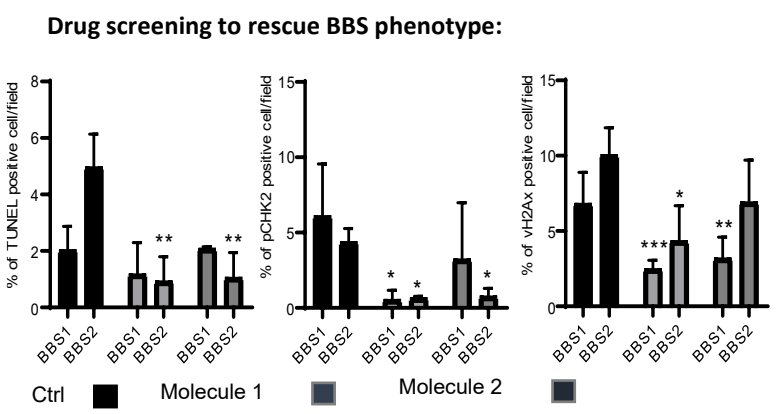

Figure 3: Targeted drug screening reveals compounds able to prevent BBS PR progenitors degeneration

To evaluate the effect of different compounds on genomic stability during mitosis, we treated cells at early time points of the differentiation process when there is still a high percentage of dividing RPCs in the cell culture (Figure 3 Chapter 4). The molecules were selected based on a thoughtful bibliographic search for compounds expected to interfere with the pathways resulted from our transcriptomic analyzes. Cells were treated with the drugs at different concentrations for 72h and then analyzed by microscopy to quantify apoptotic cells (TUNEL +) and the presence of γH2Ax and p-CHK2 positive foci (Barabino *et al.* In preparation).

In this way, we observed that two distinct compounds, MolA and MolB, were able to rescue apoptosis and the number of Chk2 and γH2Ax foci in BBS PRs progenitors from both patients.

To further confirm our results, we also used a Bbs10 KO mouse model in collaboration with Dr. Arlene Drack. In Bbs10 KO mice, we found accumulation of γH2Ax and 53bp1 foci only in cones, pointing out to a previously unappreciated selectivity of the disease for cones (Figure 4 Chapter 4) (Barabino *et al.* In preparation). Indeed, most BBS patients showed severe macular degeneration. This mouse model could be helpful to confirm our screening results in an independent *in vivo* model and for further toxicity studies in the context of a preclinical trial.

We have provided a new model to explore candidate therapeutic approaches in the context of PRs and, more specifically, cones degeneration. We thus provided proof of principle that these cells can be used to screen drugs with therapeutic properties and could eventually be adapted to HTS systems for screening thousands of molecules simultaneously.

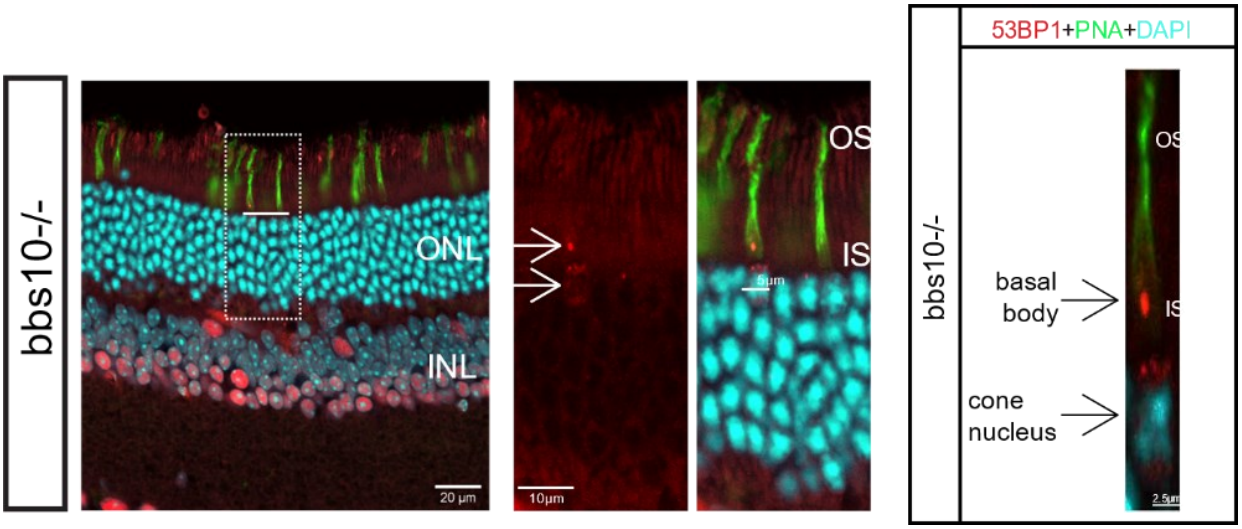

Figure 4: Bbs10 KO mice display cone specific activation of DNA damage response proteins and their accumulation at the PRs' CC

4.2.2.2 Application of iPSC retinal cells in HTS automated platforms

Nowadays, tens of millions of different active compounds are available, with a few thousand already been approved by the FDA, with ever-growing numbers.

Banks of FDA-approved molecules and a vast number of specialized panels of active compounds specially developed for drug discovery processes are now accessible from various companies at low cost and in different multiwell formats ready to be applied in drug screening. This guarantees easy access to these compounds even to academic research laboratories, while before, this type of approach was almost exclusively restricted to large pharmaceutical companies.

This has generated an increasing tendency to choose the HTS system over traditional and targeted approaches. While a well-thought-out targeted approach is generally preferable and more likely to continue clinical development, it also has some risks and limitations. First, moving forward one target at a time is a time-consuming process, and a targeted approach assumes that a target is already known.

The advantage of an HTS is that it can be applied indiscriminately despite the knowledge or not of the biological process underlying the disease of interest. It also allows the generation of multiple hits at a time. For these reasons, HTS can be very useful in an early discovery phase, especially for diseases where the mechanism is still obscure and a targeted approach is difficult or impossible.

From the point of view of drug discovery for clinical use, FDA-approved drug libraries also offer enormous advantages. These compounds have well-characterized biological activity, clear targets, safety, and bioavailability—these properties could dramatically accelerate drug development and optimization. Furthermore, in case of success and advancement towards commercialization, these drugs can be approved quickly and at lower costs.

There are various examples of successes achieved using an HTS approach. HTS permitted the discovery of an FDA-approved drug as a new treatment against Staphylococcus aureus Small-Colony Variants (1185). Another HTS of an FDA-approved drug library identifies inhibitors against Arenaviruses and SARS-CoV-2 (1186).

To date, however, these HTS systems still have many limitations and low success rates, as shown by the minimal number of molecules currently arriving on the market. HTS systems have proven effective mostly in specific cases using simple models, such as testing candidate antibiotic drugs on bacterial cultures. Furthermore, these studies have high costs and require specialized platforms.

In my opinion, another significant limitation of these systems is that they generally tend to use ultra-simplistic in vitro systems. These systems often do not reflect the complexity of the patients, such as immortalized human cell lines grown in standard 2d culture systems, and are far from mimicking human physiology. Therefore, it is not surprising if there is a very high percentage of failures in the transition from in vitro studies to in vivo models and human trials.

The advancement of cell culture techniques combined with iPSCs and new technologies will soon allow us to apply complex and physiologically relevant in vitro models in HTS to reduce failures in the transition to the clinical phase.

With broad access to these extensive collections of compounds, the limiting point for the practical application of iPSC *in vitro* systems in HTS is to adapt differentiation techniques to large-scale automated systems without sacrificing stability, efficiency, reproducibility. Furthermore, it is necessary to establish strict automated quality controls integrated with this process.

The application of multiwell plates implemented with automated steps using robotized systems allows the simultaneous screening of thousands of molecules. These permit to increase the throughput while reducing the cost of reagents and the waste related to material overproduction of the standard culture formats because of the smaller volumes used. 384-well and 1536-well microplates can accommodate at least 5000–20,000 cells and 1000–5000 cells per well, respectively. These are sufficient materials for analysis with new technologies and high sensitivity systems or single-cell analysis.

Some studies have shown the scalability of these iPSC-based systems in HTS.

Swaroop's group in 2016 reported the adaptation of their previous protocol to generate 3D retinal organoids into 1536-well multiwell format for application in drug screening. To identify chemical compounds that can accelerate differentiation in PRs, they used a CRXp-GFP H9 hESC line to visualize the endogenous expression of CRX in real-time to track retinal neurons that self-organize in a 3D retina-like tissue.

They have screened three targeted libraries of active compounds: drug repurposing collection (~ 3000 compounds), the library of pharmacologically active compounds (LOPAC, 1280 compounds), and an NIH mechanism interrogation plate (MIPE) collection of annotated compounds (1900). After the first screening with a fluorescent reporter-based approach, they confirm their primary hits by transcriptomic analysis. Overall, their work reveals the feasibility of HTS using iPSC-derived retinal cells and highlights the importance of establishing a reproductive process and using appropriate controls as critical steps for success (1187).

Cai et al. used iPSC-derived RPE cells from patients with AMD and an induced stress model to identify active compounds that can protect RPE from oxidative stress. They used an HTS system to screen 5065 bioactive compounds of an FDA-approved library to identify potential hits that can prevent RPE degeneration in AMD (1188).

More recently, a group from the Max Planck Institute presented a scalable, HTS-compatible workflow for the automated generation, maintenance, and analysis of human midbrain organoids in standard 96-well-plates that could be applied to 3D retinal organoids or other 3D cultures. Through automation of the whole process, from iPSC generation and differentiation, up to the analysis, they generated highly homogeneous organoids regarding morphology, gene expression, cellular composition, and structure.

This approach permitted to obtain results with more consistency and reproducibility. Integrating automated optical imaging, transcriptomic profiles, and electrophysiological analysis of single cells by patch-clamping, they were able to determine the effect of compounds at the single cells' level (1189).

Another laboratory from Barkley University uses a miniaturized system that increased the throughput of 3D hPSC culture. They use special microculture chips and microwell format plates

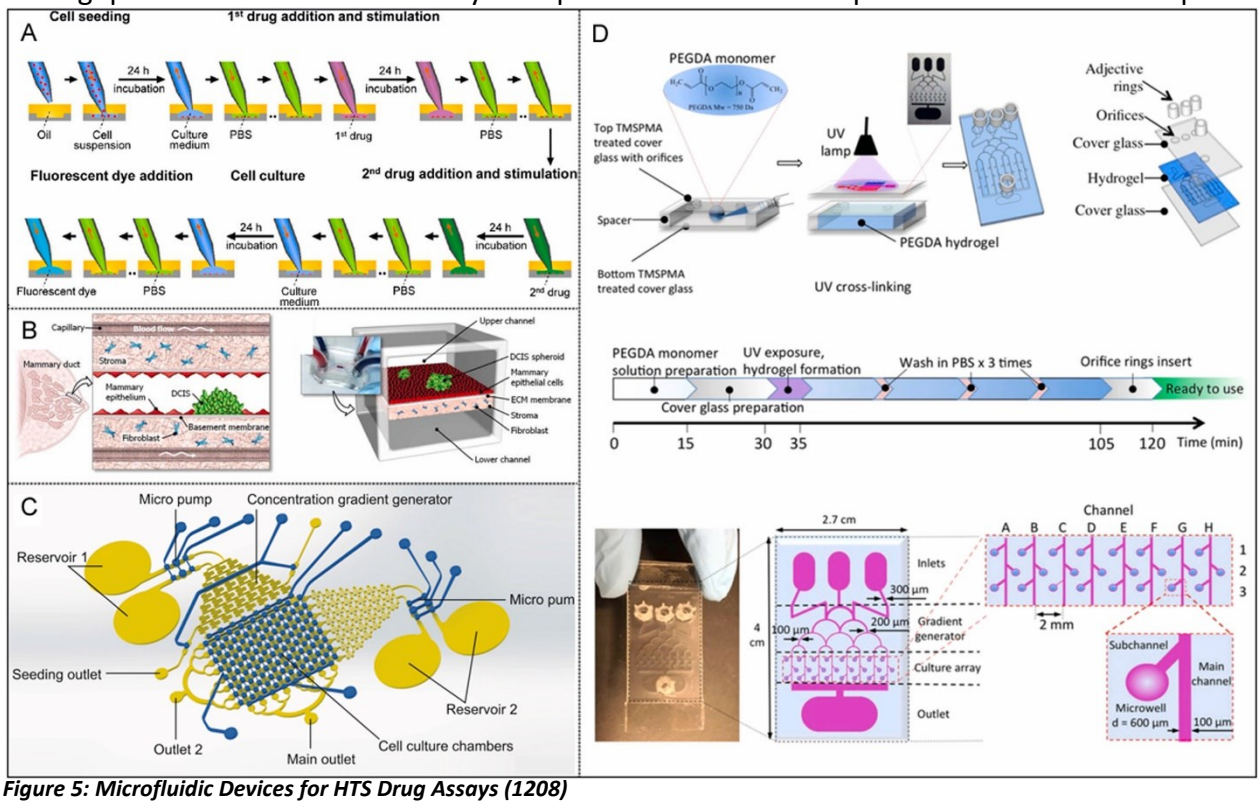

Figure 5: Microfluidic Devices for HTS Drug Assays (1208)

Application of microfluidic chip in drug screening. (A) An illustration of a drug combination assay in the droplet array system in which the cells in the droplets were sequentially stimulated by two drugs (1209)*; (B) Human breast cancer-on-a-chip, left is a diagram of ductal carcinoma in situ(DCIS) embedded in a mammary duct and right is a microdevice reproduction of the microarchitecture of DCIS and the surrounding tissue layers* (1210)*; (C) Different concentrations of sensitizer and drug are sequentially generated in the diffusive gradient mixers sequentially to perfuse cells cultured in downstream microchambers* (1211)*; (D) Brain cancer chip design and preparation that contains a schematic of the layers, chip preparation time protocol, Christmas tree-shaped channel system and final hydrogel device with microchannels and microwells* (1212).

with an automated platform to screen molecules capable of improving hPSCs differentiation in oligodendrocyte progenitor cells (OPCs). They demonstrated the usefulness of microculture platforms, which allowed them to investigate 1200 unique differentiation timelines, and a total of over 4800 independent samples using 0.2% of the reagent volumes required in a standard 96-well plate format (1190).

These works openly show the continuous and impressive advances in the field and highlight several limitations that need to be addressed for the successful future application of these technologies. Still, a few hurdles need to be overcome before a broader application of iPSCs in HTS.

For example, the use of increasingly informative and complex systems requires developing new approaches to analyze the massive quantity of data from which it derives. Machine learning and AI interfaces have already shown great promises in this regard and will be needed to maximize the outcome of biological, chemical and bioinformatics assays.

Implementing these new systems will increase the effectiveness and decrease the time required to find new pharmacological targets, thus allowing the discovery of more effective compounds and find new therapies for currently incurable diseases.

Continuous technological advancement and the use of state-of-the-art technologies are fundamental for the rapid and efficient application of iPSC-derived 3D tissues in HTS.

4.2.3 Retinal sheet application in therapy

RDs are retinal disorders affecting millions of people worldwide, and PRs degeneration is the leading cause of vision loss, and most RDs, such as MD, are considered as unmet medical needs.

Transplantation of iPSC-induced PRs has been considered, a possible clinical approach. It has proven not to be an easy task, as demonstrated by the absence, of successful reports in restoring visual functions, despite the numerous research groups sharing this goal and the significant investments made in the sector.

Multiple groups have recently reported transplantation of PRs progenitors, generated from iPSC, in rodent and non-human primate models (995,1036,1191–1193). Although their ability to

maturate, integrate, and form connections with the underlying bipolar cells, dissociated RPCs can not migrate and correctly polarize, which results in a non-functional tissue.

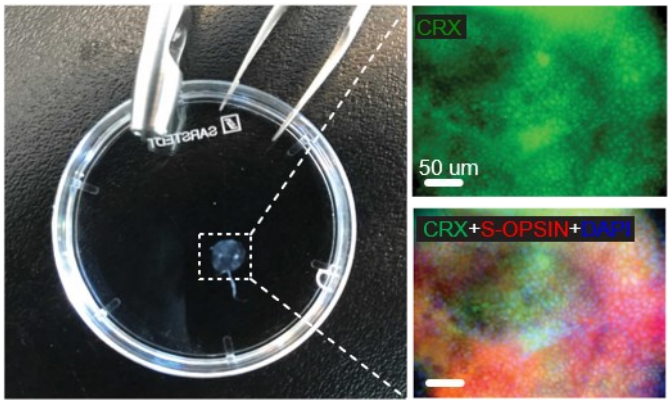

Figure 6: Retinal sheet patch

A group has recently come to partially restore visual functions in a mouse model of severe retinal degeneration by transplanting iPSC-derived PRs. To overcome current problems that prevent PRs from being functional, they introduce optogenetic light sensors into PRs. These optogenetically-transformed PRs could not correctly localize and polarize as reported by other groups, but since their functions are based on microbial opsin activity, which does not require properly formed OS or RPE support, they were able to rescue visual functions partially. This study underlines the procedure's feasibility and highlights the central current limit, which is indubitably the incorrect localization and polarization of the PRs (1035). The work conducted in Dr. Roska's laboratory has led to the first success in restoring some visual abilities to a patient with RP and complete blindness (1194). GenSight's optogenetic therapy skips the damaged photoreceptor cells entirely by using a virus to deliver light-sensitive bacterial proteins into the RGCs, allowing them to detect images directly. Although it could be an effective strategy for restoring some visual perception in blind people, this strategy could hardly bring back "normal" vision. High definition vision is a result of a complex system given by the intercommunication of multiple cells in the retina. It is nowadays unthinkable to restore high-definition visual perception while bypassing the entire visual transmission system by starting the signal directly from the ganglion cells. The addition of a superior level of complexity, such as optogenetically modified photoreceptors, could instead be a more effective strategy. Optogenetically modified PRs could capture the signal even in the absence of a functional OS.and could be applied in diseases characterized by a loss/dysfunction of the OS but without PRs degeneration.

Replacing the visual system with a bionic eye represents another option. Currently, retinal implants are the only approved and commercially available therapy. Four have recently finished

human trials, three have conducted multi- or single-center human trials, and three are in the preclinical animal testing stage. FDA has approved Argus II (FDA 2013, CE 2011); the Alpha-IMS (CE 2013) has been approved and obtained BCVA with Landolt-C test and has taken into a multicenter clinical research program (1195). The Argus II has been used to restore some level of visual perception to hundreds of individuals with severe retinitis pigmentosa and, in 2021, has also been applied to geographic atrophy in age-related macular degeneration (1196,1197). To date, the Argus II device has been implanted in the eyes of more than 350 individuals worldwide.

4.2.3.1 Retinal sheet transplantation

The transplantation of an already polarized ONL-like tissue, composed chiefly by PRs, could, in principle, overcome the limitations of migration and orientation observed previously using injections of dissociated cells, thus allowing the restoration of visual functions. Retinal sheets seem particularly suitable for this use. In fact, after 30-40 days in culture, polarized retinal sheets can be cut to the wanted size and shape, and the resulted patch is strong enough to be handled. It can then be loaded into an injector and released under the retina without using a scaffold or any kind of support.

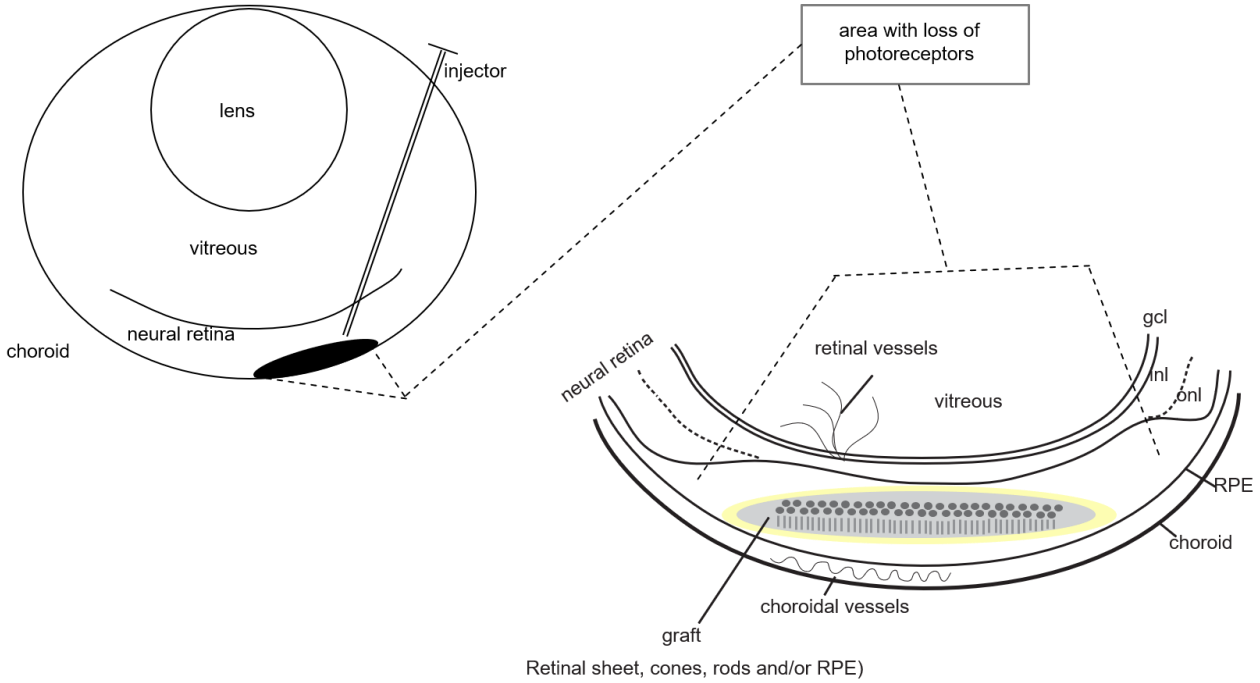

Figure 7: Graphic rappresentation subretinal injection of human iPS-derived retinal sheets

For this purpose, using an iPSC line carrying a fluorescent reporter could help subsequent analysis and trace the cells within the retina. Instead, the application of natural, non-toxic dyes, such as lutein and Zeaxanthin, can be used to color the patch to facilitate the surgical procedure while providing an antioxidant environment, with pro-survival effects, on both transplanted tissue and resident retinal neurons in the site of insertion (1198–1200).

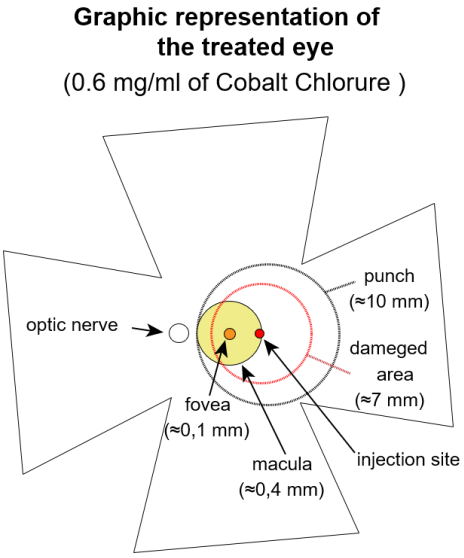

Figure 8: Graphic rappresentation of the treated eye in a non-human primate model of chemically induced macular degeneration

Considering the difficulties of the highly experimental surgical techniques, porcine or non-human primate models are the most suitable for this purpose due to their size and anatomical similarity with the human eye. In these models, selective PRs degeneration can be induced by cobalt chloride injection in the subretinal space. This allows the complete disruption of the ONL, leaving intact all other retinal layers (1193).

Subretinal transplantation of a correctly polarized retinal sheet's patch in the damaged site could restore visual function. This approach may allow the proper formation of connections between cells in the INL with the newly transplanted PRs, while maintaining their correct polarizations and architecture, thus overcoming the limitations encountered with other strategies.

This would represent the first proof of principle that PRs replacement can be used effectively to treat advanced RDs. This approach could open new insights towards the cure of MDs and other PRs dystrophies.

4.3 Final remarks

RDs are a serious burden in our society, with hundreds of millions of cases worldwide having no treatment options and a continuous upward trend. Despite the enormous capital and effort invested, advances are slow, and the results remain inconclusive considering from a clinical point of view. This lack of effective therapies reflects the large gaps in understanding the mechanisms underlying these diseases, highlighting the inadequacy of current model systems.

While animal models have shown their value on several fronts, they have also shown many limitations as it appears from the high ratio of failures during the transition to the human clinical stage. This emphasizes the need for new and improved human in-vitro models. Human iPSCs represent an almost unlimited source of cells that could be used from R&D to the clinic.

Although they still concern a minimal number of cases, some advancements in the treatment of RDs have been recently made possible using iPSCs and new gene-editing techniques, thus giving hope in the battle of these still incurable diseases. iPSCs and tissue engineering techniques are growing enormously during the last few years and hold the potential to bridge the gaps between *in vitro* and *in vivo* models.

A better understanding of the iPSCs biology, the differentiation and developmental process, and the continuous emergence of new experimental tools will help us better understand the disease's mechanisms and find new treatments.

We used hiPSC-based models to study retinal degenerative disease and ciliary dysfunctions in PRs from patients with retinal ciliopathies. Considering that ciliopathies represent one of the largest classes of RDs, these results are relevant for other diseases, and the same approach could be applied to study other mutations. Finally, we demonstrated that retinal sheets could be used as a model for retinal pathologies and to screen for molecules with therapeutic properties. However, there are still many challenges in modeling retinal diseases and their application in drug screening.

The fight against blindness is a tough battle, and it cannot be done alone or on a single front. A productive and close collaboration of multiple research centers and active communication between researchers and physicians are indispensable to defeat these diseases once and for all.

The support of national and international partnerships that support stem cell research, regenerative medicine, and specific sectors such as RDs is fundamental to scientific advancement and translates scientific discoveries from the bench to the clinic. Networks and consortiums that work in close collaborations with research, healthcare, industry representatives, health charities, government, and non-government organizations to finance research are also crucial to build the foundations for more effective scientific advancement in the sector.

To accelerate scientific discovery, avoid wasting resources, and reduce results duplication, we need to enlarge freely accessible databases and develop new systems for depositing and sharing research data. Complete and standardize health data repositories to access for research purposes and better management of human tissues donated to the research could grant more manageable access to patient samples, thus favoring the advancement of research in RDs.

Public datasets containing different data types ranging from ophthalmological imaging, genomic and transcriptomic analysis, and electrophysiological recordings are precious materials that can be reused in other studies when standardized and easily accessible. These large datasets can be extremely useful, especially when considering the concomitant advances in bioinformatics and machine learning, which will permit the application of these pieces of information in HTS and in-depth analysis in a more efficient way.

Improving metadata reporting would enable researchers to access the most appropriate datasets for their needs and maximize such resources' potential.

Large collaborative projects such as the 1000 and 100,000 Genomes Projects or the NHLBI NextGen consortium, which analyzed the retina differentiation from more than 100 different iPSC lines, have contributed significantly to the knowledge of the heterogeneity and differentiation capacity of different iPSCs. They have also allowed the individuation of a multitude of new genetic variations, including rare genetic variants, thus allowing a better comprehension of the genetics

and mechanisms behind RDs. They now represent the reference for all genome-wide bioinformatics analyzes.

To conclude, iPSCs and tissue engineering's potential is clear, and the excitement about it is undoubtedly justified. On the other hand, many obstacles still need to be overcome to generate and manipulate patient-derived iPSCs in a high-standard, reproducible and controlled environment so that they can finally be reliably introduced in both research and clinic.

5. BIBLIOGRAPHY

1. Hutmacher, F. Why Is There So Much More Research on Vision Than on Any Other Sensory Modality? *Front. Psychol.* **10**, 2246 (2019) DOI:10.3389/fpsyg.2019.02246.

2. Foster, R. G. & Hankins, M. W. Circadian vision. *Current Biology* vol. 17 (2007) DOI:10.1016/j.cub.2007.07.007.

3. Van Gelder, R. N. Nonvisual ocular photoreception in the mammal. *Methods Enzymol.* **393**, 746–55 (2005) DOI:10.1016/S0076-6879(05)93039-5.

4. Fernald, R. D. Casting a genetic light on the evolution of eyes. *Science* **313**, 1914–8 (2006) DOI:10.1126/science.1127889.

5. Gehring, W. J. & Ikeo, K. Pax 6: Mastering eye morphogenesis and eye evolution. *Trends in Genetics* vol. 15 371–377 (1999) DOI:10.1016/S0168-9525(99)01776-X.

6. Hanson, I. & Van Heyningen, V. Pax6: more than meets the eye. *Trends in Genetics* vol. 11 268–272 (1995) DOI:10.1016/S0168-9525(00)89073-3.

7. Kamachi, Y., Uchikawa, M., Tanouchi, A., Sekido, R. & Kondoh, H. Pax6 and SOX2 form a co-DNA-binding partner complex that regulates initiation of lens development. *Genes Dev.* **15**, 1272–86 (2001) DOI:10.1101/gad.887101.

8. Fernald, R. D. The evolution of eyes. *Brain. Behav. Evol.* **50**, 253–9 (1997) DOI:10.1159/000113339.

9. Fernald, R. D. Eyes: Variety, development and evolution. in *Brain, Behavior and Evolution* vol. 64 141–147 (Brain Behav Evol, 2004). DOI:10.1159/000079743.

10. Jonasova, K. & Kozmik, Z. Eye evolution: Lens and cornea as an upgrade of animal visual system. *Seminars in Cell and Developmental Biology* vol. 19 71–81 (2008) DOI:10.1016/j.semcdb.2007.10.005.

11. Ogura, A. *et al.* Loss of the six3/6 controlling pathways might have resulted in pinhole-eye evolution in Nautilus. *Sci. Rep.* **3**, 1–7 (2013) DOI:10.1038/srep01432.

12. Graw, J. Eye development. in *Current Topics in Developmental Biology* vol. 90 343–386 (Academic Press Inc., 2010). DOI:10.1016/S0070-2153(10)90010-0.

13. Stenkamp, D. L. Development of the Vertebrate Eye and Retina. in *Progress in Molecular Biology and Translational Science* vol. 134 397–414 (Elsevier B.V., 2015). DOI:10.1016/bs.pmbts.2015.06.006.

14. Jackson, E. Function and Structure of the Eye. *Trans. Am. Ophthalmol. Soc.* **38**, 226–35 (1940).

15. Skeie, J. M., Roybal, C. N. & Mahajan, V. B. Proteomic insight into the molecular function of the vitreous. *PLoS One* **10**, 127567 (2015) DOI:10.1371/journal.pone.0127567.

16. Hoshino, A. *et al.* Molecular anatomy of the developing human retina. *Dev. Cell* **43**, 763 (2017) DOI:10.1016/J.DEVCEL.2017.10.029.

17. Weil, D. *et al.* Usher syndrome type I G (USH1G) is caused by mutations in the gene encoding SANS, a protein that associates with the USH1C protein, harmonin. *Hum. Mol. Genet.* **12**, 463–71 (2003).

18. Frøen, R. *et al.* Does the Adult Human Ciliary Body Epithelium Contain '"True"' Retinal Stem Cells? *Biomed Res. Int.* **2013**, (2013) DOI:10.1155/2013/531579.

19. Lamb, T. D., Collin, S. P. & Pugh, E. N. Evolution of the vertebrate eye: Opsins, photoreceptors, retina and eye cup. *Nature Reviews Neuroscience* vol. 8 960–976 (2007) DOI:10.1038/nrn2283.

20. Chen, J., Sampath, A. P. & Jeannie Chen, A. P. S. Structure and Function of Rod and Cone Photoreceptors. in *Elsevier: Retina* vol. 1 342–359 (Elsevier Inc., 2012). DOI:10.1016/B978-1-4557-0737-9.00014-X.

21. Curcio, C. A. *et al.* Distribution and morphology of human cone photoreceptors stained with anti-blue opsin. *J. Comp. Neurol.* **312**, 610–624 (1991) DOI:10.1002/cne.903120411.

22. Viets, K., Eldred, K. C. & Johnston, R. J. Mechanisms of Photoreceptor Patterning in Vertebrates and Invertebrates. *Trends in Genetics* vol. 32 638–659 (2016)

DOI:10.1016/j.tig.2016.07.004.

23. Spraul, C. W., Lang, G. E., Grossniklaus, H. E. & Lang, G. K. Histologic and morphometric analysis of the choroid, Bruch's membrane, and retinal pigment epithelium in postmortem eyes with age-related macular degeneration and histologic examination of surgically excised choroidal neovascular membranes. *Survey of Ophthalmology* vol. 44 (1999) DOI:10.1016/S0039-6257(99)00086-7.

24. Purves, D. *et al.* Anatomical Distribution of Rods and Cones. (2001).

25. Masland, R. H. The fundamental plan of the retina. *Nature Neuroscience* vol. 4 877–886 (2001) DOI:10.1038/nn0901-877.

26. Boycott, B. B. & Wässle, H. Morphological Classification of Bipolar Cells of the Primate Retina. *Eur. J. Neurosci.* **3**, 1069–1088 (1991) DOI:10.1111/j.1460-9568.1991.tb00043.x.

27. Cohen, E. & Sterling, P. Demonstration of cell types among cone bipolar neurons of cat retina. *Philos. Trans. R. Soc. Lond. B. Biol. Sci.* **330**, 305–321 (1990) DOI:10.1098/rstb.1990.0201.

28. Martin, P. R. & Grünert, U. Spatial density and immunoreactivity of bipolar cells in the macaque monkey retina. *J. Comp. Neurol.* **323**, 269–287 (1992) DOI:10.1002/cne.903230210.

29. Dacey, D. M., Lee, B. B., Stafford, D. K., Pokomy, J. & Smith, V. C. Horizontal cells of the primate retina: Cone specificity without spectral opponency. *Science (80-.).* **271**, 656–659 (1996) DOI:10.1126/science.271.5249.656.

30. Hack, I. & Peichl, L. Horizontal cells of the rabbit retina are non-selectively connected to the cones. *Eur. J. Neurosci.* **11**, 2261–2274 (1999) DOI:10.1046/j.1460-9568.1999.00647.x.

31. Elshatory, Y. *et al.* Islet-1 controls the differentiation of retinal bipolar and cholinergic amacrine cells. *J. Neurosci.* **27**, 12707–12720 (2007) DOI:10.1523/JNEUROSCI.3951-07.2007.

32. MacNeil, M. A. & Masland, R. H. Extreme diversity among amacrine cells: Implications for

function. *Neuron* **20**, 971–982 (1998) DOI:10.1016/S0896-6273(00)80478-X.

33. Awatramani, G. B. & Slaughter, M. M. Origin of transient and sustained responses in ganglion cells of the retina. *J. Neurosci.* **20**, 7087–7095 (2000) DOI:10.1523/jneurosci.20-18-07087.2000.

34. Wassle, H. & Boycott, B. B. Functional architecture of the mammalian retina. *Physiological Reviews* vol. 71 447–480 (1991) DOI:10.1152/physrev.1991.71.2.447.

35. Calkins, D. J., Schein, S. J., Tsukamoto, Y. & Sterling, P. M and L cones in macaque fovea connect to midget ganglion cells by different numbers of excitatory synapses. *Nature* **371**, 70–72 (1994) DOI:10.1038/371070a0.

36. Curcio, C. A. & Allen, K. A. Topography of ganglion cells in human retina. *J. Comp. Neurol.* **300**, 5–25 (1990) DOI:10.1002/cne.903000103.

37. Boycott, B. B. & Hopkins, J. M. Microglia in the retina of monkey and other mammals; Its distinction from other types of glia and horizontal cells. *Neuroscience* **6**, 679–688 (1981) DOI:10.1016/0306-4522(81)90151-2.

38. Goldman, D. Müller glial cell reprogramming and retina regeneration. *Nature Reviews Neuroscience* vol. 15 431–442 (2014) DOI:10.1038/nrn3723.

39. Strauss, O. The retinal pigment epithelium in visual function. *Physiological Reviews* vol. 85 845–881 (2005) DOI:10.1152/physrev.00021.2004.

40. Marmorstein, A. D. The polarity of the retinal pigment epithelium. *Traffic* vol. 2 867–872 (2001) DOI:10.1034/j.1600-0854.2001.21202.x.

41. Miceli, M. V., Liles, M. R. & Newsome, D. A. Evaluation of oxidative processes in human pigment epithelial cells associated with retinal outer segment phagocytosis. *Exp. Cell Res.* **214**, 242–249 (1994) DOI:10.1006/excr.1994.1254.

42. Salem, M. A. Structure and function of the retinal pigment epithelium, photoreceptors and cornea in the eye of Sardinella aurita (Clupeidae, Teleostei). *J. Basic Appl. Zool.* **75**, 1–12 (2016) DOI:10.1016/j.jobaz.2015.12.001.

43. Tanihara, H., Inatani, M. & Honda, Y. Growth factors and their receptors in the retina and pigment epithelium. *Progress in Retinal and Eye Research* vol. 16 271–301 (1997) DOI:10.1016/S1350-9462(96)00028-6.

44. Baehr, W., Wu, S. M., Bird, A. C. & Palczewski, K. The retinoid cycle and retina disease. *Vision Research* vol. 43 2957–2958 (2003) DOI:10.1016/j.visres.2003.10.001.

45. Tarau, I. S., Berlin, A., Curcio, C. A. & Ach, T. The Cytoskeleton of the Retinal Pigment Epithelium: from Normal Aging to Age-Related Macular Degeneration. *International Journal of Molecular Sciences* vol. 20 (2019) DOI:10.3390/ijms20143578.

46. Zhu, D. H., Wu, J., Spee, C., Ryan, S. J. & Hinton, D. R. BMP4 mediates oxidative stress-induced retinal pigment epithelial cell senescence and is overexpressed in age-related macular degeneration. *J. Biol. Chem.* **284**, 9529–9539 (2009) DOI:10.1074/jbc.M809393200.

47. Bernier, G. *et al.* Expanded retina territory by midbrain transformation upon overexpression of Six6 (Optx2) in Xenopus embryos. *Mech. Dev.* **93**, 59–69 (2000) DOI:10.1016/S0925-4773(00)00271-9.

48. Bovolenta, P., MallaMacI, A., Puelles, L. & Boncinelli, E. Expression pattern of cSix3, a member of the Six/sine oculis family of transcription factors. *Mech. Dev.* **70**, 201–203 (1998) DOI:10.1016/S0925-4773(97)00183-4.

49. Chow, R. L. *Ectopic eyes in response to Pax6*. (1999).

50. Lagutin, O. V. *et al.* Six3 repression of Wnt signaling in the anterior neuroectoderm is essential for vertebrate forebrain development. *Genes Dev.* **17**, 368–379 (2003) DOI:10.1101/gad.1059403.

51. Loosli, F., Winkler, S. & Wittbrodt, J. Six3 overexpression initiates the formation of ectopic retina. *Genes Dev.* **13**, 649–654 (1999) DOI:10.1101/gad.13.6.649.

52. Marquardt, T. *et al.* Pax6 is required for the multipotent state of retinal progenitor cells. *Cell* **105**, 43–55 (2001) DOI:10.1016/S0092-8674(01)00295-1.

53. Mathers, P. H., Grinberg, A., Mahon, K. A. & Jamrich, M. The Rx homeobox gene is essential for vertebrate eye development. *Nature* **387**, 603–607 (1997) DOI:10.1038/42475.

54. Taranova, O. V. *et al.* SOX2 is a dose-dependent regulator of retinal neural progenitor competence. *Genes Dev.* **20**, 1187–1202 (2006) DOI:10.1101/gad.1407906.

55. Tétreault, N., Champagne, M.-P. & Bernier, G. The LIM homeobox transcription factor Lhx2 is required to specify the retina field and synergistically cooperates with Pax6 for Six6 trans-activation. *Dev. Biol.* **327**, 541–50 (2009) DOI:10.1016/j.ydbio.2008.12.022.

56. Glaser, T. *et al.* PAX6 gene dosage effect in a family with congenital cataracts, aniridia, anophthalmia and central nervous system defects. *Nat. Genet.* **7**, 463–471 (1994) DOI:10.1038/ng0894-463.

57. Lequeux, L. *et al.* Confirmation of RAX gene involvement in human anophthalmia. *Clin. Genet.* **74**, 392–395 (2008) DOI:10.1111/j.1399-0004.2008.01078.x.

58. Ragge, N. K., Subak-Sharpe, I. D. & Collin, J. R. O. A practical guide to the management of anophthalmia and microphthalmia. in *Eye* vol. 21 1290–1300 (Nature Publishing Group, 2007). DOI:10.1038/sj.eye.6702858.

59. Ragge, N. K. *et al.* SOX2 anophthalmia syndrome. *Am. J. Med. Genet.* **135 A**, 1–7 (2005) DOI:10.1002/ajmg.a.30642.

60. Ragge, N. K. *et al.* Heterozygous mutations of OTX2 cause severe ocular malformations. *Am. J. Hum. Genet.* **76**, 1008–1022 (2005) DOI:10.1086/430721.

61. Adler, R. & Canto-Soler, M. V. Molecular mechanisms of optic vesicle development: Complexities, ambiguities and controversies. *Developmental Biology* vol. 305 1–13 (2007) DOI:10.1016/j.ydbio.2007.01.045.

62. Cvekl, A. & Wang, W. L. Retinoic acid signaling in mammalian eye development. *Experimental Eye Research* vol. 89 280–291 (2009) DOI:10.1016/j.exer.2009.04.012.

63. Hou, P.-S. *et al.* LHX2 regulates the neural differentiation of human embryonic stem cells via transcriptional modulation of PAX6 and CER1. *Nucleic Acids Res* (2013)

doi:10.1093/nar/gkt567 DOI:10.1093/nar/gkt567.

64. Bell, E., Muñoz-Sanjuán, I., Altmann, C. R., Vonica, A. & Brivanlou, A. H. Cell fate specification and competence by Coco, a maternal BMP, TGFβ and Wnt inhibitor. *Development* vol. 130 1381–1389 (2003) DOI:10.1242/dev.00344.

65. Bouwmeester, T., Kim, S. H., Sasai, Y., Lu, B. & De Robertis, E. M. Cerberus is a head-inducing secreted factor expressed in the anterior endoderm of Spemann's organizer. *Nature* **382**, 595–601 (1996) DOI:10.1038/382595a0.

66. Hsu, D. R., Economides, A. N., Wang, X., Eimon, P. M. & Harland, R. M. The Xenopus dorsalizing factor Gremlin identifies a novel family of secreted proteins that antagonize BMP activities. *Mol. Cell* **1**, 673–683 (1998) DOI:10.1016/S1097-2765(00)80067-2.

67. Piccolo, S. *et al.* The head inducer cerberus is a multifunctional antagonist of Nodal, BMP and Wnt signals. *Nature* **397**, 707–710 (1999) DOI:10.1038/17820.

68. Piccolo, S., Sasai, Y., Lu, B. & De Robertis, E. M. Dorsoventral patterning in Xenopus: Inhibition of ventral signals by direct binding of chordin to BMP-4. *Cell* **86**, 589–598 (1996) DOI:10.1016/S0092-8674(00)80132-4.

69. Schmidt, J. E., Suzuki, A., Ueno, N. & Kimelman, D. Localized BMP-4 Mediates Dorsal/Ventral Patterning in the Early Xenopus Embryo. *Dev. Biol.* **169**, 37–50 (1995) DOI:10.1006/dbio.1995.1124.

70. Suzuki, A. *et al.* A truncated bone morphogenetic protein receptor affects dorsal-ventral patterning in the early Xenopus embryo. *Proc. Natl. Acad. Sci. U. S. A.* **91**, 10255–10259 (1994) DOI:10.1073/pnas.91.22.10255.

71. Weiss, A. & Attisano, L. The TGFbeta Superfamily Signaling Pathway. *Wiley Interdiscip. Rev. Dev. Biol.* **2**, 47–63 (2013) DOI:10.1002/wdev.86.

72. Bates, T. J. D., Vonica, A., Heasman, J., Brivanlou, A. H. & Bell, E. Coco regulates dorsoventral specification of germ layers via inhibition of TGFβ signalling. *Dev.* **140**, 4177–4181 (2013) DOI:10.1242/dev.095521.

73. Evans, A. L. & Gage, P. J. Expression of the homeobox gene Pitx2 in neural crest is required for optic stalk and ocular anterior segment development. *Hum. Mol. Genet.* **14**, 3347–3359 (2005) DOI:10.1093/hmg/ddi365.

74. Sowden, J. C. Molecular and developmental mechanisms of anterior segment dysgenesis. in *Eye* vol. 21 1310–1318 (Nature Publishing Group, 2007). DOI:10.1038/sj.eye.6702852.

75. Markitantova, Y. V. *et al.* Analysis of expression of regulatory genes Pax6, Prox1, and Pitx2 in differentiating eye cells in human fetus. *Biol. Bull.* **33**, 339–346 (2006) DOI:10.1134/S1062359006040042.

76. Eiraku, M. *et al.* Self-organizing optic-cup morphogenesis in three-dimensional culture. *Nature* **472**, 51–58 (2011) DOI:10.1038/nature09941.

77. Sakami, S., Etter, P. & Reh, T. A. Activin signaling limits the competence for retinal regeneration from the pigmented epithelium. *Mech. Dev.* **125**, 106–116 (2008) DOI:10.1016/j.mod.2007.10.001.

78. Fuhrmann, S., Levine, E. M. & Reh, T. A. Extraocular mesenchyme patterns the optic vesicle during early eye development in the embryonic chick. *Development* **127**, 4599–4609 (2000).

79. Fuhrmann, S., Zou, C. J. & Levine, E. M. Retinal pigment epithelium development, plasticity, and tissue homeostasis. *Experimental Eye Research* vol. 123 141–150 (2014) DOI:10.1016/j.exer.2013.09.003.

80. Volland, S., Esteve-Rudd, J., Hoo, J., Yee, C. & Williams, D. S. A Comparison of Some Organizational Characteristics of the Mouse Central Retina and the Human Macula. (2015) doi:10.1371/journal.pone.0125631 DOI:10.1371/journal.pone.0125631.

81. Belecky-Adams, T., Cook, B. & Adler, R. Correlations between terminal mitosis and differentiated fate of retinal precursor cells in vivo and in vitro: Analysis with the 'window-labeling' technique. *Dev. Biol.* **178**, 304–315 (1996) DOI:10.1006/dbio.1996.0220.

82. Cepko, C. L., Austin, C. P., Yang, X., Alexiades, M. & Ezzeddine, D. Cell fate determination in

the vertebrate retina. *Proc. Natl. Acad. Sci. U. S. A.* **93**, 589–595 (1996) DOI:10.1073/pnas.93.2.589.

83. Ohsawa, R. & Kageyama, R. Regulation of retinal cell fate specification by multiple transcription factors. *Brain Research* vol. 1192 90–98 (2008) DOI:10.1016/j.brainres.2007.04.014.

84. Reh, T. A. & Kijavin, I. J. Age of differentiation determines rat retinal germinal cell phenotype: Induction of differentiation by dissociation. *J. Neurosci.* **9**, 4179–4189 (1989) DOI:10.1523/jneurosci.09-12-04179.1989.

85. Watanabe, T. & Raff, M. C. Rod photoreceptor development in vitro: Intrinsic properties of proliferating neuroepithelial cells change as development proceeds in the rat retina. *Neuron* **4**, 461–467 (1990) DOI:10.1016/0896-6273(90)90058-N.

86. Burmeister, M. *et al.* Ocular retardation mouse caused by Chx10 homeobox null allele: Impaired retinal progenitor proliferation and bipolar cell differentiation. *Nat. Genet.* **12**, 376–384 (1996) DOI:10.1038/ng0496-376.

87. Ferda Percin, E. *et al.* Human microphthalmia associated with mutations in the retinal homeobox gene CHX10. *Nat. Genet.* **25**, 397–401 (2000) DOI:10.1038/78071.

88. Horsford, D. J. *et al.* Chx10 repression of Mitf is required for the maintenance of mammalian neuroretinal identity. *Development* **132**, 177–187 (2005) DOI:10.1242/dev.01571.

89. Nadean L. Brown *et al.* Math5 encodes a murine basic helix-loop-helix transcription factor expressed during early stages of retinal neurogenesis. *Development* (1998).

90. Riesenberg, A. N., Liu, Z., Kopan, R. & Brown, N. L. Rbpj cell autonomous regulation of retinal ganglion cell and cone photoreceptor fates in the mouse retina. *J. Neurosci.* **29**, 12865–12877 (2009) DOI:10.1523/JNEUROSCI.3382-09.2009.

91. Moshiri, A. *et al.* Near complete loss of retinal ganglion cells in the math5/brn3b double knockout elicits severe reductions of other cell types during retinal development. *Dev. Biol.*

316, 214–227 (2008) DOI:10.1016/j.ydbio.2008.01.015.

92. Fujitani, Y. *et al.* Ptf1a determines horizontal and amacrine cell fates during mouse retinal development. *Development* **133**, 4439–4450 (2006) DOI:10.1242/dev.02598.

93. Liu, H. *et al.* An isoform of retinoid-related orphan receptor β directs differentiation of retinal amacrine and horizontal interneurons. *Nat. Commun.* **4**, (2013) DOI:10.1038/ncomms2793.

94. Dyer, M. A., Livesey, F. J., Cepko, C. L. & Oliver, G. Prox1 function controls progenitor cell proliferation and horizontal cell genesis in the mammalian retina. *Nat. Genet.* **34**, 53–58 (2003) DOI:10.1038/ng1144.

95. Rapaport, D. H., Wong, L. L., Wood, E. D., Yasumura, D. & Lavail, M. M. Timing and topography of cell genesis in the rat retina. *J. Comp. Neurol.* **474**, 304–324 (2004) DOI:10.1002/cne.20134.

96. Wässle, H., Koulen, P., Brandstätter, J. H., Fletcher, E. L. & Becker, C. M. Glycine and GABA receptors in the mammalian retina. in *Vision Research* vol. 38 1411–1430 (Vision Res, 1998). DOI:10.1016/S0042-6989(97)00300-3.

97. Young, R. W. Cell differentiation in the retina of the mouse. *Anat. Rec.* **212**, 199–205 (1985) DOI:10.1002/ar.1092120215.

98. Green, E. S., Stubbs, J. L. & Levine, E. M. Genetic rescue of cell number in a mouse model of microphthalmia: Interactions between Chx10 and G1-phase cell cycle regulators. *Development* vol. 130 539–552 (2003) DOI:10.1242/dev.00275.

99. Livne-bar, I. *et al. Chx10 is required to block photoreceptor differentiation but is dispensable for progenitor proliferation in the postnatal retina*. www.pnas.orgcgidoi10.1073pnas.0600083103 (2006).

100. Ohsawa, R., Ohtsuka, T. & Kageyama, R. Mash1 and Math3 are required for development of branchiomotor neurons and maintenance of neural progenitors. *J. Neurosci.* **25**, 5857–5865 (2005) DOI:10.1523/JNEUROSCI.4621-04.2005.

101. Satow, T. *et al. The Basic Helix-Loop-Helix Gene hesr2 Promotes Gliogenesis in Mouse Retina*. (2001).

102. Wu, F. *et al.* Onecut1 is essential for horizontal cell genesis and retinal integrity. *J. Neurosci.* **33**, 13053–13065 (2013) DOI:10.1523/JNEUROSCI.0116-13.2013.

103. Westheimer, G. *The ON-OFF dichotomy in visual processing: From receptors to perception*. *Progress in Retinal and Eye Research* vol. 26 636–648 (Pergamon, 2007). DOI:10.1016/j.preteyeres.2007.07.003.

104. Swaroop, A., Kim, D. & Forrest, D. Transcriptional regulation of photoreceptor development and homeostasis in the mammalian retina. *Nature Reviews Neuroscience* vol. 11 563–576 (2010) DOI:10.1038/nrn2880.

105. Nishida, A. *et al.* Otx2 homeobox gene controls retinal photoreceptor cell fate and pineal gland development. *Nat. Neurosci.* **6**, 1255–1263 (2003) DOI:10.1038/nn1155.

106. Yamamoto, H., Kon, T., Omori, Y. & Furukawa, T. Functional and Evolutionary Diversification of Otx2 and Crx in Vertebrate Retinal Photoreceptor and Bipolar Cell Development. *Cell Rep.* **30**, 658-671.e5 (2020) DOI:10.1016/j.celrep.2019.12.072.

107. Chen, S. *et al.* Crx, a novel Otx-like paired-homeodomain protein, binds to and transactivates photoreceptor cell-specific genes. *Neuron* **19**, 1017–1030 (1997) DOI:10.1016/S0896-6273(00)80394-3.

108. Freund, C. L. *et al.* Cone-rod dystrophy due to mutations in a novel photoreceptor-specific homeobox gene (CRX) essential for maintenance of the photoreceptor. *Cell* **91**, 543–553 (1997) DOI:10.1016/S0092-8674(00)80440-7.

109. Furukawa, T., Morrow, E. M. & Cepko, C. L. Crx, a novel otx-like homeobox gene, shows photoreceptor-specific expression and regulates photoreceptor differentiation. *Cell* **91**, 531–541 (1997) DOI:10.1016/S0092-8674(00)80439-0.

110. Ng, L., Ma, M., Curran, T. & Forrest, D. Developmental expression of thyroid hormone receptor β2 protein in cone photoreceptors in the mouse. *Neuroreport* **20**, 627–631 (2009)

DOI:10.1097/WNR.0b013e32832a2c63.

111. Yasuo Yanagi, Shin-Ichiro Takezawa & Shigeaki Kato. Distinct functions of photoreceptor cell-specific nuclear receptor, thyroid hormone receptor beta2 and CRX in one photoreceptor development - PubMed. *Invest Ophthalmol Vis Sci* (2002).

112. Ahmad, I., Zagouras, P. & Artavanis-Tsakonas, S. Involvement of Notch-1 in mammalian retinal neurogenesis: association of Notch-1 activity with both immature and terminally differentiated cells. *Mech. Dev.* **53**, 73–85 (1995) DOI:10.1016/0925-4773(95)00425-4.

113. Jadhav, A. P., Mason, H. A. & Cepko, C. L. Notch 1 inhibits photoreceptor production in the developing mammalian retina. *Development* **133**, 913–923 (2006) DOI:10.1242/dev.02245.

114. Jia, L. *et al.* Retinoid-related orphan nuclear receptor RORβ is an early-acting factor in rod photoreceptor development. *Proc. Natl. Acad. Sci. U. S. A.* **106**, 17534–17539 (2009) DOI:10.1073/pnas.0902425106.

115. Mears, A. J. *et al.* Nrl is required for rod photoreceptor development. *Nat. Genet.* **29**, 447–452 (2001) DOI:10.1038/ng774.

116. Yaron, O., Farhy, C., Marquardt, T., Applebury, M. & Ashery-Padan, R. Notch1 functions to suppress cone-photoreceptor fate specification in the developing mouse retina. *Development* **133**, 1367–1378 (2006) DOI:10.1242/dev.02311.

117. Bumsted O'Brien, K. M. *et al.* Expression of photoreceptor-specific nuclear receptor NR2E3 in rod photoreceptors of fetal human retina. *Investig. Ophthalmol. Vis. Sci.* **45**, 2807–2812 (2004) DOI:10.1167/iovs.03-1317.

118. Chen, J., Rattner, A. & Nathans, J. The rod photoreceptor-specific nuclear receptor Nr2e3 represses transcription of multiple cone-specific genes. *J. Neurosci.* **25**, 118–129 (2005) DOI:10.1523/JNEUROSCI.3571-04.2005.

119. Roberts, M. R., Hendrickson, A., McGuire, C. R. & Reh, T. A. Retinoid X receptor γ is necessary to establish the S-opsin gradient in cone photoreceptors of the developing mouse retina. *Investig. Ophthalmol. Vis. Sci.* **46**, 2897–2904 (2005) DOI:10.1167/iovs.05-

0093.

120. Suzuki, S. C. *et al.* Cone photoreceptor types in zebrafish are generated by symmetric terminal divisions of dedicated precursors. *Proc. Natl. Acad. Sci. U. S. A.* **110**, 15109–15114 (2013) DOI:10.1073/pnas.1303551110.

121. Roberts, M. R., Srinivas, M., Forrest, D., De Escobar, G. M. & Reh, T. A. Making the gradient: Thyroid hormone regulates cone opsin expression in the developing mouse retina. *Proc. Natl. Acad. Sci. U. S. A.* **103**, 6218–6223 (2006) DOI:10.1073/pnas.0509981103.

122. Mey, J., McCaffery, P. & Dräger, U. C. Retinoic acid synthesis in the developing chick retina. *J. Neurosci.* **17**, 7441–7449 (1997) DOI:10.1523/jneurosci.17-19-07441.1997.

123. Stevens, C. B., Cameron, D. A. & Stenkamp, D. L. Plasticity of photoreceptor-generating retinal progenitors revealed by prolonged retinoic acid exposure. *BMC Dev. Biol.* **11**, (2011) DOI:10.1186/1471-213X-11-51.

124. Emerson, M. M., Surzenko, N., Goetz, J. J., Trimarchi, J. & Cepko, C. L. Otx2 and Onecut1 promote the fates of cone photoreceptors and horizontal cells and repress rod photoreceptors. *Dev. Cell* **26**, 59–72 (2013) DOI:10.1016/j.devcel.2013.06.005.

125. Sapkota, D. *et al.* Onecut1 and Onecut2 redundantly regulate early retinal cell fates during development. *Proc. Natl. Acad. Sci. U. S. A.* **111**, E4086–E4095 (2014) DOI:10.1073/pnas.1405354111.

126. Sorokin S. Centrioles and the formation of rudimentary cilia by fibroblasts and smooth muscle cells. *J. Cell Biol.* **15**, 363–377 (1962) DOI:10.1083/jcb.15.2.363.

127. Nonaka, S. *et al.* Randomization of Left–Right Asymmetry due to Loss of Nodal Cilia Generating Leftward Flow of Extraembryonic Fluid in Mice Lacking KIF3B Motor Protein. *Cell* **95**, 829–837 (1998) DOI:10.1016/S0092-8674(00)81705-5.

128. Satir, P., Guerra, C. & Bell, A. J. Evolution and persistence of the cilium. *Cell Motil. Cytoskeleton* **64**, 906–913 (2007) DOI:10.1002/cm.20238.

129. Hua, K. & Ferland, R. J. Primary cilia proteins: ciliary and extraciliary sites and functions.

Cell. Mol. Life Sci. **75**, 1521–1540 (2018) DOI:10.1007/s00018-017-2740-5.

130. Plotnikova, O. V., Pugacheva, E. N. & Golemis, E. A. Primary cilia and the cell cycle. *Methods Cell Biol.* **94**, 137–160 (2009) DOI:10.1016/S0091-679X(08)94007-3.

131. Nigg, E. A. & Stearns, T. The centrosome cycle: Centriole biogenesis, duplication and inherent asymmetries. *Nature Cell Biology* vol. 13 1154–1160 (2011) DOI:10.1038/ncb2345.

132. Heydeck, W., Fievet, L., Davis, E. E. & Katsanis, N. The complexity of the cilium: spatiotemporal diversity of an ancient organelle. *Curr. Opin. Cell Biol.* **55**, 139–149 (2018) DOI:10.1016/J.CEB.2018.08.001.

133. Nigg, E. A. & Holland, A. J. Once and only once: mechanisms of centriole duplication and their deregulation in disease. *Nat. Rev. Mol. Cell Biol. 2018 195* **19**, 297–312 (2018) DOI:10.1038/nrm.2017.127.

134. Werner, S., Pimenta-Marques, A. & Bettencourt-Dias, M. Maintaining centrosomes and cilia. *J. Cell Sci.* **130**, 3789–3800 (2017) DOI:10.1242/jcs.203505.

135. JM, K., A, M., L, M. & DA, A. Microtubule nucleation by γ-tubulin complexes. *Nat. Rev. Mol. Cell Biol.* **12**, 709–721 (2011) DOI:10.1038/NRM3209.

136. Rehman, I., Gulani, A., Farooq, M. & Simpson, B. Genetics, Mitosis. *StatPearls* (2021).

137. P, L.-G., FG, W. & SS, T. The spindle assembly checkpoint. *Curr. Biol.* **22**, (2012) DOI:10.1016/J.CUB.2012.10.006.

138. Nigg, E. A. Centrosome aberrations: cause or consequence of cancer progression? *Nat. Rev. Cancer 2002 211* **2**, 815–825 (2002) DOI:10.1038/nrc924.

139. Storchova, Z. & Pellman, D. From polyploidy to aneuploidy, genome instability and cancer. *Nat. Rev. Mol. Cell Biol. 2004 51* **5**, 45–54 (2004) DOI:10.1038/nrm1276.

140. Nigg, E. A. Centrosome duplication: of rules and licenses. *Trends Cell Biol.* **17**, 215–221 (2007) DOI:10.1016/J.TCB.2007.03.003.

141. Fry, A. M. & Hames, R. S. The Role of the Centrosome in Cell Cycle Progression. *Centrosomes Dev. Dis.* 143–166 (2005) doi:10.1002/3527603808.CH8 DOI:10.1002/3527603808.CH8.

142. Lacey, K., … P. J.-P. of the & 1999, undefined. Cyclin-dependent kinase control of centrosome duplication. *Natl. Acad Sci.* **96**, 2817–2822 (1999).

143. P, M., J, L., AM, F., J, B. & EA, N. Centrosome duplication in mammalian somatic cells requires E2F and Cdk2-cyclin A. *Nat. Cell Biol.* **1**, 88–93 (1999) DOI:10.1038/10054.

144. EH, H., C, L., EA, T., JL, M. & G, S. Requirement of Cdk2-cyclin E activity for repeated centrosome reproduction in Xenopus egg extracts. *Science* **283**, 851–854 (1999) DOI:10.1126/SCIENCE.283.5403.851.

145. Kawakami, M. *et al.* Polo-like kinase 4 inhibition produces polyploidy and apoptotic death of lung cancers. *Proc. Natl. Acad. Sci.* **115**, 201719760 (2018) DOI:10.1073/pnas.1719760115.

146. Zeng, X., Xu, W. K., Lok, T. M., Ma, H. T. & Poon, R. Y. C. Imbalance of the spindle-assembly checkpoint promotes spindle poison-mediated cytotoxicity with distinct kinetics. *Cell Death Dis.* **10**, 1–15 (2019) DOI:10.1038/s41419-019-1539-8.

147. Tan, F. E. *et al.* Myb promotes centriole amplification and later steps of the multiciliogenesis program. *Development* **140**, 4277–86 (2013) DOI:10.1242/dev.094102.

148. Tachibana, K. e. K., Gonzalez, M. A., Guarguaglini, G., Nigg, E. A. & Laskey, R. A. Depletion of licensing inhibitor geminin causes centrosome overduplication and mitotic defects. *EMBO Rep.* **6**, 1052–1057 (2005) DOI:10.1038/SJ.EMBOR.7400527.

149. Mori, D. *et al.* NDEL1 phosphorylation by Aurora-A kinase is essential for centrosomal maturation, separation, and TACC3 recruitment. *Mol. Cell. Biol.* **27**, 352–67 (2007) DOI:10.1128/MCB.00878-06.

150. Jackman, M., Lindon, C., Nigg, E. A. & Pines, J. Active cyclin B1–Cdk1 first appears on centrosomes in prophase. *Nat. Cell Biol. 2003 52* **5**, 143–148 (2003) DOI:10.1038/ncb918.

151. Tsou, M. F. B. *et al.* Polo Kinase and Separase Regulate the Mitotic Licensing of Centriole Duplication in Human Cells. *Dev. Cell* **17**, 344–354 (2009) DOI:10.1016/J.DEVCEL.2009.07.015.

152. Bettencourt-Dias, M. *et al.* SAK/PLK4 is required for centriole duplication and flagella development. *Curr. Biol.* **15**, 2199–2207 (2005) DOI:10.1016/j.cub.2005.11.042.

153. Leidel, S., Delattre, M., Cerutti, L., biology, K. B.-N. cell & 2005, undefined. SAS-6 defines a protein family required for centrosome duplication in C. elegans and in human cells. *nature.com* **7**, (2005) DOI:10.1038/ncb1220.

154. Habedanck, R., Stierhof, Y. D., Wilkinson, C. J. & Nigg, E. A. The Polo kinase Plk4 functions in centriole duplication. *Nat. Cell Biol.* **7**, 1140–1146 (2005) DOI:10.1038/ncb1320.

155. Gotow, T. & Nishi, T. A new photosensory function for simple photoreceptors, the intrinsically photoresponsive neurons of the sea slug Onchidium. *Frontiers in Cellular Neuroscience* vol. 3 (2009) DOI:10.3389/neuro.03.018.2009.

156. Deretic, D., Schmerl, S., Hargrave, P. A., Arendt, A. & McDowell, J. H. Regulation of sorting and post-Golgi trafficking of rhodopsin by its C-terminal sequence QVS(A)PA. *Proc. Natl. Acad. Sci. U. S. A.* **95**, 10620–5 (1998).

157. Deretic, D. A role for rhodopsin in a signal transduction cascade that regulates membrane trafficking and photoreceptor polarity. *Vision Res.* **46**, 4427–4433 (2006) DOI:10.1016/j.visres.2006.07.028.

158. Pearring, J. N., Salinas, R. Y., Baker, S. A. & Arshavsky, V. Y. Protein sorting, targeting and trafficking in photoreceptor cells. **36**, 24–51 (2013) DOI:10.1016/j.preteyeres.2013.03.002.

159. Deretic, D. *et al.* Rhodopsin C terminus, the site of mutations causing retinal disease, regulates trafficking by binding to ADP-ribosylation factor 4 (ARF4). *Proc. Natl. Acad. Sci. U. S. A.* **102**, 3301–3306 (2005) DOI:10.1073/pnas.0500095102.

160. Khanna, H. Photoreceptor Sensory Cilium: Traversing the Ciliary Gate. *Cells* **4**, 674–686 (2015) DOI:10.3390/cells4040674.

161. Insinna, C. & Besharse, J. C. Intraflagellar transport and the sensory outer segment of vertebrate photoreceptors. *Developmental Dynamics* vol. 237 1982–1992 (2008) DOI:10.1002/dvdy.21554.

162. DE ROBERTIS, E. Electron microscope observations on the submicroscopic organization of the retinal rods. *J. Biophys. Biochem. Cytol.* **2**, 319–330 (1956) DOI:10.1083/jcb.2.3.319.

163. Wong-Riley, M. Energy metabolism of the visual system. *Eye Brain* **2**, 99 (2010) DOI:10.2147/eb.s9078.

164. Pazour, G. J. *et al.* The intraflagellar transport protein, IFT88, is essential for vertebrate photoreceptor assembly and maintenance. **157**, (2002) DOI:10.1083/jcb.200107108.

165. Baker, K. & Beales, P. L. Making sense of cilia in disease: The human ciliopathies. *American Journal of Medical Genetics, Part C: Seminars in Medical Genetics* vol. 151 281–295 (2009) DOI:10.1002/ajmg.c.30231.

166. Roepman, R. & Wolfrum, U. Protein networks and complexes in photoreceptor cilia. *Subcell. Biochem.* **43**, 209–235 (2007) DOI:10.1007/978-1-4020-5943-8_10.

167. Rosenbaum, J. Intraflagellar transport. *Curr. Biol.* **12**, R125 (2002) DOI:10.1016/S0960-9822(02)00703-0.

168. Kanie, T. *et al.* The CEP19-RABL2 GTPase Complex Binds IFT-B to Initiate Intraflagellar Transport at the Ciliary Base. *Dev. Cell* **42**, 22-36.e12 (2017) DOI:10.1016/j.devcel.2017.05.016.

169. Williams, D. S. Transport to the photoreceptor outer segment by myosin VIIa and kinesin II. *Vision Res.* **42**, 455–462 (2002) DOI:10.1016/S0042-6989(01)00228-0.

170. Jiang, L. *et al.* Heterotrimeric Kinesin-2 (KIF3) mediates transition zone and axoneme formation of mouse photoreceptors. *J. Biol. Chem.* **290**, 12765–12778 (2015) DOI:10.1074/jbc.M115.638437.

171. Malicki, J. & Besharse, J. C. Kinesin-2 family motors in the unusual photoreceptor cilium. *Vision Res.* **75**, 33–6 (2012) DOI:10.1016/j.visres.2012.10.008.

172. Crouse, J. A. *et al.* Distinct functions for IFT140 and IFT20 in opsin transport. *Cytoskeleton* **71**, 302–310 (2014) DOI:10.1002/cm.21173.

173. Follit, J. A., Tuft, R. A., Fogarty, K. E. & Pazour, G. J. The intraflagellar transport protein IFT20 is associated with the Golgi complex and is required for cilia assembly. *Mol. Biol. Cell* **17**, 3781–3792 (2006) DOI:10.1091/mbc.E06-02-0133.

174. Hollingsworth, T. J. & Gross, A. K. The severe autosomal dominant retinitis pigmentosa rhodopsin mutant Ter349Glu mislocalizes and induces rapid rod cell death. *J. Biol. Chem.* **288**, 29047–29055 (2013) DOI:10.1074/jbc.M113.495184.

175. Concepcion, F., Mendez, A. & Chen, J. The carboxyl-terminal domain is essential for rhodopsin transport in rod photoreceptors. *Vision Res.* **42**, 417–426 (2002) DOI:10.1016/S0042-6989(01)00195-X.

176. Weil, D. *et al.* The autosomal recessive isolated deafness, DFNB2, and the Usher 1B syndrome are allelic defects of the myosin-VIIA gene. *Nat. Genet.* **16**, 191–193 (1997) DOI:10.1038/ng0697-191.

177. McGee, T. L., Seyedahmadi, B. J., Sweeney, M. O., Dryja, T. P. & Berson, E. L. Novel mutations in the long isoform of the USH2A gene in patients with Usher syndrome type II or non-syndromic retinitis pigmentosa. *J. Med. Genet.* **47**, 499–506 (2010) DOI:10.1136/jmg.2009.075143.

178. Well, D. *et al.* Defective myosin VIIA gene responsible for Usher syndrome type IB. *Nature* **374**, 60–61 (1995) DOI:10.1038/374060a0.

179. Audo, I. *et al.* RP1 and autosomal dominant rod-cone dystrophy: Novel mutations, a review of published variants, and genotype-phenotype correlation. *Hum. Mutat.* **33**, 73–80 (2012) DOI:10.1002/humu.21640.

180. Gao, J. *et al.* Progressive photoreceptor degeneration, outer segment dysplasia, and rhodopsin mislocalization in mice with targeted disruption of the retinitis pigmentosa-1 (Rp1) gene. *Proc. Natl. Acad. Sci. U. S. A.* **99**, 5698–5703 (2002) DOI:10.1073/pnas.042122399.

181. Liu, Q., Lyubarsky, A., Skalet, J. H., Pugh, E. N. & Pierce, E. A. RP1 is required for the correct stacking of outer segment discs. *Investig. Ophthalmol. Vis. Sci.* **44**, 4171–4183 (2003) DOI:10.1167/iovs.03-0410.

182. Liu, Q., Zuo, J. & Pierce, E. A. The retinitis pigmentosa 1 protein is a photoreceptor microtubule- associated protein. *J. Neurosci.* **24**, 6427–6436 (2004) DOI:10.1523/JNEUROSCI.1335-04.2004.

183. Hong, D.-H. *et al.* A retinitis pigmentosa GTPase regulator (RPGR)- deficient mouse model for X-linked retinitis pigmentosa (RP3). *Proc. Natl. Acad. Sci.* **97**, 3649–3654 (2000) DOI:10.1073/pnas.060037497.

184. Mavlyutov, T. A., Zhao, H. & Ferreira, P. A. Species-specific subcellular localization of RPGR and RPGRIP isoforms: Implications for the phenotypic variability of congenital retinopathies among species. *Hum. Mol. Genet.* **11**, 1899–1907 (2002) DOI:10.1093/hmg/11.16.1899.

185. Chang, P., Giddings, T. H., Winey, M. & Stearns, T. ε-Tubulin is required for centriole duplication and microtubule organization. *Nat. Cell Biol.* **5**, 71–76 (2003) DOI:10.1038/ncb900.

186. Boisvieux-Ulrich, E., Lainé, M. C. & Sandoz, D. Cytochalasin D inhibits basal body migration and ciliary elongation in quail oviduct epithelium. *Cell Tissue Res.* **259**, 443–454 (1990) DOI:10.1007/BF01740770.

187. Pan, J., You, Y., Huang, T. & Brody, S. L. RhoA-mediated apical actin enrichment is required for ciliogenesis and promoted by Foxj1. *J. Cell Sci.* **120**, 1868–1876 (2007) DOI:10.1242/jcs.005306.

188. Ramsey, M. & Perkins, B. D. Basal bodies exhibit polarized positioning in zebrafish cone photoreceptors. *J. Comp. Neurol.* **521**, 1803–1816 (2013) DOI:10.1002/cne.23260.

189. Ou, Y. Y. & Rattner, J. B. A subset of centrosomal proteins are arranged in a tubular conformation that is reproduced during centrosome duplication. **115**, (2000) DOI:10.1002/1097-0169(200009)47:1<13::AID-CM2>3.0.CO;2-C.

190. Hehnly, H., Chen, C. T., Powers, C. M., Liu, H. L. & Doxsey, S. The centrosome regulates the Rab11- dependent recycling endosome pathway at appendages of the mother centriole. *Curr. Biol.* **22**, 1944–1950 (2012) DOI:10.1016/j.cub.2012.08.022.

191. Burnicka-Turek, O. *et al.* Cilia gene mutations cause atrioventricular septal defects by multiple mechanisms. *Hum. Mol. Genet.* **25**, 3011–3028 (2016) DOI:10.1093/hmg/ddw155.

192. Trojan, P. *et al.* Centrins in retinal photoreceptor cells: Regulators in the connecting cilium. *Progress in Retinal and Eye Research* vol. 27 237–259 (2008) DOI:10.1016/j.preteyeres.2008.01.003.

193. Dean, S., Moreira-Leite, F., Varga, V. & Gull, K. Cilium transition zone proteome reveals compartmentalization and differential dynamics of ciliopathy complexes. *Proc. Natl. Acad. Sci. U. S. A.* **113**, E5135–E5143 (2016) DOI:10.1073/pnas.1604258113.

194. Williams, C. L. *et al.* MKS and NPHP modules cooperate to establish basal body/transition zone membrane associations and ciliary gate function during ciliogenesis. *J. Cell Biol.* **192**, 1023–1041 (2011) DOI:10.1083/jcb.201012116.

195. Gilula, N. B. & Satir, P. The ciliary necklace a ciliary membrane specialization. *J. Cell Biol.* **53**, 494–509 (1972) DOI:10.1083/jcb.53.2.494.

196. Chih, B. *et al.* A ciliopathy complex at the transition zone protects the cilia as a privileged membrane domain. *Nat. Cell Biol.* **14**, 61–72 (2012) DOI:10.1038/ncb2410.

197. Garcia-Gonzalo, F. R. *et al.* A transition zone complex regulates mammalian ciliogenesis and ciliary membrane composition. *Nat. Genet.* **43**, 776–784 (2011) DOI:10.1038/ng.891.

198. Sang, L. *et al.* Mapping the NPHP-JBTS-MKS protein network reveals ciliopathy disease genes and pathways. *Cell* **145**, 513–528 (2011) DOI:10.1016/j.cell.2011.04.019.

199. Roberson, E. C. *et al.* TMEM231, mutated in orofaciodigital and Meckel syndromes, organizes the ciliary transition zone. *J. Cell Biol.* **209**, 129–142 (2015) DOI:10.1083/jcb.201411087.

200. Shi, X. *et al.* Super-resolution microscopy reveals that disruption of ciliary transition-zone

architecture causes Joubert syndrome. *Nat. Cell Biol.* **19**, 1178–1188 (2017) DOI:10.1038/ncb3599.

201. Jenkins, D. & Hernandez-Hernandez, V. Advances in the understanding of the BBSome complex structure and function. *Res. Rep. Biol.* **6**, 191 (2015) DOI:10.2147/rrb.s65700.

202. Loktev, A. V. *et al.* A BBSome Subunit Links Ciliogenesis, Microtubule Stability, and Acetylation. *Dev. Cell* **15**, 854–865 (2008) DOI:10.1016/j.devcel.2008.11.001.

203. Nachury, M. V. *et al.* A Core Complex of BBS Proteins Cooperates with the GTPase Rab8 to Promote Ciliary Membrane Biogenesis. *Cell* **129**, 1201–1213 (2007) DOI:10.1016/j.cell.2007.03.053.

204. Wei, Q. *et al.* The BBSome controls IFT assembly and turnaround in cilia. *Nat. Cell Biol.* **14**, 950–957 (2012) DOI:10.1038/ncb2560.

205. Lechtreck, K. F. *et al.* The Chlamydomonas reinhardtii BBSome is an IFT cargo required for export of specific signaling proteins from flagella. *J. Cell Biol.* **187**, 1117–1132 (2009) DOI:10.1083/jcb.200909183.

206. Ou, G., Blacque, O. E., Snow, J. J., Leroux, M. R. & Scholey, J. M. Functional coordination of intraflagellar transport motors. *Nature* **436**, 583–587 (2005) DOI:10.1038/nature03818.

207. Pan, X. *et al.* Mechanism of transport of IFT particles in C. elegans cilia by the concerted action of kinesin-II and OSM-3 motors. *J. Cell Biol.* **174**, 1035–1045 (2006) DOI:10.1083/jcb.200606003.

208. Novas, R., Cardenas-Rodriguez, M., Irigoín, F. & Badano, J. L. Bardet-Biedl syndrome: Is it only cilia dysfunction? *FEBS Letters* vol. 589 3479–3491 (2015) DOI:10.1016/j.febslet.2015.07.031.

209. Nachury, M. V. Tandem Affinity Purification of the BBSome, a Critical Regulator of Rab8 in Ciliogenesis. *Methods in Enzymology* vol. 439 501–513 (2008) DOI:10.1016/S0076-6879(07)00434-X.

210. Zhang, D. & Aravind, L. Novel transglutaminase-like peptidase and C2 domains elucidate

the structure, biogenesis and evolution of the ciliary compartment. *Cell Cycle* **11**, 3861–3875 (2012) DOI:10.4161/cc.22068.

211. Álvarez-Satta, M., Castro-Sánchez, S. & Valverde, D. Bardet-Biedl Syndrome as a Chaperonopathy: Dissecting the Major Role of Chaperonin-Like BBS Proteins (BBS6-BBS10-BBS12). *Front. Mol. Biosci.* **4**, 1–7 (2017) DOI:10.3389/fmolb.2017.00055.

212. Smith, T. S. *et al.* Light-dependent phosphorylation of Bardet-Biedl syndrome 5 in photoreceptor cells modulates its interaction with arrestin1. *Cell. Mol. Life Sci.* **70**, 4603–4616 (2013) DOI:10.1007/s00018-013-1403-4.

213. Price, H. P. *et al.* A role for the vesicle-associated tubulin binding protein ARL6 (BBS3) in flagellum extension in Trypanosoma brucei. *Biochim. Biophys. Acta - Mol. Cell Res.* **1823**, 1178–1191 (2012) DOI:10.1016/j.bbamcr.2012.05.007.

214. Zhang, Q. *et al.* Bardet-Biedl syndrome 3 (Bbs3) knockout mouse model reveals common BBS-associated phenotypes and Bbs3 unique phenotypes. *Proc. Natl. Acad. Sci. U. S. A.* **108**, 20678–20683 (2011) DOI:10.1073/pnas.1113220108.

215. Mouraõ, A., Nager, A. R., Nachury, M. V. & Lorentzen, E. Structural basis for membrane targeting of the BBSome by ARL6. *Nat. Struct. Mol. Biol.* **21**, 1035–1041 (2014) DOI:10.1038/nsmb.2920.

216. Kim, J. C. *et al.* MKKS/BBS6, a divergent chaperonin-like protein linked to the obesity disorder Bardet-Biedl syndrome, is a novel centrosomal component required for cytokinesis. *J. Cell Sci.* **118**, 1007–1020 (2005) DOI:10.1242/jcs.01676.

217. Marion, V. *et al.* Transient ciliogenèsis involving Bardet-Biedl syndrome proteins is a fundamental characteristic of adipogenic differentiation. *Proc. Natl. Acad. Sci. U. S. A.* **106**, 1820–1825 (2009) DOI:10.1073/pnas.0812518106.

218. Seo, S. *et al.* BBS6, BBS10, and BBS12 form a complex with CCT/TRiC family chaperonins and mediate BBSome assembly. *Proc. Natl. Acad. Sci. U. S. A.* **107**, (2010) DOI:10.1073/pnas.0910268107.

219. Stoetzel, C. *et al.* Identification of a novel BBS gene (BBS12) highlights the major role of a vertebrate-specific branch of chaperonin-related proteins in Bardet-Biedl syndrome. *Am. J. Hum. Genet.* **80**, 1–11 (2007) DOI:10.1086/510256.

220. Stoetzel, C. *et al.* BBS10 encodes a vertebrate-specific chaperonin-like protein and is a major BBS locus. *Nat. Genet.* **38**, 521–524 (2006) DOI:10.1038/ng1771.

221. Marion, V. *et al.* Exome sequencing identifies mutations in LZTFL1, a bbsome and smoothened trafficking regulator, in a family with bardetebiedl syndrome with situs inversus and insertional polydactyly. *J. Med. Genet.* **49**, 317–321 (2012) DOI:10.1136/jmedgenet-2012-100737.

222. Schaefer, E. *et al.* Mesoaxial polydactyly is a major feature in Bardet-Biedl syndrome patients with LZTFL1 (BBS17) mutations. *Clin. Genet.* **85**, 476–481 (2014) DOI:10.1111/cge.12198.

223. Seo, S. *et al.* A novel protein LZTFL1 regulates ciliary trafficking of the BBSome and smoothened. *PLoS Genet.* **7**, (2011) DOI:10.1371/journal.pgen.1002358.

224. Chen, J. *et al.* Molecular analysis of Bardet-Biedl syndrome families: Report of 21 novel mutations in 10 genes. *Investig. Ophthalmol. Vis. Sci.* **52**, 5317–5324 (2011) DOI:10.1167/iovs.11-7554.

225. Coppieters, F., Lefever, S., Leroy, B. P. & De Baere, E. CEP290, a gene with many faces: Mutation overview and presentation of CEP290base. *Hum. Mutat.* **31**, 1097–1108 (2010) DOI:10.1002/humu.21337.

226. Pereiro, I. *et al.* New mutations in BBS genes in small consanguineous families with Bardet-Biedl syndrome: detection of candidate regions by homozygosity mapping. *Mol. Vis.* **16**, 137–43 (2010).

227. Rachel, R. A., Li, T. & Swaroop, A. Photoreceptor sensory cilia and ciliopathies: Focus on CEP290, RPGR and their interacting proteins. *Cilia* **1**, 1–15 (2012) DOI:10.1186/2046-2530-1-22.

228. Klinger, M. *et al.* The novel centriolar satellite protein SSX2IP targets Cep290 to the ciliary transition zone. *Mol. Biol. Cell* **25**, 495–507 (2014) DOI:10.1091/mbc.E13-09-0526.

229. Kim, K., Lee, K. & Rhee, K. CEP90 Is Required for the Assembly and Centrosomal Accumulation of Centriolar Satellites, Which Is Essential for Primary Cilia Formation. *PLoS One* **7**, e48196 (2012) DOI:10.1371/journal.pone.0048196.

230. Garcia-Gonzalo, F. R. & Reiter, J. F. Scoring a backstage pass: Mechanisms of ciliogenesis and ciliary access. *J. Cell Biol.* **197**, 697–709 (2012) DOI:10.1083/jcb.201111146.

231. Reiter, J. F., Blacque, O. E. & Leroux, M. R. The base of the cilium: roles for transition fibres and the transition zone in ciliary formation, maintenance and compartmentalization. *EMBO Rep.* **13**, 608–18 (2012) DOI:10.1038/embor.2012.73.

232. Hopp, K. *et al.* B9d1 is revealed as a novel Meckel syndrome (MKS) gene by targeted exon-enriched next-generation sequencing and deletion analysis. *Hum. Mol. Genet.* **20**, 2524–2534 (2011) DOI:10.1093/hmg/ddr151.

233. Weatherbee, S. D., Niswander, L. A. & Anderson, K. V. A mouse model for Meckel syndrome reveals Mks1 is required for ciliogenesis and Hedgehog signaling. *Hum. Mol. Genet.* **18**, 4565–4575 (2009) DOI:10.1093/hmg/ddp422.

234. Leitch, C. C. *et al.* Hypomorphic mutations in syndromic encephalocele genes are associated with Bardet-Biedl syndrome. *Nat. Genet.* **40**, 443–448 (2008) DOI:10.1038/ng.97.

235. Smith, U. M. *et al.* The transmembrane protein meckelin (MKS3) is mutated in Meckel-Gruber syndrome and the wpk rat. *Nat. Genet.* **38**, 191–196 (2006) DOI:10.1038/ng1713.

236. Dawe, H. R. *et al.* Nesprin-2 interacts with meckelin and mediates ciliogenesis via remodelling of the actin cytoskeleton. *J. Cell Sci.* **122**, 2716–2726 (2009) DOI:10.1242/jcs.043794.

237. Hildebrandt, F., Benzing, T. & Katsanis, N. Ciliopathies. *New England Journal of Medicine* vol. 364 1533–1543 (2011) DOI:10.1056/NEJMra1010172.

238. Wallingford, J. B. & Mitchell, B. Strange as it may seem: The many links between Wnt signaling, planar cell polarity, and cilia. *Genes and Development* vol. 25 201–213 (2011) DOI:10.1101/gad.2008011.

239. Adams, M. *et al.* A meckelin-filamin A interaction mediates ciliogenesis. *Hum. Mol. Genet.* **21**, 1272–86 (2012) DOI:10.1093/hmg/ddr557.

240. Gupta, G. D. *et al.* A Dynamic Protein Interaction Landscape of the Human Centrosome-Cilium Interface. *Cell* **163**, 1484–99 (2015) DOI:10.1016/j.cell.2015.10.065.

241. Bergmann, C. *et al.* Loss of Nephrocystin-3 Function Can Cause Embryonic Lethality, Meckel-Gruber-like Syndrome, Situs Inversus, and Renal-Hepatic-Pancreatic Dysplasia. *Am. J. Hum. Genet.* **82**, 959–970 (2008) DOI:10.1016/j.ajhg.2008.02.017.

242. Delous, M. *et al.* The ciliary gene RPGRIP1L is mutated in cerebello-oculo-renal syndrome (Joubert syndrome type B) and Meckel syndrome. *Nat. Genet.* **39**, 875–881 (2007) DOI:10.1038/ng2039.

243. Mollet, G. *et al.* Characterization of the nephrocystin/nephrocystin-4 complex and subcellular localization of nephrocystin-4 to primary cilia and centrosomes. *Hum. Mol. Genet.* **14**, 645–656 (2005) DOI:10.1093/hmg/ddi061.

244. Olbrich, H. *et al.* Mutations in a novel gene, NPHP3, cause adolescent nephronophthisis, tapeto-retinal degeneration and hepatic fibrosis. *Nat. Genet.* **34**, 455–459 (2003) DOI:10.1038/ng1216.

245. Omran, H. NPHP proteins: Gatekeepers of the ciliary compartment. *Journal of Cell Biology* vol. 190 715–717 (2010) DOI:10.1083/jcb.201008080.

246. Lin, H., Guo, S. & Dutcher, S. K. RPGRIP1L helps to establish the ciliary gate for entry of proteins. *J. Cell Sci.* **131**, (2018) DOI:10.1242/jcs.220905.

247. Murga-Zamalloa, C. A., Desai, N. J., Hildebrandt, F. & Khanna, H. Interaction of ciliary disease protein retinitis pigmentosa GTPase regulator with nephronophthisis-associated proteins in mammalian retinas. *Mol. Vis.* **16**, 1373–1381 (2010).

248. Remans, K., Bü, M., Vetter, I. R. & Wittinghofer, A. C2 Domains as Protein-Protein Interaction Modules in the Ciliary Transition Zone. *CellReports* **8**, 1–9 (2014) DOI:10.1016/j.celrep.2014.05.049.

249. Jensen, V. L. *et al.* Formation of the transition zone by Mks5/Rpgrip1L establishes a ciliary zone of exclusion (CIZE) that compartmentalises ciliary signalling proteins and controls PIP 2 ciliary abundance . *EMBO J.* **34**, 2537–2556 (2015) DOI:10.15252/embj.201488044.

250. Dowdle, W. E. *et al.* Disruption of a ciliary B9 protein complex causes meckel syndrome. *Am. J. Hum. Genet.* **89**, 94–110 (2011) DOI:10.1016/j.ajhg.2011.06.003.

251. Coutton, C. *et al.* Mutations in CFAP43 and CFAP44 cause male infertility and flagellum defects in Trypanosoma and human. *Nat. Commun.* **9**, 1–18 (2018) DOI:10.1038/s41467-017-02792-7.

252. HUGO. Cilia and flagella associated (CFAP) Gene Family | HUGO Gene Nomenclature Committee. https://www.genenames.org/cgi-bin/genefamilies/set/1491 (2019).

253. McKenzie, C. W. *et al.* CFAP54 is required for proper ciliary motility and assembly of the central pair apparatus in mice. *Mol. Biol. Cell* **26**, 3140–3149 (2015) DOI:10.1091/mbc.E15-02-0121.

254. Sironen, A., Shoemark, A., Patel, M., Loebinger, M. R. & Mitchison, H. M. Sperm defects in primary ciliary dyskinesia and related causes of male infertility. *Cellular and Molecular Life Sciences* vol. 77 2029–2048 (2020) DOI:10.1007/s00018-019-03389-7.

255. Ware, S. M., Gunay-Aygun, M. & Hildebrandt, F. Spectrum of clinical diseases caused by disorders of primary cilia. in *Proceedings of the American Thoracic Society* vol. 8 444–450 (2011). DOI:10.1513/pats.201103-025SD.

256. Duquesnoy, P. *et al.* Loss-of-Function Mutations in the Human Ortholog of Chlamydomonas reinhardtii ODA7 Disrupt Dynein Arm Assembly and Cause Primary Ciliary Dyskinesia. *Am. J. Hum. Genet.* **85**, 890–896 (2009) DOI:10.1016/j.ajhg.2009.11.008.

257. Höben, I. M. *et al.* Mutations in C11orf70 Cause Primary Ciliary Dyskinesia with

Randomization of Left/Right Body Asymmetry Due to Defects of Outer and Inner Dynein Arms. *Am. J. Hum. Genet.* **102**, 973–984 (2018) DOI:10.1016/j.ajhg.2018.03.025.

258. Jaffe, K. M. *et al.* C21orf59/kurly Controls Both Cilia Motility and Polarization. *Cell Rep.* **14**, 1841–1849 (2016) DOI:10.1016/j.celrep.2016.01.069.

259. Thomas, L. *et al.* TTC12 Loss-of-Function Mutations Cause Primary Ciliary Dyskinesia and Unveil Distinct Dynein Assembly Mechanisms in Motile Cilia Versus Flagella. *Am. J. Hum. Genet.* **106**, 153–169 (2020) DOI:10.1016/j.ajhg.2019.12.010.

260. Li, K. *et al.* Drosophila centrosomin protein is required for male meiosis and assembly of the flagellar axoneme. *J. Cell Biol.* **141**, 455–467 (1998) DOI:10.1083/jcb.141.2.455.

261. Suga, A. *et al.* Identification of novel mutations in the LRR-Cap domain of C21orf2 in Japanese patients with retinitis pigmentosa and cone–rod dystrophy. *Investig. Ophthalmol. Vis. Sci.* **57**, 4255–4263 (2016) DOI:10.1167/iovs.16-19450.

262. Gregory-Evans, K. & Bhattacharya, S. S. Genetic blindness: Current concepts in the pathogenesis of human outer retinal dystrophies. *Trends in Genetics* vol. 14 103–108 (1998) DOI:10.1016/S0168-9525(98)01402-4.

263. Aboshiha, J., Dubis, A. M., Carroll, J., Hardcastle, A. J. & Michaelides, M. The cone dysfunction syndromes. *Br. J. Ophthalmol.* **100**, 115–21 (2016) DOI:10.1136/bjophthalmol-2014-306505.

264. Nash, B. M., Wright, D. C., Grigg, J. R., Bennetts, B. & Jamieson, R. V. Retinal dystrophies, genomic applications in diagnosis and prospects for therapy. *Transl. Pediatr.* **4**, 139–13963 (2015) DOI:10.3978/j.issn.2224-4336.2015.04.03.

265. Michaelides, M., Hardcastle, A. J., Hunt, D. M. & Moore, A. T. Progressive Cone and Cone-Rod Dystrophies: Phenotypes and Underlying Molecular Genetic Basis. *Surv. Ophthalmol.* **51**, 232–258 (2006) DOI:10.1016/J.SURVOPHTHAL.2006.02.007.

266. Kiel, C., Lastrucci, C., Luthert, P. J. & Serrano, L. Simple and complex retinal dystrophies are associated with profoundly different disease networks. *Sci. Rep.* **7**, (2017)

DOI:10.1038/srep41835.

267. Sadagopan, K. A. Practical approach to syndromic pediatric retinal dystrophies. *Current Opinion in Ophthalmology* vol. 28 416–429 (2017) DOI:10.1097/ICU.0000000000000404.

268. Werdich, X. Q., Place, E. M. & Pierce, E. A. Systemic diseases associated with retinal dystrophies. *Semin. Ophthalmol.* **29**, 319–28 (2014) DOI:10.3109/08820538.2014.959202.

269. Suspitsin, E. N. & Imyanitov, E. N. Bardet-Biedl Syndrome. *Molecular Syndromology* vol. 7 62–71 (2016) DOI:10.1159/000445491.

270. Tsang, S. H., Aycinena, A. R. P. & Sharma, T. Ciliopathy: Usher syndrome. in *Advances in Experimental Medicine and Biology* vol. 1085 167–170 (Springer New York LLC, 2018). DOI:10.1007/978-3-319-95046-4_32.

271. Wright, A. F., Chakarova, C. F., Abd El-Aziz, M. M. & Bhattacharya, S. S. Photoreceptor degeneration: genetic and mechanistic dissection of a complex trait. *Nat. Rev. Genet.* **11**, 273–284 (2010) DOI:10.1038/nrg2717.

272. Hamel, C. P. Cone rod dystrophies. *Orphanet J. Rare Dis.* **2**, 7 (2007) DOI:10.1186/1750-1172-2-7.

273. Moore, A. T. Cone and cone-rod dystrophies. *J. Med. Genet.* **29**, 289–290 (1992).

274. den Hollander, A. I., Roepman, R., Koenekoop, R. K. & Cremers, F. P. M. Leber congenital amaurosis: Genes, proteins and disease mechanisms. *Progress in Retinal and Eye Research* vol. 27 391–419 (2008) DOI:10.1016/j.preteyeres.2008.05.003.

275. Haider, N. B., Cruz, N. M., Allocca, M. & Yuan, J. Pathobiology of the Outer Retina: Genetic and Nongenetic Causes of Disease. in *Pathobiology of Human Disease: A Dynamic Encyclopedia of Disease Mechanisms* 2084–2114 (Elsevier Inc., 2014). doi:10.1016/B978-0-12-386456-7.04706-7 DOI:10.1016/B978-0-12-386456-7.04706-7.

276. Estrada-Cuzcano, A., Roepman, R., Cremers, F. P. M., Hollander, A. I. Den & Mans, D. A. Non-syndromic retinal ciliopathies: Translating gene discovery into therapy. *Hum. Mol. Genet.* **21**, (2012) DOI:10.1093/hmg/dds298.

277. Thompson, J. A., De Roach, J. N., McLaren, T. L. & Lamey, T. M. A mini-review: Leber congenital amaurosis: Identification of disease-causing variants and personalised therapies. in *Advances in Experimental Medicine and Biology* vol. 1074 265–271 (Springer New York LLC, 2018). DOI:10.1007/978-3-319-75402-4_32.

278. Den Hollander, A. I. *et al.* Mutations in the CEP290 (NPHP6) gene are a frequent cause of leber congenital amaurosis. *Am. J. Hum. Genet.* **79**, 556–561 (2006) DOI:10.1086/507318.

279. Morimura, H. *et al.* Mutations in the RPE65 gene in patients with autosomal recessive retinitis pigmentosa or Leber congenital amaurosis. *Proc. Natl. Acad. Sci. U. S. A.* **95**, 3088–3093 (1998) DOI:10.1073/pnas.95.6.3088.

280. Berger, W., Kloeckener-Gruissem, B. & Neidhardt, J. The molecular basis of human retinal and vitreoretinal diseases. *Progress in Retinal and Eye Research* vol. 29 335–375 (2010) DOI:10.1016/j.preteyeres.2010.03.004.

281. van Huet, R. A. C. *et al.* Clinical characteristics of rod and cone photoreceptor dystrophies in patients with mutations in the C8orf37 gene. *Investig. Ophthalmol. Vis. Sci.* **54**, 4683–4690 (2013) DOI:10.1167/iovs.12-11439.

282. Daiger, S. P., Bowne, S. J. & Sullivan, L. S. Perspective on genes and mutations causing retinitis pigmentosa. *Arch. Ophthalmol. (Chicago, Ill. 1960)* **125**, 151–158 (2007) DOI:10.1001/archopht.125.2.151.

283. Hartong, D. T., Berson, E. L. & Dryja, T. P. Retinitis pigmentosa. *Lancet* vol. 368 1795–1809 (2006) DOI:10.1016/S0140-6736(06)69740-7.

284. Chang, S., Vaccarella, L., Olatunji, S., Cebulla, C. & Christoforidis, J. Diagnostic Challenges in Retinitis Pigmentosa: Genotypic Multiplicity and Phenotypic Variability. *Curr. Genomics* **12**, 267–275 (2011) DOI:10.2174/138920211795860116.

285. Bertelsen, M., Jensen, H., Bregnhøj, J. F. & Rosenberg, T. Prevalence of Generalized Retinal Dystrophy in Denmark. *Ophthalmic Epidemiol.* **21**, 217–223 (2014) DOI:10.3109/09286586.2014.929710.

286. Hamel, C. Retinitis pigmentosa. *Orphanet Journal of Rare Diseases* vol. 1 (2006) DOI:10.1186/1750-1172-1-40.

287. Parmeggiani, F. *et al.* Retinitis Pigmentosa: Genes and Disease Mechanisms. *Curr. Genomics* **12**, 238–249 (2011) DOI:10.2174/138920211795860107.

288. Silva, R. S., Salles, M. V., Motta, F. L. & Sallum, J. M. F. Retinitis Pigmentosa Due to Rp1 Biallelic Variants. *Sci. Rep.* **10**, 1–6 (2020) DOI:10.1038/s41598-020-58243-9.

289. Takahashi, V. K. L. *et al.* Comparison of structural progression between ciliopathy and non-ciliopathy associated with autosomal recessive retinitis pigmentosa. *Orphanet J. Rare Dis.* **14**, 187 (2019) DOI:10.1186/s13023-019-1163-9.

290. Al-khersan, H. *et al.* A novel MERTK mutation causing retinitis pigmentosa. *Graefe's Arch. Clin. Exp. Ophthalmol.* **255**, 1613–1619 (2017) DOI:10.1007/s00417-017-3679-9.

291. Sultan, N. *et al.* A novel mutation in RDH5 gene causes retinitis pigmentosa in consanguineous Pakistani family. *Genes and Genomics* **40**, 553–559 (2018) DOI:10.1007/s13258-018-0657-5.

292. Sweeney, M. O., McGee, T. L., Berson, E. L. & Dryja, T. P. Low prevalence of lecithin retinol acyltransferase mutations in patients with Leber congenital amaurosis and autosomal recessive retinitis pigmentosa. *Mol. Vis.* **13**, 588–93 (2007).

293. Liu, M. M. & Zack, D. J. Alternative splicing and retinal degeneration. *Clin. Genet.* **84**, 142–149 (2013) DOI:10.1111/cge.12181.

294. Valdés-Sánchez, L. *et al.* Retinal pigment epithelium degeneration caused by aggregation of PRPF31 and the role of HSP70 family of proteins. *Mol. Med.* **26**, (2019) DOI:10.1186/s10020-019-0124-z.

295. Zhong, Z. *et al.* Two novel mutations in PRPF3 causing autosomal dominant retinitis pigmentosa. *Sci. Rep.* **6**, (2016) DOI:10.1038/srep37840.

296. Megaw, R. & Hurd, T. W. Photoreceptor actin dysregulation in syndromic and non-syndromic retinitis pigmentosa. *Biochemical Society Transactions* vol. 46 1463–1473 (2018)

DOI:10.1042/BST20180138.

297. Priya, S., Nampoothiri, S., Sen, P. & Sripriya, S. Bardet-Biedl syndrome: Genetics, molecular pathophysiology, and disease management. *Indian Journal of Ophthalmology* vol. 64 620–627 (2016) DOI:10.4103/0301-4738.194328.

298. Mathur, P. & Yang, J. Usher syndrome: Hearing loss, retinal degeneration and associated abnormalities. *Biochimica et Biophysica Acta - Molecular Basis of Disease* vol. 1852 406–420 (2015) DOI:10.1016/j.bbadis.2014.11.020.

299. Mockel, A. *et al.* Retinal dystrophy in Bardet-Biedl syndrome and related syndromic ciliopathies. *Prog. Retin. Eye Res.* **30**, 258–274 (2011) DOI:10.1016/j.preteyeres.2011.03.001.

300. Chiang, J. P. W. & Trzupek, K. The current status of molecular diagnosis of inherited retinal dystrophies. *Current Opinion in Ophthalmology* vol. 26 346–351 (2015) DOI:10.1097/ICU.0000000000000185.

301. Allikmets, R. *et al.* A photoreceptor cell-specific ATP-binding transporter gene (ABCR) is mutated in recessive Stargardt macular dystrophy. *Nat. Genet.* **15**, 236–246 (1997) DOI:10.1038/ng0397-236.

302. Lambertus, S. *et al.* Early-onset stargardt disease: Phenotypic and genotypic characteristics. *Ophthalmology* **122**, 335–344 (2015) DOI:10.1016/j.ophtha.2014.08.032.

303. Tanna, P., Strauss, R. W., Fujinami, K. & Michaelides, M. Stargardt disease: Clinical features, molecular genetics, animal models and therapeutic options. *British Journal of Ophthalmology* vol. 101 25–30 (2017) DOI:10.1136/bjophthalmol-2016-308823.

304. Haji Abdollahi, S. & Hirose, T. Stargardt-fundus flavimaculatus: Recent advancements and treatment. *Semin. Ophthalmol.* **28**, 372–376 (2013) DOI:10.3109/08820538.2013.825286.

305. Telegina, D. V., Kozhevnikova, O. S. & Kolosova, N. G. Molecular mechanisms of cell death in retina during development of age-related macular degeneration. *Adv. Gerontol.* **7**, 17–24 (2017) DOI:10.1134/S2079057017010155.

306. National Eye Institute. Age-Related Macular Degeneration (AMD) Data and Statistics | National Eye Institute. *National Eye Institute* https://www.nei.nih.gov/learn-about-eye-health/resources-for-health-educators/eye-health-data-and-statistics/age-related-macular-degeneration-amd-data-and-statistics (2019).

307. Wong, W. L. *et al.* Global prevalence of age-related macular degeneration and disease burden projection for 2020 and 2040: A systematic review and meta-analysis. *Lancet Glob. Heal.* **2**, e106–e116 (2014) DOI:10.1016/S2214-109X(13)70145-1.

308. Pool, F. M., Kiel, C., Serrano, L. & Luthert, P. J. Repository of proposed pathways and protein–protein interaction networks in age-related macular degeneration. *npj Aging Mech. Dis.* **6**, 1–11 (2020) DOI:10.1038/s41514-019-0039-5.

309. Ardeljan, D. & Chan, C. C. Aging is not a disease: Distinguishing age-related macular degeneration from aging. *Progress in Retinal and Eye Research* vol. 37 68–89 (2013) DOI:10.1016/j.preteyeres.2013.07.003.

310. Tomany, S. C. *et al.* Risk factors for incident age-related macular degeneration: Pooled findings from 3 continents. *Ophthalmology* **111**, 1280–1287 (2004) DOI:10.1016/j.ophtha.2003.11.010.

311. Cheung, C. M. G. & Wong, T. Y. Is age-related macular degeneration a manifestation of systemic disease? New prospects for early intervention and treatment. *J. Intern. Med.* **276**, 140–153 (2014) DOI:10.1111/joim.12227.

312. Cho, B. J. *et al.* Epidemiological association between systemic diseases and age-related macular degeneration: The Korea national health and nutrition examination survey 2008-2011. *Investig. Ophthalmol. Vis. Sci.* **55**, 4430–4437 (2014) DOI:10.1167/iovs.14-14379.

313. Roy, M. *et al.* Retinal Findings in Bardet-Biedl Syndrome. *J. ASEAN Fed. Endocr. Soc.* **29**, 194–196 (2014) DOI:10.15605/jafes.029.02.15.

314. Chaitankar, V. *et al.* Next generation sequencing technology and genomewide data analysis: Perspectives for retinal research. *Progress in Retinal and Eye Research* vol. 55 1–31 (2016) DOI:10.1016/j.preteyeres.2016.06.001.

315. Roberts, L. *et al.* Molecular diagnosis of inherited retinal diseases in indigenous African populations by whole-exome sequencing. *Investig. Ophthalmol. Vis. Sci.* **57**, 6374–6381 (2016) DOI:10.1167/iovs.16-19785.

316. Den Hollander, A. I., Black, A., Bennett, J. & Cremers, F. P. M. Lighting a candle in the dark: Advances in genetics and gene therapy of recessive retinal dystrophies. *Journal of Clinical Investigation* vol. 120 3042–3053 (2010) DOI:10.1172/JCI42258.

317. Sawyer, S. L. *et al.* Utility of whole-exome sequencing for those near the end of the diagnostic odyssey: Time to address gaps in care. *Clinical Genetics* vol. 89 275–284 (2016) DOI:10.1111/cge.12654.

318. Daiger, S. P., Sullivan, L. S. & Bowne, S. J. Genes and mutations causing retinitis pigmentosa. *Clinical Genetics* vol. 84 132–141 (2013) DOI:10.1111/cge.12203.

319. Bujakowska, K. M., Liu, Q. & Pierce, E. A. Photoreceptor cilia and retinal ciliopathies. *Cold Spring Harb. Perspect. Biol.* **9**, (2017) DOI:10.1101/cshperspect.a028274.

320. Murphy, D., Singh, R., Kolandaivelu, S., Ramamurthy, V. & Stoilov, P. Alternative Splicing Shapes the Phenotype of a Mutation in BBS8 To Cause Nonsyndromic Retinitis Pigmentosa . *Mol. Cell. Biol.* **35**, 1860–1870 (2015) DOI:10.1128/mcb.00040-15.

321. May-Simera, H. L. & Kelley, M. W. Cilia, Wnt signaling, and the cytoskeleton. *Cilia* **1**, 7 (2012) DOI:10.1186/2046-2530-1-7.

322. R. Sparrrow, J., Hicks, D. & P. Hamel, C. The Retinal Pigment Epithelium in Health and Disease. *Curr. Mol. Med.* **10**, 802–823 (2010) DOI:10.2174/156652410793937813.

323. Kunchithapautham, K. & Rohrer, B. Apoptosis and autophagy in photoreceptors exposed to oxidative stress. *Autophagy* **3**, 433–441 (2007) DOI:10.4161/auto.4294.

324. Tanito, M. *et al.* Identification of 4-hydroxynonenal-modified retinal proteins induced by photooxidative stress prior to retinal degeneration. *Free Radic. Biol. Med.* **41**, 1847–1859 (2006) DOI:10.1016/J.FREERADBIOMED.2006.09.012.

325. Beatty, S., Koh, H. H., Phil, M., Henson, D. & Boulton, M. The role of oxidative stress in the

pathogenesis of age-related macular degeneration. *Surv. Ophthalmol.* **45**, 115–134 (2000) DOI:10.1016/S0039-6257(00)00140-5.

326. Bellezza, I. Oxidative stress in age-related macular degeneration: NRF2 as therapeutic target. *Front. Pharmacol.* **9**, (2018) DOI:10.3389/fphar.2018.01280.

327. Cortina, M. S., Gordon, W. C., Lukiw, W. J. & Bazan, N. G. Light-induced photoreceptor damage triggers DNA repair: Differential fate of rods and cones. in *Advances in Experimental Medicine and Biology* vol. 533 229–240 (Springer, Boston, MA, 2003). DOI:10.1007/978-1-4615-0067-4_29.

328. Domènech, E. B. & Marfany, G. The relevance of oxidative stress in the pathogenesis and therapy of retinal dystrophies. *Antioxidants* vol. 9 (2020) DOI:10.3390/antiox9040347.

329. Masuda, T., Shimazawa, M. & Hara, H. Retinal Diseases Associated with Oxidative Stress and the Effects of a Free Radical Scavenger (Edaravone). *Oxidative Medicine and Cellular Longevity* vol. 2017 (2017) DOI:10.1155/2017/9208489.

330. Specht, S., Leffak, M., Darrow, R. M. & Organisciak, D. T. Damage to rat retinal DNA induced in vivo by visible light. *Photochem. Photobiol.* **69**, 91–98 (1999) DOI:10.1111/j.1751-1097.1999.tb05311.x.

331. Vindigni, A. & Gonzalo, S. The two faces of DNA repair: disease and therapy. *Mo. Med.* **110**, 314–9 (2013).

332. Fu, D., Calvo, J. A. & Samson, L. D. Balancing repair and tolerance of DNA damage caused by alkylating agents. *Nature Reviews Cancer* vol. 12 104–120 (2012) DOI:10.1038/nrc3185.

333. Allocca, M., Corrigan, J. J., Mazumder, A., Fake, K. R. & Samson, L. D. Inflammation, necrosis, and the kinase RIP3 are key mediators of AAG-dependent alkylation-induced retinal degeneration. *Sci. Signal.* **12**, (2019) DOI:10.1126/scisignal.aau9216.

334. Meira, L. B. *et al.* Aag-initiated base excision repair drives alkylation-induced retinal degeneration in mice. *Proc. Natl. Acad. Sci. U. S. A.* **106**, 888–893 (2009) DOI:10.1073/pnas.0807030106.

335. Kosmaoglou, M., Schwarz, N., Bett, J. S. & Cheetham, M. E. Molecular chaperones and photoreceptor function. *Progress in Retinal and Eye Research* vol. 27 434–449 (2008) DOI:10.1016/j.preteyeres.2008.03.001.

336. Smith, H. L., Li, W. & Cheetham, M. E. Molecular chaperones and neuronal proteostasis. *Semin. Cell Dev. Biol.* **40**, 142–52 (2015) DOI:10.1016/j.semcdb.2015.03.003.

337. Behnen, P. *et al.* A Small Chaperone Improves Folding and Routing of Rhodopsin Mutants Linked to Inherited Blindness. (2018) doi:10.1016/j.isci.2018.05.001 DOI:10.1016/j.isci.2018.05.001.

338. Ferreira, P. A., Nakayama, T. A., Pak, W. L. & Travis, G. H. Cyclophilin-related protein RanBP2 acts as chaperone for red/green opsin. *Nature* **383**, 637–640 (1996) DOI:10.1038/383637a0.

339. Fort, P. E. & Lampi, K. J. New focus on alpha-crystallins in retinal neurodegenerative diseases. *Exp. Eye Res.* **92**, 98–103 (2011) DOI:10.1016/J.EXER.2010.11.008.

340. Wistow, G. The human crystallin gene families. *Hum. Genomics* **6**, 26 (2012) DOI:10.1186/1479-7364-6-26.

341. Xi, J. & Kern, T. S. A comprehensive analysis of the expression of crystallins in mouse retina. (2003).

342. Yaung, J. *et al.* alpha-Crystallin distribution in retinal pigment epithelium and effect of gene knockouts on sensitivity to oxidative stress. *Mol. Vis.* **13**, 566–77 (2007) DOI:v13/a61 [pii].

343. Chapple, J. P. *et al.* Unfolding retinal dystrophies: A role for molecular chaperones? *Trends in Molecular Medicine* vol. 7 414–421 (2001) DOI:10.1016/S1471-4914(01)02103-7.

344. Chapple, J. P. & Cheetham, M. E. The chaperone environment at the cytoplasmic face of the endoplasmic reticulum can modulate rhodopsin processing and inclusion formation. *J. Biol. Chem.* **278**, 19087–19094 (2003) DOI:10.1074/jbc.M212349200.

345. Kosmaoglou, M., Novoselova, T. V. & Cheetham, M. E. The Role of Chaperones and Co-Chaperones in Retinal Degenerative Diseases. in *Heat Shock Proteins and the Brain:*

Implications for Neurodegenerative Diseases and Neuroprotection 109–123 (Springer Netherlands, 2008). doi:10.1007/978-1-4020-8231-3_5 DOI:10.1007/978-1-4020-8231-3_5.

346. Hirayama, S. *et al.* MKKS is a centrosome-shuttling protein degraded by disease-causing mutations via CHIP-mediated ubiquitination. *Mol. Biol. Cell* **19**, 899–911 (2008) DOI:10.1091/mbc.E07-07-0631.

347. Ross, A. J. *et al.* Disruption of Bardet-Biedl syndrome ciliary proteins perturbs planar cell polarity in vertebrates. *Nat. Genet.* **37**, 1135–1140 (2005) DOI:10.1038/ng1644.

348. Slavotinek, A. M. *et al.* Mutations in MKKS cause Bardet-Biedl syndrome. *Nat. Genet.* **26**, 15–16 (2000) DOI:10.1038/79116.

349. Liu, X. *et al.* AIPL1, the protein that is defective in Leber congenital amaurosis, is essential for the biosynthesis of retinal rod cGMP phosphodiesterase. *Proc. Natl. Acad. Sci. U. S. A.* **101**, 13903–13908 (2004) DOI:10.1073/pnas.0405160101.

350. Ramamurthy, V. *et al.* AIPL1, a protein implicated in Leber's congenital amaurosis, interacts with and aids in processing of farnesylated proteins. *Proc. Natl. Acad. Sci. U. S. A.* **100**, 12630–12635 (2003) DOI:10.1073/pnas.2134194100.

351. Sohocki, M. M. *et al.* Mutations in a new photoreceptor-pineal gene on 17p cause Leber congenital amaurosis. *Nat. Genet.* **24**, 79–83 (2000) DOI:10.1038/71732.

352. Bartolini, F. *et al.* Functional Overlap between Retinitis Pigmentosa 2 Protein and the Tubulin-specific Chaperone Cofactor C. *J. Biol. Chem.* **277**, 14629–14634 (2002) DOI:10.1074/jbc.M200128200.

353. Hardcastle, A. J. *et al.* Mutations in the RP2 gene cause disease in 10% of families with familial X-linked retinitis pigmentosa assessed in this study [2]. *American Journal of Human Genetics* vol. 64 1210–1215 (1999) DOI:10.1086/302325.

354. Rosenberg, T., Schwahn, U., Feil, S. & Berger, W. Genotype-phenotype correlation in X-linked retinitis pigmentosa 2 (RP2). *Ophthalmic Genet.* **20**, 161–172 (1999)

DOI:10.1076/opge.20.3.161.2278.

355. Han, Z., Conley, S. M. & Naash, M. I. Gene therapy for stargardt disease associated with ABCA4 gene. *Adv. Exp. Med. Biol.* **801**, 719–724 (2014) DOI:10.1007/978-1-4614-3209-8_90.

356. Sun, D. *et al.* Non-viral Gene Therapy for Stargardt Disease with ECO/pRHO-ABCA4 Self-Assembled Nanoparticles. *Mol. Ther.* **28**, 293–303 (2019) DOI:10.1016/j.ymthe.2019.09.010.

357. Poprzeczko, M. *et al.* Rare Human Diseases: Model Organisms in Deciphering the Molecular Basis of Primary Ciliary Dyskinesia. *Cells* **8**, 1614 (2019) DOI:10.3390/cells8121614.

358. Budny, B. *et al.* A novel X-linked recessive mental retardation syndrome comprising macrocephaly and ciliary dysfunction is allelic to oral-facial-digital type I syndrome. *Hum. Genet.* **120**, 171–178 (2006) DOI:10.1007/s00439-006-0210-5.

359. Moore, A. *et al.* RPGR is mutated in patients with a complex X linked phenotype combining primary ciliary dyskinesia and retinitis pigmentosa. *J. Med. Genet.* **43**, 326–333 (2006) DOI:10.1136/jmg.2005.034868.

360. Reiter, J. F. & Leroux, M. R. Genes and molecular pathways underpinning ciliopathies. *Nat. Rev. Mol. Cell Biol.* **18**, 533–547 (2017) DOI:10.1038/nrm.2017.60.

361. Wheway, G. *et al.* Opportunities and challenges for molecular understanding of ciliopathies–the 100,000 genomes project. *Frontiers in Genetics* vol. 10 127 (2019) DOI:10.3389/fgene.2019.00127.

362. Loncarek, J. & Bettencourt-Dias, M. Building the right centriole for each cell type. *J. Cell Biol.* **217**, 823–835 (2018) DOI:10.1083/jcb.201704093.

363. Vertii, A., Bright, A., Delaval, B., Hehnly, H. & Doxsey, S. New frontiers: discovering cilia-independent functions of cilia proteins. *EMBO Rep.* **16**, 1275–87 (2015) DOI:10.15252/embr.201540632.

364. Schmidts, M. *et al.* Exome sequencing identifies DYNC2H1 mutations as a common cause

of asphyxiating thoracic dystrophy (Jeune syndrome) without major polydactyly, renal or retinal involvement. *J. Med. Genet.* **50**, 309–23 (2013) DOI:10.1136/jmedgenet-2012-101284.

365. Bachmann-Gagescu, R. *et al.* KIAA0586 is Mutated in Joubert Syndrome. *Hum. Mutat.* **36**, 831–835 (2015) DOI:10.1002/humu.22821.

366. Knopp, C. *et al.* Syndromic ciliopathies: From single gene to multi gene analysis by SNP arrays and next generation sequencing. *Mol. Cell. Probes* **29**, 299–307 (2015) DOI:10.1016/j.mcp.2015.05.008.

367. Shamseldin, H. E. *et al.* The morbid genome of ciliopathies: an update. *Genet. Med.* **22**, 1051–1060 (2020) DOI:10.1038/s41436-020-0761-1.

368. Doherty, D. Joubert Syndrome: Insights Into Brain Development, Cilium Biology, and Complex Disease. *Seminars in Pediatric Neurology* vol. 16 143–154 (2009) DOI:10.1016/j.spen.2009.06.002.

369. Karmous-Benailly, H. *et al.* Antenatal presentation of Bardet-Biedl syndrome may mimic Meckel syndrome. *Am. J. Hum. Genet.* **76**, 493–504 (2005) DOI:10.1086/428679.

370. Frank, V. *et al.* Mutations of the CEP290 gene encoding a centrosomal protein cause meckel-gruber syndrome. *Hum. Mutat.* **29**, 45–52 (2008) DOI:10.1002/humu.20614.

371. Valente, E. M. *et al.* Mutations in CEP290, which encodes a centrosomal protein, cause pleiotropic forms of Joubert syndrome. *Nat. Genet.* **38**, 623–625 (2006) DOI:10.1038/ng1805.

372. Turnbull, C. *et al.* The 100 000 Genomes Project: Bringing whole genome sequencing to the NHS. *BMJ* **361**, (2018) DOI:10.1136/bmj.k1687.

373. Nikopoulos, K. *et al.* A frequent variant in the Japanese population determines quasi-Mendelian inheritance of rare retinal ciliopathy. *Nat. Commun.* **10**, 19 (2019) DOI:10.1038/s41467-019-10746-4.

374. Shaheen, R. *et al.* Characterizing the morbid genome of ciliopathies. *Genome Biol.* **17**,

(2016) DOI:10.1186/s13059-016-1099-5.

375. Harris, P. C. 2008 Homer W. Smith award: Insights into the pathogenesis of polycystic kidney disease from gene discovery. *Journal of the American Society of Nephrology* vol. 20 1188–1198 (2009) DOI:10.1681/ASN.2009010014.

376. Zaki, M. S., Sattar, S., Massoudi, R. A. & Gleeson, J. G. Co-occurrence of distinct ciliopathy diseases in single families suggests genetic modifiers. *Am. J. Med. Genet. Part A* **155**, 3042–3049 (2011) DOI:10.1002/ajmg.a.34173.

377. Zhang, Y. *et al.* BBS mutations modify phenotypic expression of CEP290-related ciliopathies. *Hum. Mol. Genet.* **23**, 40–51 (2014) DOI:10.1093/hmg/ddt394.

378. Ma, M. Cilia and polycystic kidney disease. *Seminars in Cell and Developmental Biology* (2020) doi:10.1016/j.semcdb.2020.05.003 DOI:10.1016/j.semcdb.2020.05.003.

379. Zhang, Z. Y., Wang, Z. M. & Huang, Y. Polycystic liver disease: Classification, diagnosis, treatment process, and clinical management. *World J. Hepatol.* **12**, 72–83 (2020) DOI:10.4254/wjh.v12.i3.72.

380. Bergmann, C. Early and Severe Polycystic Kidney Disease and Related Ciliopathies: An Emerging Field of Interest. *Nephron* **141**, 50–60 (2019) DOI:10.1159/000493532.

381. Adamiok-Ostrowska, A. & Piekiełko-Witkowska, A. Ciliary Genes in Renal Cystic Diseases. *Cells* vol. 9 (2020) DOI:10.3390/cells9040907.

382. Kothari, T. H., Khara, S. S., Kothari, D. B. & Schiano, T. Caroli disease. *Consultant* **48**, 391 (2008) DOI:10.5958/2454-2652.2017.00075.0.

383. Zhong, Y., Peng, S. & Yang, Y. Hepatobiliary and Pancreatic: Caroli syndrome: Egg-like sign on CT. *Journal of Gastroenterology and Hepatology (Australia)* vol. 35 180 (2020) DOI:10.1111/jgh.14822.

384. Gunay-Aygun, M. Liver and kidney disease in ciliopathies. *American Journal of Medical Genetics, Part C: Seminars in Medical Genetics* vol. 151 296–306 (2009) DOI:10.1002/ajmg.c.30225.

385. Helou, J. *et al.* Mutation analysis of NPHP6/CEP290 in patients with Joubert syndrome ana Senior-Løken syndrome. *J. Med. Genet.* **44**, 657–663 (2007) DOI:10.1136/jmg.2007.052027.

386. Devlin, L. A. & Sayer, J. A. Renal ciliopathies. *Current Opinion in Genetics and Development* vol. 56 49–60 (2019) DOI:10.1016/j.gde.2019.07.005.

387. Adams, N. A., Awadein, A. & Toma, H. S. The Retinal Ciliopathies. *Ophthalmic Genet.* **28**, 113–125 (2007) DOI:10.1080/13816810701537424.

388. Savige, J. *et al.* Ocular features in Alport syndrome: Pathogenesis and clinical significance. *Clinical Journal of the American Society of Nephrology* vol. 10 703–709 (2015) DOI:10.2215/CJN.10581014.

389. Koyanagi, Y. *et al.* Genetic characteristics of retinitis pigmentosa in 1204 Japanese patients. *J. Med. Genet.* **56**, 662–670 (2019) DOI:10.1136/jmedgenet-2018-105691.

390. Rivolta, C., Sweklo, E. A., Berson, E. L. & Dryja, T. P. Missense mutation in the USH2A gene: Association with recessive retinitis pigmentosa without hearing loss. *Am. J. Hum. Genet.* **66**, 1975–1978 (2000) DOI:10.1086/302926.

391. Grudzinska Pechhacker, M. K. *et al.* CRB1-related retinopathy overlapping the ocular phenotype of S-adenosylhomocysteine hydrolase deficiency. *Ophthalmic Genet.* 1–8 (2020) doi:10.1080/13816810.2020.1790013 DOI:10.1080/13816810.2020.1790013.

392. Minegishi, Y. *et al.* CCT2 mutations evoke leber congenital amaurosis due to chaperone complex instability. *Sci. Rep.* **6**, (2016) DOI:10.1038/srep33742.

393. Tsang, S. H. *et al.* Whole exome sequencing identifies CRB1 defect in an unusual maculopathy phenotype. *Ophthalmology* **121**, 1773–1782 (2014) DOI:10.1016/j.ophtha.2014.03.010.

394. Wang, Y., Uraki, R., Hwang, J. & Fikrig, E. TRiC/CCT complex, a binding partner of NS1 protein, supports the replication of Zika virus in both mammalians and mosquitoes. *Viruses* **12**, (2020) DOI:10.3390/v12050519.

395. Collin, R. W. *et al.* Antisense oligonucleotide (AON)-based therapy for leber congenital amaurosis caused by a frequent mutation in CEP290. *Mol. Ther. - Nucleic Acids* **1**, e14 (2012) DOI:10.1038/mtna.2012.3.

396. Littink, K. W. *et al.* A novel nonsense mutation in CEP290 induces exon skipping and leads to a relatively mild retinal phenotype. *Investig. Ophthalmol. Vis. Sci.* **51**, 3646–3652 (2010) DOI:10.1167/iovs.09-5074.

397. Heon, E. *et al.* Mutations in C8ORF37 cause Bardet Biedl syndrome (BBS21). *Hum. Mol. Genet.* **25**, 2283–2294 (2016) DOI:10.1093/hmg/ddw096.

398. Demirci, F. Y. K. *et al.* X-linked cone-rod dystrophy (Locus COD1): Identification of mutations in RPGR exon ORF15. *Am. J. Hum. Genet.* **70**, 1049–1053 (2002) DOI:10.1086/339620.

399. Hameed, A. *et al.* Evidence of RPGRIP1 gene mutations associated with recessive cone-rod dystrophy. *J. Med. Genet.* **40**, 616–619 (2003) DOI:10.1136/jmg.40.8.616.

400. Ba-Abbad, R. *et al.* Clinical characteristics of early retinal disease due to CDHR1 mutation. *Mol. Vis.* **19**, 2250–2259 (2013).

401. Bessette, A. P., DeBenedictis, M. J. & Traboulsi, E. I. Clinical characteristics of recessive retinal degeneration due to mutations in the CDHR1 gene and a review of the literature. *Ophthalmic Genet.* **39**, 51–55 (2018) DOI:10.1080/13816810.2017.1363244.

402. Nakajima, D. *et al.* Identification of three novel non-classical cadherin genes through comprehensive analysis of large cDNAs. *Mol. Brain Res.* **94**, 85–95 (2001) DOI:10.1016/S0169-328X(01)00218-2.

403. Rattner, A. *et al.* A photoreceptor-specific cadherin is essential for the structural integrity of the outer segment and for photoreceptor survival. *Neuron* **32**, 775–786 (2001) DOI:10.1016/S0896-6273(01)00531-1.

404. Rattner, A., Chen, J. & Nathans, J. Proteolytic shedding of the extracellular domain of photoreceptor cadherin: Implications for outer segment assembly. *J. Biol. Chem.* **279**,

42202–42210 (2004) DOI:10.1074/jbc.M407928200.

405. Namburi, P. *et al.* Bi-allelic Truncating Mutations in CEP78, Encoding Centrosomal Protein 78, Cause Cone-Rod Degeneration with Sensorineural Hearing Loss. *Am. J. Hum. Genet.* **99**, 777–784 (2016) DOI:10.1016/j.ajhg.2016.07.010.

406. Hayashi, T. *et al.* Autosomal dominant occult macular dystrophy with an RP1L1 mutation (R45W). *Optom. Vis. Sci.* **89**, 684–691 (2012) DOI:10.1097/OPX.0b013e31824eea32.

407. Akahori, M. *et al.* Dominant Mutations in RP1L1 Are Responsible for Occult Macular Dystrophy. *Am J Hum Genet* **87**, (2010) DOI:10.1016/j.ajhg.2010.08.009.

408. Papageorgiou, E. *et al.* Retinal and optic nerve changes in microcephaly. *Neurology* **91**, e571–e585 (2018) DOI:10.1212/WNL.0000000000005950.

409. Ponting, C. P. A novel domain suggests a ciliary function for ASPM, a brain size determining gene. *Bioinformatics* **22**, 1031–1035 (2006) DOI:10.1093/bioinformatics/btl022.

410. Murga-Zamalloa, C. A., Swaroop, A. & Khanna, H. RPGR-containing protein complexes in syndromic and non-syndromic retinal degeneration due to ciliary dysfunction. *J. Genet.* **88**, 399–407 (2009) DOI:10.1007/s12041-009-0061-7.

411. Hong, D.-H., Yue, G., Adamian, M. & Li, T. Retinitis Pigmentosa GTPase Regulator (RPGR)-interacting Protein Is Stably Associated with the Photoreceptor Ciliary Axoneme and Anchors RPGR to the Connecting Cilium. *J. Biol. Chem.* **276**, 12091–12099 (2001) DOI:10.1074/jbc.M009351200.

412. Wright, R. N., Hong, D. H. & Perkins, B. Rpgr ORF15 connects to the usher protein network through direct interactions with multiple whirlin isoforms. *Investig. Ophthalmol. Vis. Sci.* **53**, 1519–1529 (2012) DOI:10.1167/iovs.11-8845.

413. Zhao, Y. *et al.* The retinitis pigmentosa GTPase regulator (RPGR)- interacting protein: Subserving RPGR function and participating in disk morphogenesis. *Proc. Natl. Acad. Sci.* **100**, 3965–3970 (2003) DOI:10.1073/pnas.0637349100.

414. Lentz, J. & Keats, B. *Usher Syndrome Type II*. *GeneReviews®* (University of Washington,

Seattle, 1993).

415. Mathur, P. D. & Yang, J. Usher syndrome and non-syndromic deafness: Functions of different whirlin isoforms in the cochlea, vestibular organs, and retina. *Hearing Research* vol. 375 14–24 (2019) DOI:10.1016/j.heares.2019.02.007.

416. Khaliq, S. *et al.* Mutation screening of Pakistani families with congenital eye disorders. *Exp. Eye Res.* **76**, 343–348 (2003) DOI:10.1016/S0014-4835(02)00304-4.

417. Quinn, P. M., Pellissier, L. P. & Wijnholds, J. The CRB1 complex: Following the trail of crumbs to a feasible gene therapy strategy. *Frontiers in Neuroscience* vol. 11 175 (2017) DOI:10.3389/fnins.2017.00175.

418. Gamundi, M. J. *et al.* Sequence variations in the retinal fascin FSCN2 gene in a Spanish population with autosomal dominant retinitis pigmentosa or macular degeneration. *Mol. Vis.* **11**, 922–928 (2005).

419. Wada, Y. *et al.* Autosomal Dominant Macular Degeneration Associated With 208delG Mutation in the FSCN2 Gene. *Arch. Ophthalmol.* **121**, 1613–1620 (2003) DOI:10.1001/archopht.121.11.1613.

420. Zhang, Q., Li, S., Xiao, X., Jia, X. & Guo, X. The 208delG mutation in FSCN2 does not associate with retinal degeneration in Chinese individuals. *Invest. Ophthalmol. Vis. Sci.* **48**, 530–3 (2007) DOI:10.1167/iovs.06-0669.

421. Liang, J. *et al.* Identification of novel PROM1 mutations responsible for autosomal recessive maculopathy with rod-cone dystrophy. *Graefe's Arch. Clin. Exp. Ophthalmol.* **257**, 619–628 (2019) DOI:10.1007/s00417-018-04206-w.

422. Cehajic-Kapetanovic, J. *et al.* Clinical and Molecular Characterization of PROM1-Related Retinal Degeneration. *JAMA Netw. open* **2**, e195752 (2019) DOI:10.1001/jamanetworkopen.2019.5752.

423. Michaelides, M. *et al.* The PROM1 mutation p.R373C causes an autosomal dominant bull's eye maculopathy associated with rod, rod-cone, and macular dystrophy. *Investig.*

Ophthalmol. Vis. Sci. **51**, 4771–4780 (2010) DOI:10.1167/iovs.09-4561.

424. Tobin, J. L. & Beales, P. L. The nonmotile ciliopathies. *Genetics in Medicine* vol. 11 386–402 (2009) DOI:10.1097/GIM.0b013e3181a02882.

425. Romani, M. *et al.* Mutations in B9D1 and MKS1 cause mild Joubert syndrome: Expanding the genetic overlap with the lethal ciliopathy Meckel syndrome. *Orphanet J. Rare Dis.* **9**, (2014) DOI:10.1186/1750-1172-9-72.

426. Brunham, L. Cilia get serious: Meckel-Gruber and Bardet-Biedl syndromes represent a spectrum of allelic disorders. *Clin. Genet.* **75**, 40–41 (2009) DOI:10.1111/j.1399-0004.2008.01139_2.x.

427. Goetz, S. C., Bangs, F., Barrington, C. L., Katsanis, N. & Anderson, K. V. The Meckel syndrome- associated protein MKS1 functionally interacts with components of the BBSome and IFT complexes to mediate ciliary trafficking and hedgehog signaling. *PLoS One* **12**, e0173399 (2017) DOI:10.1371/journal.pone.0173399.

428. Parisi, M. & Glass, I. *Joubert Syndrome*. *GeneReviews®* (University of Washington, Seattle, 1993).

429. Baala, L. *et al.* The Meckel-Gruber Syndrome Gene, MKS3, Is Mutated in Joubert Syndrome. *Am. J. Hum. Genet.* **80**, 186–194 (2007) DOI:10.1086/510499.

430. Phelps, I. G. *et al.* Interpreting the clinical significance of combined variants in multiple recessive disease genes: Systematic investigation of Joubert syndrome yields little support for oligogenicity. *Genet. Med.* **20**, 223–233 (2018) DOI:10.1038/gim.2017.94.

431. Brancati, F., Dallapiccola, B. & Valente, E. M. Joubert Syndrome and related disorders. *Orphanet Journal of Rare Diseases* vol. 5 (2010) DOI:10.1186/1750-1172-5-20.

432. Mougou-Zerelli, S. *et al.* CC2D2A mutations in Meckel and Joubert syndromes indicate a genotype-phenotype correlation. *Hum. Mutat.* **30**, 1574–1582 (2009) DOI:10.1002/humu.21116.

433. Chakrabarty, S., Savantre, S. B., Ramachandra Bhat, C. & Satyamoorthy, K. Multiple genetic

mutations implicate spectrum of phenotypes in Bardet-Biedl syndrome. *Gene* **725**, 144164 (2020) DOI:10.1016/j.gene.2019.144164.

434. Mykytyn, K. *et al.* Identification of the gene (BBS1) most commonly involved in Bardet-Biedl syndrome, a complex human obesity syndrome. *Nat. Genet.* **31**, 435–438 (2002) DOI:10.1038/ng935.

435. Nishimura, D. Y. *et al. Positional cloning of a novel gene on chromosome 16q causing Bardet-Biedl syndrome (BBS2)*. *Human Molecular Genetics* vol. 10 (2001).

436. Nishimura, D. Y. *et al.* Bbs2-null mice have neurosensory deficits, a defect in social dominance, and retinopathy associated with mislocalization of rhodopsin. *Proc. Natl. Acad. Sci. U. S. A.* **101**, 16588–93 (2004) DOI:10.1073/pnas.0405496101.

437. Chiang, A. P. *et al.* Comparative genomic analysis identifies an ADP-ribosylation factor-like gene as the cause of Bardet-Biedl syndrome (BBS3). *Am. J. Hum. Genet.* **75**, 475–484 (2004) DOI:10.1086/423903.

438. Mykytyn, K. *et al.* Identification of the gene that, when mutated, causes the human obesity syndrome BBS4. *Nat. Genet.* **28**, 188–191 (2001) DOI:10.1038/88925.

439. Hjortshøj, T. D. *et al.* Novel mutations in BBS5 highlight the importance of this gene in non-caucasian Bardet-Biedl syndrome patients [3]. *American Journal of Medical Genetics, Part A* vol. 146 517–520 (2008) DOI:10.1002/ajmg.a.32136.

440. Li, J. B. *et al.* Comparative genomics identifies a flagellar and basal body proteome that includes the BBS5 human disease gene. *Cell* **117**, 541–552 (2004) DOI:10.1016/S0092-8674(04)00450-7.

441. Goyal, S., Singh, I. R. & Vanita, V. Novel mutation in MKKS/BBS6 linked with arRP and polydactyly in a family of North Indian origin. *Clin. Exp. Ophthalmol.* **48**, 343–355 (2020) DOI:10.1111/ceo.13719.

442. Badano, J. L. *et al.* Identification of a novel Bardet-Biedl syndrome protein, BBS7, that shares structural features with BBS1 and BBS2. *Am. J. Hum. Genet.* **72**, 650–658 (2003)

DOI:10.1086/368204.

443. Ansley, S. J. *et al.* Basal body dysfunction is a likely cause of pleiotropic Bardet-Biedl syndrome. *Nature* **425**, 628–633 (2003) DOI:10.1038/nature02030.

444. Nishimura, D. Y. *et al.* Comparative genomics and gene expression analysis identifies BBS9, a new Bardet-Biedl syndrome gene. *Am. J. Hum. Genet.* **77**, 1021–1033 (2005) DOI:10.1086/498323.

445. Chiang, A. P. *et al.* Homozygosity mapping with SNP arrays identifies TRIM32, an E3 ubiquitin ligase, as a Bardet-Biedl syndrome gene (BBS11). *Proc. Natl. Acad. Sci. U. S. A.* **103**, 6287–6292 (2006) DOI:10.1073/pnas.0600158103.

446. Aliferis, K. *et al.* Differentiating Alström from Bardet-Biedl syndrome (BBS) using systematic ciliopathy genes sequencing. *Ophthalmic Genet.* **33**, 18–22 (2012) DOI:10.3109/13816810.2011.620055.

447. Kim, S. K. *et al.* Planar cell polarity acts through septins to control collective cell movement and ciliogenesis. *Science (80-.).* **329**, (2010) DOI:10.1126/science.1191184.

448. Otto, E. A. *et al.* Candidate exome capture identifies mutation of SDCCAG8 as the cause of a retinal-renal ciliopathy. *Nat. Genet.* **42**, 840–850 (2010) DOI:10.1038/ng.662.

449. Scheidecker, S. *et al.* Exome sequencing of Bardet-Biedl syndrome patient identifies a null mutation in the bbsome subunit BBIP1 (BBS18). *J. Med. Genet.* **51**, 132–136 (2014) DOI:10.1136/jmedgenet-2013-101785.

450. Aldahmesh, M. A. *et al.* IFT27, encoding a small GTPase component of IFT particles, is mutated in a consanguineous family with bardet-biedl syndrome. *Hum. Mol. Genet.* **23**, 3307–3315 (2014) DOI:10.1093/hmg/ddu044.

451. Liew, G. M. *et al.* The intraflagellar transport protein ift27 promotes bbsome exit from cilia through the gtpase ARL6/BBS3. *Dev. Cell* **31**, 265–278 (2014) DOI:10.1016/j.devcel.2014.09.004.

452. Schaefer, E. *et al.* Identification and characterization of known biallelic mutations in the

IFT27 (BBS19) gene in a novel family with Bardet-Biedl syndrome. *Front. Genet.* **10**, (2019) DOI:10.3389/fgene.2019.00021.

453. Kleinendorst, L. *et al.* Second case of Bardet–Biedl syndrome caused by biallelic variants in IFT74. *Eur. J. Hum. Genet.* (2020) doi:10.1038/s41431-020-0594-z DOI:10.1038/s41431-020-0594-z.

454. Lindstrand, A. *et al.* Copy-Number Variation Contributes to the Mutational Load of Bardet-Biedl Syndrome. *Am. J. Hum. Genet.* **99**, 318–336 (2016) DOI:10.1016/j.ajhg.2015.04.023.

455. Khan, A. O., Decker, E., Bachmann, N., Bolz, H. J. & Bergmann, C. C8orf37 is mutated in Bardet-Biedl syndrome and constitutes a locus allelic to non-syndromic retinal dystrophies. *Ophthalmic Genet.* **37**, 290–293 (2016) DOI:10.3109/13816810.2015.1066830.

456. Bujakowska, K. M. *et al.* Mutations in IFT172 cause isolated retinal degeneration and Bardet-Biedl syndrome. *Hum. Mol. Genet.* **24**, 230–242 (2015) DOI:10.1093/hmg/ddu441.

457. Schaefer, E. *et al.* Identification of a novel mutation confirms the implication of IFT172 (BBS20) in Bardet-Biedl syndrome. *J. Hum. Genet.* **61**, 447–450 (2016) DOI:10.1038/jhg.2015.162.

458. Ylldlz Bölükbasi, E. E. *et al.* Homozygous mutation in CEP19, a gene mutated in morbid obesity, in Bardet-Biedl syndrome with predominant postaxial polydactyly. *J. Med. Genet.* **55**, 189–197 (2018) DOI:10.1136/jmedgenet-2017-104758.

459. Morisada, N. *et al.* Bardet–Biedl syndrome in two unrelated patients with identical compound heterozygous SCLT1 mutations. *CEN Case Reports* (2020) doi:10.1007/s13730-020-00472-y DOI:10.1007/s13730-020-00472-y.

460. Castro-Sánchez, S. *et al.* Exploring genotype-phenotype relationships in Bardet-Biedl syndrome families. *J. Med. Genet.* **52**, 503–513 (2015) DOI:10.1136/jmedgenet-2015-103099.

461. Riazuddin, S. A. *et al.* A Splice-Site Mutation in a Retina-Specific Exon of BBS8 Causes Nonsyndromic Retinitis Pigmentosa. *Am. J. Hum. Genet.* **86**, 805–812 (2010)

DOI:10.1016/j.ajhg.2010.04.001.

462. Putoux, A. *et al.* KIF7 mutations cause fetal hydrolethalus and acrocallosal syndromes. *Nat. Genet.* **43**, 601–606 (2011) DOI:10.1038/ng.826.

463. Khanna, H. *et al.* A common allele in RPGRIP1L is a modifier of retinal degeneration in ciliopathies. *Nat. Genet.* **41**, 739 (2009) DOI:10.1038/NG.366.

464. Coene, K. L. M. *et al.* The ciliopathy-associated protein homologs RPGRIP1 and RPGRIP1L are linked to cilium integrity through interaction with Nek4 serine/threonine kinase. *Hum. Mol. Genet.* **20**, 3592–3605 (2011) DOI:10.1093/hmg/ddr280.

465. Young, I. D., Rickett, A. B. & Clarket, M. *High incidence of Meckel's syndrome in Gujarati Indians*. *Journal of Medical Genetics* vol. 22 (1985).

466. Hartill, V., Szymanska, K., Sharif, S. M., Wheway, G. & Johnson, C. A. Meckel–Gruber Syndrome: An Update on Diagnosis, Clinical Management, and Research Advances. *Front. Pediatr.* **5**, 1–9 (2017) DOI:10.3389/fped.2017.00244.

467. Stoll, C., Dott, B., Alembik, Y. & Roth, M. P. Associated malformations among infants with anophthalmia and microphthalmia. *Birth Defects Res. Part A - Clin. Mol. Teratol.* **94**, 147–152 (2012) DOI:10.1002/bdra.22877.

468. Richards, N. Q., Pflugrath, A., Pande, C. & Couser, N. L. Genetic Abnormalities With Anophthalmia, Microphthalmia, and Colobomas. in *Ophthalmic Genetic Diseases* 41–52 (Elsevier, 2019). doi:10.1016/b978-0-323-65414-2.00003-9 DOI:10.1016/b978-0-323-65414-2.00003-9.

469. Macrae, D. W., Howard, R. O., Albert, D. M. & Hsia, Y. E. Ocular Manifestations of the Meckel Syndrome. *Arch. Ophthalmol.* **88**, 106–113 (1972) DOI:10.1001/archopht.1972.01000030108028.

470. Raj, M., Dhanuka, S., Agarwal, P., Reddy, S. L. & Vivekananthan, S. Meckel Gruber syndrome – a case report. *Surg. Exp. Pathol.* **3**, 11 (2020) DOI:10.1186/s42047-020-00062-3.

471. Kyttälä, M. *et al.* MKS1, encoding a component of the flagellar apparatus basal body

proteome, is mutated in Meckel syndrome. *Nat. Genet.* **38**, 155–157 (2006) DOI:10.1038/ng1714.

472. Tammachote, R. *et al.* No Title. **18**, (2009) DOI:10.1093/hmg/ddp272.

473. Valente, E. M. *et al.* Mutations in TMEM216 perturb ciliogenesis and cause Joubert, Meckel and related syndromes. *Nat. Genet.* **42**, 619–625 (2010) DOI:10.1038/ng.594.

474. Tallila, J., Jakkula, E., Peltonen, L., Salonen, R. & Kestilä, M. Identification of CC2D2A as a Meckel Syndrome Gene Adds an Important Piece to the Ciliopathy Puzzle. **82**, 1361–1367 (2008) DOI:10.1016/j.ajhg.2008.05.004.

475. Shaheen, R. *et al.* A TCTN2 mutation defines a novel Meckel Gruber syndrome locus. *Hum. Mutat.* **32**, 573–578 (2011) DOI:10.1002/humu.21507.

476. Maglic, D. *et al.* TMEM231 Gene Conversion Associated with Joubert and Meckel–Gruber Syndromes in the Same Family. *Hum. Mutat.* **37**, 1144–1148 (2016) DOI:10.1002/humu.23054.

477. Shaheen, R., Ansari, S., Mardawi, E. A. L., Alshammari, M. J. & Alkuraya, F. S. Mutations in TMEM231 cause Meckel-Gruber syndrome. *J. Med. Genet.* **50**, 160–162 (2013) DOI:10.1136/jmedgenet-2012-101431.

478. Makrythanasis, P. *et al.* Biallelic variants in KIF14 cause intellectual disability with microcephaly. *Eur. J. Hum. Genet.* **26**, 330–339 (2018) DOI:10.1038/s41431-017-0088-9.

479. Meier, N. *et al.* Exome sequencing of fetal anomaly syndromes: novel phenotype–genotype discoveries. *Eur. J. Hum. Genet.* **27**, 730–737 (2019) DOI:10.1038/s41431-018-0324-y.

480. Reilly, M. L. *et al.* Loss-of-function mutations in KIF14 cause severe microcephaly and kidney development defects in humans and zebrafish. *Hum. Mol. Genet.* **28**, 778–795 (2019) DOI:10.1093/hmg/ddy381.

481. Shaheen, R. *et al.* Identification of a novel MKS locus defined by TMEM107 mutation. *Hum. Mol. Genet.* **24**, 5211–5218 (2015) DOI:10.1093/hmg/ddv242.

482. Paavola, P. *et al.* Clinical and genetic heterogeneity in Meckel syndrome. *Hum. Genet.* **101**, 88–92 (1997) DOI:10.1007/s004390050592.

483. Salvi, S. M., Akhtar, S. & Currie, Z. Ageing changes in the eye. *Postgraduate Medical Journal* vol. 82 581–587 (2006) DOI:10.1136/pgmj.2005.040857.

484. Kurtz, A. & Oh, S. J. Age related changes of the extracellular matrix and stem cell maintenance. *Preventive Medicine* vol. 54 (2012) DOI:10.1016/j.ypmed.2012.01.003.

485. Licastro, F. *et al.* Innate immunity and inflammation in ageing: A key for understanding age-related diseases. *Immunity and Ageing* vol. 2 (2005) DOI:10.1186/1742-4933-2-8.

486. Berghmans, L. V. *et al.* Discordance for retinitis pigmentosa in two monozygotic twin pairs. *Retina* **31**, 1164–1169 (2011) DOI:10.1097/IAE.0b013e3181fbcf2b.

487. Nakamura, M., Lin, J. & Miyake, Y. Young monozygotic twin sisters with fundus albipunctatus and cone dystrophy. *Arch. Ophthalmol.* **122**, 1203–1207 (2004) DOI:10.1001/archopht.122.8.1203.

488. Walia, S. *et al.* Discordant phenotypes in fraternal twins having an identical mutation in exon ORF15 of the RPGR gene. *Arch. Ophthalmol.* **126**, 379–384 (2008) DOI:10.1001/archophthalmol.2007.72.

489. Calkins, K. & Devaskar, S. U. Fetal origins of adult disease. *Curr. Probl. Pediatr. Adolesc. Health Care* **41**, 158–176 (2011) DOI:10.1016/j.cppeds.2011.01.001.

490. Mathew, V. & Ayyar, Sv. Developmental origins of adult diseases. *Indian J. Endocrinol. Metab.* **16**, 532 (2012) DOI:10.4103/2230-8210.98005.

491. Nicolas, G. & Veltman, J. A. The role of de novo mutations in adult-onset neurodegenerative disorders. *Acta Neuropathologica* vol. 137 183–207 (2019) DOI:10.1007/s00401-018-1939-3.

492. Mohana Devi, S., Mahalaxmi, I., Kaavya, J., Chinnkulandhai, V. & Balachandar, V. Does epigenetics have a role in age related macular degeneration and diabetic retinopathy? *Genes and Diseases* (2020) doi:10.1016/j.gendis.2020.01.003

DOI:10.1016/j.gendis.2020.01.003.

493. M. Liu, M., Chan, C.-C. & Tuo, J. Epigenetics in Ocular Diseases. *Curr. Genomics* **14**, 166–172 (2013) DOI:10.2174/1389202911314030002.

494. Corso-Díaz, X., Jaeger, C., Chaitankar, V. & Swaroop, A. Epigenetic control of gene regulation during development and disease: A view from the retina. *Progress in Retinal and Eye Research* vol. 65 1–27 (2018) DOI:10.1016/j.preteyeres.2018.03.002.

495. Aldiri, I. *et al.* The Dynamic Epigenetic Landscape of the Retina During Development, Reprogramming, and Tumorigenesis. *Neuron* **94**, 550-568.e10 (2017) DOI:10.1016/j.neuron.2017.04.022.

496. Spitz, F. & Furlong, E. E. M. Transcription factors: From enhancer binding to developmental control. *Nature Reviews Genetics* vol. 13 613–626 (2012) DOI:10.1038/nrg3207.

497. Freund, C., Horsford, D. J. & Mcinnes, R. R. *Transcription factor genes and the developing eye: a genetic perspective*. *Human Molecular Genetics* vol. 5 https://academic.oup.com/hmg/article-abstract/5/Supplement_1/1471/662986 (1996).

498. Avila-Fernandez, A. *et al.* Whole-exome sequencing reveals ZNF408 as a new gene associated with autosomal recessive retinitis pigmentosa with vitreal alterations. *Hum. Mol. Genet.* **24**, 4037–4048 (2015) DOI:10.1093/hmg/ddv140.

499. Corton, M. *et al.* Identification of the photoreceptor transcriptional Co-Repressor SAMD11 as novel cause of autosomal recessive retinitis pigmentosa. *Sci. Rep.* **6**, 1–13 (2016) DOI:10.1038/srep35370.

500. Collin, R. W. J. *et al.* ZNF408 is mutated in familial exudative vitreoretinopathy and is crucial for the development of zebrafish retinal vasculature. *Proc. Natl. Acad. Sci. U. S. A.* **110**, 9856–9861 (2013) DOI:10.1073/pnas.1220864110.

501. Qiao, F. & Bowie, J. U. The many faces of SAM. *Science's STKE : signal transduction knowledge environment* vol. 2005 (2005) DOI:10.1126/stke.2862005re7.

502. Schultz, J., Bork, P., Ponting, C. P. & Hofmann, K. SAM as a protein interaction domain

involved in developmental regulation. *Protein Sci.* **6**, 249–253 (2008) DOI:10.1002/pro.5560060128.

503. Inoue, T. *et al.* Cloning and characterization of mr-s, a novel SAM domain protein, predominantly expressed in retinal photoreceptor cells. *BMC Dev. Biol.* **6**, 15 (2006) DOI:10.1186/1471-213X-6-15.

504. X, Y., Z, L. & Y, C. Regulation of TGF-beta signaling by Smad7. *Acta Biochim. Biophys. Sin. (Shanghai).* **41**, (2009) DOI:10.1093/ABBS/GMP018.

505. Yu, Y. *et al.* Smad7 enables STAT3 activation and promotes pluripotency independent of TGF-β signaling. *Proc. Natl. Acad. Sci. U. S. A.* **114**, 10113–10118 (2017) DOI:10.1073/pnas.1705755114.

506. Luo, C., Hajkova, P. & Ecker, J. R. Dynamic DNA methylation: In the right place at the right time. *Science* vol. 361 1336–1340 (2018) DOI:10.1126/science.aat6806.

507. Moore, L. D., Le, T. & Fan, G. DNA methylation and its basic function. *Neuropsychopharmacology* vol. 38 23–38 (2013) DOI:10.1038/npp.2012.112.

508. Wu, X. & Zhang, Y. TET-mediated active DNA demethylation: Mechanism, function and beyond. *Nature Reviews Genetics* vol. 18 517–534 (2017) DOI:10.1038/nrg.2017.33.

509. Alfano, G. *et al.* Natural antisense transcripts associated with genes involved in eye development. *Hum. Mol. Genet.* **14**, 913–923 (2005) DOI:10.1093/hmg/ddi084.

510. Rapicavoli, N. A. & Blackshaw, S. New meaning in the message: Noncoding RNAs and their role in retinal development. *Developmental Dynamics* vol. 238 2103–2114 (2009) DOI:10.1002/dvdy.21844.

511. Zentner, G. E. & Henikoff, S. Regulation of nucleosome dynamics by histone modifications. *Nature Structural and Molecular Biology* vol. 20 259–266 (2013) DOI:10.1038/nsmb.2470.

512. Jambhekar, A., Dhall, A. & Shi, Y. Roles and regulation of histone methylation in animal development. *Nature Reviews Molecular Cell Biology* vol. 20 625–641 (2019) DOI:10.1038/s41580-019-0151-1.

513. Lessard, J. A. & Crabtree, G. R. Chromatin regulatory mechanisms in pluripotency. *Annual Review of Cell and Developmental Biology* vol. 26 503–532 (2010) DOI:10.1146/annurev-cellbio-051809-102012.

514. Chen, S., Yang, J., Wei, Y. & Wei, X. Epigenetic regulation of macrophages: from homeostasis maintenance to host defense. *Cellular and Molecular Immunology* vol. 17 36–49 (2020) DOI:10.1038/s41423-019-0315-0.

515. Cheedipudi, S., Genolet, O. & Dobreva, G. Epigenetic inheritance of cell fates during embryonic development. *Frontiers in Genetics* vol. 5 (2014) DOI:10.3389/fgene.2014.00019.

516. Miroshnikova, Y. A., Cohen, I., Ezhkova, E. & Wickström, S. A. Epigenetic gene regulation, chromatin structure, and force-induced chromatin remodelling in epidermal development and homeostasis. *Current Opinion in Genetics and Development* vol. 55 46–51 (2019) DOI:10.1016/j.gde.2019.04.014.

517. Ghirlando, R. & Felsenfeld, G. Chromatin structure outside and inside the nucleus. *Biopolymers* vol. 99 225–232 (2013) DOI:10.1002/bip.22157.

518. Luger, K., Mäder, A. W., Richmond, R. K., Sargent, D. F. & Richmond, T. J. Crystal structure of the nucleosome core particle at 2.8 Å resolution. *Nature* **389**, 251–260 (1997) DOI:10.1038/38444.

519. Simpson, R. T., Thoma, F. & Brubaker, J. M. Chromatin reconstituted from tandemly repeated cloned DNA fragments and core histones: A model system for study of higher order structure. *Cell* **42**, 799–808 (1985) DOI:10.1016/0092-8674(85)90276-4.

520. Clapier, C. R. & Cairns, B. R. The Biology of Chromatin Remodeling Complexes. *Annu. Rev. Biochem.* **78**, 273–304 (2009) DOI:10.1146/annurev.biochem.77.062706.153223.

521. Voigt, P., Tee, W. W. & Reinberg, D. A double take on bivalent promoters. *Genes and Development* vol. 27 1318–1338 (2013) DOI:10.1101/gad.219626.113.

522. Huang, H., Sabari, B. R., Garcia, B. A., David Allis, C. & Zhao, Y. SnapShot: Histone

modifications. *Cell* vol. 159 458-458.e1 (2014) DOI:10.1016/j.cell.2014.09.037.

523. Zhang, T., Cooper, S. & Brockdorff, N. The interplay of histone modifications – writers that read. *EMBO Rep.* **16**, 1467–1481 (2015) DOI:10.15252/embr.201540945.

524. Vissers, J. H. A., Nicassio, F., van Lohuizen, M., Di Fiore, P. P. & Citterio, E. The many faces of ubiquitinated histone H2A: Insights from the DUBs. *Cell Division* vol. 3 8 (2008) DOI:10.1186/1747-1028-3-8.

525. Azuara, V. *et al.* Chromatin signatures of pluripotent cell lines. *Nat. Cell Biol.* **8**, 532–538 (2006) DOI:10.1038/ncb1403.

526. Bernhart, S. H. *et al.* Changes of bivalent chromatin coincide with increased expression of developmental genes in cancer. *Sci. Rep.* **6**, 1–18 (2016) DOI:10.1038/srep37393.

527. Bernstein, B. E. *et al.* A Bivalent Chromatin Structure Marks Key Developmental Genes in Embryonic Stem Cells. *Cell* **125**, 315–326 (2006) DOI:10.1016/j.cell.2006.02.041.

528. Mimura, T., Kaji, Y., Noma, H., Funatsu, H. & Okamoto, S. The role of SIRT1 in ocular aging. *Experimental Eye Research* vol. 116 17–26 (2013) DOI:10.1016/j.exer.2013.07.017.

529. Pelzel, H. R., Schlamp, C. L. & Nickells, R. W. Histone H4 deacetylation plays a critical role in early gene silencing during neuronal apoptosis. *BMC Neurosci.* **11**, (2010) DOI:10.1186/1471-2202-11-62.

530. Q.D. Wang, X., L. Crutchley, J. & Dostie, J. Shaping the Genome with Non-Coding RNAs. *Curr. Genomics* **12**, 307–321 (2011) DOI:10.2174/138920211796429772.

531. Wu, Z. *et al.* Regulation of lncRNA expression. *Cell. Mol. Biol. Lett.* **19**, 561–575 (2014) DOI:10.2478/s11658-014-0212-6.

532. Blackshaw, S. *et al.* Genomic analysis of mouse retinal development. *PLoS Biol.* **2**, (2004) DOI:10.1371/journal.pbio.0020247.

533. Maiorano, N. A. & Hindges, R. Non-coding RNAs in retinal development. *Int. J. Mol. Sci.* **13**, 558–578 (2012) DOI:10.3390/ijms13010558.

534. Dinescu, S. *et al.* Epitranscriptomic signatures in lncRNAs and their possible roles in cancer. *Genes* vol. 10 (2019) DOI:10.3390/genes10010052.

535. Yan, N. *et al.* Postnatal onset of retinal degeneration by loss of embryonic Ezh2 repression of Six1. *Sci. Rep.* **6**, 1–15 (2016) DOI:10.1038/srep33887.

536. Aldiri, I. & Vetter, M. L. PRC2 during vertebrate organogenesis: A complex in transition. *Developmental Biology* vol. 367 91–99 (2012) DOI:10.1016/j.ydbio.2012.04.030.

537. Margueron, R. & Reinberg, D. The Polycomb complex PRC2 and its mark in life. *Nature* vol. 469 343–349 (2011) DOI:10.1038/nature09784.

538. Shao, Z. *et al.* Stabilization of chromatin structure by PRC1, a polycomb complex. *Cell* **98**, 37–46 (1999) DOI:10.1016/S0092-8674(00)80604-2.

539. Pickart, C. M. Mechanisms Underlying Ubiquitination. *http://dx.doi.org/10.1146/annurev.biochem.70.1.503* **70**, 503–533 (2003) DOI:10.1146/ANNUREV.BIOCHEM.70.1.503.

540. David, Y. *et al.* E3 Ligases Determine Ubiquitination Site and Conjugate Type by Enforcing Specificity on E2 Enzymes *. *J. Biol. Chem.* **286**, 44104–44115 (2011) DOI:10.1074/JBC.M111.234559.

541. Di Croce, L. & Helin, K. Transcriptional regulation by Polycomb group proteins. *Nature Structural and Molecular Biology* vol. 20 1147–1155 (2013) DOI:10.1038/nsmb.2669.

542. Swigut, T. & Wysocka, J. H3K27 Demethylases, at Long Last. *Cell* vol. 131 29–32 (2007) DOI:10.1016/j.cell.2007.09.026.

543. Schuettengruber, B. *et al.* Functional anatomy of polycomb and trithorax chromatin landscapes in Drosophila embryos. *PLoS Biol.* **7**, (2009) DOI:10.1371/journal.pbio.1000013.

544. Kuzmichev, A., Nishioka, K., Erdjument-Bromage, H., Tempst, P. & Reinberg, D. Histone methyltransferase activity associated with a human multiprotein complex containing the enhancer of zeste protein. *Genes Dev.* **16**, 2893–2905 (2002) DOI:10.1101/gad.1035902.

545. Aloia, L., Di Stefano, B. & Di Croce, L. Polycomb complexes in stem cells and embryonic development. *Development (Cambridge)* vol. 140 2525–2534 (2013) DOI:10.1242/dev.091553.

546. Aranda, S., Mas, G. & Di Croce, L. Regulation of gene transcription by Polycomb proteins. *Sci. Adv.* **1**, (2015) DOI:10.1126/sciadv.1500737.

547. Lewis, E. B. A gene complex controlling segmentation in Drosophila. *Nature* vol. 276 565–570 (1978) DOI:10.1038/276565a0.

548. Classen, A. K., Bunker, B. D., Harvey, K. F., Vaccari, T. & Bilder, D. A tumor suppressor activity of Drosophila Polycomb genes mediated by JAK-STAT signaling. *Nat. Genet.* **41**, 1150–1155 (2009) DOI:10.1038/ng.445.

549. Martinez, A. M. *et al.* Polyhomeotic has a tumor suppressor activity mediated by repression of Notch signaling. *Nat. Genet.* **41**, 1076–1082 (2009) DOI:10.1038/ng.414.

550. Dovey, J. S., Zacharek, S. J., Kim, C. F. & Lees, J. A. Bmi1 is critical for lung tumorigenesis and bronchioalveolar stem cell expansion. *Proc. Natl. Acad. Sci. U. S. A.* **105**, 11857–11862 (2008) DOI:10.1073/pnas.0803574105.

551. Richter, G. H. S. *et al.* EZH2 is a mediator of EWS/FLI1 driven tumor growth and metastasis blocking endothelial and neuro-ectodermal differentiation. *Proc. Natl. Acad. Sci. U. S. A.* **106**, 5324–5329 (2009) DOI:10.1073/pnas.0810759106.

552. Amoyel, M., Anderson, A. M. & Bach, E. A. JAK/STAT pathway dysregulation in tumors: A Drosophila perspective. *Seminars in Cell and Developmental Biology* vol. 28 96–103 (2014) DOI:10.1016/j.semcdb.2014.03.023.

553. Arap, W. *et al. Functional analysis of wild-type and malignant glioma derived CDKN2Ab alleles: Evidence for an RB-independent growth suppressive pathway*. (1997).

554. Leung, C. *et al.* Bmi1 is essential for cerebellar development and is overexpressed in human medulloblastomas. *Nature* **428**, 337–341 (2004) DOI:10.1038/nature02385.

555. Rocco, J. W. & Ahrendt, S. A. *p16 and pl6IJ Are Potent Growth Suppressors of Head and*

Neck Squamous Carcinoma Cells in Vitro1. http://cancerres.aacrjournals.org/content/56/18/4119 (1996).

556. Gluckman, P. D., Hanson, M. A., Cooper, C. & Thornburg, K. L. Effect of in utero and early-life conditions on adult health and disease. *New England Journal of Medicine* vol. 359 61 (2008) DOI:10.1056/NEJMra0708473.

557. Cao, R. & Zhang, Y. The functions of E(Z)/EZH2-mediated methylation of lysine 27 in histone H3. *Current Opinion in Genetics and Development* vol. 14 155–164 (2004) DOI:10.1016/j.gde.2004.02.001.

558. Pereira, J. D. *et al.* Ezh2, the histone methyltransferase of PRC2, regulates the balance between self-renewal and differentiation in the cerebral cortex. *Proc. Natl. Acad. Sci. U. S. A.* **107**, 15957–15962 (2010) DOI:10.1073/pnas.1002530107.

559. Ahmed, M., Xu, J. & Xu, P.-X. EYA1 and SIX1 drive the neuronal developmental program in cooperation with the SWI/SNF chromatin-remodeling complex and SOX2 in the mammalian inner ear. *Development* **139**, 1965–77 (2012) DOI:10.1242/dev.071670.

560. Gao, Z. *et al.* PCGF Homologs, CBX Proteins, and RYBP Define Functionally Distinct PRC1 Family Complexes. *Mol. Cell* **45**, 344–356 (2012) DOI:10.1016/j.molcel.2012.01.002.

561. Wani, A. H. *et al.* Chromatin topology is coupled to Polycomb group protein subnuclear organization. *Nat. Commun.* **7**, (2016) DOI:10.1038/ncomms10291.

562. Voncken, J. W. *et al.* Rnf2 (Ring1b) deficiency causes gastrulation arrest and cell cycle inhibition. *Proc. Natl. Acad. Sci. U. S. A.* **100**, 2468–2473 (2003) DOI:10.1073/pnas.0434312100.

563. Loubiere, V. *et al.* Coordinate redeployment of PRC1 proteins suppresses tumor formation during Drosophila development. *Nat. Genet.* **48**, 1436–1442 (2016) DOI:10.1038/ng.3671.

564. Dorafshan, E., Kahn, T. G. & Schwartz, Y. B. Hierarchical recruitment of Polycomb complexes revisited. *Nucleus* vol. 8 496–505 (2017) DOI:10.1080/19491034.2017.1363136.

565. Koppens, M. & Van Lohuizen, M. Context-dependent actions of Polycomb repressors in

cancer. *Oncogene* vol. 35 1341–1352 (2016) DOI:10.1038/onc.2015.195.

566. Park, I.-K., Morrison, S. J. & Clarke, M. F. Bmi1, stem cells, and senescence regulation. *J. Clin. Invest.* **113**, 175–179 (2004) DOI:10.1172/jci20800.

567. Cao, R., Tsukada, Y. I. & Zhang, Y. Role of Bmi-1 and Ring1A in H2A ubiquitylation and hox gene silencing. *Mol. Cell* **20**, 845–854 (2005) DOI:10.1016/j.molcel.2005.12.002.

568. Francis, N. J., Kingston, R. E. & Woodcock, C. L. Chromatin compaction by a polycomb group protein complex. *Science (80-.).* **306**, 1574–1577 (2004) DOI:10.1126/science.1100576.

569. Brunk, B. P., Martin, E. C. & Adler, P. N. Drosophila genes Posterior Sex Combs and Suppressor two of zeste encode proteins with homology to the murine bmi-1 oncogene. *Nature* **353**, 351–353 (1991) DOI:10.1038/353351a0.

570. Haupt, Y., Alexander, W. S., Barri, G., Peter Klinken, S. & Adams, J. M. Novel zinc finger gene implicated as myc collaborator by retrovirally accelerated lymphomagenesis in Eμ-myc transgenic mice. *Cell* **65**, 753–763 (1991) DOI:10.1016/0092-8674(91)90383-A.

571. van Lohuizen, M. *et al.* Identification of cooperating oncogenes in Eμ-myc transgenic mice by provirus tagging. *Cell* **65**, 737–752 (1991) DOI:10.1016/0092-8674(91)90382-9.

572. Jacobs, J. L., Kieboom, K., Marino, S., DePinho, R. A. & Van Lohuizen, M. The oncogene and Polycombgroup gene bmi-1 regulates cell proliferation and senescence through the ink4a locus. *Nature* **397**, 164–168 (1999) DOI:10.1038/16476.

573. Molofsky, A. V. *et al.* Bmi-1 dependence distinguishes neural stem cell self-renewal from progenitor proliferation. *Nature* **425**, 962–967 (2003) DOI:10.1038/nature02060.

574. Abdouh, M. *et al.* BMI1 sustains human glioblastoma multiforme stem cell renewal. *J. Neurosci.* **29**, 8884–8896 (2009) DOI:10.1523/JNEUROSCI.0968-09.2009.

575. Zencak, D. *et al.* Bmi1 loss produces an increase in astroglial cells and a decrease in neural stem cell population and proliferation. *J. Neurosci.* **25**, 5774–5783 (2005) DOI:10.1523/JNEUROSCI.3452-04.2005.

576. Fasano, C. A. *et al.* shRNA Knockdown of Bmi-1 Reveals a Critical Role for p21-Rb Pathway in NSC Self-Renewal during Development. *Cell Stem Cell* **1**, 87–99 (2007) DOI:10.1016/j.stem.2007.04.001.

577. Sherr, C. J. The INK4a/ARF network in tumour suppression. *Nature Reviews Molecular Cell Biology* vol. 2 731–737 (2001) DOI:10.1038/35096061.

578. Vousden, K. H. & Prives, C. Blinded by the Light: The Growing Complexity of p53. *Cell* **137**, 413–431 (2009) DOI:10.1016/J.CELL.2009.04.037.

579. Solá, S., Morgado, A. L. & Rodrigues, C. M. P. Death receptors and mitochondria: Two prime triggers of neural apoptosis and differentiation. *Biochim. Biophys. Acta - Gen. Subj.* **1830**, 2160–2166 (2013) DOI:10.1016/J.BBAGEN.2012.09.021.

580. Hock, A. K. & Vousden, K. H. The role of ubiquitin modification in the regulation of p53. *Biochim. Biophys. Acta - Mol. Cell Res.* **1843**, 137–149 (2014) DOI:10.1016/J.BBAMCR.2013.05.022.

581. Molofsky, A. V., He, S., Bydon, M., Morrison, S. J. & Pardal, R. Bmi-1 promotes neural stem cell self-renewal and neural development but not mouse growth and survival by repressing the p16Ink4a and p19 Arf senescence pathways. *Genes Dev.* **19**, 1432–1437 (2005) DOI:10.1101/gad.1299505.

582. Mao, L. *et al.* Cyclin E1 is a common target of BMI1 and MYCN and a prognostic marker for neuroblastoma progression. *Oncogene* **31**, 3785 (2012) DOI:10.1038/ONC.2011.536.

583. Cao, L. *et al.* BMI1 as a novel target for drug discovery in cancer. *J. Cell. Biochem.* **112**, 2729–2741 (2011) DOI:10.1002/jcb.23234.

584. Arora, M., Packard, C. Z., Banerjee, T. & Parvin, J. D. RING1A and BMI1 bookmark active genes via ubiquitination of chromatin-associated proteins. *Nucleic Acids Res.* **44**, 2136–2144 (2016) DOI:10.1093/NAR/GKV1223.

585. S, B. *et al.* DNA damage triggers nucleotide excision repair-dependent monoubiquitylation of histone H2A. *Genes Dev.* **20**, 1343–1352 (2006) DOI:10.1101/GAD.373706.

586. Q, Z. *et al.* Chromatin restoration following nucleotide excision repair involves the incorporation of ubiquitinated H2A at damaged genomic sites. *DNA Repair (Amst).* **8**, 262–273 (2009) DOI:10.1016/J.DNAREP.2008.11.007.

587. JA, M. *et al.* Nucleotide excision repair-induced H2A ubiquitination is dependent on MDC1 and RNF8 and reveals a universal DNA damage response. *J. Cell Biol.* **186**, 835–847 (2009) DOI:10.1083/JCB.200902150.

588. Ismail, I. H., Andrin, C., McDonald, D. & Hendzel, M. J. BMI1-mediated histone ubiquitylation promotes DNA double-strand break repair. *J. Cell Biol.* **191**, 45–60 (2010) DOI:10.1083/JCB.201003034.

589. Chagraoui, J., Hébert, J., Girard, S. & Sauvageau, G. An anticlastogenic function for the Polycomb Group gene Bmi1. *Proc. Natl. Acad. Sci. U. S. A.* **108**, 5284–5289 (2011) DOI:10.1073/pnas.1014263108.

590. Ginjala, V. *et al.* BMI1 Is Recruited to DNA Breaks and Contributes to DNA Damage-Induced H2A Ubiquitination and Repair. *Mol. Cell. Biol.* **31**, 1972–1982 (2011) DOI:10.1128/MCB.00981-10.

591. TT, P. *et al.* A critical role for histone H2AX in recruitment of repair factors to nuclear foci after DNA damage. *Curr. Biol.* **10**, 886–895 (2000) DOI:10.1016/S0960-9822(00)00610-2.

592. Celeste, A. *et al.* Genomic Instability in Mice Lacking Histone H2AX. *Science* **296**, 922 (2002) DOI:10.1126/SCIENCE.1069398.

593. J, C., J, H., S, G. & G, S. An anticlastogenic function for the Polycomb Group gene Bmi1. *Proc. Natl. Acad. Sci. U. S. A.* **108**, 5284–5289 (2011) DOI:10.1073/PNAS.1014263108.

594. Facchino, S., Abdouh, M., Chatoo, W. & Bernier, G. BMI1 confers radioresistance to normal and cancerous neural stem cells through recruitment of the DNA damage response machinery. *J. Neurosci.* **30**, 10096–10111 (2010) DOI:10.1523/JNEUROSCI.1634-10.2010.

595. GS, S. *et al.* The RIDDLE syndrome protein mediates a ubiquitin-dependent signaling cascade at sites of DNA damage. *Cell* **136**, 420–434 (2009)

DOI:10.1016/J.CELL.2008.12.042.

596. MS, H. *et al.* RNF8 transduces the DNA-damage signal via histone ubiquitylation and checkpoint protein assembly. *Cell* **131**, 901–914 (2007) DOI:10.1016/J.CELL.2007.09.041.

597. C, D. *et al.* RNF168 binds and amplifies ubiquitin conjugates on damaged chromosomes to allow accumulation of repair proteins. *Cell* **136**, 435–446 (2009) DOI:10.1016/J.CELL.2008.12.041.

598. Wei, F. *et al.* BMI1 attenuates etoposide-induced G2/M checkpoints via reducing ATM activation. *Oncogene 2015 3423* **34**, 3063–3075 (2014) DOI:10.1038/onc.2014.235.

599. Flamier, A. *et al.* Modeling Late-Onset Sporadic Alzheimer's Disease through BMI1 Deficiency. *Cell Rep.* **23**, 2653–2666 (2018) DOI:10.1016/j.celrep.2018.04.097.

600. Cao, G. *et al.* Bmi-1 absence causes premature brain degeneration. *PLoS One* **7**, (2012) DOI:10.1371/journal.pone.0032015.

601. Chatoo, W. *et al.* The polycomb group gene Bmi1 regulates antioxidant defenses in neurons by repressing p53 pro-oxidant activity. *J. Neurosci.* **29**, 529–542 (2009) DOI:10.1523/JNEUROSCI.5303-08.2009.

602. Calao, M. *et al.* Direct effects of Bmi1 on p53 protein stability inactivates oncoprotein stress responses in embryonal cancer precursor cells at tumor initiation. *Oncogene* **32**, 3616–3626 (2013) DOI:10.1038/onc.2012.368.

603. Krishnamurthy, J. *et al.* Ink4a/Arf expression is a biomarker of aging. *J. Clin. Invest.* **114**, 1299–1307 (2004) DOI:10.1172/JCI22475.

604. Ressler, S. *et al.* p16INK4A is a robust in vivo biomarker of cellular aging in human skin. *Aging Cell* **5**, 379–389 (2006) DOI:10.1111/j.1474-9726.2006.00231.x.

605. Li, L. U., Zhao, Y. & Zhang, H. P16INK4a upregulation mediated by TBK1 induces retinal ganglion cell senescence in ischemic injury. *Cell Death Dis.* **8**, (2017) DOI:10.1038/cddis.2017.169.

606. Skowronska-Krawczyk, D. *et al.* P16INK4a Upregulation Mediated by SIX6 Defines Retinal Ganglion Cell Pathogenesis in Glaucoma. *Mol. Cell* **59**, 931–940 (2015) DOI:10.1016/j.molcel.2015.07.027.

607. Mishima, K. *et al.* Senescence-associated β-galactosidase histochemistry for the primate eye. *Investig. Ophthalmol. Vis. Sci.* **40**, 1590–1593 (1999).

608. El Hajjar, J. *et al.* Heterochromatic genome instability and neurodegeneration sharing similarities with Alzheimer's disease in old Bmi1+/− mice. *Sci. Rep.* **9**, 1–16 (2019) DOI:10.1038/s41598-018-37444-3.

609. Jeck, W. R., Siebold, A. P. & Sharpless, N. E. Review: A meta-analysis of GWAS and age-associated diseases. *Aging Cell* vol. 11 727–731 (2012) DOI:10.1111/j.1474-9726.2012.00871.x.

610. Chatoo, W., Abdouh, M., Duparc, R. H. & Bernier, G. Bmi1 distinguishes immature retinal progenitor/stem cells from the main progenitor cell population and is required for normal retinal development. *Stem Cells* **28**, 1412–1423 (2010) DOI:10.1002/stem.462.

611. Zencak, D. *et al.* Retinal degeneration depends on Bmi1 function and reactivation of cell cycle proteins. *Proc. Natl. Acad. Sci. U. S. A.* **110**, E593–E601 (2013) DOI:10.1073/pnas.1108297110.

612. Mbefo, M. K. & Arsenijevic, Y. The evaluation of BMI1 posttranslational modifications during retinal degeneration to understand BMI1 action on photoreceptor death execution. in *Advances in Experimental Medicine and Biology* vol. 1074 359–365 (Springer New York LLC, 2018). DOI:10.1007/978-3-319-75402-4_44.

613. Galluzzi, L. *et al.* Molecular mechanisms of cell death: Recommendations of the Nomenclature Committee on Cell Death 2018. *Cell Death and Differentiation* vol. 25 486–541 (2018) DOI:10.1038/s41418-017-0012-4.

614. Tait, S. W. G., Ichim, G. & Green, D. R. Die another way - non-apoptotic mechanisms of cell death. *J. Cell Sci.* **127**, 2135–2144 (2014) DOI:10.1242/jcs.093575.

615. Yan, G., Elbadawi, M. & Efferth, T. Multiple cell death modalities and their key features (Review). *World Acad. Sci. J.* **2**, 39–48 (2020) DOI:10.3892/wasj.2020.40.

616. Syntichaki, P. & Tavernarakis, N. Death by necrosis. Uncontrollable catastrophe, or is there order behind the chaos? *EMBO Rep.* **3**, 604–609 (2002) DOI:10.1093/embo-reports/kvf138.

617. Hajra, K. M. & Liu, J. R. Apoptosome dysfunction in human cancer. *Apoptosis* **9**, 691–704 (2004) DOI:10.1023/B:APPT.0000045786.98031.1d.

618. Ashkenazi, A. & Salvesen, G. Regulated Cell Death: Signaling and Mechanisms. *Annu. Rev. Cell Dev. Biol.* **30**, 337–356 (2014) DOI:10.1146/annurev-cellbio-100913-013226.

619. Maślińska, D. Apoptosis: physiological cell death and its role in pathogenesis of diseases. *Neurologia i neurochirurgia polska* vol. 37 315–326 (2003).

620. Taylor, R. C., Cullen, S. P. & Martin, S. J. Apoptosis: Controlled demolition at the cellular level. *Nature Reviews Molecular Cell Biology* vol. 9 231–241 (2008) DOI:10.1038/nrm2312.

621. Borges, H. L., Linden, R. & Wang, J. Y. J. DNA damage-induced cell death: Lessons from the central nervous system. *Cell Res.* **18**, 17–26 (2008) DOI:10.1038/cr.2007.110.

622. Norbury, C. J. & Zhivotovsky, B. DNA damage-induced apoptosis. *Oncogene* vol. 23 2797–2808 (2004) DOI:10.1038/sj.onc.1207532.

623. Roos, W. P. & Kaina, B. DNA damage-induced cell death by apoptosis. *Trends in Molecular Medicine* vol. 12 440–450 (2006) DOI:10.1016/j.molmed.2006.07.007.

624. Lou, Z. & Chen, J. Cellular senescence and DNA repair. *Experimental Cell Research* vol. 312 2641–2646 (2006) DOI:10.1016/j.yexcr.2006.06.009.

625. Wang, H. & Xu, X. Microhomology-mediated end joining: New players join the team. *Cell and Bioscience* vol. 7 6 (2017) DOI:10.1186/s13578-017-0136-8.

626. Agarwal, M. L., Agarwal, A., Taylor, W. R. & Stark, G. R. p53 controls both the G2/M and the G1 cell cycle checkpoints and mediates reversible growth arrest in human fibroblasts. *Proc. Natl. Acad. Sci. U. S. A.* **92**, 8493–8497 (1995) DOI:10.1073/pnas.92.18.8493.

627. Barak, Y., Juven, T., Haffner, R. & Oren, M. mdm2 expression is induced by wild type p53 activity. *EMBO J.* **12**, 461–468 (1993) DOI:10.1002/j.1460-2075.1993.tb05678.x.

628. Bunz, F. *et al.* Requirement for p53 and p21 to sustain G2 arrest after DNA damage. *Science (80-.).* **282**, 1497–1501 (1998) DOI:10.1126/science.282.5393.1497.

629. Fiscella, M. *et al.* Wip1, a novel human protein phosphatase that is induced in response to ionizing radiation in a p53-dependent manner. *Proc. Natl. Acad. Sci. U. S. A.* **94**, 6048–6053 (1997) DOI:10.1073/pnas.94.12.6048.

630. Lu, X., Nannenga, B. & Donehower, L. A. PPM1D dephosphorylates Chk1 and p53 and abrogates cell cycle checkpoints. *Genes Dev.* **19**, 1162–1174 (2005) DOI:10.1101/gad.1291305.

631. Lu, X. *et al.* The Wip1 Phosphatase Acts as a Gatekeeper in the p53-Mdm2 Autoregulatory Loop. *Cancer Cell* **12**, 342–354 (2007) DOI:10.1016/j.ccr.2007.08.033.

632. Wade, M., Li, Y. C. & Wahl, G. M. MDM2, MDMX and p53 in oncogenesis and cancer therapy. *Nature Reviews Cancer* vol. 13 83–96 (2013) DOI:10.1038/nrc3430.

633. Bakalkin, G. *et al.* p53 binds single-stranded DNA ends and catalyzes DNA renaturation and strand transfer. *Proc. Natl. Acad. Sci. U. S. A.* **91**, 413–417 (1994) DOI:10.1073/pnas.91.1.413.

634. Marchenko, N. D., Zaika, A. & Moll, U. M. Death signal-induced localization of p53 protein to mitochondria: A potential role in apoptotic signaling. *J. Biol. Chem.* **275**, 16202–16212 (2000) DOI:10.1074/jbc.275.21.16202.

635. Mihara, M. *et al.* p53 has a direct apoptogenic role at the mitochondria. *Mol. Cell* **11**, 577–590 (2003) DOI:10.1016/S1097-2765(03)00050-9.

636. Yu, J. & Zhang, L. No PUMA, no death: Implications for p53-dependent apoptosis. *Cancer Cell* vol. 4 248–249 (2003) DOI:10.1016/S1535-6108(03)00249-6.

637. Abu-Qare, A. W. & Abou-Donia, M. B. Biomarkers of apoptosis: Release of cytochrome c, activation of caspase-3, induction of 8-hydroxy-2'-deoxyguanosine, increased 3-

nitrotyrosine, and alteration of p53 gene. *J. Toxicol. Environ. Heal. - Part B Crit. Rev.* **4**, 313–332 (2001) DOI:10.1080/109374001301419737.

638. Stewart, G. S., Wang, B., Bigneli, C. R., Taylor, A. M. R. & Elledge, S. J. MDC1 is a mediator of the mammalian DNA damage checkpoint. *Nature* **421**, 961–966 (2003) DOI:10.1038/nature01446.

639. Stucki, M. *et al.* MDC1 directly binds phosphorylated histone H2AX to regulate cellular responses to DNA double-strand breaks. *Cell* **123**, 1213–1226 (2005) DOI:10.1016/j.cell.2005.09.038.

640. Sperka, T., Wang, J. & Rudolph, K. L. DNA damage checkpoints in stem cells, ageing and cancer. *Nature Reviews Molecular Cell Biology* vol. 13 579–590 (2012) DOI:10.1038/nrm3420.

641. Bartek, J. & Lukas, J. Chk1 and Chk2 kinases in checkpoint control and cancer. *Cancer Cell* vol. 3 421–429 (2003) DOI:10.1016/S1535-6108(03)00110-7.

642. Lukas, C. *et al.* DNA Damage-activated Kinase Chk2 Is Independent of Proliferation or Differentiation Yet Correlates with Tissue Biology. *Cancer Res.* **61**, (2001).

643. Cho, Y. S. *et al.* Phosphorylation-Driven Assembly of the RIP1-RIP3 Complex Regulates Programmed Necrosis and Virus-Induced Inflammation. *Cell* **137**, 1112–1123 (2009) DOI:10.1016/j.cell.2009.05.037.

644. He, S. *et al.* Receptor Interacting Protein Kinase-3 Determines Cellular Necrotic Response to TNF-α. *Cell* **137**, 1100–1111 (2009) DOI:10.1016/j.cell.2009.05.021.

645. Vandenabeele, P., Galluzzi, L., Vanden Berghe, T. & Kroemer, G. Molecular mechanisms of necroptosis: An ordered cellular explosion. *Nature Reviews Molecular Cell Biology* vol. 11 700–714 (2010) DOI:10.1038/nrm2970.

646. Zhang, D. W. *et al.* RIP3, an energy metabolism regulator that switches TNF-induced cell death from apoptosis to necrosis. *Science (80-.).* **325**, 332–336 (2009) DOI:10.1126/science.1172308.

647. Cho, Y. S., McQuade, T., Zhang, H., Zhang, J. & Chan, F. K. M. RIP1-dependent and independent effects of necrostatin-1 in necrosis and T cell activation. *PLoS One* **6**, (2011) DOI:10.1371/journal.pone.0023209.

648. Kaiser, W. J., Upton, J. W. & Mocarski, E. S. Viral modulation of programmed necrosis. *Current Opinion in Virology* vol. 3 296–306 (2013) DOI:10.1016/j.coviro.2013.05.019.

649. Degterev, A. *et al.* Identification of RIP1 kinase as a specific cellular target of necrostatins. *Nat. Chem. Biol.* **4**, 313–321 (2008) DOI:10.1038/nchembio.83.

650. Smith, C. C. T. *et al.* Necrostatin: A potentially novel cardioprotective agent? *Cardiovasc. Drugs Ther.* **21**, 227–233 (2007) DOI:10.1007/s10557-007-6035-1.

651. Lin, J. *et al.* A Role of RIP3-Mediated Macrophage Necrosis in Atherosclerosis Development. *Cell Rep.* **3**, 200–210 (2013) DOI:10.1016/j.celrep.2012.12.012.

652. Linkermann, A. *et al.* Rip1 (Receptor-interacting protein kinase 1) mediates necroptosis and contributes to renal ischemia/reperfusion injury. *Kidney Int.* **81**, 751–761 (2012) DOI:10.1038/ki.2011.450.

653. Oerlemans, M. I. F. J. *et al.* Inhibition of RIP1-dependent necrosis prevents adverse cardiac remodeling after myocardial ischemia-reperfusion in vivo. *Basic Res. Cardiol.* **107**, (2012) DOI:10.1007/s00395-012-0270-8.

654. Wu, J. *et al.* Mlkl knockout mice demonstrate the indispensable role of Mlkl in necroptosis. *Cell Res.* **23**, 994–1006 (2013) DOI:10.1038/cr.2013.91.

655. Günther, C. *et al.* Caspase-8 regulates TNF-α-induced epithelial necroptosis and terminal ileitis. *Nature* **477**, 335–339 (2011) DOI:10.1038/nature10400.

656. Welz, P. S. *et al.* FADD prevents RIP3-mediated epithelial cell necrosis and chronic intestinal inflammation. *Nature* **477**, 330–334 (2011) DOI:10.1038/nature10273.

657. Cho, Y. S. The role of necroptosis in the treatment of diseases. *BMB Reports* vol. 51 219–224 (2018) DOI:10.5483/BMBRep.2018.51.5.074.

658. Kaiser, W. J. *et al.* RIP3 mediates the embryonic lethality of caspase-8-deficient mice. *Nature* **471**, 368–373 (2011) DOI:10.1038/nature09857.

659. Kim, S. J. & Li, J. Caspase blockade induces RIP3-mediated programmed necrosis in Toll-like receptor-activated microglia. *Cell Death Dis.* **4**, (2013) DOI:10.1038/cddis.2013.238.

660. Seya, T. *et al.* TLR3/TICAM-1 signaling in tumor cell RIP3-dependent necroptosis. *Oncoimmunology* **1**, 917–923 (2012) DOI:10.4161/onci.21244.

661. Upton, J. W., Kaiser, W. J. & Mocarski, E. S. DAI/ZBP1/DLM-1 complexes with RIP3 to mediate virus-induced programmed necrosis that is targeted by murine cytomegalovirus vIRA. *Cell Host Microbe* **11**, 290–297 (2012) DOI:10.1016/j.chom.2012.01.016.

662. Welz, P. S. & Pasparakis, M. A way to DAI. *Cell Host and Microbe* vol. 11 223–225 (2012) DOI:10.1016/j.chom.2012.02.003.

663. Seo, J. *et al.* The roles of ubiquitination in extrinsic cell death pathways and its implications for therapeutics. *Biochemical Pharmacology* vol. 162 21–40 (2019) DOI:10.1016/j.bcp.2018.11.012.

664. Ding, J. *et al.* Rapamycin Inhibited Photoreceptor Necroptosis and Protected the Retina by Activation of Autophagy in Experimental Retinal Detachment. *Curr. Eye Res.* **44**, 739–745 (2019) DOI:10.1080/02713683.2019.1588331.

665. Chen, W. *et al.* Diverse sequence determinants control human and mouse receptor interacting protein 3 (RIP3) and mixed lineage kinase domain-like (MLKL) interaction in necroptotic signaling. *J. Biol. Chem.* **288**, 16247–16261 (2013) DOI:10.1074/jbc.M112.435545.

666. Chen, X. *et al.* Translocation of mixed lineage kinase domain-like protein to plasma membrane leads to necrotic cell death. *Cell Res.* **24**, 105–121 (2014) DOI:10.1038/cr.2013.171.

667. Wang, H. *et al.* Mixed Lineage Kinase Domain-like Protein MLKL Causes Necrotic Membrane Disruption upon Phosphorylation by RIP3. *Mol. Cell* **54**, 133–146 (2014)

DOI:10.1016/j.molcel.2014.03.003.

668. Quarato, G. *et al.* Sequential Engagement of Distinct MLKL Phosphatidylinositol-Binding Sites Executes Necroptosis. *Mol. Cell* **61**, 589–601 (2016) DOI:10.1016/j.molcel.2016.01.011.

669. Seo, J. *et al.* Beclin 1 functions as a negative modulator of MLKL oligomerisation by integrating into the necrosome complex. *Cell Death Differ.* 1–17 (2020) doi:10.1038/s41418-020-0561-9 DOI:10.1038/s41418-020-0561-9.

670. Das, G., Shravage, B. V. & Baehrecke, E. H. Regulation and function of autophagy during cell survival and cell death. *Cold Spring Harb. Perspect. Biol.* **4**, 1–14 (2012) DOI:10.1101/cshperspect.a008813.

671. DeMartino, G. N. Introduction to the Thematic Minireview Series: Autophagy. *Journal of Biological Chemistry* vol. 293 5384–5385 (2018) DOI:10.1074/jbc.TM118.002429.

672. Galluzzi, L., Bravo-San Pedro, J. M., Blomgren, K. & Kroemer, G. Autophagy in acute brain injury. *Nature Reviews Neuroscience* vol. 17 467–484 (2016) DOI:10.1038/nrn.2016.51.

673. Mizushima, N. Autophagy in protein and organelle turnover. *Cold Spring Harb. Symp. Quant. Biol.* **76**, 397–402 (2011) DOI:10.1101/sqb.2011.76.011023.

674. Sharma, K., Le, N., Alotaibi, M. & Gewirtz, D. A. Cytotoxic autophagy in cancer therapy. *International Journal of Molecular Sciences* vol. 15 10034–10051 (2014) DOI:10.3390/ijms150610034.

675. Zhang, H. & Baehrecke, E. H. Eaten alive: Novel insights into autophagy from multicellular model systems. *Trends in Cell Biology* vol. 25 376–387 (2015) DOI:10.1016/j.tcb.2015.03.001.

676. Klionsky, D. J. & Emr, S. D. Autophagy as a regulated pathway of cellular degradation. *Science* vol. 290 1717–1721 (2000) DOI:10.1126/science.290.5497.1717.

677. Levine, B. & Klionsky, D. J. Development by self-digestion: Molecular mechanisms and biological functions of autophagy. *Developmental Cell* vol. 6 463–477 (2004)

DOI:10.1016/S1534-5807(04)00099-1.

678. Doria, A., Gatto, M. & Punzi, L. Autophagy in human health and disease. *New England Journal of Medicine* vol. 368 1845–1846 (2013) DOI:10.1056/NEJMc1303158.

679. Bravo-San Pedro, J. M., Kroemer, G. & Galluzzi, L. Autophagy and Mitophagy in Cardiovascular Disease. *Circulation Research* vol. 120 1812–1824 (2017) DOI:10.1161/CIRCRESAHA.117.311082.

680. Gatica, D., Chiong, M., Lavandero, S. & Klionsky, D. J. Molecular mechanisms of autophagy in the cardiovascular system. *Circulation Research* vol. 116 456–467 (2015) DOI:10.1161/CIRCRESAHA.114.303788.

681. Menzies, F. M. *et al.* Autophagy and Neurodegeneration: Pathogenic Mechanisms and Therapeutic Opportunities. *Neuron* vol. 93 1015–1034 (2017) DOI:10.1016/j.neuron.2017.01.022.

682. Menzies, F. M., Fleming, A. & Rubinsztein, D. C. Compromised autophagy and neurodegenerative diseases. *Nature Reviews Neuroscience* vol. 16 345–357 (2015) DOI:10.1038/nrn3961.

683. Shimizu, S. *et al.* Role of Bcl-2 family proteins in a non-apoptopic programmed cell death dependent on autophagy genes. *Nat. Cell Biol.* **6**, 1221–1228 (2004) DOI:10.1038/ncb1192.

684. Elgendy, M., Sheridan, C., Brumatti, G. & Martin, S. J. Oncogenic Ras-Induced Expression of Noxa and Beclin-1 Promotes Autophagic Cell Death and Limits Clonogenic Survival. *Mol. Cell* **42**, 23–35 (2011) DOI:10.1016/j.molcel.2011.02.009.

685. Galluzzi, L. *et al.* Autophagy in malignant transformation and cancer progression. *EMBO J.* **34**, 856–880 (2015) DOI:10.15252/embj.201490784.

686. Levy, J. M. M., Towers, C. G. & Thorburn, A. Targeting autophagy in cancer. *Nature Reviews Cancer* vol. 17 528–542 (2017) DOI:10.1038/nrc.2017.53.

687. Levy, J. M. M. *et al.* Autophagy inhibition overcomes multiple mechanisms of resistance to BRAF inhibition in brain tumors. *Elife* **6**, (2017) DOI:10.7554/eLife.19671.

688. Liu, P. *et al.* High autophagic flux guards ESC identity through coordinating autophagy machinery gene program by FOXO1. *Cell Death Differ.* **24**, 1672–1680 (2017) DOI:10.1038/cdd.2017.90.

689. Pagotto, A. *et al.* Autophagy inhibition reduces chemoresistance and tumorigenic potential of human ovarian cancer stem cells. *Cell Death Dis.* **8**, e2943 (2017) DOI:10.1038/cddis.2017.327.

690. Sica, V. *et al.* Organelle-Specific Initiation of Autophagy. *Molecular Cell* vol. 59 522–539 (2015) DOI:10.1016/j.molcel.2015.07.021.

691. Frost, L. S., Mitchell, C. H. & Boesze-Battaglia, K. Autophagy in the eye: Implications for ocular cell health. *Experimental Eye Research* vol. 124 56–66 (2014) DOI:10.1016/j.exer.2014.04.010.

692. Serageldin, I. Ancient Alexandria and the dawn of medical science. *Glob. Cardiol. Sci. Pract.* **2013**, 47 (2013) DOI:10.5339/gcsp.2013.47.

693. Blits, K. C. Aristotle: Form, function, and comparative anatomy. *Anat. Rec.* **257**, 58–63 (1999) DOI:10.1002/(SICI)1097-0185(19990415)257:2<58::AID-AR6>3.0.CO;2-I.

694. Bourne, M. C., Campbell, D. A. & Tansley, K. HEREDITARY DEGENERATION OF THE RAT RETINA. *Br. J. Ophthalmol.* **22**, 613–623 (1938) DOI:10.1136/bjo.22.10.613.

695. Chatztnoff, A., Millman, N., Oroshnik, W. & Rosen, F. 11-Cis vitamin A in the prevention of retinal rod degeneration. An animal study. *Am. J. Ophthalmol.* **46**, 205–210 (1958) DOI:10.1016/0002-9394(58)90799-2.

696. Hawkins, R. K., Jansen, H. G. & Sanyal, S. Development and degeneration of retina in rds mutant mice: Photoreceptor abnormalities in the heterozygotes. *Exp. Eye Res.* **41**, 701–720 (1985) DOI:10.1016/0014-4835(85)90179-4.

697. Sanyal, S., De Ruiter, A. & Hawkins, R. K. Development and degeneration of retina in rds mutant mice: Light microscopy. *J. Comp. Neurol.* **194**, 193–207 (1980) DOI:10.1002/cne.901940110.

698. Sidman, R. L. & Green, M. C. Retinal degeneration in the mouse: Location of the rd locus in linkage group xvii. *J. Hered.* **56**, 23–29 (1965) DOI:10.1093/oxfordjournals.jhered.a107364.

699. Collin, G. B. *et al.* Mouse Models of Inherited Retinal Degeneration with Photoreceptor Cell Loss. *Cells* vol. 9 (2020) DOI:10.3390/cells9040931.

700. Thomas, K. R. & Capecchi, M. R. Site-directed mutagenesis by gene targeting in mouse embryo-derived stem cells. *Cell* **51**, 503–512 (1987) DOI:10.1016/0092-8674(87)90646-5.

701. Hall, B., Limaye, A. & Kulkarni, A. B. Overview: Generation of Gene Knockout Mice. *Current Protocols in Cell Biology* vol. CHAPTER Unit (2009) DOI:10.1002/0471143030.cb1912s44.

702. Yoshimi, K. & Mashimo, T. Application of genome editing technologies in rats for human disease models review-article. *Journal of Human Genetics* vol. 63 115–123 (2018) DOI:10.1038/s10038-017-0346-2.

703. Gurumurthy, C. B. & Kent Lloyd, K. C. Generating mouse models for biomedical research: Technological advances. *DMM Dis. Model. Mech.* **12**, (2019) DOI:10.1242/dmm.029462.

704. Davies, B. *et al.* Site Specific Mutation of the Zic2 Locus by Microinjection of TALEN mRNA in Mouse CD1, C3H and C57BL/6J Oocytes. *PLoS One* **8**, e60216 (2013) DOI:10.1371/journal.pone.0060216.

705. Sander, J. D. *et al.* Targeted gene disruption in somatic zebrafish cells using engineered TALENs. *Nature Biotechnology* vol. 29 697–698 (2011) DOI:10.1038/nbt.1934.

706. Jinek, M. *et al.* A programmable dual-RNA-guided DNA endonuclease in adaptive bacterial immunity. *Science (80-.).* **337**, 816–821 (2012) DOI:10.1126/science.1225829.

707. Kim, H. & Kim, J. S. A guide to genome engineering with programmable nucleases. *Nature Reviews Genetics* vol. 15 321–334 (2014) DOI:10.1038/nrg3686.

708. Maxam, A. M. & Gilbert, W. A new method for sequencing DNA. *Proc. Natl. Acad. Sci. U. S. A.* **74**, 560–564 (1977) DOI:10.1073/pnas.74.2.560.

709. Sanger, F. & Coulson, A. R. A rapid method for determining sequences in DNA by primed

synthesis with DNA polymerase. *J. Mol. Biol.* **94**, 441–448 (1975) DOI:10.1016/0022-2836(75)90213-2.

710. Heather, J. M. & Chain, B. The sequence of sequencers: The history of sequencing DNA. *Genomics* vol. 107 1–8 (2016) DOI:10.1016/j.ygeno.2015.11.003.

711. Slijkerman, R. W. N. *et al.* The pros and cons of vertebrate animal models for functional and therapeutic research on inherited retinal dystrophies. *Progress in Retinal and Eye Research* vol. 48 137–159 (2015) DOI:10.1016/j.preteyeres.2015.04.004.

712. Winkler, P. A., Occelli, L. M. & Petersen-Jones, S. M. Large Animal Models of Inherited Retinal Degenerations: A Review. *Cells* **9**, 882 (2020) DOI:10.3390/cells9040882.

713. Grünert, U. & Martin, P. R. Cell types and cell circuits in human and non-human primate retina. *Progress in Retinal and Eye Research* 100844 (2020) doi:10.1016/j.preteyeres.2020.100844 DOI:10.1016/j.preteyeres.2020.100844.

714. Samardzija, M. & Grimm, C. Mouse models for cone degeneration. *Adv. Exp. Med. Biol.* **801**, 567–573 (2014) DOI:10.1007/978-1-4614-3209-8_72.

715. Le Meur, G. *et al.* Safety and Long-Term Efficacy of AAV4 Gene Therapy in Patients with RPE65 Leber Congenital Amaurosis. *Mol. Ther.* **26**, 256–268 (2018) DOI:10.1016/j.ymthe.2017.09.014.

716. Chang, B. *et al.* Retinal degeneration mutants in the mouse. *Vision Res.* **42**, 517–525 (2002) DOI:10.1016/S0042-6989(01)00146-8.

717. Fletcher, E. L. *et al.* Animal models of retinal disease. in *Progress in Molecular Biology and Translational Science* vol. 100 211–286 (Elsevier B.V., 2011). DOI:10.1016/B978-0-12-384878-9.00006-6.

718. RetNet - Retinal Information Network. https://sph.uth.edu/retnet/home.htm.

719. Cook, S. A. *et al.* A mouse model for Meckel syndrome type 3. *J. Am. Soc. Nephrol.* **20**, 753–64 (2009) DOI:10.1681/ASN.2008040412.

720. Mookherjee, S. *et al.* A CEP290 C-Terminal Domain Complements the Mutant CEP290 of Rd16 Mice In Trans and Rescues Retinal Degeneration. *Cell Rep.* **25**, 611-623.e6 (2018) DOI:10.1016/j.celrep.2018.09.043.

721. Chang, B. *et al.* In-frame deletion in a novel centrosomal/ciliary protein CEP290/NPHP6 perturbs its interaction with RPGR and results in early-onset retinal degeneration in the rd16 mouse. *Hum. Mol. Genet.* **15**, 1847–1857 (2006) DOI:10.1093/hmg/ddl107.

722. May-Simera, H. L. *et al.* Primary Cilium-Mediated Retinal Pigment Epithelium Maturation Is Disrupted in Ciliopathy Patient Cells. *Cell Rep.* **22**, 189–205 (2018) DOI:10.1016/j.celrep.2017.12.038.

723. Stowe, T. R., Wilkinson, C. J., Iqbal, A. & Stearns, T. The centriolar satellite proteins Cep72 and Cep290 interact and are required for recruitment of BBS proteins to the cilium. *Mol. Biol. Cell* **23**, 3322–3335 (2012) DOI:10.1091/mbc.E12-02-0134.

724. Collin, G. B. *et al.* Mutations in ALMS1 cause obesity, type 2 diabetes and neurosensory degeneration in Alström syndrome. *Nat. Genet.* **31**, 74–78 (2002) DOI:10.1038/ng867.

725. Hearn, T. *et al.* Mutation of ALMS1, a large gene with a tandem repeat encoding 47 amino acids, causes Alström syndrome. *Nat. Genet.* **31**, 79–83 (2002) DOI:10.1038/ng874.

726. Collin, G. B. *et al.* Alms1-disrupted mice recapitulate human Alström syndrome. *Hum. Mol. Genet.* **14**, 2323–2333 (2005) DOI:10.1093/hmg/ddi235.

727. Lewis, W. R. *et al.* Mks6 mutations reveal tissue- and cell type-specific roles for the cilia transition zone. *FASEB J.* **33**, 1440–1455 (2019) DOI:10.1096/fj.201801149R.

728. Liu, X. *et al. Usherin is required for maintenance of retinal photoreceptors and normal development of cochlear hair cells*. www.sph.uth.tmc.edu/Retnet (2007).

729. Vervoort, R. & Wright, A. F. Mutations ofRPGR in X-linked retinitis pigmentosa (RP3). *Hum. Mutat.* **19**, 486–500 (2002) DOI:10.1002/humu.10057.

730. Charng, J. *et al.* Variegated yet non-random rod and cone photoreceptor disease patterns in RPGR-ORF15-associated retinal degeneration. *Hum. Mol. Genet.* **25**, 5444–5459 (2016)

DOI:10.1093/hmg/ddw361.

731. Fischer, M. D. *et al.* Codon-Optimized RPGR Improves Stability and Efficacy of AAV8 Gene Therapy in Two Mouse Models of X-Linked Retinitis Pigmentosa. *Mol. Ther.* **25**, 1854–1865 (2017) DOI:10.1016/j.ymthe.2017.05.005.

732. Wu, Z. *et al.* A long-term efficacy study of gene replacement therapy for RPGR-associated retinal degeneration. *Hum. Mol. Genet.* **24**, 3956–3970 (2015) DOI:10.1093/hmg/ddv134.

733. Schlegel, J. *et al.* Toward genome editing in X-linked RP—development of a mouse model with specific treatment relevant features. *Transl. Res.* **203**, 57–72 (2019) DOI:10.1016/j.trsl.2018.08.006.

734. Agassandian, M., Patel, M., Bakotic, B. & Agassandian, K. Ciliary Defects in a Mouse Model of Bardet–Biedl Syndrome are Selectively Pronounced in Brain Regions Involved in Cardiovascular Regulation. *Neurosci. Behav. Physiol.* **48**, 28–38 (2018) DOI:10.1007/s11055-017-0526-8.

735. Zhang, Q. *et al.* Bardet-Biedl syndrome 3 (Bbs3) knockout mouse model reveals common BBS-associated phenotypes and Bbs3 unique phenotypes. *Proc. Natl. Acad. Sci. U. S. A.* **108**, 20678–20683 (2011) DOI:10.1073/pnas.1113220108.

736. Davis, R. E. *et al.* A knockin mouse model of the Bardet-Biedl syndrome 1 M390R mutation has cilia defects, ventriculomegaly, retinopathy, and obesity. *Proc. Natl. Acad. Sci. U. S. A.* **104**, 19422–19427 (2007) DOI:10.1073/pnas.0708571104.

737. Hsu, Y., Garrison, J. E., Seo, S. & Sheffield, V. C. The absence of BBSome function decreases synaptogenesis and causes ectopic synapse formation in the retina. *Sci. Rep.* **10**, (2020) DOI:10.1038/s41598-020-65233-4.

738. Brun, A. *et al.* In vivo phenotypic and molecular characterization of retinal degeneration in mouse models of three ciliopathies. *Exp. Eye Res.* **186**, 107721 (2019) DOI:10.1016/j.exer.2019.107721.

739. Haq, N. *et al.* Loss of Bardet-Biedl syndrome proteins causes synaptic aberrations in

principal neurons. *PLoS Biol.* **17**, (2019) DOI:10.1371/journal.pbio.3000414.

740. Mykytyn, K. *et al.* Bardet-Bledl syndrome type 4 (BBS4)-null mice implicate Bbs4 in flagella formation but not global cilia assembly. *Proc. Natl. Acad. Sci. U. S. A.* **101**, 8664–8669 (2004) DOI:10.1073/pnas.0402354101.

741. Eichers, E. R. *et al.* Phenotypic characterization of Bbs4 null mice reveals age-dependent penetrance and variable expressivity. *Hum. Genet.* **120**, 211–226 (2006) DOI:10.1007/s00439-006-0197-y.

742. Cortellino, S. *et al.* Defective ciliogenesis, embryonic lethality and severe impairment of the Sonic Hedgehog pathway caused by inactivation of the mouse complex A intraflagellar transport gene Ift122/Wdr10, partially overlapping with the DNA repair gene Med1/Mbd4. *Dev. Biol.* **325**, 225–237 (2009) DOI:10.1016/j.ydbio.2008.10.020.

743. Murcia, N., Richards, W., Yoder, B., … M. M.- & 2000, undefined. The Oak Ridge Polycystic Kidney (orpk) disease gene is required for left-right axis determination. *dev.biologists.org*.

744. Stottmann, R. W., Tran, P. V., Turbe-Doan, A. & Beier, D. R. Ttc21b is required to restrict sonic hedgehog activity in the developing mouse forebrain. *Dev. Biol.* **335**, 166–178 (2009) DOI:10.1016/j.ydbio.2009.08.023.

745. Gorivodsky, M. *et al.* Intraflagellar transport protein 172 is essential for primary cilia formation and plays a vital role in patterning the mammalian brain. *Dev. Biol.* **325**, 24–32 (2009) DOI:10.1016/j.ydbio.2008.09.019.

746. Rix, S., Calmont, A., … P. S.-H. molecular & 2011, undefined. An Ift80 mouse model of short rib polydactyly syndromes shows defects in hedgehog signalling without loss or malformation of cilia. *academic.oup.com*.

747. Berbari, N. F., O'Connor, A. K., Haycraft, C. J. & Yoder, B. K. The Primary Cilium as a Complex Signaling Center. *Current Biology* vol. 19 R526 (2009) DOI:10.1016/j.cub.2009.05.025.

748. Bangs, F. & Anderson, K. V. Primary Cilia and Mammalian Hedgehog Signaling. *Cold Spring Harb. Perspect. Biol.* **9**, (2017) DOI:10.1101/cshperspect.a028175.

749. Ko, H. W., Liu, A. & Eggenschwiler, J. T. Analysis of Hedgehog Signaling in Mouse Intraflagellar Transport Mutants. in *Methods in cell biology* vol. 93 347–369 (2009). DOI:10.1016/S0091-679X(08)93017-X.

750. Pazour, G. J. *et al.* The intraflagellar transport protein, IFT88, is essential for vertebrate photoreceptor assembly and maintenance. *J. Cell Biol.* **157**, 103–113 (2002) DOI:10.1083/jcb.200107108.

751. Gupta, P., Pendse, N., … S. G.-H. molecular & 2018, undefined. Ift172 conditional knock-out mice exhibit rapid retinal degeneration and protein trafficking defects. *academic.oup.com*.

752. Keady, B. T., Le, Y. Z. & Pazour, G. J. IFT20 is required for opsin trafficking and photoreceptor outer segment development. *Mol. Biol. Cell* **22**, 921–930 (2011) DOI:10.1091/mbc.E10-09-0792.

753. Corso-Díaz, X., Jaeger, C., Chaitankar, V. & Swaroop, A. Epigenetic control of gene regulation during development and disease: A view from the retina. *Progress in Retinal and Eye Research* vol. 65 1–27 (2018) DOI:10.1016/j.preteyeres.2018.03.002.

754. Pennington, K. L. & DeAngelis, M. M. Epigenetic mechanisms of the aging human retina. *Journal of Experimental Neuroscience* vol. 9s2 51–79 (2015) DOI:10.4137/JEN.S25513.

755. O'Sullivan, R. J. & Karlseder, J. The great unravelling: Chromatin as a modulator of the aging process. *Trends in Biochemical Sciences* vol. 37 466–476 (2012) DOI:10.1016/j.tibs.2012.08.001.

756. Collin, G. B. *et al.* Mouse Models of Inherited Retinal Degeneration with Photoreceptor Cell Loss. *Cells* vol. 9 (2020) DOI:10.3390/cells9040931.

757. Zelinger, L. & Swaroop, A. RNA Biology in Retinal Development and Disease. *Trends in Genetics* vol. 34 341–351 (2018) DOI:10.1016/j.tig.2018.01.002.

758. Hakem, R. DNA-damage repair; the good, the bad, and the ugly. *EMBO J.* **27**, 589–605 (2008) DOI:10.1038/emboj.2008.15.

759. Susaki, K. *et al.* Musashi-1, an RNA-binding protein, is indispensable for survival of photoreceptors. *Exp. Eye Res.* **88**, 347–355 (2009) DOI:10.1016/j.exer.2008.06.019.

760. Li, Y. *et al.* Top2b is involved in the formation of outer segment and synapse during late-stage photoreceptor differentiation by controlling key genes of photoreceptor transcriptional regulatory network. *J. Neurosci. Res.* **95**, 1951–1964 (2017) DOI:10.1002/jnr.24037.

761. Calderwood, S. K. A critical role for topoisomerase IIb and DNA double strand breaks in transcription. *Transcription* **7**, 75–83 (2016) DOI:10.1080/21541264.2016.1181142.

762. Peshti, V. *et al.* Characterization of physiological defects in adult SIRT6-/- mice. *PLoS One* **12**, (2017) DOI:10.1371/journal.pone.0176371.

763. Lim, D., Park, C. W., Ryu, K. Y. & Chung, H. Disruption of the polyubiquitin gene Ubb causes retinal degeneration in mice. *Biochem. Biophys. Res. Commun.* **513**, 35–40 (2019) DOI:10.1016/j.bbrc.2019.03.164.

764. Spoor, M. *et al.* Accelerated loss of hearing and vision in the DNA-repair deficient Ercc1 δ/- mouse. *Mech. Ageing Dev.* **133**, 59–67 (2012) DOI:10.1016/j.mad.2011.12.003.

765. Gorgels, T. G. M. F. *et al.* Retinal Degeneration and Ionizing Radiation Hypersensitivity in a Mouse Model for Cockayne Syndrome. *Mol. Cell. Biol.* **27**, 1433–1441 (2007) DOI:10.1128/mcb.01037-06.

766. Semenova, E., Wang, X. F., Jablonski, M. M., Levorse, J. & Tilghman, S. M. An engineered 800 kilobase deletion of Uchl3 and Lmo7 on mouse chromosome 14 causes defects in viability, postnatal growth and degeneration of muscle and retina. *Hum. Mol. Genet.* **12**, 1301–1312 (2003) DOI:10.1093/hmg/ddg140.

767. Valdés-Sánchez, L. *et al.* ATR localizes to the photoreceptor connecting cilium and deficiency leads to severe photoreceptor degeneration in mice. *Hum. Mol. Genet.* **22**, 1507–1515 (2013) DOI:10.1093/hmg/dds563.

768. Pacione, L. R., Szego, M. J., Ikeda, S., Nishina, P. M. & McInnes, R. R. Progress toward

understanding the genetic and biochemical mechanisms of inherited photoreceptor degenerations. *Annu. Rev. Neurosci.* **26**, 657–700 (2003) DOI:10.1146/annurev.neuro.26.041002.131416.

769. Pinelli, M. *et al.* An atlas of gene expression and gene co-regulation in the human retina. *Nucleic Acids Res.* **44**, 5773–5784 (2016) DOI:10.1093/nar/gkw486.

770. Hoshino, A. *et al.* Molecular Anatomy of the Developing Human Retina. *Dev. Cell* **43**, 763-779.e4 (2017) DOI:10.1016/j.devcel.2017.10.029.

771. Graziotto, J. J. *et al.* Three gene-targeted mouse models of RNA splicing factor RP show late-onset RPE and retinal degeneration. *Investig. Ophthalmol. Vis. Sci.* **52**, 190–198 (2011) DOI:10.1167/iovs.10-5194.

772. Xu, M. *et al.* Mutations in the Spliceosome Component CWC27 Cause Retinal Degeneration with or without Additional Developmental Anomalies. *Am. J. Hum. Genet.* **100**, 592–604 (2017) DOI:10.1016/j.ajhg.2017.02.008.

773. Baehr, W. & Frederick, J. M. Naturally occurring animal models with outer retina phenotypes. *Vision Res.* **49**, 2636–2652 (2009) DOI:10.1016/j.visres.2009.04.008.

774. Kostic, C. & Arsenijevic, Y. Animal modelling for inherited central vision loss. *Journal of Pathology* vol. 238 300–310 (2016) DOI:10.1002/path.4641.

775. Roosing, S. *et al.* Causes and consequences of inherited cone disorders. *Prog. Retin. Eye Res.* **42**, 1–26 (2014) DOI:10.1016/j.preteyeres.2014.05.001.

776. Jakobsson, C., Othman, I. S., Munier, F. L., Schorderet, D. F. & Abouzeid, H. Cone-rod dystrophy caused by a novel homozygous RPE65 mutation in Leber congenital amaurosis. *Klin. Monbl. Augenheilkd.* **231**, 405–10 (2014) DOI:10.1055/s-0034-1368221.

777. Al-Khayer, K. *et al.* Thirty-year follow-up of a patient with leber congenital amaurosis and novel RPE65 mutations. *Am. J. Ophthalmol.* **137**, 375–7 (2004) DOI:10.1016/S0002-9394(03)00913-9.

778. Samardzija, M. *et al.* R91W mutation in Rpe65 leads to milder early-onset retinal dystrophy

due to the generation of low levels of 11-cis-retinal. *Hum. Mol. Genet.* **17**, 281–292 (2008) DOI:10.1093/hmg/ddm304.

779. Samardzija, M., Barben, M., Geiger, P. & Grimm, C. The consequences of hypomorphic RPE65 for rod and cone photoreceptors. in *Advances in Experimental Medicine and Biology* vol. 854 341–346 (Springer New York LLC, 2016). DOI:10.1007/978-3-319-17121-0_45.

780. Pang, J. J. *et al.* Retinal degeneration 12 (rd12): A new, spontaneously arising mouse model for human Leber congenital amaurosis (LCA). *Mol. Vis.* **11**, 152–162 (2005).

781. Redmond, T. M. *et al.* Rpe65 is necessary for production of 11-cis-vitamin A in the retinal visual cycle. *Nat. Genet.* **20**, 344–351 (1998) DOI:10.1038/3813.

782. Fan, J., Rohrer, B., Frederick, J. M., Baehr, W. & Crouch, R. K. Rpe65-/- and Lrat-/- mice: Comparable models of Leber congenital amaurosis. *Investig. Ophthalmol. Vis. Sci.* **49**, 2384–2389 (2008) DOI:10.1167/iovs.08-1727.

783. Lorenz, B. *et al.* A comprehensive clinical and biochemical functional study of a novel RPE65 hypomorphic mutation. *Investig. Ophthalmol. Vis. Sci.* **49**, 5235–5242 (2008) DOI:10.1167/iovs.07-1671.

784. Chang, B. *et al.* Cone photoreceptor function loss-3, a novel mouse model of achromatopsia due to a mutation in Gnat2. *Investig. Ophthalmol. Vis. Sci.* **47**, 5017–5021 (2006) DOI:10.1167/iovs.05-1468.

785. Allen, A. E., Cameron, M. A., Brown, T. M., Vugler, A. A. & Lucas, R. J. Visual Responses in Mice Lacking Critical Components of All Known Retinal Phototransduction Cascades. *PLoS One* **5**, e15063 (2010) DOI:10.1371/journal.pone.0015063.

786. Alexander, J. J. *et al.* Restoration of cone vision in a mouse model of achromatopsia. *Nat. Med.* **13**, 685–687 (2007) DOI:10.1038/nm1596.

787. Jobling, A. I., Vessey, K. A., Waugh, M., Mills, S. A. & Fletcher, E. L. A naturally occurring mouse model of achromatopsia: Characterization of the mutation in cone transducin and subsequent retinal phenotype. *Investig. Ophthalmol. Vis. Sci.* **54**, 3350–3359 (2013)

DOI:10.1167/iovs.13-11831.

788. Biel, M. *et al.* Selective loss of cone function in mice lacking the cyclic nucleotide-gated channel CNG3. *Proc. Natl. Acad. Sci. U. S. A.* **96**, 7553–7557 (1999) DOI:10.1073/pnas.96.13.7553.

789. Ding, X. Q. *et al.* Impaired cone function and cone degeneration resulting from CNGB3 deficiency: Down-regulation of CNGA3 biosynthesis as a potential mechanism. *Hum. Mol. Genet.* **18**, 4770–4780 (2009) DOI:10.1093/hmg/ddp440.

790. Arango-Gonzalez, B. *et al.* Identification of a common non-apoptotic cell death mechanism in hereditary retinal degeneration. *PLoS One* **9**, e112142 (2014) DOI:10.1371/journal.pone.0112142.

791. Khan, N. W., Wissinger, B., Kohl, S. & Sieving, P. A. CNGB3 achromatopsia with progressive loss of residual cone function and impaired rod-mediated function. *Investig. Ophthalmol. Vis. Sci.* **48**, 3864–3871 (2007) DOI:10.1167/iovs.06-1521.

792. Kohl, S. *et al.* CNGB3 mutations account for 50% of all cases with autosomal recessive achromatopsia. *Eur. J. Hum. Genet.* **13**, 302–308 (2005) DOI:10.1038/sj.ejhg.5201269.

793. Bernstein, P. S. *et al.* Diverse macular dystrophy phenotype caused by a novel complex mutation in the ELOVL4 gene. *Investig. Ophthalmol. Vis. Sci.* **42**, (2001).

794. Vasireddy, V. *et al.* Elovl4 5-bp-deletion knock-in mice develop progressive photoreceptor degeneration. *Investig. Ophthalmol. Vis. Sci.* **47**, 4558–4568 (2006) DOI:10.1167/iovs.06-0353.

795. Vasireddy, V., Wong, P. & Ayyagari, R. Genetics and molecular pathology of Stargardt-like macular degeneration. *Prog. Retin. Eye Res.* **29**, 191–207 (2010) DOI:10.1016/j.preteyeres.2010.01.001.

796. Schori, C. *et al.* Elovl4 5-bp deletion does not accelerate cone photoreceptor degeneration in an all-cone mouse. *PLoS One* **13**, (2018) DOI:10.1371/journal.pone.0190514.

797. Li, W. *et al.* Elovl4 haploinsufficiency does not induce early onset retinal degeneration in

mice. *Vision Res.* **47**, (2007) DOI:10.1016/j.visres.2006.10.023.

798. Raz-Prag, D. *et al.* Haploinsufficiency is not the key mechanism of pathogenesis in a heterozygous Elovl4 knockout mouse model of STGD3 disease. *Investig. Ophthalmol. Vis. Sci.* **47**, (2006) DOI:10.1167/iovs.05-1527.

799. Karan, G. *et al.* Lipofuscin accumulation, abnormal electrophysiology, and photoreceptor degeneration in mutant ELOVL4 transgenic mice: A model for macular degeneration. *Proc. Natl. Acad. Sci. U. S. A.* **102**, (2005) DOI:10.1073/pnas.0407698102.

800. Harkewicz, R. *et al.* Essential role of ELOVL4 protein in very long chain fatty acid synthesis and retinal function. *J. Biol. Chem.* **287**, (2012) DOI:10.1074/jbc.M111.256073.

801. Radu, R. A. *et al.* Complement system dysregulation and inflammation in the retinal pigment epithelium of a mouse model for Stargardt macular degeneration. *J. Biol. Chem.* **286**, 18593–18601 (2011) DOI:10.1074/jbc.M110.191866.

802. Weng, J. *et al.* Insights into the function of rim protein in photoreceptors and etiology of Stargardt's disease from the phenotype in abcr knockout mice. *Cell* **98**, 13–23 (1999) DOI:10.1016/S0092-8674(00)80602-9.

803. Buch, P. K. *et al.* Dominant Cone-Rod Dystrophy: A Mouse Model Generated by Gene Targeting of the GCAP1/Guca1a Gene. *PLoS One* **6**, e18089 (2011) DOI:10.1371/journal.pone.0018089.

804. Marino, V. *et al.* A novel p.(Glu111Val) missense mutation in GUCA1A associated with cone-rod dystrophy leads to impaired calcium sensing and perturbed second messenger homeostasis in photoreceptors. *Hum. Mol. Genet.* **27**, (2018) DOI:10.1093/hmg/ddy311.

805. Bösl, M. R. *et al.* Male germ cells and photoreceptors, both dependent on close cell-cell interactions, degenerate upon ClC-2 Cl- channel disruption. *EMBO J.* **20**, 1289–1299 (2001) DOI:10.1093/emboj/20.6.1289.

806. Ng, L. *et al.* Type 3 deiodinase, a thyroid-hormone-inactivating enzyme, controls survival and maturation of cone photoreceptors. *J. Neurosci.* **30**, (2010)

DOI:10.1523/JNEUROSCI.5267-09.2010.

807. Ng, L. *et al.* A thyroid hormone receptor that is required for the development of green cone photoreceptors. *Nat. Genet.* **27**, (2001) DOI:10.1038/83829.

808. Tsang, S. H. & Sharma, T. Congenital stationary night blindness. in *Advances in Experimental Medicine and Biology* vol. 1085 61–64 (Springer New York LLC, 2018). DOI:10.1007/978-3-319-95046-4_13.

809. Kimchi, A. *et al.* An Ashkenazi Jewish founder mutation in CACNA1F causes retinal phenotype in both hemizygous males and heterozygous female carriers. *Ophthalmic Genet.* **40**, 443–448 (2019) DOI:10.1080/13816810.2019.1681008.

810. Pasutto, F., Ekici, A., Reis, A., Kremers, J. & Huchzermeyer, C. Novel truncating mutation in CACNA1F in a young male patient diagnosed with optic atrophy. *Ophthalmic Genet.* **39**, 741–748 (2018) DOI:10.1080/13816810.2018.1520263.

811. Waldner, D. M. *et al.* Cone dystrophy and ectopic synaptogenesis in a cacna1f loss of function model of congenital stationary night blindness (CSNB2A). *Channels* **12**, 17–33 (2018) DOI:10.1080/19336950.2017.1401688.

812. Regus-Leidig, H. *et al.* Photoreceptor degeneration in two mouse models for congenital stationary night blindness type 2. *PLoS One* **9**, (2014) DOI:10.1371/journal.pone.0086769.

813. Dai, X. *et al.* Photoreceptor degeneration in a new Cacna1f mutant mouse model. *Exp. Eye Res.* **179**, 106–114 (2019) DOI:10.1016/j.exer.2018.11.010.

814. Dai, X. *et al.* Photoreceptor degeneration in a new Cacna1f mutant mouse model. *Exp. Eye Res.* **179**, 106–114 (2019) DOI:10.1016/j.exer.2018.11.010.

815. Ashery-Padan, R. Somatic gene targeting in the developing and adult mouse retina. *Methods* **28**, 457–464 (2002) DOI:10.1016/S1046-2023(02)00265-7.

816. Li, L. *et al.* Ablation of the X-linked retinitis pigmentosa 2 (Rp2) gene in mice results in opsin mislocalization and photoreceptor degeneration. *Investig. Ophthalmol. Vis. Sci.* **54**, (2013) DOI:10.1167/iovs.13-12140.

817. Li, L. *et al.* Loss of retinitis pigmentosa 2 (RP2) protein affects cone photoreceptor sensory cilium elongation in mice. *Cytoskeleton* **72**, 447–454 (2015) DOI:10.1002/cm.21255.

818. Mookherjee, S. *et al.* Long-term rescue of cone photoreceptor degeneration in retinitis pigmentosa 2 (RP2)-knockout mice by gene replacement therapy. *Hum. Mol. Genet.* **24**, 6446–6458 (2015) DOI:10.1093/hmg/ddv354.

819. Samardzija, M. *et al.* A mouse model for studying cone photoreceptor pathologies. *Investig. Ophthalmol. Vis. Sci.* **55**, 5304–5313 (2014) DOI:10.1167/iovs.14-14789.

820. Ng, L. *et al.* Two transcription factors can direct three photoreceptor outcomes from rod precursor cells in mouse retinal development. *J. Neurosci.* **31**, 11118–11125 (2011) DOI:10.1523/JNEUROSCI.1709-11.2011.

821. Mustafi, D. *et al.* Defective photoreceptor phagocytosis in a mouse model of enhanced S-cone syndrome causes progressive retinal degeneration. *FASEB J.* **25**, 3157–3176 (2011) DOI:10.1096/fj.11-186767.

822. Oh, E. C. T. *et al.* Transformation of cone precursors to functional rod photoreceptors by bZIP transcription factor NRL. *Proc. Natl. Acad. Sci. U. S. A.* **104**, 1679–1684 (2007) DOI:10.1073/pnas.0605934104.

823. Godara, P. *et al.* Assessing retinal structure in complete congenital stationary night blindness and oguchi disease. *Am. J. Ophthalmol.* **154**, (2012) DOI:10.1016/j.ajo.2012.06.003.

824. Teke, M. Y., Citirik, M., Kabacam, S., Demircan, S. & Alikasifoglu, M. A novel missense mutation of the GRK1 gene in Oguchi disease. *Mol. Med. Rep.* **14**, 3129–3133 (2016) DOI:10.3892/mmr.2016.5620.

825. Mucciolo, D. P. *et al.* A novel GRK1 mutation in an Italian patient with Oguchi disease. *Ophthalmic Genetics* vol. 39 137–138 (2018) DOI:10.1080/13816810.2017.1323341.

826. Yetemian, R. M., Brown, B. M. & Craft, C. M. Neovascularization, enhanced inflammatory response, and age-related cone dystrophy in the Nrl -/-Grk1 -/- mouse retina. *Investig.*

Ophthalmol. Vis. Sci. **51**, 6196–6206 (2010) DOI:10.1167/iovs.10-5452.

827. Nathans, J., Thomas, D. & Hogness, D. Molecular genetics of human color vision: the genes encoding blue, green, and red pigments. *Science (80-.).* **232**, 193–202 (1986) DOI:10.1126/science.2937147.

828. Dominy, N. J. & Lucas, P. W. Ecological importance of trichromatic vision to primates. *Nature* **410**, 363–366 (2001) DOI:10.1038/35066567.

829. Jacobs, G. H., Neitz, M., Deegan, J. F. & Neitz, J. Trichromatic colour vision in New World monkeys. *Nature* **382**, 156–158 (1996) DOI:10.1038/382156a0.

830. Yokoyama, S. & Yokoyama, R. Molecular evolution of human visual pigment genes. *Mol. Biol. Evol.* **6**, 186–197 (1989) DOI:10.1093/oxfordjournals.molbev.a040537.

831. Marshak, D. W. & Mills, S. L. Short-wavelength cone-opponent retinal ganglion cells in mammals. *Visual Neuroscience* vol. 31 165–175 (2014) DOI:10.1017/S095252381300031X.

832. Puller, C. & Haverkamp, S. Bipolar cell pathways for color vision in non-primate dichromats. *Visual Neuroscience* vol. 28 51–60 (2011) DOI:10.1017/S0952523810000271.

833. Jacobs, G. H. The distribution and nature of colour vision among the mammals. *Biological Reviews of the Cambridge Philosophical Society* vol. 68 413–471 (1993) DOI:10.1111/j.1469-185x.1993.tb00738.x.

834. Nadal-Nicolás, F. M. *et al.* True S-cones are concentrated in the ventral mouse retina and wired for color detection in the upper visual field. *Elife* **9**, 1–30 (2020) DOI:10.7554/eLife.56840.

835. Bumsted, K. & Hendrickson, A. Distribution and development of short-wavelength cones differ between Macaca monkey and human fovea. *J. Comp. Neurol.* **403**, 502–516 (1999) DOI:10.1002/(SICI)1096-9861(19990125)403:4<502::AID-CNE6>3.0.CO;2-N.

836. Hunt, D. M. & Peichl, L. S cones: Evolution, retinal distribution, development, and spectral sensitivity. *Visual Neuroscience* vol. 31 115–138 (2014) DOI:10.1017/S0952523813000242.

837. Ahnelt, P. K. & Kolb, H. The mammalian photoreceptor mosaic-adaptive design. *Progress in Retinal and Eye Research* vol. 19 711–777 (2000) DOI:10.1016/S1350-9462(00)00012-4.

838. Denman, D. J. *et al.* Mouse color and wavelength-specific luminance contrast sensitivity are non- uniform across visual space. *Elife* **7**, (2018) DOI:10.7554/eLife.31209.

839. Kam, J. H. *et al.* Fundamental differences in patterns of retinal ageing between primates and mice. *Sci. Rep.* **9**, 1–14 (2019) DOI:10.1038/s41598-019-49121-0.

840. Packer, O., Hendrickson, A. E. & Curcio, C. A. Photoreceptor topography of the retina in the adult pigtail macaque (Macaca nemestrina). *J. Comp. Neurol.* **288**, 165–83 (1989) DOI:10.1002/cne.902880113.

841. Sahly, I. *et al.* Localization of Usher 1 proteins to the photoreceptor calyceal processes, which are absent from mice. *J. Cell Biol.* **199**, 381–399 (2012) DOI:10.1083/jcb.201202012.

842. Williams, D. S. Usher syndrome: Animal models, retinal function of Usher proteins, and prospects for gene therapy. *Vision Res.* **48**, 433–441 (2008) DOI:10.1016/j.visres.2007.08.015.

843. Liu, X., Udovichenko, I. P., Brown, S. D. M., Steel, K. P. & Williams, D. S. Myosin VIIa participates in opsin transport through the photoreceptor cilium. *J. Neurosci.* **19**, 6267–6274 (1999) DOI:10.1523/jneurosci.19-15-06267.1999.

844. Libby, R. T., Kitamoto, J., Holme, R. H., Williams, D. S. & Steel, K. P. Cdh23 mutations in the mouse are associated with retinal dysfunction but not retinal degeneration. *Exp. Eye Res.* **77**, 731–739 (2003) DOI:10.1016/j.exer.2003.07.007.

845. Palma, F. Di *et al.* Mutations in Cdh23, encoding a new type of cadherin, cause stereocilia disorganization in waltzer, the mouse model for Usher syndrome type 1D. *Nat. Genet.* **27**, 103–107 (2001) DOI:10.1038/83660.

846. Lefèvre, G. *et al.* A core cochlear phenotype in USH1 mouse mutants implicates fibrous links of the hair bundle in its cohesion, orientation and differential growth. *Development* **135**, 1427–1437 (2008) DOI:10.1242/dev.012922.

847. Purcell, P., Oliver, G., Mardon, G., Donner, A. L. & Maas, R. L. Pax6-dependence of Six3, Eya1 and Dach1 expression during lens and nasal placode induction. *Gene Expr. Patterns* **6**, 110–8 (2005) DOI:10.1016/j.modgep.2005.04.010.

848. Rapicavoli, N. A., Poth, E. M., Zhu, H. & Blackshaw, S. The long noncoding RNA Six3OS acts in trans to regulate retinal development by modulating Six3 activity. *Neural Dev.* **6**, (2011) DOI:10.1186/1749-8104-6-32.

849. Borsani, G. *et al.* EYA4, a novel vertebrate gene related to Drosophila eyes absent. *Hum. Mol. Genet.* **8**, 11–23 (1999) DOI:10.1093/hmg/8.1.11.

850. Söker, T. *et al.* Pleiotropic effects in Eya3 knockout mice. *BMC Dev. Biol.* **8**, 118 (2008) DOI:10.1186/1471-213X-8-118.

851. Azuma, N., Hirakiyama, A., Inoue, T., Asaka, A. & Yamada, M. Mutations of a human homologue of the Drosophila eyes absent gene (EYA1) detected in patients with congenital cataracts and ocular anterior segment anomalies. *Hum. Mol. Genet.* **9**, 363–366 (2000) DOI:10.1093/hmg/9.3.363.

852. Ohto, H. *et al.* Cooperation of Six and Eya in Activation of Their Target Genes through Nuclear Translocation of Eya. *Mol. Cell. Biol.* **19**, 6815–6824 (1999) DOI:10.1128/mcb.19.10.6815.

853. Perez-Carro, R. *et al.* Panel-based NGS Reveals Novel Pathogenic Mutations in Autosomal Recessive Retinitis Pigmentosa. *Sci. Rep.* **6**, 19531 (2016) DOI:10.1038/srep19531.

854. Collin, R. W. J. *et al.* Identification of a 2 Mb Human Ortholog of Drosophila eyes shut/spacemaker that Is Mutated in Patients with Retinitis Pigmentosa. doi:10.1016/j.ajhg.2008.10.014 DOI:10.1016/j.ajhg.2008.10.014.

855. Abd El-Aziz, M. M. *et al.* EYS, encoding an ortholog of Drosophila spacemaker, is mutated in autosomal recessive retinitis pigmentosa. *Nat. Genet.* **40**, 1285–1287 (2008) DOI:10.1038/ng.241.

856. Yuan, R., Peters, L. L. & Paigen, B. Mice as a mammalian model for research on the genetics

of aging. *ILAR Journal* vol. 52 4–15 (2011) DOI:10.1093/ilar.52.1.4.

857. Kenyon, C. J. The genetics of ageing. *Nature* vol. 464 504–512 (2010) DOI:10.1038/nature08980.

858. Van Zant, G. & de Haan, G. Genetic control of lifespan: Studies from animal models. *Expert Rev. Mol. Med.* **1**, 1–12 (1999) DOI:10.1017/S1462399499001441.

859. Ackert-Bicknell, C. L. *et al.* Aging Research Using Mouse Models. *Curr. Protoc. Mouse Biol.* **5**, 95–133 (2015) DOI:10.1002/9780470942390.mo140195.

860. Williams, K. & Roman, J. Studying human respiratory disease in animals - Role of induced and naturally occurring models. *Journal of Pathology* vol. 238 220–232 (2016) DOI:10.1002/path.4658.

861. Gong, B., Levine, S., Barnum, S. & Pasinetti, G. Role of Complement Systems in IVIG Mediated Attenuation of Cognitive Deterioration in Alzheimer's Disease. *Curr. Alzheimer Res.* **11**, 637–644 (2014) DOI:10.2174/1567205011666140812113707.

862. Kudlow, B. A., Kennedy, B. K. & Monnat, R. J. Werner and Hutchinson-Gilford progeria syndromes: Mechanistic basis of human progeroid diseases. *Nature Reviews Molecular Cell Biology* vol. 8 394–404 (2007) DOI:10.1038/nrm2161.

863. Santulli, G. *et al.* Models for preclinical studies in aging-related disorders: One is not for all. *Transl. Med. @ UniSa* **13**, 4–12 (2015).

864. Bracken, M. B. Why animal studies are often poor predictors of human reactions to exposure. *Journal of the Royal Society of Medicine* vol. 102 120–122 (2009) DOI:10.1258/jrsm.2008.08k033.

865. Van Norman, G. A. Limitations of Animal Studies for Predicting Toxicity in Clinical Trials: Is it Time to Rethink Our Current Approach? *JACC Basic to Transl. Sci.* **4**, 845–854 (2019) DOI:10.1016/j.jacbts.2019.10.008.

866. Bailey, J., Thew, M. & Balls, M. Predicting human drug toxicity and safety via animal tests: Can any one species predict drug toxicity in any other, and do monkeys help? *ATLA Altern.*

to Lab. Anim. **43**, 393–403 (2015) DOI:10.1177/026119291504300607.

867. Bailey, J., Thew, M. & Balls, M. An analysis of the use of animal models in predicting human toxicology and drug safety. *ATLA Altern. to Lab. Anim.* **42**, 181–199 (2014) DOI:10.1177/026119291404200306.

868. Van Norman, G. A. Drugs, Devices, and the FDA: Part 1: An Overview of Approval Processes for Drugs. *JACC Basic to Transl. Sci.* **1**, 170–179 (2016) DOI:10.1016/j.jacbts.2016.03.002.

869. Van Norman, G. A. Phase II Trials in Drug Development and Adaptive Trial Design. *JACC Basic to Transl. Sci.* **4**, 428–437 (2019) DOI:10.1016/j.jacbts.2019.02.005.

870. Hackam, D. G. & Redelmeier, D. A. Translation of research evidence from animals to humans [9]. *Journal of the American Medical Association* vol. 296 1731–1732 (2006) DOI:10.1001/jama.296.14.1731.

871. Perel, P. *et al.* Comparison of treatment effects between animal experiments and clinical trials: Systematic review. *Br. Med. J.* **334**, 197–200 (2007) DOI:10.1136/bmj.39048.407928.BE.

872. Wang, B. & Gray, G. Concordance of Noncarcinogenic Endpoints in Rodent Chemical Bioassays. *Risk Anal.* **35**, 1154–1166 (2015) DOI:10.1111/risa.12314.

873. Grandy, R., Tomaz, R. A. & Vallier, L. Modeling Disease with Human Inducible Pluripotent Stem Cells. *Annual Review of Pathology: Mechanisms of Disease* vol. 14 449–468 (2019) DOI:10.1146/annurev-pathol-020117-043634.

874. Haeckel, E. *Natürliche Schöpfungsgeschichte. Gemeinverständliche wissenschaftliche Vorträge über die Entwickelungslehre im Allgemeinen und diejenige von Darwin*. (1868).

875. Ramalho-Santos, M. & Willenbring, H. On the Origin of the Term 'Stem Cell'. *Cell Stem Cell* vol. 1 35–38 (2007) DOI:10.1016/j.stem.2007.05.013.

876. Haeckel, E. *Anthropogenie oder entwickelungsgeschichte des menschen*. (1874).

877. Haeckel, E. *Anthropogenie: oder, Entwickelungsgeschichte des menschen, Keimes-und*

stammesgeschichte. (1877).

878. Befruchtung ... - Theodor Boveri - Google Books. https://books.google.ca/books?hl=en&lr=&id=qucOAQAAIAAJ&oi=fnd&pg=PA383&dq=boveri+1892&ots=5shf1OBSN1&sig=lhQCK97hUdlMCI-6dMTVBBsjo-k&redir_esc=y#v=onepage&q=boveri 1892&f=false.

879. Haecker, V. Die Kerntheilungsvorgänge bei der Mesodermund Entodermbildung von Cyclops. *Arch. für mikroskopische Anat.* **39**, 556–581 (1892) DOI:10.1007/BF02961538.

880. Gurdon, J. B., Elsdale, T. R. & Fischberg, M. Sexually mature individuals of Xenopus laevis from the transplantation of single somatic nuclei. *Nature* **182**, 64–65 (1958) DOI:10.1038/182064a0.

881. GURDON, J. B. The developmental capacity of nuclei taken from intestinal epithelium cells of feeding tadpoles. *J. Embryol. Exp. Morphol.* **10**, (1962).

882. TILL, J. E. & McCULLOCH, E. A. A direct measurement of the radiation sensitivity of normal mouse bone marrow cells. *Radiat. Res.* **14**, (1961) DOI:10.2307/3570892.

883. J E TILL & E A McCULLOCH. Early repair processes in marrow cells irradiated and proliferating in vivo - PubMed. *Radiat Res* (1963).

884. Becker, A. J., McCulloch, E. A. & Till, J. E. Cytological demonstration of the clonal nature of spleen colonies derived from transplanted mouse marrow cells. *Nature* **197**, 452–454 (1963) DOI:10.1038/197452a0.

885. Worton, R. G., McCulloch, E. A. & Till, J. E. Physical separation of hemopoietic stem cells differing in their capacity for self-renewal. *J. Exp. Med.* **130**, 91–103 (1969) DOI:10.1084/jem.130.1.91.

886. Vos, O. & Dolmans, M. J. A. S. SELF-RENEWAL OF COLONY FORMING UNITS (CFU) IN SERIAL BONE MARROW TRANSPLANTATION EXPERIMENTS. *Cell Prolif.* **5**, 371–385 (1972) DOI:10.1111/j.1365-2184.1972.tb00376.x.

887. Thomson, J. A. *et al.* Embryonic stem cell lines derived from human blastocysts. *Science*

282, 1145–7 (1998).

888. Singh, V. K., Saini, A., Kalsan, M., Kumar, N. & Chandra, R. Describing the stem cell potency: The various methods of functional assessment and in silico diagnostics. *Frontiers in Cell and Developmental Biology* vol. 4 134 (2016) DOI:10.3389/fcell.2016.00134.

889. de Kretser, D. Totipotent, pluripotent or unipotent stem cells: a complex regulatory enigma and fascinating biology. *J. Law Med.* **15**, (2007).

890. Donovan, P. J. The germ cell - The mother of all stem cells. *Int. J. Dev. Biol.* **42**, 1043–1050 (1998) DOI:10.1387/ijdb.9853836.

891. Baker, C. L. & Pera, M. F. Capturing Totipotent Stem Cells. *Cell Stem Cell* vol. 22 25–34 (2018) DOI:10.1016/j.stem.2017.12.011.

892. Abu-Dawud, R., Graffmann, N., Ferber, S., Wruck, W. & Adjaye, J. Pluripotent stem cells: induction and self-renewal. *Philos. Trans. R. Soc. B Biol. Sci.* **373**, 20170213 (2018) DOI:10.1098/rstb.2017.0213.

893. Sobhani, A. *et al.* Multipotent stem cell and current application. *Acta Medica Iranica* vol. 55 (2017).

894. Khanlarkhani, N. *et al.* Multipotent Stem Cell and Reproduction. *J. Stem Cells* **11**, 219–229 (2016).

895. Andreotti, J. P. *et al.* Neural stem cell niche heterogeneity. *Seminars in Cell and Developmental Biology* vol. 95 42–53 (2019) DOI:10.1016/j.semcdb.2019.01.005.

896. Zhang, Q. *et al.* Expression and regulation of long noncoding RNAs during the osteogenic differentiation of periodontal ligament stem cells in the inflammatory microenvironment. *Sci. Rep.* **7**, 13991 (2017) DOI:10.1038/s41598-017-14451-4.

897. Takahashi, K. & Yamanaka, S. Induction of Pluripotent Stem Cells from Mouse Embryonic and Adult Fibroblast Cultures by Defined Factors. *Cell* **126**, 663–676 (2006) DOI:10.1016/j.cell.2006.07.024.

898. Takahashi, K. *et al.* Induction of Pluripotent Stem Cells from Adult Human Fibroblasts by Defined Factors. *Cell* **131**, 861–872 (2007) DOI:10.1016/j.cell.2007.11.019.

899. Lo, B. & Parham, L. Ethical issues in stem cell research. *Endocrine Reviews* vol. 30 204–213 (2009) DOI:10.1210/er.2008-0031.

900. Liu, G., David, B. T., Trawczynski, M. & Fessler, R. G. Advances in Pluripotent Stem Cells: History, Mechanisms, Technologies, and Applications. *Stem Cell Reviews and Reports* vol. 16 3–32 (2020) DOI:10.1007/s12015-019-09935-x.

901. Feng, B. *et al.* Reprogramming of fibroblasts into induced pluripotent stem cells with orphan nuclear receptor Esrrb. *Nat. Cell Biol.* **11**, 197–203 (2009) DOI:10.1038/ncb1827.

902. Fong, Y. W. *et al.* A DNA repair complex functions as an Oct4/Sox2 coactivator in embryonic stem cells. *Cell* **147**, 120–131 (2011) DOI:10.1016/j.cell.2011.08.038.

903. Mali, P. *et al.* Improved Efficiency and Pace of Generating Induced Pluripotent Stem Cells from Human Adult and Fetal Fibroblasts. *Stem Cells* **26**, 1998–2005 (2008) DOI:10.1634/stemcells.2008-0346.

904. Theunissen, T. W. *et al.* Systematic Identification of Culture Conditions for Induction and Maintenance of Naive Human Pluripotency. *Cell Stem Cell* **15**, 471–487 (2014) DOI:10.1016/j.stem.2014.07.002.

905. Shi, Y. *et al.* A Combined Chemical and Genetic Approach for the Generation of Induced Pluripotent Stem Cells. *Cell Stem Cell* vol. 2 525–528 (2008) DOI:10.1016/j.stem.2008.05.011.

906. Huangfu, D. *et al.* Induction of pluripotent stem cells by defined factors is greatly improved by small-molecule compounds. *Nat. Biotechnol.* **26**, 795–797 (2008) DOI:10.1038/nbt1418.

907. Shi, Y. *et al.* Induction of Pluripotent Stem Cells from Mouse Embryonic Fibroblasts by Oct4 and Klf4 with Small-Molecule Compounds. *Cell Stem Cell* **3**, 568–574 (2008) DOI:10.1016/j.stem.2008.10.004.

908. Li, W. *et al.* Generation of Rat and Human Induced Pluripotent Stem Cells by Combining

Genetic Reprogramming and Chemical Inhibitors. *Cell Stem Cell* vol. 4 16–19 (2009) DOI:10.1016/j.stem.2008.11.014.

909. Silva, J. *et al.* Promotion of reprogramming to ground state pluripotency by signal inhibition. *PLoS Biol.* **6**, 2237–2247 (2008) DOI:10.1371/journal.pbio.0060253.

910. Huangfu, D. *et al.* Induction of pluripotent stem cells from primary human fibroblasts with only Oct4 and Sox2. *Nat. Biotechnol.* **26**, 1269–1275 (2008) DOI:10.1038/nbt.1502.

911. Fusaki, N., Ban, H., Nishiyama, A., Saeki, K. & Hasegawa, M. Efficient induction of transgene-free human pluripotent stem cells using a vector based on Sendai virus, an RNA virus that does not integrate into the host genome. *Proc. Japan Acad. Ser. B Phys. Biol. Sci.* **85**, 348–362 (2009) DOI:10.2183/pjab.85.348.

912. Gonzalez, F. *et al.* Generation of mouse-induced pluripotent stem cells by transient expression of a single nonviral polycistronic vector. *Proc. Natl. Acad. Sci. U. S. A.* **106**, 8918–8922 (2009) DOI:10.1073/pnas.0901471106.

913. Yusa, K., Rad, R., Takeda, J. & Bradley, A. Generation of transgene-free induced pluripotent mouse stem cells by the piggyBac transposon. *Nat. Methods* **6**, 363–369 (2009) DOI:10.1038/nmeth.1323.

914. Stadtfeld, M., Nagaya, M., Utikal, J., Weir, G. & Hochedlinger, K. Induced pluripotent stem cells generated without viral integration. *Science (80-.).* **322**, 945–949 (2008) DOI:10.1126/science.1162494.

915. Marson, A. *et al.* Wnt Signaling Promotes Reprogramming of Somatic Cells to Pluripotency. *Cell Stem Cell* vol. 3 132–135 (2008) DOI:10.1016/j.stem.2008.06.019.

916. Mikkelsen, T. S. *et al.* Dissecting direct reprogramming through integrative genomic analysis. *Nature* **454**, 49–55 (2008) DOI:10.1038/nature07056.

917. Anokye-Danso, F. *et al.* Highly efficient miRNA-mediated reprogramming of mouse and human somatic cells to pluripotency. *Cell Stem Cell* **8**, 376–388 (2011) DOI:10.1016/j.stem.2011.03.001.

918. Kim, D. *et al.* Generation of Human Induced Pluripotent Stem Cells by Direct Delivery of Reprogramming Proteins. *Cell Stem Cell* vol. 4 472–476 (2009) DOI:10.1016/j.stem.2009.05.005.

919. Weltner, J. *et al.* Human pluripotent reprogramming with CRISPR activators. *Nat. Commun.* **9**, (2018) DOI:10.1038/s41467-018-05067-x.

920. Brons, I. G. M. *et al.* Derivation of pluripotent epiblast stem cells from mammalian embryos. *Nature* **448**, 191–195 (2007) DOI:10.1038/nature05950.

921. Tesar, P. J. *et al.* New cell lines from mouse epiblast share defining features with human embryonic stem cells. *Nature* **448**, 196–199 (2007) DOI:10.1038/nature05972.

922. Nichols, J. & Smith, A. Naive and Primed Pluripotent States. *Cell Stem Cell* vol. 4 487–492 (2009) DOI:10.1016/j.stem.2009.05.015.

923. Gafni, O. *et al.* Derivation of novel human ground state naive pluripotent stem cells. *Nature* **504**, 282–286 (2013) DOI:10.1038/nature12745.

924. Kilens, S. *et al.* Parallel derivation of isogenic human primed and naive induced pluripotent stem cells. *Nat. Commun.* **9**, 360 (2018) DOI:10.1038/s41467-017-02107-w.

925. Davis, R. L., Weintraub, H. & Lassar, A. B. Expression of a single transfected cDNA converts fibroblasts to myoblasts. *Cell* **51**, 987–1000 (1987) DOI:10.1016/0092-8674(87)90585-X.

926. Graf, T. & Enver, T. Forcing cells to change lineages. *Nature* vol. 462 587–594 (2009) DOI:10.1038/nature08533.

927. Mertens, J. *et al.* Directly Reprogrammed Human Neurons Retain Aging-Associated Transcriptomic Signatures and Reveal Age-Related Nucleocytoplasmic Defects. *Cell Stem Cell* **17**, 705–718 (2015) DOI:10.1016/j.stem.2015.09.001.

928. Home - ClinicalTrials.gov. https://www.clinicaltrials.gov/.

929. Cunha-Vaz, J., Bernardes, R. & Lobo, C. Blood-retinal barrier. *Eur. J. Ophthalmol.* **21**, 3–9 (2011) DOI:10.5301/EJO.2010.6049.

930. Chen, M.-S., Hou, P.-K., Tai, T.-Y. & Lin, B. J. *Blood-Ocular Barriers*. *Tzu Chi Med J* vol. 20 http://ajws.elsevier.com/tcmj (2008).

931. Zhou, R. & Caspi, R. R. Ocular immune privilege. *F1000 Biology Reports* vol. 2 3 (2010) DOI:10.3410/B2-3.

932. Díaz-Coránguez, M., Ramos, C. & Antonetti, D. A. The inner blood-retinal barrier: Cellular basis and development. *Vision Res.* **139**, 123–137 (2017) DOI:10.1016/j.visres.2017.05.009.

933. Liu, C., Oikonomopoulos, A., Sayed, N. & Wu, J. C. Modeling human diseases with induced pluripotent stem cells: from 2D to 3D and beyond. *Development* **145**, dev156166 (2018) DOI:10.1242/dev.156166.

934. Hall, C. E. *et al.* Progressive Motor Neuron Pathology and the Role of Astrocytes in a Human Stem Cell Model of VCP-Related ALS. *Cell Rep.* **19**, 1739–1749 (2017) DOI:10.1016/j.celrep.2017.05.024.

935. Weed, L. S. & Mills, J. A. Strategies for retinal cell generation from human pluripotent stem cells. *Stem Cell Investigation* vol. 4 65–65 (2017) DOI:10.21037/sci.2017.07.02.

936. Zahumenska, R. *et al.* Induced pluripotency: A powerful tool for in vitro modeling. *International Journal of Molecular Sciences* vol. 21 1–19 (2020) DOI:10.3390/ijms21238910.

937. Zhou, T. *et al.* Generation of human induced pluripotent stem cells from urine samples. *Nat. Protoc.* **7**, 2080–2089 (2012) DOI:10.1038/nprot.2012.115.

938. Malik, N. & Rao, M. S. A review of the methods for human iPSC derivation. in *Methods in Molecular Biology* vol. 997 23–33 (Methods Mol Biol, 2013). DOI:10.1007/978-1-62703-348-0_3.

939. Teshigawara, R., Cho, J., Kameda, M. & Tada, T. Mechanism of human somatic reprogramming to iPS cell. *Laboratory Investigation* vol. 97 1152–1157 (2017) DOI:10.1038/labinvest.2017.56.

940. Sullivan, S. *et al.* Quality control guidelines for clinical-grade human induced pluripotent

stem cell lines. *Regen. Med.* **13**, (2018) DOI:10.2217/rme-2018-0095.

941. Tran, H. T., Leonardo, T. R. & Peterson, S. E. Generation of Human Pluripotent Stem Cell-Derived Teratomas. in *Human Stem Cell Manual* 337–343 (Elsevier Inc., 2012). doi:10.1016/B978-0-12-385473-5.00021-7 DOI:10.1016/B978-0-12-385473-5.00021-7.

942. Attwood, S. & Edel, M. iPS-Cell Technology and the Problem of Genetic Instability—Can It Ever Be Safe for Clinical Use? *J. Clin. Med.* **8**, 288 (2019) DOI:10.3390/jcm8030288.

943. Yoshihara, M., Hayashizaki, Y. & Murakawa, Y. Genomic Instability of iPSCs: Challenges Towards Their Clinical Applications. *Stem Cell Reviews and Reports* vol. 13 7–16 (2017) DOI:10.1007/s12015-016-9680-6.

944. Liang, G. & Zhang, Y. Genetic and epigenetic variations in iPSCs: Potential causes and implications for application. *Cell Stem Cell* vol. 13 149–159 (2013) DOI:10.1016/j.stem.2013.07.001.

945. Meijer, M. *et al.* A Single-Cell Model for Synaptic Transmission and Plasticity in Human iPSC-Derived Neurons. *Cell Rep.* **27**, 2199-2211.e6 (2019) DOI:10.1016/j.celrep.2019.04.058.

946. Steichen, C., Hannoun, Z., Luce, E., Hauet, T. & Dubart-Kupperschmitt, A. Genomic integrity of human induced pluripotent stem cells: Reprogramming, differentiation and applications. *World J. Stem Cells* **11**, 729–747 (2019) DOI:10.4252/wjsc.v11.i10.729.

947. Zhu, Z. & Huangfu, D. Human pluripotent stem cells: An emerging model in developmental biology. *Development (Cambridge)* vol. 140 705–717 (2013) DOI:10.1242/dev.086165.

948. Hong, Y. J. & Do, J. T. Neural Lineage Differentiation From Pluripotent Stem Cells to Mimic Human Brain Tissues. *Frontiers in Bioengineering and Biotechnology* vol. 7 (2019) DOI:10.3389/fbioe.2019.00400.

949. Lewandowski, J., Kolanowski, T. J. & Kurpisz, M. Techniques for the induction of human pluripotent stem cell differentiation towards cardiomyocytes. *Journal of Tissue Engineering and Regenerative Medicine* vol. 11 1658–1674 (2017) DOI:10.1002/term.2117.

950. Vazin, T. & Freed, W. J. Human embryonic stem cells: Derivation, culture, and

differentiation: A review. *Restorative Neurology and Neuroscience* vol. 28 589–603 (2010) DOI:10.3233/RNN-2010-0543.

951. Tang, Z. *et al.* Progress of stem/progenitor cell-based therapy for retinal degeneration. *Journal of Translational Medicine* vol. 15 99 (2017) DOI:10.1186/s12967-017-1183-y.

952. Ikeda, H. *et al.* Generation of Rx+/Pax6+ neural retinal precursors from embryonic stem cells. *Proc. Natl. Acad. Sci. U. S. A.* **102**, 11331–6 (2005) DOI:10.1073/pnas.0500010102.

953. Osakada, F. *et al.* Toward the generation of rod and cone photoreceptors from mouse, monkey and human embryonic stem cells. *Nat. Biotechnol.* **26**, 215–224 (2008) DOI:10.1038/nbt1384.

954. Osakada, F. *et al.* In vitro differentiation of retinal cells from human pluripotent stem cells by small-molecule induction. *J. Cell Sci.* **122**, 3169–79 (2009) DOI:10.1242/jcs.050393.

955. Kawasaki, H. *et al.* Generation of dopaminergic neurons and pigmented epithelia from primate ES cells by stromal cell-derived inducing activity. *Proc. Natl. Acad. Sci. U. S. A.* **99**, 1580–1585 (2002) DOI:10.1073/pnas.032662199.

956. Buchholz, D. E. *et al.* Derivation of functional retinal pigmented epithelium from induced pluripotent stem cells. *Stem Cells* **27**, 2427–2434 (2009) DOI:10.1002/stem.189.

957. Haruta, M. *et al.* In vitro and in vivo characterization of pigment epithelial cells differentiated from primate embryonic stem cells. *Investig. Ophthalmol. Vis. Sci.* **45**, 1020–1025 (2004) DOI:10.1167/iovs.03-1034.

958. Klimanskaya, I. *et al.* Derivation and comparative assessment of retinal pigment epithelium from human embryonic stem cells using transcriptomics. *Cloning Stem Cells* **6**, 217–245 (2004) DOI:10.1089/clo.2004.6.217.

959. Idelson, M. *et al.* Directed Differentiation of Human Embryonic Stem Cells into Functional Retinal Pigment Epithelium Cells. *Cell Stem Cell* **5**, 396–408 (2009) DOI:10.1016/j.stem.2009.07.002.

960. Hirami, Y. *et al.* Generation of retinal cells from mouse and human induced pluripotent

stem cells. *Neurosci. Lett.* **458**, 126–131 (2009) DOI:10.1016/j.neulet.2009.04.035.

961. Torrez, L. B. *et al.* Derivation of neural progenitors and retinal pigment epithelium from common marmoset and human pluripotent stem cells. *Stem Cells Int.* **2012**, (2012) DOI:10.1155/2012/417865.

962. Idelson, M. *et al.* Directed Differentiation of Human Embryonic Stem Cells into Functional Retinal Pigment Epithelium Cells. *Cell Stem Cell* **5**, 396–408 (2009) DOI:10.1016/J.STEM.2009.07.002.

963. Zahabi, A. *et al.* A new efficient protocol for directed differentiation of retinal pigmented epithelial cells from normal and retinal disease induced pluripotent stem cells. *Stem Cells Dev.* **21**, 2262–2272 (2012) DOI:10.1089/scd.2011.0599.

964. Reichman, S. *et al.* Generation of Storable Retinal Organoids and Retinal Pigmented Epithelium from Adherent Human iPS Cells in Xeno-Free and Feeder-Free Conditions. *Stem Cells* **35**, 1176–1188 (2017) DOI:10.1002/stem.2586.

965. Perron, M. *et al.* A novel function for Hedgehog signalling in retinal pigment epithelium differentiation. *Development* vol. 130 1565–1577 (2003) DOI:10.1242/dev.00391.

966. Spence, J. R. *et al.* The hedgehog pathway is a modulator of retina regeneration. *Development* **131**, 4607–4621 (2004) DOI:10.1242/dev.01298.

967. Leach, L. L. *et al.* Induced pluripotent stem cell-derived retinal pigmented epithelium: A comparative study between cell lines and differentiation methods. *J. Ocul. Pharmacol. Ther.* **32**, 317–330 (2016) DOI:10.1089/jop.2016.0022.

968. Nadar, V. P., Buchholz, D. E., Lowenstein, S. E., Clegg, D. O. & Clegg, D. O. Canonical/β-catenin wnt pathway activation improves retinal pigmented epithelium derivation from human embryonic stem cells. *Investig. Ophthalmol. Vis. Sci.* **56**, 1002–1013 (2015) DOI:10.1167/iovs.14-15835.

969. Maruotti, J. *et al.* Small-molecule-directed, efficient generation of retinal pigment epithelium from human pluripotent stem cells. *Proc. Natl. Acad. Sci. U. S. A.* **112**, 10950–

10955 (2015) DOI:10.1073/pnas.1422818112.

970. Cyranoski, D. Stem cells cruise to clinic. *Nature* vol. 494 413 (2013) DOI:10.1038/494413a.

971. Wang, Y., Tang, Z. & Gu, P. Stem/progenitor cell-based transplantation for retinal degeneration: a review of clinical trials. *Cell Death and Disease* vol. 11 1–14 (2020) DOI:10.1038/s41419-020-02955-3.

972. Harada, T., Harada, C. & Parada, L. F. Molecular regulation of visual system development: More than meets the eye. *Genes and Development* vol. 21 367–378 (2007) DOI:10.1101/gad.1504307.

973. Martin-Belmonte, F. & Perez-Moreno, M. Epithelial cell polarity, stem cells and cancer. *Nature Reviews Cancer* vol. 12 23–38 (2012) DOI:10.1038/nrc3169.

974. Lamba, D. A., Karl, M. O., Ware, C. B. & Reh, T. A. Efficient generation of retinal progenitor cells from human embryonic stem cells. *Proc. Natl. Acad. Sci. U. S. A.* **103**, 12769–12774 (2006) DOI:10.1073/pnas.0601990103.

975. Lamba, D. A. *et al.* Generation, purification and transplantation of photoreceptors derived from human induced pluripotent stem cells. *PLoS One* **5**, (2010) DOI:10.1371/journal.pone.0008763.

976. Zhu, J. & Lamba, D. Small Molecule-Based Retinal Differentiation of Human Embryonic Stem Cells and Induced Pluripotent Stem Cells. *BIO-PROTOCOL* **8**, (2018) DOI:10.21769/bioprotoc.2882.

977. Meyer, J. S. *et al.* Optic vesicle-like structures derived from human pluripotent stem cells facilitate a customized approach to retinal disease treatment. *Stem Cells* **29**, 1206–1218 (2011) DOI:10.1002/stem.674.

978. Bussian, T. J. *et al.* Clearance of senescent glial cells prevents tau-dependent pathology and cognitive decline. *Nature* **562**, 578–582 (2018) DOI:10.1038/s41586-018-0543-y.

979. Meyer, J. S. *et al.* Modeling early retinal development with human embryonic and induced pluripotent stem cells. *Proc. Natl. Acad. Sci. U. S. A.* **106**, 16698–16703 (2009)

DOI:10.1073/pnas.0905245106.

980. Amirpour, N. *et al.* Differentiation of human embryonic stem cell-derived retinal progenitors into retinal cells by sonic hedgehog and/or retinal pigmented epithelium and transplantation into the subretinal space of sodium iodate-injected rabbits. *Stem Cells Dev.* **21**, 42–53 (2012) DOI:10.1089/scd.2011.0073.

981. Boucherie, C., Mukherjee, S., Henckaerts, E., Thrasher, A. J. & Sowden, J. C. Brief report: Self-organizing neuroepithelium from human pluripotent stem cells facilitates derivation of photoreceptors. *Stem Cells* **31**, 408–414 (2013) DOI:10.1002/stem.1268.

982. Krohne, T. U. *et al.* Generation of Retinal Pigment Epithelial Cells from Small Molecules and OCT4 Reprogrammed Human Induced Pluripotent Stem Cells . *Stem Cells Transl. Med.* **1**, 96–109 (2012) DOI:10.5966/sctm.2011-0057.

983. Mellough, C. B., Sernagor, E., Moreno-Gimeno, I., Steel, D. H. W. & Lako, M. Efficient stage-specific differentiation of human pluripotent stem cells toward retinal photoreceptor cells. *Stem Cells* **30**, 673–686 (2012) DOI:10.1002/stem.1037.

984. Tucker, B. A. *et al.* Patient-specifc iPSC-derived photoreceptor precursor cells as a means to investigate retinitis pigmentosa. *Elife* **2013**, (2013) DOI:10.7554/eLife.00824.001.

985. Yanai, A. *et al.* Differentiation of human embryonic stem cells using size-controlled embryoid bodies and negative cell selection in the production of photoreceptor precursor cells. *Tissue Eng. - Part C Methods* **19**, 755–764 (2013) DOI:10.1089/ten.tec.2012.0524.

986. Bottenstein, J. E. & Sato, G. H. Growth of a rat neuroblastoma cell line in serum free supplemented medium. *Proc. Natl. Acad. Sci. U. S. A.* **76**, 514–517 (1979) DOI:10.1073/pnas.76.1.514.

987. Brewer, G. J., Torricelli, J. R., Evege, E. K. & Price, P. J. Optimized survival of hippocampal neurons in B27-supplemented neurobasal™, a new serum-free medium combination. *J. Neurosci. Res.* **35**, 567–576 (1993) DOI:10.1002/jnr.490350513.

988. Svendsen, C. N., Fawcett, J. W., Bentlage, C. & Dunnett, S. B. Increased survival of rat EGF-

generated CNS precursor cells using B27 supplemented medium. *Exp. Brain Res.* **102**, 407–414 (1995) DOI:10.1007/BF00230645.

989. Chichagova, V. *et al.* Differentiation of Retinal Organoids from Human Pluripotent Stem Cells. *Curr. Protoc. Stem Cell Biol.* **50**, (2019) DOI:10.1002/cpsc.95.

990. Zerti, D. *et al.* Developing a simple method to enhance the generation of cone and rod photoreceptors in pluripotent stem cell-derived retinal organoids. *Stem Cells* **38**, 45–51 (2020) DOI:10.1002/stem.3082.

991. Phillips, M. J. *et al.* Blood-derived human iPS cells generate optic vesicle-like structures with the capacity to form retinal laminae and develop synapses. *Invest. Ophthalmol. Vis. Sci.* **53**, 2007–2019 (2012) DOI:10.1167/iovs.11-9313.

992. Nakano, T. *et al.* Self-Formation of Optic Cups and Storable Stratified Neural Retina from Human ESCs. *Cell Stem Cell* **10**, 771–785 (2012) DOI:10.1016/j.stem.2012.05.009.

993. Zhong, X. *et al.* Generation of three-dimensional retinal tissue with functional photoreceptors from human iPSCs. *Nat. Commun.* **5**, (2014) DOI:10.1038/ncomms5047.

994. Kuwahara, A. *et al.* Generation of a ciliary margin-like stem cell niche from self-organizing human retinal tissue. *Nat. Commun.* **6**, 6286 (2015) DOI:10.1038/ncomms7286.

995. Gonzalez-Cordero, A. *et al.* Photoreceptor precursors derived from three-dimensional embryonic stem cell cultures integrate and mature within adult degenerate retina. *Nat. Biotechnol.* **31**, 741–747 (2013) DOI:10.1038/nbt.2643.

996. Decembrini, S., Koch, U., Radtke, F., Moulin, A. & Arsenijevic, Y. Derivation of traceable and transplantable photoreceptors from mouse embryonic stem cells. *Stem Cell Reports* **2**, 853–865 (2014) DOI:10.1016/j.stemcr.2014.04.010.

997. Völkner, M. *et al.* Retinal Organoids from Pluripotent Stem Cells Efficiently Recapitulate Retinogenesis. *Stem Cell Reports* **6**, 525–538 (2016) DOI:10.1016/j.stemcr.2016.03.001.

998. Völkner, M., Kurth, T. & Karl, M. O. The Mouse Retinal Organoid Trisection Recipe: Efficient Generation of 3D Retinal Tissue from Mouse Embryonic Stem Cells. in *Methods in*

Molecular Biology vol. 1834 119–141 (Humana Press Inc., 2019). DOI:10.1007/978-1-4939-8669-9_9.

999. Wahlin, K. J. *et al.* Photoreceptor Outer Segment-like Structures in Long-Term 3D Retinas from Human Pluripotent Stem Cells. *Sci. Rep.* **7**, 1–15 (2017) DOI:10.1038/s41598-017-00774-9.

1000. Kaewkhaw, R. *et al.* Transcriptome Dynamics of Developing Photoreceptors in Three-Dimensional Retina Cultures Recapitulates Temporal Sequence of Human Cone and Rod Differentiation Revealing Cell Surface Markers and Gene Networks. *Stem Cells* **33**, 3504–3518 (2015) DOI:10.1002/stem.2122.

1001. Parfitt, D. A. *et al.* Identification and Correction of Mechanisms Underlying Inherited Blindness in Human iPSC-Derived Optic Cups. *Cell Stem Cell* **18**, 769–81 (2016) DOI:10.1016/j.stem.2016.03.021.

1002. Reichman, S. *et al.* From confluent human iPS cells to self-forming neural retina and retinal pigmented epithelium. *Proc. Natl. Acad. Sci. U. S. A.* **111**, 8518–8523 (2014) DOI:10.1073/pnas.1324212111.

1003. Barnea-Cramer, A. O. *et al.* Function of human pluripotent stem cell-derived photoreceptor progenitors in blind mice. *Sci. Rep.* **6**, 1–15 (2016) DOI:10.1038/srep29784.

1004. Bhattacharya, S. *et al.* Involvement of Ath3 in CNTF-mediated differentiation of the late retinal progenitors. *Mol. Cell. Neurosci.* **27**, 32–43 (2004) DOI:10.1016/j.mcn.2004.05.004.

1005. Rhee, K. Do, Goureau, O., Chen, S. & Yang, X. J. Cytokine-induced activation of signal transducer and activator of transcription in photoreceptor precursors regulates rod differentiation in the developing mouse retina. *J. Neurosci.* **24**, 9779–9788 (2004) DOI:10.1523/JNEUROSCI.1785-04.2004.

1006. Gonzalez-Cordero, A. *et al.* Recapitulation of Human Retinal Development from Human Pluripotent Stem Cells Generates Transplantable Populations of Cone Photoreceptors. *Stem Cell Reports* **9**, 820–837 (2017) DOI:10.1016/j.stemcr.2017.07.022.

1007. Zhou, S. *et al.* Differentiation of human embryonic stem cells into cone photoreceptors through simultaneous inhibition of BMP, TGFβ and Wnt signaling. *Development* **142**, 3294–306 (2015) DOI:10.1242/dev.125385.

1008. Smith, J. C., Price, B. M. J., Van Nimmen, K. & Huylebroeck, D. Identification of a potent Xenopus mesoderm-inducing factor as a homologue of activin A. *Nature* **345**, 729–731 (1990) DOI:10.1038/345729a0.

1009. Eldred, K. C. *et al.* Thyroid hormone signaling specifies cone subtypes in human retinal organoids. *Science (80-.).* **362**, (2018) DOI:10.1126/science.aau6348.

1010. Vancamp, P., Bourgeois, N. M. A., Houbrechts, A. M. & Darras, V. M. Knockdown of the thyroid hormone transporter MCT8 in chicken retinal precursor cells hampers early retinal development and results in a shift towards more UV/blue cones at the expense of green/red cones. *Exp. Eye Res.* **178**, 135–147 (2019) DOI:10.1016/j.exer.2018.09.018.

1011. Pan, D. *et al.* COCO enhances the efficiency of photoreceptor precursor differentiation in early human embryonic stem cell-derived retinal organoids. *Stem Cell Res. Ther.* **11**, (2020) DOI:10.1186/s13287-020-01883-5.

1012. Ballios, B. G., Khalili, S., Shoichet, M. S. & van der Kooy, D. Induction of Rod and Cone Photoreceptor-Specific Progenitors from Stem Cells. in *Advances in Experimental Medicine and Biology* vol. 1185 551–555 (Springer, 2019). DOI:10.1007/978-3-030-27378-1_90.

1013. Pan, D. *et al.* COCO enhances the efficiency of photoreceptor precursor differentiation in early human embryonic stem cell-derived retinal organoids. *Stem Cell Res. Ther.* **11**, (2020) DOI:10.1186/s13287-020-01883-5.

1014. Khalili, S. *et al.* Induction of rod versus cone photoreceptor-specific progenitors from retinal precursor cells. *Stem Cell Res.* **33**, 215–227 (2018) DOI:10.1016/j.scr.2018.11.005.

1015. Shrestha, R., Wen, Y.-T., Ding, D.-C. & Tsai, R.-K. Aberrant hiPSCs-Derived from Human Keratinocytes Differentiates into 3D Retinal Organoids that Acquire Mature Photoreceptors. *Cells* **8**, 36 (2019) DOI:10.3390/cells8010036.

1016. Kaya, K. D. *et al.* Transcriptome-based molecular staging of human stem cell-derived retinal organoids uncovers accelerated photoreceptor differentiation by 9-cis retinal. *Mol. Vis.* **25**, 663–678 (2019).

1017. Kelley, R. A., Chen, H. Y., Swaroop, A. & Li, T. Accelerated Development of Rod Photoreceptors in Retinal Organoids Derived from Human Pluripotent Stem Cells by Supplementation with 9-cis Retinal. *STAR Protoc.* **1**, 100033 (2020) DOI:10.1016/j.xpro.2020.100033.

1018. German, O. L., Insua, M. F., Gentili, C., Rotstein, N. P. & Politi, L. E. Docosahexaenoic acid prevents apoptosis of retina photoreceptors by activating the ERK/MAPK pathway. *J. Neurochem.* **98**, 1507–1520 (2006) DOI:10.1111/j.1471-4159.2006.04061.x.

1019. Brooks, M. J. *et al.* Improved Retinal Organoid Differentiation by Modulating Signaling Pathways Revealed by Comparative Transcriptome Analyses with Development In Vivo. *Stem Cell Reports* **13**, 891–905 (2019) DOI:10.1016/j.stemcr.2019.09.009.

1020. Shrestha, R., Wen, Y.-T., Ding, D.-C. & Tsai, R.-K. Aberrant hiPSCs-Derived from Human Keratinocytes Differentiates into 3D Retinal Organoids that Acquire Mature Photoreceptors. *Cells* **8**, 36 (2019) DOI:10.3390/cells8010036.

1021. Völkner, M., Kurth, T. & Karl, M. O. The Mouse Retinal Organoid Trisection Recipe: Efficient Generation of 3D Retinal Tissue from Mouse Embryonic Stem Cells. in *Methods in Molecular Biology* vol. 1834 119–141 (Humana Press Inc., 2019). DOI:10.1007/978-1-4939-8669-9_9.

1022. Bae, D. *et al.* Hypoxia enhances the generation of retinal progenitor cells from human induced pluripotent and embryonic stem cells. *Stem Cells Dev.* **21**, 1344–1355 (2012) DOI:10.1089/scd.2011.0225.

1023. Chen, H. Y., Kaya, K. D., Dong, L. & Swaroop, A. Three-dimensional retinal organoids from mouse pluripotent stem cells mimic in vivo development with enhanced stratification and rod photoreceptor differentiation. *Mol. Vis.* **22**, 1077–1094 (2016).

1024. Chen, H. Y., Kelley, R. A. & Swaroop, A. HIPRO: A High-Efficiency, Hypoxia-Induced Protocol

for Generation of Photoreceptors in Retinal Organoids from Mouse Pluripotent Stem Cells. *STAR Protoc.* **1**, 100018 (2020) DOI:10.1016/j.xpro.2020.100018.

1025. DiStefano, T. *et al.* Accelerated and Improved Differentiation of Retinal Organoids from Pluripotent Stem Cells in Rotating-Wall Vessel Bioreactors. *Stem cell reports* **10**, 300–313 (2018) DOI:10.1016/j.stemcr.2017.11.001.

1026. Ovando-Roche, P. *et al.* Use of bioreactors for culturing human retinal organoids improves photoreceptor yields. *Stem Cell Res. Ther.* **9**, (2018) DOI:10.1186/s13287-018-0907-0.

1027. Luo, Z. *et al.* An Optimized System for Effective Derivation of Three-Dimensional Retinal Tissue via Wnt Signaling Regulation. *Stem Cells* **36**, 1709–1722 (2018) DOI:10.1002/stem.2890.

1028. Kuwahara, A. *et al.* Preconditioning the Initial State of Feeder-free Human Pluripotent Stem Cells Promotes Self-formation of Three-dimensional Retinal Tissue. *Sci. Rep.* **9**, (2019) DOI:10.1038/s41598-019-55130-w.

1029. Lakowski, J. *et al.* Isolation of Human Photoreceptor Precursors via a Cell Surface Marker Panel from Stem Cell-Derived Retinal Organoids and Fetal Retinae. *Stem Cells* **36**, 709–722 (2018) DOI:10.1002/stem.2775.

1030. Collin, J. *et al.* Deconstructing Retinal Organoids: Single Cell RNA-Seq Reveals the Cellular Components of Human Pluripotent Stem Cell-Derived Retina. *Stem Cells* **37**, 593–598 (2019) DOI:10.1002/stem.2963.

1031. Kim, S. *et al.* Generation, transcriptome profiling, and functional validation of cone-rich human retinal organoids. *Proc. Natl. Acad. Sci. U. S. A.* **166**, 10824–10833 (2019) DOI:10.1073/pnas.1901572116.

1032. Lukowski, S. W. *et al.* A single-cell transcriptome atlas of the adult human retina. *EMBO J.* **38**, (2019) DOI:10.15252/embj.2018100811.

1033. Peng, Y. R. *et al.* Molecular Classification and Comparative Taxonomics of Foveal and Peripheral Cells in Primate Retina. *Cell* **176**, 1222-1237.e22 (2019)

DOI:10.1016/j.cell.2019.01.004.

1034. Gagliardi, G. *et al.* Characterization and Transplantation of CD73-Positive Photoreceptors Isolated from Human iPSC-Derived Retinal Organoids. *Stem Cell Reports* **11**, 665–680 (2018) DOI:10.1016/j.stemcr.2018.07.005.

1035. Garita-Hernandez, M. *et al.* Restoration of visual function by transplantation of optogenetically engineered photoreceptors. *Nat. Commun.* **10**, (2019) DOI:10.1038/s41467-019-12330-2.

1036. Gagliardi, G., Ben M'Barek, K. & Goureau, O. Photoreceptor cell replacement in macular degeneration and retinitis pigmentosa: A pluripotent stem cell-based approach. *Progress in Retinal and Eye Research* vol. 71 1–25 (2019) DOI:10.1016/j.preteyeres.2019.03.001.

1037. Akhtar, T. *et al.* Accelerated photoreceptor differentiation of hiPSC-derived retinal organoids by contact co-culture with retinal pigment epithelium. *Stem Cell Res.* **39**, 101491 (2019) DOI:10.1016/j.scr.2019.101491.

1038. Lowe, A., Harris, R., Bhansali, P., Cvekl, A. & Liu, W. Intercellular Adhesion-Dependent Cell Survival and ROCK-Regulated Actomyosin-Driven Forces Mediate Self-Formation of a Retinal Organoid. *Stem Cell Reports* **6**, 743–756 (2016) DOI:10.1016/j.stemcr.2016.03.011.

1039. E, C. *et al.* NRL -/- gene edited human embryonic stem cells generate rod-deficient retinal organoids enriched in S-cone-like photoreceptors. *Stem Cells* (2021) doi:10.1002/STEM.3325 DOI:10.1002/STEM.3325.

1040. Leite, N. C. *et al.* Modeling Type 1 Diabetes In Vitro Using Human Pluripotent Stem Cells. *Cell Rep.* **32**, 107894 (2020) DOI:10.1016/j.celrep.2020.107894.

1041. Byers, B., Lee, H. L. & Pera, R. R. Modeling Parkinson's disease using induced pluripotent stem cells. *Curr. Neurol. Neurosci. Rep.* **12**, 237–242 (2012) DOI:10.1007/s11910-012-0270-y.

1042. Tanaka, T. *et al.* Generation of retinal ganglion cells with functional axons from human induced pluripotent stem cells. *Sci. Rep.* **5**, 1–11 (2015) DOI:10.1038/srep08344.

1043. Qiu, X. *et al.* Efficient generation of lens progenitor cells from cataract patient-specific induced pluripotent stem cells. *PLoS One* **7**, 32612 (2012) DOI:10.1371/journal.pone.0032612.

1044. Deng, W. L. *et al.* Gene Correction Reverses Ciliopathy and Photoreceptor Loss in iPSC-Derived Retinal Organoids from Retinitis Pigmentosa Patients. *Stem Cell Reports* **10**, 1267–1281 (2018) DOI:10.1016/j.stemcr.2018.02.003.

1045. Shimada, H. *et al.* In Vitro Modeling Using Ciliopathy-Patient-Derived Cells Reveals Distinct Cilia Dysfunctions Caused by CEP290 Mutations. *Cell Rep.* **20**, 384–396 (2017) DOI:10.1016/j.celrep.2017.06.045.

1046. Sanjurjo-Soriano, C. *et al.* Genome Editing in Patient iPSCs Corrects the Most Prevalent USH2A Mutations and Reveals Intriguing Mutant mRNA Expression Profiles. *Mol. Ther. - Methods Clin. Dev.* **17**, 156–173 (2020) DOI:10.1016/j.omtm.2019.11.016.

1047. Teotia, P. *et al.* Modeling Glaucoma: Retinal Ganglion Cells Generated from Induced Pluripotent Stem Cells of Patients with *SIX6* Risk Allele Show Developmental Abnormalities. *Stem Cells* **35**, 2239–2252 (2017) DOI:10.1002/stem.2675.

1048. Volpato, V. & Webber, C. Addressing variability in iPSC-derived models of human disease: guidelines to promote reproducibility. (2020) doi:10.1242/dmm.042317 DOI:10.1242/dmm.042317.

1049. Germain, P. L. & Testa, G. Taming Human Genetic Variability: Transcriptomic Meta-Analysis Guides the Experimental Design and Interpretation of iPSC-Based Disease Modeling. *Stem Cell Reports* **8**, 1784–1796 (2017) DOI:10.1016/j.stemcr.2017.05.012.

1050. Jin, Z. B. *et al.* Modeling retinal degeneration using patient-specific induced pluripotent stem cells. *PLoS One* **6**, 17084 (2011) DOI:10.1371/journal.pone.0017084.

1051. Jin, Z.-B., Okamoto, S., Xiang, P. & Takahashi, M. Integration-Free Induced Pluripotent Stem Cells Derived from Retinitis Pigmentosa Patient for Disease Modeling. *Stem Cells Transl. Med.* **1**, 503–509 (2012) DOI:10.5966/sctm.2012-0005.

1052. Tucker, B. A. *et al.* Exome sequencing and analysis of induced pluripotent stem cells identify the cilia-related gene male germ cell-associated kinase (MAK) as a cause of retinitis pigmentosa. *Proc. Natl. Acad. Sci. U. S. A.* **108**, (2011) DOI:10.1073/pnas.1108918108.

1053. Hull, S. *et al.* Expanding the phenotype of TRNT1-related immunodeficiency to include childhood cataract and inner retinal dysfunction. *JAMA Ophthalmol.* **134**, 1049–1053 (2016) DOI:10.1001/jamaophthalmol.2015.5833.

1054. Sharma, T. P. *et al.* Patient-specific induced pluripotent stem cells to evaluate the pathophysiology of TRNT1-associated Retinitis pigmentosa. *Stem Cell Res.* **21**, 58–70 (2017) DOI:10.1016/j.scr.2017.03.005.

1055. Megaw, R. *et al.* Gelsolin dysfunction causes photoreceptor loss in induced pluripotent cell and animal retinitis pigmentosa models. *Nat. Commun.* **8**, (2017) DOI:10.1038/s41467-017-00111-8.

1056. Schwarz, N. *et al.* Arl3 and RP2 regulate the trafficking of ciliary tip kinesins. *Hum. Mol. Genet.* **26**, 2480–2492 (2017) DOI:10.1093/hmg/ddx143.

1057. Guo, Y. *et al.* Modeling Retinitis Pigmentosa: Retinal Organoids Generated From the iPSCs of a Patient With the USH2A Mutation Show Early Developmental Abnormalities. *Front. Cell. Neurosci.* **13**, (2019) DOI:10.3389/fncel.2019.00361.

1058. Gao, M. L. *et al.* Patient-Specific Retinal Organoids Recapitulate Disease Features of Late-Onset Retinitis Pigmentosa. *Front. Cell Dev. Biol.* **8**, (2020) DOI:10.3389/fcell.2020.00128.

1059. Kim, K. *et al.* Epigenetic memory in induced pluripotent stem cells. *Nature* **467**, 285–290 (2010) DOI:10.1038/nature09342.

1060. Rouhani, F. *et al.* Genetic Background Drives Transcriptional Variation in Human Induced Pluripotent Stem Cells. *PLoS Genet.* **10**, (2014) DOI:10.1371/journal.pgen.1004432.

1061. Polo, J. M. *et al.* Cell type of origin influences the molecular and functional properties of mouse induced pluripotent stem cells. *Nat. Biotechnol.* **28**, 848–855 (2010) DOI:10.1038/nbt.1667.

1062. Fuster-García, C., García-Bohórquez, B., Rodríguez-Muñoz, A., Millán, J. M. & García-García, G. Application of crispr tools for variant interpretation and disease modeling in inherited retinal dystrophies. *Genes* vol. 11 (2020) DOI:10.3390/genes11050473.

1063. Yoshida, T. *et al.* The use of induced pluripotent stem cells to reveal pathogenic gene mutations and explore treatments for retinitis pigmentosa. *Mol. Brain* **7**, (2014) DOI:10.1186/1756-6606-7-45.

1064. Lane, A. *et al.* Modeling and Rescue of RP2 Retinitis Pigmentosa Using iPSC-Derived Retinal Organoids. *Stem Cell Reports* **15**, 67–79 (2020) DOI:10.1016/j.stemcr.2020.05.007.

1065. Ito, S. ichiro, Onishi, A. & Takahashi, M. Chemically-induced photoreceptor degeneration and protection in mouse iPSC-derived three-dimensional retinal organoids. *Stem Cell Res.* **24**, 94–101 (2017) DOI:10.1016/j.scr.2017.08.018.

1066. Kallman, A. *et al.* Investigating cone photoreceptor development using patient-derived NRL null retinal organoids. *Commun. Biol.* **3**, 82 (2020) DOI:10.1038/s42003-020-0808-5.

1067. Kim, J. W. *et al.* NRL-Regulated Transcriptome Dynamics of Developing Rod Photoreceptors. *Cell Rep.* **17**, 2460–2473 (2016) DOI:10.1016/j.celrep.2016.10.074.

1068. Burnight, E. R. *et al.* CEP290 gene transfer rescues Leber congenital amaurosis cellular phenotype. *Gene Ther.* **21**, 662–672 (2014) DOI:10.1038/gt.2014.39.

1069. Wiley, L. A. *et al.* Using Patient-Specific Induced Pluripotent Stem Cells and Wild-Type Mice to Develop a Gene Augmentation-Based Strategy to Treat *CLN3* -Associated Retinal Degeneration. *Hum. Gene Ther.* **27**, 835–846 (2016) DOI:10.1089/hum.2016.049.

1070. Deng, W. L. *et al.* Gene Correction Reverses Ciliopathy and Photoreceptor Loss in iPSC-Derived Retinal Organoids from Retinitis Pigmentosa Patients. *Stem Cell Reports* **10**, 1267–1281 (2018) DOI:10.1016/j.stemcr.2018.02.003.

1071. Huang, K. C. *et al.* Morphological and Molecular Defects in Human Three-Dimensional Retinal Organoid Model of X-Linked Juvenile Retinoschisis. *Stem Cell Reports* **13**, 906–923 (2019) DOI:10.1016/j.stemcr.2019.09.010.

1072. Bohrer, L. R. *et al.* Correction of NR2E3 Associated enhanced S-cone Syndrome Patient-specific IPSCS using CRISPR-Cas9. *Genes (Basel).* **10**, (2019) DOI:10.3390/genes10040278.

1073. Reh, T. A. & Kijavin, I. J. Age of differentiation determines rat retinal germinal cell phenotype: Induction of differentiation by dissociation. *J. Neurosci.* **9**, 4179–4189 (1989) DOI:10.1523/jneurosci.09-12-04179.1989.

1074. Carl, M., Loosli, F. & Wittbrodt, J. Six3 inactivation reveals its essential role for the formation and patterning of the vertebrate eye. *Development* **129**, (2002).

1075. Porter, F. D. *et al.* Lhx2, a LIM homeobox gene, is required for eye, forebrain, and definitive erythrocyte development. *Development* **124**, (1997).

1076. Chow, R. L., Altmann, C. R., Lang, R. A. & Hemmati-Brivanlou, A. Pax6 induces ectopic eyes in a vertebrate. *Development* **126**, (1999).

1077. Freund, C. L. *et al.* De novo mutations in the CRX homeobox gene associated with leber congenital amaurosis. *Nature Genetics* vol. 18 311–312 (1998) DOI:10.1038/ng0498-311.

1078. Furukawa, T., Morrow, E. M., Li, T., Davis, F. C. & Cepko, C. L. Retinopathy and attenuated circadian entrainment in Crx-deficient mice. *Nat. Genet.* **23**, 466–470 (1999) DOI:10.1038/70591.

1079. Swaroop, A. *et al.* Leber congenital amaurosis caused by a homozygous mutation (R90W) in the homeodomain of the retinal transcription factor CRX: Direct evidence for the involvement of CRX in the development of photoreceptor function. *Hum. Mol. Genet.* **8**, 299–305 (1999) DOI:10.1093/hmg/8.2.299.

1080. Mears, A. J. *et al.* Nrl is required for rod photoreceptor development. *Nat. Genet.* **29**, 447–452 (2001) DOI:10.1038/ng774.

1081. Hennig, A. K., Peng, G. H. & Chen, S. Transcription Coactivators p300 and CBP Are Necessary for Photoreceptor-Specific Chromatin Organization and Gene Expression. *PLoS One* **8**, (2013) DOI:10.1371/journal.pone.0069721.

1082. Valk-Lingbeek, M. E., Bruggeman, S. W. M. & Van Lohuizen, M. Stem cells and cancer: The

polycomb connection. *Cell* vol. 118 409–418 (2004) DOI:10.1016/j.cell.2004.08.005.

1083. Buchwald, G. *et al.* Structure and E3-ligase activity of the Ring-Ring complex of Polycomb proteins Bmi1 and Ring1b. *EMBO J.* **25**, 2465–2474 (2006) DOI:10.1038/sj.emboj.7601144.

1084. Li, Z. *et al.* Structure of a Bmi-1-Ring1B polycomb group ubiquitin ligase complex. *J. Biol. Chem.* **281**, 20643–20649 (2006) DOI:10.1074/jbc.M602461200.

1085. Van der Lugt, N. M. T. *et al.* Posterior transformation, neurological abnormalities, and severe hematopoietic defects in mice with a targeted deletion of the bmi-1 proto-oncogene. *Genes Dev.* **8**, 757–769 (1994) DOI:10.1101/gad.8.7.757.

1086. Sharpless, N. E., Ramsey, M. R., Balasubramanian, P., Castrillon, D. H. & DePinho, R. A. The differential impact of p16INK4a or p19ARF deficiency on cell growth and tumorigenesis. *Oncogene* **23**, 379–385 (2004) DOI:10.1038/sj.onc.1207074.

1087. Liu, J. *et al.* Bmi1 regulates mitochondrial function and the DNA damage response pathway. *Nature* **459**, 387–392 (2009) DOI:10.1038/nature08040.

1088. Haverkamp, S. & W  ssle, H. Immunocytochemical analysis of the mouse retina. *J. Comp. Neurol.* **424**, 1–23 (2000) DOI:10.1002/1096-9861(20000814)424:1<1::AID-CNE1>3.0.CO;2-V.

1089. Marquardt, T. Transcriptional control of neuronal diversification in the retina. *Progress in Retinal and Eye Research* vol. 22 567–577 (2003) DOI:10.1016/S1350-9462(03)00036-3.

1090. Ortiń-Martínez, A. *et al.* Number and distribution of mouse retinal cone photoreceptors: Differences between an albino (Swiss) and a pigmented (C57/BL6) strain. *PLoS One* **9**, (2014) DOI:10.1371/journal.pone.0102392.

1091. Solovei, I. *et al.* Nuclear Architecture of Rod Photoreceptor Cells Adapts to Vision in Mammalian Evolution. *Cell* **137**, 356–368 (2009) DOI:10.1016/j.cell.2009.01.052.

1092. Linkermann, A. & Green, D. R. Necroptosis. *N. Engl. J. Med.* **370**, 455–465 (2014) DOI:10.1056/nejmra1310050.

1093. Fodor, B. D., Shukeir, N., Reuter, G. & Jenuwein, T. Mammalian su(var) genes in chromatin control. *Annual Review of Cell and Developmental Biology* vol. 26 471–501 (2010) DOI:10.1146/annurev.cellbio.042308.113225.

1094. Karimi, M. M. *et al.* DNA methylation and SETDB1/H3K9me3 regulate predominantly distinct sets of genes, retroelements, and chimeric transcripts in mescs. *Cell Stem Cell* **8**, 676–687 (2011) DOI:10.1016/j.stem.2011.04.004.

1095. Murakami, Y. *et al.* Receptor interacting protein kinase mediates necrotic cone but not rod cell death in a mouse model of inherited degeneration. *Proc. Natl. Acad. Sci. U. S. A.* **109**, 14598–14603 (2012) DOI:10.1073/pnas.1206937109.

1096. Viringipurampeer, I. A. *et al.* Rip3 knockdown rescues photoreceptor cell death in blind pde6c zebrafish. *Cell Death Differ.* **21**, 665–675 (2014) DOI:10.1038/cdd.2013.191.

1097. Chatoo, W., Abdouh, M. & Bernier, G. P53 pro-oxidant activity in the central nervous system: Implication in aging and neurodegenerative diseases. *Antioxidants and Redox Signaling* vol. 15 1729–1737 (2011) DOI:10.1089/ars.2010.3610.

1098. Fortin, A. *et al.* APAF1 is a key transcriptional target for p53 in the regulation of neuronal cell death. *J. Cell Biol.* **155**, 207–216 (2001) DOI:10.1083/jcb.200105137.

1099. Abdouh, M. *et al.* Bmi1 Is Down-Regulated in the Aging Brain and Displays Antioxidant and Protective Activities in Neurons. *PLoS One* **7**, e31870 (2012) DOI:10.1371/journal.pone.0031870.

1100. Zhou, S. *et al.* Differentiation of human embryonic stem cells into cone photoreceptors through simultaneous inhibition of BMP, TGFβ and Wnt signaling. (2015) doi:10.1242/dev.125385 DOI:10.1242/dev.125385.

1101. Wang, H. *et al.* Role of histone H2A ubiquitination in Polycomb silencing. *Nature* **431**, 873–878 (2004) DOI:10.1038/nature02985.

1102. Jacobs, W. B., Kaplan, D. R. & Miller, F. D. The p53 family in nervous system development and disease. *Journal of Neurochemistry* vol. 97 1571–1584 (2006) DOI:10.1111/j.1471-

4159.2006.03980.x.

1103. Boyer, L. A. *et al.* Polycomb complexes repress developmental regulators in murine embryonic stem cells. *Nature* **441**, 349–353 (2006) DOI:10.1038/nature04733.

1104. Avilion, A. A. *et al.* Multipotent cell lineages in early mouse development depend on SOX2 function. *Genes Dev.* **17**, 126–140 (2003) DOI:10.1101/gad.224503.

1105. Ellis, P. *et al.* SOX2, a persistent marker for multipotential neural stem cells derived from embryonic stem cells, the embryo or the adult. *Dev. Neurosci.* **26**, 148–165 (2004) DOI:10.1159/000082134.

1106. Graham, V., Khudyakov, J., Ellis, P. & Pevny, L. SOX2 functions to maintain neural progenitor identity. *Neuron* **39**, 749–765 (2003) DOI:10.1016/S0896-6273(03)00497-5.

1107. Yan, Y. *et al.* Directed Differentiation of Dopaminergic Neuronal Subtypes from Human Embryonic Stem Cells. *Stem Cells* **23**, 781–790 (2005) DOI:10.1634/stemcells.2004-0365.

1108. Ismail, H., Andrin, C., McDonald, D. & Hendzel, M. J. BMI1-mediated histone ubiquitylation promotes DNA double-strand break repair. *J. Cell Biol.* **191**, 45–60 (2010) DOI:10.1083/jcb.201003034.

1109. Rogakou, E. P., Pilch, D. R., Orr, A. H., Ivanova, V. S. & Bonner, W. M. DNA double-stranded breaks induce histone H2AX phosphorylation on serine 139. *J. Biol. Chem.* **273**, 5858–68 (1998) DOI:10.1074/JBC.273.10.5858.

1110. Marigo, V. Programmed cell death in retinal degeneration: Targeting apoptosis in photoreceptors as potential therapy for retinal degeneration. *Cell Cycle* vol. 6 652–655 (2007) DOI:10.4161/cc.6.6.4029.

1111. Sancho-Pelluz, J. *et al.* Photoreceptor cell death mechanisms in inherited retinal degeneration. *Molecular Neurobiology* vol. 38 253–269 (2008) DOI:10.1007/s12035-008-8045-9.

1112. Sauvageau, M. & Sauvageau, G. Polycomb group proteins: Multi-faceted regulators of somatic stem cells and cancer. *Cell Stem Cell* vol. 7 299–313 (2010)

DOI:10.1016/j.stem.2010.08.002.

1113. Chang, B. *et al.* A homologous genetic basis of the murine cpfl1 mutant and human achromatopsia linked to mutations in the PDE6C gene. *Proc. Natl. Acad. Sci. U. S. A.* **106**, 19581–19586 (2009) DOI:10.1073/pnas.0907720106.

1114. Zhang, J. *et al.* Ezh2 maintains retinal progenitor proliferation, transcriptional integrity, and the timing of late differentiation. *Dev. Biol.* **403**, 128–138 (2015) DOI:10.1016/j.ydbio.2015.05.010.

1115. Katoh, K., Yamazaki, R., Onishi, A., Sanuki, R. & Furukawa, T. G9a histone methyltransferase activity in retinal progenitors is essential for proper differentiation and survival of mouse retinal cells. *J. Neurosci.* **32**, 17658–17670 (2012) DOI:10.1523/JNEUROSCI.1869-12.2012.

1116. Popova, E. Y. *et al.* Developmentally regulated linker histone H1c promotes heterochromatin condensation and mediates structural integrity of rod photoreceptors in mouse retina. *J. Biol. Chem.* **288**, 17895–17907 (2013) DOI:10.1074/jbc.M113.452144.

1117. Bhaskara, S. *et al.* Hdac3 is essential for the maintenance of chromatin structure and genome stability. *Cancer Cell* **18**, 436–447 (2010) DOI:10.1016/j.ccr.2010.10.022.

1118. Kappes, F. *et al.* The DEK oncoprotein is a Su(var) that is essential to heterochromatin integrity. *Genes Dev.* **25**, 673–678 (2011) DOI:10.1101/gad.2036411.

1119. Larson, K. *et al.* Heterochromatin formation promotes longevity and represses ribosomal RNA synthesis. *PLoS Genet.* **8**, (2012) DOI:10.1371/journal.pgen.1002473.

1120. Peng, J. C. & Karpen, G. H. Heterochromatic genome stability requires regulators of histone H3 K9 methylation. *PLoS Genet.* **5**, (2009) DOI:10.1371/journal.pgen.1000435.

1121. Rowe, H. M. *et al.* KAP1 controls endogenous retroviruses in embryonic stem cells. *Nature* **463**, 237–240 (2010) DOI:10.1038/nature08674.

1122. Lavoie, J., Maziade, M. & Hébert, M. The brain through the retina: The flash electroretinogram as a tool to investigate psychiatric disorders. *Progress in Neuro-Psychopharmacology and Biological Psychiatry* vol. 48 129–134 (2014)

DOI:10.1016/j.pnpbp.2013.09.020.

1123. Zhu, Q. *et al.* BRCA1 tumour suppression occurs via heterochromatin-mediated silencing. *Nature* **477**, 179–184 (2011) DOI:10.1038/nature10371.

1124. Wheway, G., Nazlamova, L. & Hancock, J. T. Signaling through the Primary Cilium. *Front. Cell Dev. Biol.* **6**, 1–13 (2018).

1125. OMIM. OMIM Entry Search - MECKEL-GRUBER SYNDROME. https://www.omim.org/search/?index=entry&start=1&limit=10&sort=score+desc%2C+prefix_sort+desc&search=MECKEL-GRUBER+SYNDROME (2019).

1126. OMIM. OMIM Entry Search - BARDET-BIEDL SYNDROME. https://www.omim.org/search/?index=entry&start=1&limit=10&sort=score+desc%2C+prefix_sort+desc&search=BARDET-BIEDL+SYNDROME (2019).

1127. Ou, Y. Y., Mack, G. J., Zhang, M. & Rattner, J. B. CEP110 and ninein are located in a specific domain of the centrosome associated with centrosome maturation. *J. Cell Sci.* **115**, (2002).

1128. Novarino, G., Akizu, N. & Gleeson, J. G. Modeling Human Disease in Humans: The Ciliopathies. *Cell* **147**, 70–79 (2011) DOI:10.1016/j.cell.2011.09.014.

1129. Young, R. W. Passage of newly formed protein through the connecting cilium of retina rods in the frog. *J. Ultrastruct. Res.* **23**, 462–73 (1968).

1130. Marszalek, J. R. *et al.* Genetic Evidence for Selective Transport of Opsin and Arrestin by Kinesin-II in Mammalian Photoreceptors. *Cell* **102**, 175–187 (2000) DOI:10.1016/S0092-8674(00)00023-4.

1131. Breuer, D. K. *et al.* A Comprehensive Mutation Analysis of RP2 and RPGR in a North American Cohort of Families with X-Linked Retinitis Pigmentosa. *Am. J. Hum. Genet.* **70**, 1545–1554 (2002) DOI:10.1086/340848.

1132. Li, M. *et al.* Comprehensive analysis of gene expression in human retina and supporting tissues. *Hum. Mol. Genet.* **23**, 4001–4014 (2014) DOI:10.1093/hmg/ddu114.

1133. Navarro Quiroz, E. *et al.* Cell Signaling in Neuronal Stem Cells. *Cells* **7**, (2018) DOI:10.3390/cells7070075.

1134. Ma, L. *et al.* WNT/NOTCH Pathway Is Essential for the Maintenance and Expansion of Human MGE Progenitors. *Stem Cell Reports* (2019) doi:10.1016/j.stemcr.2019.04.007 DOI:10.1016/j.stemcr.2019.04.007.

1135. Wu, W. *et al.* The role of Six1 in the genesis of muscle cell and skeletal muscle development. *Int. J. Biol. Sci.* **10**, 983–9 (2014) DOI:10.7150/ijbs.9442.

1136. Li, X. *et al.* Eya protein phosphatase activity regulates Six1–Dach–Eya transcriptional effects in mammalian organogenesis. *Nature* **426**, 247–254 (2003) DOI:10.1038/nature02083.

1137. Paradowska-Stolarz, A. MSX1 gene in the etiology orofacial deformities. *Postepy Hig. Med. Dosw. (Online)* **69**, 1499–504 (2015).

1138. Goodnough, L. H., Dinuoscio, G. J. & Atit, R. P. Twist1 contributes to cranial bone initiation and dermal condensation by maintaining Wnt signaling responsiveness. *Dev. Dyn.* **245**, 144–56 (2016) DOI:10.1002/dvdy.24367.

1139. Tzekov, R., Stein, L. & Kaushal, S. Protein misfolding and retinal degeneration. *Cold Spring Harb. Perspect. Biol.* **3**, a007492 (2011) DOI:10.1101/cshperspect.a007492.

1140. He, S. *et al.* Retinitis Pigmentosa GTPase Regulator (RPGR) protein isoforms in mammalian retina: insights into X-linked Retinitis Pigmentosa and associated ciliopathies. *Vision Res.* **48**, 366–376 (2008) DOI:10.1016/j.visres.2007.08.005.

1141. Sheth, R. *et al.* Hox genes regulate digit patterning by controlling the wavelength of a Turing-type mechanism. *Science* **338**, 1476–80 (2012) DOI:10.1126/science.1226804.

1142. Wheway, G. *et al.* Aberrant Wnt signalling and cellular over-proliferation in a novel mouse model of Meckel–Gruber syndrome. *Dev. Biol.* **377**, 55–66 (2013) DOI:10.1016/j.ydbio.2013.02.015.

1143. Zacharias, A. L., Lewandoski, M., Rudnicki, M. A. & Gage, P. J. Pitx2 is an upstream activator of extraocular myogenesis and survival. *Dev. Biol.* **349**, 395–405 (2011)

DOI:10.1016/j.ydbio.2010.10.028.

1144. Campione, M. *et al.* The homeobox gene Pitx2: mediator of asymmetric left-right signaling in vertebrate heart and gut looping. *Development* **126**, 1225–34 (1999).

1145. Kozlowski, K. & Walter, M. A. Variation in residual PITX2 activity underlies the phenotypic spectrum of anterior segment developmental disorders. *Hum. Mol. Genet.* **9**, 2131–9 (2000).

1146. Lowe, J., Mayer, J., Landon, M. & Layfield, R. Ubiquitin and the molecular pathology of neurodegenerative diseases. *Adv. Exp. Med. Biol.* **487**, 169–86 (2001).

1147. Thornell, E. & Aquilina, A. Regulation of αA- and αB-crystallins via phosphorylation in cellular homeostasis. *Cell. Mol. Life Sci.* **72**, 4127–4137 (2015) DOI:10.1007/s00018-015-1996-x.

1148. Fort, P. E., Freeman, W. M., Losiewicz, M. K., Singh, R. S. J. & Gardner, T. W. The retinal proteome in experimental diabetic retinopathy: up-regulation of crystallins and reversal by systemic and periocular insulin. *Mol. Cell. Proteomics* **8**, 767–79 (2009) DOI:10.1074/mcp.M800326-MCP200.

1149. Sakaguchi, H. *et al.* Intense light exposure changes the crystallin content in retina. *Exp. Eye Res.* **76**, 131–133 (2003) DOI:10.1016/S0014-4835(02)00249-X.

1150. Organisciak, D., Darrow, R., Gu, X., Barsalou, L. & Crabb, J. W. Genetic, Age and Light Mediated Effects on Crystallin Protein Expression in the Retina. *Photochem. Photobiol.* **82**, 1088 (2006) DOI:10.1562/2005-06-30-RA-599.

1151. Piri, N., Song, M., Kwong, J. M. K. & Caprioli, J. Modulation of alpha and beta crystallin expression in rat retinas with ocular hypertension-induced ganglion cell degeneration. *Brain Res.* **1141**, 1–9 (2007) DOI:10.1016/J.BRAINRES.2006.11.095.

1152. Liedtke, T., Schwamborn, J. C., Schröer, U. & Thanos, S. Elongation of axons during regeneration involves retinal crystallin beta b2 (crybb2). *Mol. Cell. Proteomics* **6**, 895–907 (2007) DOI:10.1074/mcp.M600245-MCP200.

1153. Gattone, V. H. *et al.* Development of multiorgan pathology in thewpk rat model of polycystic kidney disease. *Anat. Rec.* **277A**, 384–395 (2004) DOI:10.1002/ar.a.20022.

1154. Oishi, I., Kawakami, Y., Raya, Á., Callol-Massot, C. & Belmonte, J. C. I. Regulation of primary cilia formation and left-right patterning in zebrafish by a noncanonical Wnt signaling mediator, duboraya. *Nat. Genet.* **38**, 1316–1322 (2006) DOI:10.1038/ng1892.

1155. Yuan, S. & Sun, Z. Expanding horizons: ciliary proteins reach beyond cilia. *Annu. Rev. Genet.* **47**, 353–76 (2013) DOI:10.1146/annurev-genet-111212-133243.

1156. Cohen-Hadad, Y. *et al.* Marked Differences in C9orf72 Methylation Status and Isoform Expression between C9/ALS Human Embryonic and Induced Pluripotent Stem Cells. *Stem cell reports* **7**, 927–940 (2016) DOI:10.1016/j.stemcr.2016.09.011.

1157. Sharmin, S. *et al.* Human Induced Pluripotent Stem Cell–Derived Podocytes Mature into Vascularized Glomeruli upon Experimental Transplantation. *J. Am. Soc. Nephrol.* **27**, 1778 (2016) DOI:10.1681/ASN.2015010096.

1158. Jang, J. *et al.* Primary Cilium-Autophagy-Nrf2 (PAN) Axis Activation Commits Human Embryonic Stem Cells to a Neuroectoderm Fate. *Cell* **165**, 410–420 (2016) DOI:10.1016/j.cell.2016.02.014.

1159. Syrett, C. M., Sierra, I., Berry, C. L., Beiting, D. & Anguera, M. C. Sex-Specific Gene Expression Differences Are Evident in Human Embryonic Stem Cells and During In Vitro Differentiation of Human Placental Progenitor Cells. *Stem Cells Dev.* **27**, 1360–1375 (2018) DOI:10.1089/scd.2018.0081.

1160. Sun, C. *et al.* Transcriptome variations among human embryonic stem cell lines are associated with their differentiation propensity. *PLoS One* **13**, e0192625 (2018) DOI:10.1371/journal.pone.0192625.

1161. Bourne, R. R. A. *et al.* Magnitude, temporal trends, and projections of the global prevalence of blindness and distance and near vision impairment: a systematic review and meta-analysis. *Lancet Glob. Heal.* **5**, e888–e897 (2017) DOI:10.1016/S2214-109X(17)30293-0.

1162. Wong, W. L. *et al.* Global prevalence of age-related macular degeneration and disease burden projection for 2020 and 2040: A systematic review and meta-analysis. *Lancet Glob. Heal.* **2**, e106–e116 (2014) DOI:10.1016/S2214-109X(13)70145-1.

1163. Rein, D. B. *et al.* Forecasting age-related macular degeneration through the year 2050: The potential impact of new treatments. *Arch. Ophthalmol.* **127**, 533–540 (2009) DOI:10.1001/archophthalmol.2009.58.

1164. S, H. *et al.* Bmi-1 over-expression in neural stem/progenitor cells increases proliferation and neurogenesis in culture but has little effect on these functions in vivo. *Dev. Biol.* **328**, 257–272 (2009) DOI:10.1016/J.YDBIO.2009.01.020.

1165. M, S. & G, S. Polycomb group proteins: multi-faceted regulators of somatic stem cells and cancer. *Cell Stem Cell* **7**, 299–313 (2010) DOI:10.1016/J.STEM.2010.08.002.

1166. LE, S., SR, T. & LA, B. Polycomb group proteins set the stage for early lineage commitment. *Cell Stem Cell* **7**, 288–298 (2010) DOI:10.1016/J.STEM.2010.08.004.

1167. Dhuriya, Y. K. & Sharma, D. Necroptosis: A regulated inflammatory mode of cell death. *Journal of Neuroinflammation* vol. 15 1–9 (2018) DOI:10.1186/s12974-018-1235-0.

1168. Yerbury, J. J. *et al.* Walking the tightrope: Proteostasis and neurodegenerative disease. *Journal of Neurochemistry* vol. 137 489–505 (2016) DOI:10.1111/jnc.13575.

1169. Goodall, M. L. *et al.* The Autophagy Machinery Controls Cell Death Switching between Apoptosis and Necroptosis. *Dev. Cell* **37**, 337–349 (2016) DOI:10.1016/j.devcel.2016.04.018.

1170. A, D. *et al.* Inhibition of BMI1 induces autophagy-mediated necroptosis. *Autophagy* **12**, 659–670 (2016) DOI:10.1080/15548627.2016.1147670.

1171. Mirabella, A. C., Foster, B. M. & Bartke, T. Chromatin deregulation in disease. *Chromosoma* vol. 125 75–93 (2016) DOI:10.1007/s00412-015-0530-0.

1172. Jin, P. & Warren, S. T. Understanding the molecular basis of fragile X syndrome. *Human Molecular Genetics* vol. 9 901–908 (2000) DOI:10.1093/hmg/9.6.901.

1173. Lu, H., Liu, X., Deng, Y. & Qing, H. DNA methylation, a hand behind neurodegenerative diseases. *Frontiers in Aging Neuroscience* vol. 5 (2013) DOI:10.3389/fnagi.2013.00085.

1174. Hanna, R., Flamier, A., Barabino, A. & Bernier, G. G-quadruplexes originating from evolutionary conserved L1 elements interfere with neuronal gene expression in Alzheimer's disease. *Nat. Commun.* **12**, 1–14 (2021) DOI:10.1038/s41467-021-22129-9.

1175. Hey, C. A. B. *et al.* Generation of induced pluripotent stem cells, KCi002-A derived from a patient with Bardet-Biedl syndrome homozygous for the BBS10 variant c.271insT. *Stem Cell Res.* **33**, 46–50 (2018) DOI:10.1016/j.scr.2018.09.013.

1176. Hey, C. A. B. *et al.* Generation and characterization of three isogenic induced pluripotent stem cell lines from a patient with Bardet-Biedl syndrome and homozygous for the BBS5 variant. *Stem Cell Res.* **41**, (2019) DOI:10.1016/j.scr.2019.101594.

1177. Barrell, W. B. *et al.* Induction of neural crest stem cells from Bardet–Biedl syndrome patient derived hiPSCs. *Front. Mol. Neurosci.* **12**, (2019) DOI:10.3389/fnmol.2019.00139.

1178. Hey, C. A. B. *et al.* Generation of induced pluripotent stem cells, KCi001-A derived from a Bardet-Biedl syndrome patient compound heterozygous for the BBS1 variants c.1169T>G/c.1135G>C. *Stem Cell Res.* **31**, 235–239 (2018) DOI:10.1016/j.scr.2018.08.005.

1179. DL, G. *et al.* Mutations in centrosomal protein CEP152 in primary microcephaly families linked to MCPH4. *Am. J. Hum. Genet.* **87**, 40–51 (2010) DOI:10.1016/J.AJHG.2010.06.003.

1180. Mikule, K. *et al.* Loss of centrosome integrity induces p38—p53—p21-dependent G1—S arrest. *Nat. Cell Biol. 2006 92* **9**, 160–170 (2006) DOI:10.1038/ncb1529.

1181. Rannou, Y. *et al.* Localization of aurora A and aurora B kinases during interphase: role of the N-terminal domain. *Cell Cycle* **7**, 3012–20 (2008) DOI:10.4161/cc.7.19.6718.

1182. Arslanhan, M. D., Rauniyar, N., Yates, J. R. & Firat-Karalar, E. N. Aurora Kinase A proximity interactome reveals centriolar satellites as regulators of its function during primary cilium biogenesis. *bioRxiv* 2020.11.05.370320 (2020) doi:10.1101/2020.11.05.370320 DOI:10.1101/2020.11.05.370320.

1183. Cognard, N. *et al.* Comparing the Bbs10 complete knockout phenotype with a specific renal epithelial knockout one highlights the link between renal defects and systemic inactivation in mice. *Cilia* **4**, 1–12 (2015) DOI:10.1186/s13630-015-0019-8.

1184. Chang, Y. C. *et al.* The generation of induced pluripotent stem cells for macular degeneration as a drug screening platform: Identification of curcumin as a protective agent for retinal pigment epithelial cells against oxidative stress. *Front. Aging Neurosci.* **6**, (2014) DOI:10.3389/fnagi.2014.00191.

1185. Trombetta, R. P. *et al.* A High-Throughput Screening Approach To Repurpose FDA-Approved Drugs for Bactericidal Applications against Staphylococcus aureus Small-Colony Variants. (2021) doi:10.1128/mSphere.00422-18 DOI:10.1128/mSphere.00422-18.

1186. Wan, W. *et al.* High-Throughput Screening of an FDA-Approved Drug LibraryIdentifies Inhibitors against Arenaviruses and SARS-CoV-2. *ACS Infect. Dis.* (2020) doi:10.1021/ACSINFECDIS.0C00486 DOI:10.1021/ACSINFECDIS.0C00486.

1187. Kaewkhaw, R. *et al.* Treatment paradigms for retinal and macular diseases using 3-D retina cultures derived from human reporter pluripotent stem cell lines. *Investig. Ophthalmol. Vis. Sci.* **57**, ORSFl1–ORSFl11 (2016) DOI:10.1167/iovs.15-17639.

1188. Cai, H. *et al.* High-throughput screening identifies compounds that protect RPE cells from physiological stressors present in AMD. *Exp. Eye Res.* **185**, (2019) DOI:10.1016/j.exer.2019.04.009.

1189. Renner, H. *et al.* A fully automated high-throughput workflow for 3d-based chemical screening in human midbrain organoids. *Elife* **9**, 1–39 (2020) DOI:10.7554/eLife.52904.

1190. Muckom, R. *et al.* High-throughput 3D screening for differentiation of hPSC-derived cell therapy candidates. *Sci. Adv.* **6**, eaaz1457 (2020) DOI:10.1126/sciadv.aaz1457.

1191. Aboualizadeh, E. *et al.* Imaging Transplanted Photoreceptors in Living Nonhuman Primates with Single-Cell Resolution. *Stem Cell Reports* **15**, 482–497 (2020) DOI:10.1016/j.stemcr.2020.06.019.

1192. Waldron, P. V. *et al.* Transplanted Donor- or Stem Cell-Derived Cone Photoreceptors Can Both Integrate and Undergo Material Transfer in an Environment-Dependent Manner. *Stem Cell Reports* **10**, 406–421 (2018) DOI:10.1016/j.stemcr.2017.12.008.

1193. Shirai, H. *et al.* Transplantation of human embryonic stem cell-derived retinal tissue in two primate models of retinal degeneration. *Proc. Natl. Acad. Sci. U. S. A.* **113**, E81-90 (2016) DOI:10.1073/pnas.1512590113.

1194. Sahel, J.-A. *et al.* Partial recovery of visual function in a blind patient after optogenetic therapy. *Nat. Med. 2021 277* **27**, 1223–1229 (2021) DOI:10.1038/s41591-021-01351-4.

1195. K, N., E, L.-W., P, S., KE, N. & JP, S. Bionic eye review - An update. *J. Clin. Neurosci.* **78**, 8–19 (2020) DOI:10.1016/J.JOCN.2020.05.041.

1196. PE, S. *et al.* Electronic retinal prosthesis for severe loss of vision in geographic atrophy in age-related macular degeneration: First-in-human use. *Eur. J. Ophthalmol.* (2021) doi:10.1177/11206721211000680 DOI:10.1177/11206721211000680.

1197. Z, O.-A., A, D., MR, M. & A, M. Safety, effectiveness, and cost-effectiveness of Argus II in patients with retinitis pigmentosa: a systematic review. *Int. J. Ophthalmol.* **14**, 300–316 (2021) DOI:10.18240/IJO.2021.02.20.

1198. Ozawa, Y. *et al.* Neuroprotective Effects of Lutein in the Retina. *Curr. Pharm. Des.* **18**, 51–56 (2012) DOI:10.2174/138161212798919101.

1199. Li, S. Y. *et al.* Effect of lutein on retinal neurons and oxidative stress in a model of acute retinal ischemia/reperfusion. *Investig. Ophthalmol. Vis. Sci.* **50**, 836–843 (2009) DOI:10.1167/iovs.08-2310.

1200. Koushan, K., Rusovici, R., Li, W., Ferguson, L. R. & Chalam, K. V. The role of lutein in eye-related disease. *Nutrients* **5**, 1823–1839 (2013) DOI:10.3390/nu5051823.

1201. Mustafi, D., Engel, A. H. & Palczewski, K. Structure of cone photoreceptors. *Progress in Retinal and Eye Research* vol. 28 289–302 (2009) DOI:10.1016/j.preteyeres.2009.05.003.

1202. Nigg, E. A. & Raff, J. W. Centrioles, Centrosomes, and Cilia in Health and Disease. *Cell* **139**,

663–678 (2009) DOI:10.1016/J.CELL.2009.10.036.

1203. Yang, H. J., Ratnapriya, R., Cogliati, T., Kim, J. W. & Swaroop, A. Vision from next generation sequencing: Multi-dimensional genome-wide analysis for producing gene regulatory networks underlying retinal development, aging and disease. *Progress in Retinal and Eye Research* vol. 46 1–30 (2015) DOI:10.1016/j.preteyeres.2015.01.005.

1204. Goodlett, C. R. & Horn, K. H. Mechanisms of alcohol-induced damage to the developing nervous system. *Alcohol Res. Health* **25**, 175–84 (2001).

1205. Delia, D. & Mizutani, S. The DNA damage response pathway in normal hematopoiesis and malignancies. *International Journal of Hematology* vol. 106 328–334 (2017) DOI:10.1007/s12185-017-2300-7.

1206. Negroni, A., Cucchiara, S. & Stronati, L. Apoptosis, necrosis, and necroptosis in the gut and intestinal homeostasis. *Mediators of Inflammation* vol. 2015 (2015) DOI:10.1155/2015/250762.

1207. Llonch, S., Carido, M. & Ader, M. Organoid technology for retinal repair. *Developmental Biology* vol. 433 132–143 (2018) DOI:10.1016/j.ydbio.2017.09.028.

1208. Regnault, C., Dheeman, D. S. & Hochstetter, A. Microfluidic devices for drug assays. *High-Throughput* vol. 7 18 (2018) DOI:10.3390/HT7020018.

1209. Du, G.-S. *et al.* Cell-Based Drug Combination Screening with a Microfluidic Droplet Array System. *Anal. Chem.* **85**, 6740–6747 (2013) DOI:10.1021/AC400688F.

1210. Yoonseok Choi *et al.* A microengineered pathophysiological model of early-stage breast cancer. *Lab Chip* **15**, 3350–3357 (2015) DOI:10.1039/C5LC00514K.

1211. An, D., Kim, K. & Kim, J. Microfluidic System Based High Throughput Drug Screening System for Curcumin/TRAIL Combinational Chemotherapy in Human Prostate Cancer PC3 Cells. *Biomol. Ther. (Seoul).* **22**, 355 (2014) DOI:10.4062/BIOMOLTHER.2014.078.

1212. Fan, Y., Nguyen, D. T., Akay, Y., Xu, F. & Akay, M. Engineering a Brain Cancer Chip for High-throughput Drug Screening. *Sci. Reports 2016 61* **6**, 1–12 (2016) DOI:10.1038/srep25062.

6. Annex 1: Article: Differentiation of human embryonic stem cells into cone photoreceptors through simultaneous inhibition of BMP, TGFβ and Wnt signaling

© 2015. Published by The Company of Biologists Ltd | Development (2015) 142, 3294-3306 doi:10.1242/dev.125385

RESEARCH ARTICLE

STEM CELLS AND REGENERATION

Differentiation of human embryonic stem cells into cone photoreceptors through simultaneous inhibition of BMP, TGFβ and Wnt signaling

Shufeng Zhou[1,*], Anthony Flamier[1,*], Mohamed Abdouh[1], Nicolas Tétreault[1], Andrea Barabino[1], Shashi Wadhwa[2] and Gilbert Bernier[1,3,4,‡]

ABSTRACT

Cone photoreceptors are required for color discrimination and high-resolution central vision and are lost in macular degenerations, cone and cone/rod dystrophies. Cone transplantation could represent a therapeutic solution. However, an abundant source of human cones remains difficult to obtain. Work performed in model organisms suggests that anterior neural cell fate is induced 'by default' if BMP, TGFβ and Wnt activities are blocked, and that photoreceptor genesis operates through an S-cone default pathway. We report here that *Coco* (*Dand5*), a member of the Cerberus gene family, is expressed in the developing and adult mouse retina. Upon exposure to recombinant COCO, human embryonic stem cells (hESCs) differentiated into S-cone photoreceptors, developed an inner segment-like protrusion, and could degrade cGMP when exposed to light. Addition of thyroid hormone resulted in a transition from a unique S-cone population toward a mixed M/S-cone population. When cultured at confluence for a prolonged period of time, COCO-exposed hESCs spontaneously developed into a cellular sheet composed of polarized cone photoreceptors. COCO showed dose-dependent and synergistic activity with IGF1 at blocking BMP/TGFβ/Wnt signaling, while its cone-inducing activity was blocked in a dose-dependent manner by exposure to BMP, TGFβ or Wnt-related proteins. Our work thus provides a unique platform to produce human cones for developmental, biochemical and therapeutic studies and supports the hypothesis that photoreceptor differentiation operates through an S-cone default pathway during human retinal development.

KEY WORDS: Coco, Dand5, Cerl2, Differentiation, Retina, Cone photoreceptors, hES cells, Mouse, Human

INTRODUCTION

Macular degenerations, retinitis pigmentosa and retinal dystrophies affect millions of people worldwide. In most cases, loss of visual function results from death of photoreceptors, the specialized cells involved in phototransduction (Pacione et al., 2003). Macular degenerations and cone dystrophies preferentially target the macula, a cone photoreceptor-rich retinal structure involved in color discrimination and high-resolution central vision. Cell replacement therapy may stop disease progression or restore visual function. However, a reliable and abundant source of human cone photoreceptors is not currently available. This limitation may be overcome using embryonic stem cells (ESCs). ESCs originate from the inner cell mass of the blastocyst and represent the most primitive stem cells. Human ESCs (hESCs) can develop into cells and tissues of the three primary germ layers and be expanded indefinitely (Reubinoff et al., 2000; Thomson et al., 1998).

Work performed in amphibians and chick suggests that primordial cells adopt a neural fate in the absence of alternative cues (Muñoz-Sanjuán and Brivanlou, 2002). The default model of neural induction has paved the way to the differentiation of ESCs into neurons (Tropepe et al., 2001). The retina and cerebral cortex originate from the anterior portion of the neural plate, and hESCs spontaneously adopt an anterior positional identity when induced to differentiate into neurons (Banin et al., 2006; Couly and Le Douarin, 1988). However, only a fraction of these cells actually differentiate into retinal neurons, possibly because active inhibition of bone morphogenetic protein (BMP), transforming growth factor β (TGFβ) superfamily (including Nodal and Activin), and Wingless (Wnt) signaling is normally required (Liu et al., 2010). In principle, this can be partially achieved by expressing noggin and chordin, two BMP antagonists, and dickkopf 1 (Dkk1), a Wnt antagonist. Furthermore, retinal fate can be promoted using insulin like growth factor 1 (IGF1) (Pera et al., 2001; Rorick et al., 2006). Application of this rationale has led to the differentiation of hESCs into retinal progenitor cells, where ~12% of cells express CRX (Lamba et al., 2006). CRX is expressed by photoreceptor progenitors, mature photoreceptors and a subset of bipolar neurons (Chen et al., 1997; Freund et al., 1997; Furukawa et al., 1997). Although ~4% of differentiated hESCs were reported to express rhodopsin, a marker of rod photoreceptors, fewer than 0.01% express S-opsin (OPN1SW – HUGO), a marker of cone photoreceptors. Notably, transplanted cells could adopt rod and cone photoreceptor phenotypes when grafted into the retina of normal and *Crx*-deficient mice (Lamba et al., 2009). The differentiation of hESCs into cone and rod photoreceptors at a frequency of 12-20% over a 150-200 day period was also achieved using Dkk1 and LEFTY, a Nodal antagonist, as well as retinoic acid (RA) and taurine, two factors that can promote the terminal differentiation of photoreceptors (Osakada et al., 2008). In addition, directed differentiation of hESCs into retinal pigment epithelium was performed using nicotinamide (Idelson et al., 2009). More recently, differentiation of human pluripotent stem cells into retinal organoids containing rod and cone photoreceptors was also achieved (Mellough et al., 2015; Nakano et al., 2012; Tucker et al., 2013).

We report here that ~60-80% of hESCs can be differentiated within 4-5 weeks into S-cone photoreceptors using human recombinant COCO, a multifunctional BMP, TGFβ and Wnt

[1]Stem Cell and Developmental Biology Laboratory, Maisonneuve-Rosemont Hospital, 5415 Boul. l'Assomption, Montréal, Canada H1T 2M4. [2]Department of Anatomy, All India Institute of Medical Sciences, New Delhi 110029, India. [3]Department of Neuroscience, University of Montréal, Montréal H3T 1J4, Canada. [4]Department of Ophthalmology, University of Montréal, Montréal H3T 1J4, Canada. *These authors contributed equally to this work

‡Author for correspondence (gbernier.hmr@ssss.gouv.qc.ca)

Received 13 April 2015; Accepted 6 August 2015

Development (2015) 142, 3294-3306 doi:10.1242/dev.125385

antagonist, supporting the hypothesis that photoreceptor development operates through an S-cone default pathway (Jadhav et al., 2006; Mears et al., 2001; Ng et al., 2001; Swaroop et al., 2010; Yanagi et al., 2002; Yaron et al., 2006). The short wave (S) and medium wave (M) cone subtype ratio can also be manipulated by the addition of thyroid hormone and the procedure is achieved without using the embryonic body (EB) induction step. Alternatively, a self-organized and polarized 3D cone photoreceptor sheet can be derived that shows evidence of connecting cilium and outer segment formation. This work might contribute to progress toward the use of hESCs for the treatment of macular degenerations and cone dystrophies, and provides a framework with which to study the biochemistry and developmental genetics of human cones in a culture dish.

RESULTS

Mouse *Coco* is expressed in the developing CNS and retina

Members of the Cerberus/Dan family of secreted inhibitors can block BMP, Nodal/TGFβ and Wnt activities simultaneously (Bouwmeester et al., 1996; Piccolo et al., 1999). In a search for a putative 'retinal promoting' factor of this family, we analyzed the expression pattern of the mammalian ortholog of *Coco* (also known as *Dand5* or *Cerl2* in mammals). In *Xenopus*, *Coco* is expressed maternally and ubiquitously within the ectoderm prior to neural induction, but expression is not detected after gastrulation (Bell et al., 2003). However, a search of the UNIGENE and EST databases reveals that mouse *Coco* and human *COCO* transcripts are present in the eye, brain and testis cDNA libraries at embryonic and adult stages.

Coco encodes two transcripts, with one lacking the 5′ coding sequence (supplementary material Fig. S1A). We analyzed mouse *Coco* expression by RNA *in situ* hybridization. Using the full-length mouse *Coco* cDNA (which recognizes both isoforms), we observed *Coco* expression in the optic vesicle and CNS at E9.5 (Fig. 1A), in the retina and hair follicles at E14.5 and P1 (Fig. 1A), and in the photoreceptor nuclear layer at P60 (supplementary material Fig. S1B). These observations were confirmed using quantitative RT-PCR (qPCR) analysis on tissues from neonates at P3 using

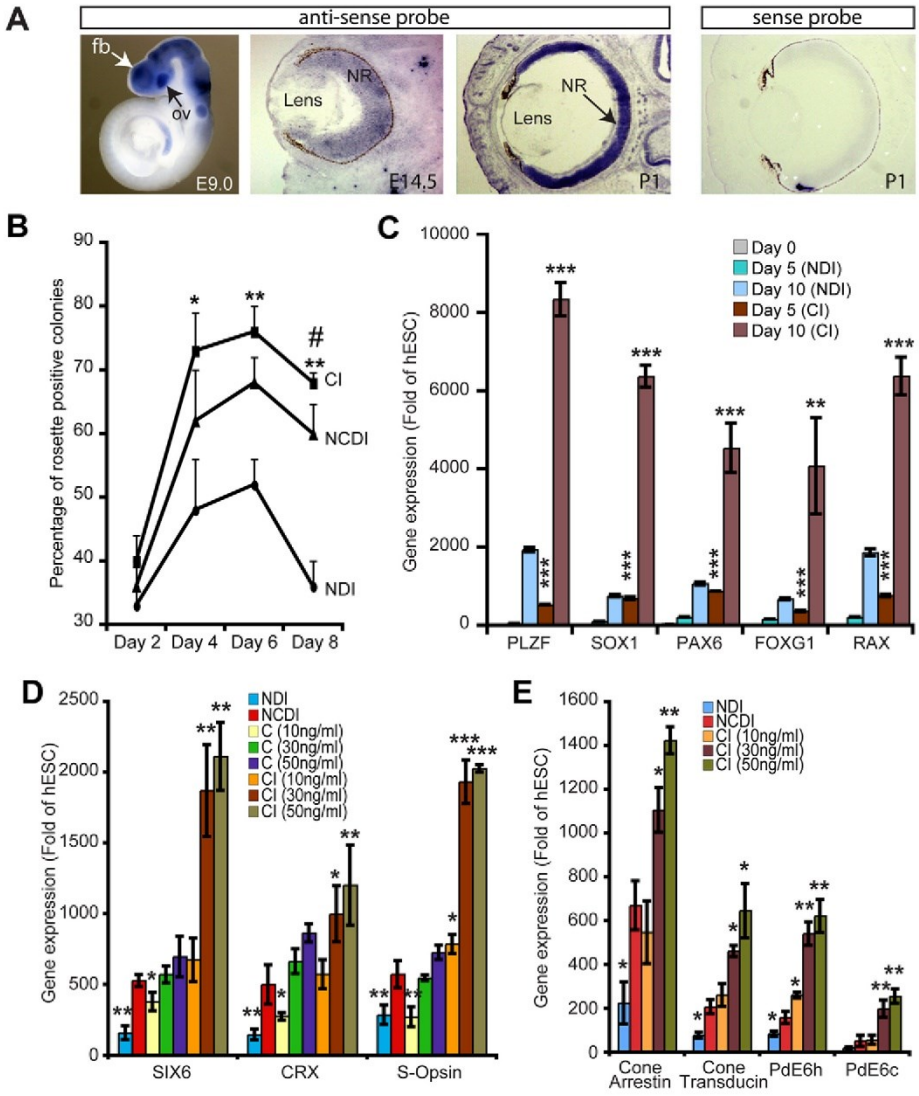

Fig. 1. COCO is a potent retinal and photoreceptor inducer. (A) *In situ* hybridization on E9.0 mouse embryos (whole mount) revealed *Coco* expression in the optic vesicle (ov), forebrain (fb) and neural tube, and in the neural retina (NR) at E14.5 and P1 (sections). The sense probe provides a negative control. (B) Analysis of neural rosette induction kinetics in NDI, NCDI, or COCO (30 ng/ml)+IGF1 (10 ng/ml) (CI) culture medium. **P*<0.05 and ***P*<0.01 when compared with NDI-treated culture and $^{\#}$*P*<0.05 when compared with NCDI-treated culture. (C) hESCs were induced to differentiate in the presence of NDI or CI media for 5 and 10 days and analyzed by qPCR. Data are expressed as fold change over gene expression in undifferentiated hESCs. ***P*<0.01 and ****P*<0.001 when comparing CI with NDI at both time points analyzed. (D,E) hESCs were induced to differentiate in the presence of NDI, NCDI, COCO alone or CI for 3 weeks. Differentiated hESCs were analyzed by qPCR. Data are expressed as fold change over gene expression in undifferentiated hESCs. **P*<0.05, ***P*<0.01, ****P*<0.001 as compared with gene expression levels in NCDI-treated cells. (B-E) Results are mean±s.d. (*n*=3).

Development (2015) 142, 3294-3306 doi:10.1242/dev.125385

oligonucleotide pairs that recognize either the 5′ coding isoform or both isoforms (supplementary material Fig. S1C).

COCO is a potent neural and photoreceptor inducer

Neural induction of hESCs can be achieved through the formation of floating EBs and subculture on a laminin or Matrigel substrate in serum-free media (supplementary material Fig. S2). Using the hESC line H9, we tested the putative neural/retinal-inducing activity of human recombinant COCO by morphological analysis of EBs maintained in suspension for 4-5 days and then subcultured on Matrigel. We quantified the frequency and kinetics of neural rosette formation (Fig. 1B). In these experiments, COCO (30 ng/ml) was used in combination with IGF1 and FGF2 (referred to as CI medium) or added at 10 ng/ml to the previously described NDI medium (referred to as NCDI medium), which contains noggin, Dkk1, IGF1 and FGF2. The original NDI medium was used as a positive control (Lamba et al., 2006). We found that although more colonies presented neural rosettes with the NCDI (~67%) than with the NDI (~50%) medium at day 6 of the differentiation protocol, this process was further improved with the CI medium (~76%). To directly compare the neural induction activity of the NDI and CI media, we analyzed the differentiated cells at early time points for the expression of neural rosette (*PLZF*; *ZBTB16* – HUGO), pan-neural (*SOX1*, *PAX6*), anterior neural/forebrain (*FOXG1*) and anterior neural/ventral forebrain/early retinal (*RAX*) cell fate markers using qPCR (Chambers et al., 2009; Mathers et al., 1997; Walther and Gruss, 1991). These results revealed that the CI medium provided robust neural and anterior neural/early retinal induction activity (Fig. 1C).

To evaluate the putative retinal-inducing activity of COCO, we tested whether COCO+FGF2 possessed early retinal (*SIX6*) and photoreceptor [*CRX*, rhodopsin (*RHO*), *NRL*, M-opsin (*OPN1MW* – HUGO) and S-opsin] inducing activity using qPCR analysis on colonies isolated at day 21 of the differentiation protocol (Gallardo et al., 1999; Jean et al., 1999). We found that COCO+FGF2 was very efficient at inducing *SIX6*, *CRX* and S-opsin gene expression, and that this effect was dose dependent (Fig. 1D). The retinal-inducing activity of COCO (30 ng/ml)+FGF2 was comparable to that of NCDI medium. When this was combined with 10 ng/ml IGF1 (the same concentration as in the NDI and NCDI media), the induction of *SIX6*, *CRX* and S-opsin was further enhanced. This effect was dose dependent, and maximal CI activity was obtained when COCO concentrations ranged between 30 and 50 ng/ml (Fig. 1D). Taken as a whole, the retinal- and photoreceptor-inducing activity of CI was ~10-fold more effective than the NDI medium and ~3- to 4-fold more effective than the NCDI medium. Expression of *RHO* and *NRL* (rods) and of M-opsin (M-cones) was not detected after 21 days of hESC differentiation in CI (supplementary material Fig. S3). However, timecourse analysis revealed weak induction (about 4-fold the hESC level) of the *NRL* and M-opsin genes at 1 week, and of *RHO* at week 2, suggesting that retinal progenitor cells might be potent to generate all types of photoreceptor cells at these early stages (supplementary material Fig. S3). Robust expression of the cone-specific genes cone arrestin [also known as arrestin 3 (*ARR3*) and X-arrestin], cone transducin (*GNAT2*), phosphodiesterase 6H (*PDE6H*) and phosphodiesterase 6C (*PDE6C*) was also observed in cells exposed to CI for 21 days (Fig. 1E) (Corbo et al., 2007), altogether suggesting a predominant S-cone photoreceptor cell population. Comparable results, but with variable efficiencies, were obtained with the hESC lines HUES1, HUES8 and HUES9 (supplementary material Fig. S4).

Generation of a highly enriched S-opsin-positive cell population

To further characterize the differentiated cell populations, we performed western blot analyses using extracts from hESCs exposed to NCDI or CI for 21 days. We observed robust expression of CRX and of the phototransduction proteins S-opsin, cone transducin and cone arrestin (Fig. 2A,B). Expression of rhodopsin and of M-opsin proteins was, however, not detected, even when thyroid hormone (T3) was added to the culture media (supplementary material Fig. S6A).

We performed intracellular labeling using an anti-S-opsin antibody combined with fluorescence activated cell sorting (FACS) analysis on cells exposed to CI for 21 days (Chatoo et al., 2010). We found that ~70±9% (n=5 independent cell differentiation experiments) of differentiated cells from the H9 cell line highly expressed S-opsin (Fig. 2C). Comparable results were obtained with the HUES1, HUES8 and HUES9 cell lines (supplementary material Fig. S6B). In a separate set of experiments, S-opsin-labeled cell populations were sorted and analyzed by qPCR for the expression of retinal, mesendodermal, ectodermal and ESC markers (Fig. 2D,E). We found that S-opsin^{high} cells (95% in experiment #1, 80% in experiment #2) expressed photoreceptor genes at levels several orders of magnitude higher than undifferentiated hESCs (Fig. 2E). The S-opsin^{low} cells (5% in experiment #1, 20% in experiment #2) were also positive for *CRX*, cone arrestin and S-opsin gene expression but at levels corresponding to 4-10% of those found in the S-opsin^{high} population (Fig. 2E, inset). Both populations were, however, negative for non-retinal lineage-specific genes (Fig. 2E).

Developmental kinetics of the differentiated cells

To study the developmental kinetics of the cell differentiation process, hESCs exposed to CI for 5, 10 and 21 days were analyzed by immunofluorescence (IF) microscopy for CHX10 (VSX1 – HUGO), SOX2, RAX and CRX expression (Burmeister et al., 1996; Ellis et al., 2004; Ferda Percin et al., 2000; Graham et al., 2003; Livne-Bar et al., 2006; Mathers et al., 1997; Taranova et al., 2006). At day 5, we observed that the large majority of the cells were positive for the retinal progenitor markers CHX10 (90%) and SOX2 (100%) (Fig. 3A,F,G). This proportion slightly declined at day 10, when numerous RAX-positive and CRX-positive cells also appeared (Fig. 3B,F,G). Yet, almost all CHX10-expressing cells also expressed SOX2 (Fig. 3D). At day 21, few cells positive for CHX10, SOX2 or RAX remained, being replaced by prospective photoreceptor cells expressing CRX (Fig. 3C,F).

Cells expressing S-opsin at the highest levels (40% of S-opsin^{high} cells) were generally located within neural rosettes (Fig. 3E). Most cells within rosettes also expressed βIII-tubulin (a marker of immature neurons) at low levels (Fig. 3E). Furthermore, ~3% of cells present in our cultures had a typical neuronal morphology and expressed βIII-tubulin at high levels (Fig. 3E). The subtype identity of these neurons remains to be established. These analyses revealed that, upon exposure to CI, the large majority of hESCs rapidly adopt a retinal progenitor cell identity, which is also rapidly lost toward a cone photoreceptor precursor cell identity.

Cone phenotype and cGMP degradation *in vitro*

In all experiments, hESCs were induced to differentiate into photoreceptors when at confluence, which in our hands improved cell survival and neural/photoreceptor induction. However, this procedure prevented the analysis of single cells. At first, we analyzed cells exposed to CI by high-resolution IF at day 21, which confirmed immunoreactivity for CRX (mean 72±7%) and ABCA4

Development (2015) 142, 3294-3306 doi:10.1242/dev.125385

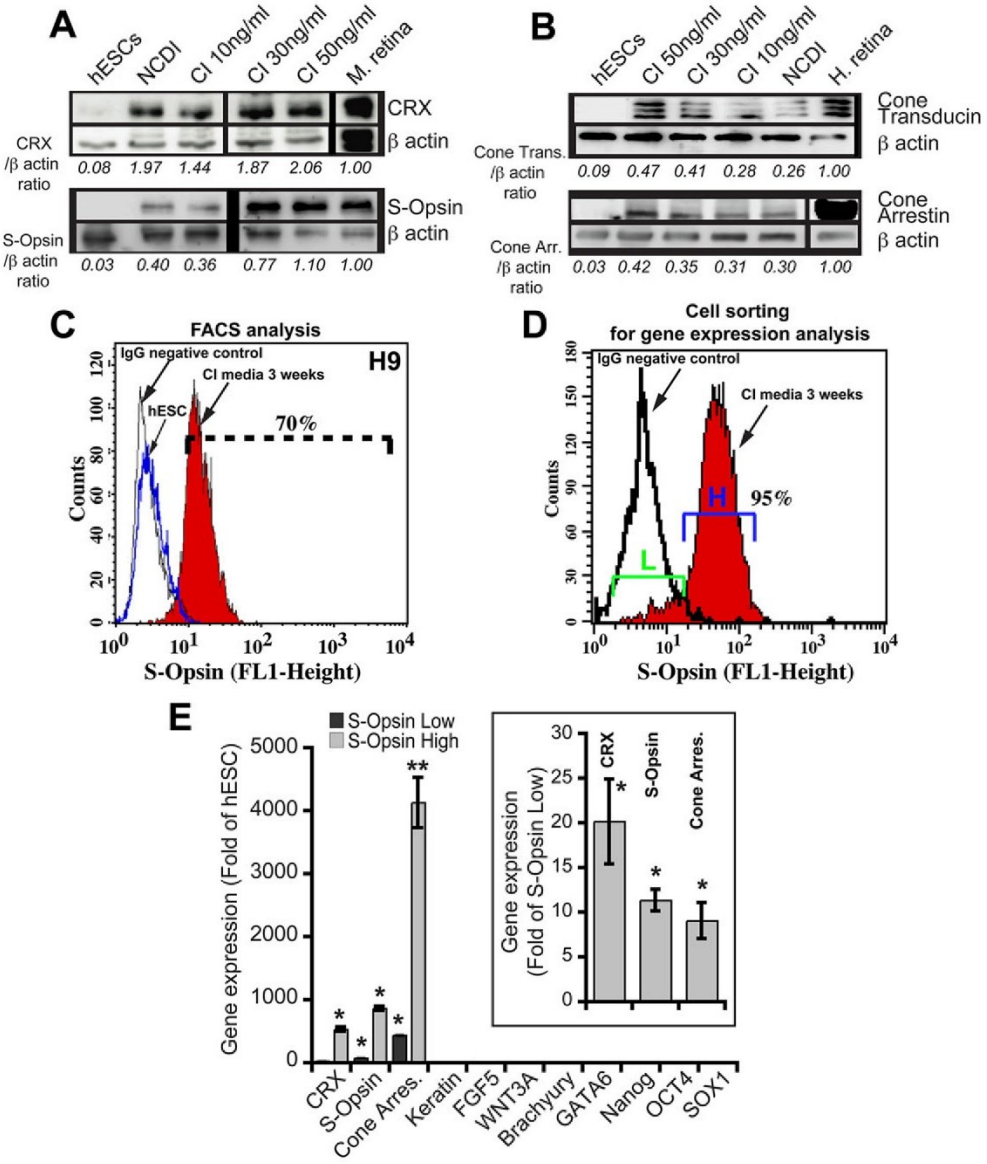

Fig. 2. COCO induces the generation of a highly enriched S-cone photoreceptor population. (A,B) hESCs cultured in NCDI or CI medium for 3 weeks were subjected to western blot analyses for the expression of CRX and S-opsin (A), or cone transducin and cone arrestin (B). β-actin was used to quantify protein loading. CRX, S-opsin, cone transducin or cone arrestin levels are expressed as a ratio over β-actin levels. Mouse or human retinas were used as positive controls. (C) Undifferentiated hESCs (blue line) or hESCs cultured in CI for 3 weeks (red) were analyzed by FACS for S-opsin expression. The black line represents the IgG isotypic control serum. (D) hESCs cultured in CI for 3 weeks were sorted by FACS for subsequent gene expression analysis on the basis of S-opsin expression levels [S-opsin^{low} (L) versus S-opsin^{high} (H)]. (E) Sorted cells were analyzed for gene expression by qPCR. Data are expressed as fold change over gene expression in undifferentiated hESCs. In the inset, a parallel analysis was performed in which gene expression in the S-opsin^{high} cell fraction is represented as fold change over that in the S-opsin^{low} cell fraction, which was set at 1. Results are mean±s.d. (n=2 cell sortings); *P<0.05 and **P<0.01 as compared with gene expression levels in undifferentiated hESCs and the S-opsin^{low} cell fraction, respectively.

(mean 67±12%) in densely packed cellular aggregates (Fig. 4A). *ABCA4* is mutated in Stargardt disease and is expressed by cone and rod photoreceptors (Allikmets et al., 1997; Molday et al., 2000). Cells differentiated for 21 days were next dissociated to single cells and plated on glass coverslips at low density. After an additional 7 days, they were analyzed by IF for the expression of cone markers. Under these conditions, most cells presented neurites and were positive for ABCA4 (mean 76±11%), S-opsin (mean 79±9%) and cone arrestin (mean 84.9±5%) (Fig. 4A). Although S-opsin immunoreactivity was diffused throughout the cell at this early stage, it was enriched in the proximal soma of the cells, suggesting possible S-opsin compartmentalization (Fig. 4A, inset).

Using the same experimental procedure, single cells were allowed to differentiate for 15 days. On rare occasions, we could observe the formation of more mature cones having an outer segment-like structure (Fig. 4A). These cells were immunoreactive

Development (2015) 142, 3294-3306 doi:10.1242/dev.125385

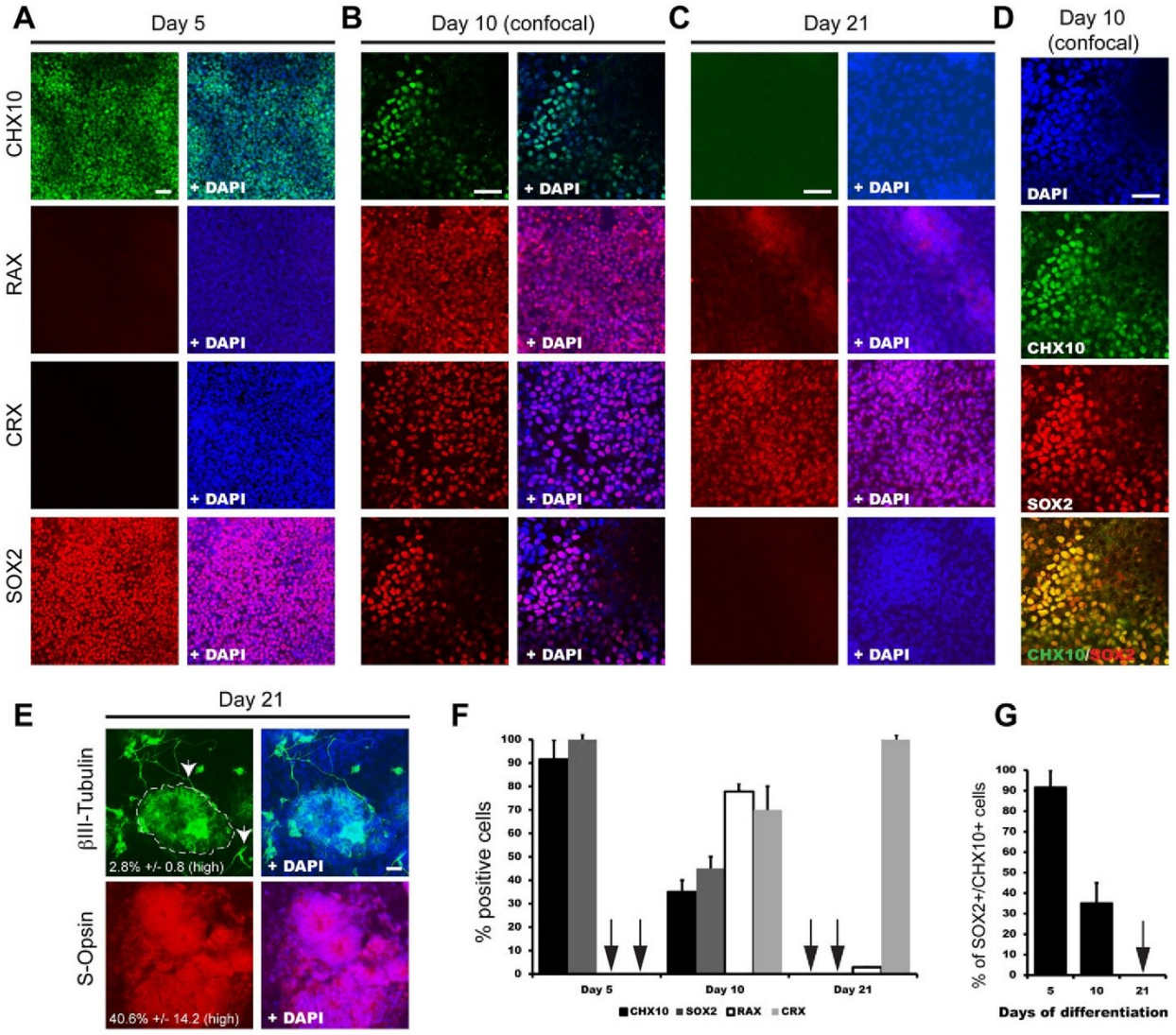

Fig. 3. Developmental kinetics of hESC differentiation into photoreceptors. (A-C) Representative immunofluorescence images of hESCs exposed to CI for 5 (A), 10 (B) or 21 (C) days using antibodies against CHX10, RAX, CRX and SOX2. (D) Co-expression of CHX10 and SOX2 after 10 days of differentiation, as revealed by confocal IF analysis. (E) Expression of βIII-tubulin and S-opsin after 21 days of differentiation. Arrowheads indicate neurons expressing βIII-tubulin at high levels. The dashed line delineates a neural rosette. Values indicate the percentage of cells expressing high levels of βIII-tubulin or S-opsin. (F) Quantitative analysis of cells positive for CHX10, SOX2, RAX or CRX. (G) Quantitative analysis of CHX10/SOX2 double-positive cells after 5, 10 and 21 days of differentiation. Results are mean±s.d. (*n*=3 experiments). Arrows (F,G) indicate the absence of positive cells for the corresponding antibody. Scale bars: 40 µm.

for ABCA4 at the presumptive junction between the inner and outer segments, a localization possibly corresponding to the nascent disk (Fig. 4A). We also observed polarized accumulation of S-opsin at one side of the cells, also suggesting cone maturation (Fig. 4A). Using scanning electron microscopy at day 35 of the differentiation protocol, we observed that cells within these aggregates displayed a buttonhead-like morphology reminiscent of the head-like morphology of week 15 human embryonic cones when viewed vertically (Fig. 4B). In immature cones, this structure corresponds to the apex of the inner segment (Narayanan and Wadhwa, 1998). The morphological similarity was also noticeable when cells were viewed in the horizontal plane, revealing the presence of an inner segment-like protrusion in the *in vitro* generated cones (Fig. 4B).

One of the unique properties of photoreceptors is to degrade cGMP in response to the activation of photosensitive opsin pigments by light. This process occurs through release of the α-transducin subunit, which can activate the cGMP phosphodiesterase, ultimately resulting in membrane hyperpolarization (Michaelides et al., 2006). To establish if cells could degrade cGMP in response to light exposure, we measured cGMP levels by immunoassay in cells differentiated for 35 days in NDI or CI medium (Jomary and Jones, 2008). Extracts were isolated from cells exposed to a bright light for 1 min or maintained in the dark for 2 days. No difference in cGMP levels was observed in undifferentiated hESCs between light and dark conditions, in contrast to hESCs differentiated with NDI or CI medium (Fig. 4C). To evaluate the total amount of cGMP

Development (2015) 142, 3294-3306 doi:10.1242/dev.125385

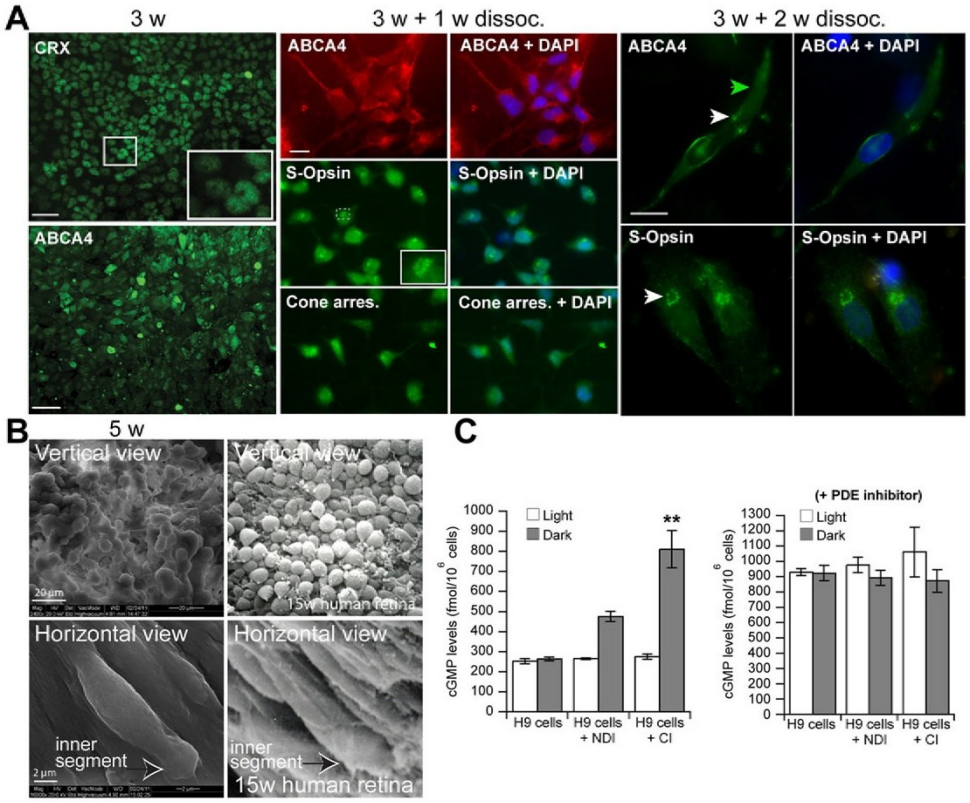

Fig. 4. Differentiated cells develop neurites and an outer segment-like structure and can degrade cGMP upon light exposure. (A) hESCs differentiated for 21 days (3 w) in CI medium were analyzed by IF. hESCs were differentiated for 3 weeks at confluence in CI medium and then dissociated to single cells and plated on glass coverslips at low density. Cells were analyzed 7 days later (3 w+1 w) by IF, revealing the broad cellular distribution of S-opsin at this early maturation stage but with stronger accumulation in the cell soma (inset), and expression of ABCA4 and cone arrestin. Note the presence of neurites. Cells were further analyzed 15 days later (3 w+2 w) by IF. Note the localization of ABCA4 at the presumptive inner/outer segment junction (white arrowhead) and the presence of an outer segment-like structure (green arrowhead). Note also the polarized accumulation of S-opsin (arrowhead). Scale bars: 5 µm, except 50 µm in 3 w. (B) hESCs differentiated for 35 days were analyzed by scanning electron microscopy. 15-week-old human embryonic retina is shown for comparison. (C) hESCs were cultured in NDI or CI medium for 35 days and cGMP concentrations were measured. (Left) Cells were kept in the dark or exposed to light. (Right) cGMP concentrations were measured in cells cultured in the presence of the PDE inhibitor IBMX. cGMP levels are presented as mean±s.d. (n=3); $^{**}P$<0.01 as compared with cGMP levels in undifferentiated hESCs cultured in NDI medium.

hydrolyzed by all phosphodiesterases (PDEs) present in the cells, we applied a non-specific PDE inhibitor (IBMX). The addition of IBMX abolished the difference of cGMP levels between light and dark conditions (Fig. 4C). The level of cGMP hydrolyzed by light-sensitive PDE corresponds to the difference between the levels in light and dark conditions and represented 240 femtomoles/10^6 cells in NDI medium and 560 femtomoles/10^6 cells in CI medium. The total amount of cGMP hydrolyzed by all PDEs (the difference between the cGMP levels in the presence and absence of IBMX in the light) corresponds to 650 femtomoles/10^6 cells. Therefore, light-sensitive PDEs account for 36% (240/650) of the total PDE activity in NDI-differentiated cells and for 86% (560/650) in CI-differentiated cells.

Cone phenotype upon cell transplantation in mouse eyes

To test the capacity of the cells to migrate and adopt a cone phenotype *in vivo*, we performed cell transplantation experiments by injecting hESCs differentiated with CI for 2, 3 or 4 weeks into the vitreous of wild-type mouse pups (Lamba et al., 2009). A fraction of the cells that underwent differentiation for 2 weeks, but not for 3 or 4 weeks, could migrate into various layers of the host retina, as detected using a human-specific mitochondrial antigen antibody (1.4±0.5% from the 10,000 cells injected) (supplementary material Fig. S5A,B). Notably, rare human cells present in the photoreceptor nuclear layer were positive for S-opsin and adopted a morphology that was similar to that of endogenous photoreceptors (supplementary material Fig. S5B,B′). The non-rodent identity of the double-positive cells was further confirmed by the unique pattern of chromatin condensation and the larger nuclei of human cells, as visualized with DAPI (supplementary material Fig. S5B′). These features were not present in PBS-injected eyes (supplementary material Fig. S5C). These results suggested that a fraction of the immature human cone progenitors or precursors differentiated with CI could migrate into the mouse retina outer nuclear layer and adopt an S-cone photoreceptor fate *in vivo*.

Thyroid hormone signaling allows M-cone genesis

During mouse retinal development, cone differentiation into the M-cone subtype is induced by T3 through activation of the thyroid hormone receptor β2 (Thrβ2). Thrβ2 can repress the S-opsin promoter while activating the M-opsin gene (Roberts et al., 2006; Swaroop et al., 2010). In previous assays using the EB induction

Development (2015) 142, 3294-3306 doi:10.1242/dev.125385

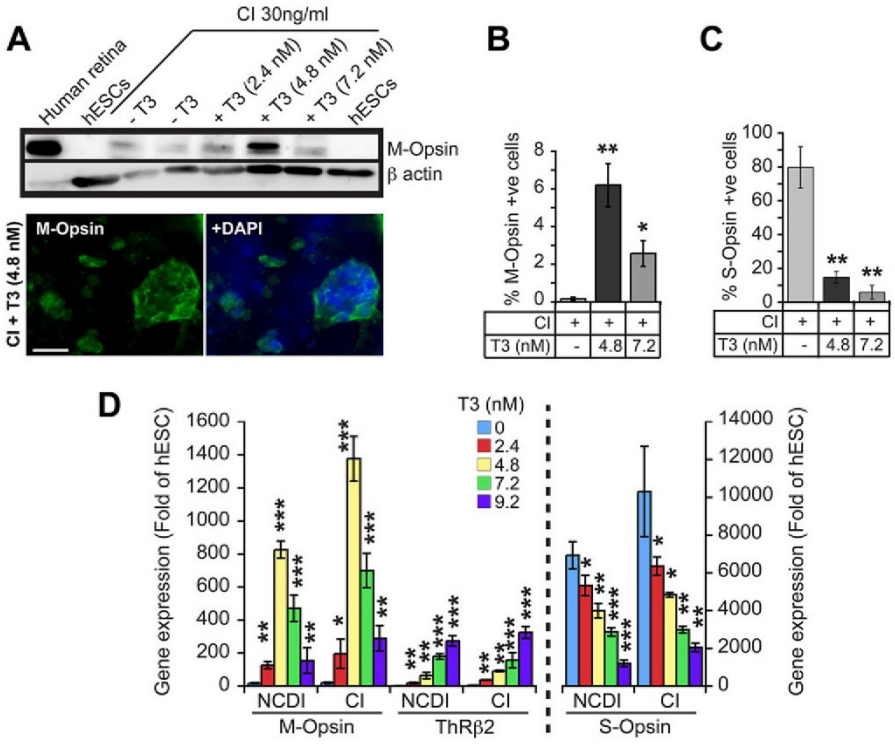

Fig. 5. Exposure to thyroid hormone can induce the generation of M-cone photoreceptors. (A) hESCs were cultured in CI medium with or without thyroid hormone (T3) for 3 weeks and analyzed by western blot and IF for M-opsin expression. Scale bar: 40 µm. (B,C) hESCs cultured as in A were labeled with anti-M-opsin (B) or anti-S-opsin (C) antibodies. The percentage of cells positive for M-opsin or S-opsin among total DAPI-stained nuclei are shown. Results are mean±s.d. (n=4); *P<0.05, **P<0.01 as compared with cells not treated with T3. (D) hESCs were cultured in NCDI or CI medium with or without T3, and analyzed by qPCR. Data are expressed as fold change over gene expression in undifferentiated hESCs. Results are mean±s.d. (n=3); *P<0.05, **P<0.01, ***P<0.001 as compared with gene expression levels in cells not treated with T3.

protocol and CI, we were unable to detect M-opsin and *Thrb2* expression by qPCR or western blot, even when cells were exposed to various concentrations of T3 (supplementary material Fig. S3 and Fig. S6A). To test if this limitation could be overcome, we induced hESCs predifferentiation by plating them directly on reduced growth factor Matrigel for 5-7 days in hESC medium until they reached confluence, and then added CI medium (thus bypassing the EB induction step) (Chambers et al., 2009). With this modification, addition of T3 to the CI medium resulted in a dose-dependent activation of M-opsin and *Thrb2* expression (Fig. 5A-D). M-opsin gene expression reached maximum levels at T3 concentrations of 4-5 nM, decreasing dramatically at higher concentrations (Fig. 5A-D). This result was expected since T3 is toxic for cones at high concentrations (Ng et al., 2010). In contrast to *Thrb2*, S-opsin gene expression decreased steadily with the addition of T3, which is suggestive of a binary cell fate choice between S- and M-cones (Fig. 5D). However, because the maximal proportion of M-cones generated (6%) never compensated for the observed reduction in S-cones at 4-5 nM T3 (Fig. 5B,C), S-cone differentiation might also be substantially inhibited by the addition of T3.

Spontaneous development of polarized cellular sheets containing cone photoreceptors

To test for self-organization of retinal tissue, we cultured COCO-exposed hESCs at confluence for 60 days, without additional manipulations (Fig. 6A). This generated a whitish and uniform cellular sheet (or tissue) that could be manipulated (see supplementary material Movie 1). The sheet could be grown to cover an entire well of a 6-well plate or cell culture dish, totaling ~6×10^6 cells. Pigmented cells were not observed on either side of the sheet, suggesting the absence of retinal pigment epithelium. Quantitative analyses revealed that ~80% of the cells were positive for CRX (Fig. 6B). Confocal IF combined with 3D reconstruction analyses revealed that the sheet was polarized and that peanut agglutinin (PNA) staining, which labels the inner and outer segment membrane of cones, was located at the opposite side of the DAPI-stained nuclear layer (Fig. 6C) (Blanks and Johnson, 1983). The presumptive PNA^+ outer segment of cones thus connected with the Matrigel-coated Petri dish surface (Fig. 6A). On average, the sheet was 150 µm thick and the nuclear layer was composed of ~5 nuclei, with additional sparse nuclei randomly distributed (Fig. 6C). Notably, immunolabeling for S-opsin was predominantly observed at the opposite side of the nuclei-rich layer (Fig. 6C).

Formation of the photoreceptor outer segment requires the presence of a connecting cilium (Novarino et al., 2011; Rachel et al., 2012). To test for this, we used three antibodies against proteins located at the connecting cilium, namely RP2, RPGR and acetylated α-tubulin (Ghosh et al., 2010; Hurd et al., 2010; Rachel et al., 2012). These antibodies, and especially RPGR, decorated a unique rod-shaped structure located in between the S-opsin-labeled outer segments and CRX-labeled nuclei (Fig. 6D). IF analyses of flat-mount P17 mouse retinas and human retinal sections were used to validate the specificity of all antibodies (supplementary material Fig. S7A-C). We used transmission electron microscopy to analyze cellular morphology and observed in longitudinal sections the presence of cells having a well-developed inner segment-like structure containing numerous mitochondria and a large Golgi apparatus (Fig. 6E). These cells had an additional protrusion resembling an immature outer segment, since membrane stacks were not present (Fig. 6E). The presence of a connecting cilium was not observed in the limited number of samples analyzed. In transverse sections and at the level of the mitochondria-rich inner segment, we also observed groups of cells with a rosette-like organization (Fig. 6E).

Development (2015) 142, 3294-3306 doi:10.1242/dev.125385

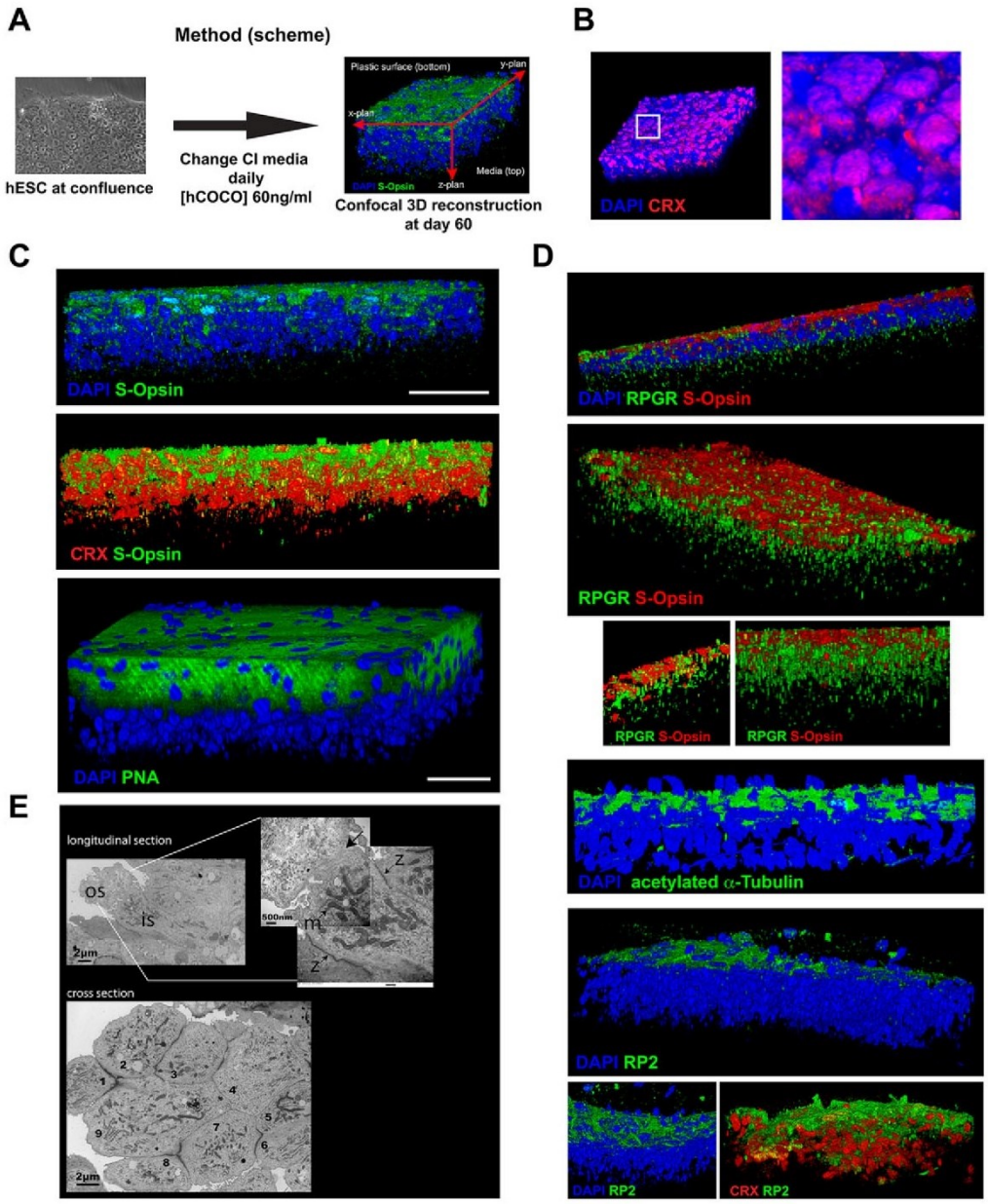

Fig. 6. Spontaneous development of a cellular sheet containing polarized cones. (A) Method for the derivation of a cellular sheet containing polarized cones. hESCs at confluence were exposed to CI medium (60 ng/ml COCO, daily media change) for 60 days and analyzed by confocal microscopy for 3D reconstruction, and by transmission electron microscopy. (B) Cellular sheet stained for CRX and analyzed by confocal microscopy. The boxed region is magnified to the right. (C) Cellular sheet stained for CRX, S-opsin and PNA. Scale bars: 40 µm. (D) Cellular sheet stained for connecting cilium markers (RPGR, acetylated α-tubulin and RP2). (E) Cellular sheets analyzed by transmission electron microscopy. Numbers on the transverse section reveal cells organized in a rosette-like conformation. Arrows indicate the junction between the inner (is) and outer (os) segment. m, mitochondria; z, stratum limitans junction.

Antagonism between COCO and BMP/TGFβ/Wnt activities

To address the mechanism of COCO activity, hESCs cultured under a constant concentration of FGF2, BMP4, activin A and WNT1 recombinant proteins were exposed, or not, to increasing concentrations of COCO, or of COCO+10 ng/ml IGF1, for a period of 7 days. Because SMAD2/3 proteins are stabilized through phosphorylation, we used β-actin to establish the phospho (p)-SMAD2/3 and p-SMAD1/5/8 ratio (Funaba et al., 2002). We found that phosphorylation of SMAD2/3 (a readout of BMP signaling) and of SMAD1/5/8 (a readout of TGFβ signaling) was inhibited in a dose-dependent manner by COCO, and that addition of IGF1 greatly increased COCO inhibitory activity (Fig. 7A).

p-β-catenin, which represents the β-catenin pool targeted for proteosomal degradation, was also greatly increased by the addition of COCO, while addition of IGF1 ultimately resulted in a net reduction in p-β-catenin (at 50 and 100 ng/ml COCO), which

Development (2015) 142, 3294-3306 doi:10.1242/dev.125385

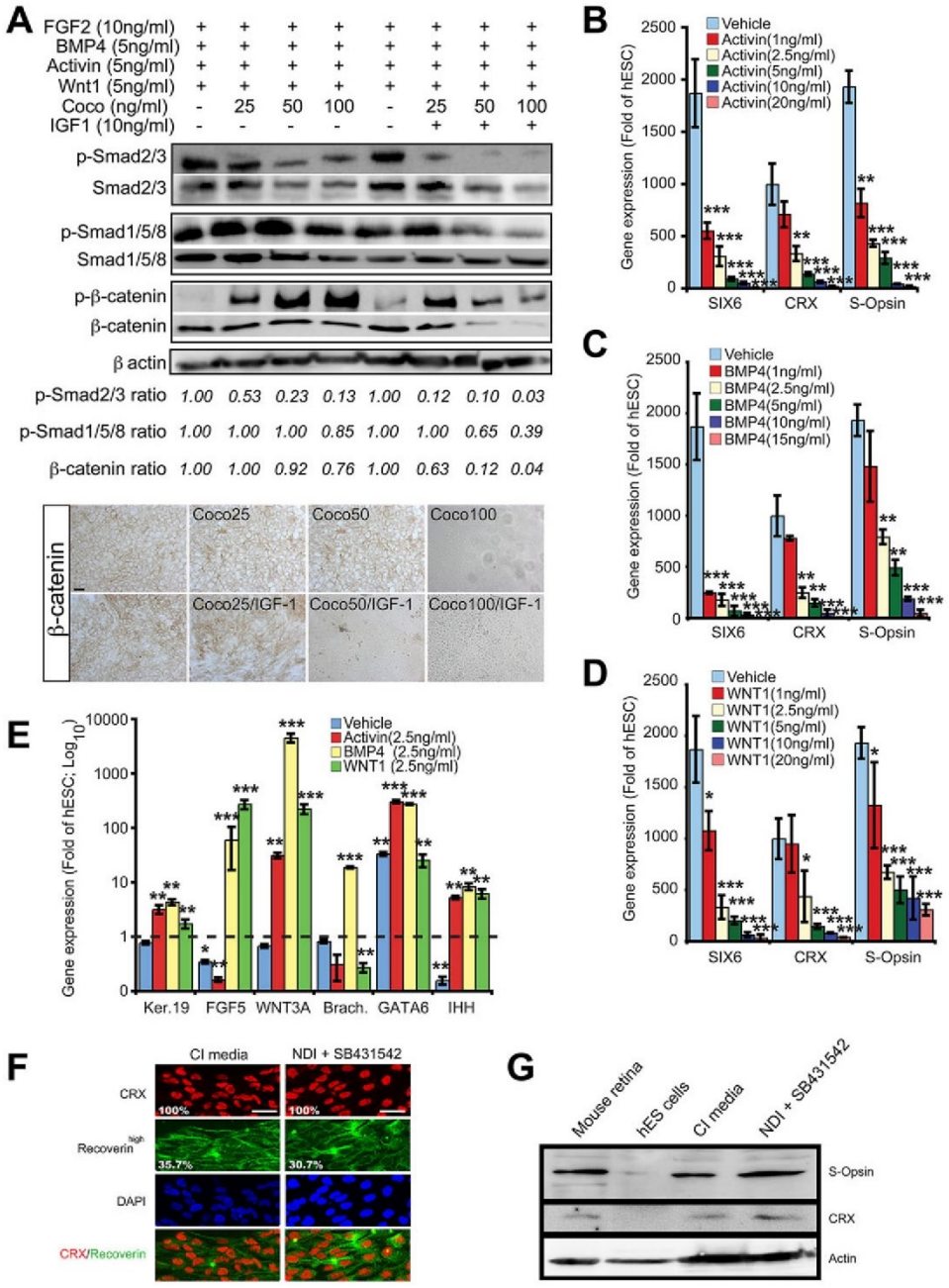

Fig. 7. COCO cooperates with IGF1 to inhibit BMP/TGFβ/Wnt activities. (A) hESCs cultured as indicated for 7 days were subjected to western blot (top) or immunohistochemistry (bottom) analyses. β-actin was used to quantify protein loading. p-SMAD2/3, p-SMAD1/5/8 or β-catenin levels are expressed as a ratio over β-actin levels. (B-D) hESCs were cultured for 21 days in CI without (vehicle, PBS) or with increasing concentrations of activin A, BMP4 or WNT1 and analyzed by qPCR. Data are expressed as fold change over gene expression in undifferentiated hESCs. Results are mean±s.d. (n=3); *P<0.05, **P<0.01, ***P<0.001 as compared with gene expression levels in vehicle-treated cells. (E) hESCs were cultured in CI for 21 days with the addition of 2.5 ng/ml activin A, BMP4 or WNT1, and then analyzed by qPCR. Data are expressed as fold change over gene expression in undifferentiated hESCs. Results are mean±s.d. (n=3); *P<0.05, **P<0.01, ***P<0.001 as compared with gene expression levels in undifferentiated cells. (F,G) hESCs cultured in CI or NDI+SB431542 (TGFβ inhibitor) for 21 days were analyzed by IF (F) or western blot (G). The percentage of positive cells is indicated (F). Scale bars: 40 µm.

is likely to reflect depletion of the β-catenin pool. Accordingly, the total level of β-catenin (a readout of Wnt signaling) progressively decreased with the addition of COCO, while β-catenin expression was nearly abolished with 50-100 ng/ml COCO+10 ng/ml IGF1 (Fig. 7A). Comparable results were also obtained by immunohistochemistry analysis (Fig. 7A, lower panel).

In converse experiments, hESCs differentiated with CI were exposed to increasing concentrations of activin A, BMP4 or WNT1

Development (2015) 142, 3294-3306 doi:10.1242/dev.125385

for 3 weeks. We observed that even 1 ng/ml BMP4, activin A or WNT1 was sufficient to inhibit CI retinal-inducing activity and that this effect was dose dependent (Fig. 7B-D). Accordingly, adding a fixed concentration (2.5 ng/ml) of activin A, BMP4 or WNT1 to CI-treated cells induced differentiation of hESCs toward the epidermal (*FGF5* and *KRT19*) and mesendodermal [*WNT3A*, brachyury (*T*), *GATA6* and *IHH*] cell lineages (Fig. 7E). Conversely, hESCs exposed to NDI+TGFβ inhibitor (SB431542) could differentiate as efficiently into S-cones as those exposed to CI when analyzed for CRX, recoverin and S-opsin expression (Fig. 7F,G).

Taken together, these results support the notion that COCO can promote neural and retinal cell fate from hESCs by simultaneous inhibition of BMP/TGFβ/Wnt signaling, and are consistent with the previously described inhibitory function of COCO on these pathways (Bell et al., 2003). They also suggest that IGF1 can greatly enhance the inhibitory activity of COCO on BMP/TGFβ/Wnt signaling.

DISCUSSION

We report on the rapid and efficient differentiation of hESCs into cone photoreceptors. ESCs were cultured under chemically defined, feeder-free conditions, and cell differentiation was induced under serum-free culture conditions without preselection procedures. Although COCO (+FGF2) displayed robust neuronal and retinal inducing activity, S-cone photoreceptor cell fate was induced to unprecedented levels when COCO was used in combination with IGF1. Differentiated cells expressed cone-specific genes and key proteins involved in phototransduction. After 35 days, *in vitro* generated cells were similar in morphology to week 15 human embryonic cones and could degrade cGMP when exposed to light. Bypassing the EB induction step also allowed manipulation of S- and M-cone cell fate by the addition of T3. After 60 days, *in vitro* generated cells self-organized into a cellular sheet with polarized cone photoreceptors and showing evidence of connecting cilium and outer segment formation.

In the developing mouse retina, photoreceptor development apparently follows an S-cone default pathway that is determined by Crx and Thrβ2; Crx induces the expression of S-opsin by default, whereas Thrβ2 suppresses it and instead induces the expression of M-opsin (Ng et al., 2001; Swaroop et al., 2010; Yanagi et al., 2002). Likewise, both Nrl and Notch1 inhibit cone formation to promote genesis of other retinal cell types (Jadhav et al., 2006; Mears et al., 2001; Yaron et al., 2006). We found here that most retinal progenitors derived from hESCs become S-cones upon exposure to COCO, FGF2 and IGF1. Notably, using a simplified neural induction protocol, M-cone genesis could also be induced by adding T3. During this process, 9-cis RA is, in principle, required to activate RA receptor γ (Rarγ), which cooperates with Thrβ2 to repress S-opsin expression (Roberts et al., 2006; Swaroop et al., 2010). Although we did not add RA to our cultures, the precursor of RA synthesis, retinyl acetate, is present in the B27 supplement.

We showed that antagonism between COCO and BMP4, Activin and WNT1 activities is required to allow hESC differentiation into retinal and photoreceptor cells. More surprisingly, we found that COCO (+FGF2) was sufficient to promote hESC differentiation into retinal and photoreceptor progenitors, with comparable efficiency to NCDI. This is notable because noggin and Dkk1 are unable to induce retinal cell fate from hESCs in the absence of IGF1 (Lamba et al., 2006). One explanation is that COCO, in contrast to noggin and Dkk1, is also able to block TGFβ signaling. Hence, pharmaceutical inhibition of TGFβ in combination with NDI provided comparable efficiency to CI (Fig. 7). Likewise, the relatively low efficiency of Dkk1 and LEFTY at inducing hESC differentiation into photoreceptors might be explained by the inability of LEFTY to block Activin signaling (Schier, 2009), combined with the absence of BMP inhibition (Osakada et al., 2008). This raises the possibility that Wnt, BMP and TGFβ/Nodal/Activin signaling also exert cone-inhibitory activities during normal retinal development. Accordingly, in the $Nrl^{-/-}$ mouse retina, which is composed of an excessively large number of cones, the *Bmp4*, *Smad4* and Wnt/Ca^{2+} signaling pathway genes are downregulated, and Nrl was found to directly activate these genes in order to promote rods genesis at the expense of cones (Yu et al., 2004). Finally, both Wnt and Activin can promote rod genesis (Davis et al., 2000).

These findings suggest a working model whereby inhibition of Wnt, BMP and TGFβ/Nodal/Activin is required to allow cone genesis at the expense of rods (and possibly of other retinal cell types), and suggest that S-cones are generated by default if all inhibitory factors are blocked. Our data also support the possibility that retinal cell fate can be actively promoted, as evidenced by the improved differentiation of hESCs into S-cones when IGF1 was used in combination with COCO. Likewise, although early neural induction efficiency was similar when using either COCO+IGF1 or COCO+FGF2, anterior neural and retinal induction was more efficient with IGF1. However, the mechanism by which IGF1 operates in this context is still unclear. IGF1 retinal fate-promoting activity may in part be through inhibition of Smad signaling (Pera et al., 2001). Indeed, we observed robust cooperation between COCO and IGF1 in blocking SMAD2/3 and SMAD1/5/8 phosphorylation, as well as in reducing β-catenin stabilization.

In eye diseases in which cones are severely affected, such as macular degenerations, cone dystrophies and cone-rod dystrophies, differentiation of hESCs into cones is of particular interest for cell therapy by transplantation (Michaelides et al., 2006). Although most forms of retinitis pigmentosa primarily affect rods, the disease is followed by loss of cones, possibly because of a reduction in the trophic support normally provided by rods to cones and/or increased metabolic stress (Mohand-Said et al., 2000; Punzo et al., 2009). Thus, the efficiency of cell replacement therapy to treat retinitis pigmentosa may also depend on our capacity to generate rods and cones. Using scanning electron microscopy, we observed that cells differentiated for 35 days developed a protruding inner segment and displayed morphological similarities to week 15 human embryonic cones. Prolonging the cell culture time to 60 days resulted in the formation of a cellular sheet composed of polarized cones with evidence of connecting cilium and outer segment formation. Self-organization of hESCs into a cone tissue sheet is reminiscent of the self-formation of hESCs into an optic cup (Nakano et al., 2012). Human cone tissue sheets may be used as a retinal patch for the treatment of macular degenerations, as shown for mouse retinal sheets transplanted into a retinitis pigmentosa mouse model (Assawachananont et al., 2014).

In conclusion, the availability of a highly enriched human cone photoreceptor population opens new avenues to study cone biochemistry and developmental genetics. Using induced pluripotent stem cell technology, it will also be possible to generate cones from cone-affected disease patients in order to study the disease mechanism and perform drug-screening assays (Jin et al., 2011).

MATERIALS AND METHODS

Ethics statement

The Animal Care Committee of the Maisonneuve-Rosemont Hospital Research Centre approved the use of the animals in this study. Post-mortem

Development (2015) 142, 3294-3306 doi:10.1242/dev.125385

human eyes (see the supplementary Materials and Methods) were provided by the Banque d'yeux du Québec du Centre Michel-Mathieu and were used with approbation of the Comité d'Éthique à la Recherche de l'Hôpital Maisonneuve-Rosemont. hESCs were used in accordance with Canadian Institute Health Research (CIHR) guidelines and approved by the Comité de Surveillance de la Recherche sur les Cellules Souches (CSRCS) of the CIHR.

Cell cultures

The hESC line H9 (WiCell) was cultured on a Matrigel-coated plate (BD Biosciences) with a daily change of mTeSR medium according to the manufacturer's instruction (Stemcell Technologies) (Thomson et al., 1998). The H9 hESC line was first established on mouse embryonic fibroblasts (MEFs) and then cultured on Matrigel in mTeSR medium. Undifferentiated hESC colonies were treated with dispase and induced to form EBs in ultra-low attachment plates (VWR) in neural induction medium, which consists of the NDI mix [DMEM-F12 medium (Invitrogen) containing 10% KnockOut serum, 2% B27, 1 ng/ml noggin, 1 ng/ml Dkk1 and 5 ng/ml IGF1], essentially as described (Lamba et al., 2006). Otherwise, cells were cultured in NCDI mix (NDI supplemented with 10 ng/ml COCO) using COCO alone or together with 10 ng/ml IGF1. EBs were plated 3 days later into Matrigel- or laminin-coated plates and cultured in DMEM-F12 medium supplemented with 2% B27, 1% N2, 10 ng/ml noggin, 10 ng/ml Dkk1, 10 ng/ml IGF1, 10 ng/ml COCO and 5 ng/ml FGF2 for an additional 4 weeks. The media were changed every 2 days. Unless otherwise stated, COCO was used at 30 ng/ml in CI media. Recombinant proteins were purchased from R&D Systems.

Western blot

Total protein extracts were prepared in the Complete Mini Protease Inhibitor Cocktail solution (Roche Diagnostics) and sonicated. Protein content was quantified using the Bradford reagent. Proteins in Laemmli buffer were resolved by SDS-PAGE and transferred to a nitrocellulose blotting membrane (Pall). Membranes were blocked for 1 h in 5% non-fat milk in 1×TBS containing 0.05% Tween 20 and incubated overnight with primary antibodies: mouse anti-CRX (1:1000; Genetex, GTX91782), rabbit anti-S-opsin (1:1000; Abcam, ab81017), mouse anti-rhodopsin (4D2) (1:50, provided by the Robert S. Molday Laboratory, University of British Columbia, Canada), rabbit anti-M-opsin (1:500; Chemicon, AB5405), rabbit anti-Smad1/5/8 (1:250; Santa Cruz, sc-6031-R), rabbit anti-p-Smad1/5/8 (1:250; #9516), rabbit anti-Smad2/3 (1:300; #8685), rabbit anti-p-Smad2/3 (1:300; #8828), rabbit anti-β-catenin (1:300; #8480), rabbit anti-p-β-catenin (1:300; #4176) (all from Cell Signaling), and mouse anti-β-actin (1:1000; Abcam, ab8226). Membranes were treated with the appropriate horseradish peroxidase-conjugated secondary antibodies (anti-rabbit, 1:15,000, A9169; anti-mouse, 1:10,000, A8924; Sigma) and developed using Immobilon western reagents (Millipore).

Immunohistochemistry

Fixed/permeabilized cells were incubated with primary antibodies overnight at 4°C, and analyzed using the Vectastain ABC Kit (Vector Laboratories); DAB (Sigma) was used as the peroxidase substrate. For grafting analyses, eye sections were incubated overnight with primary antibody solutions at 4°C, washed and incubated with Rhodamine-conjugated and FITC-conjugated secondary antibodies for 1 h at room temperature. Slides were mounted on coverslips in DAPI-containing mounting medium (Vector Laboratories). Observations were made under a Leica DMRE fluorescence microscope with a Retiga EX digital camera. For further details of sample preparation and the antibodies used, see the supplementary Materials and Methods.

In situ hybridization

For *in situ* hybridizations on slices, tissues were dissected in PBS, embedded in CRYOMATRIX embedding medium (Thermo Shandon), snap frozen in liquid nitrogen and sections (8 µm) were cut and dried onto Superfrost glass slides (Fisher Scientific). For *in situ* hybridizations on whole embryos, embryos were dissected in PBS, then fixed overnight in 4% paraformaldehyde at 4°C. Whole embryos and slices were hybridized with digoxigenin-labeled RNA probes [*Dand5* (*Coco*), accession #BC115659] and revealed with alkaline phosphatase-coupled anti-digoxigenin antibody (1:2000; Roche, 11093274910) and NBT/BCIP substrate (Boehringer) at pH 9.5.

RT-PCR

Total RNA (1 µg) was reverse transcribed with M-MLV reverse transcriptase (Invitrogen) and used in quantitative real-time PCR (qPCR) using Platinum SYBR Green SuperMix (Invitrogen) and an ABI Prism 7000 apparatus, with *GAPDH* as an internal standard. Experiments were performed at least in triplicate. For further details and primer sequences, see the supplementary Materials and Methods.

Phototransduction analysis

Phototransduction activity was assessed by measuring the light-induced hydrolysis of cyclic (c) GMP with an enzyme immunoassay kit (Biotrack EIA system) according to the manufacturer's instructions (Amersham Bioscience GE Healthcare). Undifferentiated H9 hESCs and cells cultured in NDI, COCO and IGF1 were kept in the dark or exposed to ambient light. The PDE inhibitor IBMX (3-isobutyl-1-methylxanthine, Sigma) was added (1 mM) 72 h before determination of cGMP levels.

Fluorescence-activated cell sorting

For cell membrane epitope staining, dispase-dissociated cells were stained with Rhodamine-coupled PNA (1:500; Vector Laboratories, RL-1072). Cells were then fixed/permeabilized with the CytoFix/Cytoperm Kit according to the manufacturer's instructions (BD Biosciences). Cells were incubated with rabbit anti-S-opsin antibody (1:2000; Chemicon, A5407) or Alexa-conjugated isotypic control goat anti-rabbit IgG antibody (1:500; Molecular Probes, A-11037). The primary antibody was visualized using FITC-conjugated goat anti-rabbit serum (1:500; Chemicon, AP124F). Sorting employed a FACSVantage flow cytometer (Becton-Dickinson) at a flow rate of less than 3000 cells/s. Dead cells and cell debris were excluded from acquisition by gating with FCS and SSC biparametric plot. After sorting, an aliquot of sorted cells was always reanalyzed to check for purity, which was usually greater than 95%.

Cell transplantation

Cell clamps (1 µl) containing ~10,000 cells were injected into the vitreous of anesthetized neonatal (P1) mice as described in the supplementary Materials and Methods.

Statistical analysis

Statistical differences were analyzed using Student's *t*-test for unpaired samples. An analysis of variance (ANOVA) followed by the Dunnett test was used for multiple comparisons with one control group. *P*-values are given in the figure legends.

Acknowledgements

We are grateful to D. Melton and the Harvard Stem Cell Institute for the HUES1, HUES8 and HUES9 cell lines, and to M. Nelea and S. Breault for technical assistance with electron microscopy.

Competing interests

The authors declare no competing or financial interests.

Author contributions

Conceived and designed the study and wrote the paper: G.B. Performed the experiments: S.Z., A.F., M.A., N.T., A.B., S.W. Analyzed the data: G.B., S.Z., A.F., M.A.

Funding

This work was supported by grants from the Foundation Fighting Blindness Canada, Turmel Family Foundation for Macular Degeneration Research, Canadian Stem Cell Network, C. Durand Foundation, the GO Foundation, and Natural Science and Engineering Research Council of Canada [grant #250970-2012]. A.F. was supported by fellowships from the Réseau Vision du Québec and from University of Montreal Molecular Biology Program. G.B. was supported by the Fonds de Recherche en Santé du Québec.

Supplementary material

Supplementary material available online at
http://dev.biologists.org/lookup/suppl/doi:10.1242/dev.125385/-/DC1

References

Allikmets, R., Singh, N., Sun, H., Shroyer, N. F., Hutchinson, A., Chidambaram, A., Gerrard, B., Baird, L., Stauffer, D., Peiffer, A. et al. (1997). A photoreceptor cell-specific ATP-binding transporter gene (ABCR) is mutated in recessive Starqardt macular dystrophy. *Nat. Genet.* **15**, 236-246.

Assawachananont, J., Mandai, M., Okamoto, S., Yamada, C., Eiraku, M., Yonemura, S., Sasai, Y. and Takahashi, M. (2014). Transplantation of embryonic and induced pluripotent stem cell-derived 3D retinal sheets into retinal degenerative mice. *Stem Cell Rep.* **2**, 662-674.

Banin, E., Obolensky, A., Idelson, M., Hemo, I., Reinhardtz, E., Pikarsky, E., Ben-Hur, T. and Reubinoff, B. (2006). Retinal incorporation and differentiation of neural precursors derived from human embryonic stem cells. *Stem Cells* **24**, 246-257.

Bell, E., Muñoz-Sanjuán, I., Altmann, C. R., Vonica, A. and Brivanlou, A. H. (2003). Cell fate specification and competence by Coco, a maternal BMP, TGFbeta and Wnt inhibitor. *Development* **130**, 1381-1389.

Blanks, J. C. and Johnson, L. V. (1983). Selective lectin binding of the developing mouse retina. *J. Comp. Neurol.* **221**, 31-41.

Bouwmeester, T., Kim, S.-H., Sasai, Y., Lu, B. and De Robertis, E. M. (1996). Cerberus is a head-inducing secreted factor expressed in the anterior endoderm of Spemann's organizer. *Nature* **382**, 595-601.

Burmeister, M., Novak, J., Liang, M.-Y., Basu, S., Ploder, L., Hawes, N. L., Vidgen, D., Hoover, F., Goldman, D., Kalnins, V. I. et al. (1996). Ocular retardation mouse caused by Chx10 homeobox null allele: impaired retinal progenitor proliferation and bipolar cell differentiation. *Nat. Genet.* **12**, 376-384.

Chambers, S. M., Fasano, C. A., Papapetrou, E. P., Tomishima, M., Sadelain, M. and Studer, L. (2009). Highly efficient neural conversion of human ES and iPS cells by dual inhibition of SMAD signaling. *Nat. Biotechnol.* **27**, 275-280.

Chatoo, W., Abdouh, M., Duparc, R.-H. and Bernier, G. (2010). Bmi1 distinguishes immature retinal progenitor/stem cells from the main progenitor cell population and is required for normal retinal development. *Stem Cells* **28**, 1412-1423.

Chen, S., Wang, Q.-L., Nie, Z., Sun, H., Lennon, G., Copeland, N. G., Gilbert, D. J., Jenkins, N. A. and Zack, D. J. (1997). Crx, a novel Otx-like paired-homeodomain protein, binds to and transactivates photoreceptor cell-specific genes. *Neuron* **19**, 1017-1030.

Corbo, J. C., Myers, C. A., Lawrence, K. A., Jadhav, A. P. and Cepko, C. L. (2007). A typology of photoreceptor gene expression patterns in the mouse. *Proc. Natl. Acad. Sci. USA* **104**, 12069-12074.

Couly, G. and Le Douarin, N. M. (1988). The fate map of the cephalic neural primordium at the presomitic to the 3-somite stage in the avian embryo. *Development* **103**, 101-113.

Davis, A. A., Matzuk, M. M. and Reh, T. A. (2000). Activin A promotes progenitor differentiation into photoreceptors in rodent retina. *Mol. Cell. Neurosci.* **15**, 11-21.

Ellis, P., Fagan, B. M., Magness, S. T., Hutton, S., Taranova, O., Hayashi, S., McMahon, A., Rao, M. and Pevny, L. (2004). SOX2, a persistent marker for multipotential neural stem cells derived from embryonic stem cells, the embryo or the adult. *Dev. Neurosci.* **26**, 148-165.

Ferda Percin, E., Ploder, L. A., Yu, J. J., Arici, K., Horsford, D. J., Rutherford, A., Bapat, B., Cox, D. W., Duncan, A. M. V., Kalnins, V. I. et al. (2000). Human microphthalmia associated with mutations in the retinal homeobox gene CHX10. *Nat. Genet.* **25**, 397-401.

Freund, C. L., Gregory-Evans, C. Y., Furukawa, T., Papaioannou, M., Looser, J., Ploder, L., Bellingham, J., Ng, D., Herbrick, J.-A. S., Duncan, A. et al. (1997). Cone-rod dystrophy due to mutations in a novel photoreceptor-specific homeobox gene (CRX) essential for maintenance of the photoreceptor. *Cell* **91**, 543-553.

Funaba, M., Zimmerman, C. M. and Mathews, L. S. (2002). Modulation of Smad2-mediated signaling by extracellular signal-regulated kinase. *J. Biol. Chem.* **277**, 41361-41368.

Furukawa, T., Morrow, E. M. and Cepko, C. L. (1997). Crx, a novel otx-like homeobox gene, shows photoreceptor-specific expression and regulates photoreceptor differentiation. *Cell* **91**, 531-541.

Gallardo, M. E., Lopez-Rios, J., Fernaud-Espinosa, I., Granadino, B., Sanz, R., Ramos, C., Ayuso, C., Seller, M. J., Brunner, H. G., Bovolenta, P. et al. (1999). Genomic cloning and characterization of the human homeobox gene SIX6 reveals a cluster of SIX genes in chromosome 14 and associates SIX6 hemizygosity with bilateral anophthalmia and pituitary anomalies. *Genomics* **61**, 82-91.

Ghosh, A. K., Murga-Zamalloa, C. A., Chan, L., Hitchcock, P. F., Swaroop, A. and Khanna, H. (2010). Human retinopathy-associated ciliary protein retinitis pigmentosa GTPase regulator mediates cilia-dependent vertebrate development. *Hum. Mol. Genet.* **19**, 90-98.

Graham, V., Khudyakov, J., Ellis, P. and Pevny, L. (2003). Sox2 functions to maintain neural progenitor identity. *Neuron* **39**, 749-765.

Hurd, T., Zhou, W., Jenkins, P., Liu, C.-J., Swaroop, A., Khanna, H., Martens, J., Hildebrandt, F. and Margolis, B. (2010). The retinitis pigmentosa protein RP2 interacts with polycystin 2 and regulates cilia-mediated vertebrate development. *Hum. Mol. Genet.* **19**, 4330-4344.

Idelson, M., Alper, R., Obolensky, A., Ben-Shushan, E., Hemo, I., Yachimovich-Cohen, N., Khaner, H., Smith, Y., Wiser, O., Gropp, M. et al. (2009). Directed differentiation of human embryonic stem cells into functional retinal pigment epithelium cells. *Cell Stem Cell* **5**, 396-408.

Jadhav, A. P., Mason, H. A. and Cepko, C. L. (2006). Notch 1 inhibits photoreceptor production in the developing mammalian retina. *Development* **133**, 913-923.

Jean, D., Bernier, G. and Gruss, P. (1999). Six6 (Optx2) is a novel murine Six3-related homeobox gene that demarcates the presumptive pituitary/hypothalamic axis and the ventral optic stalk. *Mech. Dev.* **84**, 31-40.

Jin, Z.-B., Okamoto, S., Osakada, F., Homma, K., Assawachananont, J., Hirami, Y., Iwata, T. and Takahashi, M. (2011). Modeling retinal degeneration using patient-specific induced pluripotent stem cells. *PLoS ONE* **6**, e17084.

Jomary, C. and Jones, S. E. (2008). Induction of functional photoreceptor phenotype by exogenous Crx expression in mouse retinal stem cells. *Invest. Ophthalmol. Vis. Sci.* **49**, 429-437.

Lamba, D. A., Karl, M. O., Ware, C. B. and Reh, T. A. (2006). Efficient generation of retinal progenitor cells from human embryonic stem cells. *Proc. Natl. Acad. Sci. USA* **103**, 12769-12774.

Lamba, D. A., Gust, J. and Reh, T. A. (2009). Transplantation of human embryonic stem cell-derived photoreceptors restores some visual function in Crx-deficient mice. *Cell Stem Cell* **4**, 73-79.

Liu, W., Lagutin, O., Swindell, E., Jamrich, M. and Oliver, G. (2010). Neuroretina specification in mouse embryos requires Six3-mediated suppression of Wnt8b in the anterior neural plate. *J. Clin. Invest.* **120**, 3568-3577.

Livne-Bar, I., Pacal, M., Cheung, M. C., Hankin, M., Trogadis, J., Chen, D., Dorval, K. M. and Bremner, R. (2006). Chx10 is required to block photoreceptor differentiation but is dispensable for progenitor proliferation in the postnatal retina. *Proc. Natl. Acad. Sci. USA* **103**, 4988-4993.

Mathers, P. H., Grinberg, A., Mahon, K. A. and Jamrich, M. (1997). The Rx homeobox gene is essential for vertebrate eye development. *Nature* **387**, 603-607.

Mears, A. J., Kondo, M., Swain, K. S., Takada, Y., Bush, R. A., Saunders, T. L., Sieving, P. A. and Swaroop, A. (2001). Nrl is required for rod photoreceptor development. *Nat. Genet.* **29**, 447-452.

Mellough, C. B., Collin, J., Khazim, M., White, K., Sernagor, E., Steel, D. H. and Lako, M. (2015). IGF-1 signaling plays an important role in the formation of three-dimensional laminated neural retina and other ocular structures from human embryonic stem cells. *Stem Cells* **33**, 2416-2430.

Michaelides, M., Hardcastle, A. J., Hunt, D. M. and Moore, A. T. (2006). Progressive cone and cone-rod dystrophies: phenotypes and underlying molecular genetic basis. *Surv. Ophthalmol.* **51**, 232-258.

Mohand-Said, S., Hicks, D., Dreyfus, H. and Sahel, J. A. (2000). Selective transplantation of rods delays cone loss in a retinitis pigmentosa model. *Arch. Ophthalmol.* **118**, 807-811.

Molday, L. L., Rabin, A. R. and Molday, R. S. (2000). ABCR expression in foveal cone photoreceptors and its role in stargardt macular dystrophy. *Am. J. Ophthalmol.* **130**, 689.

Muñoz-Sanjuán, I. and Brivanlou, A. H. (2002). Neural induction, the default model and embryonic stem cells. *Nat. Rev. Neurosci.* **3**, 271-280.

Nakano, T., Ando, S., Takata, N., Kawada, M., Muguruma, K., Sekiguchi, K., Saito, K., Yonemura, S., Eiraku, M. and Sasai, Y. (2012). Self-formation of optic cups and storable stratified neural retina from human ESCs. *Cell Stem Cell* **10**, 771-785.

Narayanan, K. and Wadhwa, S. (1998). Photoreceptor morphogenesis in the human retina: a scanning electron microscopic study. *Anat. Rec.* **252**, 133-139.

Ng, L., Hurley, J. B., Dierks, B., Srinivas, M., Saltó, C., Vennström, B., Reh, T. A. and Forrest, D. (2001). A thyroid hormone receptor that is required for the development of green cone photoreceptors. *Nat. Genet.* **27**, 94-98.

Ng, L., Lyubarsky, A., Nikonov, S. S., Ma, M., Srinivas, M., Kefas, B., St. Germain, D. L., Hernandez, A., Pugh, E. N., Jr and Forrest, D. (2010). Type 3 deiodinase, a thyroid-hormone-inactivating enzyme, controls survival and maturation of cone photoreceptors. *J. Neurosci.* **30**, 3347-3357.

Novarino, G., Akizu, N. and Gleeson, J. G. (2011). Modeling human disease in humans: the ciliopathies. *Cell* **147**, 70-79.

Osakada, F., Ikeda, H., Mandai, M., Wataya, T., Watanabe, K., Yoshimura, N., Akaike, A., Sasai, Y. and Takahashi, M. (2008). Toward the generation of rod and cone photoreceptors from mouse, monkey and human embryonic stem cells. *Nat. Biotechnol.* **26**, 215-224.

Pacione, L. R., Szego, M. J., Ikeda, S., Nishina, P. M. and McInnes, R. R. (2003). Progress toward understanding the genetic and biochemical mechanisms of inherited photoreceptor degenerations. *Annu. Rev. Neurosci.* **26**, 657-700.

Pera, E. M., Wessely, O., Li, S.-Y. and De Robertis, E. M. (2001). Neural and head induction by insulin-like growth factor signals. *Dev. Cell* **1**, 655-665.

Piccolo, S., Agius, E., Leyns, L., Bhattacharyya, S., Grunz, H., Bouwmeester, T. and De Robertis, E. M. (1999). The head inducer Cerberus is a multifunctional antagonist of Nodal, BMP and Wnt signals. *Nature* **397**, 707-710.

Punzo, C., Kornacker, K. and Cepko, C. L. (2009). Stimulation of the insulin/mTOR pathway delays cone death in a mouse model of retinitis pigmentosa. *Nat. Neurosci.* **12**, 44-52.

Rachel, R. A., Li, T. and Swaroop, A. (2012). Photoreceptor sensory cilia and ciliopathies: focus on CEP290, RPGR and their interacting proteins. *Cilia* **1**, 22.

Reubinoff, B. E., Pera, M. F., Fong, C. Y., Trounson, A. and Bongso, A. (2000). Embryonic stem cell lines from human blastocysts: somatic differentiation in vitro. *Nat. Biotechnol.* **18**, 399-404.

Roberts, M. R., Srinivas, M., Forrest, D., Morreale de Escobar, G. and Reh, T. A. (2006). Making the gradient: thyroid hormone regulates cone opsin expression in the developing mouse retina. *Proc. Natl. Acad. Sci. USA* **103**, 6218-6223.

Rorick, A. M., Mei, W., Liette, N. L., Phiel, C., El-Hodiri, H. M. and Yang, J. (2006). PP2A:B56epsilon is required for eye induction and eye field separation. *Dev. Biol.* **302**, 477-493.

Schier, A. F. (2009). Nodal morphogens. *Cold Spring Harb. Perspect. Biol.* **1**, a003459.

Swaroop, A., Kim, D. and Forrest, D. (2010). Transcriptional regulation of photoreceptor development and homeostasis in the mammalian retina. *Nat. Rev. Neurosci.* **11**, 563-576.

Taranova, O. V., Magness, S. T., Fagan, B. M., Wu, Y., Surzenko, N., Hutton, S. R. and Pevny, L. H. (2006). SOX2 is a dose-dependent regulator of retinal neural progenitor competence. *Genes Dev.* **20**, 1187-1202.

Thomson, J. A., Itskovitz-Eldor, J., Shapiro, S. S., Waknitz, M. A., Swiergiel, J. J., Marshall, V. S. and Jones, J. M. (1998). Embryonic stem cell lines derived from human blastocysts. *Science* **282**, 1145-1147.

Tropepe, V., Hitoshi, S., Sirard, C., Mak, T. W., Rossant, J. and van der Kooy, D. (2001). Direct neural fate specification from embryonic stem cells: a primitive mammalian neural stem cell stage acquired through a default mechanism. *Neuron* **30**, 65-78.

Tucker, B. A., Mullins, R. F., Streb, L. M., Anfinson, K., Eyestone, M. E., Kaalberg, E., Riker, M. J., Drack, A. V., Braun, T. A. and Stone, E. M. (2013). Patient-specific iPSC-derived photoreceptor precursor cells as a means to investigate retinitis pigmentosa. *Elife* **2**, e00824.

Walther, C. and Gruss, P. (1991). Pax-6, a murine paired box gene, is expressed in the developing CNS. *Development* **113**, 1435-1449.

Yanagi, Y., Takezawa, S. and Kato, S. (2002). Distinct functions of photoreceptor cell-specific nuclear receptor, thyroid hormone receptor beta2 and CRX in one photoreceptor development. *Invest. Ophthalmol. Vis. Sci.* **43**, 3489-3494.

Yaron, O., Farhy, C., Marquardt, T., Applebury, M. and Ashery-Padan, R. (2006). Notch1 functions to suppress cone-photoreceptor fate specification in the developing mouse retina. *Development* **133**, 1367-1378.

Yu, J., He, S., Friedman, J. S., Akimoto, M., Ghosh, D., Mears, A. J., Hicks, D. and Swaroop, A. (2004). Altered expression of genes of the Bmp/Smad and Wnt/calcium signaling pathways in the cone-only Nrl-/- mouse retina, revealed by gene profiling using custom cDNA microarrays. *J. Biol. Chem.* **279**, 42211-42220.

SUPPLEMENTARY MATERIALS AND METHODS

Quantitative RT-PCR

All primers were designed to flank individual exons and tested by PCR in RT+ and RT- control extracts. Total RNA was isolated using TRIzol reagent (Invitrogen). Reverse transcription (RT) was performed using 1 µg of total RNA and the MML-V reverse transcriptase (Invitrogen). Quantitative real-time PCR (qPCR) was performed using the Platinum SYBRGreen SuperMix (Invitrogen) and a real-time PCR apparatus (ABI Prism 7000). GAPDH was used as an internal standard for data calibration. The 2^{-DDCt} formula was used for the calculation of differential gene expression. All experiments were performed at least in triplicates. Primers sequences are: SIX3 (F; CCCACACAAGATGGCAACTG and R; GTTACCGAGAGGATGGAGGT), SIX6 (F; CCTGCAGGATCCATACCCTA and R; ACCTGCTGCTGGAGTCTGTT), CRX (F; CCTTCTGACAGCTCGGTGTT and R; CCACTTTCTGAAGCCTGGAG), S-opsin (F; TGTGCCTCTCTCCCTCATCT and R; GGCACGTAGCAGACACAGAA), PAX6 (F; AGATTTCAGAGCCCCATATTCG and R; CCATTTGGCCCTTCGATTAG), Cone Arrestin (F; CCCAGAGCTTTGCAGTAACC and R; CACAGGACACCATCAGGTTG), M-opsin (F; GCTACACCGTCTCCCTGTGT and R; ACCTGCTCCAACCAAAGATG), Rhodopsin (F; TAAGCCCATGAGCAACTTCC and R; GCTGCCCATAGCAGAAAAAG), PdEb (F; CAGTGATGAACACCGACACC and R; ATTTGACCAGGTCCAGTTCG), Arrestin3 (F; CCCAGAGCTTTGCAGTAACC and R; CACAGGACACCATCAGGTTG), PdE6h (F; TACTCTGCCTGCTCCAGCTT and R; GAGAGTGGCAGAACCTCTGG), PdE6c (F; TTGGGAACAAGGAGATCTGG and R; GGCTCCTCCTTCTTGCTTTT), Recoverin (F; AGCTCCTTCCAGACGATGAA and R; CAAACTGGATCAGTCGCAGA), Keratin19 (F; TTTGAGACGGAACAGGCTCT and R; AATCCACCTCCACACTGACC), FGF5 (F; CTTGGAGCAGAGCAGTTTCC and R;

ACAATCCCCTGAGACACAGC), Brachyury (F; CCGTCTCCTTCAGCAAAGTC and R; CACCGCTATGAACTGGGTCT), Indian Hedgehog (IHH) (F; CCTGAACTCGCTGGCTATCT and R; CGGTCTGATGTGGTGATGTC), WNT3A (F; CAAGATTGGCATCCAGGAGT and R; ATGAGCGTGTCACTGCAAAG), GATA6 (F; GCCAACTGTCACACCACAAC and R; AGTTGGAGTCATGGGAATGG), SOX1 (F; AAAGTCAAAACGAGGCGAGA and R; AAGTGCTTGGACCTGCCTTA), FOXG1 (F; GAACGGCAAGTACGAGAAGC and R; TCACGAAGCACTTGTTGAGG), RAX (F; GGCAAGGTCAACCTACCAGA and R; GCTTCATGGAGGACACTTCC), PLZF (F; CAAGGCTGACGCTGTATTGA and R; AGTGGGATGAAGACGTACGG), and GAPDH (F; TCACCAGGGCTGCTTTTAAC and R ATCCACAGTCTTCTGGGTGG). On the other hand, for 5'- and 3'-Coco (Dand5) transcripts amplification, the primers sequences used are: 5'-transcript (F; CTGCACAGCCAAGTGATGTT and R; CACTTCTTGAGGAGCCAAGG), and 3'-transcript (F; GCAGCTGCTAGGAAAACCTG and R; TTTATGGTTCCCACGGAATG).

Immunohistochemistry

Cells were fixed/permeabilized in 4% paraformaldehyde (PFA) containing 0.01% Tween 20 at room temperature for 15 minutes, and blocked with 5% horse serum in 1xPBS/0.1 % Tween 20 at room temperature for 1 hour. Slides were incubated with the primary antibodies overnight at 4°C, and analyzed using the Vectastain® ABC kit (Vector Laboratories, CA) according to the manufacturer instructions. DAB (Sigma) was used as the peroxidase substrate. For grafting analyses, eyes were immersed for 1 h at room temperature in 4% PFA/3% sucrose in 0.1 M phosphate buffer, pH 7.4. Samples were washed three times in PBS, cryoprotected in PBS/30% sucrose, and frozen in CRYOMATRIX embedding medium (CEM) (Thermo Shandon, Pittsburgh, PA). 7 µm thick sections were mounted on Super-Frost

glass slides (Fisher Scientific) and processed for immunofluorescence. Sections were incubated overnight with primary antibody solutions at 4ºC in a humidified chamber. After three washes in PBS, sections were incubated with secondary antibodies for 1 h at room temperature. Slides were mounted on coverslips in DAPI-containing mounting medium (Vector). Observations were made under a fluorescence microscope (Leica DMRE, Leica Microsystems) and images were captured with a digital camera (Retiga EX; QIMAGING; with OpenLab, ver.3.1.1 software; Open-Lab, Canada). Antibodies used in this study were: mouse anti-CRX (1:250; Genetex), mouse anti-S-opsin (1:500; Chemicon) and mouse anti-ABCA4 (1:25; SantaCruz Biotech.). For immunofluorescence, the secondary antibodies used were rhodamine-conjugated donkey anti-rabbit, and FITC-conjugated donkey anti-mouse (Chemicon).

Cell transplantation

Neonatal (P1) mice were anesthetized by hypothermia. The eyelid was opened using a scalpel, and a hole was made in the cornea using a 26G needle to have access to the vitreous. Cell clamps (1µl) containing ~10 000 cells were injected using a 5 µl Hamilton syringe with a 33G needle (Hamilton Company, Reno, NV). For the immunosuppressive regimen, mothers of neonatal pups were injected with Cyclosporine A (10 mg/kg/day) from the day before surgery until tissue preparation. For each experimental condition (2, 3 and 4 weeks of hES cell differentiation using CI at 30ng/ml of Coco (n = 15); and 2 weeks of hES cell differentiation using CI at 50ng/ml of Coco (n = 5)), pups were injected on the left eye. Animals were handled in accordance with the Animal Care Committee of Maisonneuve-Rosemont Hospital.

Human eyes specimens

Retinas were dissected and fixed in 4% paraformaldehyde, then cryopreserved in 30% sucrose. Retinas were frozen until use.

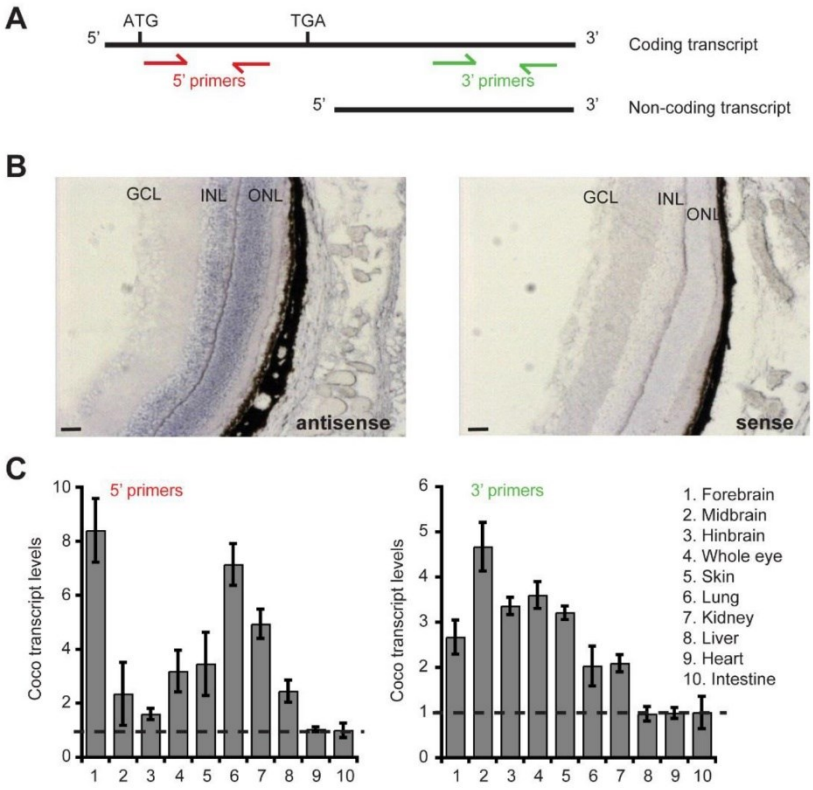

Figure S1. Coco/Cerl2 is expressed in the mouse retina

(A) Schematic representation of the coding and non-coding *Coco/Cerl2* transcripts. The PCR primers locations are highlighted, where the 5'primers (red) amplify only the coding transcript, while the 3'primers (green) amplify both transcripts. (B) *In situ* hybridization on adult mouse eye sections with antisense and sense *Coco/Cerl2* RNA probes showing robust expression of *Coco* transcripts in the photoreceptor nuclear layer (ONL; outer nuclear layer), and the inner nuclear layer (INL). *Coco* transcripts were not detected in the ganglion cell layer (GCL). (C) Post-natal day 3 mouse tissues were analyzed by qPCR for the expression of *Coco* transcripts using the 5'primers or the 3'primers. Data are expressed as fold change over gene expression in intestine, which was set at 1. Results are Mean +/- s.d. (n = 3). Scale bars: 30 μm.

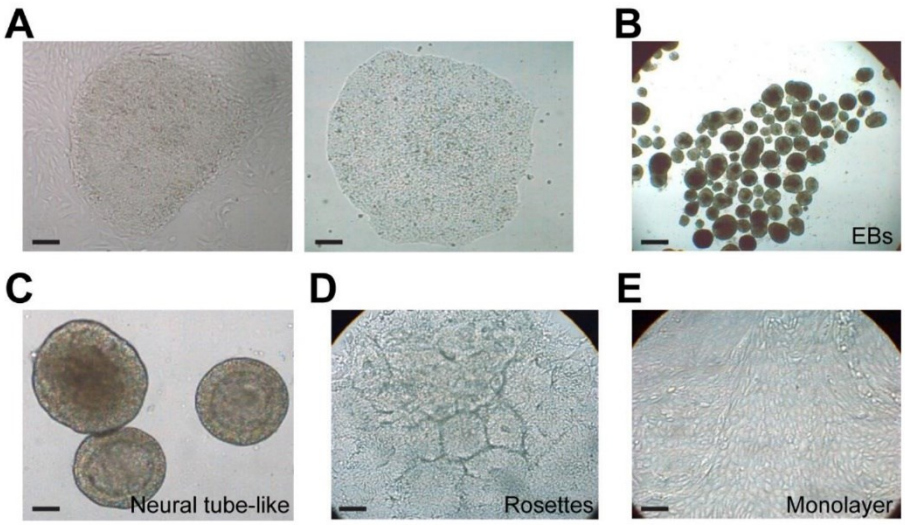

Figure S2. Stepwise neural induction of hES cells

(A) hES cultured on mouse fibroblasts feeders (left) or on matrigel (right). (B) Floating embryoid bodies (EBs). (C) EBs cultured on a matrigel surface showing neural tube-like appearance. (D) Neural rossettes. (E) Neuroepithelial monolayer. Scale bars: 50 μm (A and E), 100 μm (B and C), 200 μm (D).

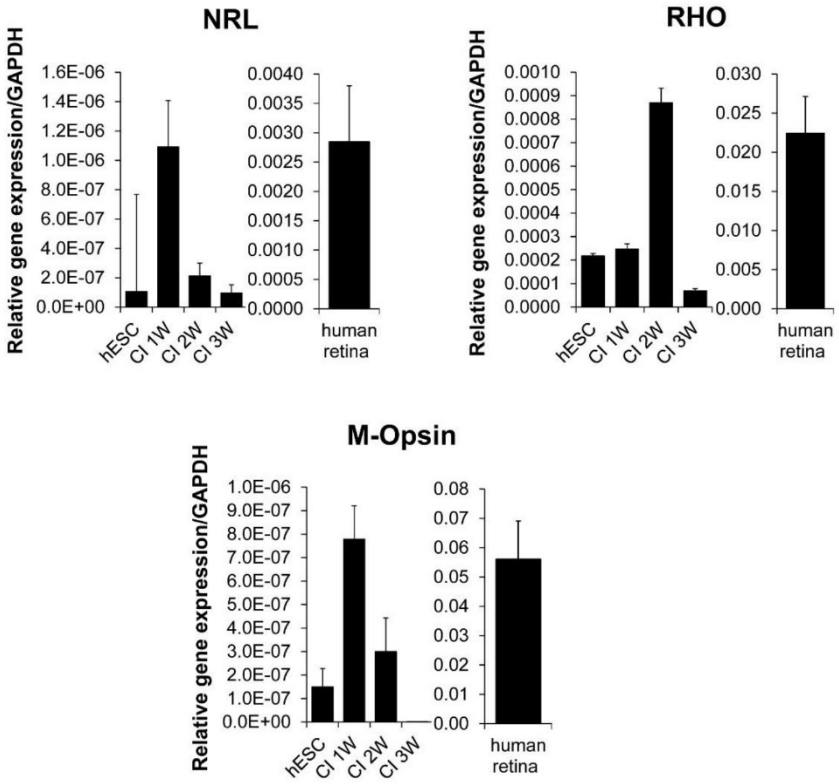

Figure S3. Analysis of rod and m-cone specific transcripts

hES cells were induced to differentiate in the presence of CI media for 1, 2 or 3 weeks and analyzed by qPCR. Data are expressed as relative gene expression over *GAPDH*. Whole human retina was used as positive control.

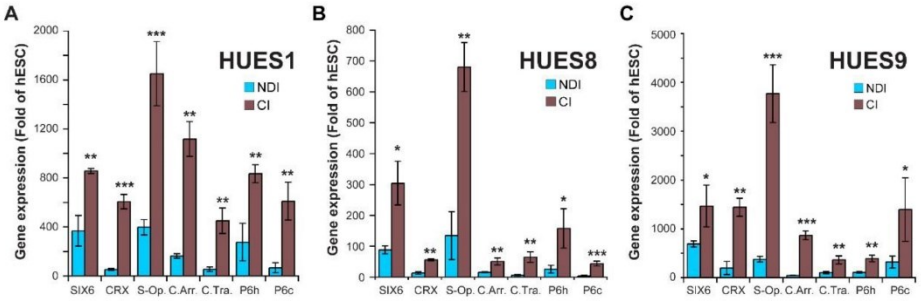

Figure S4. Expression of cone-specific transcripts across various hES cell lines

EBs derived from 3 hES cell lines (HUES1, HUES8 and HUES9) were differentiated in the presence of NDI or CI media for 3 weeks. Differentiated hES cells were analyzed by qPCR for the expression of *SIX6*, *CRX*, *S-Opsin* (*S-Op.), Cone Arrestin* (*C.Arr.), Cone transducin* (*GNAT2*), *PDE6h* (*P6h*) and *PDE6c* (*P6c*). Data are normalized over *GAPDH* and expressed as fold change of hESC. Results are Mean +/- s.d. (n = 3; *P<0.05; **P<0.01; ***P<0.001 as compared to gene expression levels in NDI-treated cells).

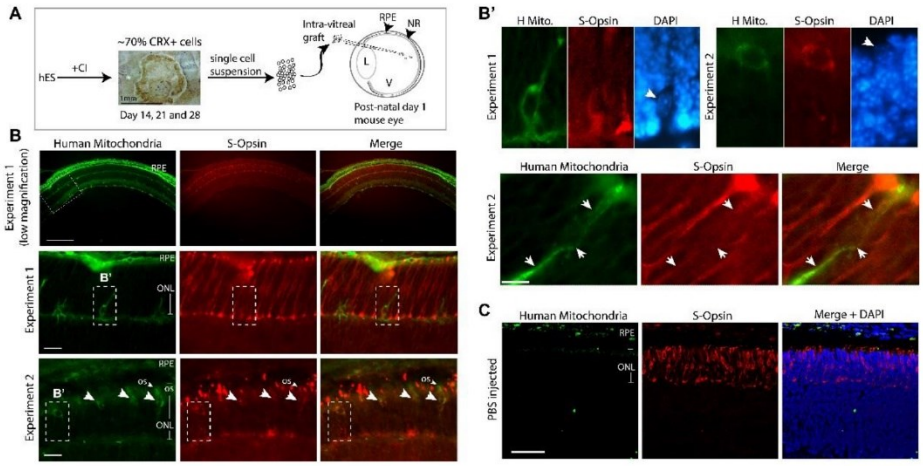

Figure S5. Differentiated hES can integrate the developing mouse retina

(A) Scheme describing the engraftment method. (B) 10 days (experiment 1) or 14 days (experiment 2) after transplantation, eye sections were labeled with anti-human mitochondria (H Mito.; green) and anti-S-Opsin (red) antibodies and mounted with DAPI (blue). Top: low magnification images from experiment 1. Percentage of grafted cells having migrated in the host retina was 1.4 +/- 0.5% in both experimental settings. Note that S-Opsin is mostly localized to the newly formed outer segment of endogenous cones in 14-day old grafted mice (experiment 2). Arrowheads point to grafted human cells that are S-Opsin positive. The smaller arrowhead in Experiment 2 indicates a human cell displaying S-Opsin immuno-reactivity in its outer segment. There may be more than a single human cell positive for S-Opsin in this particular region of the host retina. (B') The higher magnifications of cells selected in (B) revealed that double-positive cells have a larger nuclei and a unique chromatin condensation pattern (top arrowheads) when compared to that of endogenous mouse photoreceptors. They are also positive for S-Ospin. Bottom: high magnification images of engrafted cells (white arrows). (C) IF analysis of mouse eyes only injected with PBS (negative control). Scale bars: 800 µm (low magnification in B), 40 µm (higher magnification in experiments 1 and 2), 50 µm (PBS injected eyes in C). ONL: outer nuclear layer, RPE: retinal pigment epithelium, os: outer segment of photoreceptors.

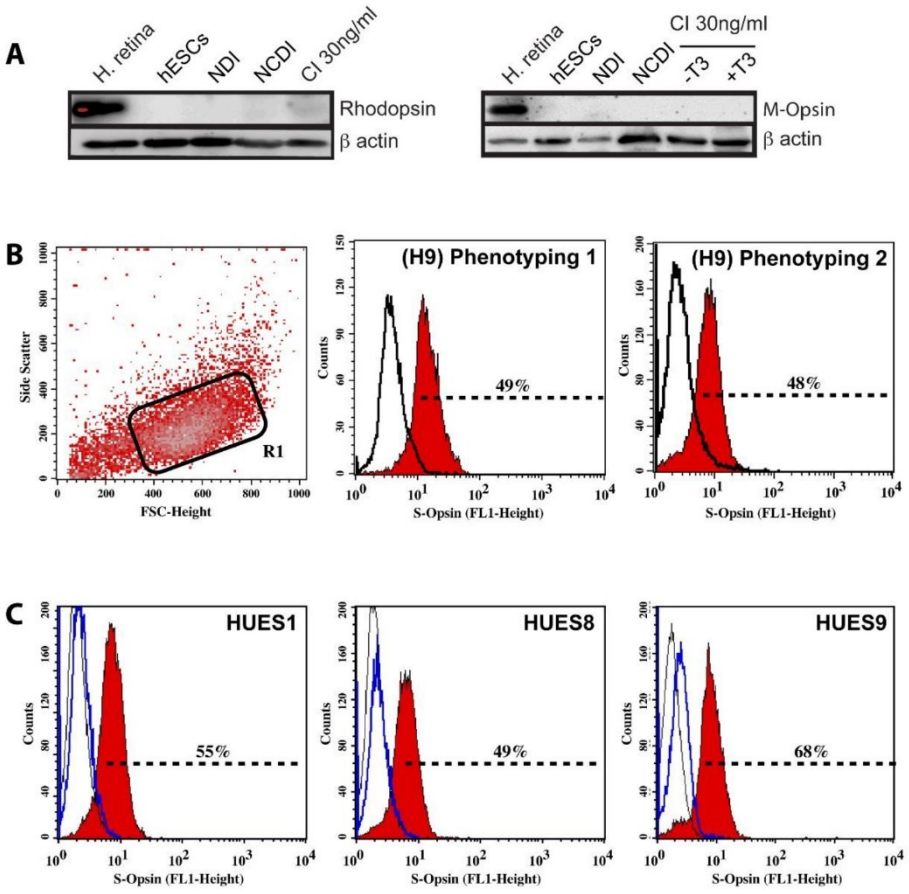

Figure S6. Generation of S-cones across various hES cell lines

(A) hES cell-derived EBs cultured in the NDI, NCDI, or CI media for 3 weeks were subjected to Western blot analysis for the expression of Rhodopsin. hES cell-derived EBs cultured in the presence or absence of thyroid hormone (T3; 4.8 nM) were subjected to Western blot analysis for the expression of M-Opsin. β actin was used for the quantification of protein loading. Human retinas were used as a positive control. (B-C) In the Side Scatter/Forward Scatter biparametric diagram, the R1 gate delineates the cell population analyzed. We analyzed by FACS using an anti-S-Opsin antibody either naive hES cells (blue line) or hES cells cultured in CI media for 3 weeks (red line). The isotypic control serum is represented by the black line. These uniparametric panels show data obtained with 4 different hES cell lines.

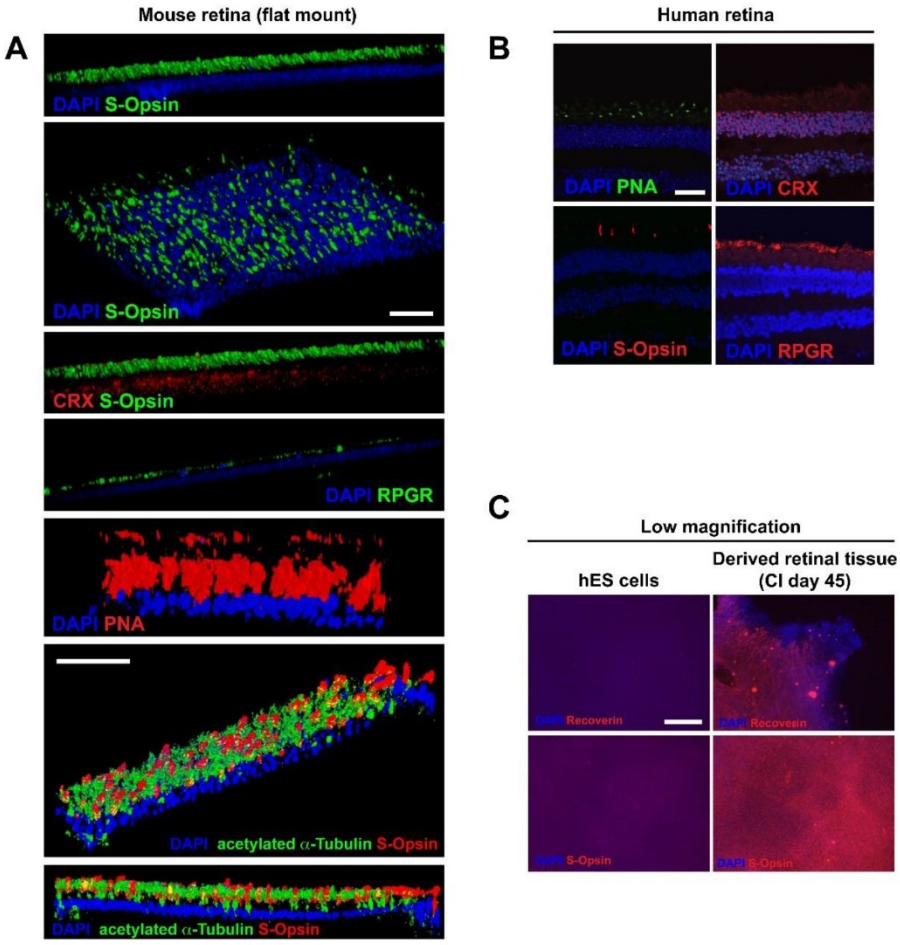

Figure S7. Antibodies specificity validated on mouse and human retinas

(A) Immunofluorescence on whole mount P17 mouse retina for photoreceptor markers (CRX, S-Opsin and PNA) and connecting cilium markers (RPGR and acetylated α-Tubulin). Tissues were reconstructed in 3D using confocal microscopy. (B) Immunofluorescence on adult human retina for the photoreceptor markers CRX, S-Opsin and PNA, and the connecting cilium marker RPGR using confocal microscopy. (C) Immunofluorescence on undifferentiated hES cells and cellular sheet obtained after 45 days with the CI media (10X magnification). Scale bars: 40µm (3D images) and 400µm (low magnification in C).

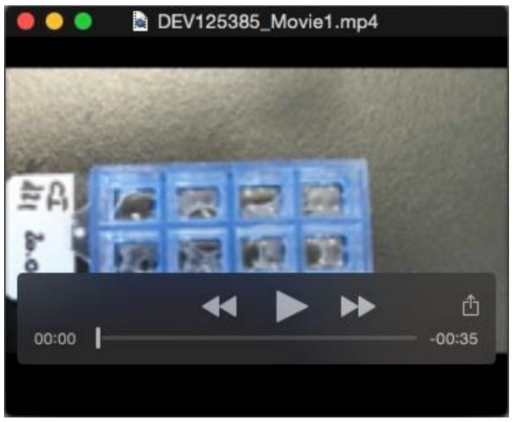

Supplementary Movie 1. Manipulation of hES cells-derived retinal sheet

hES cells were differentiated for 60 days in CI media with a daily media change. Cellular sheets are then detached from the chamber slides using nippers and placed on a microscopy slide.